Thèse

NUMERICAL ANALYSES OF SEGMENTAL TUNNEL LINING UNDER STATIC AND DYNAMIC LOADS

ANALYSES NUMERIQUES DE REVETEMENT ARTICULE DE TUNNEL SOUS CHARGES STATIQUE ET DYNAMIQUE

Présentée devant

L'INSTITUT NATIONAL DES SCIENCES APPLIQUEES DE LYON

Pour obtenir

LE GRADE DE DOCTEUR

ECOLE DOCTORALE : MEGA – Mécanique, Energétique, <u>Génie Civil</u>, Acoustique

Par

Ngoc Anh DO

Ingénieur et Master en Construction des Ouvrages Souterrains et des Mines
Ecole supérieure des Mines et de Géologie, Hanoi, Vietnam

Soutenue le 07 Juillet 2014 devant la Commission d'Examen

Jury Mme. et MM.

Richard KASTNER	Professeur	Président - INSA de Lyon
Tarcisio CELESTINO	Professeur	Rapporteur - University of São Paulo
Günther MESCHKE	Professeur	Rapporteur - Ruhr-Universität Bochum
Pierpaolo ORESTE	Professeur associé	Examinateur - Politecnico di Torino
Daniel DIAS	Professeur	Directeur de thèse - Grenoble Alpes Université
Irini DJERAN-MAIGRE	Professeur	Directrice de thèse - INSA de Lyon

Cette thèse a été effectuée au Laboratoire L.G.C.I.E. de l'INSA de LYON

INSA Direction de la Recherche - Ecoles Doctorales - Quinquennal 2011-2015

SIGLE	ECOLE DOCTORALE	NOM ET COORDONNEES DU RESPONSABLE
CHIMIE	**CHIMIE DE LYON** **http://www.edchimie-lyon.fr** Sec :Renée EL MELHEM Bat Blaise Pascal 3e etage Insa : R. GOURDON	M. Jean Marc LANCELIN Université de Lyon – Collège Doctoral Bât ESCPE 43 bd du 11 novembre 1918 69622 VILLEURBANNE Cedex Tél : 04.72.43 13 95 directeur@edchimie-lyon.fr
E.E.A.	**ELECTRONIQUE, ELECTROTECHNIQUE, AUTOMATIQUE** **http://edeea.ec-lyon.fr** Secrétariat : M.C. HAVGOUDOUKIAN eea@ec-lyon.fr	M. Gérard SCORLETTI Ecole Centrale de Lyon 36 avenue Guy de Collongue 69134 ECULLY Tél : 04.72.18 60.97 Fax : 04 78 43 37 17 Gerard.scorletti@ec-lyon.fr
E2M2	EVOLUTION, ECOSYSTEME, MICROBIOLOGIE, MODELISATION http://e2m2.universite-lyon.fr **Insa : H. CHARLES**	Mme Gudrun BORNETTE CNRS UMR 5023 LEHNA Université Claude Bernard Lyon 1 Bât Forel 43 bd du 11 novembre 1918 69622 VILLEURBANNE Cédex Tél : 06.07.53.89.13 e2m2@ univ-lyon1.fr
EDISS	**INTERDISCIPLINAIRE SCIENCES- SANTE** **http://www.ediss-lyon.fr** Sec : Insa : M. LAGARDE	Mme Emmanuelle CANET-SOULAS INSERM U1060, CarMeN lab, Univ. Lyon 1 Bâtiment IMBL 11 avenue Jean Capelle INSA de Lyon 696621 Villeurbanne Tél : 04.72.68.49.09 Fax :04 72 68 49 16 Emmanuelle.canet@univ-lyon1.fr
INFOMATHS	**INFORMATIQUE ET MATHEMATIQUES** **http://infomaths.univ-lyon1.fr** Sec :Renée EL MELHEM Bat Blaise Pascal 3e etage infomaths@univ-lyon1.fr	Mme Sylvie CALABRETTO LIRIS – INSA de Lyon Bat Blaise Pascal 7 avenue Jean Capelle 69622 VILLEURBANNE Cedex Tél : 04.72. 43. 80. 46 Fax 04 72 43 16 87 Sylvie.calabretto@insa-lyon.fr
Matériaux	**MATERIAUX DE LYON** **http://ed34.universite-lyon.fr** Secrétariat : M. LABOUNE PM : 71.70 –Fax : 87.12 Bat. Saint Exupéry Ed.materiaux@insa-lyon.fr	M. Jean-Yves BUFFIERE INSA de Lyon MATEIS Bâtiment Saint Exupéry 7 avenue Jean Capelle 69621 VILLEURBANNE Cedex Tél : 04.72.43 83 18 Fax 04 72 43 85 28 Jean-yves.buffiere@insa-lyon.fr
MEGA	**MECANIQUE, ENERGETIQUE, GENIE CIVIL, ACOUSTIQUE** **http://mega.universite-lyon.fr** Secrétariat : M. LABOUNE PM : 71.70 –Fax : 87.12 Bat. Saint Exupéry mega@insa-lyon.fr	M. Philippe BOISSE INSA de Lyon Laboratoire LAMCOS Bâtiment Jacquard 25 bis avenue Jean Capelle 69621 VILLEURBANNE Cedex Tél :04.72 .43.71.70 Fax : 04 72 43 72 37 Philippe.boisse@insa-lyon.fr
ScSo	**ScSo*** **http://recherche.univ-lyon2.fr/scso/** Sec : Viviane POLSINELLI Brigitte DUBOIS Insa : J.Y. TOUSSAINT	M. OBADIA Lionel Université Lyon 2 86 rue Pasteur 69365 LYON Cedex 07 Tél : 04.78.77.23.86 Fax : 04.37.28.04.48 Lionel.Obadia@univ-lyon2.fr

*ScSo : Histoire, Géographie, Aménagement, Urbanisme, Archéologie, Science politique, Sociologie, Anthropologie

ACKNOWDLEGEMENTS

The work described within this thesis was conducted at Laboratory LGCIE, INSA of Lyon, University of Lyon, France, from September 2011 to July 2014.

Foremost, I am particularly grateful to my supervisors, Professor Daniel Dias, Professor Irini Djeran-Maigre. They have been very supportive, given me invaluable advices on the preparation of this thesis and research articles. I would like to thank Professor Daniel Dias for his constant support. He pushed me to achieve my full potential. His professional guidance and willingness to make himself constantly available have been crucial to the completion of this research. I would like to thank Professor Irini Djeran-Maigre for her invaluable guidance, supervision, encouragement and support throughout this study. I would like to state my sincere appreciation to my collaborator, Professor Pierpaolo Oreste, for his professional support, discussion and for his original Hyperstatic Reaction Method on which some new solutions presented in this study are based. I wish to record my sincere appreciation of their help and I will never forget three years of my PhD study under their direction.

I would also like to thank every member of the Laboratory LGCIE, INSA of Lyon for their encouragement. Special thanks to Mr. Vu Xuan Hong for nominating me as a PhD candidate.

The financial support of the Vietnamese Ministry of Education and Training, Vietnam and of the Laboratory LGCIE, INSA of Lyon, France is gratefully acknowledged.

I would like to give thanks to my friends for their support during the hardest parts of this research.

Finally, I am deeply indebted to my family, who made this research possible by their support, patience and love. Particularly, this research would not have started, could not have been undertaken and would never have been completed without the support of my wife, Ngoc and my two daughters, Chau Giang and Minh Chau. Nothing would have been possible without their support and it is to them that I dedicate this thesis.

Ngoc Anh DO

Lyon, July 2014

iii

SUMMARY

This PhD thesis has the aim to study the behaviour of segmental tunnel lining by developing a new numerical approach to the Hyperstatic Reaction Method (HRM) and producing two-dimensional (2D) and three-dimensional (3D) numerical models using the finite difference method (FDM). The study first deals with under static loads, and then performs under dynamic loads.

Firstly, a literature review has been conducted. A new numerical approach applied to the HRM has then been developed. At the same time, a 2D numerical model is programmed regarding static loading conditions in order to evaluate the influence of the segmental joints, in terms of both joint distribution and joint stiffness characteristics, on the tunnel lining behaviour. After that, full 3D models of a single tunnel, twin horizontal tunnels and twin tunnels stacked over each other, excavated in close proximity in which the joint pattern is simulated, have been developed. These 3D models allow one to investigate the behaviour of not only the tunnel lining but also the displacement of the ground surrounding the tunnel during the tunnel excavation. A simplified 3D numerical model has then been produced in order to validate the new numerical approach applied to the HRM.

In the last part of the manuscript, the performance of the segmental tunnel lining exposed to dynamic loading is taken into consideration through quasi-static and full dynamic analyses using 2D numerical models (FDM). A new HRM model has also been developed considering quasi-static loads. The differences of the tunnel behaviour under static and seismic loadings are highlighted.

Keywords: Tunnel; Segmental lining; Hyperstatic Reaction Method; Numerical model; Quasi static; Dynamic; Soft ground.

v

RÉSUMÉ

Cette thèse vise à étudier le comportement de revêtement articulé du tunnel en développant une nouvelle approche numérique à la Méthode de Réaction Hyperstatique (HRM) et la production des modèles numériques en deux dimensions et trois dimensions à l'aide de la méthode des différences finies (FDM). L'étude a été traitée d'abord sous charges statiques, puis effectuée sous charges dynamiques.

Tout d'abord, une étude bibliographique a été effectuée. Une nouvelle approche numérique appliquée à la méthode HRM a ensuite été développée. En même temps, un modèle numérique en deux dimensions est programmé sur les conditions de charge statique dans le but d'évaluer l'influence des joints, en termes de la distribution et des caractéristiques des joints, sur le comportement du revêtement articulé de tunnel. Après cela, des modèles complets en trois dimensions d'un seul tunnel, de deux tunnels horizontaux et de deux tunnels empilés, dans lesquels le système des joints est simulé, ont été développés. Ces modèles en trois dimensions permettent d'étudier le comportement non seulement du revêtement du tunnel, mais encore le déplacement du sol entourant le tunnel lors de l'excavation. Un modèle numérique en trois dimensions simplifié a ensuite été réalisé afin de valider la nouvelle approche numérique appliquée à la méthode HRM.

Dans la dernière partie de ce mémoire, la performance du revêtement articulé du tunnel sous chargements dynamiques est prise en compte par l'analyse quasi-statique et dynamique complète en utilisant le modèle numérique en deux dimensions (FDM). Un modèle HRM a également été développé prenant en compte des charges quasi-statiques. Les différences de comportement de tunnel sous chargements statiques et sismiques sont mises en évidence et expliquées.

Mots-clés: Tunnel; Revêtement articulé; Méthode de Réaction Hyperstatiques; Modèle numérique; Quasi statique; Dynamique; Sol souple.

TABLE OF CONTENTS

ix

LIST OF FIGURES

xix

xxi

xxiii

LIST OF TABLES

xxvii

GENERAL INTRODUCTION

xxviii

Background and Problematic

The application range of mechanized tunnelling has been remarkably extended in recent years. Segmental linings are usually utilized in these tunnels. One of the most important factors in the design of a segmental tunnel lining is the influence of the segmental joints on its overall behaviour.

Nowadays, many design methods for segmental lining have been developed and can be classified into three main groups which include empirical methods, analytical methods and numerical methods.

As far as empirical/analytical methods are concerned, the effects of segmental joints on tunnel lining behaviour have usually been considered in literature through direct and indirect methods. In indirect methods, the segmental tunnel lining is considered as a continuous lining ring embedded in a continuous soil mass. The effect of the joints is usually taken into account through the reduction factor, η, of the flexural rigidity of the lining, which can be determined empirically, analytically or experimentally. Due to their simplicity, these indirect methods are still considered very useful for the dimensioning of a segmental lining. In direct methods, segmental joints are added directly to the tunnel lining structure. The main drawback of this solution is the symmetrical assumption of external load and joint distribution over the vertical tunnel axis. In addition, the behaviour of the segment joints is usually taken into account through a linear rotational stiffness relationship.

Rapid progress in the development of user friendly computer codes and the limitations of analytical methods have led to an increase in the use of numerical methods for the design of tunnel lining. The numerical models could be built by using in-house finite element software or commercial software packages which allow one to take the complex interaction between the tunnel lining and the surrounding ground and elements of the tunnelling process into account. Great efforts in numerical modelling have been made by researchers over the world in order to study the effect of the joints on the segmental tunnel lining behaviour and ground surrounding the tunnel. There is however still no complex numerical modelling that is able to focus on this problem and the behaviour of segmental tunnel lining has not been yet thoroughly clarified.

During service time, a tunnel could be exposed to dynamic loads. While tunnels generally performed better than above ground structures during earthquakes, damage to some of important structures during previous earthquake events highlights the need to account for seismic loads in the design of underground structures. Despite the multitude of studies that have been carried out over the years, the behaviour of segmental tunnel lining under seismic loads is still far from being fully understood. Consequently, current engineering practice lacks conclusive information that may be used in the design of tunnel lining structures.

Obviously, there is a necessity to improve the existing methods and/or develop new approaches for the purpose of segmental lining design under both static and dynamic loading conditions. In addition, development of new numerical models taken into consideration the presence of the joints in the lining will be very helpful in order to highlight their effects on the behaviour of segmental lining.

Scope

The Hyperstatic Reaction Method (HRM), which is part of the numerical method category, is particularly suitable for the design of support structures. Present work has the aim of introducing new numerical approaches applied to the HRM in order to realize a calculation code for the analysis of segmental lining under both static and dynamic loading conditions. Two-dimensional (2D) and three-dimensional (3D) numerical models developed using the finite difference program FLAC^{3D} have been used to validate the new proposed HRM. Also using these 2D and 3D models, numerical investigation will be carried out in order to highlight the effect of the joints, mechanical parameters of the ground, and elements of construction procedure on the behaviour of segmental tunnel lining and the ground surrounding the tunnel.

The adequate achievement of the main goals is planed through the accomplishment of the partial targets listed below:

As far as static analyses are concerned:

- Development of 2D and 3D numerical models and assessment of the influence of joint stiffness parameters on the tunnel lining behaviour;
- Development of a new numerical approach to the Hyperstatic Reaction Method for the design of segmental tunnel lining; Validation of this new method with numerical models on the prediction of segmental concrete lining response;
- Study of the behaviour of tunnel when using simplified 2D methods in order to take into consideration 3D effects during tunnelling and point out which one is the better method;
- Study of the behaviour during excavation of a single tunnel, twin horizontal tunnels and twin stacked tunnels using corresponding full 3D models;

As far as dynamic analyses are concerned:

- Development of a 2D numerical model which allows simulating the segmental tunnel lining exposed to dynamic circumstances in both quasi-static and full dynamic conditions. Determination of the segmental tunnel lining behaviour under dynamic loads;
- Implementation of a new numerical approach in the HRM for the dynamic purpose. Validation of this new method with numerical models on the prediction of segmental concrete lining response;

It should be noted that all analyses presented in this research are performed for the case of circular tunnels excavated through soft grounds. However, the new HRM approaches and 2D or 3D numerical models can also be used for circular tunnels excavated through other types of ground (i.e., hard rock).

Original Features

For the best of the author's knowledge, the original features of the present work are:

- Generation of a 2D numerical model and investigation the influence of the joints in

lining, including joint stiffnesses and joint distribution, and geo-mechanical parameters of the ground mass on the behaviour of a segmental tunnel lining under both static and dynamic (quasi-static) loading conditions;

- Determination of the impacts between twin horizontal tunnels under the influence of the joints and tunnel distance;

- Generation of a full 3D model and description of the phenomena involved in mechanized tunnelling process of a single tunnel, especially the effect of both longitudinal and circumferential joints on the tunnel behaviour has been studied in detail;

- Generation of full 3D models and description of the phenomena involved in mechanized tunnelling process of twin horizontal tunnels and twin stacked tunnels;

- Generation of a simplified 3D model which allow the presence of the joints in segmental lining to be simulated;

- Performance of a new technique of simulation on the basis of the Volume Loss Method by using FLAC^{3D} software;

- Determination of the effect of simplified 2D simulation techniques (Convergence - Confinement Method and Volume Loss Method) on the tunnel behaviour taking into account the presence of the joints;

- Validation of simplified 2D models by using 3D model in order to indicate the better 2D model;

- Generation of a new numerical approach on the basis of the Hyperstatic Reaction Method for the design of segmental tunnel linings under both static and dynamic (quasi-static) loading conditions;

- Generation of a 2D numerical model and deep investigation the influence of the joints in lining on the behaviour of a segmental tunnel lining under full dynamic condition.

Outline and Contents

This thesis is composed of **9 chapters** decomposed in **3 parts**. Part 1 presents a bibliography study. **Part 2** aims to study the segmental tunnel lining behaviour under static loads, while **Part 3** focuses on estimating that of the tunnel exposed to dynamic loads.

In the first part, literature study presents the contents useful to the understanding of this thesis and is composed of 3 separate chapters as follows:
- **Chapter 1** focuses on the influence of segmental joints on the tunnel lining behaviour, studied using analytical methods, numerical methods and experimental analyses;

- **Chapter 2** pays attention to the interaction between tunnels excavated in close proximity to each other. Two typical cases, that is, twin horizontal tunnels and twin stacked tunnels, have been taken into consideration;

- In **Chapter 3**, methods used to study seismic-induced stress developed in the tunnel lining during seismic loads are presented.

The second part is composed of 3 chapters that present the segmental tunnel lining behaviour under static loads:

- In **Chapter 4**, a 2D numerical analysis of the segmental tunnel lining behaviour in which the effects of the joint stiffness, Young's modulus of the ground and the lateral earth pressure factor are taken into consideration. A 2D numerical investigation has been conducted in order to highlight the influence of two equivalent approaches, that is, the convergence-confinement method and the volume loss method, on the behaviour of a tunnel built in an urban area, in terms of not only the surface settlement but also the structural lining forces, taking into account the effect of segment joints. A technique that can be used to simulate the tunnel wall displacement process, based on the principles of the Volume Loss Method, has been developed using the FLAC^{3D} finite difference program.

  Another 2D model has been developed for twin horizontal tunnels**,** which allow the impacts between two tunnels during excavation to be highlighted. Parametric analyses considering the change in the joint distribution and tunnel distance have been performed.

- **Chapter 5** present 3D numerical models of a single tunnel and of twin (horizontal/stacked) tunnels, which would allow the tunnel lining behaviour, the displacement of the ground surrounding the tunnel and the interaction between tunnels to be evaluated. Most of the main processes that occur during mechanized excavation are simulated in this model. The influence of the joint pattern of the lining has in particular been taken into consideration. Numerical studies performed by using these models help to achieve significant conclusions about the impacts of the boundaries of the model, the constitutive model of the ground, the behaviour during the advancement of the tunnel face, and the influence of the joint pattern in particular. Additionally, the interaction between the new tunnel and the existing tunnel or between two tunnels excavated simultaneously has been highlighted in terms of both lining structural forces and displacement of the ground surrounding the tunnel.

- A new numerical approach applied to the HRM is developed and presented in **Chapter 6**. In the new approach, the influence of segmental joints has been considered directly using a fixity ratio that is determined on the basis of the rotational stiffness. The parameters necessary for the calculation are presented. A specific implementation has been developed using a finite element method (FEM) framework, which is able to consider the 3D effect of segment joints in successive rings on the tunnel lining behaviour. Comparison between results of the new HRM and simplified FLAC^{3D} model has been presented which allow the new HRM to be validated.

During its service time, the tunnel could be exposed to dynamic loads. Estimation of the segmental tunnel lining behaviour under dynamic loads is goal of the third part:

- **Chapter 7** introduces a 2D model in which the ovaling deformation of the tunnel cross-section has been adopted to simulate dynamic conditions. The influence of parameters, that is, the rotational, axial and radial stiffness of longitudinal joints, the lateral earth pressure factor, the deformability of the soil and the maximum shear strain, on the tunnel behaviour under seismic loadings is considered in detail.

- Full dynamic analysis is introduced in **Chapter 8**. Two different ground motions have been applied in the model, which allow highlighting the effect of the joints on the

tunnel lining during a seismic event with different maximum amplitude of the input signal.

- Finally, **Chapter 9** introduces the new HRM which is developed on the basis of the model presented in **Chapter 6** and taking into consideration the impact of dynamic loads by using quasi-static method.

The results presented in this manuscript have been several publications in international journals with peer review (Do et al. [2013a, 2013b, 2014a, 2014b, 2014c, 2014d, 2014e, 2014f]). Basically, the content of the articles are originally kept. However, some modifications and re-organizations of these articles have been made in order to ensure the continuity of the manuscript. The general organization of the present PhD thesis is illustrated in the figure below.

Static Analyses

Dynamic Analyses

Single tunnel

2D Model

Twin tunnels

Comparision

Numerical Analyses (FLAC^{3D})

Single tunnel

3D Model

Twin tunnels

Stacked tunnels

Validation

2D Model

Quasi-Static

Full Dynamic

Comparison

Hyperstatic Reaction Method (HRM)

xxxiv
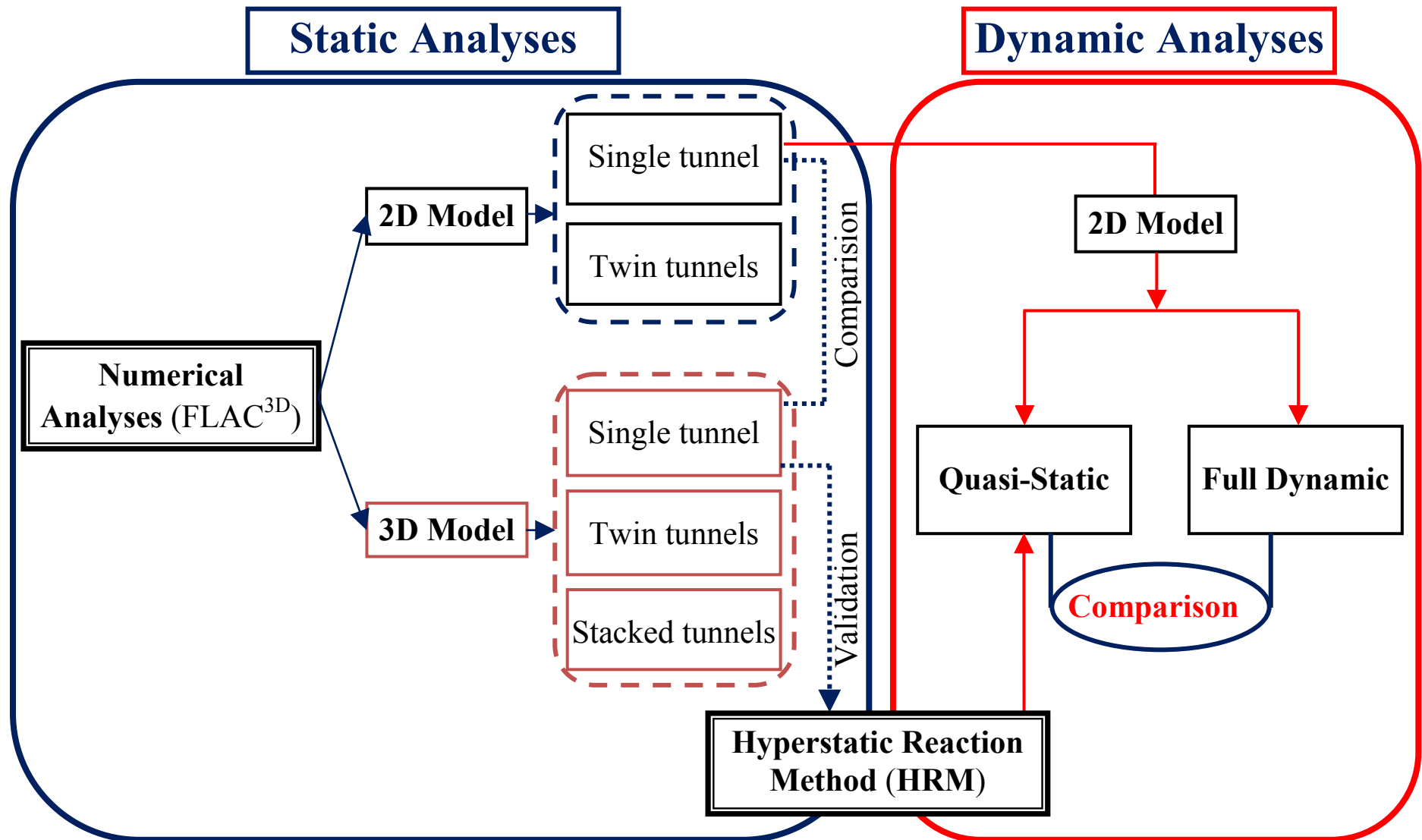
Contexte et Problématique

Le domaine d'application des tunnels mécanisés a été étendu ces dernières années. Les revêtements articules sont généralement utilisés dans ces tunnels. L'un des facteurs les plus importants dans la conception d'un revêtement articulé de tunnel est l'influence des joints de segments sur son comportement global.

Aujourd'hui, de nombreuses méthodes de conception pour le revêtement articulé ont été développées et peuvent être classés en trois groupes principaux qui comprennent des méthodes empiriques, des méthodes d'analyse et des méthodes numériques.

En ce qui concerne les méthodes empiriques et analytiques, les effets de joints de segments sur le comportement de revêtement du tunnel ont généralement été considérés dans la littérature par des méthodes directes et indirectes. Dans les méthodes indirectes, le revêtement articulé de tunnel est considéré comme un anneau de revêtement continu placé dans une masse de sol continu. L'effet des joints est généralement prise en compte par un facteur intermédiaire de réduction, η, de la rigidité à la flexion du revêtement, qui peut être déterminé empiriquement, analytiquement, ou expérimentale. En raison de leur simplicité, ces méthodes indirectes sont toujours très utiles pour la conception d'un revêtement articulé. Dans les méthodes directes, les joints de segments sont ajoutés directement à la structure du revêtement du tunnel. Le principal inconvénient de cette solution est l'hypothèse symétrique des charges externes et de la distribution des joints sur l'axe vertical du tunnel. De plus, le comportement des joints de segment est généralement pris en compte par une rigidité en rotation linéaire.

Le développement rapide des codes informatiques et la limite des méthodes d'analyse ont conduit à une augmentation de l'utilisation de méthodes numériques pour la conception de revêtement du tunnel. Les modèles numériques permettent de prendre en compte l'interaction complexe entre le revêtement du tunnel et le sol environnant et les éléments du processus de l'excavation mécanisé du tunnel. Des grands efforts dans la modélisation numérique ont été faits par des chercheurs autour du monde afin d'étudier l'effet des joints sur le comportement de revêtement articulé du tunnel et le sol environnant. Cependant, il n'y a pas encore de modélisation numérique complexe qui est capable de se concentrer sur ce problème; et le comportement de revêtement articulé du tunnel n'a pas encore été complètement clarifié.

Au cours du temps de service, un tunnel peut être exposé à des charges dynamiques. Alors que les tunnels réalisés généralement mieux que les structures de surface lors de séismes, les dommages de structures lors d'événements sismiques précédentes mettent en évidence la nécessité de tenir compte des charges sismiques dans la conception d'ouvrages souterrains. Malgré la multitude d'études qui ont été menées au fil des ans, le comportement de revêtement articulé du tunnel sous charges sismiques est encore loin d'être entièrement compris. Par conséquent, la pratique de l'ingénierie actuelle manque de données concluantes qui peut être utilisé dans la conception de revêtement du tunnel.

Évidemment, il y a une nécessité d'améliorer les méthodes existantes et /ou de développer de nouvelles approches en vue de la conception du revêtement articulé dans des conditions de chargement statique et dynamique. En outre, le développement de nouveaux modèles numériques prises en considération la présence des joints dans le revêtement sera très utile pour mettre en évidence leurs effets sur le comportement du revêtement articulé.

Cadre d'étude

La Méthode Réaction Hyperstatique (HRM), qui fait partie de la catégorie de la méthode numérique, est particulièrement adapté pour la conception des structures de soutien. Le présent travail a pour but d'introduire une nouvelle approche numérique appliquée à la méthode HRM afin de réaliser un code de calcul pour l'analyse du revêtement articulé dans des conditions de chargement statique et dynamique. Les modèles numériques en deux dimensions (2D) et trois dimensions (3D) développés en utilisant le programme de différences finies FLAC^{3D} ont été utilisées pour valider la nouvelle méthode HRM proposé. De plus, en utilisant ces modèles 2D et 3D, analyse numérique sera réalisée afin de mettre en évidence l'effet des joints, des paramètres mécaniques du sol et des éléments de la procédure de construction sur le comportement de revêtement articulé du tunnel et le sol entourant le tunnel.

La réalisation des principaux objectifs est prévue par la réalisation des objectifs partiels ci-dessous:

En ce qui concerne les analyses statiques:

- Le développement de modèles numériques 2D et 3D; l'évaluation de l'influence des paramètres de rigidités du joints sur le comportement de revêtement du tunnel;
- Le développement d'une nouvelle approche numérique appliquée à la méthode HRM pour la conception de revêtement articulé du tunnel; validation de cette nouvelle méthode avec les modèles numériques;
- L'étude de comportement du tunnel lors de l'utilisation des méthodes 2D simplifiées afin de tenir compte des effets de 3D lors de l'excavation du tunnel et souligner ce qui est la méthode mieux;
- L'étude de comportement du tunnel lors de l'excavation d'un seul tunnel, de deux tunnels horizontaux et de deux tunnels empilés en utilisant des modèles 3D complets correspondant.

En ce qui concerne les analyses dynamiques:

- Le développement d'un modèle numérique 2D qui permet de simuler le revêtement articulé du tunnel exposé à des circonstances dynamiques qui sont les conditions quasi-statique et dynamiques complets. La détermination du comportement de revêtement articulé de tunnel sous des charges dynamiques;
- Le développement d'une nouvelle approche numérique appliquée la méthode HRM

pour la conception de revêtement articulé du tunnel. La validation de cette nouvelle méthode avec les modèles numériques.

Caractéristiques originales

A la connaissance de l'auteur, les caractéristiques originales de ce travail sont:

- La génération d'un modèle numérique 2D et enquête sur l'influence des joints de revêtement, y compris les paramètres de rigidités et la distribution du joint, et les paramètres de géo-mécanique du sol sur le comportement d'un revêtement articulé du tunnel sous les chargements statiques et dynamiques (quasi-statiques);
- La détermination des impacts entre les deux tunnels horizontaux en tenant compte de l'influence des joints et de la distance du tunnel;
- La génération d'un modèle 3D complet et une description des phénomènes impliqués dans le processus de tunneling mécanisée d'un seul tunnel. En particulier, l'effet des joints longitudinaux et des joints circonférentiels sur le comportement de tunnel a été étudiée en détail;
- La génération de modèles 3D complets et la description complète des phénomènes impliqués dans le processus de tunneling mécanisée de deux tunnels horizontaux et de deux tunnels empilés;
- La génération d'un modèle simplifié en 3D qui permet à la présence des joints dans le revêtement articulé à simuler;
- La réalisation d'une nouvelle technique de simulation numérique sur la base de la méthode de perte de volume en utilisant le logiciel de FLAC3D;
- La détermination de l'effet de techniques simplifiés de simulation numérique 2D (la méthode de convergence-confinement et la méthode de perte de volume) sur le comportement du tunnel en tenant compte de la présence des joints;
- La validation des modèles 2D simplifiés en utilisant le modèle 3D afin d'indiquer la meilleure modèle 2D;
- La génération d'une nouvelle approche numérique sur la base de la méthode HRM pour la conception de revêtement articulé du tunnel sous les conditions de chargement statiques et dynamiques (quasi-statique);
- La génération d'un modèle numérique 2D et enquête sur l'influence des joints sur le comportement d'un revêtement articulé du tunnel sous la condition dynamique complète.

Plan et Contenu

Cette thèse est composée de 9 chapitres décomposés en 3 parties. Partie 1 présente une étude de la bibliographie. Partie 2 vise à étudier le comportement de revêtement articulé du tunnel sous charges statiques, tandis que la partie 3 se concentre sur l'estimation le comportement du tunnel exposés à des charges dynamiques.

Dans la première partie, l'étude de la littérature présente les contenus utiles à la compréhension de cette thèse et composé de 3 chapitres distincts comme suit:

- Le **chapitre** 1 se concentre sur l'influence des joints sur le comportement du revêtement articulé du tunnel, en utilisant des méthodes analytiques, numériques et des analyses de laboratoire.
- Le **chapitre** 2 accorde une attention à l'interaction entre les tunnels creusés à proximité de l'autre. Deux cas typiques, les deux tunnels horizontaux et empilés, ont été pris en considération.
- Dans le **chapitre** 3, les méthodes utilisées pour étudier les contraines sismiques développé dans le revêtement du tunnel sous les charges sismiques.

La deuxième partie est composée de 3 chapitres qui présentent le comportement de revêtement articulé du tunnel sous charges statiques :

- Dans le **chapitre 4**, une analyse numérique 2D du comportement de revêtement articulé du tunnel dans lequel les effets de la rigidité de joint, du module d'Young du sol et du coefficient de pression latérale des terres sont pris en considération. Une réduction significative du moment de flexion induit dans le revêtement du tunnel lorsque le nombre augmente de joint a été démontrée. On a vu que l'influence de la rigidité en rotation de joint, de la diminution de rigidité en rotation dans le cadre du moment de flexion négatif, du coefficient de pression latérale des terres et du module de sol entourant le tunnel ne doit pas être négligée. D'autre part, les résultats ont aussi montré une influence négligeable de la rigidité axiale et radiale des joints sur le comportement du revêtement articulé de tunnel. Une étude numérique 2D a été réalisée afin de mettre en évidence l'influence de deux approches équivalentes, ce sont la méthode convergence-confinement et la méthode de perte de volume, sur le comportement d'un tunnel construit dans une zone urbaine, en termes non seulement le tassement de surface mais aussi les forces de revêtement, en tenant compte de l'effet des joints. Une technique qui peut être utilisée pour simuler le processus de déplacement de la périphérie du tunnel, sur la base des principes de la méthode de perte de volume, a été développé en utilisant le programme de différences finies FLAC^{3D}.

  Un autre modèle 2D a été développé pour des tunnels horizontaux, qui permet les impacts entre les deux tunnels à souligner. La paramétrique analyse compte tenu de change de la distribution de joints et la distance de tunnel ont été réalisés.

- **Chapitre 5** présente les modèles numériques 3D d'un seul tunnel et de deux tunnels horizontales/empilées qui permettent le comportement de revêtement du tunnel, le déplacement du sol entourant le tunnel et l'interaction entre les tunnels à évaluer. La plupart des principaux processus qui se produisent lors de l'excavation mécanisée de tunnel sont simulés dans ce modèle. L'influence des joints a en particulier été prise en considération. Les résultats numériques ont montré une influence négligeable de l'état

initial de l'excavation de tunnel sur le comportement de tunnel. En revanche, une grande influence du modèle constitutif du sol sur le comportement de tunnel et le déplacement de sol a été soulignée. L'impact des processus en cours d'excavation mécanisée, tels que la pression d'injection et les forces des jacks, sur les efforts internes induits dans le revêtement du tunnel dépend de l'avancement du tunnel.

Une influence négligeable des joints sur le champ de déplacement du sol entourant le tunnel a été observée. En général, une variation des efforts internes induits dans des anneaux successifs le long de l'axe du tunnel a été trouvée dans revêtements articules en quinconce, ce qui indique la nécessité de simuler les joints dans le revêtement de tunnel et en utilisant un modèle numérique complet en 3D pour obtenir une estimation précise. En outre, l'influence de l'effet de couplage entre les anneaux successifs sur le comportement du revêtement a été mise en évidence.

Dans le cas de tunnels empilés, les résultats de l'analyse numérique ont indiqué un grand impact de la construction d'un nouveau tunnel sur un tunnel existant. Les plus grands effets sont observés lorsque le tunnel supérieur est creusé en premier. Le tunnel supérieur est également affecté à une plus grande mesure par la procédure d'excavation. L'excavation du tunnel supérieur conduit généralement à de plus grandes tassements de surface que ceux obtenus pour le cas où le tunnel inférieur est creusé en premier. D'autre part, les efforts internes induits dans les tunnels empilés, quand ils sont creusés simultanément, sont supérieures à celles obtenues dans les autres cas. Le développement de champ de contraintes verticales σ_{zz} et de zones plastiques autour des tunnels à l'état final dépend surtout de l'excavation du tunnel inférieur.

En ce qui concerne les tunnels horizontaux, les résultats de l'analyse numérique ont également indiqué un grand impact de la construction d'un nouveau tunnel sur un tunnel existant. En générale, l'excavation simultanée de tunnels provoque plus petit efforts internes et déplacements de revêtement que ceux induits dans le cas de tunnels creusés à une grande distance. Cependant, l'excavation simultanée de tunnels pourrait aboutir à un tassement au-dessus des deux tunnels plus élevé.

- Bien que les analyses numériques à l'aide de logiciels commerciaux permettent la plupart des processus complexes au cours du tunneling mécanisé à simuler, ils sont généralement la consommation de temps. La méthode HRM est particulièrement adaptée pour l'estimation du comportement de revêtement du tunnel, en termes d'efforts internes, déplacement de revêtement, et la pression passive du sol le long du profil de tunnel. Cette méthode permet d'obtenir des résultats avec un peu de temps de calcul. Une nouvelle approche numérique appliquée à la méthode HRM a été élaborée et présenté dans le **chapitre 6**.

Tout d'abord, une approche numérique amélioré pour la méthode HRM, qui a d'abord été développé en utilisant le facteur de réduction, η, sur la base du modèle proposé par Oreste [2007], a été présenté. Une analyse paramétrique a permis d'estimer le

xxxix

comportement de revêtement articulé du tunnel dans un grand nombre de cas qui couvrent les conditions qui sont généralement rencontrés dans la pratique de l'excavation de tunnel. L'influence de trois types typiques de terrain, qui est la terre faibles, la terre moyen, et la terrain solide; de deux valeurs du coefficient de pression latérale des terres, K_0; de deux valeurs de profondeur du tunnel, H, qui correspondent à un tunnel faible profond et un tunnel profonde; de trois valeurs du rayon du tunnel, R; de trois valeurs d'épaisseur de revêtement de tunnel, t, et de quatre valeurs de coefficient de réduction, η, ont été étudiés. Les résultats qui sont présentés comme des figures de conception peuvent être utilisé pour une estimation préliminaire d'efforts internes, de déplacement de revêtement, et de pression passive du sol.

Sur la base du modèle HRM ci-dessus, une nouvelle approche de la méthode HRM appliquée à un revêtement articulé de tunnel a été présentée. L'influence des joints a été considérée directement utilisant un printemps de rotation, qui est représenté par un ratio de fixité qui a été déterminée sur la base de la rigidité en rotation non linéaire. Une exécution spécifique a été développée en utilisant FEM. Ce code est capable d'examiner l'effet de joints en anneaux successifs de revêtement articulé du tunnel. La méthode présente HRM permet la distribution des joints le long de la périphérie de tunnel à prendre en compte. En outre, la rigidité en rotation a été simulée en utilisant un comportement non linéaire, qui est plus proche du comportement réel d'un joint que le comportement linéaire ou bilinéaire. Cette nouvelle approche HRM a été validée en utilisant un modèle numérique 3D simplifiée.

Pendant son temps de service, le tunnel peut être exposé à des charges dynamiques. Estimation du comportement de revêtement articulé du tunnel sous charges dynamiques est l'objectif de la troisième partie:

- Tout d'abord, un modèle numérique 2D dans lequel la déformation ovale de la section transversale du tunnel est adoptée pour simuler des conditions dynamiques a été développée dans le **chapitre 7**. Les influences de la distribution de joint, des rigidités de joint (y compris la rigidité en rotation, la rigidité axiale et la rigidité radiale attribuée aux joints), les conditions du sol (le module d'Young et le coefficient de pression latérale des terres), et les charges sismiques représentées par la déformation maximale de cisaillement, ont été étudiés en détail. Les résultats ont indiqué que l'influence de la distribution des joints sur le revêtement articulé du tunnel dans les conditions sismiques et statiques n'est pas similaire. Le moment de flexion et les efforces normales induite dans un revêtement articule de tunnel sont généralement plus petits que ceux correspondants au revêtement continu, à l'exception des efforces normales minimales. Ceci signifie que d'un revêtement articulé peut effectuer mieux qu'un revêtement continu pendant tremblement de terre.

- L'analyse dynamique complète est introduite dans le **chapitre 8**. Par rapport aux

modèles quasi-statiques, l'analyse dynamique complète est évidemment le niveau le plus complexe des analyses dynamiques, qui est donc aussi la méthode la plus précise. Dans cette étude, deux différentes excitations sismiques du sol ont été appliquées dans le modèle numérique 2D, ce qui permet de mettre en évidence l'effet des joints sur le revêtement du tunnel lors d'un événement sismique aux différentes amplitudes maximales du signal d'entrée. Bien qu'il existe des différences entre le comportement d'un revêtement articulé et celle d'un revêtement continu, l'effet des joints sous une faible excitation sismique peut être négligé. L'effet du modèle constitutif de sol sur le comportement de tunnel dépend dans une large mesure de l'amplitude de l'excitation sismique et il pourrait être négligé sous faible excitation sismique. Cependant, cet effet doit être pris en considération sous une grande excitation sismique. Les résultats indiquent également que l'analyse élastique n'est pas suffisante pour déterminer la réponse d'un système sol-tunnel sous les charges séismiques et une solution statique équivalente donnerait efforts internes de revêtement inférieur à celles d'une solution dynamique complète.

- Enfin, le **chapitre 9** présente la nouvelle approche HRM qui est développé sur la base du modèle présenté au chapitre 6 et en tenant compte de l'impact des charges dynamiques en utilisant la méthode quasi-statique. Cette nouvelle approche HRM permet aux effets de contrainte cisaillement induit par les charges sismiques sur les revêtements articules de tunnels être étudiés. Les résultats paramétriques indiquent que l'effet des joints sur les efforces internes doit être considérée pour obtenir une conception économique du revêtement articulé exposés à des charges sismiques.

Les résultats présentés dans ce manuscrit ont fait l'objet de plusieurs publications en revues internationales à comités de lecture (Do et al. [2013a, 2013b, 2014a, 2014b, 2014c, 2014d, 2014e, 2014f]). Il reste néanmoins dans cette thèse un certain nombre de recherches à valoriser par d'autres publications. Fondamentalement, les contenus de ces articles sont initialement maintenus. Toutefois, certaines modifications et réorganisations de ces articles ont été réalisées afin d'assurer la continuité du manuscrit. Le contenu principal de la mémoire est illustré dans la figure ci-dessous.
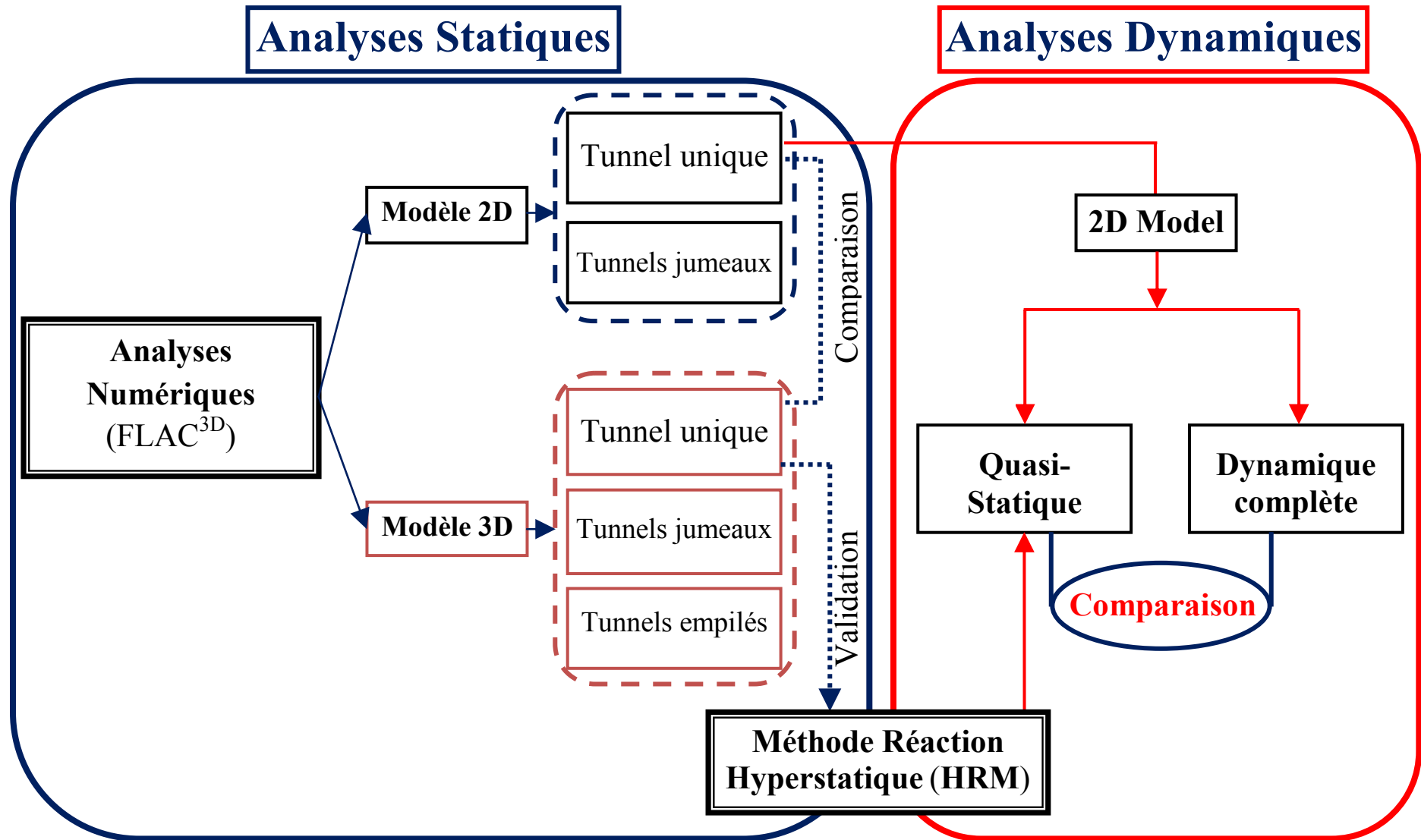
First part

Bibliography Study

Introduction

Application range of segmental tunnel linings have extended more and more, especially in mechanized tunnelling. One of the most important factors in the design of a segmental tunnel lining is the influence of the segmental joints on its overall behaviour.

Apart from single tunnels, the increase in transportation in large cities makes it necessary to construct twin tunnels at shallow depths. In these cases, the prediction of the influence of a new tunnel construction on an already existing one plays a key role in the optimal design and construction of close parallel shield tunnels.

During service time, a tunnel could be exposed to dynamic loads. While tunnels generally performed better than above ground structures during earthquakes, damage to some of important structures during previous earthquake events highlights the need to account for seismic loads in the design of underground structures.

This first part provides a state of the art to the understanding of this thesis. In Chapter 1, methods of study the segmental tunnel lining, that is, analytical, numerical and experimental methods, and the main results are described. An emphasis is placed on the influence of segmental joints on the tunnel lining behaviour. Some experimental test results, which allow determining stiffness parameters of the joints, are shown.

Chapter 2 pays attention to the interaction between tunnels excavated in close proximity to each other. Two typical cases, that is, twin horizontal tunnels and twin stacked tunnels, have been taken into consideration. It appears that most of reported cases focus on the ground displacement (surface settlement) and the influence of the segmental joints is not considered.

In Chapter 3, methods used to study seismic-induced stress developed in the tunnel lining during seismic events are presented. An emphasis is placed on the tunnel lining behaviour in the transverse section study using quasi-static and full dynamic analyses. The effects of segmental joints and soil constitutive model are also detailed.

Chapter 1

Influence of Segmental Joints on the Tunnel Lining Behaviour

1.1. Introduction

The existence of joints between the segments is a main characteristic of segmental linings. There are two types of joints in segmental lining, that is:

- Ring or circumferential joints between two successive rings;

- Longitudinal or segmental joints between segments in a ring.

Nomenclature of elements in a segmental tunnel lining is illustrated in **Figure** 1-1 (Nguyen [2006]).
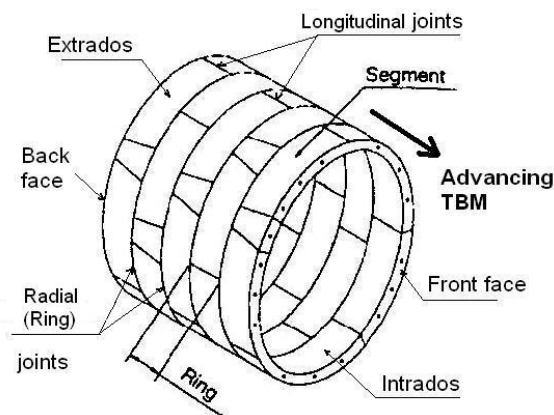
Figure 1-1. Segmental lining nomenclature (Nguyen [2006])

The development of a realistic calculation model for a precast lining requires a correct modelling of the joints between the segments, whose influence is very important upon the sectional dimensions. The static action of the lining will be determined in a large measure by its rigidity, i.e. by the overall capacity to resist deformation, the combined effect of deformation of the segments and deformation at the joints. In majority of the reinforced concrete precast linings, the deformation at the joints has a significant effect on the deformation of the segments. Thus, the magnitude and distribution of the internal forces depend to a great extent upon the distribution and characteristic of the joints. Consequently, one of the most important factors in designing a segmental tunnel lining is the influence of the segmental joints on its overall behaviour.

In structural analyses, a segmental joint can be considered as an elastic pin and its stiffness characteristics are influenced by rotational stiffness K_{RO}, axial (normal) stiffness K_A, and radial (shear) stiffness K_R. The K_{RO} value is defined as the bending moment-per-unit length required to develop a unit rotation angle along the joints of the assembled segments. Similarly, axial stiffness, K_A, and radial stiffness, K_R, are defined as the axial force and the shear force-per-unit length required developing a unit axial and radial displacement at a given joint, respectively. Although many well documented experimental, numerical and analytical results exist in literature concerning the functioning of segmental tunnel linings, their behaviour under the influence of joints is still not clear.

1.2. Consideration of the effect of the joint connection

1.2.1. Effect of segmental joint studied by analytical methods

In the literature, the effects of segmental joints on tunnel lining behaviour are usually considered in both indirect and direct methods. As far as indirect methods are concerned, the tunnel structure is perceived as a rigid lining ring embedded on a continuous ground model (Muir Wood [1975], Einstein and Schwartz [1979], Duddeck and Erdmann [1985], Takano [2000], Oreste [2007]). The effect of joints is usually taken into account through a reduced rigidity of the tunnel structure. The ground-structure interaction is usually considered by means of so-called bedded ring models, in which the ground reaction is taken into consideration by means of discrete springs according to Winkler's theory (e.g. Schulze and Duddek [1964]). These simplified analytical methods can neither take into account the complexities of the joint characteristics, including joint stiffness and joint distribution, nor analyse complex situations of the surrounding ground (e.g. tunnel excavated through different ground layers). In direct methods, segmental joints are added directly to the tunnel lining structure (Lee et al. [2002], Blom [2002], Ding et al. [2004], Naggar and Hinchberger [2008]). Ding et al. [2004] proposed a numerical method in which joint behaviour is simulated by means of all three joint stiffnesses, that is, the rotational stiffness, the axial stiffness and the radial stiffness. However, the influence of joint stiffness has not been investigated in detail. Apart from the method by Ding et al. [2004], most direct models consider joint behaviour through rotational springs at the joints. In addition, these methods cannot be applied to cases in which the joint distribution is asymmetrical to the vertical axis of the tunnel.

1.2.1.1. Indirect methods using continuous lining models

Generally, the presence of joints causes a reduction of the stiffness of segmental lining. In other words, the deformability of segmental lining is higher than the one of a continuous lining.

One way to apply design methods built based on the continuous lining for designing the segmental lining is to consider the segmental lining as a continuous ring with a reduced rigidity by applying a reduction factor, η, to the bending rigidity (EI) of the tunnel lining:

$$\eta = \frac{(EI)_{eq}}{EI} \qquad (1\text{-}1)$$

where $(EI)_{eq}$ is the bending stiffness of the segmental lining and EI is the bending stiffness of the continuous lining without joints.

Wood [1975] suggested that the segmental joint behaved like a set of partial hinges in lining structure. Therefore, the effective moment of inertia of the overall lining, I_e, should be reduced to take into account of joint characteristics and can be written as follows:

$$I_e = I_j + \left(\frac{4}{n}\right)^2 I \qquad \left(I_e \leq I, n > 4\right) \qquad (1\text{-}2)$$

where I and I_j are the moment of inertia of the intact liner and segmental joint and n is the number of joints in the liner.

The Japanese Society of Civil Engineers (JSCE [1996]) descriptively recommends reducing the rigidity of the continuous liner structure by 20 - 40%. Most of the Japanese tunnelling projects however required a full scale prototype test to verify the bending moment reduction factor.

Liu and Hou [1991] proposed an analytical correlation for moment reduction factor based on the maximum horizontal displacement of a continuous ring:

$$\eta = \frac{1}{1+b} \qquad (1\text{-}3)$$

with
$$b = \frac{3EI}{RK_{RO}} \sum_{i=1}^{m} \cos\varphi_i \cos 2\varphi_i \qquad \left(0 < \varphi_i < \frac{\pi}{2}\right) \qquad (1\text{-}4)$$

where EI is the bending rigidity of the tunnel lining per unit length; K_{RO} is the rotational spring stiffness of the joints, which is defined as the bending moment per unit length required to develop a unit rotation angle along a joint of the assembled segments; φ_i is the angle measured from the vertical direction around the tunnel of the i_{th} joint in the range 0 - 90°; m is the number of joints in the range of 0-90°; and R is the tunnel calculation radius.

It should be noted that both of the above approaches were developed for evenly distribution joints around the segmental tunnel lining.

Through analytical analysis, Lee and Ge [2001] provided graphical relations between the effective segmental lining stiffness, reduction factor of the bending rigidity (η) and soil resistance (K_s). In order to illustrate the relationship between the reduction factor of the bending rigidity (η) and the joint stiffness, a dimensionless parameter called the joint stiffness ratio, $\lambda = K_\theta l / EI$, is introduced to represent the relative stiffness of the joint over the rigidity of the lining segment. The calculation length, l, is usually taken as 1 m to represent a typical unit length of a lining segment. K_θ is the flexural (rotational) stiffness of the joint (per unit length), which is assumed to be a constant. **Figure 1-2** shows the effective rigidity ratio (η) against stiffness ratio in logarithmic scale ($\log\lambda$) for different soil resistance (K_s).

For the tunnel embedded in soft ground (i.e., $K_s \leq 30,000$ kN/m^3), the effective rigidity ratio is less affected by soil resistance. Within the typical range of λ, the effective rigidity ratio η in soft ground is in the range of about $0.1 \div 0.4$.

The results shown in **Figure 1-2** is rearranged in terms of effective rigidity ratios η versus soil resistance coefficient K_s at various joint stiffness ratios λ as shown in **Figure 1-3**. At a given λ value, the variation between η and K_s can be best fitted with a linear relationship. The slope of the linear relationship between η and K_s is higher for a lower value of λ, which indicates that the relationship between η and K_s is more sensitive for a lining with more flexible joints.
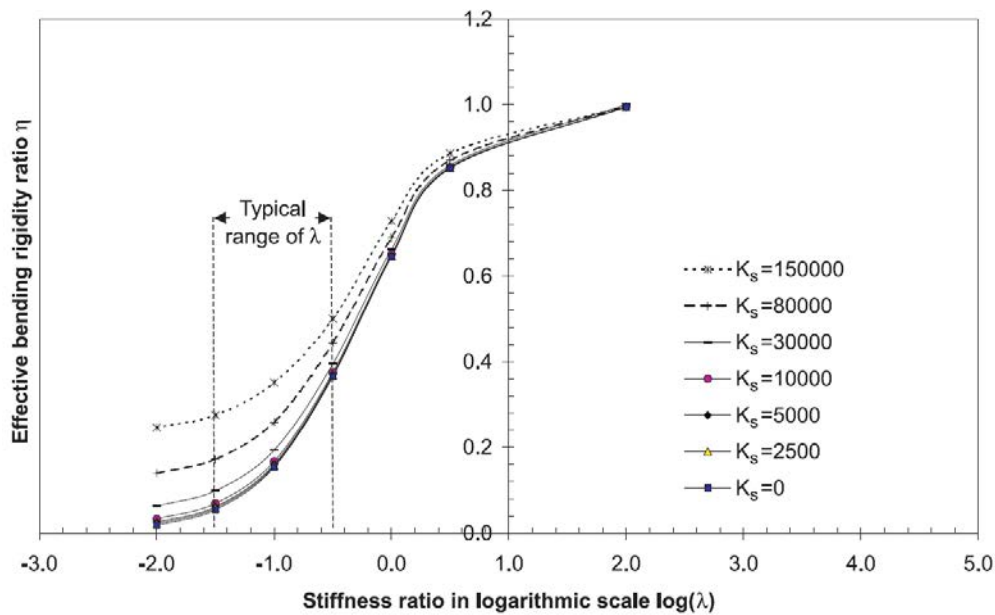
Figure 1-2. Effective bending rigidity ratios in terms of horizontal or vertical displacement (Lee and Ge [2001])
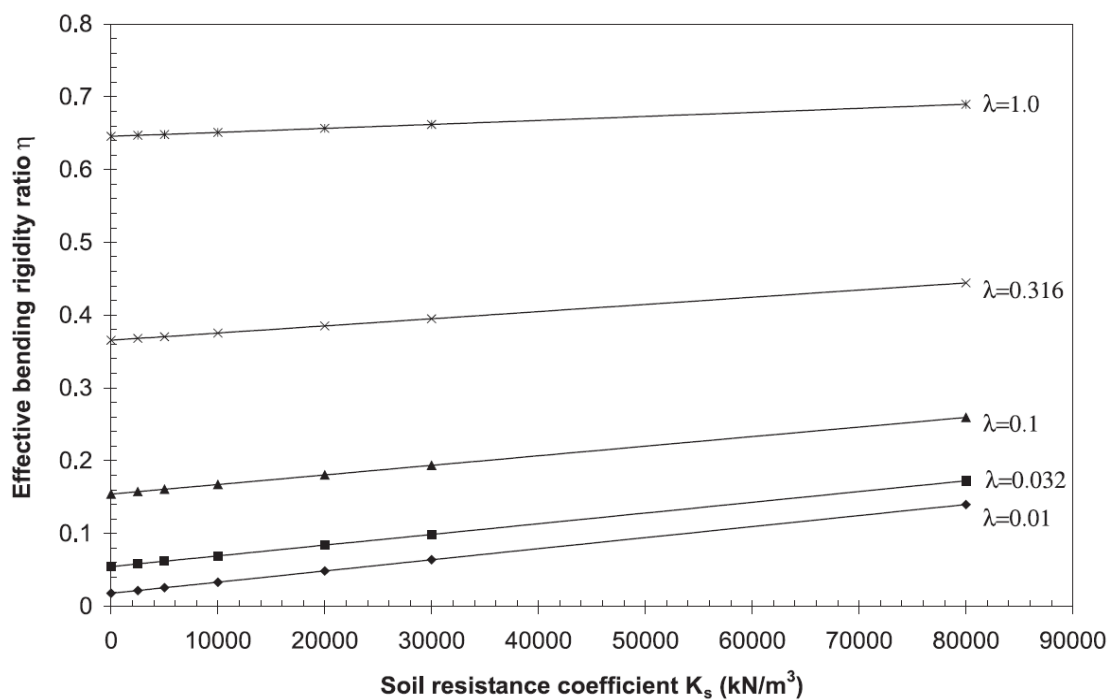
Figure 1-3. Linear relationships between the effective rigidity ratio (η) and the soil resistance coefficient (K_s) at different λ values (Lee and Ge [2001])

Chapter 1: Influence of segmental joints on the tunnel lining behaviour   10

Unlike the two methods proposed by Muir Wood [1975] and Liu and Hou [1991], this force method (Lee and Ge [2001]) can be used in the case in which the joint distribution is not even along the segmental tunnel lining. On the basis os a parametric study, the factors affecting the effective rigidity ratio are summarized in **Table 1-1**.

Table 1-1. Main factors affecting the effective rigidity ratio (Lee and Ge [2001])

Factor	Effective rigidity ratio (η)
Join stiffness ratio λ ($K_\theta l/EI$) ($\uparrow$)	Sensitive ($\uparrow$)
Soefficient of soil resistance K_s ($\uparrow$)	Not sensitive if Ks is less than 30,000 kN/m^3 ($\uparrow$)
No. of joint ($\uparrow$)	Sensitive ($\downarrow$)
Geometry	
Thickness ($\downarrow$)	Depends on total number of joints ($\uparrow$ when 3 joints; $\downarrow$ when 4 joints)
Radius ($\uparrow$)	Sensitive ($\uparrow$)
Joint stiffness reduction	Sensitive ($\downarrow$)

Note: The arrows indicate a tendency to increase ($\uparrow$), decrease ($\downarrow$). Tendency direction for the factors in the first column indicates the tendency of values for the associated factor adopted in the parametric analyses; tendency direction in the second columns indicates the tendency of results of (η) as predicted by the parametric study.

Blom [2002] introduced a reduction factor formula that can be applied to the flexural rigidity of a full continuous ring to take into account the global influence of the joint:

$$\eta = \frac{1}{1 + \frac{3}{4}\frac{t^3}{l_t^2 r}\left(C_x^* + C_y^*\right)} \tag{1-5}$$

where

$$C_x^* = \sum_{-\frac{\pi}{2}<\beta_i}^{\beta_i<\frac{\pi}{2}}\cos(\beta_i)\cos(2\beta_i) \quad and \quad C_y^* = -\sum_{0<\beta_i}^{\beta_i<\pi}\sin(\beta_i)\cos(2\beta_i) \tag{1-6}$$

where β_i is the angle at the ith joint location, measured from the tunnel crown. A diagram presenting the reduction factor η of the bending stiffness as a function of the contact area in the longitudinal joint (l_t), segmental thickness (t) and the radius (R), for several numbers of segments of a single ring was also introduced, based on this formula.

Figure 1-4 shows the results of the equation for the reduction factor, η, in general for several numbers of segments in a ring.
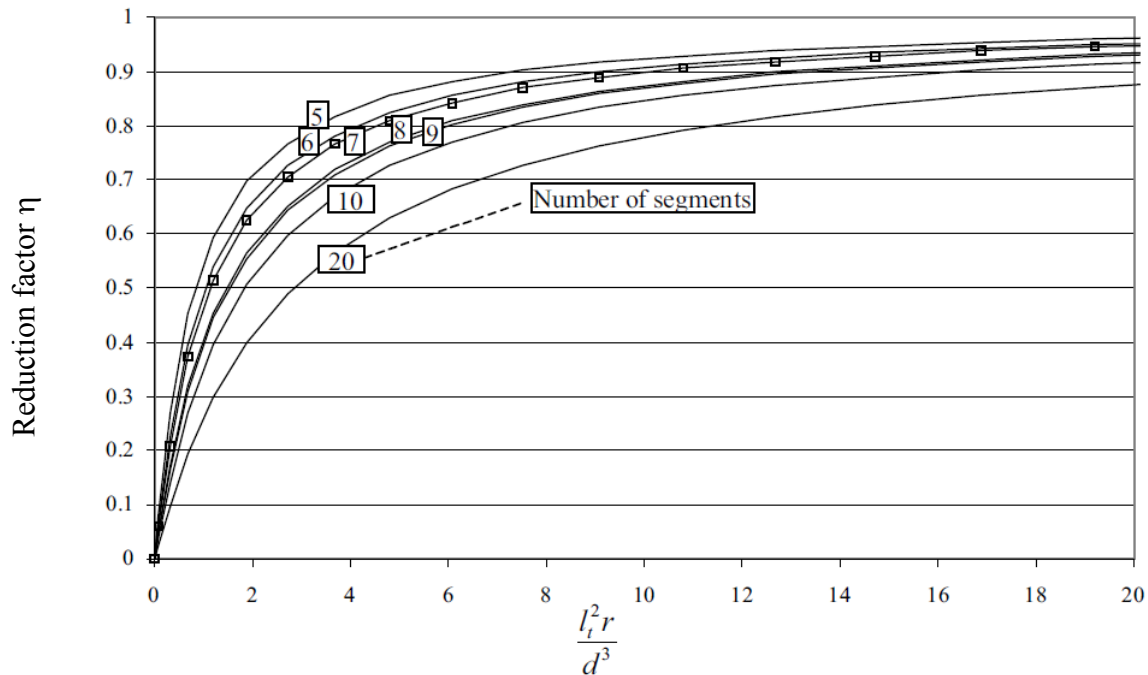
Figure 1-4. The reduction factor η for the bending stiffness as function of the contact area in the longitudinal joint (l_t), segmental thickness (d) and the radius (r), for the several numbers of segments of a single ring (Blom [2002])

1.2.1.2. Direct methods based on jointed lining models

Although one can use simple design methods in which the lining is considered as continuous lining for determining the internal force in segmental lining by using the reduction factor, η, as mentioned above, but these methods have some drawbacks that need to be drawn as follows:

- The effect of joint location on the internal forces induced in the tunnel lining is not shown;
- The dependency of the lining behaviour on the change of characteristics such as rotation stiffness K_θ between joints in a ring is not possible to taken into account.

For above reasons, it is more precise to use design methods, in which the presence of joints in the lining is considered directly.

Following Takano [2000], Lee et al. [2002] proposed an analytical method that allows one to consider segmental tunnel lining connected through elastic springs, subject to external loads which are similar to that considered by Takano, except for the load produced by the reaction of the soil in the area near to the spring line (**Figure** 1-5). This method was developed based on a «*force method*» to examine the effects of joint stiffness, joint distribution, joint number and non-equal joint stiffness (see Lee et al. [2002]).

Chapter 1: Influence of segmental joints on the tunnel lining behaviour   12
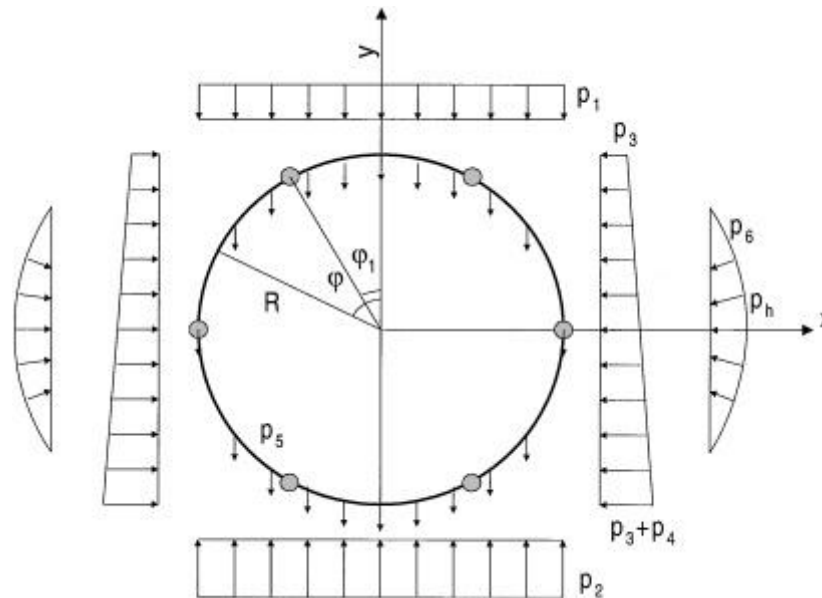
Figure 1-5. Model diagram of a jointed tunnel lining (Lee et al. [2002]) (where p_1 is the vertical overburden soil pressure, p_2 is the reaction pressure at the bottom of the lining, p_3 is the total lateral earth pressure developed at the crown level of the tunnel lining, p_4 is the additional lateral earth pressure developed at the tunnel invert level, p_5 is the self-weight of the tunnel lining and p_6 is the soil resistance pressure)

The tests carried out have allowed one to demonstrate that, in the model, the change in stiffness of joints affects only the distribution of bending moments (**Figure** 1-6 and **Figure** 1-7). In other word, the axial force developed in the lining is non-sensitive to the magnitude of the joint stiffness.
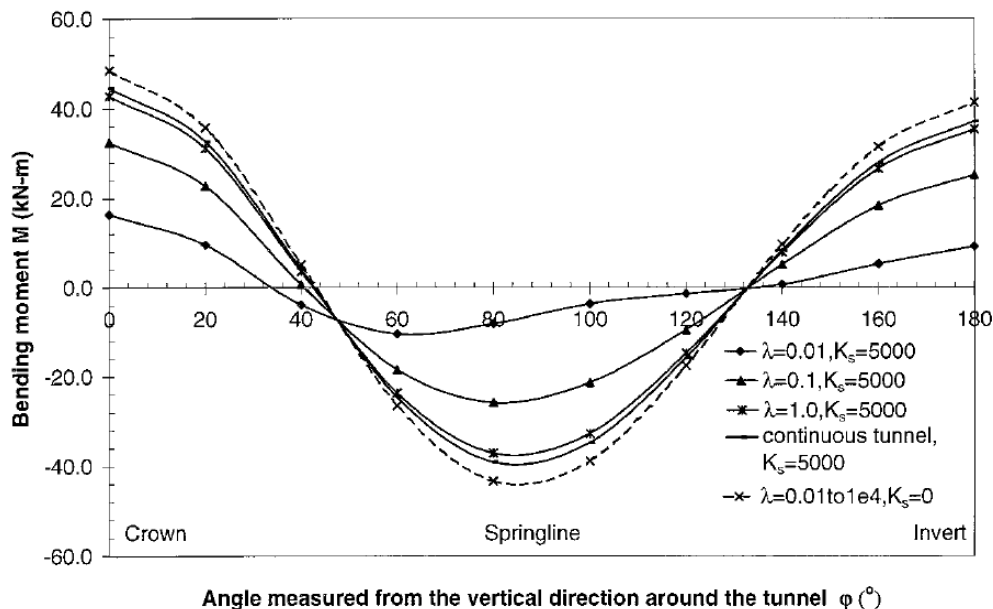
Figure 1-6. Bending moment diagram with different values of joint stiffness (Lee et al. [2002])
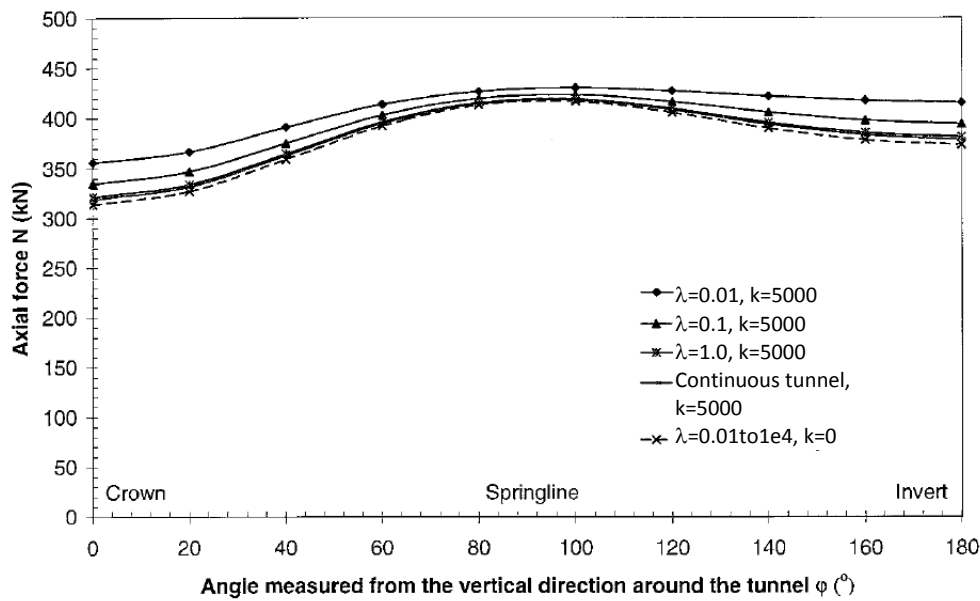
Figure 1-7. Axial force with different values of joint stiffness (Lee et al. [2002])

Lee et al. [2002] have also pointed out that when the joints are very stiff, the maximum bending moments induced in the lining is not affected to any extent by the change in soil stiffness. However, for more flexible joints, the results indicated strong variations of the maximum bending moment affected by the increase in the soil resistance coefficient, k, from 0 to 2500 kN/m^3; Beyond a k of 2500 kN/m^3, the change in the bending moment ratio, defined as the ratio of the maximum bending moment of the jointed tunnel and the maximum bending moment of the continuous tunnel, becomes more gradual (**Figure** 1-8).

Soil resistance coefficient k (kN/m^3)
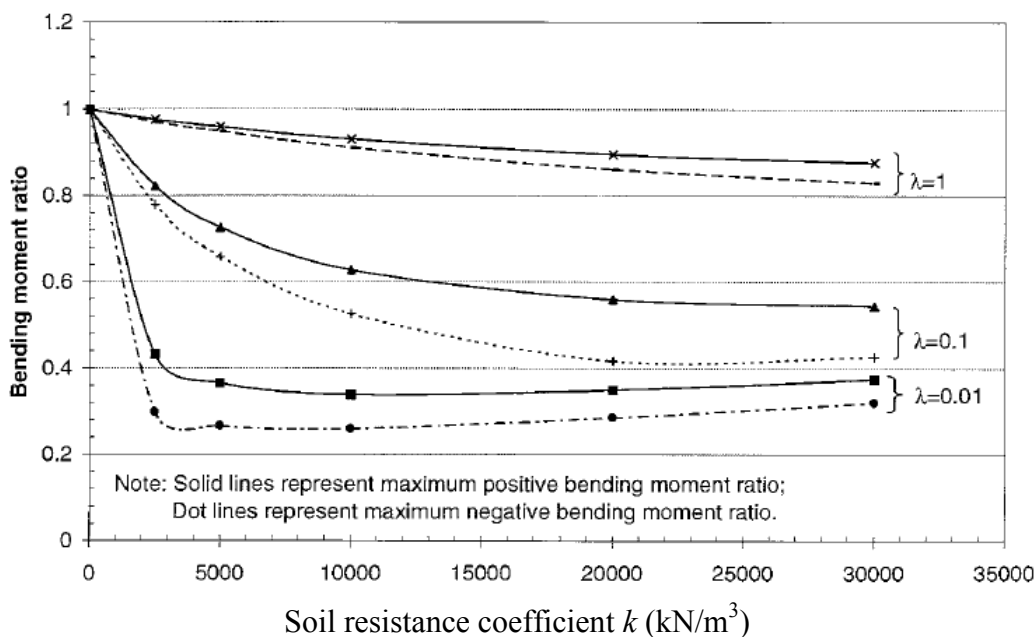
Figure 1-8. Bending moment ratio R_m at various soil resistance coefficients under different stiffness ratios (R_m = Maximum bending moment of jointed lining/Maximum bending moment of continuous lining) (Figure 10 in Lee et al. [2002])

Chapter 1: Influence of segmental joints on the tunnel lining behaviour   14

It is necessary to note that in the method of Lee et al. [2002], lining structure and surrounding loads are assumed to be symmetric with respect to vertical centerline. This method cannot apply in the case in which the distribution of joint over the vertical tunnel axis is asymmetrical. This method does not also consider the interaction between the lining rings in the longitudinal direction and the effect of construction progress (staged loads). As is previously mentioned, successive rings are mostly assembled in a so-called masonry layout. This means that the longitudinal joints of the successive rings are not in line. This characteristic of the joint pattern is not taken into consideration in this method.

To overcome some drawbacks of the methods so far expressed, Blom [2002] proposes an analytical method that takes into account both the interaction between successive rings composed of elastic jointed segments and the soil-structure interaction. In this method, the soil is modelled through a bed of constant radial spring around the lining. The author considers two sets of elastic blocks: each set forms a circular ring. The static scheme adopted by Blom [2002] is shown in **Figure** 1-9.
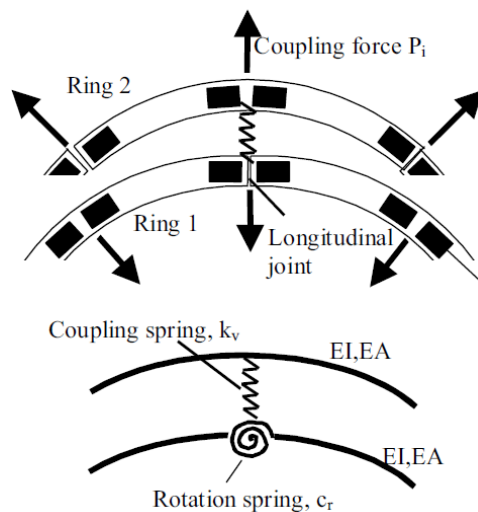
Figure 1-9. Detail of the static scheme adopted by Blom [2002]

In the model proposed by Blom, linings are subjected to an elliptical load. The load is subdivided into a uniform load (σ_0) and an ovalisation load (σ_2) (**Figure** 1-10).

The deformation of a ring with longitudinal joints is subdivided into three components:

- Uniform compression u_0 due to the uniform stress σ_0.
- Ovalisation by bending of segments u_{2EI} due to the ovalisation stresses σ_2.
- Ovalisation by rotation in the longitudinal joints u_{2lj} due to the ovalisation stresses σ_2.

The longitudinal joints are modelled using rotational spring stiffness of springs K_{RO}, while the circumferential joints between successive rings are modelled with shear springs that carry a shear force released by the displacement difference in radial direction between two successive rings.

By considering the differential displacement bient between two successive rings, assuming that the rings are initially subjected to the same loads, the interaction force and moment between

two rings can be determined. The bending moment in the lining was determined by superposition of moments caused by the effect of longitudinal joints and ring joints.
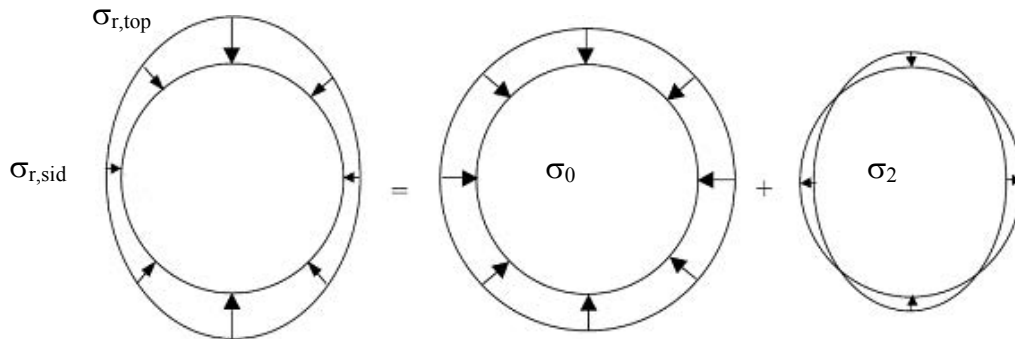
Figure 1-10. Loading subdivided into a uniform load (σ_0) and an ovalisation load (σ_2) ($\sigma_{r,\,top}$ = radial stress at the top; $\sigma_{r,\,side}$ = radial stress at the side; σ_0 = uniform radial compression stress; σ_2 = radial ovalisation stress) (Blom [2002])

It should be noted that in the method proposed by Blom [2002], due to the fact that the soil-structure interaction was modelled through a bed of radial reaction around the lining, only the full slip case between the liner and the soil was considered. In addition, for shallow tunnels the influence of the gradient of vertical stress with depth is not negligible, especially for the evaluation of bending moments. So this method is not suitable for shallow tunnels. Beside above drawbacks, similar to the methods proposed by precedent authors (Lee [2002]), one of the main disadvantages of Blom's method is the symmetrical distribution of the joints in respect to the vertical axis of the tunnel cross section.

Naggar and Hinchberger [2008] introduced an analytical solution for jointed tunnel lining that can be idealized as an inner jointed segmental lining and an outer thick-walled cylinder embedded in a homogenous infinite elastic soil and rock. **Figure 1-11** illustrates joint contribution around the tunnel considered in their analyses.
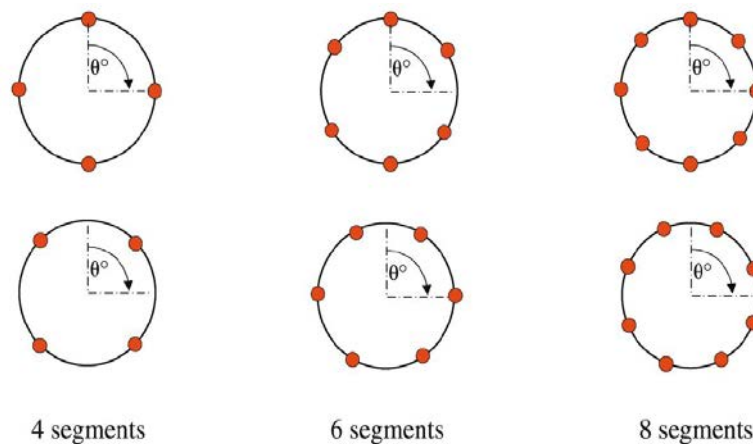
Figure 1-11. Liner configuration considered in Naggar and Hinchberger's analyses (Naggar and Hinchberger [2008])

Figure 1-12 presents an example of analytical results obtained by Naggar and Hinchberger's solution compared to the FEM results for the case of 6 joints. Similar to the methods proposed by precedent authors (Lee [2002], Blom [2002]), one of the main disadvantages of Naggar and Hinchberger's method is the symmetrical distribution of the joints in respect to the vertical axis of the tunnel cross section.
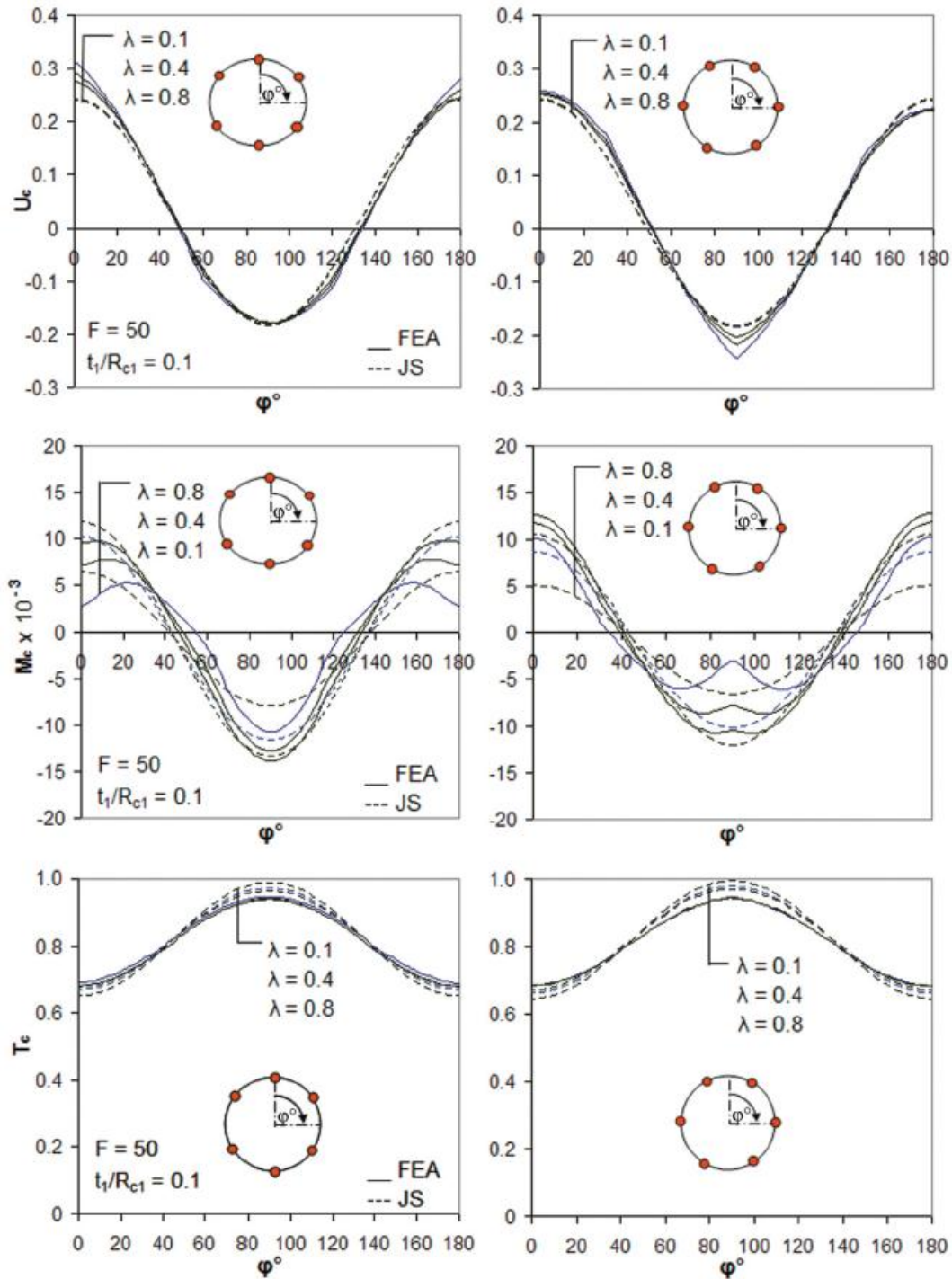
Figure 1-12. Normal displacement, moment and thrust forces for six joint configuration
(Naggar and Hinchberger [2008])

1.2.2. Effect of segmental joint studied by 2D numerical analysis

Rapid progress in the development of computer codes and the limitation of analytical methods have led to an increase in the use of numerical methods for the design of tunnel lining. A summary of the finite element models used for tunnelling analyses prior to 2000 was given by Muniz de Farias et al. [2004] and by Negro and Queiroz [1999]. They showed, after an examination of more than 65 recently published papers, that the finite element method (FEM) is the most popular approach, accounting for 96% of the published cases, while the remaining ones used the finite differences method (FDM) or others. They also noted that 92% of the published analyses were still performed in two-dimensions, under the hypothesis of plane strain conditions.

In numerical analyses, two main techniques are applied to model the ground-structure interaction. The first technique involves the use of discrete springs and is based on Winkler's theory, which focuses on the structural behaviour of the segmental lining (Blom [1999], Oreste [2007]). The second approach uses the full ground model using finite elements (Kasper [2004, 2006]). Although heavy computational efforts are required, the second approach generally provides more accurate results.

Using the first method, Teachavorasinskun and Chub-Uppakarn [2010] conducted a numerical study using a finite element analysis program on the influence of joint rotational stiffness (**Figure** 1-13), the joint number and the ground subgrade modulus on the bending moment. However, the interaction between the ground and the tunnel lining was taken into account only with regard to a set of normal subgrade reaction springs, and not tangential ones. The external loads were imposed vertically and horizontally to simulate the action of the earth pressures in corresponding directions (the lateral earth pressure factor was put equal to 0.5 and the depth equal to 20 m).
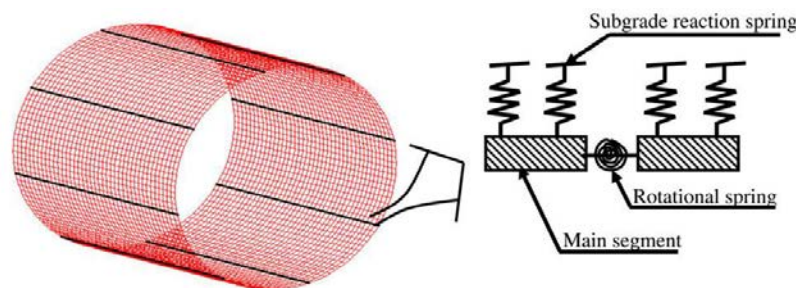
Figure 1-13. Cross section of segment model (Teachavorasinskun and Chub-Uppakarn [2010])

The influences of orientation of segmental joints were examined by rotating the joints along the tunnel's circumferential. The orientation of joints is found to greatly affect the amount of maximum bending moment acting on the lining as can be seen in **Figure** 1-14. The variation of maximum bending moment against joint location is sinusoidal in nature, at which its frequency reduces according to the number of joints.

Figure 1-15 shows the plots between the upper and lower values of the maximum bending moment against the angular joint stiffness, K_{RO}. When joints are rigid (high value of

---

Chapter 1: Influence of segmental joints on the tunnel lining behaviour   18

K_{RO}), the maximum bending moment, both upper and lower values, of the jointed lining becomes naturally approaching the non-jointed one. However, within the recommended range of the angular joint stiffness ($\approx 1000 - 3000$ kNm/rad), the maximum bending moment decreases to about $0.50 - 0.95$ (for upper value of maximum bending moment) and $0.3 - 0.90$ (for lower value of maximum bending moment) of that obtained from the non-jointed lining (Teachavorasinskun and Chub-Uppakarn [2010]).
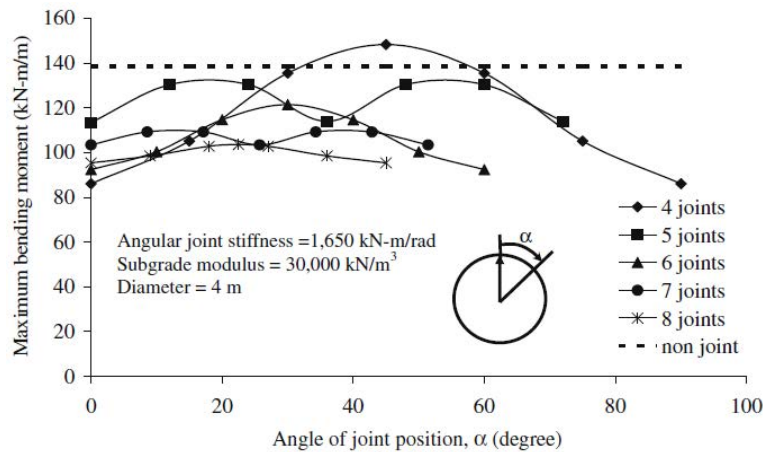
Figure 1-14. Variation of maximum bending moment with number and orientation of joints (Teachavorasinskun and Chub-Uppakarn [2010])
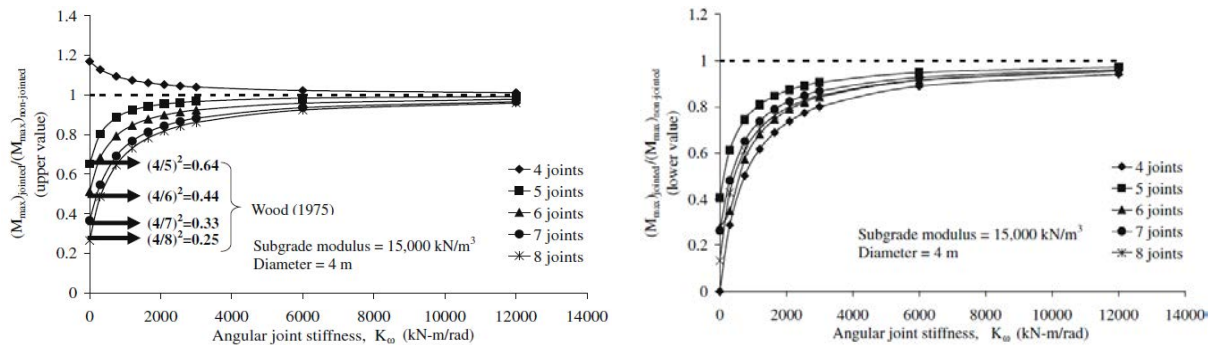
a) Upper value of maximum bending moment

b) Lower value of maximum bending moment

Figure 1-15. Moment reduction factor against the angular joint stiffness (Teachavorasinskun and Chub-Uppakarn [2010])

As far as the second method is concerned, Hefny et al. [2006] numerically studied the influence of the joint number, joint orientation, lateral earth pressure factor, and tunnel depth on the bending moment induced in a 6 m diameter segmental tunnel lining, using a finite element analysis program. In their analyses, the segmental joints were assumed to be fully hinged (the joint capacity of transmitting partial moment by the joints was not considered).

Figure 1-16a shows that increasing joint number reduces the maximum bending moment induced in the lining. The maximum bending moment induced in the lining becomes negligible small when the joint number exceeds 8 joints. In addition, it should be noted that

the most favourable orientation of 4 joints induced much lower maximum bending moment as compared to 5 joints and 6 joints. This indicates that the joint orientation significantly influence the maximum bending moment induced in the lining. However, the maximum bending moment for cases involved a minimum of 8 joints is about similar in magnitude, regardless of the joint orientations (Hefny et al. [2006]).

The results in **Figure** 1-16b shows that the maximum bending moment induced in the jointed lining is the lowest for reference joint at $\omega = 0^0$, i.e. when the reference joint is located at tunnel crown. However, the maximum bending moment developed in the lining is the largest when the reference joint is located in between the angle of $\omega = 0^0$ and the largest possible ω value for each case of joint number (Hefny et al. [2006]).

(a)

(b)
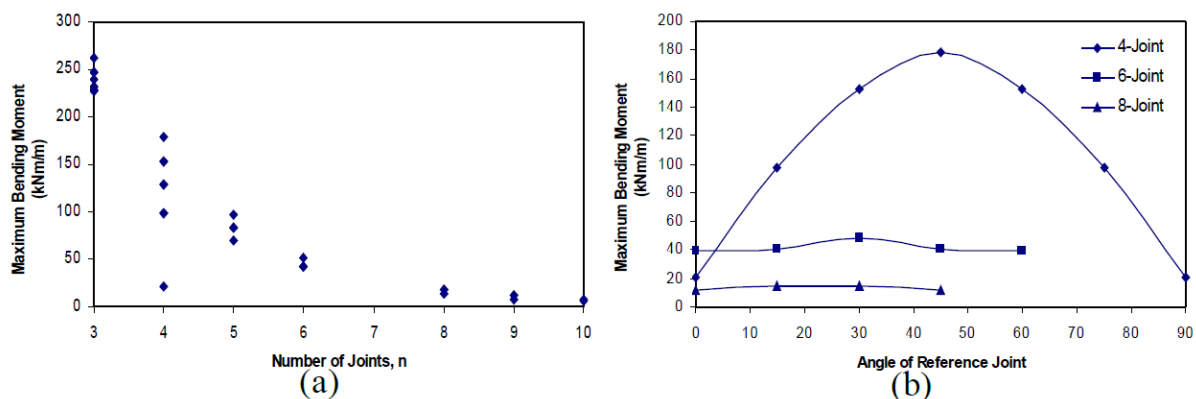
Figure 1-16. Variation of maximum bending moment with (a) Number; and (b) Orientation of joints (Hefny et al. [2006])

Hefny et al. [2006] also showed the effect of coefficient of earth pressure at rest K_0. As shown in **Figure** 1-17a, the largest maximum bending moment obtained when $K_0 = 2.0$ and the lowest value was observed for $K_0 = 1.0$ (approximately zero moment), with $K_0 = 0.5$ in between. As expected, this is attributed to the larger difference between the vertical and horizontal loads that act on the lining for $K_0 = 2.0$, as compared to $K_0 = 0.5$ and 1.0.

Figure 1-17b shows the maximum bending moment induced in the lining increases with tunnel depth. This could be attributed to the increase in the overburden pressure that acts on the lining as the depth increases. At shallower depth of tunnel, e.g. H/D of about 1.0, the maximum bending moment induced in both 6-joint and 8-joint lining is more or less similar. On the other hand, the difference becomes increasingly significant at greater tunnel depth. This indicates that the influence of the joint number is much more significant for the deep tunnel case compared to shallow tunnels (Hefny et al. [2006]).

The influence of lining flexibility on the maximum bending moment induced in the segmental tunnel lining was determined on the basis of using the flexibility ratio, F, defined by Peck [1972]. **Figure** 1-17c shows that for jointed tunnel with stiff lining, the maximum bending moment developed in the lining is significantly influenced by the number of joints. For example, as the joint number increases from 6 to 8-joint for very stiff lining case with flexibility ratio of about 0.05, the maximum bending moment in the lining reduces nearly 70 %. However, the influence of joint number becomes gradually negligible with the increase in

lining flexibility, particularly for cases involved lining with flexibility ratio of greater than 15 (Hefny et al. [2006]).
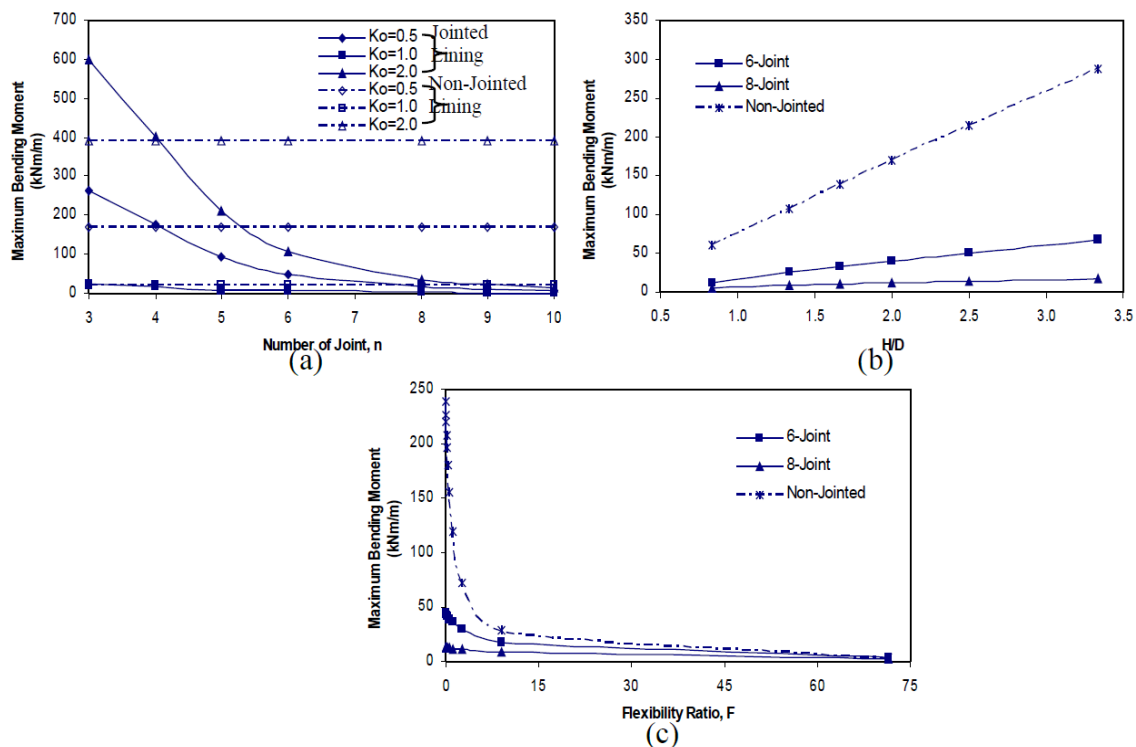
Figure 1-17. Variation of Maximum Bending Moment (most critical joint orientation) with (a) K_0-Value; (b) Tunnel Depth; and (c) Flexibility Ratio (Hefny et al. [2006])

1.2.3. Effect of segmental joint studied by 3D numerical analysis

Three-dimensional analyses are now commonly used for research, and they usually adopt in-house finite element software (Muniz de Farias et al. [2004]), while software packages such as FLAC^{3D} (Barla et al. [2005], Dias and Kastner [2000], Dias et al. [2000], Lambrughi et al. [2012], Mollon [2010] and Mollon et al. [2013]), Abaqus (Migliazza et al. [2009], Ng et al. [2004]), PLAXIS^{3D} (Afifipour et al. [2011b], Broere and Brinkgreve [2002]. Möller and Vermeer [2008]), Diana (Arnau and Molins [2011]) and Tochnog Professional (Mašin [2009], Svoboda et al. [2010]) are normally used for commercial purposes. Only a few of these codes take into account the influence of segmental lining joints on the tunnel behaviour (Arnau and Molins [2011b], Arnau and Molins [2012] Blom [2002], Hudoba [1997], Medina Rodríguez [2008], Thienert and Pulsfort [2011]). Interesting summaries of 3D tunnelling models can be found in studies presented by Franzius [2004] and Franzius and Potts [2005].

Kasper and Meschke [2004, 2006a, 2006b] presented three papers on a 3D FEM numerical investigations which focused on the influence of face pressure, grouting pressure, trailer weight and length, as well as weight and tapering of the shield machine in a homogenous, soft, cohesive soil medium below the ground water table. Unfortunately, segmentation of the tunnel lining was not considered in the model.

Lambrughi et al. [2012] introduced a 3D model using the FLAC[3D] finite difference code for mechanized excavation using an Earth Pressure Balance TBM. The main construction aspects of a mechanized excavation such as the shield machine, concrete lining, support of the excavation face, over-excavation, tail gap grouting, and progressive hardening of the cement based grout, were modelled in this model. However, like the model introduced by Kasper and Meschke [2004, 2006a, 2006b], the tunnel lining was modelled using continuous elements that neglected the discontinuities of the tunnel lining.

Recently, Chakeri et al. [2013] introduced interesting results on the effects of important properties like tunnel depth, overburden pressure, tunnel dimension and face pressure using empirical, theoretical and numerical methods used to control surface settlement. Unfortunately, also like above researches, the influence of segmental joints was not considered.

Blom et al. [1999] proposed a detailed 3D FEM analysis of tunnel structures using Ansys FEM software. This model allows the effects of the ground reaction, interaction between segments, packing material between rings, jacking forces, grout phase changes from a liquid state to a solid state, and assembly segments in a ring to be taken into account. The interaction between the segments (in all directions) was realized by applying contact elements. A staggered arrangement of the tunnel lining was also considered in this study. Some conclusions have been drawn below:

- Stresses are not uniformly distributed (stress peaks) in axial, radial and tangential directions (stress paths around the key segment) (see **Figure 1-18**);
- The long-term ring forces remain close to the level that was observed during the assembly;
- Eccentricity of the axial normal forces is obviously indicated, as can be seen from the bending moments in the longitudinal direction of the tunnels (see **Figure 1-19**);
- Maximum measured sectional forces and moments are twice the highest predicted with conventional models.
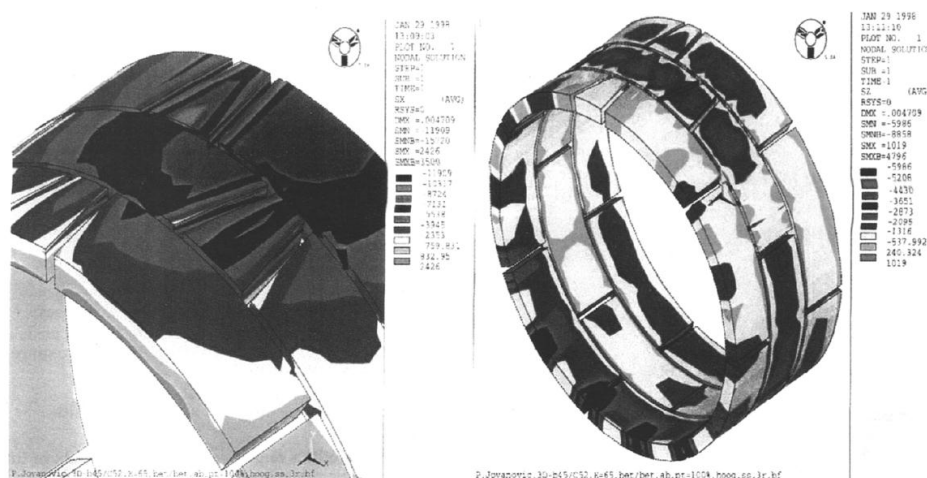
Figure 1-18. Normal stresses are not uniformly distributed in radial, axial and tangential directions (stress paths around the key segment) (Blom et al. [1999])

Obviously, their results indicate significant effects of the joints and construction loads on the lining behaviour. Unfortunately, the influence of joints (e.g., joint distribution, joint stiffness) on the tunnel lining behaviour during excavation was not dealt with in detail.
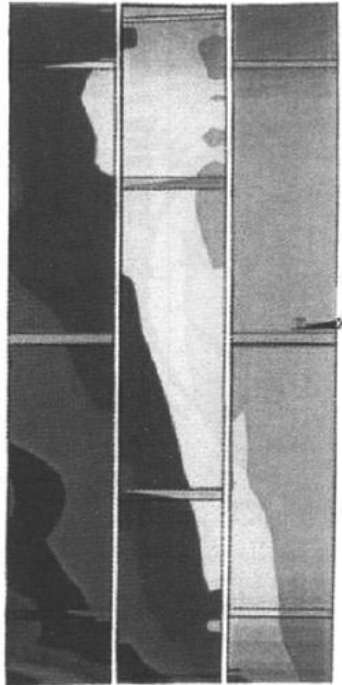
Figure 1-19. Eccentricity of the axial normal forces is obviously available (Blom et al. [1999])

In a 3D FEM model presented by Klappers et al. [2006] the segments were modelled by means of 4-node plane shell-elements. A comparison between structural forces induced in a continuous lining with the ones induced in a segmental lining obtained using a 2D FEM model and a 3D beam and spring model was presented. The results showed that the calculated bending moments of both models were in a similar range and the deformations only differed slightly. In **Figure** 1-20, the effect of the coupling of the rings is clarified. At the uncoupled system each ring deforms independently and at the coupled system the deformation of the rings is harmonized (Klappers et al. [2006]).

Hudoba [1997] presented a simplified comparative static computation of an underground metro supported with a concrete lining. Different joint patterns were used for the same dimensions of the tunnel cross-section and the same constitutive model and joints were assigned as hinges (see **Figure 1-21**). A comparison of the structural forces and deformations achieved using different plain ring (2D) and spatial (3D) computing models showed that traditional plain ring models give more accurate results than spatial (3D) models (**Table 1-2**). Unfortunately, neither of the two above models (Hudoba [1997], Klappers et al. [2006]) took into account other elements of the tunnel excavation process such as the tunnel boring machine, face pressure, grouting pressure, etc.

The segmental lining was considered in a model proposed by Medina Rodríguez [2008] using the FLAC^{3D} finite difference code. Interface elements were employed to reproduce the

contact between all the segments that formed the lining. During the advancement of the shield, the large shoving loads from the hydraulic jacks were supported by the segments in the longitudinal direction. Nevertheless, like the research of Blom et al. [1999], the influence of joints on the tunnel lining behaviour was not introduced.

a) Uncoupled   b) Coupled
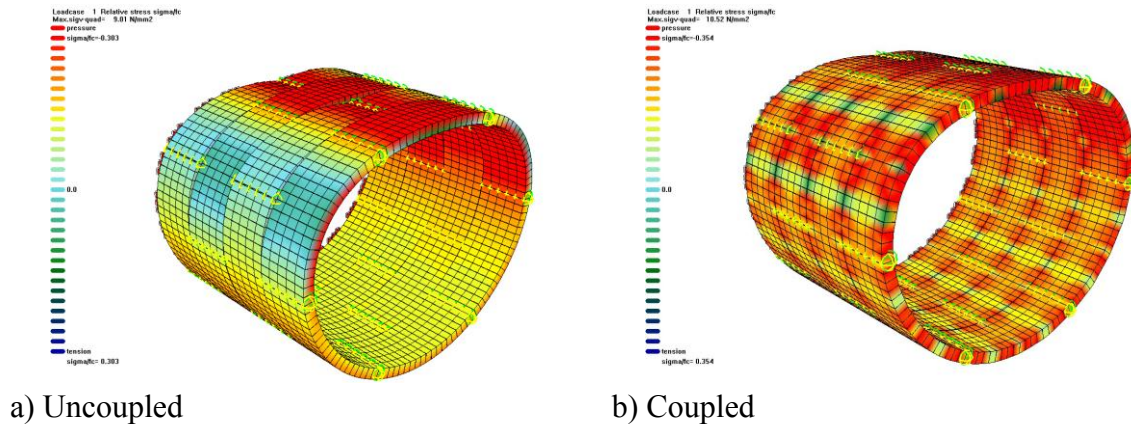
Figure 1-20. Deformed structures (scaled up) (Klappers et al. [2006])

| Model M2 | Model M3 | Model M1 | Model M4 | Model M4 |
| Straight pattern | Straight pattern | Continuous lining | Staggered pattern | Staggered pattern |
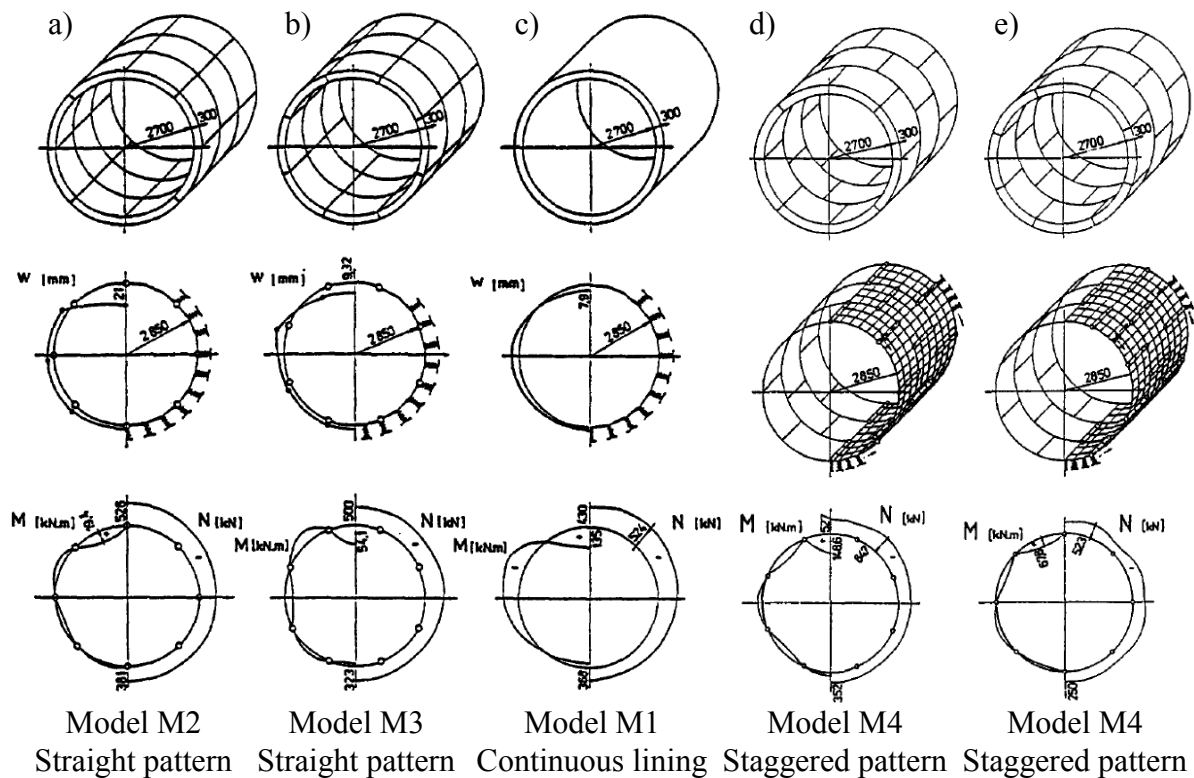
Figure 1-21. Load-bearing lining computing model, course of deformations w, bending moments M, normal forces N. a) Prefabricated reinforced concrete tunnel lining, continuous longitudinal interstice in the ring's crown; b) Prefabricated reinforced concrete tunnel lining, continuous longitudinal interstice is outside the ring's crown; c) monolithic concrete lining; d) three rings with one interstice in the crown; e) three rings with two interstices in the crown (Hudoba [1997])

Arnau and Molins [2012] analysed the influence of the interaction between adjacent rings in the structural response of segmental tunnel linings subjected to typical design loads (longitudinally uniform). A three dimensional finite element model of a real tunnel section of the new Line 9 of the Barcelona metro was set up, applying modelling techniques that allowed both the joint responses and the material behaviour to be simulated. A sensitivity analysis was carried out in order to establish the influence of some parameters, that is, the ground stiffness, the actual load and the remaining longitudinal force, on the three dimensional response of the structure. The results show significant effects of ring connection on the lining behaviour (e.g., **Figure** 1-22 and **Figure 1-23**). However, the ground-structure interaction was modelled by means of spring elements placed in radial, tangential and longitudinal directions. Furthermore, the influence of other aspects concerning the tunnel construction, such as shield machine, and construction loads (e.g. face pressure, grouting pressure), were not mentioned.

Table 1-2. Comparative results of the load-bearing concrete tunnel lining static calculations (Hudoba [1997])

Computing model	Plain ring model (2D model)			Spatial model (3D model)	
	M1	M2	M3	M4	M5
*w_{max} (mm)	7.9	21.0	9.3	3.9	3.6
c_W	1.0	2.66	1.18	0.5	0.46
M_{max} (kN.m)	135.0	19.4	54.1	142.7	67.8
c_M	1.0	0.14	0.4	1.06	0.5
Ncor (kN)	490	538	500	527	523
c_N	1.0	1.19	1.02	1.07	1.06

* Deformation values in the ring's crown are absolute. N_{cor} are corresponding values to M_{max}
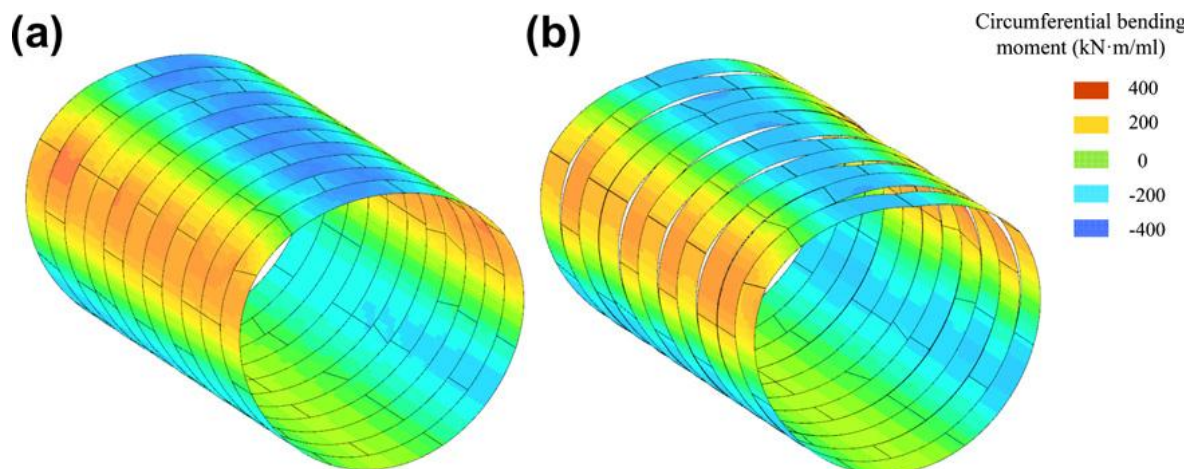
Figure 1-22. L9 Deformation and circumferential bending moment for Es = 25 MPa, K_0 = 0.5 for the coupled system (jacking forces = 40 MN) (a) and uncoupled (b) (deformation amplification factor = 18) (Arnau and Molins [2012])
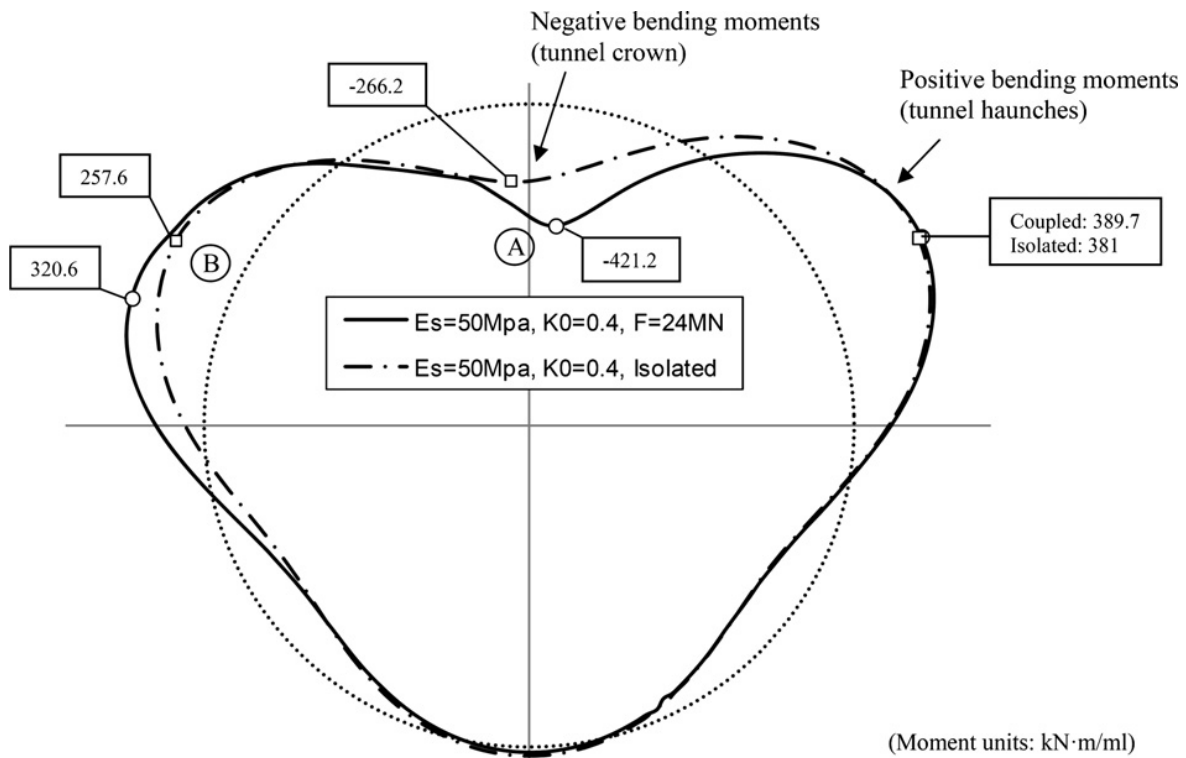
Figure 1-23. Representation of the circumferential bending moment of the central ring for Es = 50 MPa and K_0 = 0.4 in the coupled system (jacking force = 24 MN) and in the isolated ring (Arnau and Molins [2012])

The joints in a tunnel lining evidently have a great influence on the tunnel behaviour (Arnau and Molins [2012], Blom [2002], Hudoba [1997], Klappers et al. [2006], Teachavorasinskun and Chub-Uppakarn [2010], Zheng-Rong et al. [2006]). So far, this influence has not been mentioned very often and has not been clarified in the literature. There is still no complex 3D modelling that is able to focus on this problem. **Table 1-3** presents a summary of the researches in the literature that have used the FLAC^{3D} software package to model TBM tunnelling. It should be noted that most of these models have focused on studying the settlement induced by the tunnelling process. However, the segmentation of the lining has not been considered.

Table 1-3. Parameters of some numerical models using the FLAC^{3D} software package

Authors	Type of TBM	D_{ex} (m)	Depth H (m)	Type of soil	Type of stress	Ground constitutive model	Lining modelling	Shield modelling	Grout pressure (kPa)	Lateral earth pressure factor at rest K_0	Face pressure p_{face} (kPa)	Model sizes (L x W x H)
Maranha and Neves [2000]	EPB	9.71	17	Soft clay	Total stress	Mohr Coulomb	Shell element	Shell element	160-180	0.67	equal to measured earth pressure	60 x 50 x 33.855 (half of tunnel)
Melis et al. [2002]	EPB	9.38	16	Clay	-	Linear elastic; Mohr Coulomb; Modified Cam-Clay	Shell element, linear elastic	Solid volume element	250; zone element (hardened state) (E=2.57 GPa, μ = 0.286)	$K_0 = K_{ONC} OCR^{ff}$ ff = 0.54 x $10^{-PI/281}$ $K_{ONC} = 1 - \sin\varphi$	60-100 (roof); 270-300 (bottom)	-
Jenck and Dias [2003]	-	9.8	26	Silty sand	-	Mohr Coulomb	-	-	-	0.6-1.05	-	90 x 100 x 51 (half of tunnel)
Barla et al. [2005]	EPB	7.8	15-20	Sand + Gravel	Effective stress	Mohr Coulomb	Shell element	-	-	0.5	-	160 x 160 x 38 (full tunnel)
Phienwej et al. [2006]	EPB	6.4	8-25	Bankok clay + sand	Total Stress	Mohr Coulomb	Shell element;	Shell element	Highly compressible material (E = 1000 kN/m^2)	0.5 - 0.75	50-400 (average 80)	120 x 50 x 58 (half of tunnel)
Lambrughi et al. [2012]	EPB	9.38	13.81			Linear elastic; Mohr-Coulomb; Modified Cam-clay	Linear-Elastic continuous elements	Linear-Elastic continuous elements	Varied for parameter study	-	Varied for parameter study	2 (H + 4D) x 2 (H + 4D) x (H + 4D) (half of tunnel)

Note: *The given values were determined from plots, graphs and so on; PI - plasticity index; φ - friction angle; OCR - Overconsolidation ratio;*

1.2.4. Effect of segmental joint studied by experimental tests

Besides the numerical studies mentioned above, experimental studies of tunnel lining structures have also been conducted in laboratories (e.g., Cheng [1985], Hordijk and Gijsbers [1996], Lu et al. [2005], Lu et al. [2006], Nishikawa [2003] Schreyer and Winselmann [2000], Teachavorasinskun and Chub-Uppakarn [2008], Zhou [1988], Cavalaro and Aguado [2011]) or at tunnel sites (Arnau and Molins [2011a], Bilotta and Russo [2013], Blom et al. [1999]). Most of them focused on studying joint parameters, e.g. joint rotation stiffness (Cheng [1985], Hordijk and Gijsbers [1996], Nishikawa [2003], Teachavorasinskun and Chub-Uppakarn [2008], Zhou [1988]), or determining the bearing behaviour of a closed lining ring with actual segments (Arnau and Molins [2011a], Bilotta and Russo [2013], Blom et al. [1999], Lu et al. [2005], Lu et al. [2006], Schreyer and Winselmann [2000]). Unfortunately, the influence of segmentation on the global behaviour of a tunnel lining has not been dealt with in detail.

1.2.4.1. Normal Stiffness

In order to determine translation springs stiffness in tangential direction, Cavalaro and Aguado [2011] performed experimental tests to characterize the behaviour of the packer under simple stress (normal) and propose a mathematical constitutive model to describe the behaviour properly. The test configuration is presented in **Figure** 1-24. In these tests, only packers in bituminous and rubber were considered.
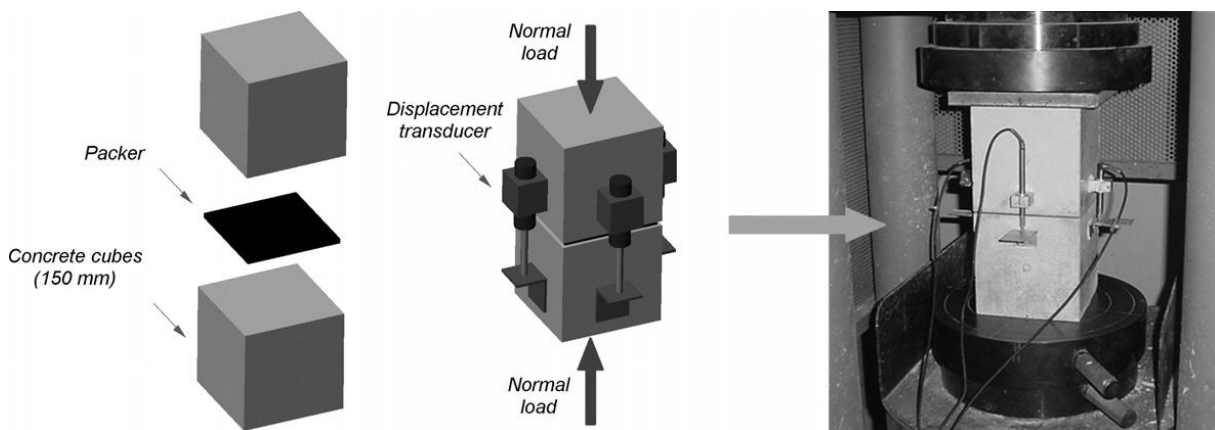
Figure 1-24. Configuration of test using concrete blocks (Cavalaro and Aguado [2011])

The packer is in direct contact with concrete blocks that could generate a certain restriction to the in plane deformation of the packer. The test setup consists of two 150 mm concrete cubes arranged vertically with a 140 mm square packer sheet placed without any adhesive between them. The maximum stress of 20 MPa is applied at a rate of 0.255 MPa/s. The stress-strain curve obtained for the third loading stage is presented in **Figure 1-25**. Using this diagram, the range of normal stiffness, K_N, can be determined. In order to determine K_N value, it is necessary to know the normal stress acting on the joint's surface.
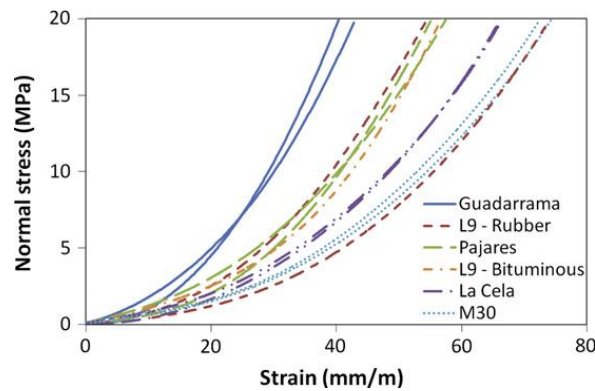
Figure 1-25. Stress-strain curve obtained for the third loading stage (Cavalaro and Aguado [2011])

1.2.4.2. Shear stiffness

Cavalaro and Aguado [2011] also performed experiments on concrete blocks under coupled stress (normal and tangential stress) (**Figure** 1-26). The testing of each of the packers was carried out for the constant normal stress level of 1.5, 8.0 and 15.0 MPa.
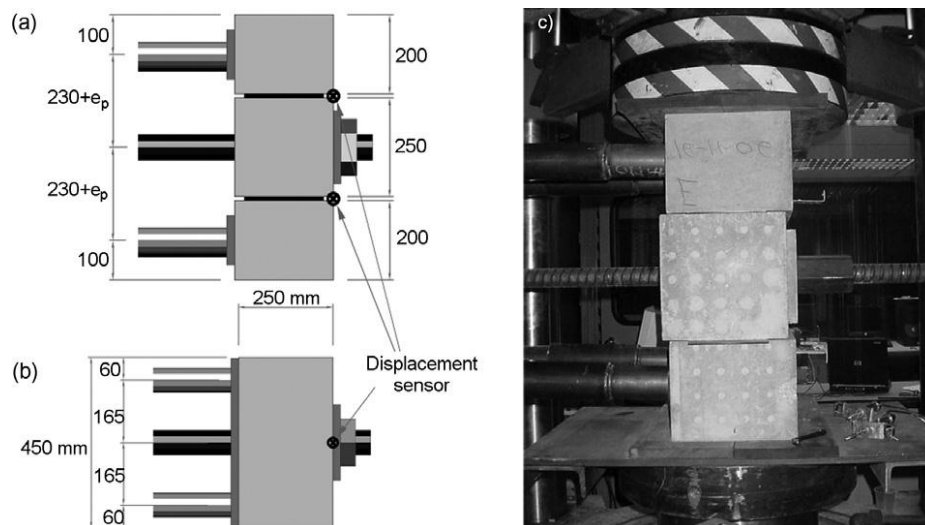
Figure 1-26. Elevation (a), plan view (b) and general view of the press (c) in the coupled stress test setup (Cavalaro and Aguado [2011])

Figure 1-27 shows the graphs that relate the tangential stress to the displacement of the middle block for the tests carried out with the packer of the Line 9 in Barcelona (rubber) at a normal stress level of 1.5, 8 and 15 MPa. In each test a maximum stress (τ_{max}) is estimated, as well as a yielding stress (τ_{2mm}) obtained with a reference relative displacement of 2 mm when the joint has already entered the yield phase (Cavalaro and Aguado [2011]).

In the tests performed with the bituminous packer of the Line 9 in Barcelona (**Figure** 1-28), the tangential stress that marks the transition between the slightly plastic phase and the yield phase is not clearly estimated. In view of this, the limit tangential stress was assumed in

a simplified way as that corresponding to a displacement of 2.0 mm for all the tests performed. As a consequent, in this case the maximum stress (τ_{max}) is considered equal to the yielding stress (τ_{2mm}) (Cavalaro and Aguado [2011]).

The test behaviour in the situation of direct contact shows an initial stiff stage in which the increase of tangential stress does not produce significant displacements (**Figure 1-29**). The friction coefficient measured for the joint without contact material is 0.56 for a normal stress of 1.5 MPa and 0.62 for a normal stress of 4.0 MPa (Cavalaro and Aguado [2011]).
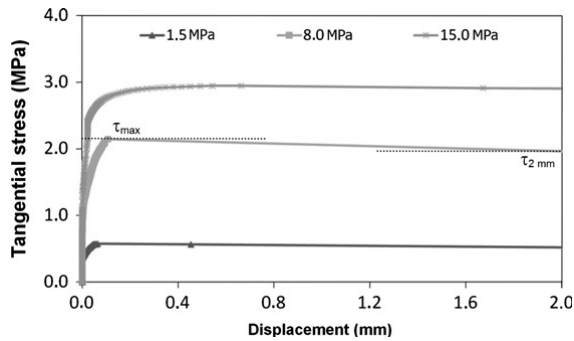
Figure 1-27. Tangential stress-displacement curves for the packer of the Line 9 in Barcelona – rubber (Cavalaro and Aguado [2011])
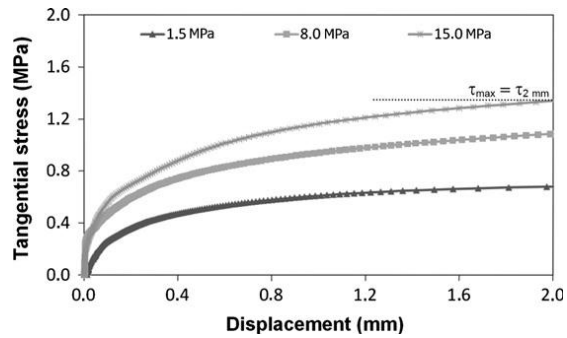
Figure 1-28. Tangential stress-displacement curves for the packer of the Line 9 in Barcelona – bituminous (Cavalaro and Aguado [2011])
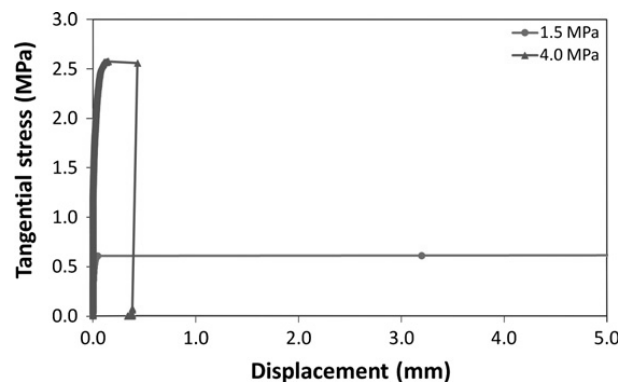
Figure 1-29. Tangential stress–displacement curves in the situation without packer (direct contact) (Cavalaro and Aguado [2011])

1.2.4.3. Rotational stiffness

Experiments on longitudinal joints without packing materials are described by Hordijk and Gijsbers [1996]. Two tunnel segments were loaded by increasing bending moments, under various normal forces. A schematic overview of the test set-up is given in **Figure** 1-30. When raising the normal force to the desired level the measurements resulted in normal force-deformation diagrams. After reaching a constant deformation the rotation test could start. For the calculation of the rotations, the measurements directly over the joint, 50 mm are used. The differences in measured rotations between 50, 600 and 1200 mm were very small so the 50

mm data is a good representation of real rotations occurring in the joint. The normal forces lay in a range varying between 0.2 kN/mm and 4.4 kN/mm. Looking at the moment-rotation diagrams a linear and a non-linear branch is recognized just like that obtained using simple theoretical model proposed by Janssen [1983] (**Figure 1-31**) (see Luttikholt [2007]).
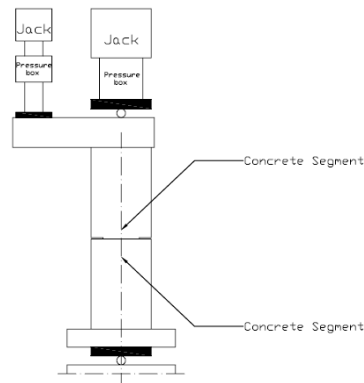
Figure 1-30. Schematic overview of test set-up (Luttikholt [2007])
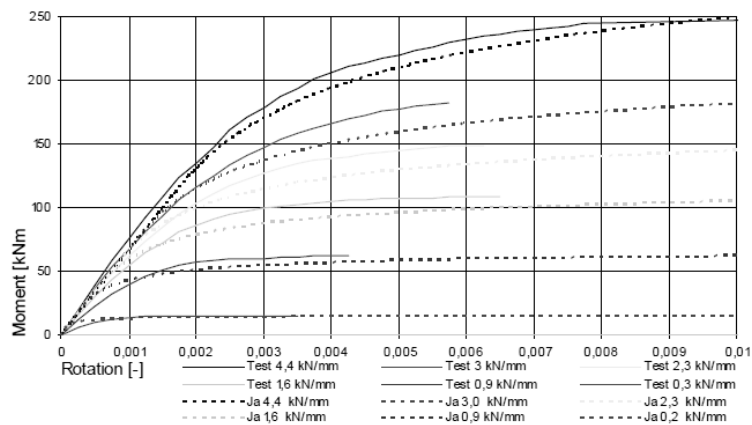
Figure 1-31. Test results (Hordijk and Gijsbers [1996]) compared to Janssen [1983] (Luttikholt [2007])

The initial rotation stiffness shows a steeper slope with increasing normal forces (**Figure 1-31**). This can be explained by the fact that the concrete contact areas are not smooth enough to guarantee ideal contact in the joint. With an increase in normal force the contact area increases. In the treated theoretical models a full contact is supposed. This is not feasible in practice, the initial stiffness will therefore always be lower than the theoretically derived stiffness. For low normal forces the discrepancies between the experimental stiffnesses and theoretical stiffnesses are large. In these areas the theoretically derived initial stiffness according to Janssen cannot be used. For a normal force in the ranch varying between 2 kN/mm and 3 kN/mm the Janssen relation shows a good approximation to the found initial stiffness in the test results. Hordijk and Gijsbers [1996] concluded that for large rotations the results are in accordance with Janssen that means Janssen's model (Janssen [1983]) may be used to simulate the joint behaviour (see Luttikholt [2007]).

1.3. Conclusions

In the literature, the effects of segmental joints have been considered using analytical, experimental and numerical analyses.

In analytical methods, the effects of segmental joints on tunnel lining behaviour are usually considered in both indirect and direct methods. As far as indirect methods are concerned, the effect of joints is usually taken into account through a reduced rigidity of the tunnel structure, which can neither take into account the complexities of the joint characteristics, including joint stiffness and joint distribution, nor analyse complex situations of the surrounding ground. In direct methods, segmental joints are added directly to the tunnel lining structure. Apart from the Ding et al. [2004] method, most direct models consider joint behaviour through rotational springs at the joints. In addition, these methods cannot be applied to cases in which the joint distribution is asymmetrical to the vertical axis of the tunnel.

In order to overcome drawbacks of analytical solutions, numerical analyses have been performed. In 2D models developed by Hefny et al. [2006] and Teachavorasinskun and Chub-Uppakarn [2010], influence of joint distribution and rotational stiffness has been taken into consideration. Unfortunately, the effects of radial and axial stiffness of the joints were not mentioned.

As far as 3D numerical model for mechanized tunnelling is concerned, some researchers have focused on studying the influence of the joint on the tunnel lining behaviour (Blom et al. [1999], Hudoba [1997], Klappers et al. [2006], Arnau and Molins [2012], etc.). However, most of them have modelled only the tunnel structure without considering the effect of surrounding ground. Obviously, there is still not yet a full model, in which the presence of the joints in the tunnel lining is simulated, that allows both ground displacement and structural lining forces to be taken into consideration.

Besides the numerical studies, experimental studies of tunnel lining structures have also been conducted in laboratories or at tunnel sites. Unfortunately, the influence of segmentation on the global behaviour of a tunnel lining has not been dealt with in detail.

Chapter 2

Twin Tunnel Interaction

2.1. Introduction

In recent years, many tunnels have been built in urban environments; this often involves the construction of twin tunnels in close proximity to each other. In addition, in many cases, the new tunnel is often excavated adjacent to an already existing one. Most of them are twin horizontal tunnels. However, in some cases, the twin tunnels are stacked over each other in order to avoid the pile foundations of existing building on the ground surface. The prediction of the influence of a new shield tunnel construction on the existing tunnel plays a key role in the optimal design and construction of close parallel shield tunnels in order to avoid any damage to the existing tunnel during and after excavation of the new tunnel.

Interactions between closely-spaced tunnels were studied in the past using a variety of approaches: physical model testing, field observations, empirical/analytical methods and numerical modelling.

2.2. Twin horizontal tunnel interaction

Interactions between closely-spaced tunnels were studied using a variety of approaches, using physical tests (Kim et al. [1996, 1998], Chapman et al. [2007], Choi and Lee [2010], He et al. [2012], Ng. et al. [2013], Ng. And Lu [2014]), field measurements (Yamaguchi et al. [1998], Suwansawat [2007], Suwansawat and Einstein [2007], Chen et al. [2011], Ocak [2012], He et al. [2012]), empirical/analytical methods (Wang et al. [2003], Hunt [2005], Suwansawat and Einstein [2007], Yang and Wang [2011]), and numerical analyses (Leca [1989], Addenbrooke and Potts [1996], Yamaguchi et al. [1998], Sagaseta et al. [1999], Hefny et al. [2004], Ng et al. [2004], Zheng and Qiu [2005], Karakus et al. [2007], Hage Chehade and Shahrour [2008], Liu et al. [2008], Li et al. [2010], Afifipour et al. [2011], Chakeri et al. [2011], Ercelebi et al. [2011], Mirhabibi and Soroush [2012], Hasanpour et al. [2012], Channabasavaraj and Vishwanath [2012], Mathew and Lehane [2013]). Interesting summaries of twin tunnel interactions can be found in study presented by Laver [2010].

Kim et al. [1996, 1998] performed physical tests to investigate the response of the first tunnel lining on the approaching of the second shield. The results of their model tests showed that the interaction effects are greater in the spring line and crown of the existing tunnel. Chapman et al. [2007] described results from a series of small-scale (1/50) laboratory model tests carried out in Speswhite kaolin clay which focused on studying the short-term ground movements associated with closely spaced multiple tunnels (**Figure 2-1**). The influence of tunnel distance, tunnel depth and tunnel number were highlighted. The results showed asymmetrical settlement troughs, greater settlement above the second of twin tunnels constructed (see an example in **Figure 2-2**). Their study also demonstrated that the commonly used semi-empirical method of predicting the short-term settlement above twin tunnels, using the summation of Gaiussian curves, will potentially give inaccuracies results.

Figure 2-1. The front Perspex window showing maker beads and tunnelling device (Fig. 3 in Chapman et al. [2007])
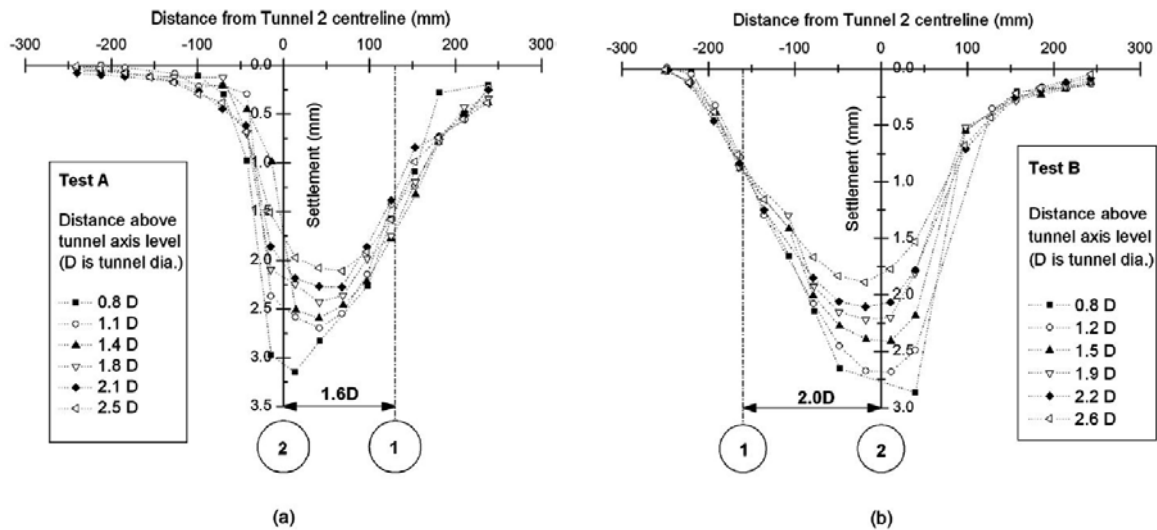
Figure 2-2. Observed ground movements above a second tunnel (a) 1.6D from the first tunnel, (b) 2.0D from the first tunnel (Fig. 7 in Chapman et al. [2007])

In the study by Choi and Lee [2010], the influence of the size of an existing tunnel, the distance between tunnel centers and the lateral earth pressure factor on mechanical behaviour of the existing and new tunnels was investigated by quantifying the displacement and crack propagation during the excavation of a new tunnel constructed near an existing tunnel. A series of experimental model tests were performed and analysed. It was found that the displacements decreased and stabilized as the distance between the tunnel centers increased, depending on the size of the existing tunnel.

A series of 3D centrifuge model tests investigating the effects of twin tunnel construction on an existing pile in dry sand has been conducted by Ng et al. [2013] and Ng and Lu [2014]. Strong impact of the tunnel construction procedure on the movement of the ground surrounding the tunnels has been highlighted through the change in internal forces induced in the existing pile and the settlement curves developed on the ground surface.

Chapter 2: Twin tunnel interaction   35

Suwansawat and Einstein [2007] introduced interesting field measurement results on ground movements induced by parallel EPB tunnels excavated in soft ground in Bangkok. They showed that the operational parameters, such as face pressure, penetration rate, grouting pressure and filling, have significant effects on the maximum settlement and extent of the settlement trough. On the basis of measurement data, the authors proposed a procedure of the superposition technique for describing the settlement trough developed over twin horizontal tunnels using the Gaussian curves:

(1) Measure the maximum surface settlement with the settlement marker installed over the centerline of the first tunnel (i.e., Point A in **Figure 2-3**) and determine the entire settlement trough induced by the first shield using the Gaussian function.

(2) Observe settlements over the second tunnel centerline (i.e., Point B in **Figure 2-3**) after the passage of the second shield.

(3) Calculate the additional or inferred settlement over the second tunnel (i.e., Point C in **Figure 2-3**) by subtracting the settlement measured after the passage of the first shield from the settlement measured after second shield passing.

(4) Determine the additional settlement curve induced by the second shield using the Gaussian curve and superimpose it on the settlement trough induced by the first shield in order to obtain the total settlement curve caused by the twin tunnels.
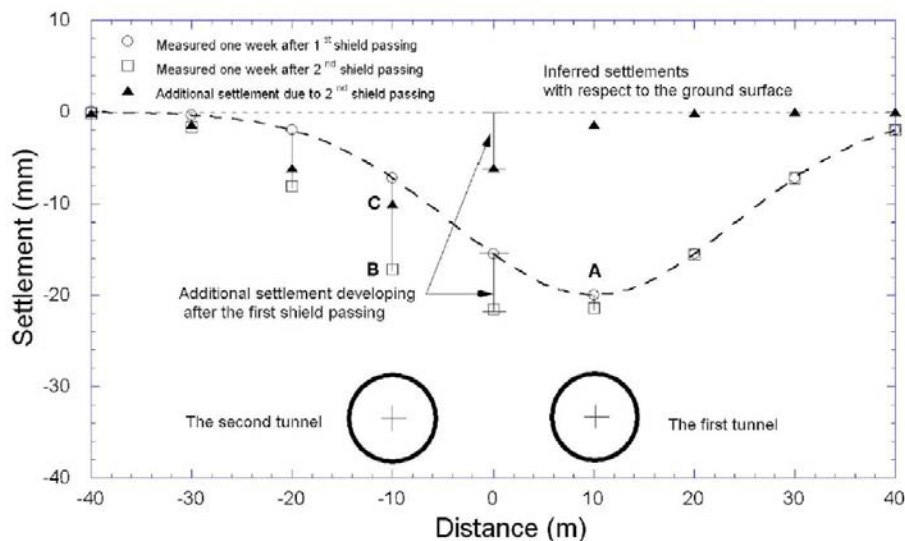
Figure 2-3 Additional settlement developing after the first shield passing (Fig. 24 in Suwansawat and Einstein [2007])

Using proposed superposition technique, total settlement trough as a result of the twin tunnels were obtained (see an example in **Figure 2-4**). The superposition curves and the observed data compare very well. Their results also showed that the maximum settlement for twin tunnels is not usually located over the midpoint between the two tunnels and that the settlement trough is often asymmetric (see **Figure 2-4**).

Chen et al. [2011] presented field measurements conducted on parallel tunnels using EPB shields in silty soil. Their results showed a great dependence of the ground movements on the distance between the second tunnel face and the monitored section. They also indicated that

the two settlement troughs caused by the construction of the first and the second tunnel had similar shapes. However, similar as that observed by Suwansawat and Einstein [2007], the second tunnel trough was shallower and wider than that of the first tunnel. The first tunnel made the symmetric axis of the final trough of the parallel tunnels incline towards the first tunnel (see **Figure 2-5**).
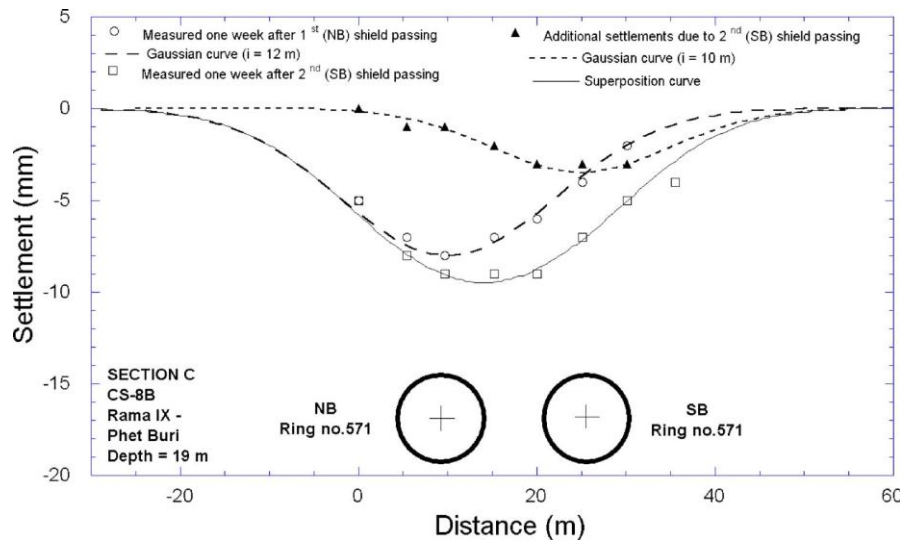
Figure 2-4. Surface settlements measured on CS-8B, settlement troughs described by Gaussian curves and superposition curve (Fig. 27 in Suwansawat and Einstein [2007])
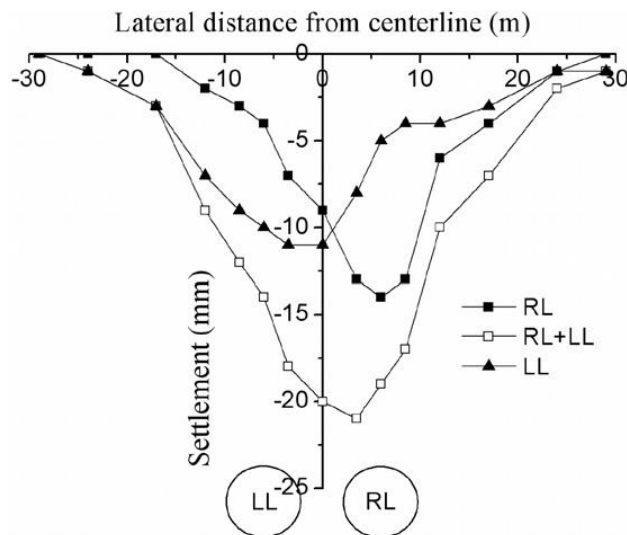
Figure 2-5. Surface settlement measured in section G2 (Fig. 6 in Chen et al. [2011])

In the study by Ocak [2012], thirty longitudinal monitoring sections, obtained through EPB tunnelling, were used to determine the interactions of the longitudinal surface settlement profiles in shallow twin tunnels. He et al. [2012] carried out field and model tests, based on the Chengdu Metro Line 1 in China, to study the surface settlement caused by twin parallel shield tunnelling in a sandy cobble strata. The surface settlement mechanism and the effect of tunnel distance on the surface settlement were also studied using the discrete element method.

They showed that when the spacing between two tunnels is higher than twice the tunnel diameter, an independent arch can be formed.

It should be noted that in any of the above studies, the resulting structural forces induced in the tunnel lining were not mentioned.

Obviously, field observations remain the key to understanding the interaction between adjacent tunnels. Unfortunately, field data are often incomplete. It is clear that model testing can only be used to study limited interaction behaviour. Empirical and analytical methods, using the superposition technique (e.g. Wang et al. [2003], Hunt [2005], Suwansawat and Einstein [2007], Yang and Wang [2011]), have been used on the basis of the prediction of each individual excavation in order to obtain the final accumulated settlement trough. Generally, superposition method cannot take into account rigorously the effect of an existing tunnel and the unloading of the ground caused by the previous excavation of the first tunnel. Therefore, the settlement curves do not represent the final displacement very well (Divall [2012]). Furthermore, empirical and analytical methods also introduce drawbacks for those cases in which complex geological conditions (e.g. multilayer strata) are expected. The use of a finite element model seems to be a promising way of addressing this issue.

Leca [1989], Addenbrooke and Potts [1996], Yamaguchi et al. [1998], Sagaseta et al. [1999], Hefny et al. [2004], Ng et al. [2004], Karakus et al. [2007], Hage Chehade and Shahrour [2008], Afifipour et al. [2011], Chakeri et al. [2011], Ercelebi et al. [2011], Mirhabibi and Soroush [2012], Hasanpour et al. [2012] have all carried out numerical analysis of this interaction problem. Most of these studies focused on considering the effect of the ground condition, tunnel size, tunnel depth, surface loads, and relative position between two tunnels on the surface settlement. Their results were similar: the influence of the second tunnel on the previously installed lining of the first one has been shown to depend on the relative position of the tunnel and on the spacing between the two tunnels.

The literature reviewed above clearly indicates that an extensive amount of research has been conducted on tunnel interactions between parallel tunnels. Most of this research has focused on the influence of twin tunnels on ground deformation. However, less work has been devoted to the influence of the interaction between tunnels on the structural forces induced in a tunnel lining.

Ng et al. [2004] performed a series of 3D numerical simulations to investigate the interactions between two parallel noncircular tunnels constructed using the new Austrian tunnelling method (NATM). Special attention was paid to the influence of the lagged distance between the excavated faces of the twin tunnels (L_F) and the load-transfer mechanism between the two tunnels. It was found that L_F has a greater influence on the horizontal movement than on the vertical movement of each tunnel and that the magnitude of the maximum settlement is independent of L_F.

An example of shifting of the settlement trough can also be clearly illustrated by plotting transverse surface settlements at various longitudinal distances in the y direction for $L_F = 3.5D$ (see **Figure 2-6**). It is clear that the settlement trough shifts gradually from the first (left) tunnel to the second (right) tunnel, and the maximum ground surface settlement offsets the centerline of the pillar. They also showed that the distributions of the bending moment induced in the tunnel linings are similar in shape, but different in magnitude in the two

tunnels (see **Figure 2-7**). It should be noted that the bending moment diagram for single tunnel is not symmetric in **Figure 2-7**. In fact, tunnel was excavated partly using NTAM method. Drift on the left side was excavated first and then followed by the drift on the right side. The tunnel support lining was constructed right after the excavation of each drift. A center support was used to close the support structure of the left drift and then it was removed during the excavation of the right drift. That is why the bending moment in a single tunnel is not symmetric.

In the study by Liu et al. [2008], the effect of tunnelling on the existing support system (i.e. shotcrete lining and rock bolts) of an adjacent tunnel was investigated through full 3D finite element calculations, coupled with an elasto-plastic material model. It was concluded that the driving of a new tunnel significantly affects the existing support system when the advancing tunnel face passes the existing support system and has less effect when the face is far from the system. It was also pointed out that the effects of tunnelling on the existing support system depend to a great extent on the relative position between the existing and new tunnels.
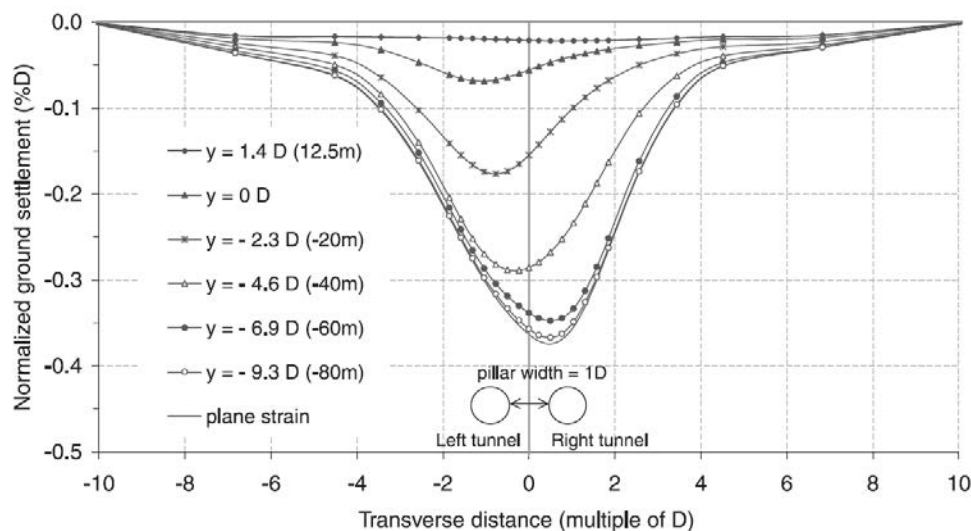
Figure 2-6. Normalized surface ground settlements at various longitudinal distances for L_F = 3.5D (Fig. 8 in Ng et al. [2004])
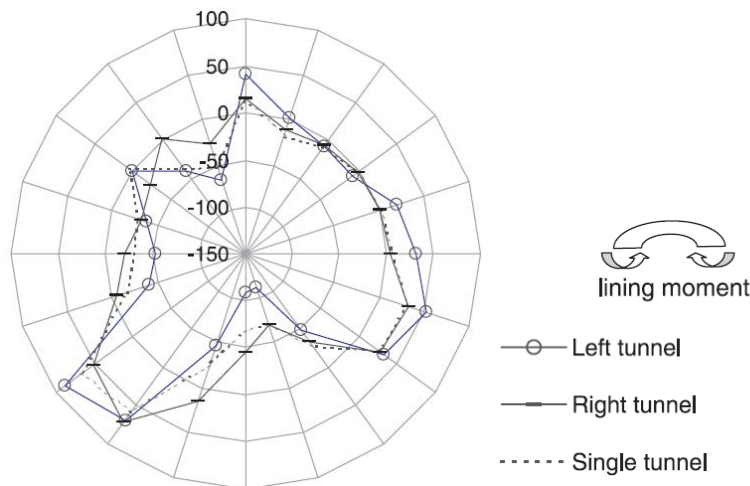
Figure 2-7. Bending moment (kN.m) in lining at section E–E ($y = -8.6D$, approaching plane strain conditions) for $L_F = 3.5D$ (Fig. 11 in Ng et al. [2004])

2.3. Stacked twin tunnel interaction

As far as the excavation of mechanized twin tunnels in close proximity is concerned, most of the cases reported in the literature have focused on considering the interaction between two horizontally driven tunnels. However, less work has been devoted to the interaction between tunnels stacked over each other (e.g., Yamaguchi et al. [1998], Hefny et al. [2004], Suwansawat and Einstein [2007], Hage Chehade and Shahrour [2008], Liu et al. [2008], Li et al. [2010], Channabasavaraj and Vishwanath [2012], Zhang and Huang [2014]).

In Yamaguchi et al. [1998], various stages of the interactions between two tunnels were dealt with: Stage 1- the succeeding shield approaches the measuring point and its thrust begins to have influence; Stage 2- the tail of the succeeding shield passes the measuring point and the influence of the falling pressure after excavation can be observed; Stage 3- the succeeding shield moves away and ceases to have any influence. Unfortunately, only the tunnel bending moment and the measurements of the earth pressure gauges in an existing tunnel when succeeding shields passed were presented (**Figure 2-8**). Their results indicate that, in case of stacked tunnels, the deformation of the existing tunnel is a vertical expansion.

On the basis of measurement data (**Figure 2-9**), Suwansawat and Einstein [2007] introduced a superposition technique using Gaussian curves to describe surface settlement troughs over twin tunnels, and dealt with stacked tunnels (see an example in **Figure 2-10**). It was found that the Gaussian curve does fit the settlement trough of the first (lower) tunnel very well as shown in **Figure 2-10**. The Gaussian curve is also applied to the settlement trough measured after second shield passing. As can be seen in **Figure 2-10**, the Gaussian curve fits the settlement trough very well and the trough width parameter (i=9 m) is equal to that of the settlement curve caused by the first tunnel. However, to study the ground response only induced by the second (upper) tunnel, one needs to determine additional surface settlements developed after the first shield passage by using the technique previously introduced in the previous section. The additional settlement trough induced by the second

shield is much smaller than the settlement trough caused by the first shield. This was somewhat unexpected as the upper tunnel is much shallower than the lower and one would expect that the surface settlements induced by the upper tunnel to be larger than those of the lower tunnel. This assumption may be true in cases of open-faced tunnelling as the ground response is mainly affected by tunnel geometry and geological conditions. On the other hand, if the tunnel is excavated using the EPB tunnelling method, one should consider operational parameters as well (Suwansawat and Einstein [2007]).

Although superposition technique using Gaussian curves proposed by Suwansawat and Einstein [2007] were successfully applied to predict the settlement trough above stacked tunnels, this method, as mentioned above, ignores the presence of an existing tunnel and the repeated unloading of the ground due to the preceding excavation of this tunnel. Additionally, this method also shows some drawbacks for the cases in which complex geological conditions (e.g. multilayer strata) can be expected.
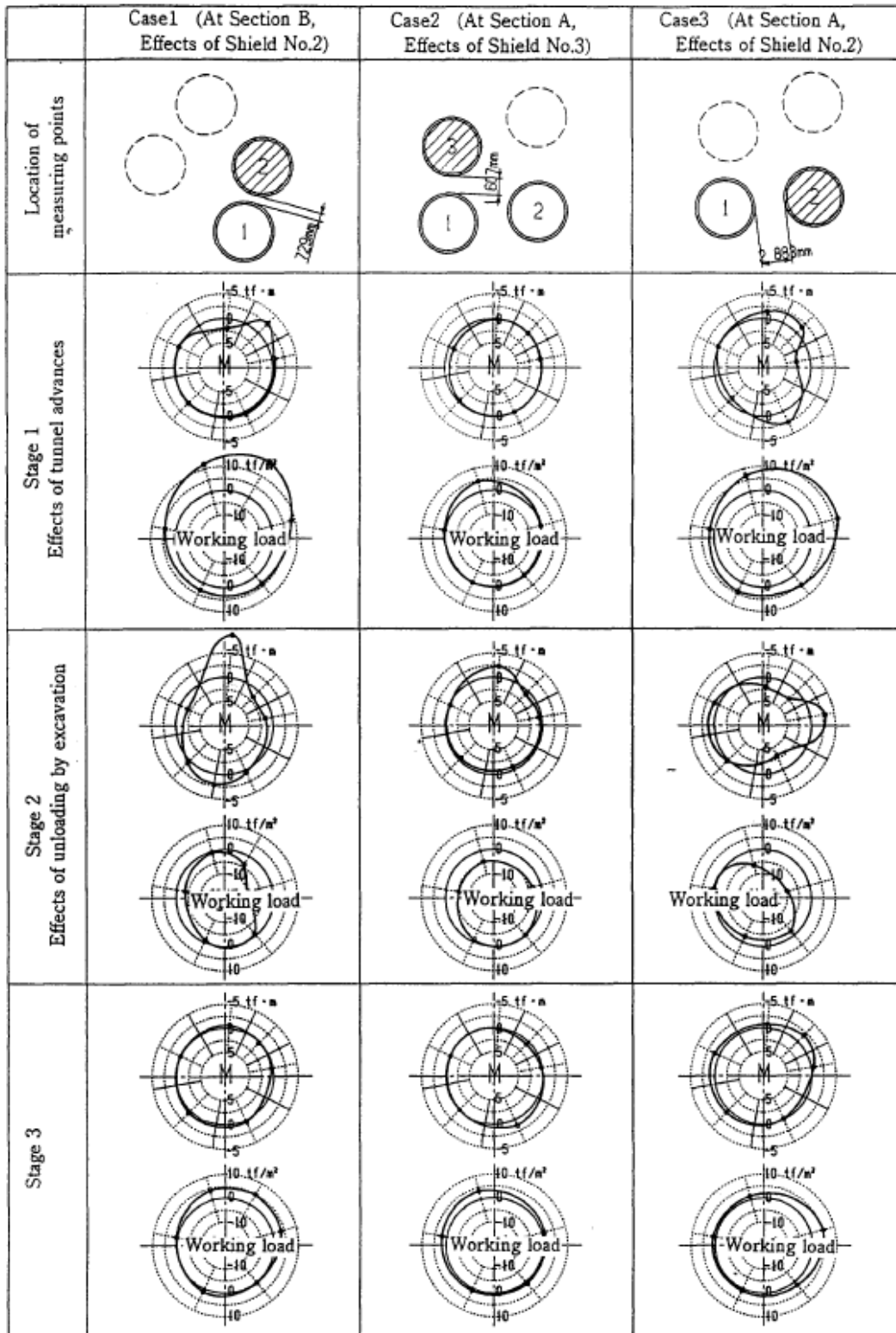
Figure 2-8. Sectional profiles of bending moment and working load (Fig. 4 in Yamaguchi et al. [1998])
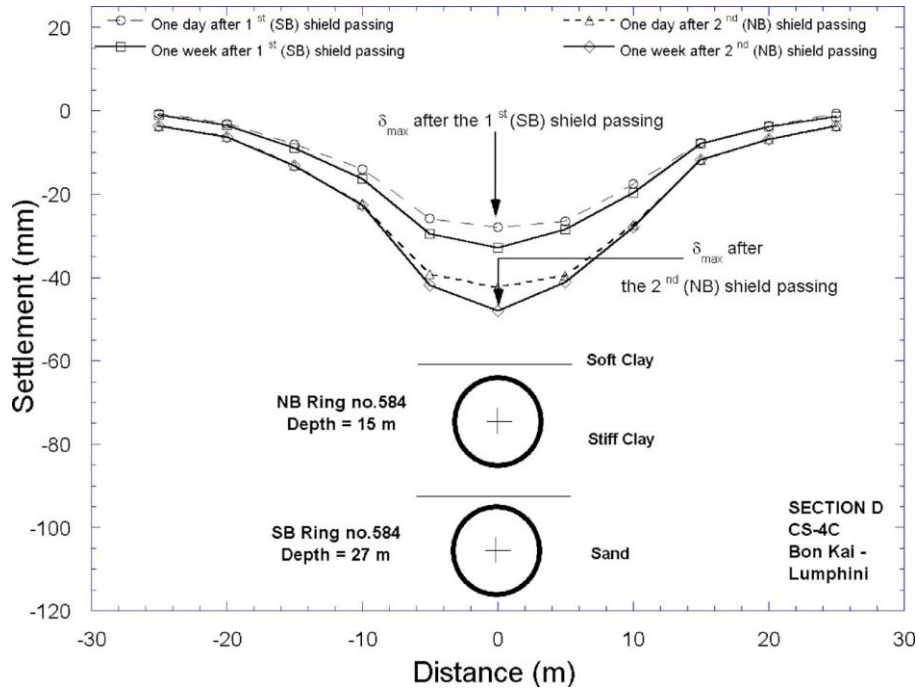
Figure 2-9. Surface settlement troughs measured in CS-4C and the instrumentation layout
(Fig. 33 in Suwansawat and Einstein [2007])
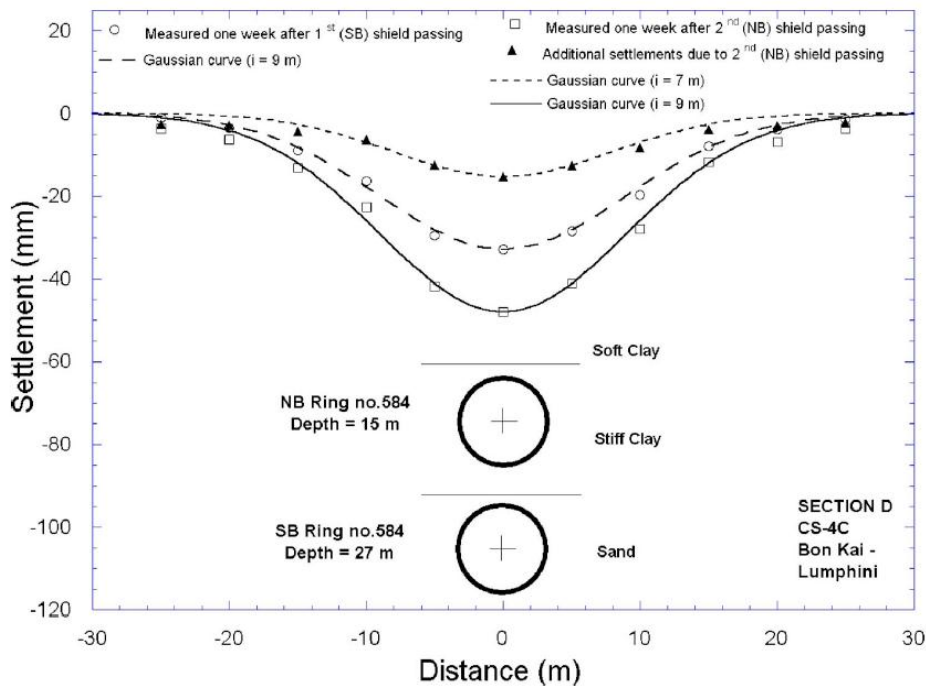
Figure 2-10. Surface settlements measured in CS-4C, settlement troughs described by
Gaussian curves (Fig. 34 in Suwansawat and Einstein [2007])

Hefny et al. [2004], Hage Chehade and Shahrour [2008] and Channabasavaraj and Vishwanath [2012] have presented 2D numerical analyses which have shown the influence of the position of a new tunnel on existing tunnel behaviour. Hage Chehade and Shahrour [2008] and Channabasavaraj and Vishwanath [2012] have indicated that the construction of an upper

tunnel at first leads to greater settlement and structural forces than those obtained when the lower tunnel is constructed first (see **Figure 2-11**).

Hefny et al. [2004] focused on investigating the effect of the angular position of a new tunnel relative to a parallel existing tunnel. The relative position was represented by the angle θ measured between the center-to center line and the crown-invert line of the existing tunnel. An angle θ of 0^0 represents a new tunnel directly above the crown of an existing tunnel, while an angle θ of 90^0 represents a new tunnel located beside and at the same depth as the existing tunnel. In their study, the distance between tunnels was kept constant at three times the tunnel radius (center-to-center). All the soil and lining properties were assumed to be unchanged throughout the analysis. Results of two cases of volume loss (VL of 0 % and 2 %) were presented.
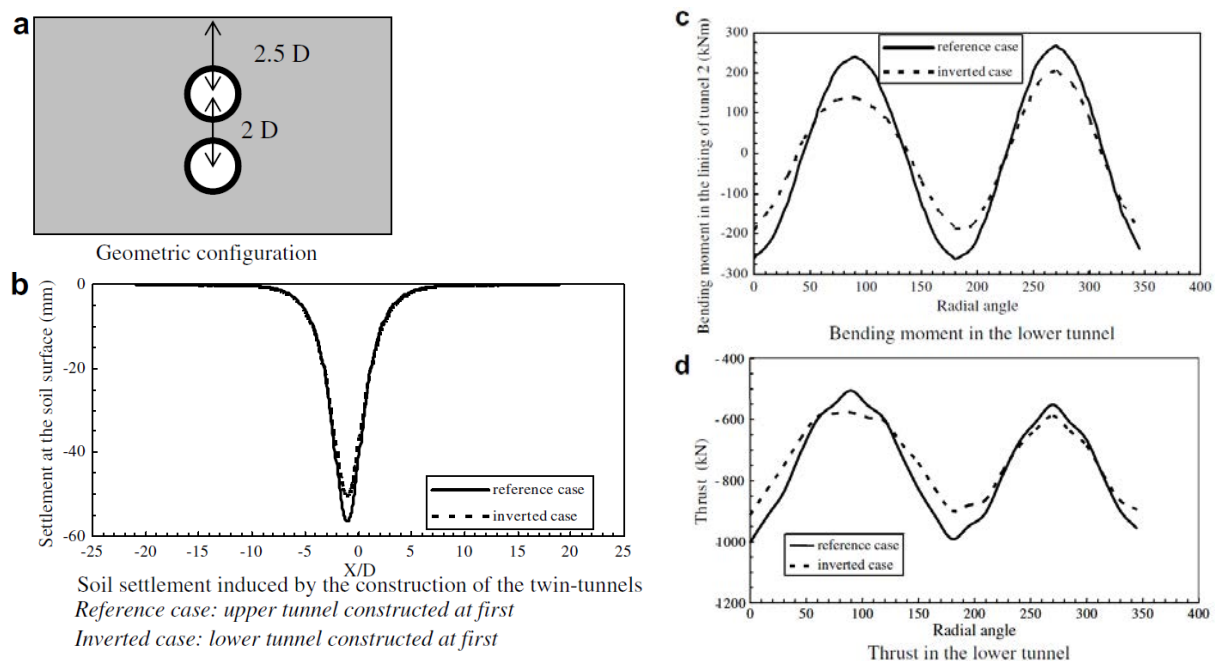
Figure 2-11. Tunnels with vertical alignment: Influence of the construction procedure on the soil settlement and internal forces (Fig. 5 in Hage Chehade and Shahrour [2008])

The results obtained by Hefny et al. [2004] showed that when the new tunnel is driven above the existing tunnel, the existing tunnel experiences a decrease in the maximum axial forces. This can be explained by the decrease in vertical pressure acting on the existing tunnel due to the removal of a mass of soil above the tunnel. It can be seen from **Figure 2-12** that the excavation of the new tunnel beside or below the existing tunnel has insignificant effect on the maximum axial force induced in the lining.

Figure 2-13 shows that the influence of angular relative position of the new tunnel on the bending moment induced in the existing tunnel is considerable compared to the axial forces. For the case of no volume loss (VL of 0 %), there is a decrease in the maximum bending moment induced in the lining of the existing tunnel after interaction with the new tunnel when the new tunnel is excavated above the existing tunnel with relative position changing from 0^0 to about 45^0. This can be attributed to the decrease in vertical pressure that acts on the existing tunnel after the new tunnel is excavated. When the new tunnel is excavated below the existing

tunnel, the bending moment developed in the lining of the existing tunnel increases substantially. This can be explained by the fact that the excavation of the new tunnel below the existing tunnel reduces the ground stiffness in the vertical direction, which leads to more vertical deformation to the lining and therefore the bending moment increases. In this case, the maximum change in bending moment induced in existing tunnel was about 30 % of that observed before interaction with the new tunnel (Hefny et al. [2004]).
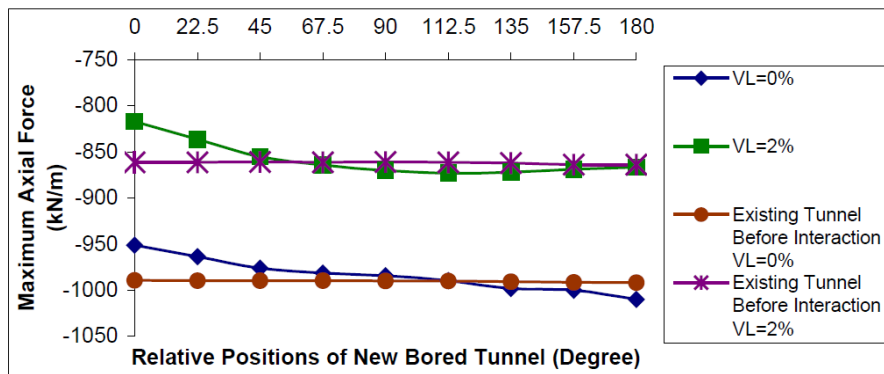
Figure 2-12. Variation of maximum axial force (existing tunnel after interaction) with relative position of new bored tunnel (Fig. 2 in Hefny et al. [2004])
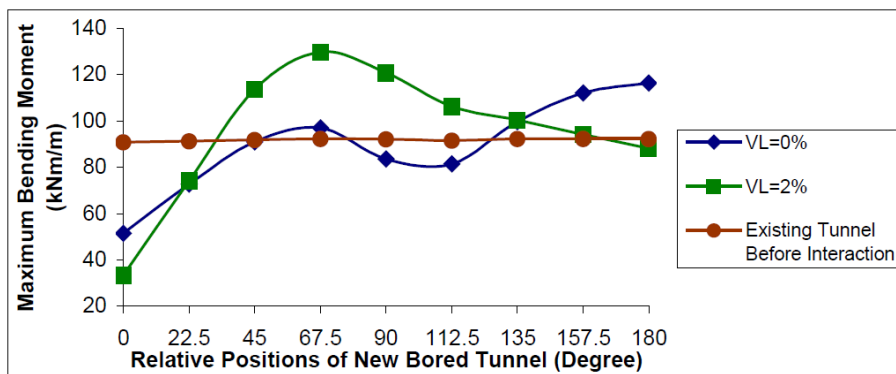
Figure 2-13. Variation of maximum bending moment (existing tunnel after interaction) with relative position of new bored tunnel (Fig. 3 in Hefny et al. [2004])

From above results, Hefny et al. [2004] drew some conclusions as follows:
- There is a decrease in the maximum bending moment developed in the lining of existing tunnel when the new tunnel is located above the existing tunnel.
- For cases of small percentage of volume loss (less than about 0.5%), the excavation of the new tunnel below the existing tunnel leads to an increase in the bending moment induced in the existing tunnel lining.
- The excavation of the new tunnel beside the existing tunnel may lead to significant increase in the bending moment in the lining of the existing tunnel.

In order to investigate the influence of a new shield tunnel excavation on the internal forces and deformations in the lining of an existing tunnel, Li et al. [2010] presented a series of 3D numerical simulations of the interaction between two shield tunnels in which the ground behaviour was modelled using the linear elastic perfectly plastic constitutive model

using the Mohr-Coulomb criteria (see **Figure 2-14** and **Figure 2-15**). Particular attention was paid to the influence of the relative position of the two parallel tunnels. A case of stacked tunnels in which the upper tunnel was driven first, was presented. The results indicated decreases in the bending moment developed in the bottom and crown region of the existing tunnel and a decrease in the normal forces around the tunnel lining. Unfortunately, the existence of joints in the segmental lining, the construction loads during shield tunnelling, that is, face pressure, jacking force and grouting pressure, were not simulated in this numerical model. Moreover, the impact of a new tunnel excavation on an existing tunnel during the advancement of the new tunnel and of the surface settlements developed above the stacked tunnels was not considered.
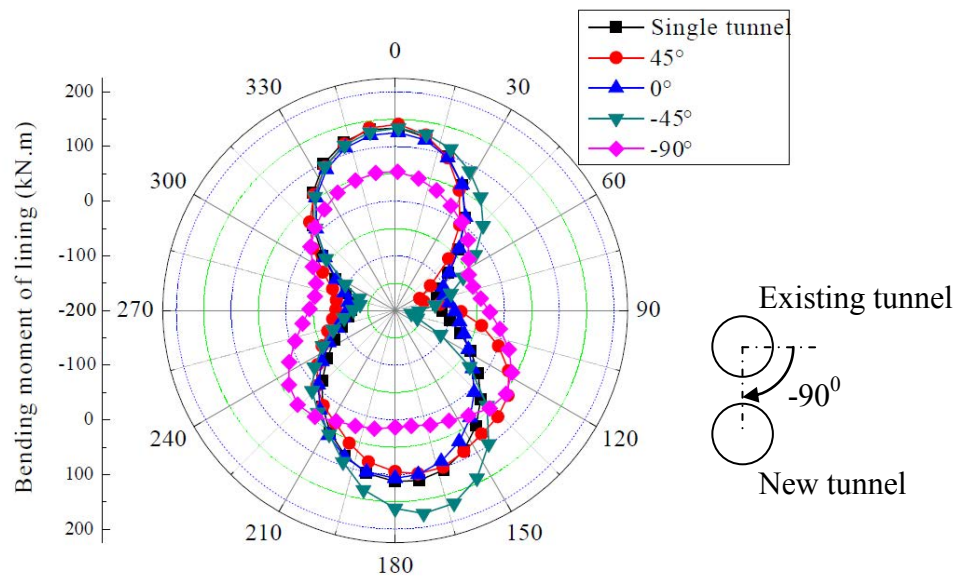
Figure 2-14. Variation of bending moment (kN.m) with different position of new tunnel (Li et al. [2010])
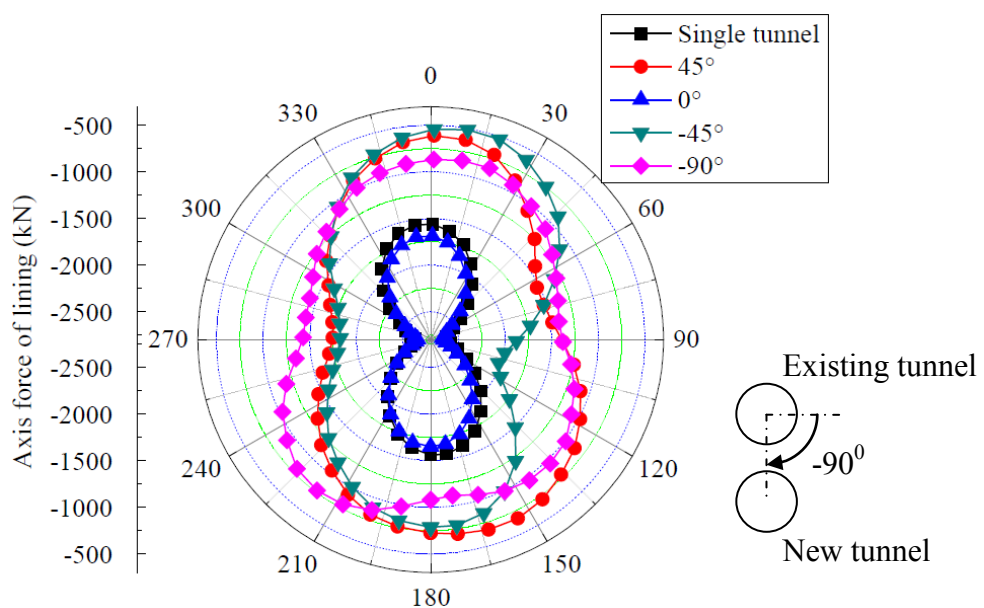
Figure 2-15. Variation of axial force (kN) with different position of new tunnel (Li et al. [2010])

Zhang and Huang [2014] performed simplified theoretical analysis and 3D FEM numerical simulation to investigate the influence of multiline overlapped tunnelling on existing tunnels. Twin new stacked tunnels were excavated cross above and below existing horizontal tunnels. Unfortunately, this study focused only on the deformation of the ground surface.

2.4. Conclusions

Interactions between closely-spaced tunnels were studied using a variety of approaches: physical model testing, field observations, empirical/analytical methods and finite element modelling. All results indicated an interaction between tunnels excavated in close proximity. Most of the research has focused on the influence of twin tunnels on ground deformation. However, less work has been devoted to the influence of the interaction between tunnels on the structural forces induced in a tunnel lining (Li et al. [2010]).

Obviously, there is not a full 3D numerical simulation for mechanized twin tunnels in soft ground, in which the segmental joints is simulated, that allows both ground displacement and structural lining forces to be taken into consideration.

Chapter 3

Behaviour of Tunnel Linings under Dynamic Loads

3.1. Introduction

Understanding the behaviour of underground structures during seismic events is one of the most interesting challenges in geotechnical engineering. While tunnels generally performed better than above ground structures during earthquakes, damage to some of these important structures during previous earthquake events, that is, the 1995 Kobe, Japan earthquake, the 1999 Chi Chi, Taiwan earthquake, the 1999 Bolu, Turkey earthquake, the 2004 Baladeh, Iran earthquake, the 2008 Sichuan, China earthquake, and recently the 2014 Valparaiso, Chile earthquake, highlights the need to account for seismic loading in the design of underground structures.

In a broad sense, earthquake effects on underground structures can be grouped into two categories: ground shaking and ground failure (Wang [1993]). The latter one is not considered in the present work.

Ground shaking refers to the vibration of the ground induced by seismic waves that propagate through the earth's crust. **Figure 3-1** shows the ground response due to the various types of seismic waves:

- Body waves travel within the earth's material. They may be either P waves (also known as primary or compressional or longitudinal waves) or S waves (also known as secondary or shear or transverse waves) and they can travel in any direction in the ground.

- Surface waves travel along the earth's surface. They may be either Rayleigh waves or Love waves. They have a slower velocity and a lower frequency than body waves.

As ground is deformed by the travelling waves, any tunnel structure in the ground will also be deformed. Owen and Scholl [1981] claimed that the behaviour of a underground structure during seismic event can be approximated to that of an elastic beam subject to deformations imposed by the surrounding ground. Three types of deformations express the response of underground structures to seismic motions (see **Figure 3-2**):

- Axial compression/extension
- Longitudinal bending
- Ovalling/racking

Axial deformation in tunnels are generated by the components of seismic waves that produce motions parallel to the axis of the tunnel and cause alternating compression and tension. Bending deformation are caused by the components of seismic waves producing particle motions perpendicular to the longitudinal axis. Design considerations for axial and bending deformations, which are not taken into account in this study, are generally in the direction along the tunnel axis (Wang [1993]).

Ovaling or racking deformations in a tunnel lining develop when shear waves propagate normal or nearly normal to the tunnel axis: circular tunnels undergo ovalisation, rectangular tunnel undergo racking. Penzien [2000], Hashash et al. [2005] indicated that the component that has the most significant influence on the tunnel lining behaviour under seismic loading, except the case of a tunnel sheared by a fault, is the ovaling or racking deformation generated

by the seismic shear wave or S-wave propagation. In other words, they are the most crucial deformation modes for the tunnel sections.
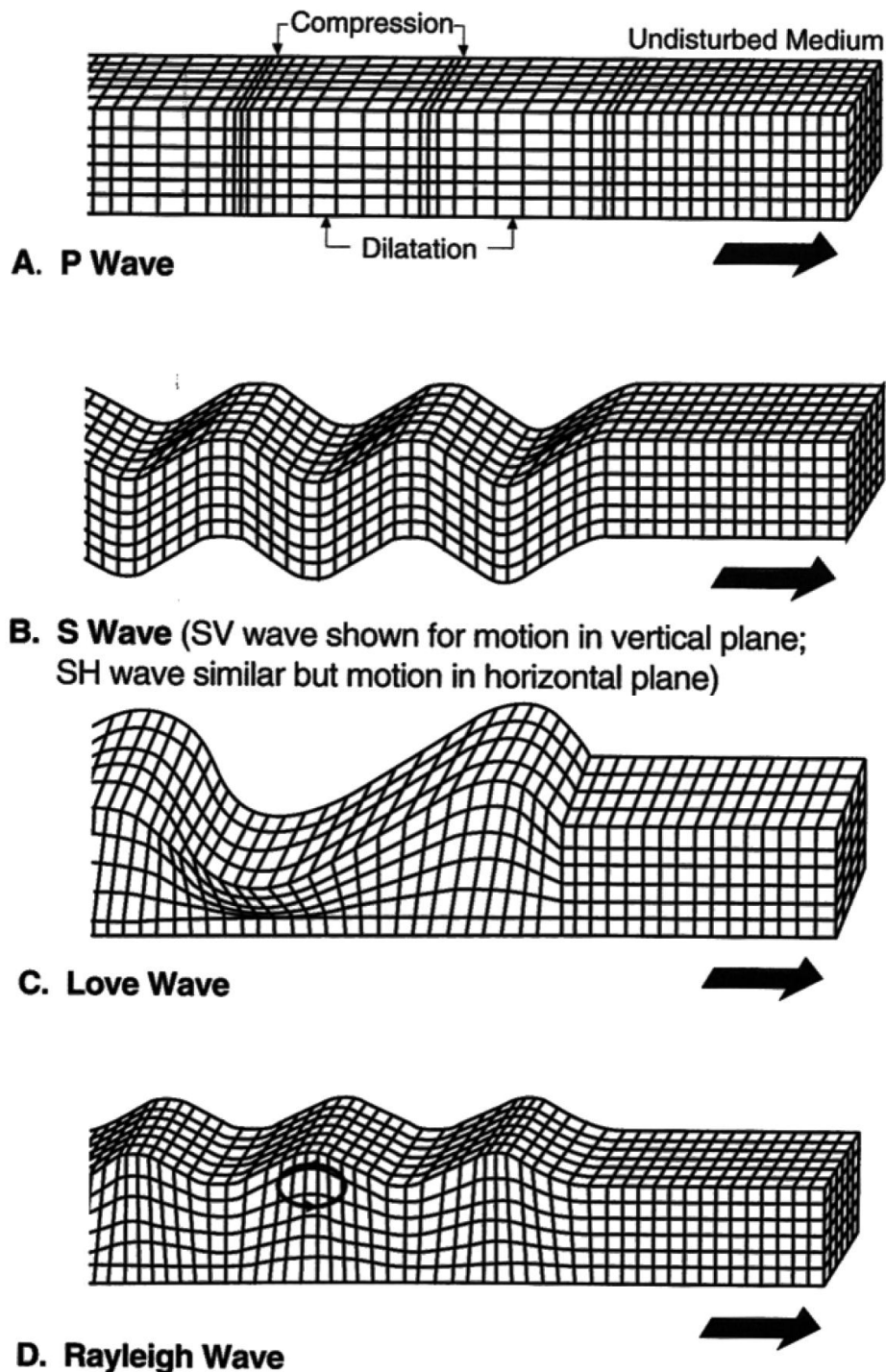
Figure 3-1. Ground response to seismic waves (Wang [1993])

In the following sections, a review of the more common methods used to calculate the seismic-induced stresses in a circular tunnel undergoing ovalisation is presented. A special attention is focused on the influence of segmental joints and soil constitutive model on the tunnel behaviour under seismic loads.

Axial deformation along tunnel   Bending (curvature) deformation along tunnel
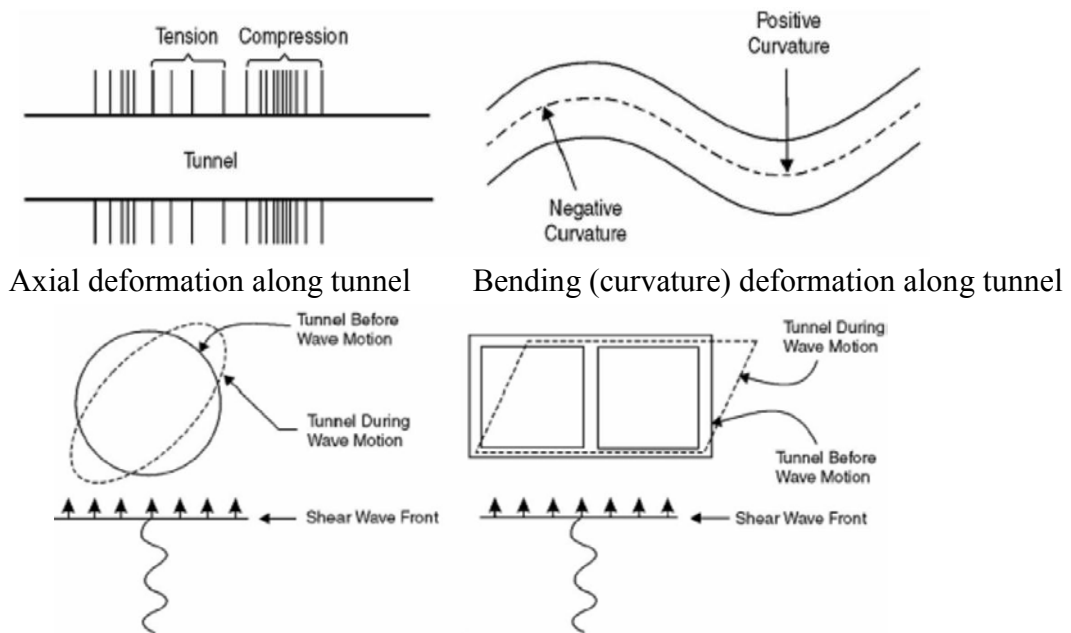
Ovaling deformation of a circular tunnel   Racking deformation of a rectangular tunnel
Figure 3-2. Type of tunnel deformations during a seismic event (Owen and Scholl [1981])

3.2. Analysis methods

The behaviour of tunnels under seismic loads has been studied using a variety of approaches: empirical and analytical methods, physical model tests and numerical modelling.

3.2.1. Closed-form solutions

The ovaling deformation is commonly simulated with a two-dimensional, plane strain configuration and usually further simplified as a quasi-static case and hence without taking into account of the seismic interaction (Hashash et al. [2005]).

Due to their simplicity, various elastic closed-form solutions have been developed to determine the structural forces induced in a circular tunnel lining due to a seismic load (e.g., Wang, [1993], Peinzen and Wu [1998], Peinzen [2000], Bobet [2003], Park et al. [2009], Corigliano et al. [2011]). Hashash et al. [2005] described the discrepancies between the Wang [1993] and Penzien and Wu [1998] methods, and used numerical analyses under the same assumptions to better understand the differences between the two solutions and their causes. The comparisons clearly demonstrated that Wang's solution provides a realistic estimation of the thrust in the tunnel lining for a no-slip condition. It has been recommended that Peinzen's solution should not be used for a no-slip condition (Hashash et al. [2005]). These differences are also reported by Park et al. [2006], Bazaz and Besharat [2008]. The works performed by Park et al. [2006] and Park et al. [2009] indicated a good agreement between their solution with the previous solutions of Wang [1993] and Bobet [2003].

Generally, the closed-form solutions are limited to the following assumptions (Sederat et al. [2009]):

- The homogenous soil mass and the tunnel lining are assumed to be linear elastic and mass-less materials;
- Tunnel is circular with uniform thickness and without joints;
- The effect of the construction sequence is not considered.

Considering a circular tunnel of radius *R* located sufficiently below the ground surface and subjected to an earthquake loading using shear waves (**Figure 3-3**), the seismic-induced stress state of the soil can be treated as a shear-type stress. This is equivalent to a compressive and a tensile free-field principal stresses at 45^0 with the direction of the pure shear, as shown in **Figure 3-4** (Park et al. [2006]).
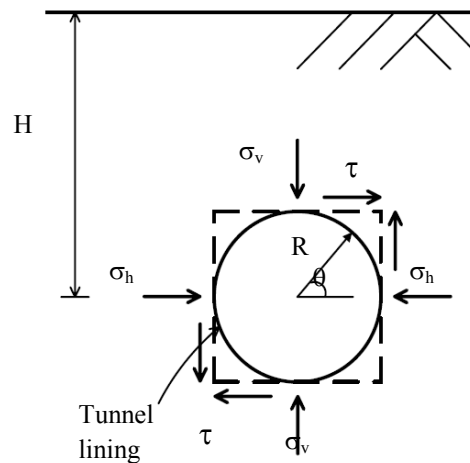
Figure 3-3. A circular tunnel (Park et al. [2006])
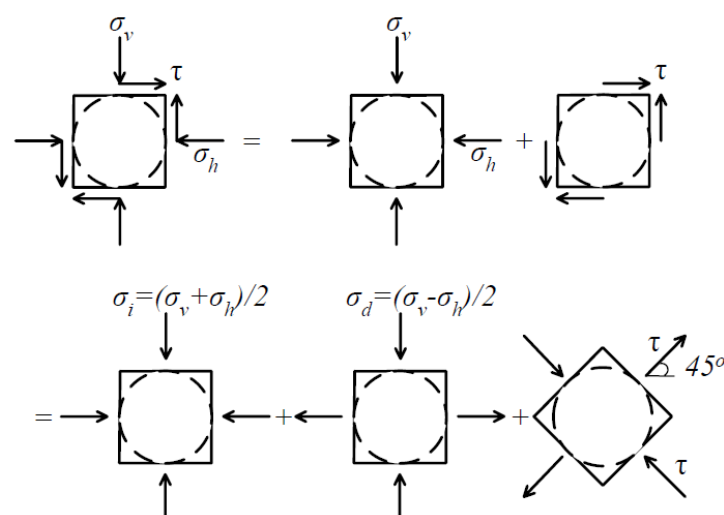
Figure 3-4. Seismic shear loading and equivalent static loading (Park et al. [2006])

The shear stress can be estimated using the free-field shear strain γ_c (Penzien and Wu [1998], Hashash et al. [2001], Hashash et al. [2005]):

$$\tau = \frac{E\gamma_c}{2(1+\nu)} \tag{3-1}$$

Where the shear strain γ_c over the depth *2R* can be determined as follows:

$$\gamma_c = \frac{u(-R,t_c) - u(R,t_c)}{2R} \tag{3-2}$$

or $\qquad \gamma_c = \dfrac{V_{max}}{V_S}$ (3-3)

Where $u(y,t_c)$ = the horizontal free-field ground displacement with depth y and time t_c which produces the maximum shear-type deformation of the soil over the depth *2R* of the intended tunnel, V_{max}= the peak shear wave velocity, V_s = the ground shear wave velocity, E = Young's modulus of the soil, and ν = Poisson's ratio of the soil.

The maximum ovaling of the circular tunnel lining in **Figure 3-3** will occur with its major and minor axes at $\theta = 45^0$ respect to the spring line (Park et al. [2009]).

3.2.1.1. Analytical solutions due to static loading (Einstein and Schwartz, [1979])

On the basis of the relative stiffness method, Einstein and Schwartz [1979] proposed the solution for the structural forces due to static loading.

No-Slip Solution: The interface boundary condition for the no-slip solution does not have any relative shear displacement between the ground and the support. The no-slip solution is given by Einstein and Schwartz [1979]:

$$\frac{N}{\sigma_v R} = \frac{1}{2}(1+K_0)(1-a_0^*) + \frac{1}{2}(1-K_0)(1+2a_2^*)\cos 2\theta \tag{3-4}$$

$$\frac{M}{\sigma_v R^2} = \frac{1}{4}(1-K_0)(1-2a_2^*+2b_2^*)\cos 2\theta \tag{3-5}$$

where: θ= angular location (counter-clockwise with respect to the right spring line);

$\qquad R$ = tunnel radius;

$\qquad \sigma_v$= vertical stress;

$\qquad K_0$= lateral earth pressure coefficient;

$\qquad E$ = Young's modulus of the ground mass;

$\qquad \nu$= Poisson's ratio of the ground mass;

$\qquad a_0^*, a_2^*, b_2^*$ = dimensionless coefficients:

$$a_0^* = \frac{C^* F^* (1-\nu)}{C^* + F^* + C^* F^* (1-\nu)} \tag{3-6}$$

$$a_2^* = \beta b_2^* \tag{3-7}$$

$$b_2^* = \frac{C^*(1-\nu)}{2\left[C^*(1-\nu)+4\nu-6\beta-3\beta C^*(1-\nu)\right]} \tag{3-8}$$

$$\beta = \frac{\left(6+F^*\right)C^*(1-\nu)+2F^*\nu}{3F^*+3C^*+2C^*F^*(1-\nu)} \tag{3-9}$$

where C^*, F^* = compressibility and flexibility ratios, respectively:

$$C^* = \frac{ER\left(1-\nu_s^2\right)}{E_s A_s\left(1-\nu^2\right)} \tag{3-10}$$

$$F^* = \frac{ER^3\left(1-\nu_s^2\right)}{E_s J_s\left(1-\nu^2\right)} \tag{3-11}$$

where: E_s = Young's modulus of the support;

ν_s = Poisson's ratio of the support;

A_s = average cross-sectional area of the support per unit length of the tunnel (for a support of constant thickness t, $A_s = t$);

J_s = inertia moment of the support per unit length of the tunnel (for a support of constant thickness t, $J_s = t^3/12$).

Full-Slip Solution: For the full-slip solution, the interface boundary condition consists of no shear stress transmission between the ground and the support. The full slip solution is given by Einstein and Schwartz [1979]:

$$\frac{N}{\sigma_v R} = \frac{1}{2}\left\{\left(1+K_0\right)\left(1-a_0^*\right)+\left(1+K_0\right)\left(1-2a_2^*\right)\cos 2\theta\right\} \tag{3-12}$$

$$\frac{M}{\sigma_v R^2} = \frac{1}{2}\left\{\left(1-K_0\right)\left(1-2a_2^*\right)\cos 2\theta\right\} \tag{3-13}$$

Where a_0^*, a_2^* = dimensionless coefficients:

$$a_0^* = \frac{C^*F^*(1-\nu)}{C^*+F^*+C^*F^*(1-\nu)} \tag{3-14}$$

$$a_2^* = \frac{(F^*+6)(1-\nu)}{2F^*(1-\nu)+6(5-6\nu)} \tag{3-15}$$

3.2.1.2. Analytical solutions due to seismic loading (Wang [1993])

Wang may be the first person who proposed a closed-form solution for the structural forces in the tunnel lining under seismic loading conditions.

For the full-slip condition at the soil-lining interface, the normal forces (T_W) and bending moment (M_W) can be expressed as Wang [1993]:

$$T_W = \frac{1}{6} K_1 \frac{E}{(1+v)} R\gamma_{max} \cos\left[2\left(\theta+\frac{\pi}{4}\right)\right] \qquad (3\text{-}16)$$

$$M_W = \frac{1}{6} K_1 \frac{E}{(1+v)} R^2\gamma_{max} \cos\left[2\left(\theta+\frac{\pi}{4}\right)\right] \qquad (3\text{-}17)$$

where

$$K_1 = \frac{12(1-v)}{2F+5-6v} \qquad (3\text{-}18)$$

For the no slip condition at the soil-lining interface, only the normal forces (T_W) can be expressed by Wang [1993]:

$$T_W = K_2 \frac{E}{2(1+v)} R\gamma_{max} \cos 2\left(\theta+\frac{\pi}{4}\right) \qquad (3\text{-}19)$$

where

$$K_2 = 1 + \frac{F\left[(1-2v)-(1-2v)C\right]-\frac{1}{2}(1-2v)^2+2}{F\left[(3-2v)+(1-2v)C\right]+C\left[\frac{5}{2}-8v+6v^2\right]+6-8v} \qquad (3\text{-}20)$$

$$C = \frac{E(1-v_s^2)R}{E_S t(1+v)(1-2v)} \qquad (3\text{-}21)$$

$$F = \frac{E(1-v_s^2)R^3}{6E_S J_S(1+v)} \qquad (3\text{-}22)$$

In equations from (3-16) to (3-22):

K_1 = full-slip lining response coefficient;

K_2 = no-slip lining response coefficient;

F = flexibility ratio of tunnel lining;

C = compressibility ratio of tunnel lining;

E_S = Young's modulus of tunnel lining;

v_S = Poisson's ratio of tunnel lining;

R = tunnel radius;

t = thickness of tunnel lining

J_S = inertia moment of tunnel lining per unit length of the tunnel (per unit width);

E = Young's modulus of ground mass;

v = Poisson's ratio of ground mass;

γ_{max} = maximum free-field shear strain;

θ = angle measured counter-clockwise from springline on the right.

Note that no solution is developed for calculating bending moments under no slip condition by Wang [1993]. It is recommended that the solutions for full slip condition be used for no slip condition. The more conservative estimations of the full slip condition are

---

Chapter 3: Behaviour of tunnel linings under dynamic loads 55

considered to offset the potential underestimation due to quasi-static representation of the dynamic problem (Wang [1993], Hashash et al. [2005]).

Recently, Kouretzis et al. [2013] proposed an expression of the maximum bending moment under no slip condition to improve the method proposed by Wang [1993]:

$$M_K = \pm\left(2 - K_3 - 2K_4\right)\tau_{max}\frac{R^2}{2} \tag{3-23}$$

where τ_{max} is the maximum free field seismic shear stress:

$$\tau_{max} = \pm V_{max}\sqrt{\rho_{max}G_{max}} \tag{3-24}$$

With ρ_{max} is density of the surround ground, G_{max} is the maximum ground shear modulus, and V_{max} is the peak seismic velocity due to shear wave propagation.

$$K_3 = 1 + \frac{(1-2v)(1-C)F - 0.5(1-2v)C + 2}{[(3-2v)+(1-2v)C]F + [0.5(5-6v)](1-2v)C + (6-8v)} \tag{3-25}$$

$$K_4 = \frac{[1+(1-2v)C]F - [0.5(1-2v)C] - 2}{[(3-2v)+(1-2v)C]F + [0.5(5-6v)](1-2v)C + (6-8v)} \tag{3-26}$$

3.2.2. Physical tests

In order to overcome the drawbacks of analytical methods, physical model tests and numerical analysis have been used to obtain a better understanding of the physical problem and in particular of the soil-structure interaction phenomenon.

Physical model tests have been carried out by many researchers to investigate the performance of underground structures and to check current design/analysis methods. Most of them have focused on data for the validation of the design models (e.g., Bilota et al. [2009], Lanzano et al. [2010], Cilingir and Madabhushi [2010], Chen et al. [2012a], Conti et al. [2013]) and on tunnel lining behaviour (e.g., He and Koizumi [2000]). Due to their complexity and the high costs of the tests, the results obtained from physical tests are still quite limited.

Cilingir and Madabhushi [2010] introduced centrifuge tests, which show the variations between the behaviour of flexible and rigid tunnels under seismic loads. The flexibility of the lining is considered by the change of its thickness. The experimental results indicated that in the case of flexible tunnels, low-frequency components of the input motion are amplified more if the tunnel is deep, whereas in the case of rigid tunnels, the amplification ratio is larger for the shallow tunnel than for the deep tunnel. The centrifuge experimental results also show that the dynamic behaviour of a circular tunnel can be divided into three stages: transient stage, steady-state cycles, and residual (post-earthquake) stage (see **Figure 3-5**). During the transient stage, which lasts for the first few cycles, the tunnel lining reaches a dynamic

equilibrium configuration. Most of the residual forces that remain after the shaking stops are built up during this period. The transient stage is followed by the steady-state cycles, during which both the earth pressures around the tunnel and the forces in the tunnel lining oscillate around a mean residual value. After the shaking stops, residual stresses are left in the tunnel lining.
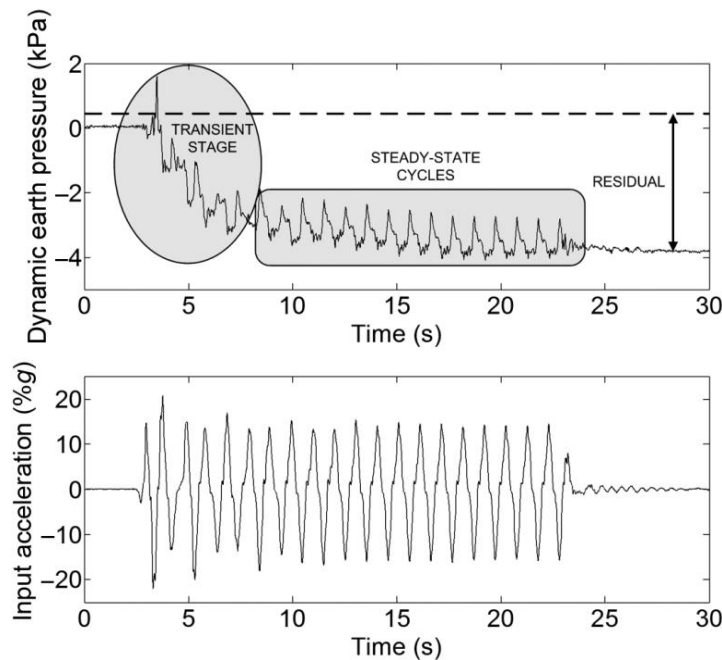
Figure 3-5. Typical earth pressure time history (Fig. 9 in Cilingir and Madabhushi [2010])

3.2.3. Numerical modelling

The recently common trend is to use 2D numerical analysis techniques (e.g. Pakbaz & Yareevand [2005], Hashash et al. [2005], Park et al. [2006], Bazaz & Besharat [2008], Sederat et al. [2009], Fahimifar & Vakilzadeh [2009], Chow et al. [2009], Torcato [2010], Shahrour et al. [2010]) or 3D numerical analyses (e.g. Kramer et al. [2007], Sliteen [2013]).

Using numerical analysis techniques, seismic loads are usually considered as quasi-static loads. Unfortunately, almost all quasi-static analyses presented in the literature incorporate the same assumptions as the closed-form solutions, and hence, have the same limited applicability. The main disadvantage of quasi-static models is that they do not take into consideration changes in the structure behaviour change in time. In addition, it has been suggested that an equivalent static solution would yield smaller structural lining forces than a true dynamic solution (Lee et al. [2007], Hung et al. [2009], Romero and Caufield [2012]). Full dynamic analysis, which is also called time history analysis, and which has been used in this study, is the most complex level of seismic analysis. Therefore it is also the most precise method. This type of analysis is generally numerical. However, this method is not economic, due to the long calculation time that is necessary. This is why full dynamic analysis applications are still limited.

3.2.3.1. *Quasi-static analysis*

Sederat et al. [2009] performed quasi-static numerical analyses to investigate the effect of the contact interface for a circular tunnel subjected to ovaling deformation supported by continuous lining. Their results underlined the influence of the interface properties on the structural forces developed in the tunnel lining. The results pointed out that the no slip condition provides the worst case of normal forces induced in the lining (**Figure 3-6**). Their results also indicated significant effects of the friction coefficient, the soil shear strain, and the lining thickness on the tunnel response (see **Figure 3-7** and **Figure 3-8**). They concluded that numerical methods should be used to determine the tunnel response.
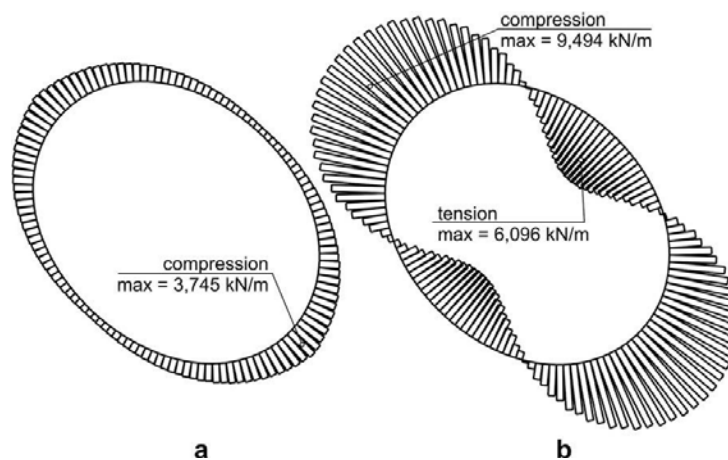
Figure 3-6. Lining total thrust at soil shear strain of 0.5%: (a) frictional contact ($f = 1.0$); (b) ''no-slip'' connection; displacement magnification factor = 20, lining flexibility ratio $F = 143$, lining thickness $t = 0.36$ m, lateral earth pressure factor $K_0 = 1.0$ (Fig. 2 in Sederat et al. [2009])
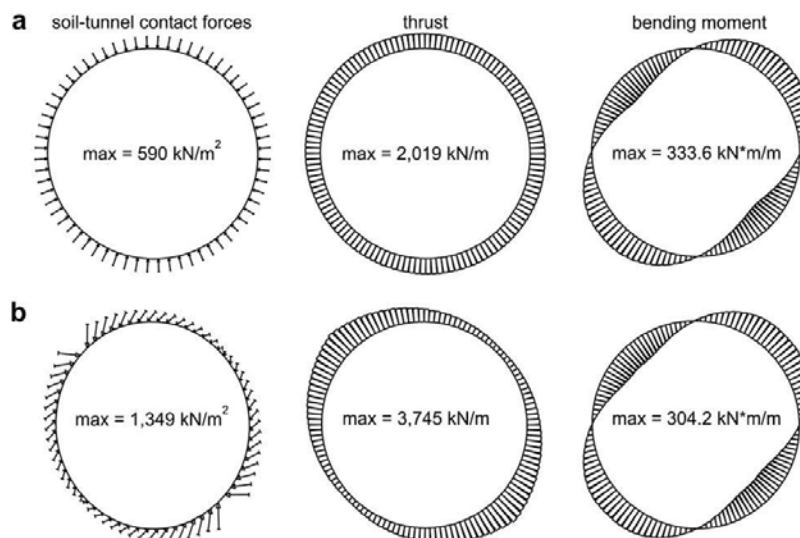
Figure 3-7. Contact tractions, lining total thrust and bending moment at soil shear strain of 0.5% under different friction coefficients: (a) f = 0 and (b) $f = 1.0$; lining flexibility ratio $F = 143$, lining thickness $t = 0.36$ m, lateral earth pressure factor $K_0 = 1.0$ (Fig. 5 in Sederat et al. [2009])
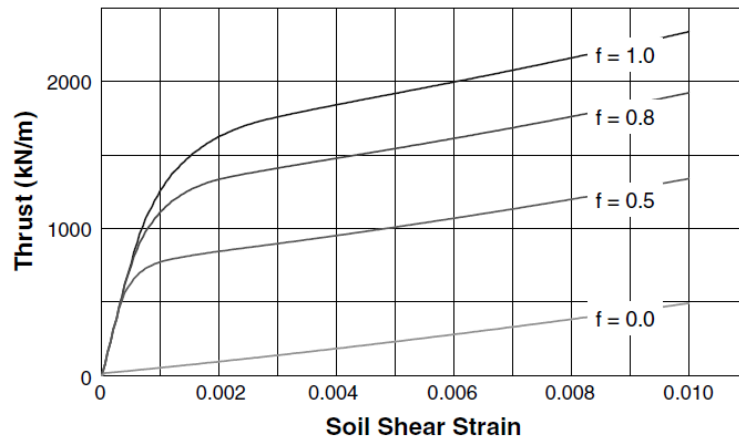
Figure 3-8. Seismic increment of lining thrust versus soil shear strain under different friction coefficients: $f = 0$, 0.5, 0.8, and 1.0; lining flexibility ratio $F = 143$, lining thickness $t = 0.36$ m, lateral earth pressure factor $K_0 = 1.0$ (Fig. 6 in Sederat et al. [2009])

Torcato et al. [2010] performed a numerical study to highlight the influence of the stratified medium surrounding the tunnel on the tunnel behaviour under seismic loadings. In addition, the effects of tunnel dimension and lining thickness were also considered. It should be noted that continuous lining was adopted in all above studies.

3.2.3.2. Full dynamic analysis

Pakbaz and Yareevand [2005] performed 2D numerical analyses using the CA2 software, in order to estimate the effect of an earthquake on circular tunnels, in an elasto-plastic medium. The tunnel was modelled as an elastic beam. The recordings of the Naghan Fars earthquake, which showed a maximum acceleration of 0.7g and an intensity of 7 in the Richter scale, were used. Two sets of parametric analyses were carried out in order to show the variation in the maximum stresses with the peak ground acceleration and with the flexibility ratio F (Wang [1993]). Additionally, the numerical results were compared with those obtained using analytical solution in order to show their similarities and differences (**Figure 3-9**).

Some general results were drawn from their study as follows (Pakbaz and Yareevand [2005]):

- The effect of an earthquake on the tunnel-ground interaction depends on various parameters, that is, intensity, peak acceleration, duration of the earthquake and relative rigidity between tunnel and ground.
- Increasing structural dimensions of lining in static design cannot always be a reliable method against earthquake loading, due to the fact that this causes an increase in the rigidity of lining (low lining flexibility factor *F*) and therefore, would increase the effect of earthquake loading.
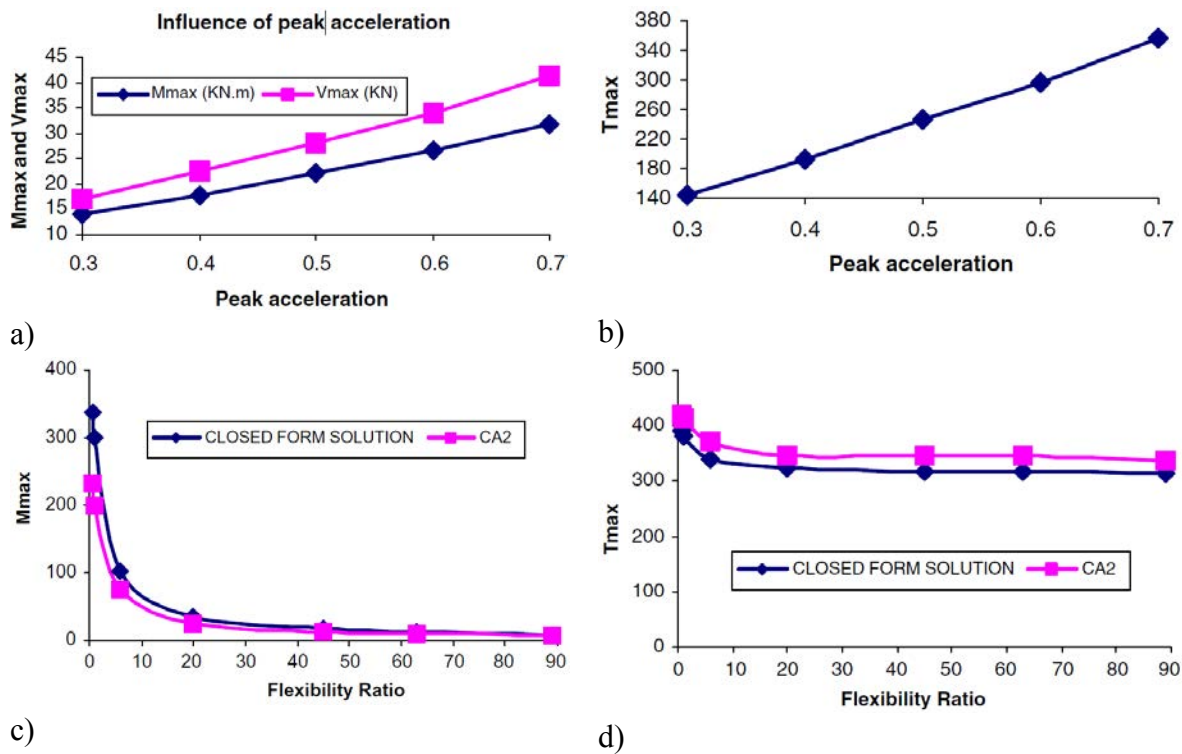
Figure 3-9. (a) Effect of peak acceleration on maximum bending moment M_{max}, and maximum shear forces V_{max}, CA2 (no-slip), (b) Effect of peak acceleration on maximum thrust force T_{max}, CA2 (no-slip), (c) Comparison of M_{max} of CA2 (no-slip) and closed form (full-slip) solution, (d) Comparison of T_{max} of CA2 (no-slip) and closed form (full-slip) solution (Pakbaz and Yareevand [2005])

Kontoe et al. [2008] presented a case study of the Bolu highway twin tunnels, which experienced extensive damage during the 1999 Duzce earthquake in Turkey. Static and full dynamic plane-strain finite element analyses were undertaken to investigate the seismic response of the tunnel and to compare the results with post-earthquake field observations. The results of the dynamic numerical analyses were also compared with those obtained from quasi-static elasto-plastic analyses. The quasi-static analyses, in which prescribed shear strains were assigned to the model boundaries, gave thrusts which were lower than the full dynamic analyses. Conversely, quasi-static analysis predicts a much higher bending moment (see **Figure 3-10** and **Figure 3-11**).
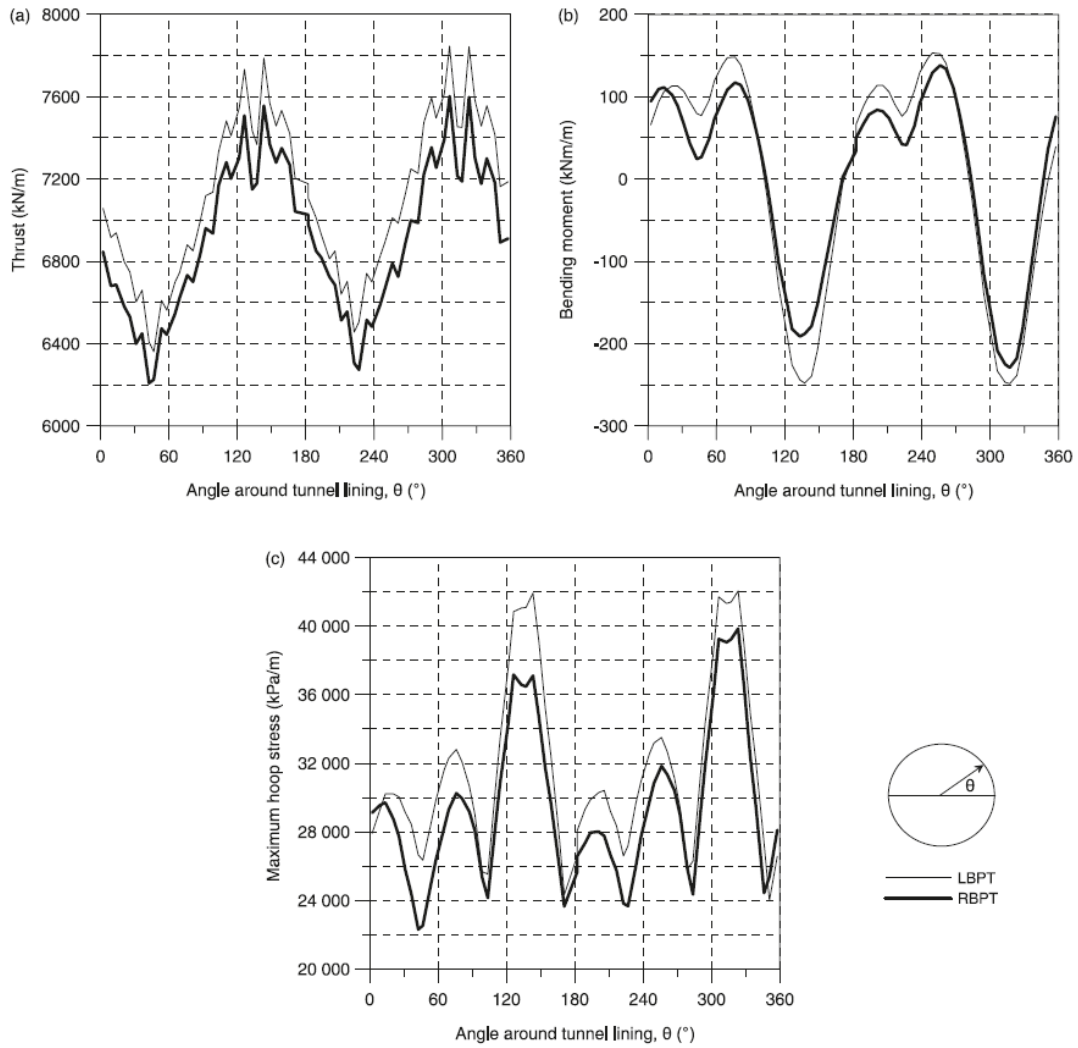
Figure 3-10. Accumulated thrust (a), bending moment (b) and maximum hoop stress (c) distribution around the lining of the tunnels at time t = 10 s (full dynamic analysis) (Fig. 15 in Kontoe et al. [2008])
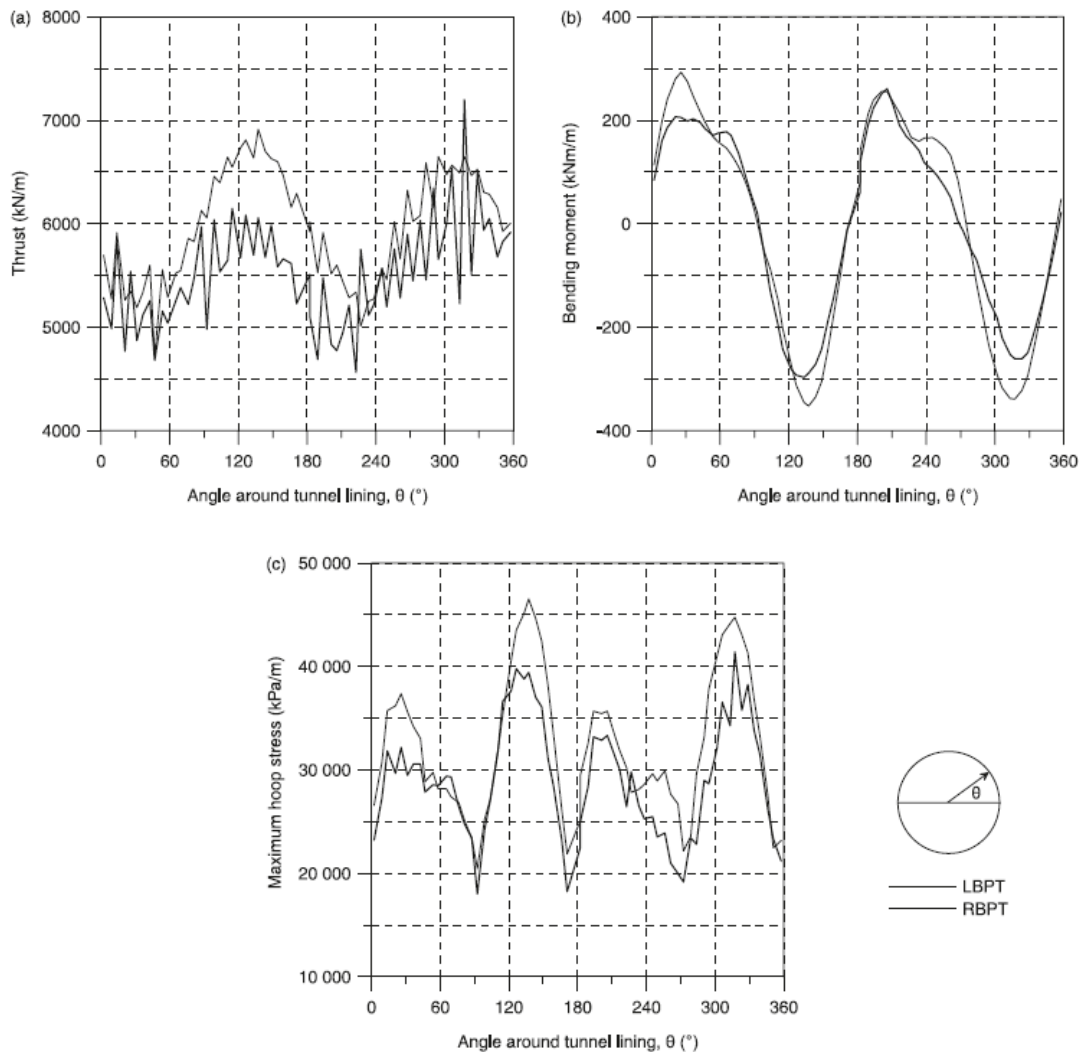
Figure 3-11. Accumulated thrust (a), bending moment (b) and maximum hoop stress (c) distribution around the lining of the tunnels at time t = 10 s (quasi-static analysis) (Fig. 20 in Kontoe et al. [2008])

Cao and Yan [2013] have conducted a study in which attempts have been made to systematically analyse tunnel responses for different degree of lining rigidity, to an earthquake and to find rules that govern the change in lining rigidity and the seismic response of tunnels. Conclusions have been drawn state that, under the impact of a seismic wave, an increase in rigidity is consistent with an increase in the maximum axial force, the maximum bending moment and the maximum combined stress of a lining structure. Therefore, it is unfeasible and uneconomic to diminish the response of tunnels to seismic motion by increasing lining rigidity. In all the above analyses, segmental linings and the effects of the joints were not considered either.

3.2.3.3. Influence of segmental joints

Segmental tunnel linings are now often used for seismic areas in many countries, such as the United States, Japan, Iran, Taiwan, Turkey, Venezuela, Spain, Portugal, Italy, Greece, India, and elsewhere (Dean et al. [2006]). As is well known, due to their higher flexibility, which is achieved through the use of joints between the segments, they can accommodate deformations with little or no damage. A segmental lining generally performs better than a continuous lining during an earthquake (Dean et al. [2006], Power et al. [2004], Kaneshiro and Sinha [2008]). The presence of segment joints in a tunnel lining can reduce the stresses and strains in the lining (Hashash et al. [2001]). An interesting estimation of the use and performance of segmental tunnel linings in seismic areas can be found in Dean et al. [2006].

Most of the presented studies that have been considered the presence of joints during the analysis of the response of a tunnel lining under seismic loads are related to immersed tunnels with rectangular cross-sections (e.g., Anastasopoulos et al. [2007], Lyngs [2008], Van Oorsouw [2010]). This kind of cross-section presents different behaviour, under seismic circumstance, from that of the circular tunnel studied in this study. It should be noted that in any of the above cited works, the effect of the joints on tunnel behaviour during a time seismic history that is different from that of a continuous lining was not mentioned in detail.

The design of circular segmental linings under seismic loads still therefore needs to be discussed. However, only a few prescriptions and guidelines specifically address the issue of seismic design (e.g., Power et al. [2004], AFPS/AFTES [2001]). Unfortunately, the effect of joints on lining behaviour has still not been quantitatively estimated.

Obviously, one of the key issues regarding the simulation of the response of a segmental tunnel lining is the necessity of taking into consideration the influence of the joints. Chen and Gui [2011] used an equivalent continuous lining with reduced stiffness (Muir Wood [1975]) to consider the presence of joints in a tunnel lining. He and Koizumi [2000] performed a series of shaking table model tests, seismic 2D FEM analysis and static analysis based on the seismic deformation method (Hashash et al. [2001], Nishida and Matsui [2004], Kramer et al. [2007]) to study the seismic behaviour and the seismic design method in the transverse direction of shield tunnels. In their static FEM analysis, the segment joints were simulated using short beam elements lowered in tension-compression rigidity and bending rigidity. As for the beam spring model, the segment joints were simulated using a rotational spring constant. Unfortunately, the influence of joint distribution and joint stiffness on tunnel behaviour under seismic loads was not introduced. In Chow et al. [2009], the segmental tunnel lining design was carried out using 2D FEM model. The tunnel linings were modelled with hinges to simulate the joints. Their results indicated that a quasi-static analysis can be carried out effectively to obtain the structural forces induced in the tunnel lining under the seismic or earthquake loading.

Naggar et al. [2008] developed a simplified analytical solution which allows the joints in the tunnel lining to be considered. The segmental joints were simulated through rotational stiffness. However, the method cannot be applied to cases in which the joint distribution is asymmetrical to the vertical axis of the tunnel. As can be seen from the results of their jointed lining analysis, the presence of joints permit the developed moments in a tunnel lining to be

reduced by up to 50% compared to an unjointed lining (see **Figure 3-12**). However, the effect of the joints on the developed thrusts was not so significant (10% or less) (see **Figure 3-13**). They concluded that the effect of joints on the internal forces needs to be considered to achieve an economic design.

Naggar and Hinchberger [2012] used a non linear FEM model and a linear elastic solution for jointed tunnel linings to examine the effects of concrete degradation on structural forces in tunnel linings under static and seismic loads. In their analyses, segment joints were simulated using thin zones of linear elastic elements with an equivalent elastic property determined on the basis of the rotational stiffness of the joints.
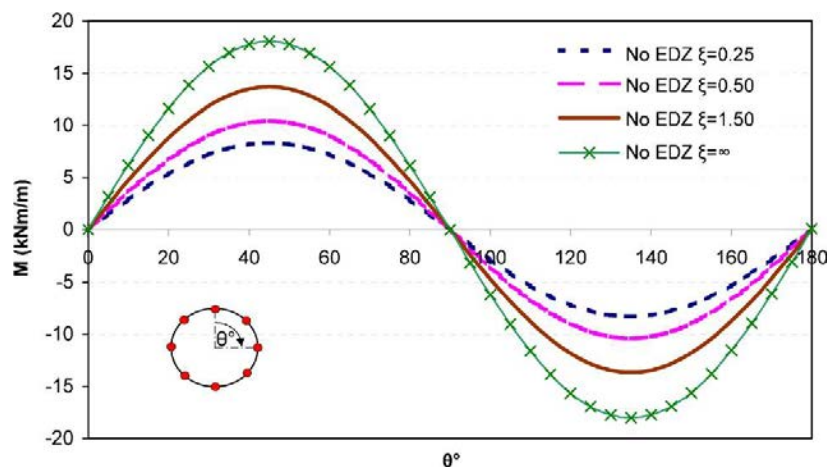
Figure 3-12. Moment distribution in the circumferential direction around the tunnel (seismically induced loads only) (Fig. 10 in Naggar et al. [2008])
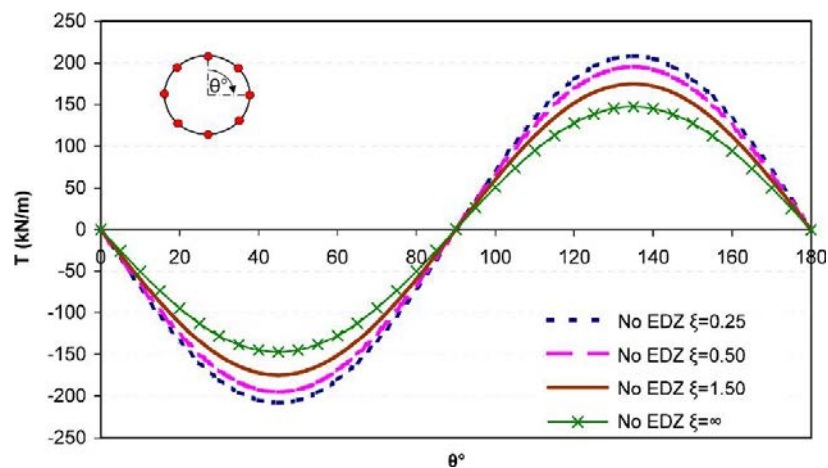
Figure 3-13. Thrust distribution in the circumferential direction around the tunnel (seismically induced loads only) (Fig. 11 in Naggar et al. [2008])

3.2.3.4. Influence of ground type

It is well known that soil exhibits non linear and irreversible behaviour, even at low strains. Under severe earthquake loading, the seismic response of a tunnel may be affected significantly by its non linear behaviour (Shahrour et al. [2010], Sliteen [2013]).

Shahrour et al. [2010] conducted an elasto-plastic finite element analysis using the advanced cyclic elasto-plastic model Modsol (Khoshnoudian and Sharour [2002]), which is based on the bounding surface concept. This constitutive model reproduces the contracting behaviour of soft soils under cyclic loading, and generally leads to good results in terms of settlements. The results of numerical simulations have shown that seismic-induced plastic deformations lead to a significant reduction in the seismic amplification, and, consequently, to an important decrease in the seismic-induced bending moment in a tunnel (**Figure 3-14**).
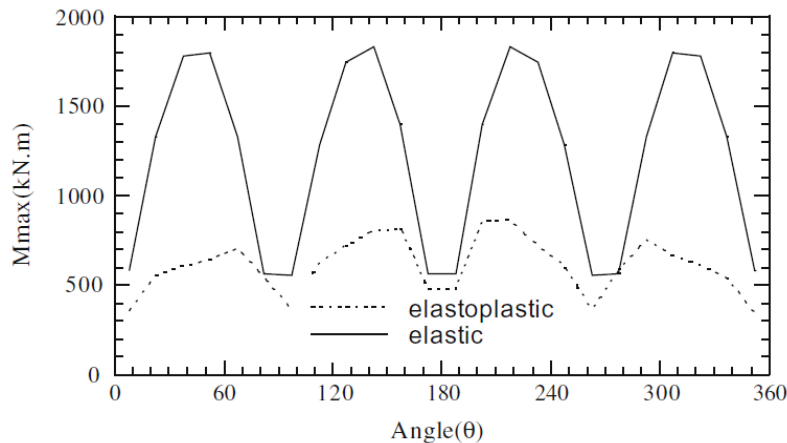
Figure 3-14. Influence of plasticity on the seismic-induced bending moment (Fig. 7 in Shahrour et al. [2010])

The 3D numerical results obtained by Sliteen [2010] and Sliteen et al. [2013] instead showed that an elastic analysis is not sufficient to determine the seismic induced response of a soil-tunnel system. In their study, the maximum bending obtained with non linear analysis using Mohr-Coulomb criteria was 24% higher than the one obtained with an elastic analysis (**Figure 3-15**).
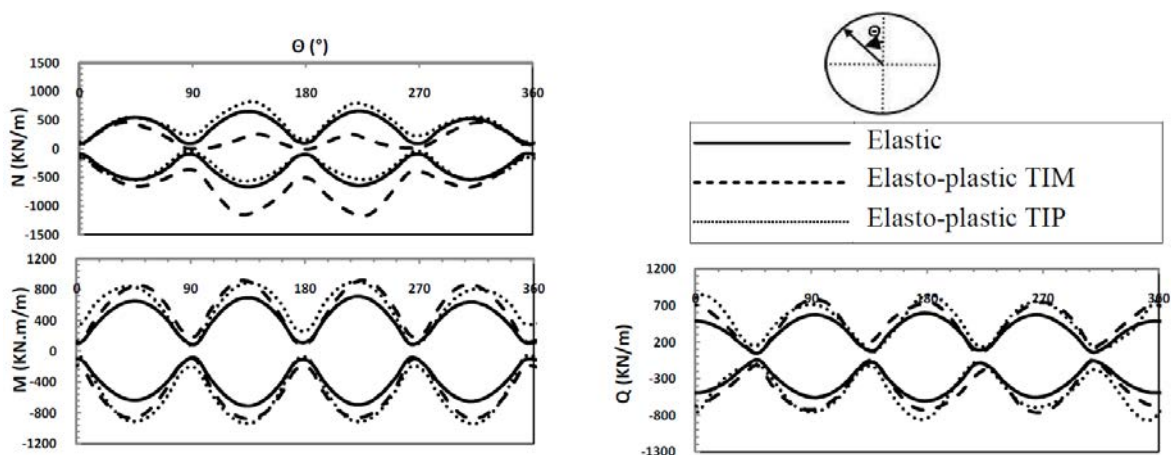
Figure 3-15. Comparison between elastic and Mohr-Coulomb models for tunnel response under dynamic loads, using Flac^{3D} (Fig. 6 in Sliteen et al. [2013])

The work of Amorosi and Boldini [2009] focused on the role of plasticity in the dynamic response of a soil-tunnel system. The responses of a tunnel lining in terms of bending

moments and normal forces under seismic excitation and in undrained conditions were pointed out. Accordingly, adding plasticity to the FEM analysis significantly modifies the stress distribution in the lining, both qualitatively and quantitatively. All the plasticity-based analyses show a noticeable accumulation of permanent loads for the time corresponding to the peak value of the accelerogram at the tunnel depth. The authors concluded that, concerning the role of plasticity in the dynamic response of the soil-tunnel system, the irreversible soil behaviour significantly modifies the tunnel loads both during the earthquake and, more importantly, after it (Amorosi and Boldini [2009]).

3.3. Conclusions

Generally, the behaviour of tunnels under seismic loads can be studied using a variety of approaches: empirical and analytical methods, physical model tests and numerical modelling. They are performed through full dynamic analysis or quasi-static analysis.

Due to their simplicity, the closed-form solutions present some drawbacks, that is the fact that: the homogeneous soil mass and the tunnel lining are assumed to be linear elastic and mass-less materials; tunnel is supposed to be circular with uniform thickness and without joints; The effect of the construction sequence is not considered; etc.

In order to overcome the drawbacks of analytical methods, physical model tests and numerical analysis have been used to obtain a better understanding of the physical problem and in particular of the soil-structure interaction phenomenon. However, due to their complexity and the high costs of the tests, the results obtained from physical tests are still quite limited.

The recently common trend is to use numerical analysis techniques. Unfortunately, the effect of segmental joints, that is joint distribution, joint stiffness, were not thoroughly studied in both quasi-static and full dynamic analyses. Some full dynamic analyses have pointed out that the influence of a soil constitutive model on tunnel behaviour under seismic loads is an important factor that should be considered to obtain a reliable design.

<div style="border:3px double navy; text-align:center;">

Second part

</div>

<div style="border:3px double navy; text-align:center;">

Static Analyses of Segmental Tunnel Linings

</div>

Introduction

This second part aims to study the segmental tunnel lining behaviour under static loads. The works have been conducted using numerical analyses, including both 2D and 3D models, and the Hyperstatic Reaction Method (HRM).

A 2D numerical analysis of the segmental tunnel lining behaviour is dealt with in **Chapter 4**. The presented models allow one to take the complete interaction between the tunnel lining and the surrounding medium into account through normal and tangential connections. A bilinear model, in which the rotational stiffness characteristics are assumed, allows the joint behaviour to be modelled in a more realistic way. The influence of certain characteristics including the rotational stiffness, the axial stiffness and the radial stiffness of longitudinal joints on the tunnel behaviour, with respect to the effect of the packing material, is considered in detail through parametric analyses. Important conclusions about the effect of the joint distribution, the role of each joint stiffness parameters and ground deformability on the overall behaviour of a segmental tunnel lining has been made.

Tunnelling process is in fact a 3D problem. Modelling this process in a 2D plane strain analysis requires a specific approach that allows a 3D tunnelling effect to be taken into consideration. A 2D numerical investigation has been conducted in order to highlight the influence of two equivalent approaches, that is, the convergence-confinement method (CCM) and the volume loss method (VLM), on the behaviour of a tunnel built in an urban area, in terms of not only the surface settlement but also the structural lining forces, taking into account the effect of segment joints. A technique that can be used to simulate the tunnel wall displacement process, based on the principles of the VLM, has been developed using the FLAC^{3D} finite difference program. A comparison with 3D numerical results has been introduced to estimate the precision of these 2D equivalent approaches. Significant conclusions about the method which give the results that are in better agreement with those of 3D numerical model are finally presented.

On the basis of the above 2D model applied for a single tunnel using the convergence-confinement method, another 2D model has been developed for twin horizontal tunnels which allow the impacts between two tunnels during excavation to be highlighted. In this model, some processes occurring during a mechanized excavation (e.g., stress relaxation process of the tunnel boundary before the installation of tunnel lining and grout injection behind the lining) have been simulated. Parametric analyses considering the change in the joint distribution and tunnel distance have been performed. The results point out the critical influence distance between two tunnels is about two times tunnel diameter.

A 3D numerical model which allows the tunnel lining behaviour and the displacement of the ground surrounding the tunnel to be evaluated has been developed in **Chapter 5**. Most of

70

the main processes that occur during mechanized excavation are simulated in this model. The influence of the joint pattern of the lining, pertaining to both segment joints and ring joints as well as their connection condition, have in particular been taken into consideration. Numerical studies performed by using this model help to achieve significant conclusions about the impacts of the starting condition at the boundary of the model, the constitutive model of the ground, the behaviour of tunnel during the advancement of the tunnel face, and the influence of the joint pattern in particular.

On the basis of the above full 3D model of a single tunnel, the construction of twin horizontal tunnels excavated in close proximity or stacked over each other has also been simulated and studied. Different cases of tunnelling excavation procedures are analysed. The interaction between the new tunnel and the existing tunnel or between two tunnels excavated simultaneously has been highlighted in terms of both lining structural forces and displacements of the ground surrounding the tunnel. Most of the phenomena have been compared with experimental and/or laboratory results and previous numerical results found in the literature. Especially, the effects of elements during tunnelling such as face pressure, grouting pressure or jacking forces, etc. on the tunnel behaviour have been explained in detail. The results indicate the role of using an appropriate tunnelling excavation procedure on the overall stability of the tunnels and provide significant recommendations for tunnelling design.

A new numerical approach applied to the HRM is developed and presented in **Chapter 6**. In the new approach, the influence of segmental joints has been considered directly using a fixity ratio that is determined on the basis of the rotational stiffness. The parameters necessary for the calculation are presented. A specific implementation has been developed using a FEM framework, which is able to consider the 3D effect of segment joints in successive rings on the tunnel lining behaviour. The present HRM allows one to take an arbitrary distribution of segment joints along the tunnel boundary into consideration. In addition, the rotational stiffness of segment joints has been simulated using nonlinear behaviour, as it is closer to the true behaviour of a joint than linear or bilinear behaviour. Comparison between results of the new HRM and simplified FLAC^{3D} model has been presented which allow the new HRM to be validated.

Chapter 4

Two-dimensional Numerical Analyses

4.1. Numerical Investigation of Segmental Tunnel Lining Behaviour

4.1.1. Introduction

Rapid progress in the development of user friendly computer codes and the limitations of analytical methods have led to an increase in the use of numerical methods for the design of tunnel linings. Tunnel advancement induces a change in the boundary conditions in localized zones that requires a 3D approach in order to accurately simulate the excavation process. However, a full 3D numerical analysis often requires excessive computational resources (both storage and time). Therefore, a tunnel excavation is often modelled in 2D.

This section presents a 2D numerical analysis of the segmental tunnel lining behaviour in which the effects of the joint stiffness, Young's modulus of the ground and the lateral earth pressure factor are taken into consideration using a finite difference program. A bilinear model, in which the rotational stiffness characteristics are assumed, allows the joint behaviour to be modelled in a more realistic way. The influence of certain characteristics including the rotational stiffness, the axial stiffness and the radial stiffness of longitudinal joints on the tunnel behaviour, with respect to the effect of the packing material, is considered in detail. The presented model is here used for the parametric analyses of a shallow tunnel in conditions in which the ground loads increase in depth due to the effect of the gravity field. In addition, this model allows the complete interaction between the tunnel lining and the surrounding medium to be taken into account through the normal and tangential connections. Parameters from the Bologna-Florence high speed railway line tunnel project in Bologna have been adopted in this numerical modelling (Croce [2011]). This case is named the reference case. The main content of this section has been published in Do et al. [2013a].

4.1.2. The Bologna-Florence railway line project

This project is a part of the Italian high speed railway network. The project involves the excavation of two tunnels in Bologna with a space distance of 15 m between the two tunnel centers. The tunnel has an external excavation diameter of 9.4 m and an internal diameter of 8.3 m for a useful section of 46 m^2. The tunnels have been excavated to a depth of between 15 m and 25 m below the ground surface (see **Figure 4-1**).

The excavation has been conducted with mechanized machines to meet design and construction requirements. Two Earth Pressure Balance Shields (EPBs) were used for the construction of the two parallel tunnels in Bologna (**Figure 4-2**). The second tunnel was driven after the first tunnel over a period of 6 months.

The tunnels were excavated through two main formations: alluvial deposits of the late Pleistocene - Pliocene era, which is mostly alluvial deposits from the Savena River with deposits of clay, and sandy soil (clayey sands and Pliocene clays). Some typical parameters of

the ring 582 section in the first tunnel, which have been adopted in this study as a reference case, are summarized in **Table** 4-1 (Croce [2011]).
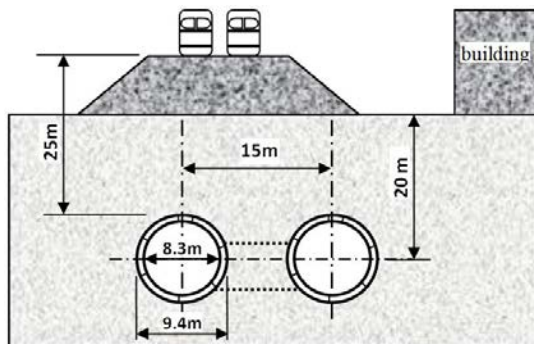
Figure 4-1. Typical cross-section of the two tunnels excavated below the old railway

Figure 4-2. EPBs used at the Bologna – Florence project

The tunnel lining is composed of precast segments made of reinforced concrete. Each 1.5 m long circular ring consists of 6 conical regularly shaped blocks and a small sized key block. Each precast concrete ring has an extrados diameter of 9.1 m and is 0.4 m thick. The mechanical characteristics of the tunnel lining are shown in **Table** 4-1.

Table 4-1. Details of the reference case

Parameter	Symbol	Value	Unit
Properties of clayey sand			
Unit weight	γ_S	17	kN/m^3
Young's modulus	E_S	150	MPa
Poisson's ratio	v_S	0.3	-
Internal friction angle	ϕ	37	degree
Lateral earth pressure factor	K_0	0.5	-
Overburden	H	20	m
Properties of tunnel lining			
Young's modulus	E_l	35,000	MPa
Poisson's ratio	v_l	0.15	-
Lining thickness	t_l	0.4	m
External diameter	D	9.1	M
Properties of the grouting layer			
Young's modulus	E_g	10	MPa
Grouting layer thickness	t_g	0.15	m
Poisson's ratio	v_g	0.22	-
Unit weight	γ_g	15	kN/m^3

4.1.3. Numerical modelling

Figure 4-3 shows a 2D numerical model which uses the plane-strain conditions. It has been used to quantify the behaviour of a segmental tunnel lining. The whole tunnel is simulated, due to the arbitrary distribution of the joints along the tunnel wall boundary.

It is assumed that the behaviour of the tunnel structure is linear-elastic and that of the ground is governed by an elastic perfectly-plastic constitutive relation, which is based on the Mohr-Coulomb failure criterion. The properties are given in **Table** 4-1.

In this study, numerical simulations have been performed by means of the FLAC^{3D} finite difference program (Itasca [2009]), which provides flexible features for the analyses of joint parameters. The volume under study is discretized into hexahedral zones. The tunnel segments are modelled using the embedded liner elements. These elements are used to model thin liners (based on the classical Kirchhoff plate theory) for which both normal-directed compressive/tensile interaction and shear-directed frictional interaction with the host medium occurs. The embedded liner element is a three-noded, flat with five degrees of freedom per node: three translational components and two rotational components. It combines a six degrees-of-freedom CST plane element to model membrane action in the shell with a nine degrees-of-freedom DKT plate element to model bending action in the shell (Itasca [2009]). This kind of liner element provides two links on each node. The first link permits a connection to be created between the lining and the ground mass, and the second link allows the segments to be connected together.
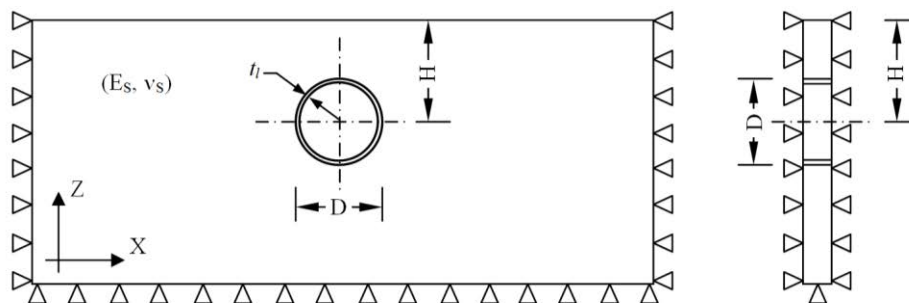
Figure 4-3. The plane strain model under consideration

The segment joint is simulated using double node connections (**Figure** 4-4). These include six degrees of freedom, which are represented by six springs: three translational components in the x, y and z directions, and three rotational components around the x, y and z directions. It is possible to assign the stiffness to each spring. One of the following four attachment conditions is used: (1) free; (2) linear spring characterized by a stiffness factor; (3) bi-linear spring characterized by a stiffness factor and yield strength; and (4) rigid.

In this study, the stiffness characteristics of the joint connection are represented by a set composed of a rotational spring (K_{RO}), an axial spring (K_A) and a radial spring (K_R), as depicted in **Figure** 4-5. The attachment conditions of the translational component in the y direction (parallel to the longitudinal axis of the tunnel) and two rotational components

around the x and z directions are assumed to be rigid for all the investigated cases. Some typical tunnel lining parameters are summarized in **Table** 4-1.
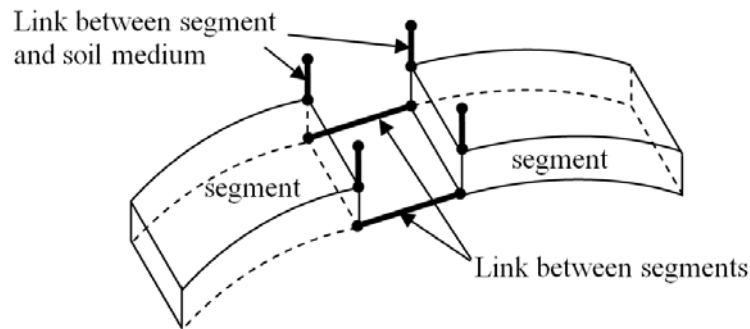
Figure 4-4. Joint connection scheme.
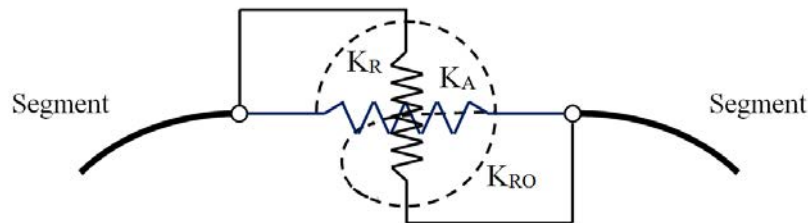
Figure 4-5. K_A, K_{RA}, K_{RO} stiffness in the axial, radial and rotational directions of a joint.

Embedded liner elements are attached to the zone faces along the tunnel boundary. The liner-zone interface stiffness (normal stiffness k_n and tangential stiffness k_s) is chosen using a rule-of-thumb in which k_n and k_s are set to one hundred times the equivalent stiffness of the stiffest neighbouring zone (Itasca [2009]). The apparent stiffness (expressed in stress-per-distance units) of a zone in the direction normal to the surface is:

$$\max \left[\frac{\left(K + \frac{4}{3} G \right)}{\Delta z_{min}} \right] \tag{4-1}$$

where: K and G are the bulk and shear modulus, respectively;

z_{min} is the smallest dimension in the normal direction of zones which contact with the liner elements.

The FLAC^{3D} model grid contains a single layer of zones in the y-direction, and the dimension of elements increases as one moves away from the tunnel (see **Figure** 4-6). The numerical model (**Figure** 4-6) is 240 m wide in the x-direction, 60 m high in the z-direction and consists of approximately 13,800 zones and 27,765 grid points.

The first calculation step of the numerical excavation process consists in setting up the model, and assigning the plane strain boundary conditions and the initial stress state taking into consideration the influence of vertical stress with depth gradient under the effect of the gravity field. Then, the tunnel is excavated, the segments have set in a ring on the tunnel

boundary and the joint link condition is assigned in the second step. Relaxation of the ground between the excavation phase and the lining setup has not been considered. This process has been adopted in order to consider the worst case for the lining stress state.

a)   b)
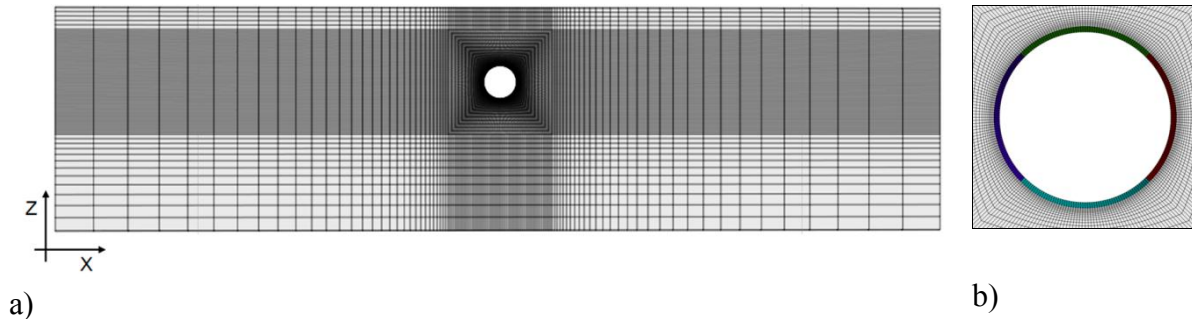
Figure 4-6. Two-dimensional numerical model (a) tunnel with 4 concrete segments (b).

4.1.4. Parametric study

4.1.4.1 Impact of the joint parameters

4.1.4.1.1 Influence of the joint distribution

The influence of the joint distribution on the behaviour of a segmental lining can be established considering the change in joint number and joint orientation in a lining ring. The location of the joints in a ring is represented by the reference joint that is closest to the tunnel crown, considering the angle "ω" between the reference joint and the crown and measuring it in the clockwise direction starting from the tunnel crown. A ω angle of zero means the reference joint has been positioned at the tunnel crown, while a ω angle of 90° means the reference joint has been located at the right spring line. The joint distribution is assumed to be uniform.

As for the relationship between the bending moment and the angular rotation at the joint, the nonlinear behaviour was back analysed on experimental data (Hordijk and Gijsbers [1996]). This means that the rotational stiffness can be considered to depend on the rotation of the longitudinal joints. However, it is difficult to analyse this nonlinear behaviour through rigorous and exact procedures. Hence, the analysis of the rotational behaviour of a joint in practical design is usually approximate and simplifications are adopted. Apart from the single-stiffness linear model, bilinear models have been proposed for the calculation of the structure to provide a better approximation (Burns et al. [2002]). In this study, a simplified bilinear relationship, which has been applied by Zhong et al. [2006], Van Oorsouw [2010] and Thienert and Pulsfort [2011] in the numerical analyses of tunnels, is used. Their works show that the moment-angular rotation relationship of a joint can be approximately fit by a bilinear model. However, without considering the reduction in rotational stiffness due to the non-linear behaviour of the longitudinal joints, the bilinear model may result in a higher

bending stiffness of the overall tunnel lining system and this can cause larger bending moments along the lining. This simplified assumption of joint stiffness can be acceptable from the design point of view.

For simplification purposes, a calculation is first performed using the input data of the reference case (**Table** 4-1) with a full hinge and a 30 cm thickness at the narrowest part of the joint, using a simplified procedure proposed by Thienert and Puslfort [2011]. The maximum limit bending moment M_{yield} is calculated from the average normal force of the tunnel lining for an angle of rotation (θ) of 0.01 radians ($\approx$ 1%), which is assumed as an approximation of the maximum permissible rotation. An identical calculated rotational stiffness of K_{RO} = 0.8 M_{yield}/θ is derived as a simplification for all of the joints in the lining ring (Thienert and Puslfort [2011]). Janssen's formulas, which are based on the investigation by Leonhardt and Reimann [1966], are used to determine the rotational stiffness of the longitudinal joints (Gruebl [2006], Groeneweg [2007]). Janssen's analytical results closely match the experimental results introduced by Hordijk and Gijsbers [1996] (see Luttikholt [2007]). The evaluation, which uses the input parameters presented in **Table** 4-1, is shown in **Figure 4-7**.

The reference case (**Table** 4-1) is adopted in this study, considering the determined joint rotational stiffness. However, the lateral earth pressure factors, K_0, of 0.5, 1, 1.5, and 2 are considered. The K_0 values of 0.5 and 1.0 were adopted to represent normally consolidated ground, while K_0 values of 1.5 and 2.0 were adopted for over-consolidated ground.

A comparative study has been performed for the tunnel lining with the joint number varying from 4 to 9. As an example, for a joint number of 4, four segmental concrete linings, which represent 90° each, were set to represent the whole lining.
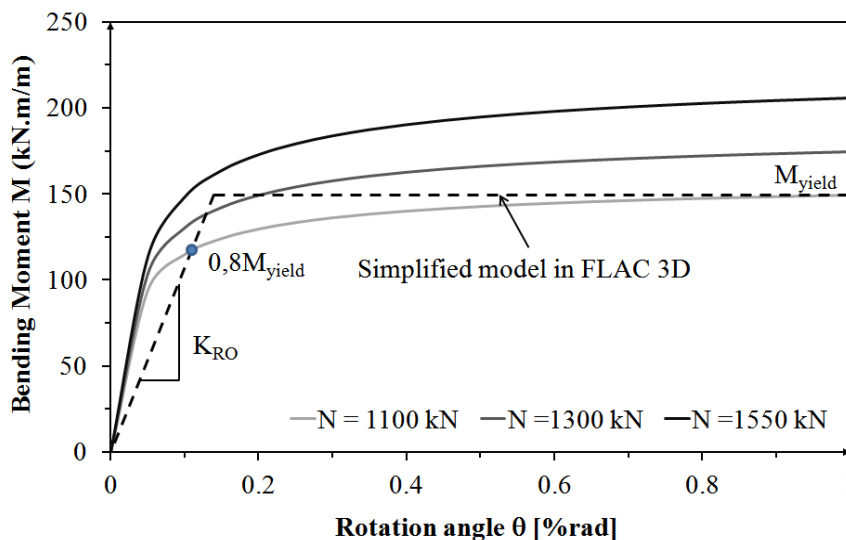
Figure 4-7. Bending moment - rotation relationship of the longitudinal joint.

M_{yield} (N = 1100 kN/m) = 150 kN.m/m   for θ = 1%

0.8*M_{yield} = 0.8 * 150 = 120 kN.m/m   for θ = 0.1212%

$\rightarrow K_{RO}$ = 120 / 0.001212 = 98,410 kN.m/rad/m

The results show the same change in tendency of the bending moment due to the variation in the joint distribution when the K_0 values are equal to 0.5, 1.5, and 2. Therefore, only the results of the maximum absolute bending moment, corresponding to different joint orientations for each joint number obtained in the case of a K_0 value of 0.5, are presented hereafter (**Figure** 4-8). The results show the great influence of joint distribution on the magnitude of the maximum absolute bending moment induced in the tunnel lining. **Figure** 4-8a shows that an increase in joint number will result in a reduction in the maximum absolute bending moment in the segmental lining and its magnitude is also affected by the joint location. Furthermore, it should be noted that the most favourable orientation of four joints (corresponding to the lowest value of the maximum absolute bending moment) induced a much lower maximum absolute bending moment than the other cases. This indicates that joint orientation has a significant influence on the maximum absolute bending moment that develops in a segmental lining. This can be attributed to the fact that the influence of a joint is less important when it is located near a point where the bending moment is equal to zero. The influence of a joint on the reduction of the bending moment will be greater when the joint is located near a point where the bending moments are maximum.

According to **Figure** 4-8a, the influence of the joint orientation is not similar to that of the joint number. In general, the difference in the maximum absolute bending moment resulting from the change in joint orientation reduces when the joint number increases. This means that the higher the number of joints, the lower the influence of the joint orientation. This phenomenon could be explained by the fact that the span of each segment becomes shorter for the tunnel ring with a greater segment number. Therefore, the loads acting on each segment become almost similar in magnitude, regardless of the joint orientation. These results are in good agreement with the ones obtained by Hefny and Chua [2006].

a)   b)
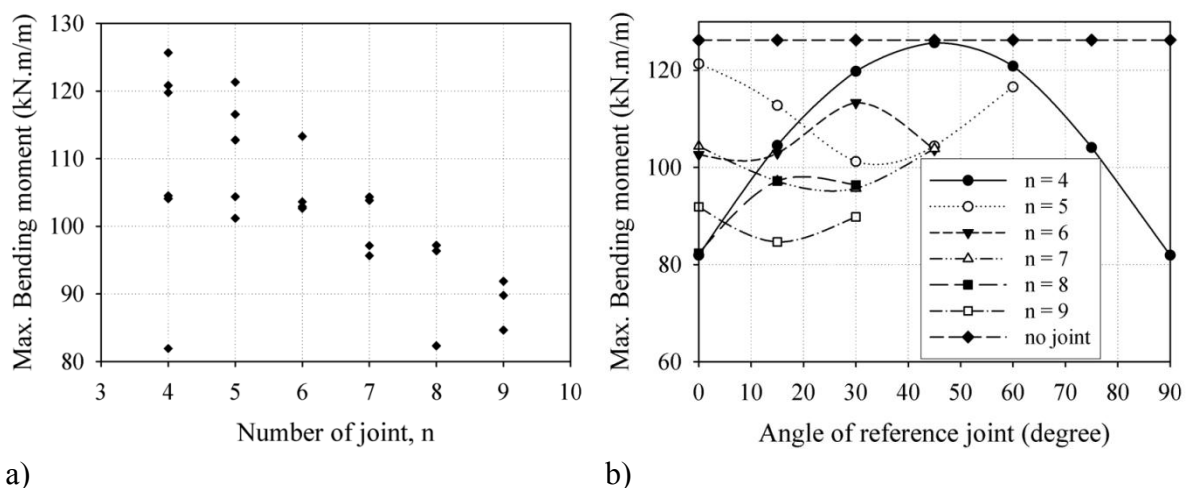
Figure 4-8. Variation of the maximum absolute bending moment with the joint number and joint orientation (K_0 values of 0.5).

Using the same calculated results presented in **Figure** 4-8a, **Figure** 4-8b shows the effect of the joint orientation on the bending moment in another way. It shows that the maximum absolute bending moment induced in the lining for all of the joint number cases, is affected to

a great extent by the location of the joints along the lining. It is very interesting to note that for cases in which the joint number is even (4-joints, 6-joints, 8-joints), the favourable orientation of the joints is referred to an angle of the reference joint (ω) of almost zero, i.e. when the reference joint is located close to the tunnel crown, and the critical orientation of the joints corresponding to the largest value of maximum absolute bending moment occur at a ω angle of 45^0, 30^0, and 22.5^0, respectively. On the other hand, when the joint number is odd (5-joints, 7-joints, 9-joints), the favourable orientation of the joints is referred to an angle of the reference joint ω of 32.5^0, 27.5^0, and 15^0, respectively, and the critical orientation of the joints is referred to an angle of the reference joint ω of zero. This behaviour is different from that obtained by Teachavorasinskun and Chub-Uppakarn [2010] for odd joint numbers. In their results, the behaviour of a segmental tunnel lining, in terms of bending moment, for odd joint numbers was similar to that obtained when the joint numbers were even. The difference is probably due to the fact that, in their study, both the vertical and lateral loads acting on the tunnel lining were assumed to be constant and symmetrical over the spring line and the vertical tunnel axis, respectively, and the increase in ground loads according to the depth due to the effect of the gravity field was not taken into consideration. This external load distribution is more suitable for deep tunnels. This assumption may not be valid for shallow tunnels such as the reference case in this study (H/D $\approx$ 2). Moreover, the tangential subgrade reaction springs were not considered in their study.

On the basis of the analysed results, **Figure** 4-9 illustrates the most favourable and critical orientations of joints corresponding to the different joint numbers in segmental tunnel linings in which the K_0 values are 0.5, 1.5, and 2.

Favourable	Critical	Favourable	Critical	Favourable	Critical
$\omega = 0^0$	$\omega = 45^0$	$\omega = 32,5^0$	$\omega = 0^0$	$\omega = 0^0$	$\omega = 30^0$
4 - joint lining		5 - joint lining		6 - joint lining	
$\omega = 27.5^0$	$\omega = 0^0$	$\omega = 0^0$	$\omega = 22.5^0$	$\omega = 15^0$	$\omega = 0^0$
7 - joint lining		8 - joint lining		9 - joint lining	
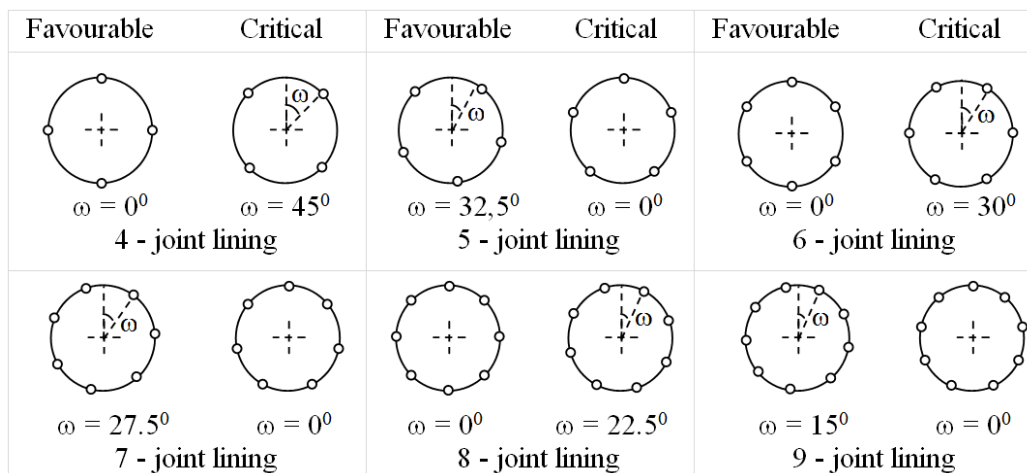
Figure 4-9. Illustration of favourable and critical cases of a segmental tunnel lining (K_0 values of 0.5, 1.5, and 2) with reference to the number and position of the joints.

However, for K_0=1, the bending moment trend caused by different joint numbers is similar (see **Figure 4-10**). This means that the favourable orientations of the joints is always referred to ω=0^0, i.e. when the reference joint is located at the tunnel crown. **Figure 4-11** illustrates the most favourable and critical orientations of the joints, corresponding to the different joint numbers, in a segmental tunnel lining in which the K_0 value is equal to unity.
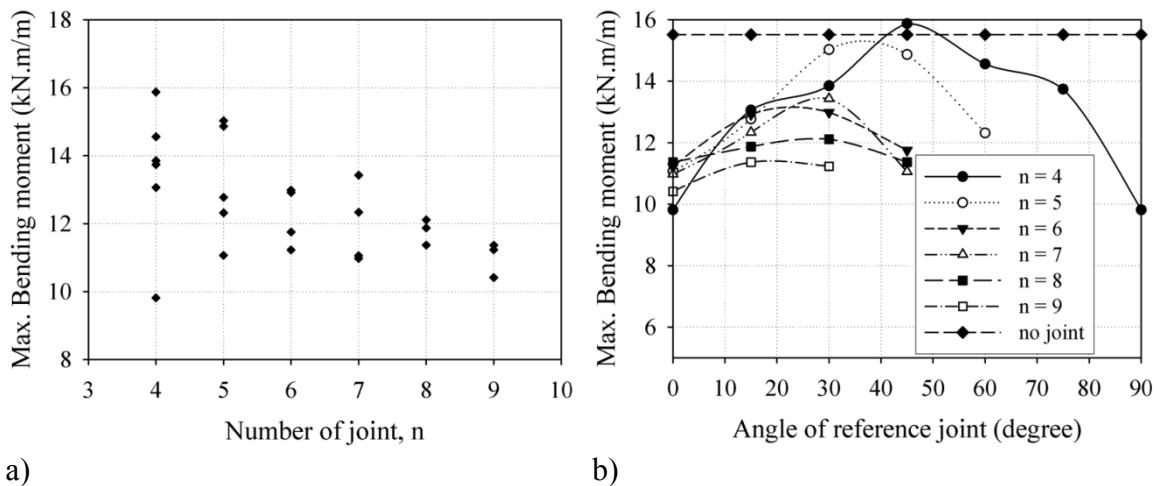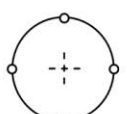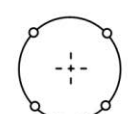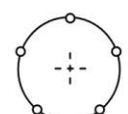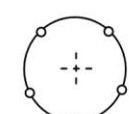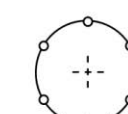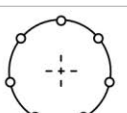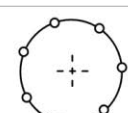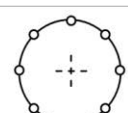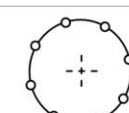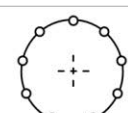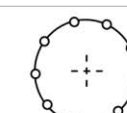
Figure 4-10. Variation of the maximum bending moment with the joint number and joint orientation (K_0 value of unity).

4.1.4.1.2 Influence of joint stiffness

Influence of rotational stiffness

In order to illustrate the relationship between the structural forces and lining displacements in function of the joint rotational stiffness, the dimensionless factor, called the rotational stiffness ratio, $\lambda = K_{RO}l/E_lI_l$, proposed by Lee et al. [2001], is adopted to represent the relative joint stiffness over the lining segment bending stiffness. The calculation length, l, of 1 m is usually taken to present a typical unit length of a lining segment.

Figure 4-11. Illustration of favourable and critical cases of a segmental tunnel lining (K_0=1) with reference to the number and position of the joints.

The reference case (**Table** 4-1), with a joint number equal to 6, has been adopted in this study. The joints are located at angles of $0°$, $60°$, $120°$, $180°$, $240°$ and $300°$ measured counter-clockwise with respect to the spring line on the right (critical orientation of the joints). For simplification purposes, the rotational stiffnesses assigned to all the joints in the lining ring are assumed to be similar. The bending moment ratio, R_M, and the normal force ratio, R_N, are defined as the ratio of the maximum absolute value of the bending moment and the maximum normal force, respectively, induced in a segmental lining to the corresponding value developed in a continuous lining. The diameter change ratio, R_{dia}, is defined as the ratio of the change in diameter induced in a segmental lining to that developed in a continuous lining (see **Figure 4-12**d for the definition of the R_{dia} value). The R_{dia} ratios determined in both the vertical axis and the spring line are considered. They allow the ovalization of the lining ring to be observed. It should be noted that since the lateral earth pressure factor K_0 is less than unity ($K_0 = 0.5$), a decrease can be observed in the diameter measured in the vertical axis. An increase in the diameter measured at the spring line can be noted (**Figure 4-12**d).

a)

b)

c)

d)
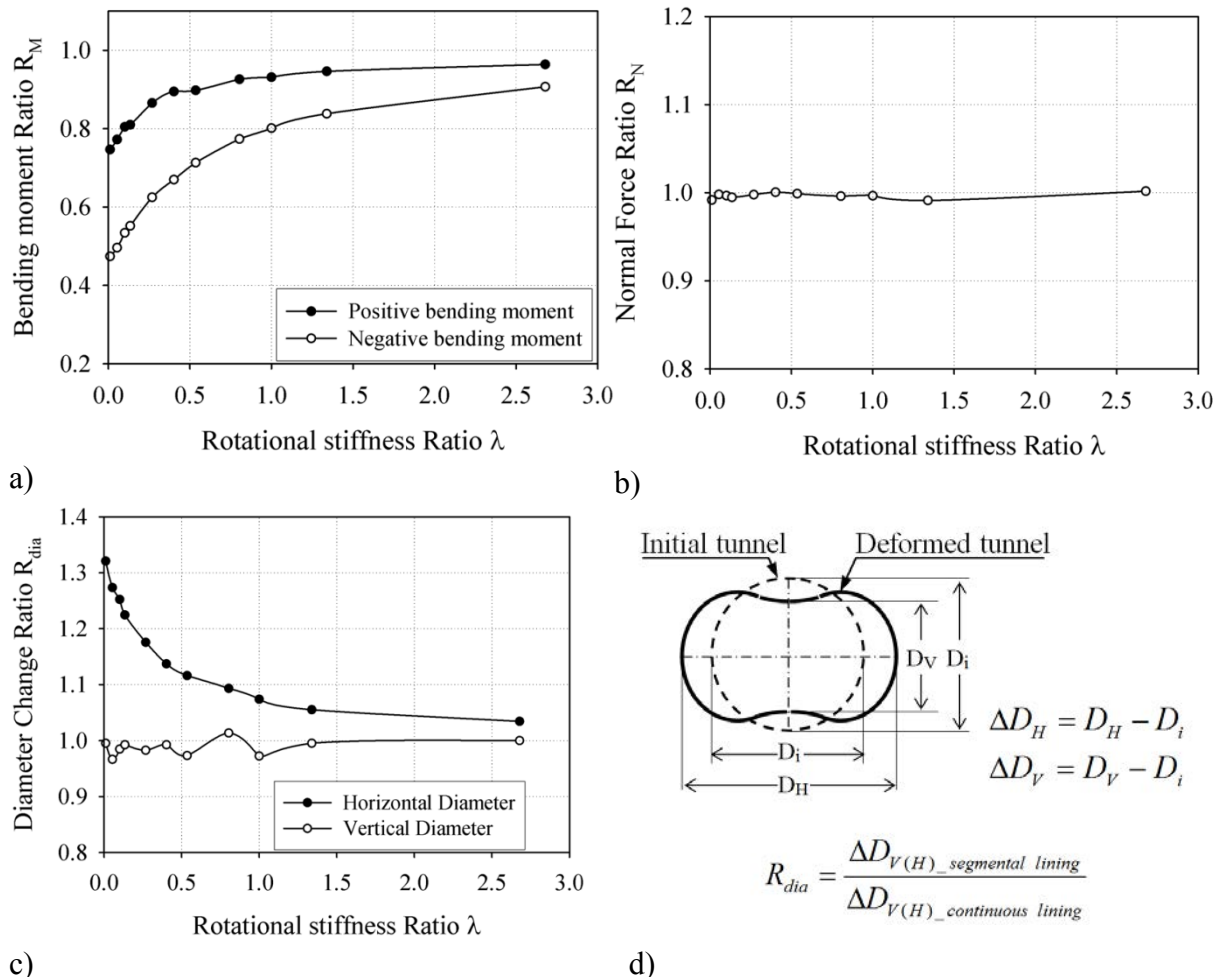
Figure 4-12. Diagrams of the bending moment (a), normal force (b) and diameter change ratios (c) under the influence of the rotational stiffness of the joints (joint number equal to 6, lateral earth pressure factor K_0 equal to 0.5).

Figure 4-12 shows the dependence of the bending moment, normal force and diameter change ratios in the tunnel lining on the rotational stiffness ratio, λ. For a given value of Young's ground modulus (E_S=150 MPa), the development of the bending moment is affected to a great extent by the rotational stiffness ratio. A higher rotational stiffness ratio results in a higher magnitude of both the positive and negative bending moment ratios (**Figure 4-12**a). These results are in good agreement with the numerical results obtained by Teachavorasinskun and Chub-Uppakarn [2010].

Unlike the bending moment, the normal force that develops in the lining is not-sensitive to the magnitude of the rotational stiffness (**Figure 4-12**b). It should be noted that the increase in the rotational stiffness of the joints results in an increase in the lining rigidity and in a considerable decrease in the horizontal displacement of the tunnel, especially when the rotational stiffness λ is lower than 0.5 as can be seen in **Figure 4-12**c. Beyond a λ value of 0.5, the horizontal diameter change ratio becomes more gradual and approaches unity. On the contrary, **Figure 4-12**c shows a negligible effect of the rotational stiffness on the vertical displacement. Despite the change in the λ value, the vertical diameter change ratio is always close to unity. It is possible to conclude that the higher the rotational stiffness of the joints, the lower the value of horizontal diameter change ratio, R_{dia}. Thus, under the action of the same loading conditions, a reduction in tunnel deformation will result in an increase in the structural forces induced in the tunnel lining. It should be mentioned that the effects of λ value on the changes in vertical and horizontal diameter ratio depend on the value of K_0. This means that the results shown in **Figure 4-12**c can only be applied to the case of the value of K_0 of 0.5.

Influence of axial stiffness

The effect of the axial stiffness (K_A) of a joint has been considered using the reference case (six joints located on the tunnel lining with the critical orientation). The rotational stiffness of the joint is assumed to be equal for each joint. The effect of radial stiffness is neglected. The range of axial stiffness, K_A, is chosen on the basis of experimental results presented by Cavalaro and Aguado [2011].

In order to determine the K_A value, it is necessary to know the normal stress that acts on the joint. Considering the input parameters of the reference case (**Table** 4-1), an average normal force of 1100 kN is adopted, which corresponds to a normal stress of 2.75 MPa. On the basis of this normal stress value, the K_A value can be deduced from the work of Cavalaro and Aguado [2011]. The K_A value is equal to 1500 MN/m for the packer made of bitumen used in the Barcelona tunnel project, and the K_A value changes over a 850 to 1500 MN/m range, for a plastic (rubber) packer that was used in five different projects.

In this study, $R_{M-axial}$, $R_{N-axial}$ and $R_{dia-axial}$ are defined as the ratio of the maximum absolute bending moment, the maximum normal force and the diameter change (measured at the vertical axis and the spring line (see **Figure 4-12**d)), respectively, induced in a segmental lining where a certain axial stiffness of the joint has been assigned, to the corresponding values developed in a segmental lining in which the axial stiffness of the joint goes to infinity.

For investigation purposes, the K_A value was chosen over a range from 100 MN/m to 3000 MN/m. **Figure 4-13** indicates that the ratios of the bending moment, the normal force and the tunnel diameter change approximate to unity. On the basis of these results, it is possible to conclude that the axial stiffness of a segment joint has a negligible effect on segmental lining behaviour.

a)

b)

c)
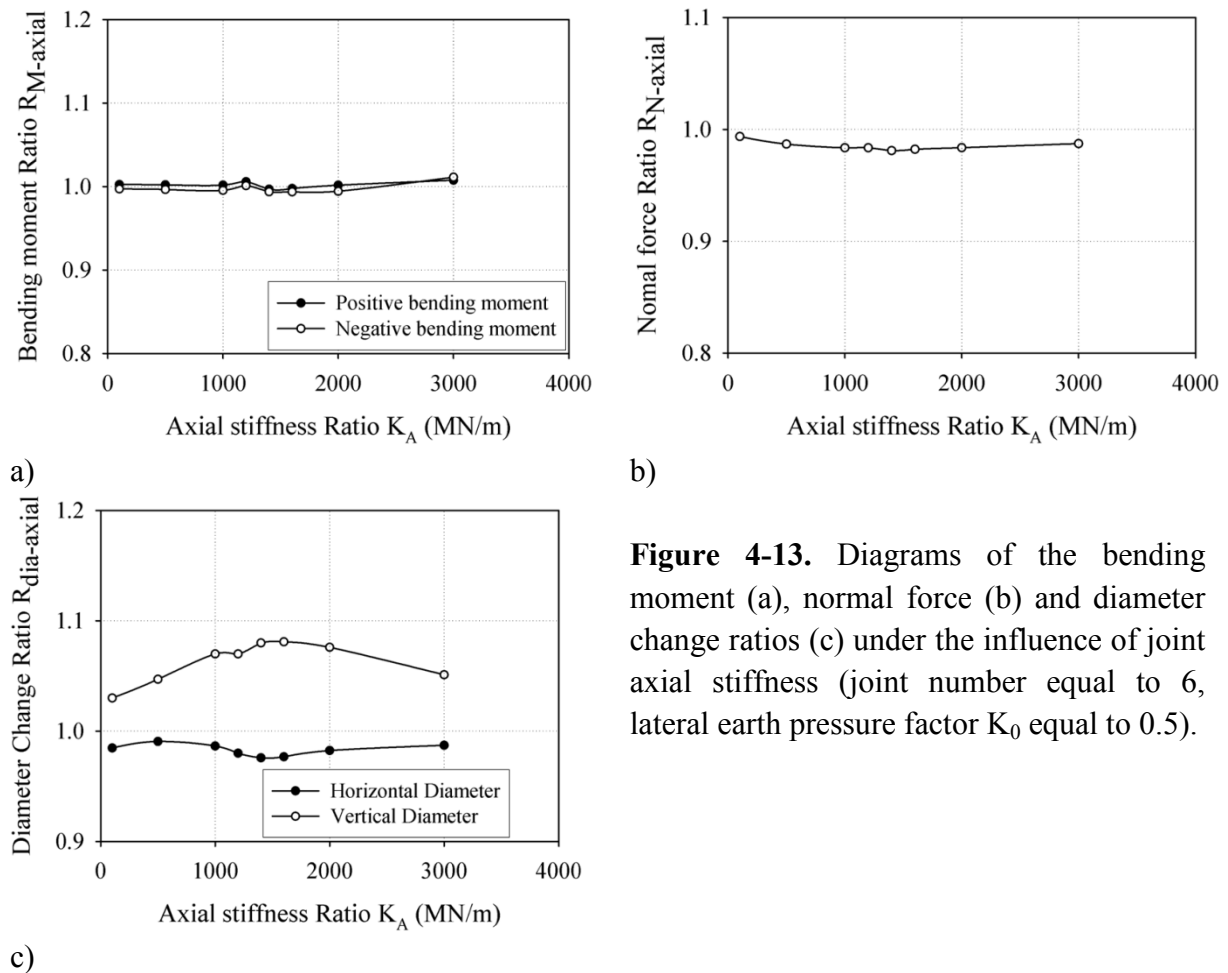
Figure 4-13. Diagrams of the bending moment (a), normal force (b) and diameter change ratios (c) under the influence of joint axial stiffness (joint number equal to 6, lateral earth pressure factor K_0 equal to 0.5).

Table 4-2. Radial stiffness parameters.

Order number	Radial stiffness K_R (MN/m)	Maximum shear stress τ_{yield} (MPa)	Type of packer
1	1050	0.55	Rubber
2	3450	2.00	Rubber
3	5500	3.15	Rubber
4	130	0.70	Bitumen
5	175	1.05	Bitumen
6	215	1.35	Bitumen
7	1190	0.60	Without packer
8	2245	2.60	Without packer

Influence of radial stiffness

In order to quantity the effect of the radial stiffness of joint, K_R, on the behaviour of a segmental tunnel lining, the experimental results presented by Cavalaro and Aguado (2011) were adopted and three main materials used for segment joints were considered: packers made of plastic (rubber), packers made of bitumen and contact without packers (direct contact between the concrete surfaces). The rotational stiffness of a joint is assumed to be equal for all the joints. The effect of axial stiffness is neglected.

The shear stress-displacement relationship curve is in fact non linear. Like the rotational stiffness, this non-linear characteristic needs to be simulated approximately by means of a bi-linear curve, represented by two main parameters: (1) the radial stiffness K_R and (2) the maximum shear stress (τ_{yield}), which is determined adopting the same principles shown in **Figure 4-7**. **Table** 4-2 presents the parameters used in this study.

Figure 4-14 shows the results of the bending moment ratio, R_{M_radial}, the normal force ratio, R_{N_radial} and the diameter change ratio, R_{dia_radial}, defined as the ratio of the maximum absolute bending moment, the maximum normal force and the diameter change (measured in the vertical axis and on the spring line, see **Figure 4-12**d), which are induced in a segmental lining, to the corresponding ones developed in a tunnel lining with an infinite radial stiffness of the joints.

a)

b)

c)
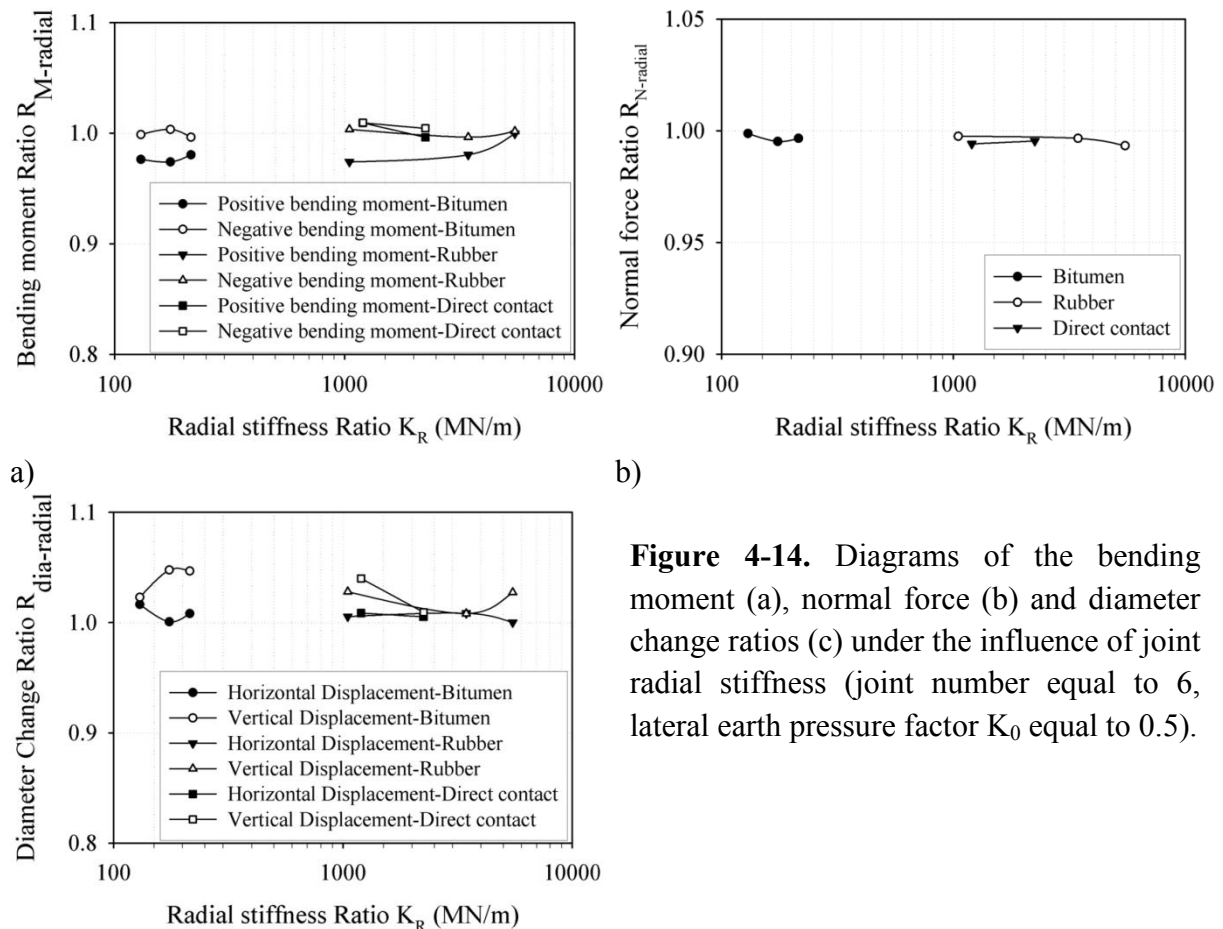
Figure 4-14. Diagrams of the bending moment (a), normal force (b) and diameter change ratios (c) under the influence of joint radial stiffness (joint number equal to 6, lateral earth pressure factor K_0 equal to 0.5).

Generally, the bending moment ratio approaches unity when the joint radial stiffness increases (**Figure 4-14**a). In the case of the bitumen packer, the change in radial stiffness causes a greater effect on the tunnel lining behaviour, due to the low capacity of shear resistance, compared to the other cases (i.e. plastic packer and without packer). The maximum bending moment induced in a segmental lining with a finite radial stiffness of the joints is usually lower than that developed in tunnel lining with an infinite radial stiffness. **Figure 4-14**b shows that the normal force ratio, R_{N_radial}, is close to unity for all the radial stiffness values and for all the packer materials. Similarly, **Figure 4-14**c shows the insignificant influence of radial stiffness on the tunnel displacements, especially in the cases in which the packer is made of rubber and the joints are in contact without a packer. In these cases, the R_{dia_radial} values change over a range of about 1.01 to 1.02. When the packer is made of bitumen, the R_{dia_radial} values change over a larger range, of about 1.02 to 1.05, also because of the low capacity of the shear resistance of the bitumen material. On the basis of the above results, it is possible to conclude that the radial stiffness assigned to the segment joint has a negligible effect on the segmental lining behaviour.

Effect of the reduction in joint rotational stiffness when a joint is subjected to a negative bending moment

Full-scale laboratory tests were performed by Cheng [1985] during the design stage of tunnels in Shanghai to determine the joint rotational stiffness of the segmental lining used to support the Shanghai subway tunnel. Furthermore, full-scale tests were also conducted by Zhou [1988] on a highway tunnel constructed in Shanghai. In these structural tests, the rotational stiffness K_{RO} of the joint was determined through two types of full-scale tests: (a) two-point bending tests on assembled concrete lining segments with a single point section, and (b) a completely assembled lining ring with applied loads, corresponding to an embedded depth of 8m. The results of the structural tests show that the rotational stiffness is higher, when the joint is subjected to a positive bending moment, than when it is subjected to a negative bending moment, that is $K_{RO}^{-} = \left(\frac{1}{2} \div \frac{1}{3} \right) K_{RO}^{+}$ (Lee et al. [2001]).

In the aforementioned cases, the rotational stiffness of the joint was assumed to be equal for each joint, and the change in joint rotational stiffness when the joints were subjected to a positive or negative bending moment was disregarded. In order to quantity this effect an additional analysis has been performed considering the parameters of the reference case (**Table** 4-1), in which the joint rotational stiffness has been reduced under a negative bending moment. The value of the rotational stiffness under a negative bending moment was assumed to be one third of the rotational stiffness used under a positive bending moment (Lee et al. [2001]).

Figure 4-15 shows the bending moment obtained with and without considering the reduction in joint rotational stiffness, corresponding to "different K_{RO}" and the "same K_{RO}". Basically, the difference in joint rotational stiffness assigned at the joints in a ring (hereafter called the non-equal joint rotational stiffness case) results in a significant reduction in the

maximum magnitude of the negative bending moment, but also a negligible reduction in the maximum bending magnitude of the positive bending moment. These results are in good agreement with the values obtained with the analytical method presented by Lee et al. [2001].
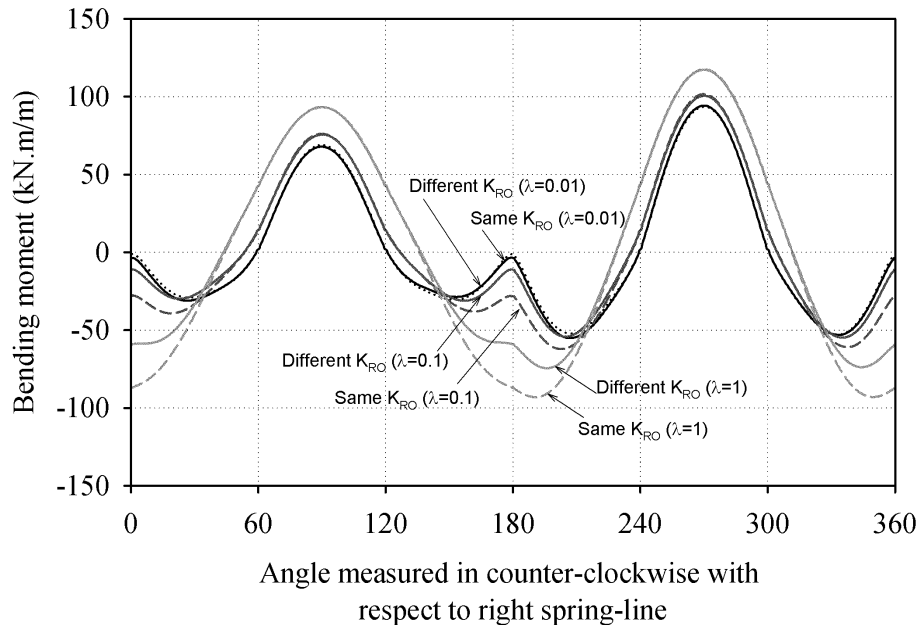
Figure 4-15. Bending moment diagram with different or with the same joint rotational stiffness assigned for the joints in a ring.

Figure 4-16 clearly shows the influence of a reduction in joint rotational stiffness on the segmental tunnel lining behaviour in function of $R_{M\text{-}SD}$, $R_{N\text{-}SD}$ and $R_{disp\text{-}SD}$. The values $R_{M\text{-}SD}$, $R_{N\text{-}SD}$ and $R_{disp\text{-}SD}$ are defined as the ratios of the maximum bending moment, normal force and displacement, respectively, induced in a segmental lining, where the reduction in joint rotational stiffness is considered, to the corresponding ones developed in a segmental lining assigned with the same joint rotational stiffness. In **Figure 4-16**, the λ value represents the joint rotational stiffness under a positive bending moment.

The effect of the non-equal joint rotational stiffness on the bending moment is negligible for the lining assigned with a low joint rotational stiffness ($\lambda = 0.01$). This effect increases in the case of intermediate joint rotation stiffness ($\lambda = 0.268 - 0.8$) (**Figure 4-16**a). The horizontal and vertical displacements of the tunnel lining in which the reduction in joint rotational stiffness is considered are about 1.76 to 6.88 and 0.21 to 3.23 per cent, respectively, that is larger than the ones induced in a segmental lining considering the same rotational stiffness for all the joints. Like the bending moment, the difference in tunnel displacement is greater for an intermediate rotational stiffness (**Figure 4-16**c). On the other hand, the normal force is only affected slightly by non-equal joint rotational stiffness (**Figure 4-16**b).

a)

b)

c)
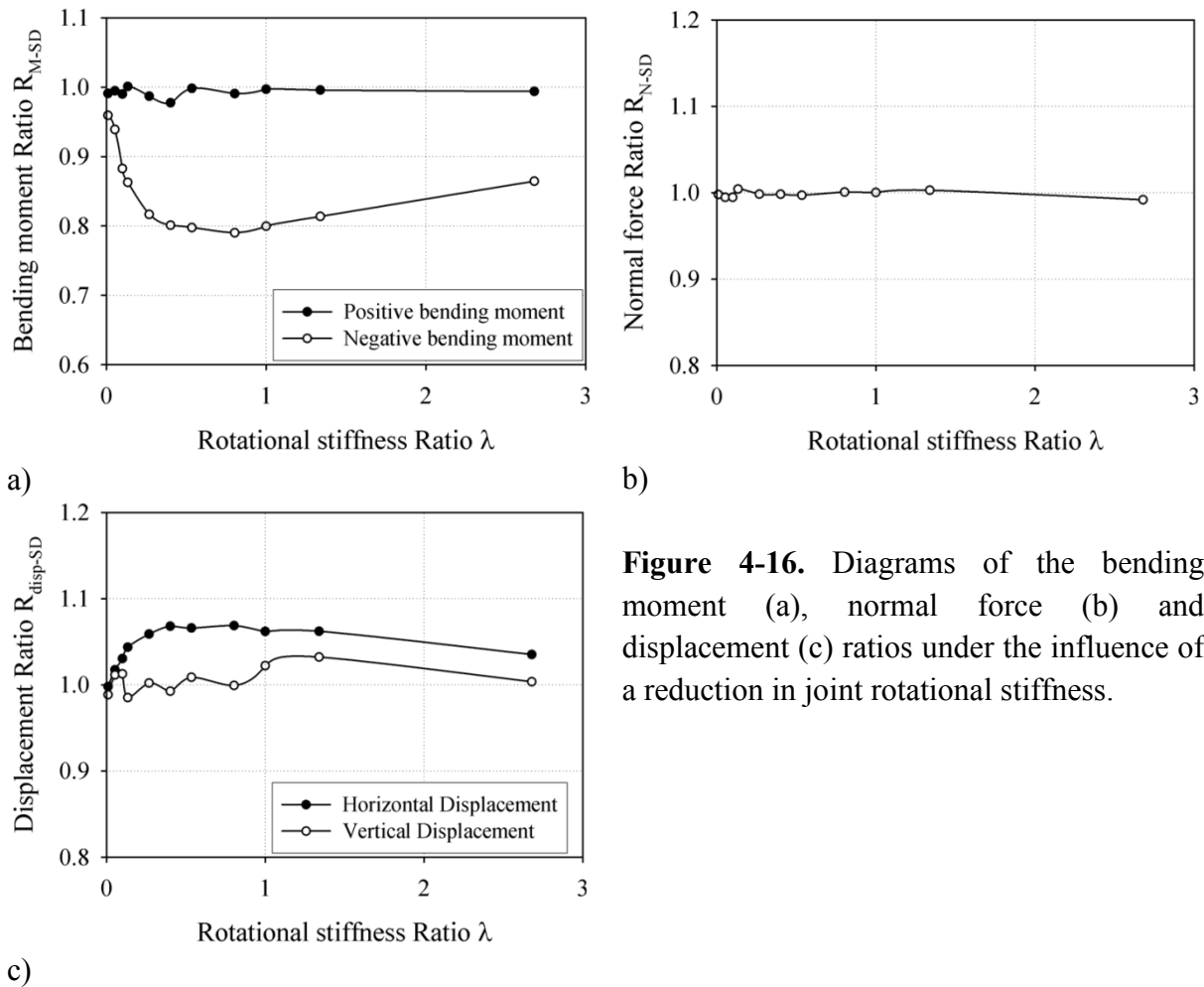
Figure 4-16. Diagrams of the bending moment (a), normal force (b) and displacement (c) ratios under the influence of a reduction in joint rotational stiffness.

4.1.4.2 Impact of the geo-mechanical parameters of the ground mass

4.1.4.2.1 Effect of the lateral earth pressure factor

The effect of the lateral earth pressure factor, K_0, on segmental tunnel lining behaviour is studied in this section. Other parameters based on the reference case have been assumed (**Table** 4-1). The effects of the joint axial and radial stiffness are neglected. Only the corresponding critical case of joint orientation is considered for each case of K_0 value and of the joint number (see **Figure** 4-9 and **Figure** 4-11).

Figure 4-17 shows that the largest maximum bending moment occurs when the K_0 value was 2.0 and the lowest one was observed when the K_0 value was unity. The largest maximum bending moments when the K_0 values are equal to 0.5 and 1.5 are similar in magnitude. This can be explained by the difference between the vertical and horizontal loads acting on the tunnel lining. The influence of the joint number on the maximum bending moment induced in the tunnel lining is considerable for cases of the K_0 values that are lower or higher than unity.

a) (Note : The solid line and dotted line represent the segmental lining and contiunuous lining values, respectively)
b)

c)   d)
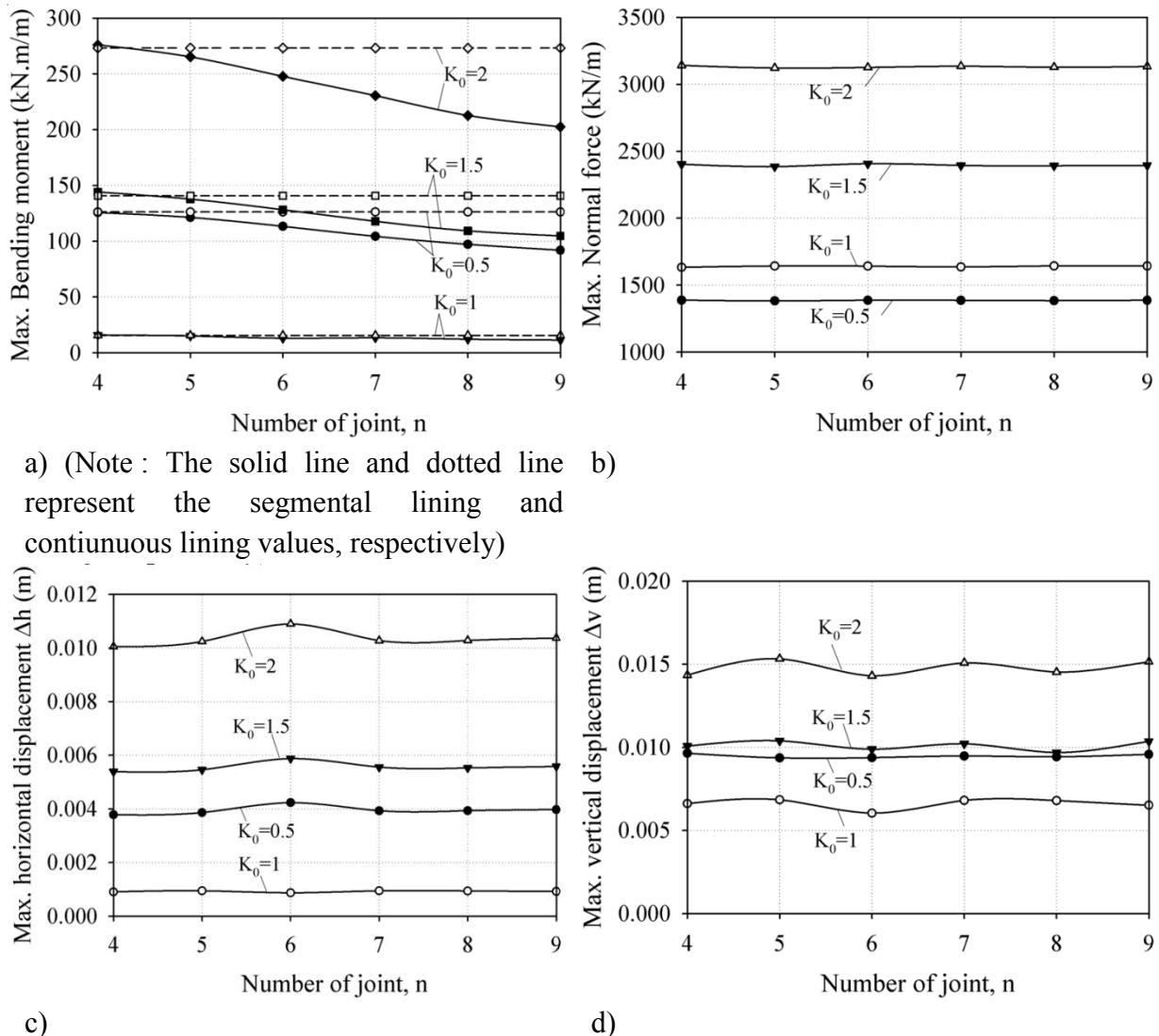
Figure 4-17. Variation of the structural forces and displacements for different joint numbers and lateral earth pressure factors.

For a given K_0 value, the maximum bending moment induced in a segmental lining with the joint number of 4 is similar in magnitude to the one induced in a continuous lining. These observations are in agreement with the statements made by Muir Wood [1975] who stated that the influence of joints on the flexibility of a segmental tunnel lining should only be considered if the number of joints in a ring is greater than 4. The same conclusion was obtained through the works performed by Hefny and Chua [2006]. It should be noted that, for the same K_0 value, the reduction in the magnitude of the maximum bending moment developed in the segmental lining is approximately linear when the joint number increases. Although the maximum bending moment has resulted to depend on the distribution of the joints, as mentioned above, for a given K_0 value, **Figure** 4-17b, c and d show that the absolute vertical displacement (Δv), the absolute horizontal displacement (Δh) and the maximum value of the normal force that have developed in the lining do not depend on the joint number. The tunnel displacement is lower at the K_0 value of unity than for the other cases.

4.1.4.2.2 Effect of ground deformability

The change in structural forces and tunnel displacements are here investigated over a Young's ground modulus range that varies from 10 MPa to 500 MPa, corresponding to a range of ground condition from soft soils to soft rocks, in order to study the effect of the ground deformability, which is represented here by Young's ground modulus, E_s, for each given value of stiffness ratio λ of 0.01, 0.1, and 1 (**Figure** 4-18). Other parameters are assumed considering the reference case (**Table** 4-1) and six joints located on the tunnel lining with the critical orientation. The axial and radial stiffness effects are neglected.

The development of the bending moment is affected to a great extent by the change in Young's modulus of the ground surrounding the tunnel for a given rotational stiffness ratio, λ. A higher E_s value results in a lower absolute magnitude of the bending moment. It is also possible to note that the influence of stiffness ratio, λ, on the bending moment decreases when Young's ground modulus increases. When the E_S values are larger than 200 MPa, the maximum bending moments for the three λ values of 0.01, 0.1, and 1 are similar.

It is interesting to note that the maximum bending moment and the maximum displacements induced in the tunnel lining are almost the same at the lower Young's modulus E_s of 10 MPa, when the rotational stiffness ratios, λ, are large ($\lambda = 0.1$ and $\lambda = 1$). Generally, for a given E_s value, the maximum bending moment increases as the rotational stiffness, λ, increases. This result agrees well with the results presented in **Figure 4-12**a. **Figure** 4-18b shows a steady linear reduction in the normal force for all three rotational stiffness values ($\lambda = 0.01$; 0.1 and 1) when the E_s value increases.

Like the bending moment, the maximum vertical displacements (Δv) and the horizontal displacements (Δh) that have developed in the tunnel lining are sensitive to Young's ground modulus, especially at the low E_s range of 10 to 50 MPa. This means that the low stiffness of the ground may also lead to an increase in the flexibility of the tunnel structure. Beyond a Young's modulus of 50 MPa, the changes in the maximum vertical and horizontal displacement become more gradual and approach Δv value of about 3.13 mm and Δh value of 1.14 mm, respectively. For a given E_s value, the maximum vertical displacements do not depend on the rotational stiffness ratio, λ, (**Figure** 4-18d), while the maximum horizontal displacement depends on the rotational stiffness ($\lambda = 0.01$) compared to other cases ($\lambda = 0.1$ and $\lambda = 1$) (**Figure** 4-18c). It should be mentioned that the maximum vertical displacements and the positive bending moment are usually observed at the top or bottom zones of a tunnel because of the lateral earth pressure factor K_0, which is less than unity ($K_0 = 0.5$). On the other hand, the maximum horizontal displacements and the negative bending moment are always observed at the two sidewalls. These displacements lead to the oval tunnel shape, which is more or less the same as the one presented in **Figure 4-12**d.

a)

b)

c)

d)
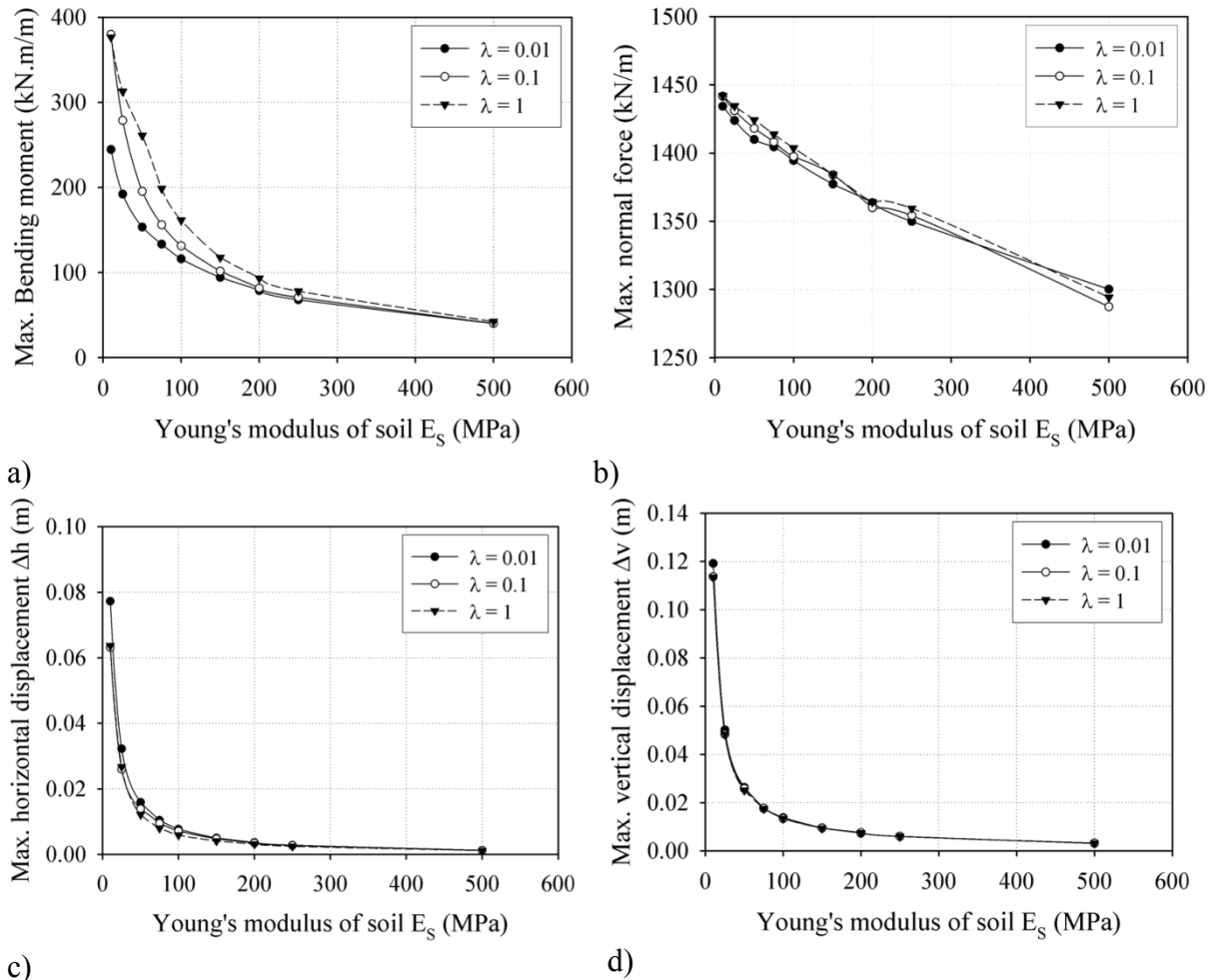
Figure 4-18. The variation in the bending moment (a), normal force (b), horizontal displacement (c) and vertical displacement (d) in function of the Young's ground modulus and for different rotational stiffness.

In order to quantify the influence of the ground deformability on the tunnel behaviour, the positive bending moment ratio R_{M+}, the negative bending moment ratio R_{M-}, the horizontal displacement ratio $R_{disp-\Delta h}$ and the vertical displacement ratio $R_{disp-\Delta v}$, defined as the ratios of the maximum absolute values induced in a segmental lining to the corresponding values developed in a continuous lining, are presented in **Figure** 4-19. **Figure** 4-19b shows that the negative bending moment ratio, R_{M-}, is significantly affected by low Young's modulus values for stiffer joints ($\lambda = 0.1$ and $\lambda = 1$). The change in the negative bending moment ratio, R_{M-}, could approximately be presented by a bilinear curve with a transition point located at E_s values of 25 MPa and 100 MPa, which correspond to λ values of 0.1 and 1. Beyond these Young's modulus values, the change in R_{M-} becomes more gradual and approaches values of 0.661 and 0.832, respectively. However, in the case of a λ value of 0.01, the R_{M-} value could approximately be represented by a steady linear function of Young's ground modulus.
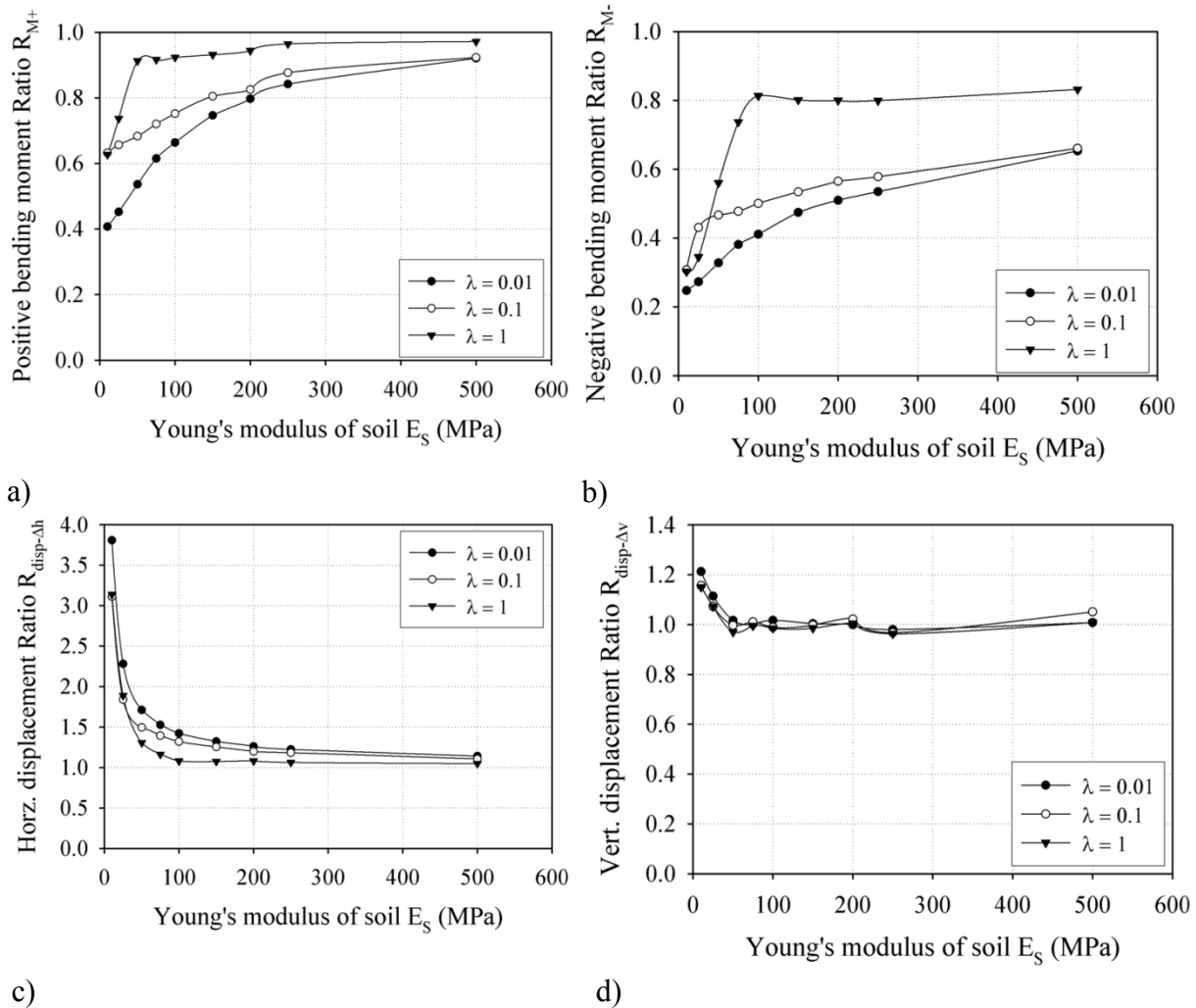
Figure 4-19. The variation in the positive bending moment ratio, R_{M+}, (a) negative bending moment ratio, R_{M-}, (b) horizontal displacement ratio, $R_{disp-\Delta h}$, (c) and vertical displacement ratio, $R_{disp-\Delta v}$, (d) depends on the various Young's ground modulus (E_s) under different rotational stiffness (λ).

For all the rotational stiffness values, the positive bending moment ratio, R_{M+}, (**Figure 4-19a**) is always higher than the negative bending moment ratio, R_{M-} (**Figure 4-19b**). The positive bending moment ratio, R_{M+}, is not affected to any extent by Young's ground modulus, for stiffer joint ($\lambda = 1$), but the R_{M+} value is almost the same of the case of $\lambda=0.1$ for a low E_s value ($E_s=10$ MPa) and this value is close to 62.7%. The positive bending moment ratio, R_{M+}, is significantly affected by the Young's ground modulus for a softer joint ($\lambda = 0.1$ and $\lambda = 0.01$): a steady increase in the R_{M+} value can be noted when the E_s value increases and R_{M+} approaches to the values of 92.3% and 92.1%, respectively. It is interesting to note that, except for low Young's ground modulus, the decrease in joint rotational stiffness results in an increase in the slope of the R_{M+} and R_{M-} curves. This means that the increase in Young's ground modulus, E_s, and the rotational stiffness, λ, causes a reduction in their influence on the bending moment ratio. It is possible to conclude that, in general, the higher the value of Young's modulus, i.e. the lower the deformability of the ground, the higher the bending

Chapter 4: Two-dimensional numerical analyses   92

moment ratio.

On the contrary, **Figure** 4-19c shows a reduction in the horizontal displacement ratio when Young's ground modulus increases to a large value. The horizontal displacement ratio, $R_{disp-\Delta h}$ is affected to a great extent by the early increase of E_s from 10 to 50 MPa and drastically reduces to a range of 1.31 to 1.71 with respect to the λ value of 1 and 0.01. Beyond an E_s value of 50 MPa, the change in the horizontal displacement ratio becomes more gradual and approaches values of about 1.05 and 1.14, corresponding to λ values of 1 and 0.01. On the other hand, **Figure** 4-19d shows that the vertical displacement ratio, $R_{disp-\Delta v}$, is not affected to any great extent by the increase in Young's ground modulus: $R_{disp-\Delta v}$ is almost constant and close to unity except for low values of the Young's ground modulus ($E_s < 50$ MPa).

4.1.5. Conclusions

A 2D numerical study has been used to investigate the factors that affect the behaviour of segmental tunnel linings. A 2D analysis does not allow the interaction between lining rings in the tunnel axis direction to be taken into account.

The influences of the joint distribution, joint stiffness (including the rotational stiffness, the axial stiffness, the radial stiffness, and the non-equal rotational stiffness assigned at the joints) and the ground conditions, such as Young's ground modulus and the lateral earth pressure factor, have been studied in detail.

The number and the orientation of joints have a significant influence on the maximum bending moment induced in a segmental lining. Generally, the higher the joint number, the lower the maximum bending moment and also the influence of the joint orientation on it. The behaviour of segmental linings, when the lateral earth pressure factor K_0 is equal to 0.5, 1.5 and 2, is similar. In other words, when the joint number is even (4-joints, 6-joints, 8-joints), the favourable orientation of the joints almost refers to a reference angle (ω) of zero, and the critical orientation of the joints occur at a ω angle of 45^0, 30^0, and 22.5^0, respectively. Instead, when the joint numbers are odd (5-joints, 7-joints, 9-joints), the favourable orientation of the joints almost refers to reference angles of 32.5°, 27.5° and 15° and the critical orientation of the joints occurs at a ω angle of zero. Unlike the above three cases, when the K_0 value is equal to unity, the bending moment trend is similar for all joint numbers. The favourable orientation of the joints always refers to a reference angle of zero.

The development of the bending moment is affected to a great extent by the rotational stiffness of the joints. A higher rotational stiffness results in a higher magnitude of both the positive and negative bending moment ratios. On the other hand, the normal force that develops in the lining is not-sensitive to the magnitude of the rotational stiffness. Generally, the higher the rotational stiffness of the joints, the lower the value of the horizontal diameter change ratio, R_{dia}.

The axial stiffness of a segment joint has a negligible effect on the segmental lining behaviour for all types of packing material.

The higher the radial stiffness of the joint, the higher the bending moment ratio. The

magnitude of the normal force ratio, R_{N_radial}, is close to unity for all the radial stiffness values and for all the packer materials. Similarly, the tunnel displacements are not affected to any extent by the radial stiffness, especially when the packer is made of rubber and when no packer is used between the joints. It is possible to conclude that the radial stiffness of the segment joint has a negligible effect on segmental lining behaviour.

The "non-equal joint rotational stiffness" results in a significant reduction in the maximum magnitude of the negative bending moment, but also in a negligible effect on the maximum magnitude of the positive bending moment. The differences in tunnel displacements are greater for intermediate joint rotational stiffness. On the other hand, the normal force is not affected to any extent by non-equal joint rotational stiffness.

When the lateral earth pressure factor, K_0, is lower or higher than unity, the influence of the joint number on the maximum bending moment induced in the tunnel lining is considerable. On the other hand, for a given K_0 value, the results show that the maximum value of the normal force, vertical displacement and horizontal displacement developed in the lining does not depend on the joint number.

For a given rotational stiffness ratio, λ, the development of the bending moment is affected to a great extent by the change in Young's ground modulus. A higher E_s value results in a lower absolute magnitude of the bending moment. The influence of the rotational stiffness ratio, λ, on the bending moment decreases when Young's ground modulus increases. The vertical and horizontal displacements developed in the tunnel lining depend on Young's ground modulus, especially for a low range of E_s varying from 10 to 50 MPa. This means that ground with a low stiffness may also lead to an increase in tunnel structure flexibility. For a given E_s value, the maximum vertical displacement does almost not depend on the rotational stiffness ratio, λ, while the maximum horizontal displacement shows a significant dependence as the rotational stiffness ratio decreases ($\lambda = 0.01$). Generally, the higher the value of Young's ground modulus, the higher the R_M ratio.

4.2. Numerical Investigation - The influence of the Simplified Excavation Method on Tunnel Behaviour

4.2.1. Introduction

Tunnel advancement induces a change in the boundary conditions in localized zones that requires a 3D approach in order to accurately simulate the excavation process. However, a full 3D numerical analysis often requires excessive computational resources (both storage and time). Therefore, a tunnel excavation is often modelled in 2D.

When the tunnelling process is modelled with a 2D plane strain model, a simplified assumption must be made. This assumption allows the pre-displacement of the ground surrounding the tunnel boundary, prior to the structural element installation, to be taken into account. This pre-displacement process of the tunnel boundary is hereafter called the deconfinement process. The available equivalent approaches that allow the deconfinement process to be controlled, include: the convergence-confinement method (Panet [1982], Bernat [1996], Hejazi et al. [2008], Janin [2012]), the gap method (Rowe et al. [1983]), the progressive softening method (Swoboda [1979]), the contraction method (Vermeer and Brinkgreve [1993], Klotz et al. [2006]), the volume loss control method (Bernat [1996], Addenbrooke et al. [1997], Jenck and Dias [2003], Hejazi et al. [2008]), the grout pressure method (Möller and Vermeer [2008]), and the modified grout pressure method (Surarak [2010]).

Most of the cases reported in the literature concerning tunnels excavated in urban areas have focused on estimating the applicability of the above methods through an evaluation of the surface settlement. Karakus [2007] used various ways of modelling tunnel excavation that took into account 3D effects in a 2D model, in order to determine the shape of the settlement trough on the ground surface. Karakus [2007] concluded that the CCM method (Panet and Guenot [1982]) leads to the best agreement with experimental results. On the basis of the settlement that develops on the ground surface and the structural forces that are induced in a continuous lining, Möller and Vermeer [2008] proposed the grout pressure method and evaluated its merits by comparing it with the CCM method and VLM method. Surarak [2010] used the contraction method, CCM method and the modified grout pressure method to predict the ground displacement and structural lining forces during shield tunnelling. In this study, numerical results of the surface settlement are compared with experimental data, referring to the Bangkok MRT blue line extension project. The results showed that the shape of the predicted settlement profiles was the same. The maximum magnitudes of the lining deformation, the bending moment and the structure forces, which were determined using the above methods, were comparable. The shape of the tunnel boundary at the final state and therefore the diagram of the bending moment of the CCM method and modified grout pressure method were similar. However, they were different from those of the contraction method. The influence of the joints on the tunnel lining has not been dealt with in the above literature. Do et al. [2012] showed that segment joints in a lining have a certain influence on

the settlement induced on the ground surface. However, Do et al. [2012] only focused on studying the effect of the joint distribution and ground deformability, and did not consider the effect on deconfinement process.

Generally, all of the above deconfinement approaches allow a certain amount of the tunnel wall displacement to take place before installation of the tunnel lining. Due to the difference in the controlling technique of the tunnel wall displacement, the shape of the tunnel boundary is different from the others after one of the above deconfinement approaches. The tunnel shape has in fact a great effect on tunnel behaviour, in terms of the structural forces and on the surrounding ground displacement. This effect should be taken into consideration during the design phase.

In this section, a numerical investigation has been performed which has made it possible to include the influence of two tunnel boundary deconfinement techniques, that is, the CCM method and VLM method, on the structural lining forces and surface settlement surrounding a tunnel built in an urban area. In addition, the effect of the segment joints has also been considered. As far as the VLM method is concerned, a technique to simulate the tunnel wall displacement process, based on the principles of the VLM method, which is hereafter called the free tunnel boundary technique, has been developed. A comparison with 3D numerical results has been introduced to estimate the precision of these 2D equivalent approaches. Analyses were carried out using the FLAC^{3D} finite difference program (Itasca [2009]). The main content of this section has been published in Do et al. [2014a].

4.2.2. 2D numerical modelling

Parameters from the Italian Bologna-Florence high speed railway line tunnel project have been adopted in this numerical modelling as the reference case (Croce [2011]). Some typical parameters of the ring 582 section in the first tunnel, which have been adopted in this study as a reference case, are summarized in **Table** 4-1 (Croce [2011]). The soil behaviour is assumed to be governed by a linear elastic perfectly-plastic constitutive relation based on the Mohr-Coulomb failure criterion. It is well known that an elastic perfectly plastic constitutive model with a Mohr-Coulomb failure criterion is not able to accurately reproduce the soil movements induced by excavation. Nevertheless, most finite element calculations are still performed using simple constitutive models, because they require a limited number of parameters and the calculation times tend to be lower than those of advanced soil models (e.g. Melis et al. [2002], Mroueh and Shahrour [2008], Migliazza et al. [2009]).

In this study, the numerical simulations have been performed by means of the FLAC^{3D} finite differences program (Itasca [2009]). The FLAC^{3D} model grid contains a single layer of zones in the y-direction, and the dimension of the elements increases as one moves away from the tunnel. The numerical model is 240 m wide in the x-direction, 60 m in the z-direction and consists of approximately 13,800 zones and 27,765 grid points. The nodes were fixed in the directions perpendicular to the x-z and the y-z planes (i.e. y = 0, y = 1, x = -120 and x = 120), while the nodes at the base of the model (z = -40) were fixed in the vertical (z) direction.

Other components of the numerical model are basically similar to those described in section 4.1.3.

The joints has been assumed to be located at angles of $0°$, $60°$, $120°$, $180°$, $240°$ and $300°$ measured counter-clockwise with respect to the spring line on the right. The segment joint parameters are presented in **Table** 4-3.

Table 4-3. Parameters of the segment joints

Rotational stiffness K_θ (MN.m/rad/m)	100
Maximum bending moment at segment joint M_{yield} (kN.m/m)	150
Axial stiffness K_A (MN/m)	500
Radial stiffness K_R (MN/m)	1050
Maximum shear forces at segment joint S_{yield} (MN/m)	0.55

Two-dimensional numerical studies using the CCM method have already been conducted by Bernat et al. [1996], Hejazi et al. [2008], Svoboda and Masin [2009], Janin [2012], Dias and Kastner [2012], Janin et al. [2013]. Their works pointed out that, in certain geotechnical and construction conditions, the CCM method can correctly simulate the final surface settlement, but it requires a priori estimation of the stress relaxation ratio. In fact, the stress relaxation ratio is usually specified on the basis of a back analysis that uses experimental data obtained from a tunnelling process. In the present study, the deconfinement process has been performed using the CCM method in two phases:

- The excavated ground inside the tunnel is deactivated and a radial pressure is simultaneously applied to the tunnel circumference towards the ground medium. The value of this pressure is calculated using Equation (4-2). This pressure depends on the value of initial stresses (see **Figure** 4-21) and is not constant around the tunnel circumference.

$$\sigma = (1 - \lambda_d)\,\sigma_0 \qquad\qquad (4\text{-}2)$$

where σ: radial pressure; kN/m^2;

               σ_0: initial stress in the ground medium; kN/m^2;

               λ_d: stress relaxation coefficient.

This radial pressure applied to the excavation circumference is reduced step by step until its value reaches the specified stress relaxation λ_d.

- The support system is activated and the total relaxation ($\lambda_d = 1$) is applied.

In De Borst et al. [1996] and Benmebarek et al. [1998], the VLM method was adopted to simulate different stages during tunnelling, using diameter variations of the excavation boundary. This approach assumes that the tunnel base is fixed. The tunnel boring machine passage, the injection process and the grout consolidation phase were simulated considering the change in diameter of the excavation boundary. Benmebarek et al. [1998] showed that this procedure was much better than applying a confinement pressure around the excavation, as in

the CCM method. However, the tunnel base could be moved under the impact of the external loads during the tunnel excavation process.

The VLM method was applied in Hejazi et al. [2008]. The tunnel wall displacement was permitted, in which the tunnel center was assumed to be fixed. This means that the shape of the tunnel wall is always circular during the deconfinement process (see **Figure** 4-20). The tunnel wall displacement process is stopped when the volume loss reaches a specified value. These uniform displacements are in good agreement with the behaviour of a tunnel that is excavated through a ground mass in which the vertical load is equal to the horizontal one. This case corresponds to the earth pressure coefficient at rest K_0 of unity. These uniform displacement processes do not seem to be realistic for other cases of K_0 values.
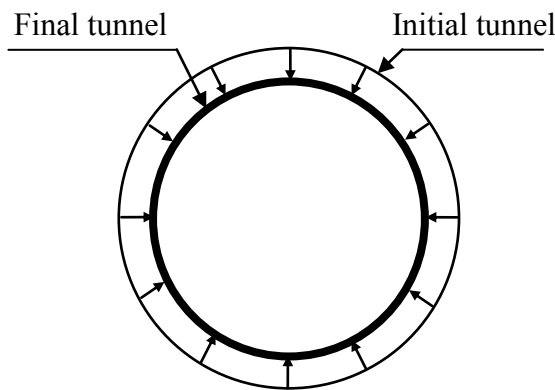
Figure 4-20. Tunnelling simulation with the volume loss method (fixed tunnel center) (Hejazi et al. [2008])
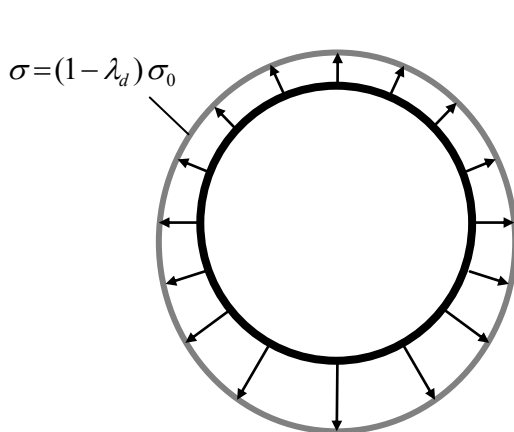
Figure 4-21. Tunnelling simulation with the CCM method (Hejazi et al. [2008])
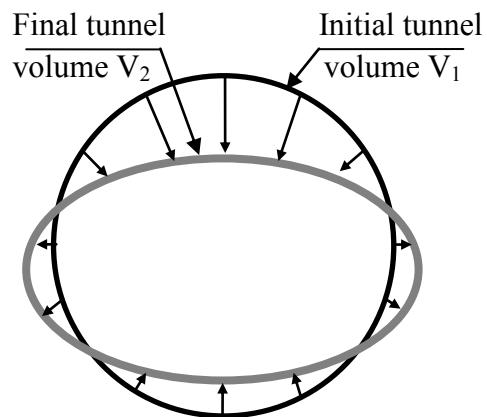
Figure 4-22. Tunnelling simulation with the VLM method (free tunnel boundary)

Another technique that uses the principles of the VLM method has been developed in this study to overcome these drawbacks. When this technique is used, the tunnel wall is allowed to move freely and is not controlled by the confinement forces or by pre-specified displacement values. After the deconfinement process, the tunnel shape may not be circular and it depends on the earth pressure coefficient at rest K_0 (see **Figure** 4-22).

In the present study, the deconfinement process has been simulated using the free tunnel boundary technique in the following steps:

- The excavated ground inside the tunnel boundary is deactivated;

- The tunnel circumference deforms freely due to the surrounding medium. The deformed area of the tunnel is continuously calculated at each computation cycle during the displacement of the tunnel boundary;

- The computation process is stopped when the volume loss value of the tunnel boundary, which is calculated, using the formula presented in **Figure** 4-22, reaches a specified value;

- Activation of the support system.

In this study, besides the CCM method, only the free tunnel boundary technique in the VLM method has been applied. For the models adopted here, we have chosen the phases of work as followed:

- Phase 0 (set up the model): The first calculation step of the numerical excavation process consists in setting up the model, and assigning the plane strain boundary conditions and the initial stress state, taking into consideration the influence of vertical stress with the depth gradient under the effect of the gravity field;

- Phase 1 - Deconfinement phase: The excavated ground is deactivated and a deconfinement technique, corresponding to one of the following methods, is simultaneously applied:

- Method 1 (CCM method): a stress relaxation ratio λ_d, which allows a proportional reduction in the stresses on the periphery of the excavation to occur, is applied to the tunnel wall (see **Figure** 4-21).

- Method 2 (VLM method): a displacement-controlled analysis, which permits the tunnel area to be reduced, has been used (see **Figure** 4-22). The displacement process is stopped when the volume loss ratio reaches a specified value.

- Phase 2 - Installation of the tunnel support: the segmental lining is activated on the tunnel boundary. The surrounding ground is in contact with the tunnel lining through a solid grout layer with elastic characteristics $E_g = 10$ MPa and $v_g = 0.22$ (Mollon [2010], Mollon et al. [2013]).

4.2.3. 2D parametric studies

The two above deconfinement techniques have been applied in this section to investigate the influence of the corresponding deconfinement parameters on tunnel behaviour, in terms of the bending moments, normal forces and surface settlements. The reference case (**Table** 4-1), which has a joint number equal to 6, has been adopted.

4.2.3.1. Convergence-confinement method

Figure 4-23 illustrates the main characteristics of the CCM method. The radial displacement of the tunnel wall is equal to zero for an internal pressure equal to the initial

stress σ_0. The radial displacement of the tunnel wall begins to appear for a reduction in the internal pressure σ. This displacement increases until the internal pressure is equal to zero and the tunnel wall can be self-stabilized without the use of a support structure (curve *a* in **Figure 4-23**) or the surrounding ground falls into a shear failure state that leads to an increase in the ground load acting on the tunnel wall (curve *b* in **Figure 4-23**). In the later case, the tunnel wall must be supported by an artificial structure. The CCM method is represented here through the stress release coefficient λ_d.
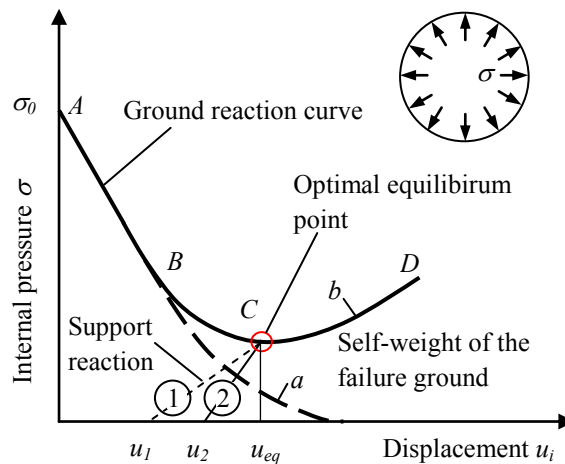
Figure 4-23. CCM method: geometry of the problem. Key: 1- support reaction line of a flexible lining; 2- support reaction line of a stiff lining; u_{eq}- tunnel wall displacement at the equilibrium state; u_1 and u_2- tunnel boundary displacements before the installation of the flexible and stiff supports.

Figure 4-24 shows the results of the CCM method. In this figure, the structural forces correspond to the maximum values determined in the tunnel lining. Since the low value of the lateral earth pressure coefficient at rest K_0 is 0.5, the maximum bending moments determined when the CCM method is used usually occur on the tunnel bottom. On the other hand, the maximum normal forces are obtained at the two tunnel sides. In this study, the stress release coefficient λ_d changed over a range of 0.1 to 0.75. Theoretically, the stress release coefficient λ_d can reach a maximum value of unity that corresponds to the case of a total relaxation of the tunnel boundary. However, during the numerical analyses in this study, as the stress release coefficient was greater than 0.75, the FLAC^{3D} model could not reach an equilibrium state. This could be attributed to the non-stop failure process that occurs in the ground surrounding the tunnel. This is why a maximum stress release coefficient of 0.75 has been used.

The results that take into consideration the effect of the segment joints have shown a significant influence of the stress release coefficient on the structural forces induced in the tunnel lining and the settlement developed on the ground surface.

The behaviour of the tunnel supported by a jointed lining is discussed first. Generally, when the λ_d value is less than 0.7, an increase in the λ_d value would result in a reduction of both the bending moment and the normal forces. This reduction can be explained by a reduction in the external loads that originates from the surrounding ground, which acts on the

tunnel lining. This reduction is caused by the stress relaxation process. The higher the λ_d value, the lower the external loads that act on the tunnel lining that is installed later (**Figure** 4-24b). This behaviour corresponds to line ABC in **Figure 4-23**. However, beyond a λ_d value of 0.7, an increase in the λ_d value would result in a greater bending moment. On the other hand, the normal forces seem to be almost constant. This phenomenon could be attributed to the fact that the stress relaxation on the tunnel boundary has caused the displacement of the surrounding ground. When these displacements reach a certain value, a failure zone develops in the ground surrounding the tunnel. As a consequence, the ground loads that act on the tunnel lining change due to the self-weight of the failure ground in this zone. In the considered case, the impact of the failure ground could be one of the factors that can lead to an increase in bending moments induced in the tunnel lining (**Figure** 4-24a).

a)

b)

c)
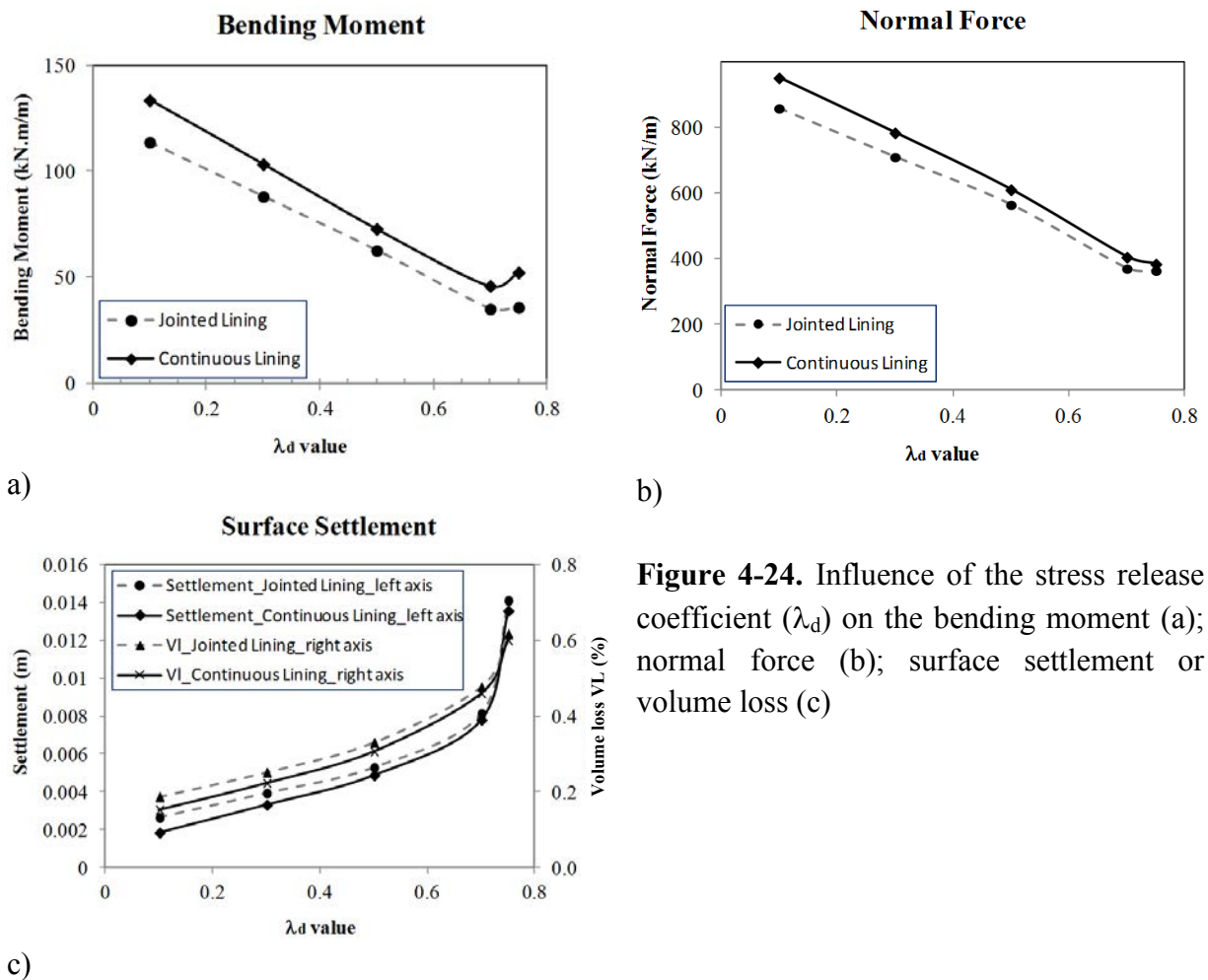
Figure 4-24. Influence of the stress release coefficient (λ_d) on the bending moment (a); normal force (b); surface settlement or volume loss (c)

The failure zone that develops around the tunnel can be highlighted by the development of the surface settlement. As can be seen in **Figure** 4-24c, the surface settlement does not depend to any great extent on the stress release coefficient. Its value is equal to 0.0081 m for a λ_d value of 0.7, which corresponds to a volume loss of about 0.48%. However, beyond this λ_d value, the development of the surface settlement is very sensitive to changes in the stress release coefficient λ_d (**Figure** 4-24c). The development illustrates large ground movements

that occur above the tunnel as a result of the formation of the failure zone (**Figure 4-25**). The increase in vertical displacements that occurs in the surrounding ground is the main reason for the increase in bending moments induced in the tunnel lining that can be seen in **Figure** 4-24a. The volume loss values presented in **Figure** 4-24c are calculated using the same formula of the *Vl* value as that illustrated in **Figure** 4-22.
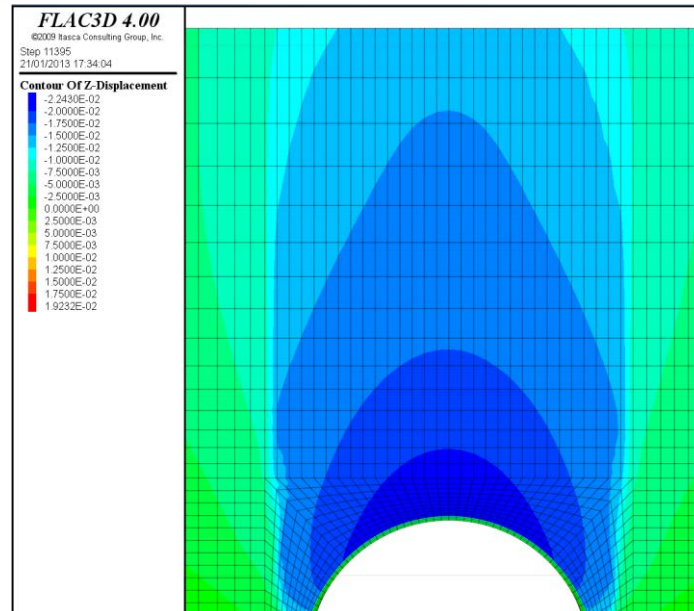
Figure 4-25. Vertical displacement above the tunnel (λ_d value of 0.75)

The results highlight the fact that the support structure should not be installed too soon when the stresses in the surrounding ground are still high. This would result in high pressures that act on the support structure. However, it is also important that the support structure is not assembled too late, when the ground surrounding the tunnel fails as this could be followed by an increase in external loads acting on the tunnel support structure caused by the self-weight of the failure ground. In other words, the tunnel support structure should be installed at the "right" time so that the requirement on its resistance capacity is minimum. In this considered case, a jointed lining should be installed before the moment that corresponds to a λ_d value of 0.7.

Figure 4-24 also shows a considerable effect of the segment joints on the bending moment, normal force, and surface settlement. Generally, a jointed lining is more flexible than a continuous one which would result in a lower value of both the bending moment (**Figure** 4-24a) and the normal force (**Figure** 4-24b), and a higher surface settlement value and therefore a greater volume loss (**Figure** 4-24c). However, the shapes of the relationship curves that present these values in two cases in which the tunnel is supported by a jointed lining and a continuous lining, respectively, are quite similar. Depending on which λ_d value is adopted, the ratios of the bending moment, normal force and surface settlement, induced in the case in which the jointed lining, is used to the ones developed in the case in which the continuous lining is used, change over ranges from 0.68 to 0.88, from 0.90 to 0.95 and from 1.04 to 1.43, respectively. It should also be noted that, for a case of a λ_d value that is less than

0.5, the variation in the structural forces, induced in a continuous lining, is more sensitive to the λ_d value than the one developed in the case of a jointed lining.

As far as the continuous lining is concerned, the optimal moment of the tunnel lining installation corresponds to a λ_d value of 0.72, which is higher than the optimal λ_d value determined in the case in which a jointed lining is used. This difference can be attributed to the fact that a jointed lining is more flexible than a continuous lining. After being installed at the tunnel boundary, the jointed lining and the surrounding ground may be passed through a greater displacement before reaching a new equilibrium state. This means that, for the same displacement of the tunnel boundary at the equilibrium state (for example the u_{eq} value at point C in **Figure 4-23**), a jointed lining that corresponds to line (1) in **Figure 4-23** must be installed earlier than a continuous one that corresponds to line (2) in **Figure 4-23**. This conclusion is in good agreement with the rule of thumb of the CCM method.

4.2.3.2. Volume loss method

Figure 4-26 shows the results obtained with the VLM method. In this figure, the structural forces correspond to the maximum values determined in the tunnel lining. Like the results obtained in the CCM method, the maximum bending moments determined when the VLM method is used are usually determined at the crown or bottom of the tunnel, depending on the volume loss ratio. On the other hand, the maximum normal forces usually occur at the two sides. The volume loss value is assumed to be changed over a range from 0.1 to 2 % (Hefny et al. [2004]). In order to have a more convenient comparison between the VLM method and the CCM method, the variations in the structural forces and surface settlement caused by the CCM method are also represented here through the corresponding volume loss value (**Figure 4-26**).

The numerical results have pointed out that the segment joints have a certain influence on the surface settlement. This influence is greater when the volume loss value is small. However, as the volume loss ratio is quite high, the influence of the joints is not so obvious. **Figure 4-26**c shows that the surface settlements obtained in both the jointed and continuous linings depend linearly on the volume loss value. As expected, the higher the volume loss value, the greater the settlement.

Figure 4-26a and b indicate a significant effect of the volume loss on the structural lining forces. Generally, the greater the volume loss, the lower the bending moment and normal force in the tunnel lining. For a volume loss that is greater than 1.5 %, the structural lining forces seem to be almost constant and they do not depend on the volume loss value.

It should be noted that the deconfinement techniques and the segment joints have a significant influence on the structural forces induced in the tunnel lining. The bending moments and the normal forces induced in a jointed lining are both lower than those developed in a continuous lining. Depending on which volume loss value is adopted, the ratios of the bending moment and normal force in the case in which a jointed lining is used to the ones developed in the case of a continuous lining change over ranges from 0.798 to 0.895, and from 0.889 to 0.923, respectively.

a)

b)

c)
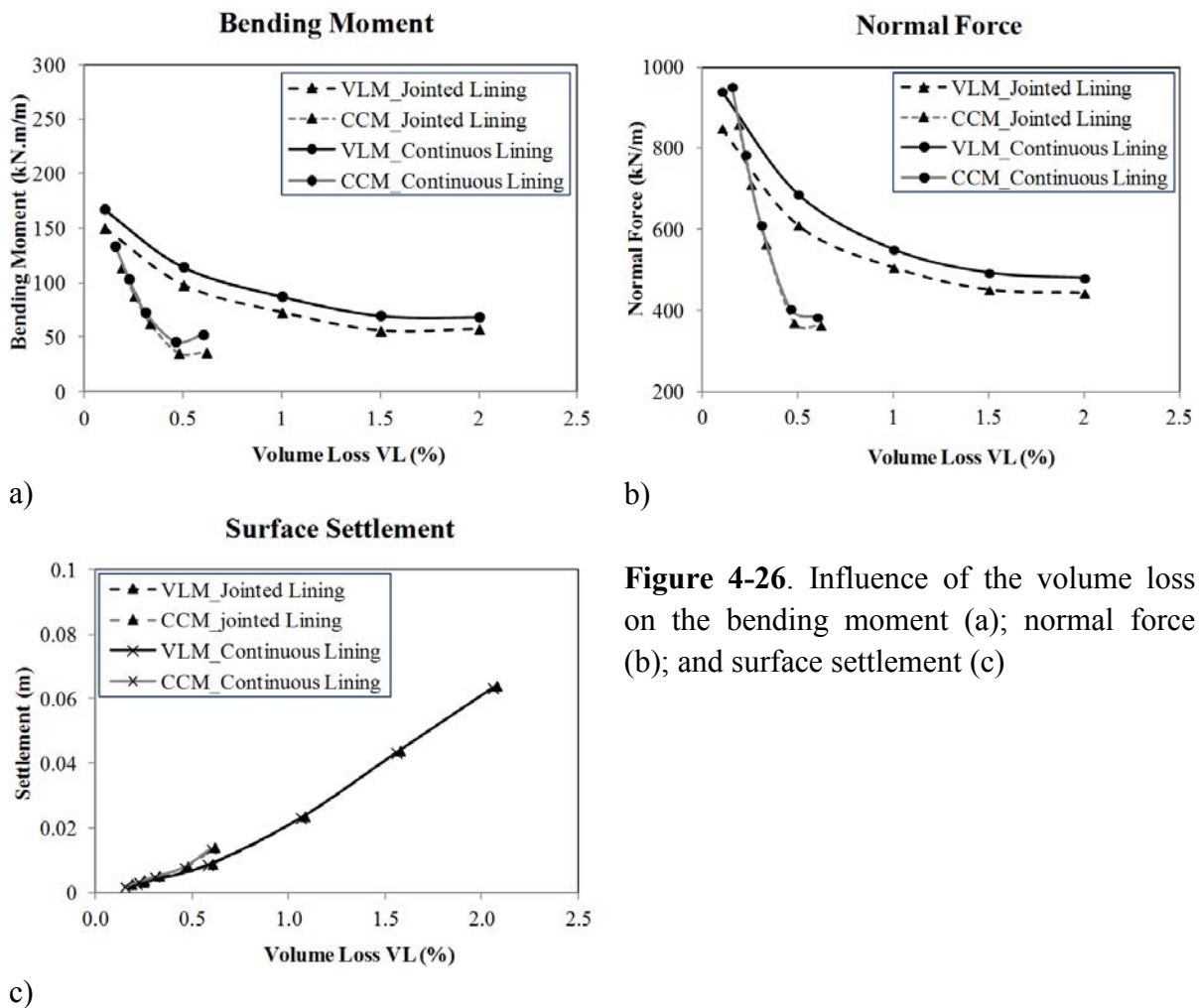
Figure 4-26. Influence of the volume loss on the bending moment (a); normal force (b); and surface settlement (c)

It should be mentioned that the volume loss value that can be obtained in the CCM method is smaller than the one determined in the VLM method. As can be seen in **Figure 4-26**, the maximum volume loss determined in the CCM method for the reference case is about 0.62 %.

Apart from the volume loss, which is less than 0.25 %, the structural lining forces obtained with the CCM method are generally smaller than those determined with the VLM method for the same volume loss value (**Figure 4-26**a, and b). The maximum differences in the bending moment are about 250 % and 300 %, for the continuous and jointed lining, respectively (**Figure 4-26**a). As far as the normal forces are concerned, the maximum differences are about 170 % and 175 %, respectively.

Figure 4-26c also shows that, for the same volume loss value, the surface settlement developed in the CCM method is generally higher than that obtained in the VLM method. With a ground dilation angle value of zero (see **Table** 4-1), this phenomenon means that the settlement trough obtained in the case in which the VLM method is applied is wider than the one obtained in the case in which the CCM method is used. This conclusion can be confirmed by the settlement troughs shown in **Figure** 4-28d, which are presented in the next section. In

other words, for the same final surface settlement value, the VLM method causes a greater volume loss ratio than that of the CCM method (**Figure 4-26**c).

4.2.4. Comparison between 2D and 3D numerical results

4.2.4.1. 3D numerical model

The objective of this 3D analysis is to estimate the precision of the two examined 2D deconfinement methods. The 3D numerical model of a slurry shield tunnelling process used in this analysis is described in detail in section 5.1.3 and not presented here.

4.2.4.2. Comparative results

Figure 4-27 illustrates the contour of the z-displacement of half of the developed 3D numerical model.
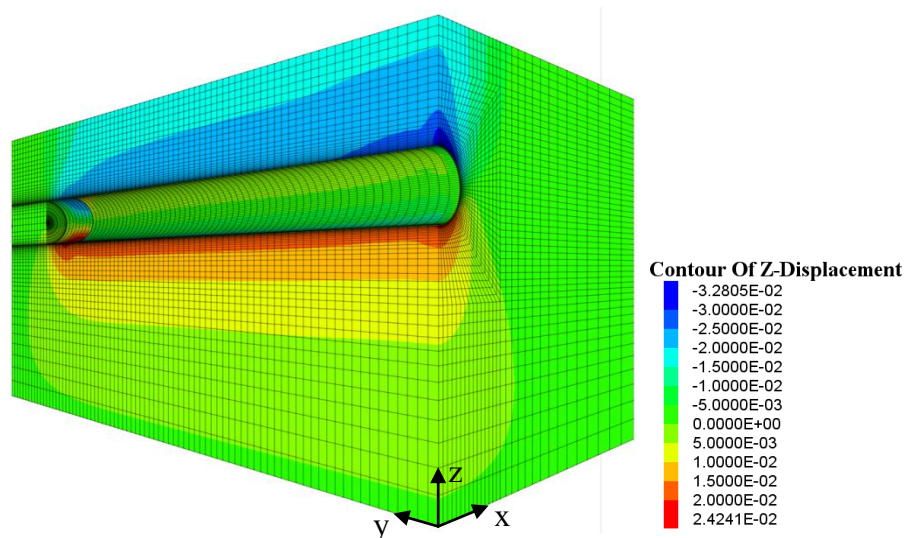
Figure 4-27. Contour of the z-displacement of half of the developed 3D numerical model introduced into FLAC^{3D}

In order to estimate the precision of the previous two deconfinement methods, **Figure 4-28** shows a comparison of the structural forces from the 2D and 3D analyses for the same surface settlement of 0.0148m, which was determined at a stationary state in the 3D numerical model. The volume loss ratio corresponding to the above settlement value is about 0.73 %. As for the CCM method, a stress relaxation ratio λ_d of 0.75 has been applied. All the results in this section have been obtained for the case in which a jointed lining is applied.

It is necessary to note that the variation in the structural lining forces, using the VLM method, is different from that of the CCM method (see **Figure 4-28**a, and b). This could be

attributed to the fact that the displacement of the tunnel wall, after the deconfinement process, using the two above deconfinement techniques, is different, as can be seen in **Figure** 4-28c, especially at the tunnel crown. The structural lining forces depend to a great extent on the movement of the surrounding ground (Möller [2006], Surarak [2010]).

Figure 4-28 shows that the 2D settlement trough matches the 3D one quite well for the CCM method. The same conclusion was also made by Karakus [2007]. He showed that the CCM method allows the best agreement with experimental results. Svoboda and Masin [2009] pointed out that, for an optimum value of the stress relaxation ratio in the CCM method, the displacement field predicted by the 2D method agreed well with the 3D simulation. In addition, the work conducted by Janin [2012] indicated that the settlement trough determined with means of the CCM method, using a couple of stress relaxation ratios which allow the influence of the multi-phase construction to be taken into account, was in good agreement not only with the 3D numerical results but also with the measured data.

a)

b)

c)

d)
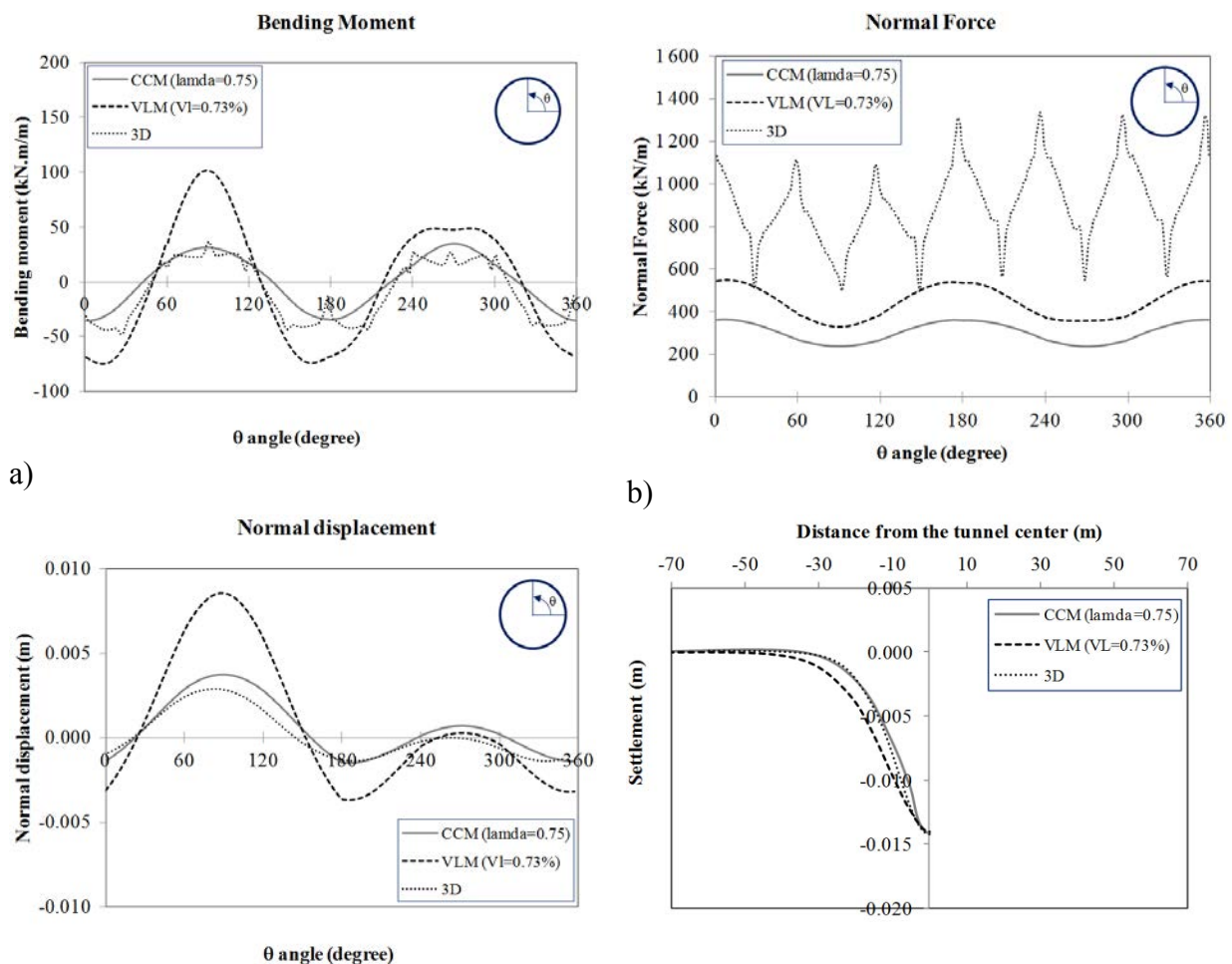
Figure 4-28. Comparison of the bending moment (a); normal force (b); normal displacement (c) surface settlement (d) from 2D and 3D analyses for the case of a jointed lining with the same surface settlement value of 0.0148m.

Besides the surface settlement, both the bending moments and normal displacements obtained with the CCM method are in better agreement with the 3D numerical results than that of the VLM method (see **Figure** 4-28a and c). However, the normal forces obtained with both 2D methods are always lower than those induced in the 3D model (see **Figure** 4-28b). This could be explained by the fact that, the influence of the construction loads in 2D models, such as the jacking forces, grouting pressure, etc, has not been included in this study. It is recognized that construction loads cause important effect on the behaviour of tunnel lining and ground surrounding the tunnel. Interesting investigations performed by Kasper and Meschke (2006) indicate that the increase in construction loads such as face pressure and grouting pressure induce smaller stress release of the ground and therefore cause an increase of the pressure acting on the tunnel lining. Consequently, the ring normal forces increase. The same observations were made from the works of Keolewijn and Verruijt [2001] and Möeller and Vermeer [2008]. They showed that the magnitude and the distribution of bending moments are on average predicted well with 2D and 3D analyses (however differences 300% or more may be observed locally). As far as the normal forces are concerned, the numerical results obtained by 3D analyses are in good agreement with experimental data. However, the 2D numerical results are greatly different from experimental data and 3D numerical results (Bilotta and Russo [2013]). Consequently, it is necessary to use a numerical model which allows the processes that take place during tunnel excavation to be taken into consideration in order to obtain realistic results for structural forces. The impact of the construction loads during tunnelling should be taken into account for mechanized tunnelling.

On the basis of the above comparative results, it is possible to conclude that, for 2D numerical analysis, the structural lining forces and surface settlement determined by the CCM method are in better agreement with the 3D numerical results than those obtained with the VLM method.

4.2.5. Conclusions

This section presents a 2D numerical investigation, in which a significant influence of the segment joints and simplified excavation methods, including the CCM method and the VLM method, on tunnel behaviour has been observed. As far as the VLM method is concerned, a free tunnel boundary technique has been developed, which allows the tunnel wall displacement process that is being controlled to be simulated on the basis of the principles of the VLM method.

As far as the CCM method is concerned, the results have shown a great impact of the stress release ratio on the tunnel behaviour, thus indicating the importance of evaluating the stress release ratio during tunnel design. For the reference case in this study, the numerical analysis using the CCM method showed a failure process that occurred in the ground above the tunnel, when the stress release ratio was greater than 0.75. A jointed lining is generally more flexible than a continuous lining, and this should result in a lower value of the bending moment, normal force and a higher surface settlement value that corresponds to a greater volume loss. However, the shapes of the relationship curves that present these values in both

lining cases are quite similar. As far as the continuous lining is concerned, the optimal moment of the tunnel lining installation corresponds to a λ_d value of 0.72, which is higher than that determined in the case in which the jointed lining is applied. This difference is in good agreement with the rule of thumb of the CCM method.

As far as the VLM method is concerned, the results have indicated a significant effect of the volume loss on the structural lining forces. As expected, the greater the volume loss, the lower the bending moment and normal force in the tunnel lining. For a greater volume loss than 1.5 %, the structural lining forces seem to be almost constant and they do not depend on the volume loss ratio. Both the bending moments and the normal forces in a jointed lining are lower than those in a continuous lining. Depending on which volume loss value is adopted, the ratios of the bending moment and normal force in the case in which the jointed lining is used to the ones developed in the case in which the continuous lining is applied change over ranges from 0.798 to 0.895, and from 0.889 to 0.923, respectively.

Since the displacement characteristics of the tunnel wall, when the volume loss method and the convergence-confinement method are used, are different, a difference has been shown between the structural lining forces and the surface settlement obtained with these two methods. For the same surface settlement, the structural lining forces obtained with the CCM method and VLM method for the continuous lining and jointed lining are different from each others. Generally, the structural lining forces obtained with the CCM method are smaller than those determined with the VLM method.

A comparison with 3D numerical results has been introduced in order to estimate the precision of these equivalent 2D approaches. For the same surface settlement, the structural lining forces determined with the CCM method are in better agreement with the 3D numerical results than those obtained with the VLM method. However, in order to obtain an accurate estimation of the structural forces when the shield tunnelling process is used, the impact of construction loads during tunnelling should be taken into account.

Further comparisons with experimental data, obtained from a real tunnel excavation, should be made in order to improve the quality of the numerical simulation.

4.3. Numerical Investigation of the Interaction between Twin Tunnels: Influence of Segment Joints and Tunnel Distance

4.3.1. Introduction

Many tunnelling projects have recently been constructed that involve the excavation of twin tunnels in close proximity to each other. Even if in many cases, the new tunnel was excavated at close distance to an existing tunnel. Therefore, it is very important to understand in detail the interaction mechanism between two tunnels during their construction processes. Obviously, the interaction between two adjacent tunnels is complex, which depends on many factors such as geometry of tunnels, lining properties, ground characteristics, and construction methods.

As far as the twin tunnels excavated in parallel are concerned, most of the reported cases considered the effect of the ground condition, tunnel size, depth, surface loads, relative position between two tunnels, and construction process on the structural forces (Hefny et al. [2004], Ng et al. [2004], Hage Chehade and Shahrour [2008], Afifipour et al. [2011], etc.). Nevertheless, the effect of the segment joints was not taken into consideration.

Two-dimensional numerical investigation performed in this study made it possible to include the influence of the segment joints and of the distance between two tunnels on the structural forces induced in both tunnels. The results showed that the critical influence distance between two tunnels is about two tunnel diameters. The structural lining forces induced in the first tunnel through various phases are considerably affected by the second tunnel construction process. Their values induced in a segmental lining are always lower than the ones developed in a continuous lining. In addition, the influence of the joint distribution in the second tunnel on the structural lining forces induced in the first tunnel is insignificant. The main content of this section has been published in Do et al. [2014e].

4.3.2. Numerical modelling

When tunnelling process is performed in 2D plane strain model, an assumption that takes into account the pre-displacement of the ground surrounding the tunnel boundary prior to the installation of structural elements must be adopted. This pre-displacement process of the tunnel wall is called here the deconfinement process. Apart from the VLM, gap method, and grouting pressure method, Karakus [2007] used various ways of tunnel excavation modelling, which take into account 3D effects in a 2D model, to determine the shape of the settlement trough on the ground surface. This work shows that the CCM allows the best agreement with experimental results. Furthermore, the results performed in section 4.2 (also see Do *et al.* [2014a]) have presented a comparison of 2D numerical analyses using both the VLM and the CCM with 3D numerical analyses, which indicated that the structural lining forces determined with the CCM are in better agreement with the 3D numerical results than those obtained with the VLM. For the above reason, the CCM has been adopted in this section.

The determination of the ground convergence, when the support system becomes active, is an essential element of the CCM. This method is also known as the "λd method". Choosing a value of the stress release ratio λd before the lining being installed is one of the difficulties when applying this method. In this study, for the purpose of the numerical investigation, a λ_d value of 0.3, which is different from the λ_d value of 0.75 indicated in section 4.2, has been adopted (Möller and Vermeer [2008]). Moller and Vermeer [2008] pointed out that different stress reduction factor, λ_d, are necessary to use to obtain good estimations in terms of surface settlement and normal forces. In their studied case, λ values of 0.6 - 0.7 were adopted for surface settlement, while a λ value of about 0.3 was adopted for normal forces. The main purpose of this section is to investigate the interaction between 2 tunnels in terms of internal forces. That is why a λ_d value of 0.3 has been preliminarily adopted.

In order to avoid a possible soil decompression that relates to the annular void appearing between the excavated soil surface and the concrete lining, the tail void grouting is performed. In general, after being injected into the void behind the shield tail, the grouting action are modelled through two phases: (1) the liquid state (state 1) represented by a certain pressure simultaneously acting on both the soil surface and the tunnel lining; (2) the solid state (state 2) (Melis *et al.* [2002], Kasper and Meschke [2004], Mollon *et al.* [2013]).

As far as the grouting pressure distribution over the tunnel height is concerned, there is no unique rule which has been accepted by researchers (Rijke 2006). However, the distribution of the grouting pressure can be generally assumed to be linearly increased with depth under the grout unit weight effect (Bezuijen and Talmon [2004]). In this study, the vertical grouting pressure gradient behind the TBM is assumed to be of 15 kPa/m, which corresponds to the density of the fresh grout. The grout pressure applied to the tail void is generally set to (Mollon *et al.* [2013]):

$$\sigma_{inj} \approx 1.2 \cdot \sigma_{vcr} \tag{4-3}$$

where σ_{vcr} is the soil overburden pressure at the tunnel crown.

Figure 4-29 shows a 2D numerical model which utilizes the plane-strain conditions. Parameters from the Bologna-Florence high-speed railway line tunnel project have been adopted in this numerical modelling as the reference case (Croce [2011]) (see **Table** 4-1).
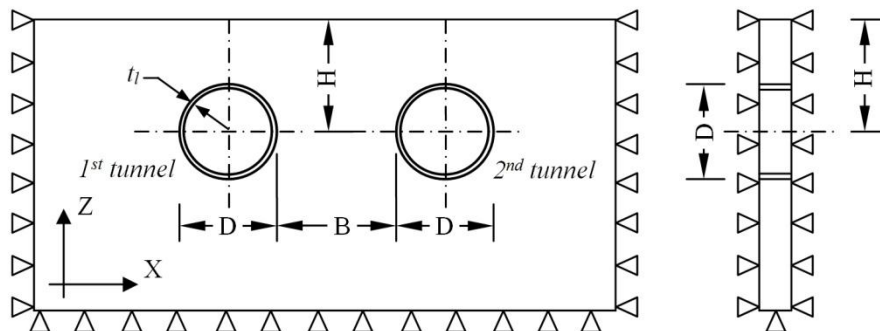
Figure 4-29. Plane strain model under consideration (not scaled)

In this section, the components of the numerical model are basically similar to those described in section 4.1.3. Some typical tunnel lining and soil parameters are summarized in **Table** 4-1. The segment joint parameters are presented in **Table** 4-3.

The FLAC^{3D} model grid contains a single layer of zones in the y-direction, and the dimension of elements increases as one moves away from the tunnel (see **Figure** 4-30). The numerical model is 60 m high in the z-direction. The width in the x-direction is varied depending on the distance between two tunnels.

Modelling of the construction process of two tunnels has been carried out in the following steps:

- Setting up the model of two tunnels, assigning the plane strain boundary conditions and the initial gravity stress state;

- Constructing the first tunnel that includes three phases as follows:

+ 1st phase: Deactivating the excavated ground, simultaneously applying a stress relaxation ratio λ_d of 0.3 to the tunnel boundary (see **Figure** 4-21);

+ 2nd phase: Activating the segments in a ring, assigning joint stiffnesses; simultaneously applying the total relaxation, and setting up the grouting pressure, which acts over the whole tunnel periphery, on both tunnel structure and ground surface.

+ 3rd phase: Consolidation of the grout: the hardened grout in the present model has been simulated by means of volume elements with perfect elastic behaviour, and with the elastic characteristics E_{grout}= 10 MPa and ν_{grout}= 0.22 (Mollon *et al.* [2013], Do *et al.* [2014c, 2014f]).

- Starting the construction of the second tunnel using the same procedure as performed for the first tunnel, which includes three phases ordered as the 4th phase, 5th phase, and 6th phase, respectively, in this study.

a)   b)
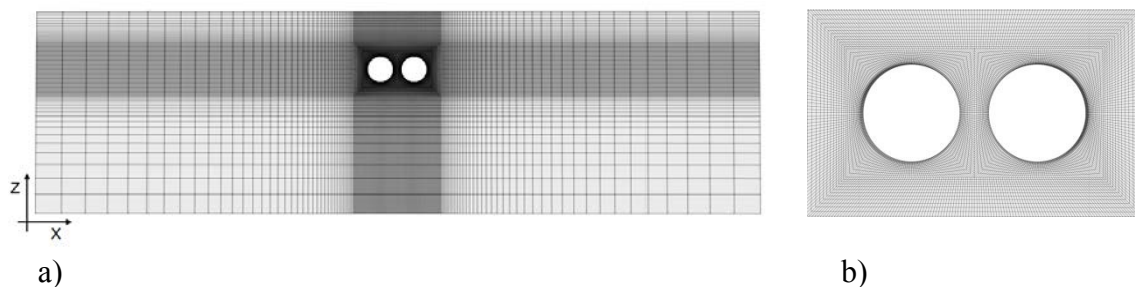
Figure 4-30. 2D numerical model (a); zoom of twin tunnels in case of tunnel distance B = 0.25 D (b)

Moller and Vermeer (2008) pointed out that different stress reduction factor, λ, are necessary to use to obtain good estimations in terms of surface settlement and normal forces. In their studied case, λ values of 0.6-0.7 were adopted for surface settlement, while λ value of about 0.3 was adopted for normal forces. For this reason, a λ value of 0.3 has been adopted in this section as mentioned above. This value is a preliminary choice but it can be acceptable due to the fact that the main purpose of parametric study introduced in this section is to show the influence of tunnel distance on the behaviour of linings in the two tunnels.

4.3.3. Parametric study

4.3.3.1. Impact of the second tunnel construction process on the first tunnel structure behaviour

The reference case (**Table** 4-1) with a joint number of 6 has been adopted in this study. Segment joints in the first tunnel are fixed at angles of 0^0, 60^0, 120^0, 180^0, 240^0, and 300^0 measured counter-clockwise from the right spring line. On the other hand, segment joint locations in the second tunnel have been changed in order to determine the effect of the joint distribution on the first tunnel behaviour.

For each tunnel distance value (B) which changes over a range from 0.25D to 3D, the numerical results, which are not presented in figures in this study, show that the joint distribution in the second tunnel has a negligible influence on both normal force and bending moment induced in the first tunnel. For this reason, all the other calculations performed in this study have conducted using a set of the segment joints in the second tunnel that are fixed at the same angle as those in the first tunnel mentioned above.

In this section, the bending moment ratio, R_M, and the normal force ratio, R_N, which are not graphed in the figures, are defined as the ratio of the maximum absolute value of the bending moment and normal force, respectively, induced in the lining of the first tunnel, that are determined at the 6th phase, to the corresponding ones developed in the first tunnel lining at the 3rd phase. It should be noted that the behaviour of the first tunnel determined at the 3rd phase can be considered as that of a single tunnel. The maximum values of the normal force and maximum/minimum values of the bending moment are presented in **Figure** 4-31, **Figure** 4-32 and **Figure** 4-33, respectively.

Figure 4-31 shows that the normal forces induced in both the jointed and continuous lining of the first tunnel, determined at the 6th phase, are considerably affected by the tunnel distance. As expected, the greater the tunnel distance, the lower the impact of the second tunnel on the normal force induced in the first tunnel. It should be noted that the normal force ratio R_N in a jointed lining is greater than that of a continuous lining when the tunnel distance is less than 1D. This means that the jointed lining in the first tunnel is more sensitive to the impact of the second tunnel construction than a continuous lining.
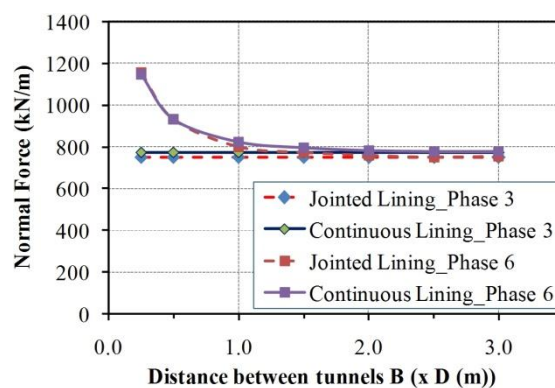
Figure 4-31. Maximum normal force induced in the first tunnel

Also at a tunnel distance that is less than 1D, **Figure** 4-31 presents a great impact of the second tunnel construction on the first tunnel, represented by high values of the R_N ratio. Generally, the magnitude of the normal forces induced in the first tunnel, after being interacted with the second tunnel, is greater than the one developed in a single tunnel. This suggests that an increase in the external load acting on the first tunnel was expected due to the excavation of the second tunnel. At a tunnel distance of about 2D, the R_N ratios, determined in both cases in which the jointed lining and continuous lining are used, are approximately unity (**Figure** 4-31). Beyond this distance, the influence of the second tunnel construction process on the first tunnel behaviour, in terms of the normal forces, can be neglected.

Figure 4-32 and **Figure** 4-33 presents a considerable influence of the tunnel distance on the bending moment induced in both jointed and continuous linings of the first tunnel. When the tunnel distance is less than 1D, an increase in the tunnel distance would result in a reduction in the absolute bending moment, determined at the 6th phase, in the first tunnel. This is consistent with the numerical results performed by Hossani *et al.* [2012]. Beyond this distance, the results show a negligible variation in the bending moment induced in the first tunnel. It should be noted that, at a tunnel distance that is less than about 0.5D, the bending moment ratio R_M is generally higher than unity. However, beyond this distance, the R_M value is always smaller than unity.
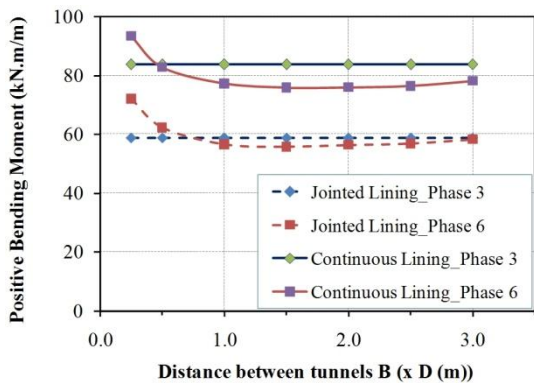
Figure 4-32. Maximum positive bending moment induced in the first tunnel.
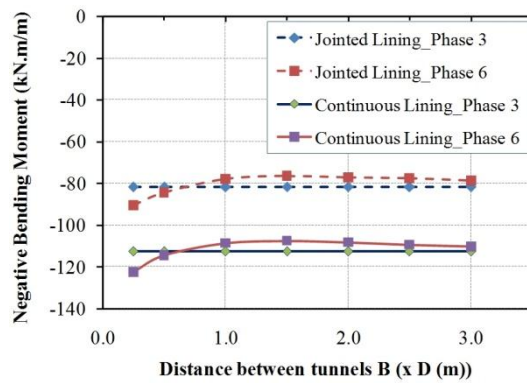
Figure 4-33. Minimum negative bending moment induced in the first tunnel.
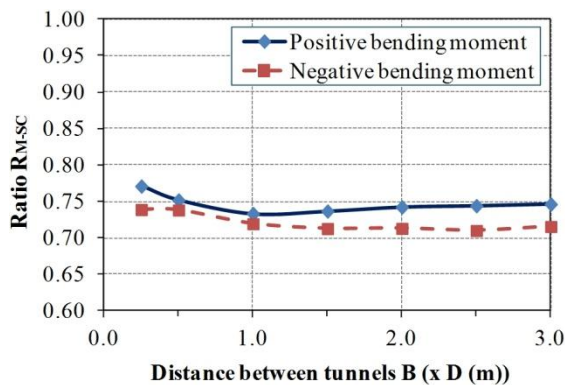
Figure 4-34. Influence of the tunnel distance on the ratio R_{M-SC}
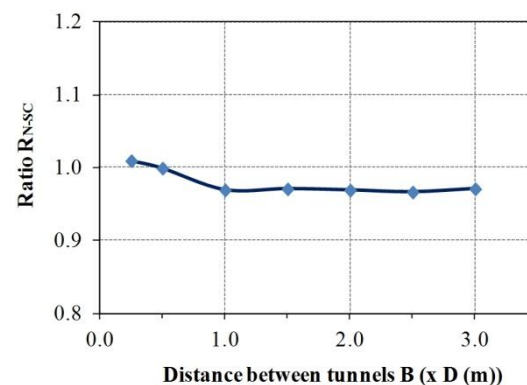
Figure 4-35. Influence of the tunnel distance on the ratio R_{N-SC}

Figure 4-34 and **Figure** 4-35 show the effect of the tunnel distance on the R_{M-SC} and R_{N-SC} ratios, which are defined as the ratio of the bending moment and normal force, respectively, induced in a jointed lining in the first tunnel, to the corresponding ones induced in a continuous lining. All of these structural lining forces were determined at the 6th phase. It should be noted that the bending moment induced in a jointed lining is always smaller than the one developed in a continuous lining due to the influence of the segment joints. The ratio R_{M-SC} changes over a range from 0.715 to 0.742 and from 0.735 to 0.77, corresponding to the negative bending moment and positive bending moment. However, the normal forces seem to be not significantly affected by the segment joints. Indeed, the R_{N-SC} ratio changes over a range from 0.969 to 1.001.

4.3.3.2 Impact of the first tunnel construction process on the second tunnel structure behaviour

Figure 4-36 to **Figure** 4-40 present the dependence of the structural lining forces induced in the two tunnels on the tunnel distance. The R_{M21} and R_{N21} ratios are defined as the ratio of the bending moment and normal force, respectively, induced in the second tunnel to the corresponding ones developed in the first tunnel. All of them were determined at the 6th phase.

As can be seen in **Figure** 4-36, due to the impact of the first tunnel excavation, the normal force developed in the second tunnel is generally higher than that induced in the first tunnel measured at the 3rd phase, which corresponds to the behaviour of a single tunnel, especially at a tunnel distance (B) which is less than 1D. The maximum differences of about 22.3 % and 21.6 % corresponding to the cases of a jointed lining and a continuous lining were obtained at a tunnel distance of 0.25D (**Figure** 4-36)
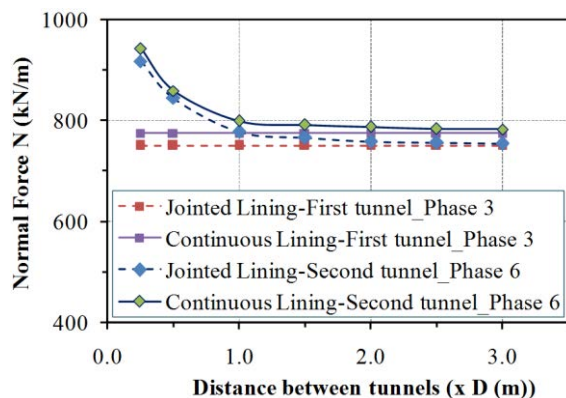
Figure 4-36. Maximum normal force induced in the second tunnel
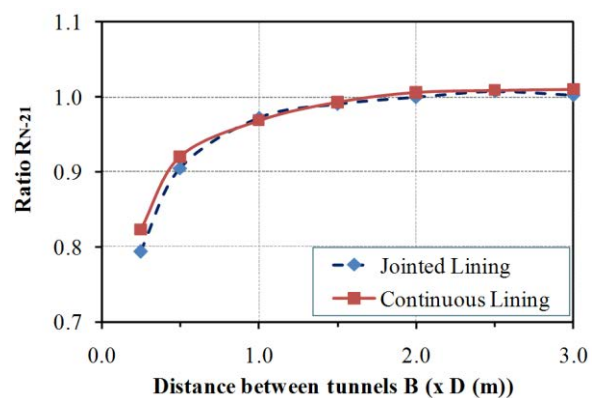
Figure 4-37. Influence of the tunnel distance on the ratio R_{N21}

Figure 4-37 shows that the normal force in the second tunnel lining is generally smaller than that in the first tunnel lining determined at the 6th phase. The R_{N21} ratio is usually less than unity. This suggests that more loads are taken by the first tunnel than by the second tunnel. Similar observations were also obtained through 3D numerical analyses of twin new

Austrian tunnelling method tunnels performed by Ng. *et al.* [2004]. For a jointed lining, the R_{N21} ratio is generally smaller than that of a continuous lining. In other words, compared to the case of continuous lining, greater difference between the normal forces induced in two parallel tunnels supported by jointed linings is expected.

Figure 4-36 and **Figure** 4-37 also show that the impact between two tunnels is more considerable when the tunnel distance (B) is less than 1D. At a tunnel distance of about 2D, the R_{N21} ratios determined in both cases in which jointed and continuous linings are used are approximately unity. One again, it is possible to conclude that, beyond this distance, the impact between two tunnels excavated in parallel, in terms of the normal force, can be ignored. This conclusion is in good agreement with the results obtained in the Hage Chehade and Shahrour [2008] study, which was also performed using a 2D model. In their study, the critical distance of the influence between two tunnels was determined on the basis of the settlement trough that developed on the ground surface. However, different from the results in Hage Chehade and Shahrour [2008] study, in which the bending moment and normal forces induced in the second tunnel were negligibly affected by the tunnel distance, a strong dependence of the normal forces induced in the second tunnel on the distance between two tunnels that obtained in this study has been shown. The above difference could be attributed to the fact that, unlike the numerical model in this study, the effect of the grouting pressure and segment joints was not taken into consideration in the study of Hage Chehade and Shahrour [2008].
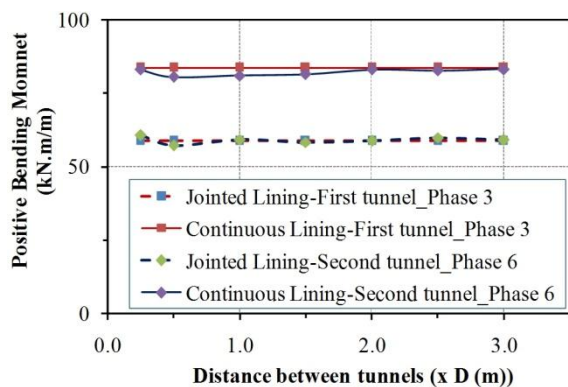
Figure 4-38. Maximum positive bending moment induced in the second tunnel.
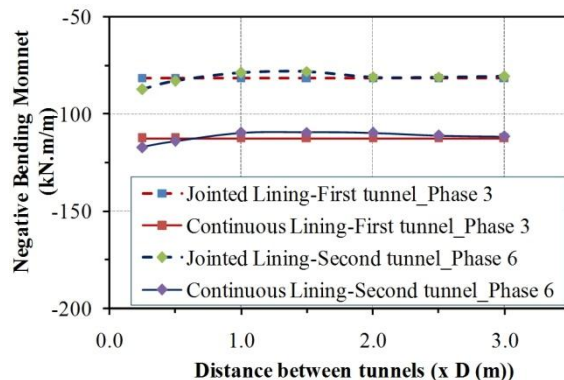
Figure 4-39. Minimum negative bending moment induced in the second tunnel.
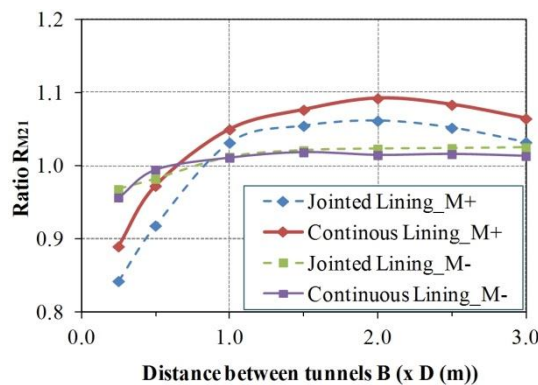
Figure 4-40. Influence of the tunnel distance on the ratio R_{M21}

Chapter 4: Two-dimensional numerical analyses   115

Figure 4-38 and **Figure** 4-39 present the bending moment in both tunnels determined at the 3rd and 6th phases, respectively. The behaviour of the first tunnel determined at the 3rd phase can be considered as that of a single tunnel. **Figure** 4-38 shows that the positive bending moment in the second tunnel is generally smaller than that developed in a single tunnel. Whereas, apart from the tunnel distance which is greater than 0.5D, the absolute negative bending moment in the second tunnel is greater than the one induced in a single tunnel (**Figure** 4-39). The maximum difference of the bending moment determined in the two tunnels is about 7 %.

As the tunnel distance is lower than 0.75D, the R_{M21} ratio is generally lower than unity. This means that for this range of the tunnel distance, the bending moments in the first tunnel are greater than that of the second tunnel (**Figure** 4-40). In contrary, beyond the tunnels distance of 0.75D, the R_{M21} ratio is generally higher than unity.

When the tunnel distance is less than 1D, an increase in the tunnel distance will result in a significant increase in the R_{M21} ratio determined in both cases of jointed and continuous linings. Apart from the tunnel distance which is less than 1D, the negative bending moment ratio determined at the tunnel side wall (due to the K_0 value of 0.5 in this reference case) is not sensitive to the change in the tunnel distance.

4.3.4. Conclusions

This section presents 2D numerical analyses of twin tunnels excavated in close proximity in order to investigate the influence of both the segment joints and tunnel distance on the structural forces induced in the tunnel lining. The impact of the second tunnel construction process on the first tunnel, and vice versa, in terms of the bending moment and normal force, has been discussed. The numerical investigation has shown a considerable effect of the segment joints and tunnel distance on the behaviour of both tunnels.

Owing to the excavation of the second tunnel, an increase in the external load acting on the first tunnel was expected. The greater the tunnel distance, the lower the impact of the second tunnel on the normal force in the first tunnel. A jointed lining in the first tunnel is more sensitive to the impact of the second tunnel construction than a continuous lining. At a tunnel distance of about 2D, the variation in the normal forces induced in the first tunnel due to the impact of the second tunnel, for both cases in which the tunnel is supported by jointed lining and continuous lining, can be ignored.

When the tunnel distance is less than 1D, an increase in the tunnel distance would result in a reduction in the absolute bending moment determined at the 6th phase in the first tunnel. Beyond this distance, the results show a negligible variation in the bending moment induced in the first tunnel.

The variation in the joint distribution in the second tunnel has a negligible influence on both normal force and bending moment induced in the first tunnel.

Due to the impact of the first tunnel excavation, the normal force in the second tunnel is generally higher than that induced in a single tunnel, especially at tunnel distance which is

less than 1D. However, the normal force determined at the 6th phase in the second tunnel is generally smaller than that induced in the first tunnel. The R_{N21} ratio is usually less than unity. For a jointed lining, the R_{N21} ratio is always smaller than that of a continuous lining.

Generally, the results show that the impact between two tunnels is more considerable when the tunnel distance is less than 1D. At a tunnel distance of about 2D, the impact of the first tunnel construction process on the second tunnel behaviour can be negligible.

Above results made it possible to conclude that beyond a tunnel distance of 2D, the impact between two tunnels excavated in close proximity, in terms of the normal force, can be ignored.

4.4. General conclusions

2D numerical analyses have been conducted to investigate:
- The factors that affect the behaviour of segmental tunnel linings;
- The simplified excavation methods, that is, the CCM method and the VLM method, that are used to represented 3D problem during tunnelling using a 2D model;
- The interaction between two tunnels excavated in close proximity to each other.

The influences of the joint distribution, joint stiffness (including the rotational stiffness, the axial stiffness, the radial stiffness, and the non-equal rotational stiffness assigned at the joints) and the ground conditions, such as Young's modulus of the ground and the lateral earth pressure factor, have been studied in detail. The numerical results show a significant reduction in the bending moment induced in the tunnel lining as the joint number increases. The tunnel behaviour in terms of the bending moment considering the effect of joint distribution, when the lateral earth pressure factor K_0 is equal to 0.5, 1.5 and 2, is almost similar and differs when K_0 is equal to unity. It has been seen that the influence of joint rotational stiffness, the reduction in joint rotation stiffness under the negative bending moment, the lateral earth pressure factor and Young's modulus of the ground surrounding the tunnel should not be neglected. On the other hand, the results have also shown an insignificant influence of the axial and radial stiffness of the joints on segmental tunnel lining behaviour.

Significant difference has been shown between the structural lining forces and the surface settlement obtained when the volume loss method and the convergence-confinement method are used. A comparison with 3D numerical results indicated that, for the same surface settlement, the structural lining forces determined with the CCM method are in better agreement with the 3D numerical results than those obtained with the VLM method.

The results show that the impact between two tunnels is more considerable when the tunnel distance is less than 1D. At a tunnel distance of about 2D, the impact of the first tunnel construction process on the second tunnel behaviour can be negligible.

The presented results indicate the necessity of considering the effect of the joints during segmental tunnel lining design.

Segmental tunnel lining is a 3D structure, in which joint pattern in successive rings is usually staggered. This means that 2D calculations mentioned above corresponds only to a

particular case where the joints in successive rings are in line along the longitudinal tunnel axis. For other cases of the joint pattern, it is necessary to use 3D calculations.

Chapter 5

Three-dimensional Numerical Analyses

5.1. Numerical Investigation of a Single Tunnel

5.1.1. Introduction

The purpose of a numerical mechanized tunnelling (TBM) model is to take into consideration the large number of processes that take place during tunnel excavation, such as the applied face pressure, the shield overcutting, the shield conicity, the annular void behind the shield, the grout injection in this void and its consolidation process, the segmental concrete lining, the TBM weight distribution and that of other equipment. In order to conduct a rigorous analysis, a 3D numerical model should be used to take into account all these processes.

Tunnel structure behaviour is a complex phenomenon in which the behaviour of the surrounding ground is one of the main aspects of a tunnel excavation that should be taken into account. Consequently, a realistic ground constitutive model is crucial to estimate the structural force induced in a tunnel structure and ground displacement. Nevertheless, most finite element calculations are still performed using simple constitutive models, because they require a limited number of parameters and the calculation times tend to be smaller than those using advanced soil constitutive models (e.g., Melis et al. [2002], Migliazza et al. [2009], Mroueh and Shahrour [2008], and **Table 1-3**). In general, simple constitutive models lead to a shallower and wider settlement trough than the one observed experimentally (Addenbrooke et al. [1997], Bolton et al. [1994], Hejazi et al. [2008], Lambrughi et al. [2012], Mašin and Herle [2005], Medina Rodríguez [2008]) or even give unrealistic predictions with a surface heave above the tunnel centerline (Mašin [2009]). In order to take into account some of the fundamental aspects of soil behaviour, such as the variation in the stiffness modulus, according to the stress state, and the difference in the modulus during the unloading and loading phases, it is at least necessary to use an elasto-plastic model with strain hardening. The cap-yield soil (CYsoil) model, which is a strain hardening constitutive model that takes into consideration hyperbolic behaviour, has been adopted. This constitutive model is available in the FLAC^{3D} software (Itasca [2009]).

The main purpose of this chapter was to provide 3D models of single tunnel, which would allow the tunnel lining behaviour, displacement of the ground surrounding the tunnels to be evaluated. Most of the main elements of a mechanized excavation are simulated in this model: the initial condition at the model boundary, the conical geometry of the shield, the face pressure, the circumferential pressure acting on the soil surface in the working chamber behind the tunnel face, the circumferential pressure due to the migration of the grout acting on the soil surface and at the shield tail, the grouting pressure acting simultaneously on the soil surface and tunnel structure after the shield tail, the progressive hardening of the grout, and the jacking force. The influence of the joint pattern of the lining, pertaining to both segment joints and ring joints as well as their connection condition, have been taken into consideration.

The Bologna-Florence railway high speed line project described in section 4.1 has been adopted in this study as a reference case. The mechanical characteristics of the tunnel lining

are shown in **Table** 4-1. All the calculations have been performed under drained conditions. The behaviour of a tunnel, during the excavation process, has been studied in detail using the developed model. In addition, the influence of the initial conditions and lining segmentation on the tunnel behaviour and ground displacement has been highlighted. The main content of this section has been published in Do et al. [2014f].

5.1.2. Constitutive models

5.1.2.1. CYsoil model

The CYsoil model is a strain-hardening constitutive model that is characterized by a frictional Mohr-Coulomb shear envelope and an elliptic volumetric cap in the (p', q) plane. Apart from the cap-hardening law and the compaction/dilation law, which allow the volumetric power law behaviour observed in isotropic compaction tests and the irrecoverable volumetric strain that occurs as a result of soil shearing to be captured, the friction hardening law in the CYsoil model offers the possibility of alternatively expressing the hyperbolic behaviour. In the CYsoil model, the stiffness is adopted as a function of the effective confinement and it leads to a higher value for unloading-reloading stiffness. For the CYsoil model, if friction hardening behaviour is adopted, the input parameters are (Itasca [2009]):

- Elastic tangent shear modulus G^e_{ref} at reference effective pressure p^{ref} (equal to 100 kPa) ($G^e_{ref} = E/(2(1+\nu))$);
- Failure ratio R_f which is a constant and smaller than 1 (0.9 in most cases);
- Ultimate friction angle ϕ_f and
- Calibration factor β.

5.1.2.2. Parameter calibration

Due to the lack of data for the calibration of the CY constitutive model parameters, several procedures have been adopted:

- For G^e_{ref}, G^e, K^e and ϕ_f: Numerical models of drained triaxial tests corresponding to the different depths (half of the overburden, top of the tunnel and bottom of the tunnel) in the reference case have been simulated in order to calibrate these parameters of the CY soil model. The calibration results are presented in **Table 5-1**. **Figure** 5-1 illustrates an example of the deviatoric stress-strain relationships obtained for a confinement pressure value σ_3 of the different depths. The CY soil model parameters applied for a confinement pressure σ_3 of 170 kPa at the tunnel spring line have been chosen for numerical analyses in this study (**Table 5-1**).

- β has been varied. A settlement point at the soil surface was used to fit in the back analysis (Croce [2011]).

- Recommendations made by Itasca [2009] have been used to fix R_f as a constant (**Table 5-1**).
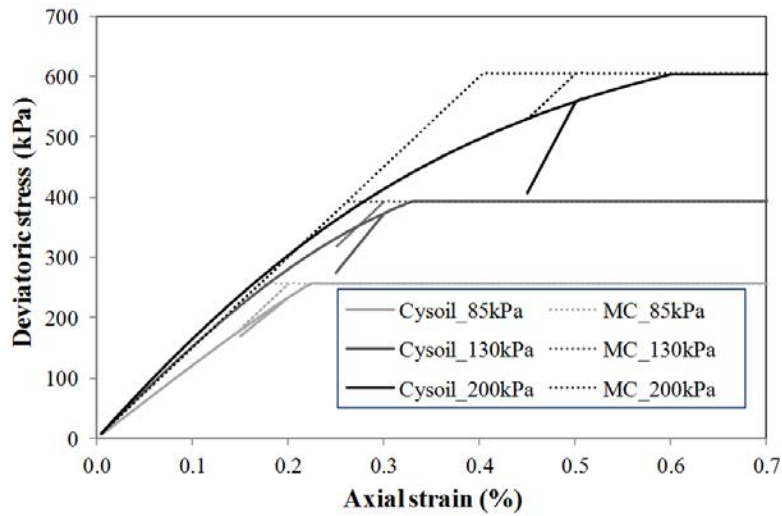
Figure 5-1. Stress-strain curves with loading-unloading phases
(MC: Mohr-Coulomb constitutive model)

Table 5-1. Ground properties

MC model	Value	CYsoil model	Value
E (Young's modulus) (MPa)	150	Reference elastic tangent shear modulus G_{ref}^e (MPa)	58
ν (Poisson ratio)	0.3	Elastic tangent shear modulus G^e (MPa) $G^e = G_{ref}^e \left(\sigma_3 / p^{ref} \right)$	98
φ (friction angle) (degrees)	37	Elastic tangent bulk modulus K^e (MPa) $K^e = K_{ref}^e \left(\sigma_3 / p^{ref} \right)$	213
ψ (dilation angle) (degrees)	0	Reference effective pressure p^{ref} (kPa)	100
c (cohesion) (kPa)	0	Failure ratio R_f	0.9
K_0 (lateral earth pressure factor)	0.5	Ultimate friction angle ϕ_f (degrees)	37
		Calibration factor β	2.35

5.1.3. The adopted numerical model

5.1.3.1. Three-dimensional numerical procedure for mechanized tunnelling

The model has been developed using the FLAC^{3D} software (Itasca [2009]). The analyses have been performed using small strain calculations.

Mechanized tunnelling is in fact a continuous process with a continuous support pressure and continuous installation of the lining segments. 3D simulation in shield tunnelling started as a simplified single-step approach (Lee and Rowe [1991]). However, the most popular trend in recent years has been to use the step-by-step procedure (Barla et al. [2005], Blom et al.

[1999], Boubou [2010], Brinkgrave and Broere [2003], Hossaini et al. [2012], Jenck and Dias [2003], Kasper and Meschke [2004], Melis et al. [2012], Möller, [2006], Mollon et al. [2013], Mroueh and Shahrour [2008], Phienwej et al. [2006], Swoboda et al. [2004]). The later procedure has been adopted in this study. Accordingly, each excavation step corresponds to an advancement of the tunnel face of 1.5m, which is equal to the width of a lining ring.

5.1.3.2. Simulation of different phases of the mechanized tunnelling process

A 3D numerical model has been developed which allows the advancement of the TBM in the ground to be simulated, taking into account the components and procedures that can occur in actual tunnel excavation as much as possible. In general, a tunnelling process consists of three main phases (Bernat and Cambou [1998], Boubou [2010], Dias and Kastner, [2012], Jenck and Dias [2004]):
  (1) Excavating the ground at the tunnel face and simultaneously applying a confinement to ensure tunnel face stability.
  (2) Installing the tunnel lining, applying the jacking force and injecting the grout behind the segments in order to fill the voids created at the shield tail.
  (3) The TBM continues to advance, and the ground begins to become stabilized, which is expressed by a consolidation phase.

5.1.3.2.1. Modelling Phase 1: tunnel face confinement and shield passing

Modelling the face support

The confinement pressure acting at the tunnel face plays an important role in ensuring tunnel stability during the excavation process; the tunnel face will not collapse and no water can penetrate the tunnel.

In this work, the face pressure has been presented as a trapezoidal profile in order to account for the density of the slurry. The unit weight of the slurry is 11 kN/m^3. The normal method to choose the value of the face pressure is based on the vertical stress σ_v in the soil mass (Maranha and Neves [2000], Mollon [2010], Mollon et al. [2013]). The value of the average face pressure (applied at the tunnel axis) is thus generally set equal to the horizontal ground pressure (Mollon [2010], Mollon et al. [2013]):

$$\sigma_t = K_0 \cdot \sigma_v \qquad\qquad (5\text{-}1)$$

In this expression, K_0 is the lateral earth pressure factor, and σ_v is the vertical soil overburden pressure at the tunnel axis. The applied pressure is taken equal to $\sigma_t = 150$ kPa for all of the presented numerical analyses.

Due to slight overcutting, a possible slurry migration could occur over a short distance behind the cutting wheel (Dias et al. [2000], Mollon [2010], Mollon et al. [2013]). Therefore,

in addition to the pressure acting on the tunnel face, a certain pressure, caused by the slurry solution, has also been applied to the cylindrical surface just behind the tunnel face. In this study, the cylindrical surface corresponds to the excavation chamber situated between the excavated face and the shield. This slurry is simulated by means of a uniform pressure diagram over a length of 1.5m and this is followed by a reduced pressure acting over a 1.5m length with a triangular distribution (see **Figure** 5-4).

Modelling the TBM shield

As far as the shield machine simulation is concerned, Chakeri et al. [2013] modelled the EPB shield machine using shell elements with elastic modulus of 200 GPa, Poisson's ratio of 0.25 and the density 7840 kg/m^3. Shell elements were also adopted to simulate shield machines by Broere and Brinkgreve [2002], Brinkgreve and Broere [2003], Swoboda et al. [2004], Klotz et al. [2006], Phienwej et al. [2006], and Ercelebi et al. [2011].

In Melis et al. [2002], solid volume elements were adopted to simulate the EPB shield. Their unit weight was the ratio between the total shield weight and its apparent volume. The shield and ground meshes were created and could deform independently due to the fact that they were separated by an interface layer. This interface, with appropriate mechanical properties, prevented the soil from penetrating the EPB mesh and allowed contact forces to be developed. A similar way of modelling a shield machine was also adopted by Kasper and Meschke [2004]; the TBM was considered as a separate body connected to the surrounding soil by means of interface elements. After each excavation step, a re-meshing procedure was employed prior to the next step.

For the sake of simplicity, the "fictive" shield introduced by Dias et al. [2000], Jenck and Dias [2004], Simic [2006], Mollon [2010], Mollon et al. [2013], has been adopted in the present model using a numerical test performed at each computation cycle (i.e. at each pseudo-time step in the Lagrangian finite-difference resolution scheme) and at any point that could be in contact with the shield during the excavation. The position of each of these points has been computed at each computation cycle, and this position has been artificially fixed when this point begins to be in contact with the "fictive" shield. The geometrical parameters of the shield are presented in **Figure 5-4**.

Modelling the jacking forces

The jacking force is one of the primary segment loads in the construction stage (JSCE [1996], Maidl et al. [1996], Takano [2000]).The distribution of the jacking force is uneven over the tunnel height. The jack force is greater at the bottom of the tunnel than at the top. This is caused by the moments the jacks have to exert (Rijke [2006]). The distribution of the jacking force used in this study has been assumed to be linear over the height of the tunnel. The jacking forces have been simulated in the present model through concentrated forces acting directly on the nodes located at the edge of the segment. These jacking forces have been set on each segment considering three plates located at 1/6, 1/2, and 5/6 of the segmental

length. A total jacking forces of about 40 MN has been adopted in the present model on the basis of the theoretical method proposed by Rijke [2006].

5.1.3.2.2. Modelling Phase 2: injection at the shield tail

In general, after being injected into the void behind the shield tail, the grouting action is modelled through two phases: (1) the liquid state (state 1) represented by a certain pressure acting on the soil surface and on the tunnel lining; (2) the solid state (state 2) (Melis et al. [2002], Mollon [2010], Mollon et al. [2013]).

As far as the grout pressure distribution over the tunnel height is concerned, there is still no unique rule that is accepted by researchers (Bezuijen and Talmon [2004], Hasimoto et al. [2004], Rijke [2006], Talmon and Bezuijen [2009]). For the sake of simplicity, the grouting pressure distribution at the shield tail in this study is assumed to linearly increase with depth due to the grout unit weight effect (Bezuijen and Talmon [2004]). This has been simulated using distributional radial pressure (Brinkgrave and Broere [2003], Kasper and Meschke [2006a], Melis et al. [2002], Mollon [2010], Mollon et al. [2013]). The grout pressure applied to the tail void is generally set to (Mollon [2010], Mollon et al. [2013]) (see Equation (4-3)). A σ_{inj} value of 180 kPa at the tunnel crown has been adopted in the present model. The grout is simulated by adopting a uniform pressure which is applied to both the cylindrical surface of the excavated soil and external surface of the tunnel lining.

As for the face pressure, the annular void between the outside surface of the shield and the excavated soil makes the migration of some grout towards the shield possible. This migration is simulated by means of a triangular pressure on a certain length (Mollon [2010], Mollon et al. [2013]). In this study, the length of grouting pressure acting on the lining and the migration length of the grouting pressure on the annulus void have been chosen arbitrarily equal to the length of one ring (1.5 m).

5.1.3.2.3. Modelling Phase 3: grout consolidation and lining installation

Modelling the grout consolidation

Generally, a linear elastic model is employed to simulate the hardening of grout (Dias and Kastner [2012], Lambrughi et al. [2012], Mollon [2010], Mollon et al. [2013], Phienwej et al. [2006]). In this study, the grout has been assumed to harden beyond the length of the grouting pressure at the shield tail mentioned above. The hardened grout in the present model has been simulated by means of volume elements with perfect elastic behaviour, and with the elastic characteristics E_{grout}= 10 MPa and ν_{grout}= 0.22 (Dias and Kastner [2012], Mollon [2010], Mollon et al. [2013]) (see **Table** 4-1).

Obviously, the above simulation is a very simple way of considering grout solidification behind the shield tail. However, it was here chosen because of its simplicity and because it has already been successfully used in Dias and Kastner [2012], Mollon [2010] and Mollon et al. [2013].

Modelling the segmental lining

In the present model, the tunnel segments have been modelled using a linear-elastic embedded liner element. Detail description of the lining model and segment joints can be found in section 4.1.3. The values of the spring constants (see **Table** 4-3) used to simulate the segment joints have been determined on the basis of the simplified procedures presented by Thienert and Pulsfort [2011] and reproduced in section 4.1 (also see Do et al. [2013a]).

Besides the simulation of the segment joints mentioned in section 4.2.2, the ring joints between successive rings along the tunnel axis have also been modelled in the 3D numerical model using double connections (**Figure 5-2**). In this study, the rigidity characteristics of the ring joint connection have been represented by a set composed of a rotational spring ($K_{\theta R}$), an axial spring (K_{AR}), and a radial spring (K_{RR}), as depicted in **Figure 5-3**. The interaction mechanism of each spring is the same as the one applied for a segment joint. The attachment conditions of the translational component in the x direction (tangential to the tunnel boundary) and two rotational components around the y and z directions have been assumed to be rigid for all the investigated cases. The interaction mechanism and stiffness value of each spring is the same as those applied for a segment joint.
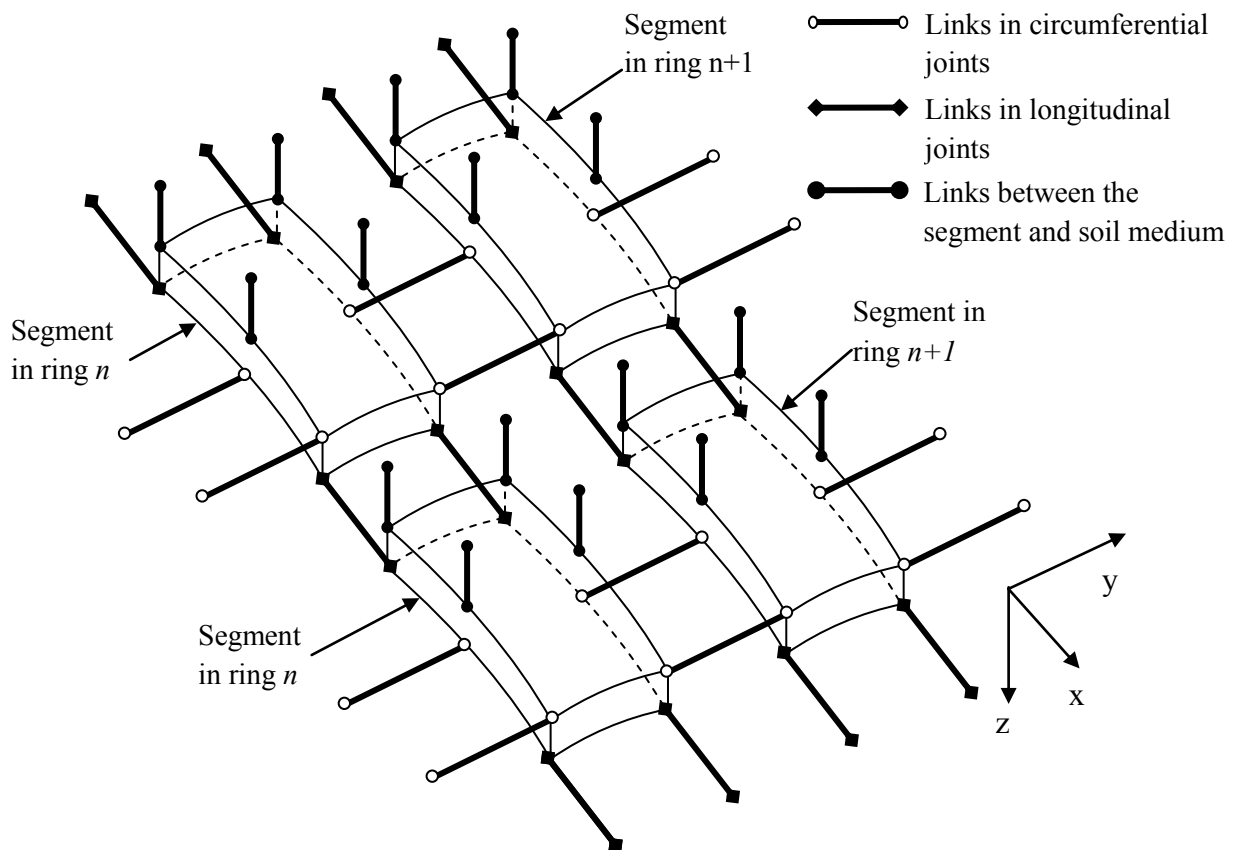
Figure 5-2. Ring joint scheme
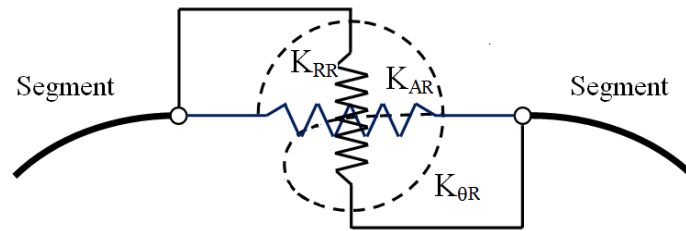
Figure 5-3. K_{AR}, K_{RR}, $K_{\theta R}$ stiffness in the axial, radial and rotational directions of a ring joint

5.1.3.3. Developed numerical model

A number of parametric studies were carried out in previous works (Medina Rodríguez, 2000) in order to evaluate the minimum dimensions of the domain size. As a result, the following values were obtained:

- (H + 4D), for the mesh height,
- (H + 3D), for the mesh length,
- 3H, for the mesh width (for half of the model).

where H is the tunnel axis depth and D is the tunnel diameter.

Owing to the arbitrary distribution of the joints in the cross section, a full 3D model is necessary. A full model with a height of 60m and a width of 120m has been adopted in the present model. The mesh length of the model is equal to 120m. This number has not been chosen arbitrarily and will be explained later on. The excavation step length is equal to 1.5 m, and corresponds to the width of a lining ring. A schematic view of the present model is provided in **Figure 5-4**. The model introduced in **Figure 5-5** is composed of around 504,627 grid points and 480,000 zones.
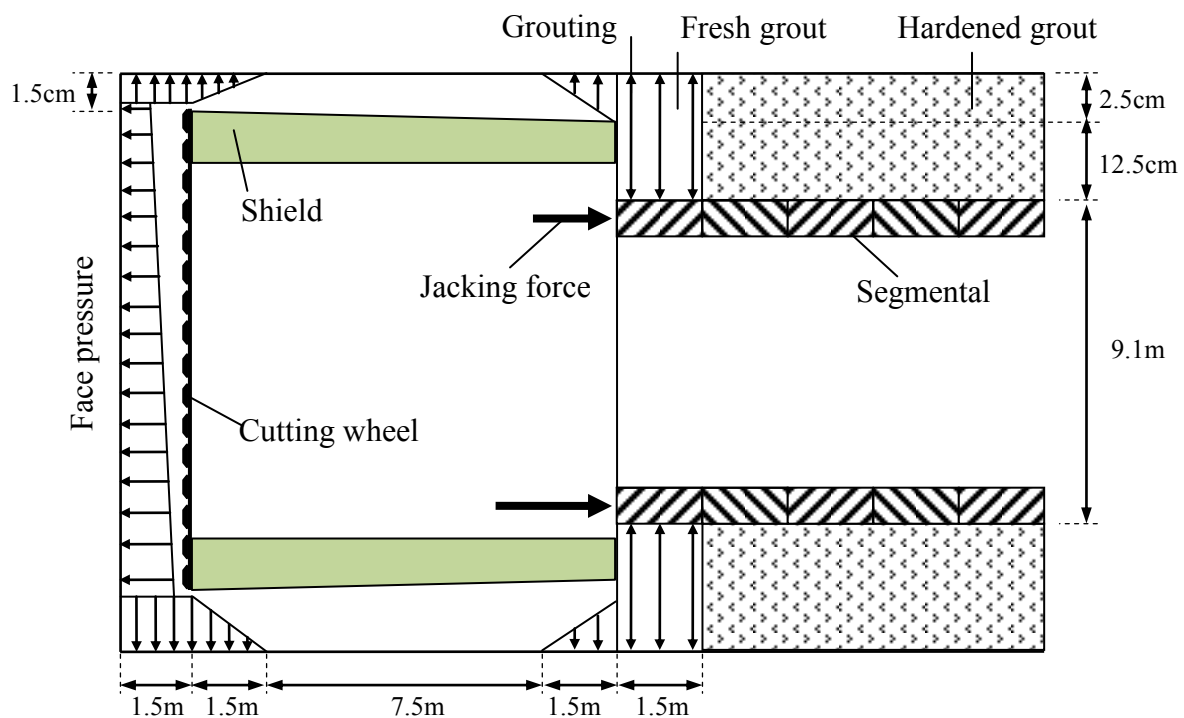
Figure 5-4. Layout of the proposed TBM model
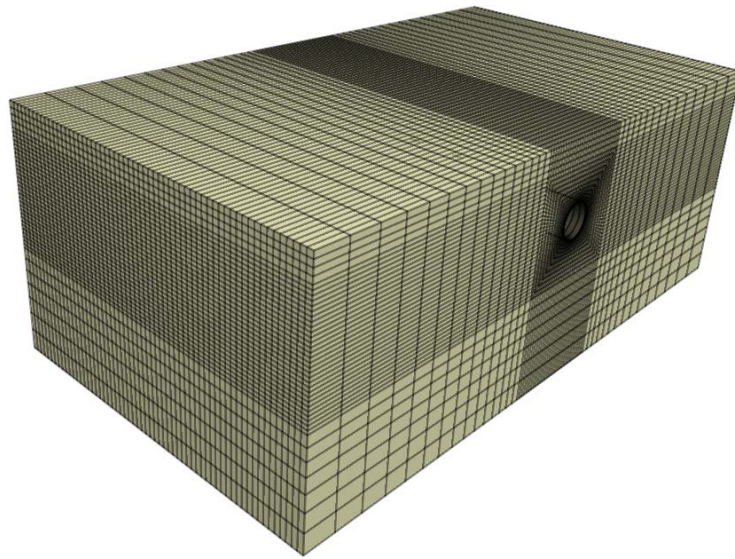
Figure 5-5. Perspective view of the developed numerical model introduced into FLAC^{3D}

Six lining models have been examined to consider the effects of the joint pattern and the coupling effect (**Figure 5-6**):

- Model M1 - Continuous lining: the attachment conditions of the joint connections, including both the segment joint and ring joint, are assumed to be rigid (**Figure 5-6**a);
- Model M2 - Straight joint (type 1 joint pattern): the segment joints of successive rings lie on a line. The rigidity characteristics of both the segment joint and ring joint have been considered (**Figure 5-6**b);
- Model M3 (the reference model) - Staggered joint (type 2 joint pattern): the segment joints between successive rings are staggered according to type 2 (**Figure 5-6**c). The rigidity characteristics of both the segment joint and ring joint have been considered (**Figure 5-6**b);
- Model M4 - Staggered joint (type 3 joint pattern): the segment joints between successive rings are staggered according to type 3 (**Figure 5-6**d). The rigidity characteristics of both the segment joint and ring joint have been considered;
- Model M5 - Staggered joint (type 2 joint pattern) with a rigid link at the ring joint: the lining conditions are similar to model M3, with one difference: the ring joints between successive rings have been assigned as rigid (**Figure 5-6**e);
- Model M6 - Staggered joint (type 2 joint pattern) with a free link at the ring joint: the lining conditions are similar to model M3, with one difference: the ring joints between successive rings have been assigned as free (**Figure 5-6**f);

The locations of the segment joints in each ring are presented in **Table 5-2**. Finally, it should be mentioned that the average time requested for one calculation is approximately 190 hours when using a 2.67GHz core i7 CPU computer.

a) **Model M1** - Continuous Lining

b) **Model M2** - Straight Rings - Type 1 joint pattern

c) **Model M3** (The reference model) - Staggered Rings - Type 2 joint pattern

d) **Model M4** - Staggered Rings - Type 3 joint pattern

e) **Model M5** - Staggered Rings - Type 2 joint pattern, Rigid link at the ring joint

f) **Model M6** - Staggered Rings - Type 2 joint pattern, Free link at the ring joint
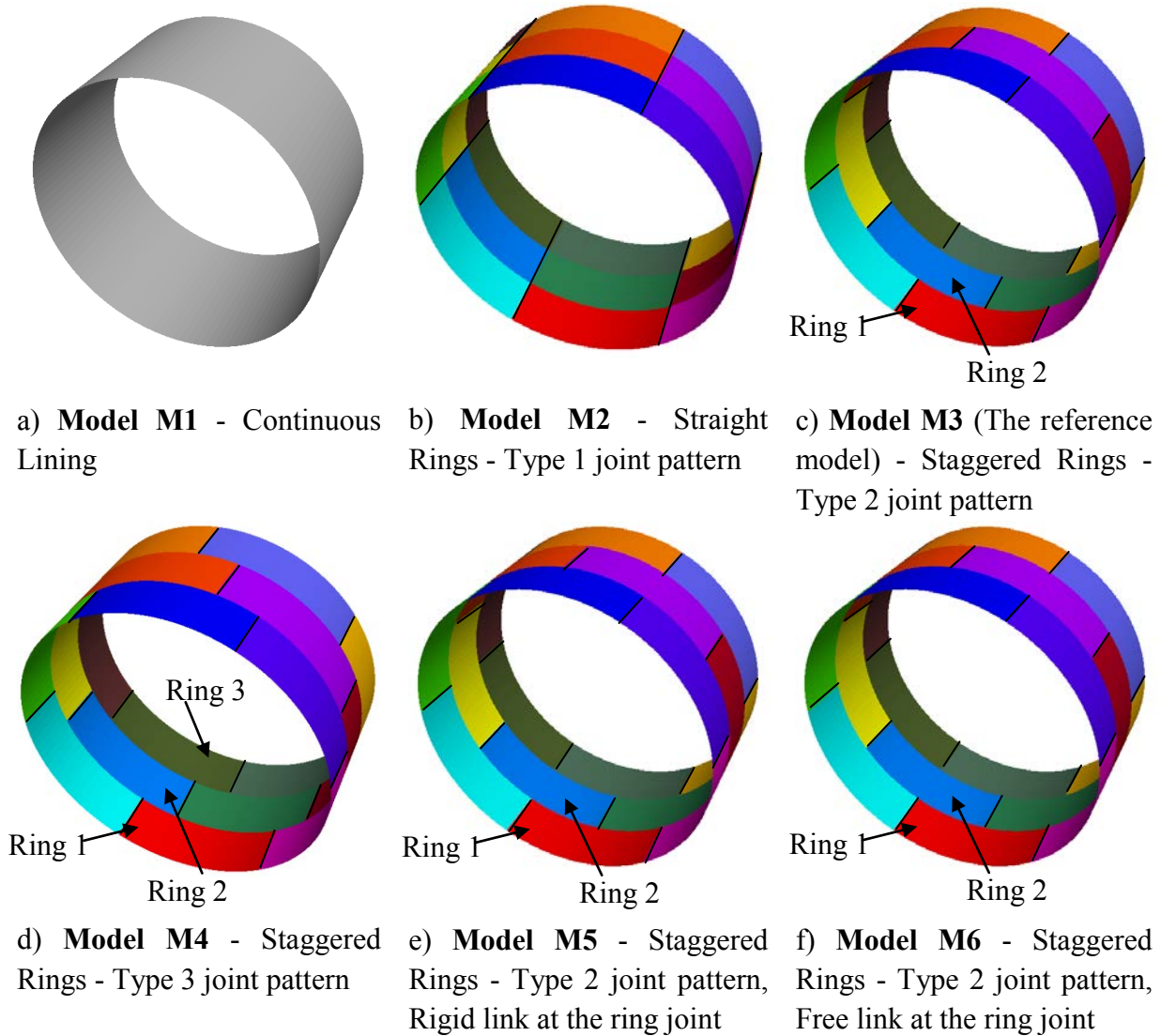
Figure 5-6. Considered lining models

Table 5-2. Location of the segment joints in a ring θ (degrees) (see **Figure 5-6** for the ring order)

Ring order	Type 1 joint pattern (model M2)	Type 2 joint pattern (model M3, M5, M6)	Type 3 joint pattern (model M4)
Ring 1	0;60;120;180;240;300	0;60;120;180;240;300	0;60;120;180;240;300
Ring 2	-	30;90;150;210;270;330	15;75;135;195;255;315
Ring 3	-	-	30;90;150;210;270;330

5.1.4. Numerical results and discussions

5.1.4.1. Settlement prediction method

Figure 5-7 present the settlement prediction results obtained using the method proposed by Mollon [2010] and Mollon et al. [2013] which allows the settlement above a tunnel to be

determined using a minimum number of excavation steps. The lining pattern of model M3 (the reference model) has been adopted during the FLAC^{3D} simulation in this section.

The total settlement above a tunnel can be evaluated on the basis of the instantaneous settlement estimated at excavation step 38, which is computed as the difference between the total settlement at step 38 and that obtained at step 37, through an integration calculation.

As in the work of Mollon [2010] and Mollon et al. [2013], this figure (especially the settlement curve at the tunnel crown) provides some interesting information on the phenomena that occur during excavation. A progressive decompression of the soil can be observed at about 5 m upstream from of the tunnel face due to face excavation. A much larger settlement appears because of the overcutting in the area surrounding the cutting wheel. A small increase in settlement, related to the conicity of the shield, appears behind this ''peak''. The grout injection pressure at the tail void induces a negative settlement (i.e., soil heave) at the end of the shield, and the grout compression induces a final settlement peak. It should be noticed here that the use of the CY constitutive soil model in the present study, represents an improvement in comparison with the use of an elastic perfectly plastic model with a shear failure criterion of Mohr Coulomb type. Due to the fact that the non linearity and the unloading-reloading behaviour are taken into account, the effects of the grout pressure and the grout solidification are less important (Mollon et al. [2013]). However, improvements would take into account the evolution of the soil density with the stress state. In addition, freshly made grout behaves as a viscous liquid. Its viscosity increases in time until the grout became a solid. The grout behaviour develops smoothly from the viscous phase to the solid one. It should then be noticed that if a more complex constitutive model (including viscous/solid phase change) of the grout were used, the effects of the grout could be much less important.

Figure 5-7 shows that the instantaneous settlement curves at the 38th step are not disturbed by the model boundaries, the instantaneous settlement being equal to zero at Y = 0 m and Y = 82.5 m. This means that, a model with the dimension of 82.5 m in the Y direction is sufficient for the purpose of settlement determination. The influence of length in the upstream from the tunnel face is therefore about 25.5 m (82.5-38*1.5=25.5). This property is the reason why 38 excavation steps were chosen to assess the final settlement.

The final settlement is obtained through a simple summation of the instantaneous settlement curves in which the settlement at any coordinate Y is equal to the sum of the previous instantaneous settlements induced at this point by all the stages that were performed (Mollon et al. [2013]). This procedure also allows the influence of model boundary conditions on the computed displacement to be eliminated, as can be seen in **Figure 5-8**.
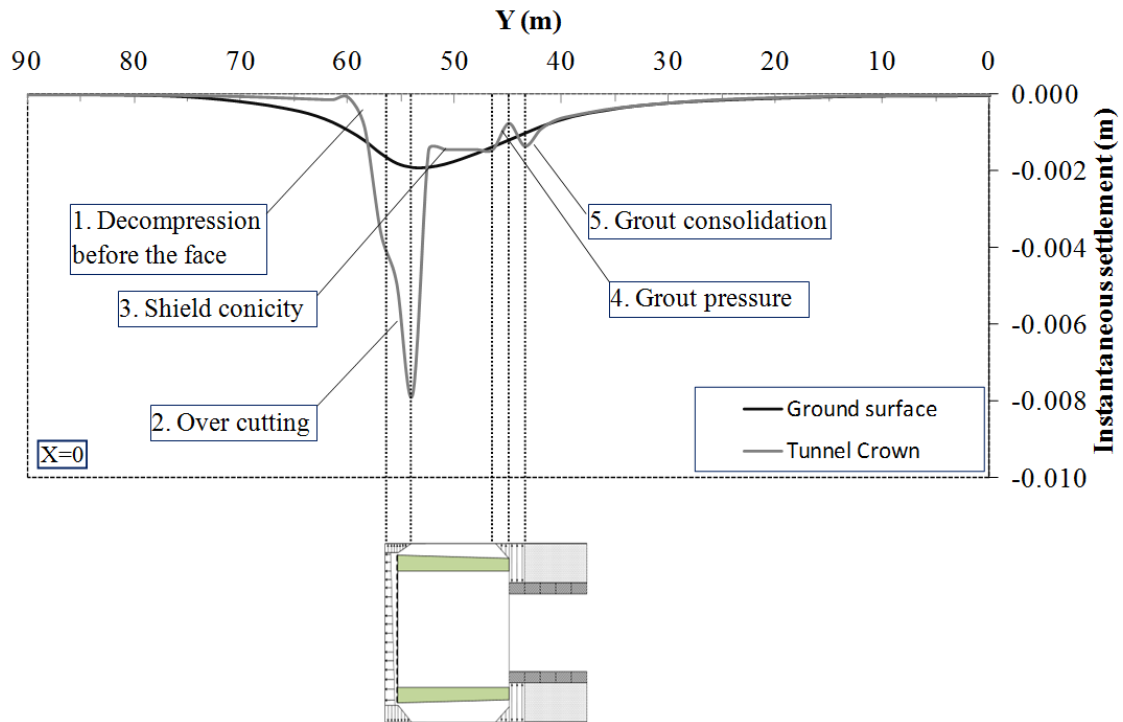
Figure 5-7. Instantaneous settlement induced along the tunnel axis by the 38th excavation step.
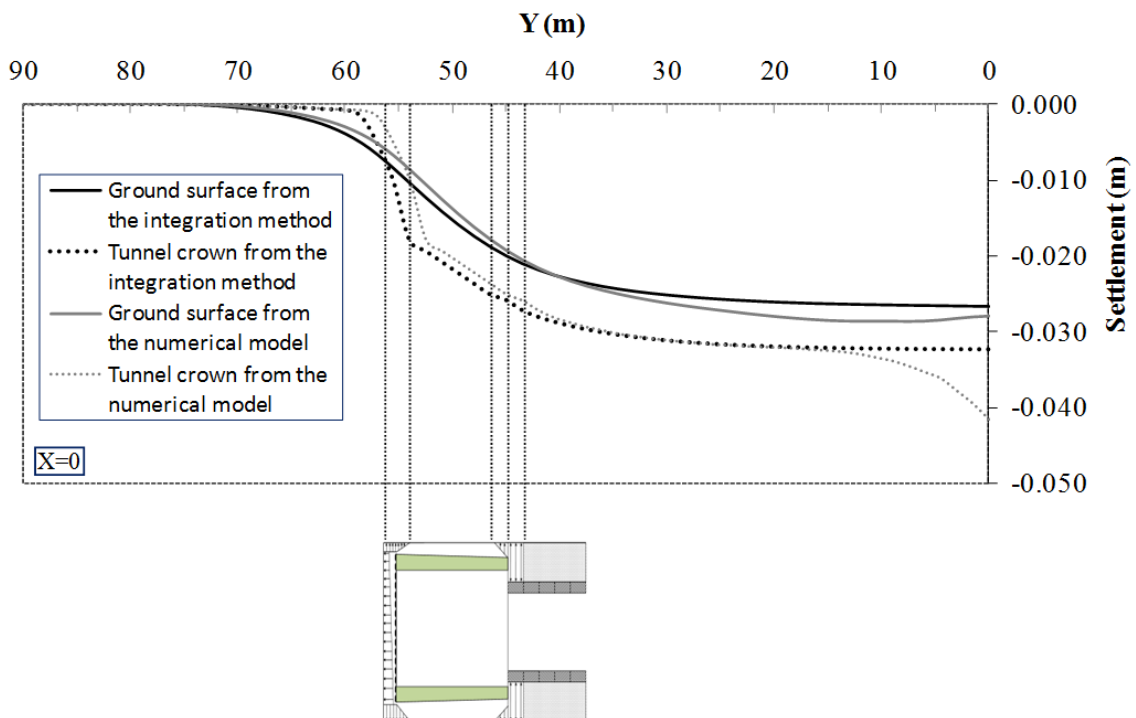
Figure 5-8. Comparison of the settlement provided directly by means of the numerical model and the integration method.

Figure 5-8 depicts the vertical displacement of the points located on the ground surface and at the tunnel crown along the y axis, which are provided directly by the FLAC[3D] model

Chapter 5: Three-dimensional numerical analyses 132

and obtained through the integration of the instantaneous settlement displacement at excavation step 38. It clearly appears that the integration method allows one to accurately estimate the final values of these displacements, despite the presence of the model boundaries. The integration method has been used in the rest of this section to obtain the final settlement above the tunnel.

5.1.4.2. *Zigzag line of the structural forces*

First, it is necessary to discuss the zigzag characteristic of the normal forces induced in a tunnel lining ring that can be seen in **Figure 5-9**. The model M3 lining pattern (the reference model) has been adopted during the FLAC^{3D} modelling for this section.

In a single lining ring of width d = 1.5 m, there is a certain difference in the structural forces obtained in the elements at the back of the ring compared to those induced in the elements at the front of the ring.

This zigzag pattern of the normal forces has also been obtained from the 3D numerical results given by Möller [2006] and can be explained by the fact that the unsupported tunnel heading arches more at the front than at the back of the tunnel segments, and this leads to a significant increase in structural forces at the front of a lining ring (Möller [2006]). In addition, when mechanized tunnelling is adopted, the impact of jacking forces on the segment is not even along the segments. This could be one of the main factors that induces the zigzag phenomenon.

The solid lines in **Figure 5-9** present the average values. Like the normal forces, the bending moment and the longitudinal force also show a zigzag pattern in a lining ring, as can be seen in **Figure 5-10** and **Figure 5-11**, respectively. For convenience, in the next sections, focus has been placed on the average value, as indicated by the solid line.
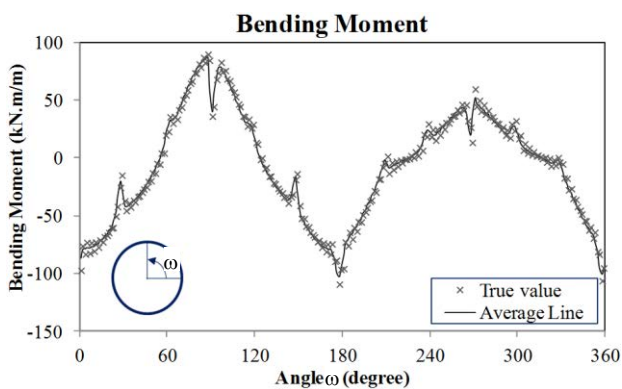
Figure 5-9. Average line of the bending moment in a lining ring
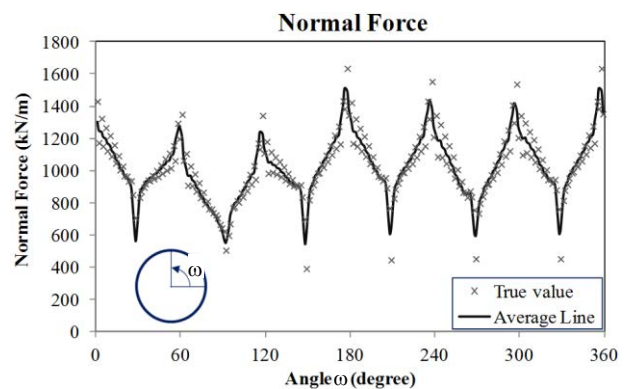
Figure 5-10. Average line of the normal forces in a lining ring
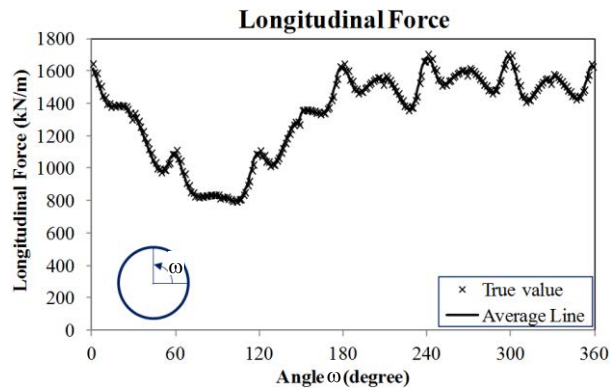
Figure 5-11. Average line of the longitudinal force in a lining ring

5.1.4.3. Influence of the initial condition

A special aspect which needs to be considered during 3D numerical modelling is the initial condition. In order to ensure that the numerical modelling is as close as possible to an actual tunnelling process, a certain number of construction steps are required to set the proper "initial" conditions and to avoid the influence of the boundary where the tunnelling process is started (Brinkgrave and Broere [2003], Hossaini et al. [2012]).

For this reason, the construction of a tunnel during the first eight steps of a numerical modelling process corresponding to a 12 m length of the shield machine only includes the excavation of soil at the tunnel face, with the face pressure and circumferential pressure being applied behind the face, but without the segmental lining being installed at the shield tail. This cycle is repeated till a shield length of 12 m is reached. After these first eight steps, the step-by-step procedure is continued. Each step of the ground excavation at the tunnel face is followed by the installation of a segmental lining ring at the shield tail.

Figure 5-12 presents the impact of the initial condition on the tunnel behaviour. The gradual condition depicts the excavation process described above, and the instantaneous condition presents the excavation process without these first eight steps being applied but through a unique step in which the excavation of the tunnel along a shield section of 12 m and the installation of the first lining ring are conducted simultaneously.

Looking at the numerical results, it can be seen that the initial condition has an insignificant effect on the tunnel lining behaviour. Compared to the maximum bending moment, normal force, longitudinal force, and normal displacement determined in a tunnel using the instantaneous initial condition, the corresponding ones obtained in the case in which the gradual initial condition is used are about 105.8 %, 100.8 %, 98.4 %, and 101.7 %, respectively (**Figure 5-12**c, d, e, and f). Instead, as can be seen in **Figure 5-12**a and b, the initial condition has a considerable influence on the longitudinal settlement at the zone near the tunnel face and on the settlement trough in the transverse section. A wider settlement trough was obtained in the case in which the instantaneous initial condition was used. However, the final settlements determined by means of both models are rather similar with a difference of about 0.5 %.

a) Settlement along the tunnel axis

b) Settlement in the transverse section

c) Bending moment

d) Normal forces

e) Longitudinal forces

f) Normal displacement
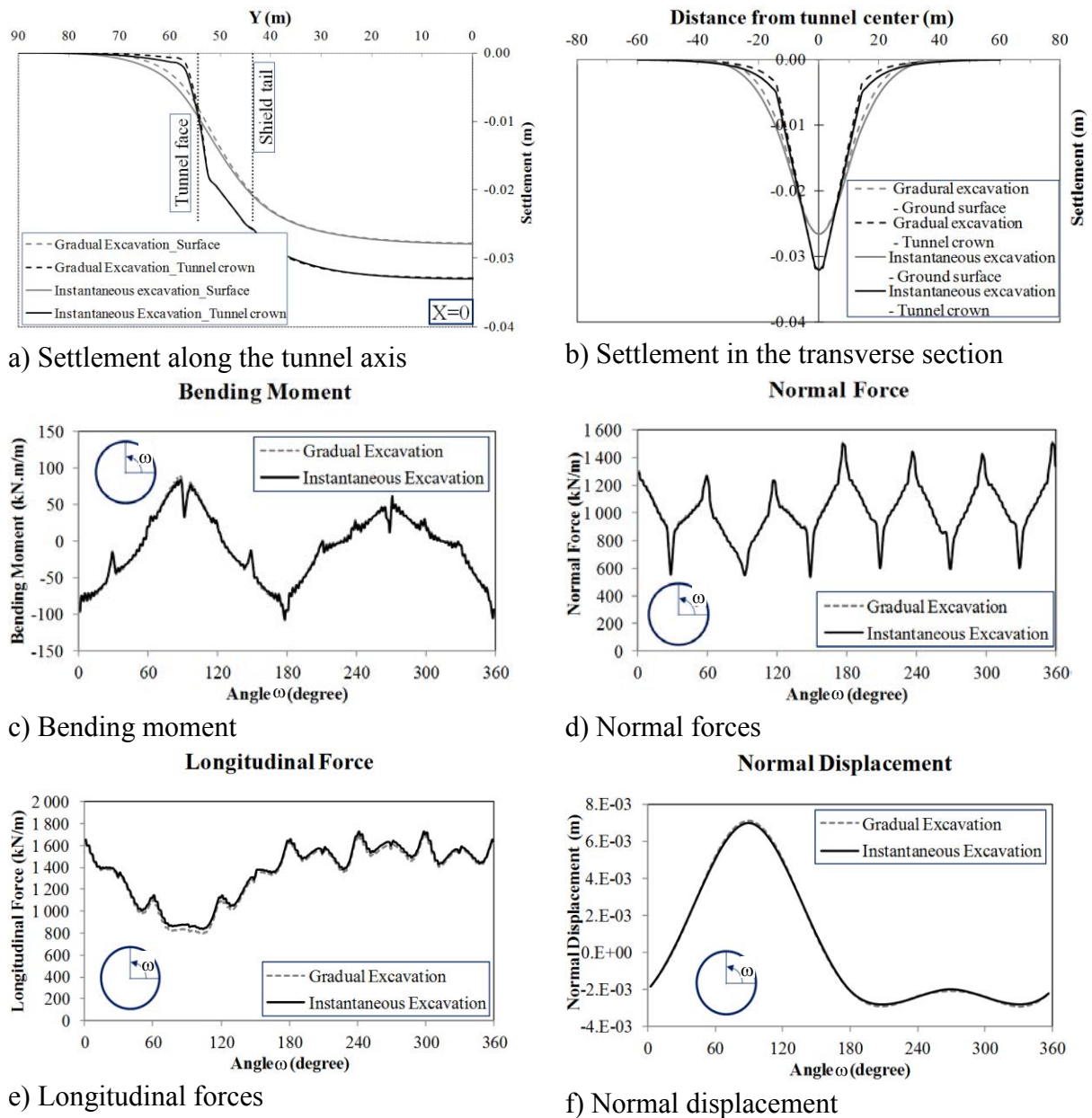
Figure 5-12. Influence of the initial condition on the structural forces in the lining and surface settlement

Although the difference between the two models is limited, all the other calculations in this section have been done using the gradual initial condition, in this way ensuring that the numerical simulation is as close as possible to real conditions.

5.1.4.4. Influence of the constitutive model

The influence of the two constitutive models adopted in the numerical analyses has been investigated using the M3 lining pattern (the reference model).

Figure 5-13 show a great impact of the constitutive model on the predicted settlements developing on the ground surface and tunnel crown. A difference of about 74 % between the

maximum surface settlements estimated by means of the CYsoil model and MC model can be seen (**Figure 5-13**a), thus indicating the importance of taking into account the variation in the stiffness modulus. The corresponding difference for the tunnel crown settlement is about 40 % (**Figure 5-13**b).

a) Surface Settlement

b) Tunnel crown Settlement

c) Surface settlement in the transverse section

d) Tunnel crown settlement in the transverse section
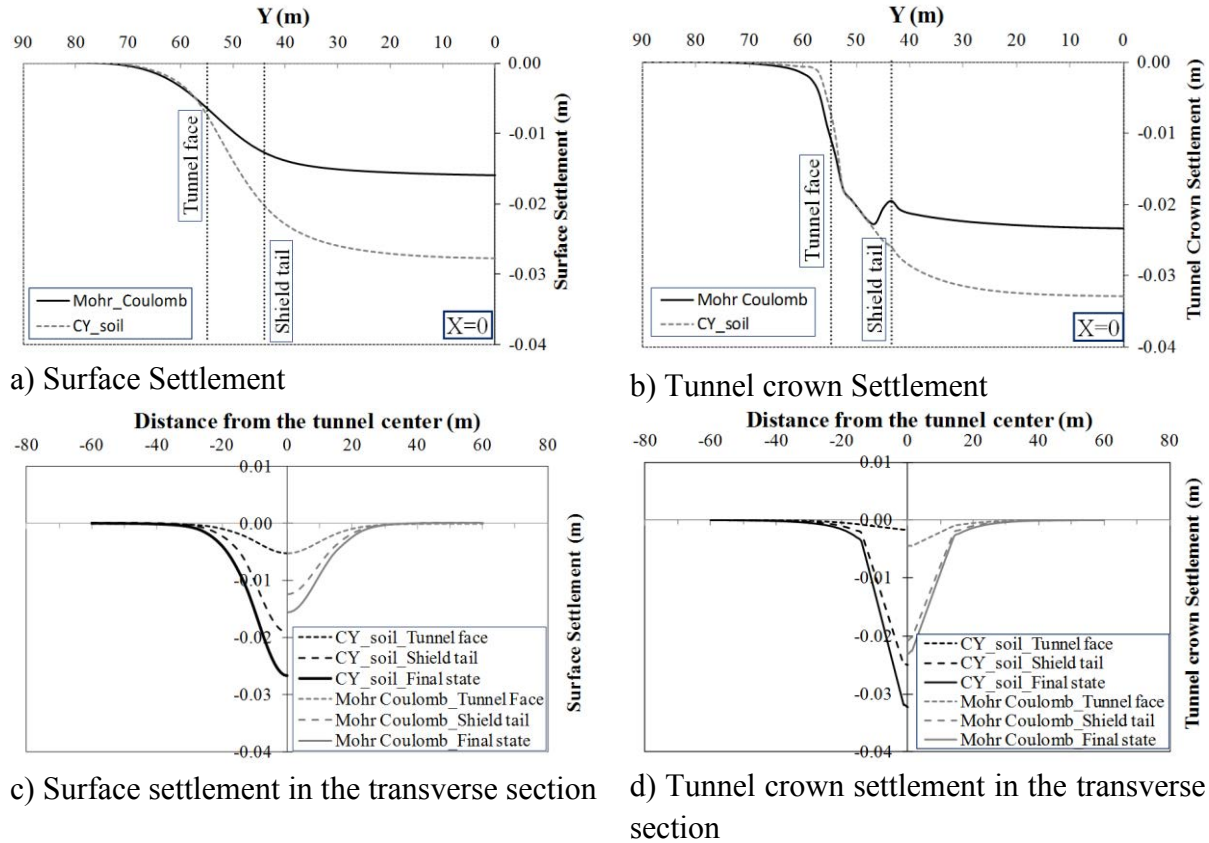
Figure 5-13. Influence of the constitutive model on the settlement field

In order to highlight the influence of constitutive model on the tunnel excavation, the plastic zones developed around the tunnel are illustrated in **Figure 5-14**. As can be seen, the plastic zone surrounding the tunnel in case of using the Cysoil model is approximately twice larger than the one observed in case of using the MC model. Both the constant stiffness of the MC model and yield characteristic at the small strain of the CYsoil model are the main reasons for the difference in the ground settlement.

Figure 5-13c indicates the impact of the constitutive model on the surface settlement in a transverse section. Large settlement differences can be observed between the two models at the shield tail and far behind the tunnel face. However, the surface movements in the two models are quiet similar at the tunnel face. Unlike the surface settlement, the movement at the tunnel crown indicates a considerable difference between the two models at each stage (**Figure 5-13**d).

In the same way as for the settlements, **Figure 5-15** indicates an important difference between the structural forces, especially the bending moment, longitudinal forces, and normal displacement induced in a tunnel lining, using the MC model and those obtained in the case of the CYsoil model. All these values are determined at the final state of the tunnel lining.
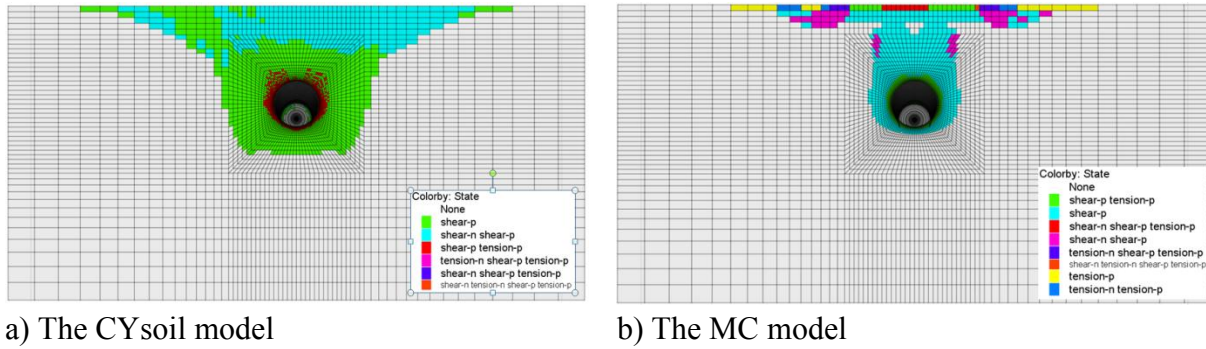
a) The CYsoil model

b) The MC model

Figure 5-14. Plastic zone around the tunnel
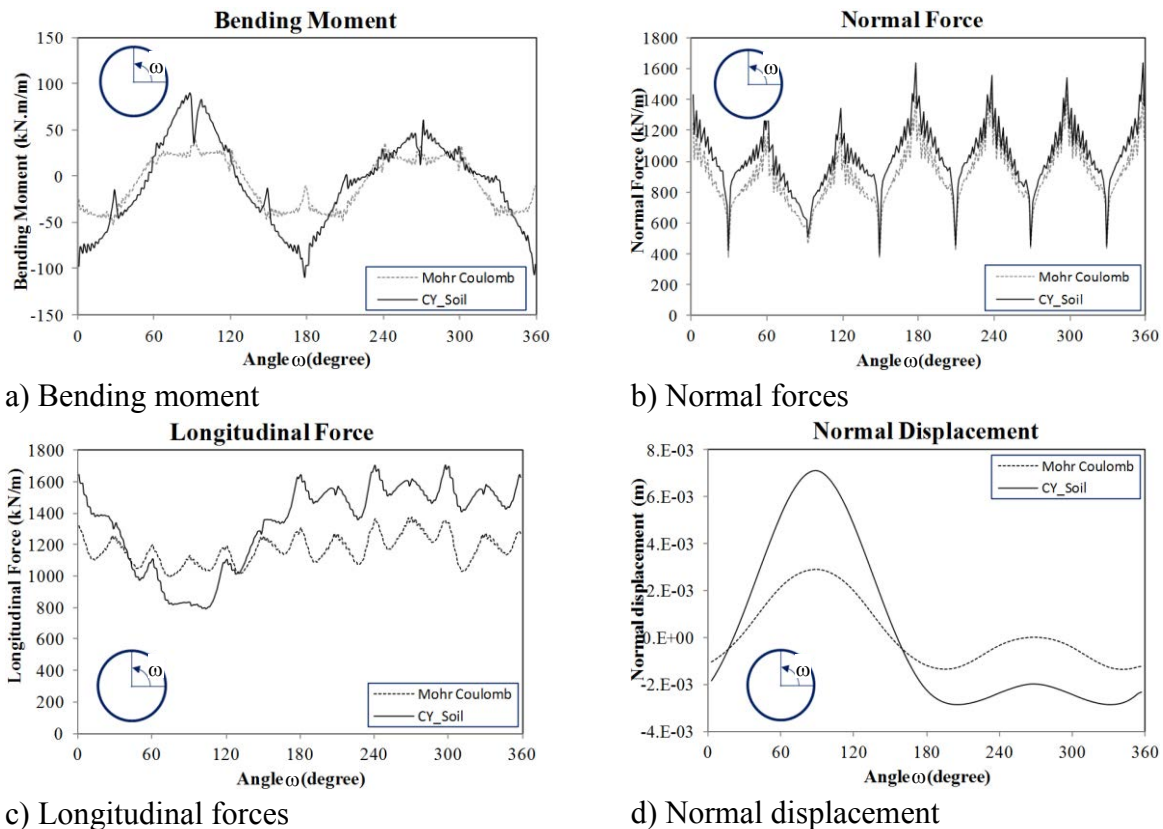
a) Bending moment

b) Normal forces

c) Longitudinal forces

d) Normal displacement

Figure 5-15. Influence of the constitutive model on the structural lining forces

As expected, due to the higher development of the plastic zones surrounding the tunnel in case of using the CYsoil model, the normal forces induced in the tunnel lining are larger than the corresponding ones obtained in the case of using the MC model (**Figure 5-15**b).

This could be attributed to the higher external loads which act on the tunnel lining in the case of the CYsoil model, caused by the self-weight of the failure ground in the surrounding plastic zone. Also, due to the higher magnitude of the external loads originating from the surrounding ground, a higher value of the longitudinal force induced the lining is observed. This is caused by the partial restraint of the transversal deformation (Poisson effect). Lower values of the longitudinal forces in the case of the CYsoil model that appear locally at the tunnel crown could be explained by the larger vertical displacement of the tunnel lining which have occurred at the tunnel crown (**Figure 5-15**d).

Chapter 5: Three-dimensional numerical analyses

Similarly, the CYsoil model produces higher bending moments and normal displacements than those predicted by the MC model (**Figure 5-15**a, d). The larger differences are observed at the crown and bottom of the tunnel and at the spring lines.

The above results reveal that the MC model does not adequately reflect realistic ground behaviour during tunnelling, due to the fact that it results induce lower structural forces. More results are illustrated in **Table** 5-3. The maximum differences in the results can be seen for the normal displacement and for the bending moment. The minimum difference is obtained for the normal forces. Considering the disadvantages of the MC model introduced in previous studies (e.g. Bolton et al. [1994], Addenbrooke et al. [1997], Mašin and Herle [2005], Hejazi et al. [2008]), the above results show the importance of the complexity of a constitutive model in tunnelling engineering. For this reason, all the other calculations performed in section 5.1 have conducted using the CYsoil model.

Table 5-3. Difference in structural forces due to the effect of the constitutive model

Parameters	CYsoil model (A)	MC model (B)	A/B (%)
Maximum positive bending moment (kN.m/m)	89.6	40.4	222
Minimum negative bending moment (kN.m/m)	-109	-53.1	205
Maximum normal force (kN/m)	1640	1450	113
Maximum longitudinal force (kN/m)	1700	1370	124
Maximum normal displacement (mm)	7.12	2.91	244
Maximum surface settlement (cm)	2.79	1.60	174
Maximum tunnel crown settlement (cm)	3.29	2.34	140

5.1.4.5. Behaviour of the tunnel during the excavation process

In order to understand the behaviour of the tunnel lining and the surrounding ground during the tunnel excavation process, **Figure 5-16** presents the variation in the structural lining forces and ground displacement during tunnel face advancement in the case of a segmental lining (model M3), considering the reference case parameters.

As mentioned above, the influence of the model boundaries on tunnel behaviour can be ignored at excavation step 38. The variations in the structural force caused by the excavation process will therefore be taken into consideration for the tunnel lining ring assembled at this step which is hereafter called the reference lining ring. **Figure 5-4** shows that the lining ring is placed at a distance of 12 m behind the tunnel face. The reference lining ring is therefore ring 30, counting from the model boundary (y = 0 m). In **Figure 5-16**, the "*i*" index represents the tunnel excavation process which corresponds to the number of lining rings that have been assembled. For example, an "*i*" value of 55 means that the result shows the behaviour of the reference lining ring after 25 (= 55 - 30) excavation cycles from the installation moment.

a) Settlement trough in the transverse section

b) Bending moment in lining ring 30

c) Normal force in lining ring 30

d) Longitudinal force in lining ring 30
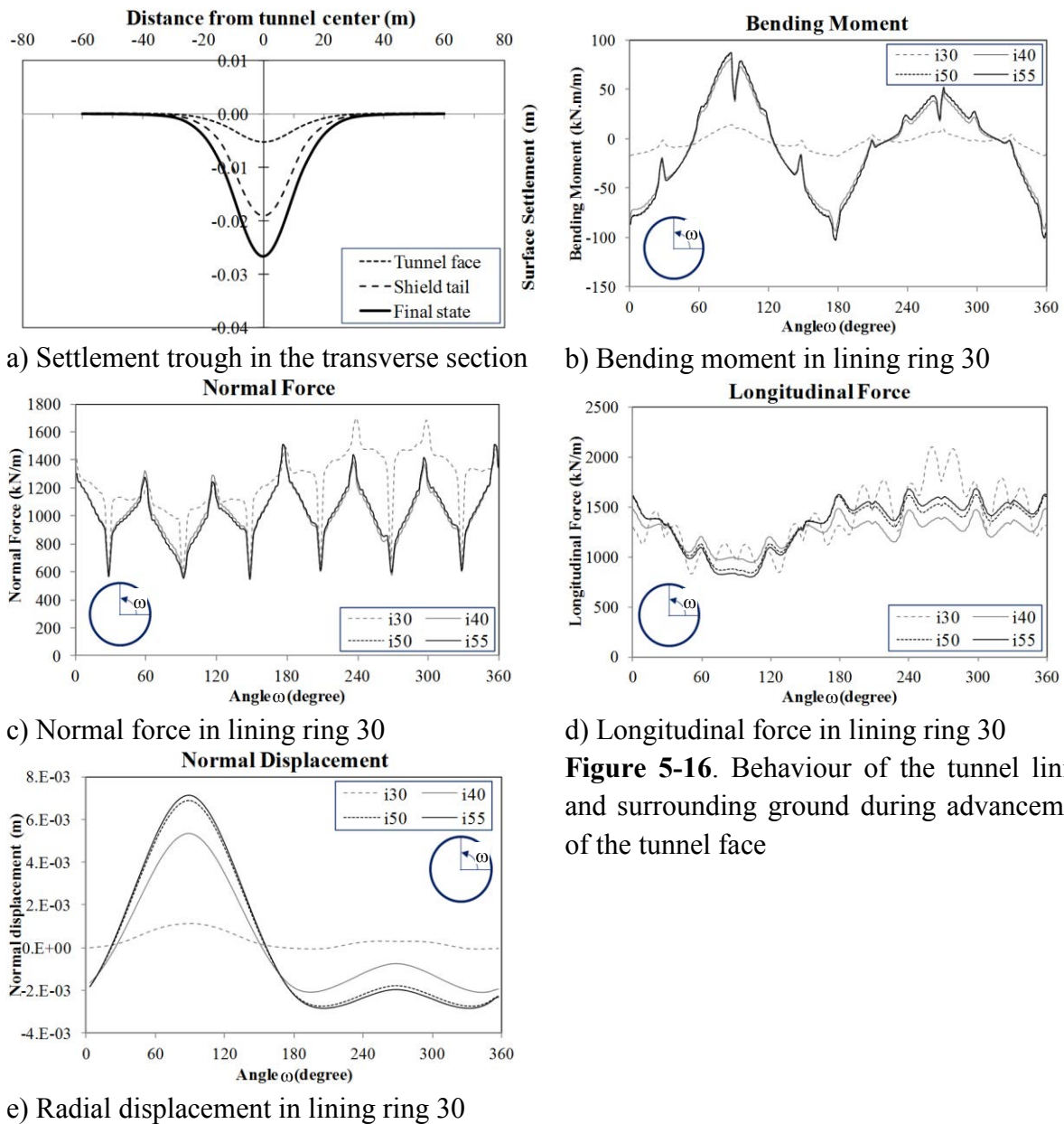
Figure 5-16. Behaviour of the tunnel lining and surrounding ground during advancement of the tunnel face

e) Radial displacement in lining ring 30

As for structural forces, the influence of the length of the tunnel advance process on the behaviour of the reference lining ring (ring 30) will be evaluated considering the instantaneous variation in structural forces between two successive steps. The numerical results show that, between the two excavation steps corresponding to the *i* value of 54 and 55, the instantaneous variation in the structural force induced in the reference lining ring is approximately zero. This means that the structural forces determined at this excavation step can be considered the final values that act on the reference lining ring in the long term. Considering a length of influence of 25.5 m upstream from the tunnel face, as mentioned in section 5.1.4.1, it is possible to determine a total necessary length in the y direction of the numerical model of 120 m (= 55 lining rings x 1.5 m/ring + 12 m shield length + 25.5 m of the influence length upstream from the tunnel face).

Figure 5-16a shows surface settlement curves along the x direction that corresponds to three main steps: settlement at the tunnel face; settlement at the shield tail; and final settlement at a large distance behind the tunnel face. This figure shows that, the settlement at the tunnel face and shield tail are about 20 % and 70%, respectively, compared to the final settlement.

Figure 5-16c presents the development of the normal forces of the tunnel lining. Because of the impact of the shield tail grouting pressure, the maximum normal forces, which are equal to 104 % of those determined at the final state (*i* step of 55), are obtained right after installation (*i* step of 30). Since the grouting pressure distribution was assumed to linearly increase with the depth gradient under the effect of the grout unit weight, the greatest normal force was obtained at the tunnel bottom. When the grout was consolidated, the main external loads acting on the tunnel lining became the ground loads. This is why the normal force in the tunnel lining decreases and becomes equal to about 94.4 % of the final value (*i* step of 35 in **Table 5-4**). After that, the increase in ground loads far behind the tunnel face due to the disappearance of the confinement grouting pressure is the main reason for the gradual increase in normal forces (**Table 5-4**).

Table 5-4. Development of the structural forces of the lining during tunnel advancement

Parameters	*i30*	*i35*	*i40*	*i45*	*i50*	*i55*
Tunnel advancement after installation (m)	0	7.5	15	22.5	30	37.5
Maximum positive bending moment (kN.m/m)	15.1	65.4	83.4	88.1	88.9	89.6
R_{M+} (%)	*16.8*	*73.0*	*93.0*	*98.2*	*99.2*	*100*
Minimum negative bending moment (kN.m/m)	-19.7	-75.7	-99.2	-106.1	-108.2	-109
R_{M-} (%)	*18.1*	*69.5*	*91.0*	*97.3*	*99.3*	*100*
Maximum normal force (kN/m)	1712	1546	1626	1636	1637	1637
R_N (%)	*104.5*	*94.4*	*99.3*	*99.9*	*100*	*100*
Maximum longitudinal force (kN/m)	2105	1644	1497	1585	1637	1701
R_{LN} (%)	*123.7*	*96.6*	*88.0*	*93.1*	*96.2*	*100*
Maximum normal displacement (mm)	1.13	3.22	5.35	6.42	6.89	7.12
R_{disp} (%)	*15.9*	*45.3*	*75.2*	*90.3*	*96.8*	*100*

Figure 5-16d shows the same change in tendency of the longitudinal force due to the advancement of the tunnel face. The largest longitudinal force, of about 123.7 %, was obtained at the shield tail, due to the impact of the forces caused by the hydraulic jacks (step *i* = 30), compared to that determined at the final state was obtained. Advancement of the tunnel face would result in a reduction in the jacking forces on the reference lining ring (lining ring 30) and therefore a reduction in the longitudinal force. After the *i* = 40 step, the numerical results present an increase tendency of the longitudinal force and this force reaches the final state at the *i* = 55 step with a maximum value of 80.8 % compared to the largest value estimated at the *i* = 30 step. The increase in the longitudinal force along the tunnel axis after

the $i = 40$ step can be explained by the fact that tunnel linings are confined by the surrounding ground. As a consequence, the gradual increase in the external loads originating from the surrounding ground can produce an increase in the longitudinal force of the lining due to the partial restraint of the transversal deformation (Poisson effect).

Figure 5-16b and e present a gradual increase in tendency of the bending moment and normal displacement, with respect to the tunnel face advancement, which is different from that of the normal forces and longitudinal forces.

It should be noted that, as the tunnel face becomes distant, the increasing velocity of the structural forces will also be gradually reduced and their values approximately approach a steady-state when the tunnel has advanced by about 22.5 m, measured from the installation time of reference lining ring 30. However, as mentioned above, the real steady state is only reached at a tunnel advancement of 37.5 m, corresponding to a step i of 55. Other results can be found in **Table 5-4**.

5.1.4.6. Influence of the joint patterns

In this section, a parametric study has been carried out using the six lining patterns illustrated in **Figure 5-6**. The other parameters of the model are those of the reference case.

The goal of this parametric investigation is to highlight the influence of the joint distribution on the tunnel lining behaviour and ground displacement. All the results introduced in this section (**Figure 5-17**) have been determined at the final state of tunnel lining ring 30, counting from the tunnel boundary (y = 0).

Apart from lining model M6, in which the coupling effect between two successive rings is neglected, **Figure 5-17** shows a negligible influence of the joint pattern on the final surface settlement. The maximum difference between the settlement obtained using four models (M2, M3, M4, and M5) compared to that of the continuous lining case is only about 0.09 cm, which corresponds to 3.3 % (**Table** 5-8).

As the segment joint arrangements in a ring, for the cases of models M1 and M2, do not change along the tunnel axis, the structural forces in the successive rings can be assumed to be similar. However, when models M3, M4, and M5 are used, segment joints in a ring are staggered around the y direction along the tunnel axis. It is therefore necessary to consider the variation in the structural forces induced in the successive rings (**Table 5-5**,

Table 5-6 and **Table 5-7**).

Looking at the results presented in **Table 5-5**,

Table 5-6 and **Table 5-7**, a considerable effect of joint pattern in a ring on the bending moment can be seen, with a maximum difference between two successive rings of about 26.1 %. However, the normal force, longitudinal force and normal displacement are in a similar range with a maximum difference between two successive rings of only 1.8 %, 3.4 %, and 0.7 %, respectively. The lower maximum bending moment is often obtained in a ring with the segment joint located at the tunnel crown (**Figure 5-6**c-e). The closer the reference joint to the tunnel crown, the lower the bending moment (i.e. ring 2 in model M3 (**Table 5-5**), ring 3 in model M4 (

Table 5-6), and ring 2 in model M5 (**Table 5-7**). The reference joint is defined as the one closest to the tunnel crown, in the clockwise direction from the tunnel crown. This means that, the stiffness of the lining ring is not similar between the successive rings along the tunnel axis, which causes a load transfer from the stiffer ring to the softer ring. This phenomenon can be attributed to the fact that, due to the lateral earth pressure factor of 0.5 used in the present model (**Table** 4-1), the maximum bending moment in a ring is measured at the tunnel crown, as can be seen in **Figure 5-17**b. Hence, in the case in which a segment joint is situated at this location, the influence of the joint on the reduction of the bending moment will be greater than the case in which the joint is situated near a point where the bending moment is equal to zero. With the six joints in the ring of all the considered lining models, this conclusion is in good agreement with the results obtained in section 4.1 (also see Do et al. [2013a]) which was performed using a 2D model. In their results, the minimum and maximum bending moments were given at reference joint angle (ω) of 0^0 and 30^0, respectively. A low bending moment for the case of a reference joint located at the tunnel crown was also found, through 3D numerical analyses, by Hudoba [1997] and Klappers et al. [2006]. The abovementioned results clearly indicate the necessity of using a full 3D numerical model to obtain an accurate estimation of the structural forces induced in a staggered segmental lining.

It should be noted that, from the three lining models that used the staggered pattern (lining model M3, M4, and M5), the minimum differences between the bending moments induced in the successive rings are obtained in the case of lining model M4 (**Table 5-5**,

Table 5-6 and **Table 5-7**). In addition, the maximum bending moment developed in the case of lining model M4 is lower than that obtained in the other cases (lining model M3 and M5). These results demonstrate that, lining model M4 is better for the lining design than the two models (M3 and M5). The same conclusion can be reached by conducting a numerical study according to the approach proposed by Klappers et al. [2006]. In other words, the use of a staggered lining with a larger number of ring types, i.e. a smaller difference in the reference angles between successive rings, would result in a decrease in the bending moment induced in the lining. This could be explained by the smaller span of concrete lining affected by the segment joints in successive rings. This causes an increase in the flexibility of the global support structure.

Table 5-5. Differences in the structural forces between the successive rings in model M3 (**Figure 5-6**c)

Parameters	Ring type 1 (A)	Ring type 2 (B)	A/B (%)
Maximum positive bending moment (kN.m/m)	113	89.6	126.1
Minimum negative bending moment (kN.m/m)	-97.7	-109	89.6
Maximum normal force (kN/m)	1630	1640	99.4
Maximum longitudinal force (kN/m)	1680	1700	98.8
Maximum normal displacement (mm)	7.11	7.12	99.9

Table 5-6. Differences in the structural forces between the successive rings in model M4 (**Figure 5-6**d)

Parameters	Ring type 1 (A)	Ring type 2 (B)	Ring type 3 (C)	A/C (%)	B/C (%)
Maximum positive bending moment (kN.m/m)	97	92.3	82.8	117.1	111.5
Minimum negative bending moment(kN.m/m)	-93.2	-80	-98	95.1	81.6
Maximum normal force (kN/m)	1650	1650	1680	98.2	98.2
Maximum longitudinal force (kN/m)	1900	1830	1770	107.3	103.4
Maximum normal displacement (mm)	7.07	7.05	7	101.0	100.7

Table 5-7. Difference in the structural forces between the successive rings in model M5 (**Figure 5-6**e)

Parameters	Ring type 1 (A)	Ring type 2 (B)	A/B (%)
Maximum positive bending moment (kN.m/m)	104	83.1	125.2
Minimum negative bending moment (kN.m/m)	-103	-117	88.0
Maximum normal force (kN/m)	1760	1770	99.4
Maximum longitudinal force (kN/m)	2130	2130	100.0
Maximum normal displacement (mm)	6.91	6.96	99.3

Because of the variation of the structural forces in the different rings along the tunnel axis, only the maximum values of structural forces are presented in **Table** 5-8 for each lining model pattern. For comparison purposes, the results obtained in the continuous lining (model M1) has been selected as a reference and considered to be 100 %. In this way, it is possible to determine the coefficients R for the other computing models. These coefficients are expressed as the ratio of the values of the positive bending moment, negative bending moment, normal forces, longitudinal forces, normal displacement, and surface settlement of model M_i, to the corresponding values of model M1.

The maximum bending moment developed in the case of a straight joint (model M2) is lower than that obtained in the other cases (**Figure 5-17**b and **Table** 5-8). This can be explained by the fact that the tunnel lining that uses a straight joint pattern has less rigidity than in the other cases. The normal forces developed in all three staggered joint lining cases are higher than the ones obtained in the case of a continuous lining and they are all greater than those determined for a straight joint pattern. The same results were also obtained by Hudoba [1997]. The largest normal force in a staggered lining was given when the ring joints were assumed to be rigid (lining model M5) (**Table** 5-8).

Figure 5-17e and **Table** 5-8 show an insignificant effect of the joint pattern on the normal displacement of the lining, which is different from that of the bending moment and normal forces. All four cases in which the segmental lining has been used (M2, M3, M4, and

M5) provide a higher displacement than the case in which a continuous lining has been used. However, the maximum difference between them is only about 6.4 %.

a) Longitudinal surface settlement

b) Bending moment at lining ring 30

c) Normal force at lining ring 30

d) Longitudinal force at lining ring 30

e) Normal displacement at lining ring 30
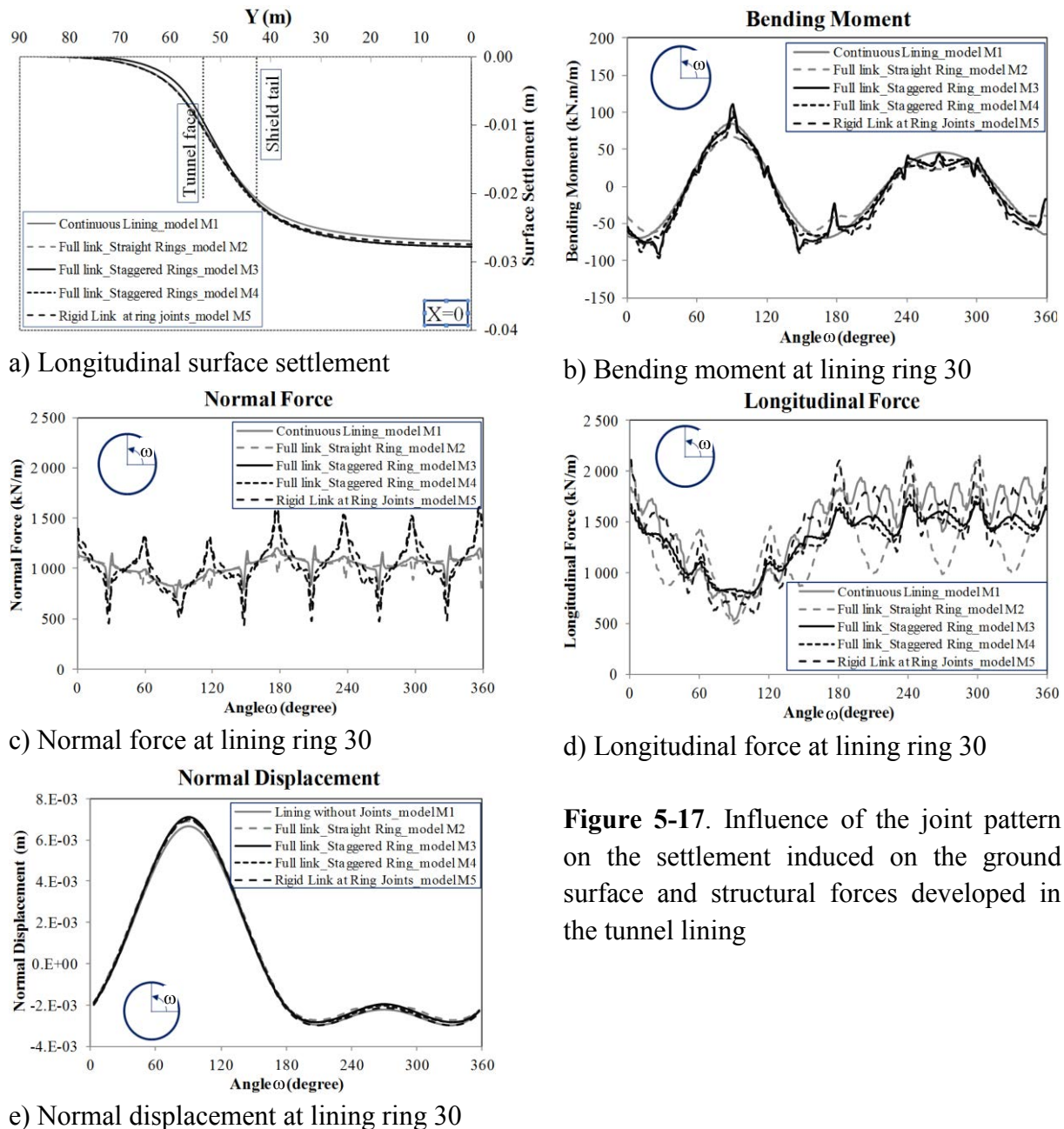
Figure 5-17. Influence of the joint pattern on the settlement induced on the ground surface and structural forces developed in the tunnel lining

A comparison has been made of the structural forces and ground settlements obtained using the three lining models M3, M5, and M6 with the same type 2 joint pattern in order to highlight the influence of the coupling effect between successive rings on tunnel behaviour (see **Table 5-9**).

Owing to the lack of connection between successive rings, the lining rings in model M6 can be considered as being isolated since the coupling effects are negligible. The coupling effects lead to a stiffer response of the lining. As a consequence, the normal deformation of the lining is reduced while the structural forces increase. These conclusions can be confirmed

through a comparison of the results obtained using model M6 (without considering the coupling effect) with those of the other models using the same joint pattern type in which the coupling effect is considered (models M3 and M5) (**Table 5-9**). Generally, the stiffer the link between two successive rings, the higher the structural forces in terms of the bending moment, normal forces, and longitudinal forces, and the lower the lining displacement (**Table 5-9**). The maximum difference in the positive bending moment, negative bending moment, normal forces, longitudinal forces, and normal displacement determined in the three above models are 39.9 %, 25 %, 25.4 %, 27.4 %, and 18.4 %, respectively. The same conclusion can be drawn from studies performed by Arnau and Molins [2012], Blom [2002], Klappers et al. [2006].

Table 5-8. Comparison of the computed results for five different lining models

Parameters	Model M1	Model M2	Model M3	Model M4	Model M5
Maximum positive bending moment (kN.m/m)	92.1	68.2	113	97	104
R_{M+} (%)	*100*	*74.0*	*122.7*	*105.3*	*112.9*
Minimum negative bending moment (kN.m/m)	-71.8	-64.3	-109	-98	-117
R_{M-} (%)	*100*	*89.6*	*151.8*	*136.5*	*163.0*
Maximum normal force (kN/m)	1380	1270	1640	1680	1770
R_N (%)	*100*	*92.0*	*118.8*	*121.7*	*128.3*
Maximum longitudinal force (kN/m)	1860	2170	1700	1900	2130
R_{LN} (%)	*100*	*116.7*	*91.4*	*102.2*	*114.5*
Maximum normal displacement (mm)	6.69	6.92	7.12	7.07	6.96
R_{disp} (%)	*100*	*103.4*	*106.4*	*105.7*	*104.0*
Maximum surface settlement (cm)	2.70	2.79	2.78	2.78	2.75
R_{set} (%)	*100*	*103.3*	*103*	*103*	*101.9*

Table 5-9. Influence of the coupling effect on tunnel behaviour

Parameters	Model M3 (A)	Model M5 (B)	Model M6 (C)	A/C (%)	B/C (%)
Maximum positive bending moment (kN.m/m)	113	104	80.8	139.9	128.7
Minimum negative bending moment (kN.m/m)	-109	-117	-93.6	116.5	125.0
Maximum normal force (kN/m)	1640	1770	1411	116.2	125.4
Maximum longitudinal force (kN/m)	1700	2130	1672	101.7	127.4
Maximum normal displacement (mm)	7.12	6.96	8.53	83.5	81.6
Maximum surface settlement (cm)	2.78	2.78	2.81	98.9	98.9

The above results show that the segment layout in successive rings and the attachment conditions of joints are two important parameters that affect structural forces and lining deformation; the bending moment and normal forces are affected in particular. For this reason, the joints in the tunnel lining should be simulated to ensure an accurate estimation of the structural forces. Furthermore, different segment layouts of a ring should be analysed through a 3D modelling in order to determine the most favourable segment configuration for the design of segmental linings.

5.1.5. Conclusions

A 3D numerical model of the mechanized tunnelling process has been developed. This model can be used to predict the ground movements and structural forces induced in a tunnel lining in which the influence of the lining joints should be taken into account. The results have shown a negligible influence of the initial condition on tunnel behaviour. In contrast, a great influence of the constitutive model of the ground on the tunnel behaviour and ground displacement has been pointed out. Generally, the CYsoil model provides higher structural forces and ground settlement than those predicted by the MC model. These results indicate the importance of using a sufficiently complex constitutive model to take into account the real soil behaviour in tunnelling engineering

The variation in the structural forces and displacement induced in the surrounding ground during the advancement of the tunnel face has also been studied. The results showed a great impact of the construction loads, such as the grouting pressure and jacking forces, on the structural forces induced in the tunnel lining. All the bending moments, normal forces, longitudinal forces, normal displacements developed in the tunnel lining and the ground displacement were seen to depend on the tunnel advancement. Generally, under the impact of jacking forces and grouting pressure, the largest values of the normal forces and longitudinal forces in a lining ring are reached right after it is installed behind a shield tail. These two structural forces are gradually reduced as the grout becomes consolidated and the shield machine advances. However, their values increase again for a gradual increase in ground loads. The real steady state of the tunnel lining was only reached after a tunnel advancement of 37.5 m.

A variation in structural forces, especially the bending moment, between successive rings along the tunnel axis has been found in a staggered segmental lining (models M3, M4, and M5), thus highlighting the necessity of using a full 3D numerical model to obtain an accurate estimation. In general, in a segmental lining, the closer the reference joint to the tunnel crown, the lower the bending moment. The results showed that, lining model M4 is better for the lining design than the two models (M3 and M5).

The results also showed, on the basis of five difference lining patterns from model M1 to M5, that the segment layout in successive rings and the attachment conditions of the joints are two important parameters that affect the structural forces and lining deformation; the bending moment and normal forces are important in particular. On the other hand, an insignificant

effect of joint pattern on the normal displacement of the lining and the surface settlement could be seen.

The coupling effect provides a stiffer response of the lining. As a consequence, the normal deformation of a lining is reduced while the structural forces increase. Furthermore, the stiffer the link between two successive rings, the higher the structural forces in terms of the bending moment, normal forces, and longitudinal forces, and the lower the lining displacement. The maximum differences in the positive bending moment, negative bending moment, normal forces, longitudinal forces, and normal displacement determined in the models, with and without considering the coupling effect, were 39.9 %, 25 %, 25.4 %, 27.4 %, and 18.4 %, respectively.

For these reasons, the joints in a tunnel lining should be simulated to ensure an accurate estimation of the structural forces. Furthermore, different segment layouts of a ring should be analysed with a 3D model in order to determine the most favourable segment configuration in the design of segmental linings.

5.2. Numerical Investigation of Twin Horizontal Tunnels

5.2.1. Introduction

Many tunnels have been built in urban environments; this often involves the construction of twin tunnels in close proximity. In addition, in many cases, the new tunnel is often excavated adjacent to an already existing one. Thus, the prediction of the influence of a new shield tunnel construction on an existing tunnel plays a key role in the optimal design and construction of close parallel shield tunnels in order to avoid any damage to the existing tunnel during and after excavation of the new tunnel.

Interactions between closely-spaced tunnels were studied in the past using a variety of approaches: physical model testing, field observations, empirical/analytical methods and finite element modelling. The literature reviewed in chapter 2 clearly indicates that an extensive amount of research have been focused on the influence of twin tunnels on ground deformation. However, less work has been devoted to the influence of the interaction between tunnels on the structural forces induced in a mechanised tunnel lining.

The main purpose of this section is to provide a full 3D model of twin horizontal tunnels which would allow to better understand the behaviour of the interaction of mechanized twin tunnels, in terms of structural forces induced in the tunnel lining and ground displacement surrounding the two tunnels. Most of the main elements of a mechanized excavation are simulated in this model: the conical geometry of the shield, the face pressure, the circumferential pressure acting on the cylindrical surface of the excavated ground in the working chamber behind the tunnel face, the circumferential pressure caused by the migration of the grout acting on the excavated ground at the shield tail, the grouting pressure acting simultaneously on the excavated ground and on the tunnel structure behind the shield tail, progressive hardening of the grout, the jacking force, the self-weight of the shield and back-up trains and the lining joint pattern, including the segment joints, the ring joints and their connection condition. The CYsoil constitutive model has been adopted. The Bologna-Florence high speed railway line has been adopted in this study as a reference case. The main content of this section has been presented in Do et al. [2014c].

5.2.2. Numerical model

5.2.2.1. Three-dimensional numerical model

The numerical model, the 3D simulation procedure of a single tunnel and the parameter calibration of the CY soil model were described in detail in section 5.1. Therefore, only a short overview is given here. However, the numerical model introduced in section 5.1 has been improved and some other components of the tunnelling process have been simulated in

the present study. It includes the weight of the shield machine and the weight of the back-up train behind the shield machine.

The tunnel construction process is modelled using a step-by-step approach. Each excavation step corresponds to an advancement of the tunnel face of 1.5m, which is equal to the width of a lining ring. A schematic view of the present model is provided in **Figure 5-18**.

Face pressure has been estimated depending on the horizontal stress induced in the ground in front of the tunnel face (Mollon et al. [2013]). This face pressure has been modelled by applying a pressure distribution to the excavation face using a trapezoidal profile in order to account for the slurry density. Owing a slight overcutting, a possible slurry migration could occur over a short distance behind the cutting wheel. Therefore, in addition to the pressure acting on the tunnel face, a pressure, caused by the slurry solution, has also been applied to the cylindrical surface just behind the tunnel face. The shield machine has been simulated using "fictive" shield introduced by Mollon et al. [2013], Dias et al. [2000], Jenck and Dias [2004]. The geometrical parameters of the shield are presented in **Figure 5-18**.
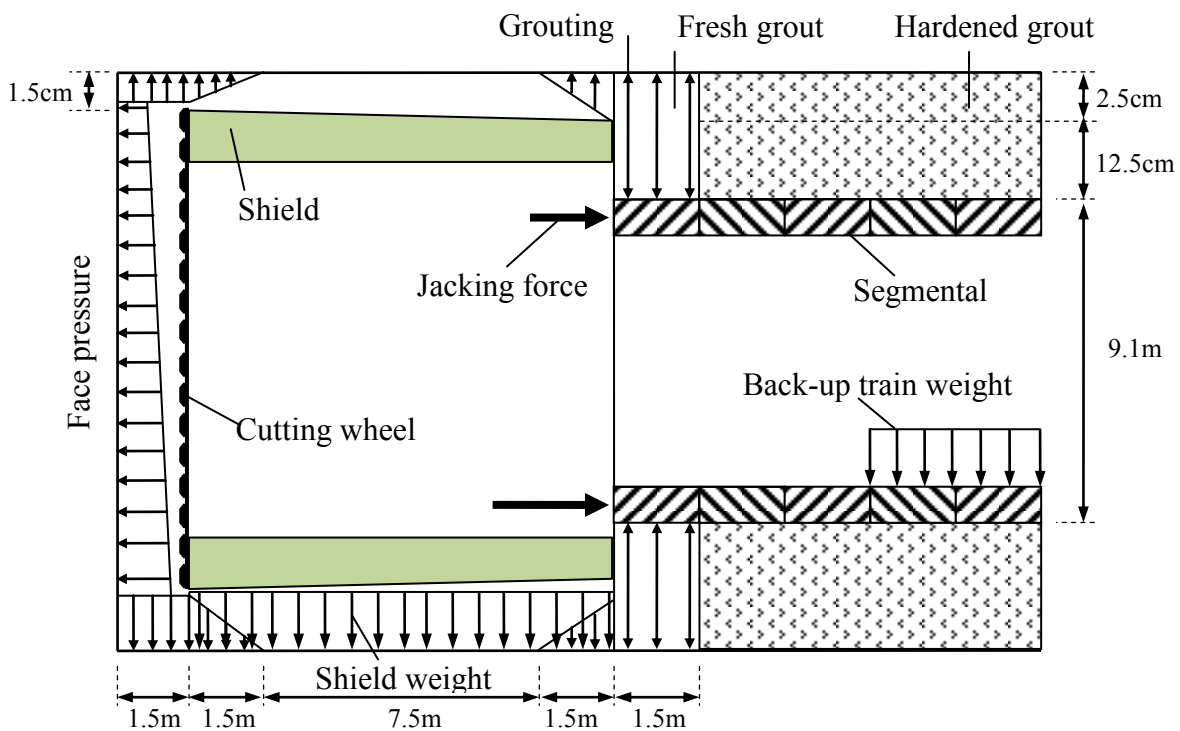
Figure 5-18. Layout of the proposed TBM model (not scaled)

The self-weight of the shield is simulated through the vertical loads acting on the grid points of the ground mesh at the tunnel bottom region over an assumed range of 90 degrees in the cross-section and over the whole shield length, as can be seen in **Figure 5-18** and **Figure 5-19**. In this study, a shield weight value of 6000 kN, which refers to a tunnel diameter of 9.4 m (JSCE [1996]), has been adopted.

The distribution of the jacking force has been assumed to be linear over the height of the tunnel. The jacking forces were set on each segment, considering three plates located at 1/6,

1/2, and 5/6 of the segment length. A total jacking force of about 40 MN was adopted in the present model on the basis of the theoretical method proposed by Rijke [2006].

The grouting action is modelled in two phases: (1) the liquid state (state 1) represented by a certain pressure acting on the ground surface and on the tunnel lining; (2) the solid state (state 2). The distributional radial pressure has been used to simulate this kind of pressure. The grouting pressure has been estimated depending on the ground overburden pressure at the crown of each tunnel (Mollon et al. [2013]). The grout was simulated by adopting a uniform pressure which was applied to both the cylindrical surface of the excavated ground and the external surface of the tunnel lining. As for the face pressure, the annular void between the outside surface of the shield and the excavated ground made the migration of some grout towards the shield possible. This migration was simulated by means of a triangular pressure over the length of one ring (1.5 m). The grout was assumed to harden beyond this length and was simulated by means of volume elements with perfect elastic behaviour, and with the elastic characteristics E_{grout}= 10 MPa and ν_{grout}= 0.22 (Dias and Kastner [2013], Mollon et al. [2013]).
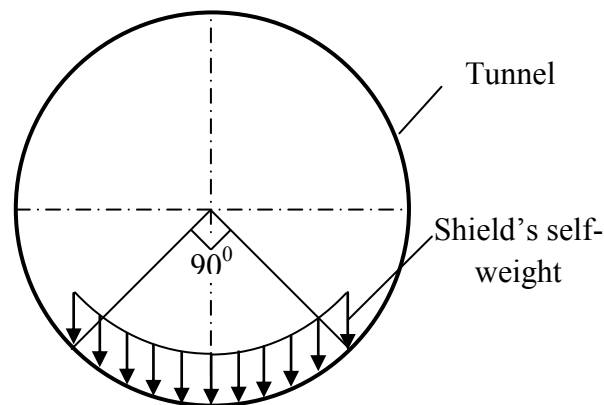
Figure 5-19. Self-weight scheme of the shield machine

In the present model, the tunnel segments have been modelled using a linear-elastic embedded liner element. The segment joints have been simulated using double node connections. The stiffness characteristics of the joint connection have been represented by a set composed of a rotational spring (K_{RO}), an axial spring (K_A) and a radial spring (K_R) (see section 4.1 and Do et al. [2013a]).

In the same way as for the segment joint, the ring joint has also been simulated using double connections. In this study, the rigidity characteristics of the ring joint connection have been represented by a set composed of a rotational spring ($K_{\theta R}$), an axial spring (K_{AR}) and a radial spring (K_{RR}). The interaction mechanism of each spring is the same as that applied for a segment joint.

Once the TBM back-up train enters the excavated tunnels during the excavation process, it is necessary to take its self-weight into consideration. In a study performed by Lambrughi et al. [2012], this weight was simulated by artificially increasing the density value of the concrete lining. Kasper and Meschke [2004, 2006a] have instead modelled the back-up train assuming a loading scheme along the tunnel axis. In the present study, a total weight of 3980

kN for the back-up train has been simulated through distributed loads which act on the lining elements at the tunnel bottom region over an assumed angle of 90 degrees in the cross-section and over a tunnel length of 72m behind the shield tail (Kasper and Meschke [2004]) (see **Figure 5-18**).

5.2.2.2. *Mechanized twin horizontal tunnel simulation procedure*

The twin tunnel excavation sequence was modelled as follows: (i) excavation of the first tunnel (left); (ii) excavation of the second tunnel (right) with a lagged distance L_F behind the face of the first tunnel. The plan view and typical cross section of the twin tunnel excavation procedure is illustrated in **Figure** 5-20 and **Figure** 5-21.
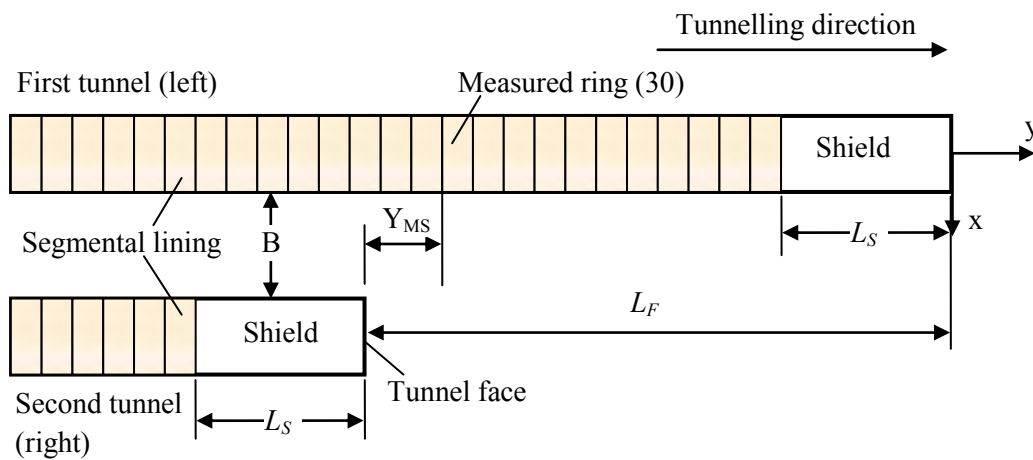
Figure 5-20. Plan view of the twin tunnels (not scaled)
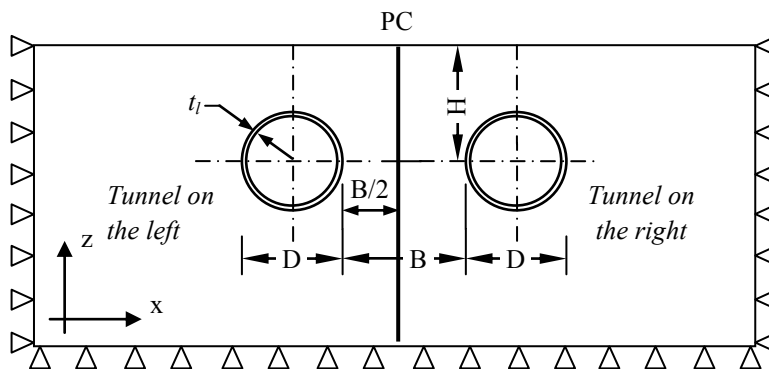
Figure 5-21. Typical cross section view of the twin tunnels with the lateral movement monitoring axis PC located in the middle between the two tubes (not scaled)

In this work, two different lagged distances (i.e., $L_F = 0D$ and $10D$) that correspond to $L_F = 0$ and $7.875L_S$, in which L_S is the shield length ($L_S = 12$ m in the present model), between the tunnel on the left and the one on the right have been adopted and analysed. The case of $L_F = 0D$ corresponds to the situation in which the two tunnel faces are excavated simultaneously

in parallel. The case of $L_F = 10D$ means that the second (new) tunnel is excavated when the lining structure behaviour and ground displacement caused by the first (existing) tunnel excavation appear to have reached a steady state. The latter case usually occurs in reality. The twin tunnels in the Bologna-Florence railway line project presented in this study is a typical example. In fact, the distance between the two tunnels in the Bologna-Florence railway line project is 15 m (Croce [2011]). However, in order to highlight the influence of the excavation process of a new tunnel on an existing tunnel, a distance from center to center of 11.75 m (1.25D) has been adopted in this study.

A full model of the twin tunnels considering a height of 60 m and a width of 131.75 m has been adopted. The mesh length of the model is equal to 120 m. The nodes at all the sides of the model were fixed in the horizontal directions on the x-z and y-z planes (i.e. y = 0, y = 120, x = -71.75 and x = 60), while the nodes at the base of the model (z = -40) were fixed in the vertical (z) direction. The perspective view of the lower part of the developed numerical model, which is composed of around 1,100,000 grid points and 900,000 zones, is presented in **Figure 5-22**.

The positions of the segment joints in each ring are presented in **Table 5-10** and **Figure 5-23**. Finally, it should be mentioned that the average time necessary for one calculation is approximately 340 hours when a 2.67GHz core i7 CPU ram 24G computer is used.
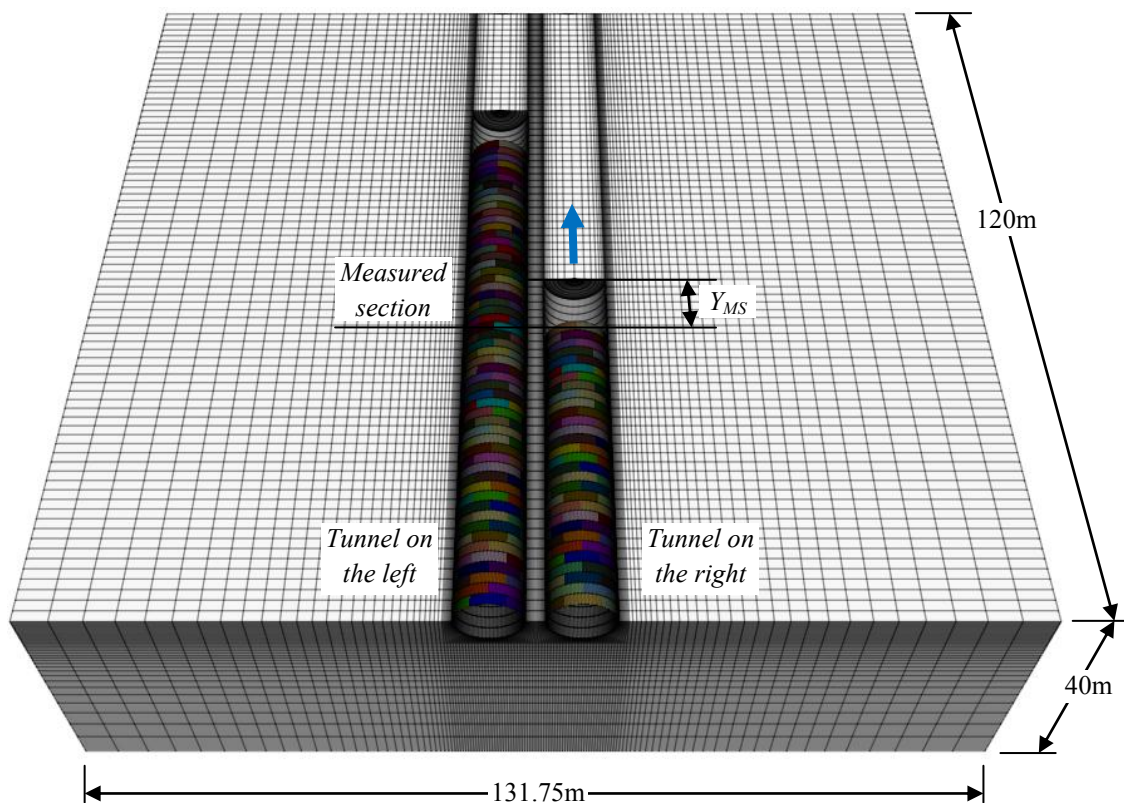
Figure 5-22. Perspective view of the developed numerical model introduced into FLAC^{3D}

Table 5-10. Location of the segment joints in a ring θ (degree) (measured counter clockwise from the right spring line)

Ring order	Joint location θ (degree)
Ring type 1	0; 60; 120; 180; 240; 300
Ring type 2	30; 90; 150; 210; 270; 330

Ring 1

Ring 2
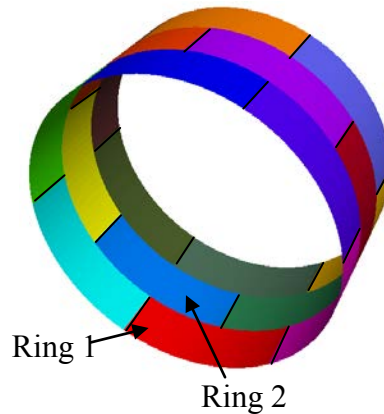
Figure 5-23. Considered lining models

5.2.3. Numerical results and discussions

In order to understand the behaviour of twin tunnels during the excavation process of the new tunnel (right), this section presents variations in the structural lining forces induced in the existing tunnel (left) and the ground displacement during new tunnel face advancement.

The variations in structural forces in the new tunnel and ground displacements have been extracted at the section corresponding to the 30th ring, which hereafter is called the measured section or measured ring, counting from the model boundary (y = 0 m). The influence of the boundary condition on the tunnel behaviour is negligible at this section. In **Figure** 5-24, **Figure** 5-25, Figure 5-26, **Figure** 5-28, **Figure** 5-30, and **Table 5-11**, the Y_{MS} value presents the distance from the new tunnel face (right)to the measured section. In **Figure** 5-27, **Figure** 5-29, **Figure** 5-31, and **Table 5-12**, the Y_{FT} value presents the distance from the faces of the two tunnels, which are excavated simultaneously, to the measured section. In **Table 5-11**, **Table 5-12**, **Table 5-13**, the R values present the ratios between the results obtained in the case of twin tunnels with L_F = 0D or 10D and the corresponding one obtained in the case of a single tunnel.

The influence of the length of the tunnel advancement on the behaviour of the measured lining ring (ring 30) has been evaluated in section 5.1 for a single (upper) tunnel, considering the instantaneous variation in structural forces between two successive steps (also see Do et al. [2014f]). The numerical results show that the instantaneous variation in the structural force induced in the measured lining ring between two excavation steps, which corresponds to the installation of rings 54 and 55, is approximately zero. This means that the structural forces determined at this excavation step can be considered as the final values that act on the measured lining ring in the long term, for the case of a single tunnel. At this point, the

distance from the tunnel face to the measured lining ring is about 5.3D, where D is the tunnel diameter.

5.2.3.1. Surface settlement

The loads caused by the excavation of the new tunnel are transmitted through the ground movements and thus affect the support of the existing tunnel. Therefore, in order to understand the twin tunnel interactions, it is very important to understand the surface settlements and especially the ground movements between the tunnels.

Figure 5-24a shows the development of the surface settlement trough in the transverse section during the face advancement of the new tunnel on the right in the case of $L_F = 10D$. This figure shows that the twin tunnels cause an increase in the surface settlement. This could be explained by the accumulated loss of the ground in both two tunnels. In the considered case, the maximum settlement measured above the twin tunnels is 47.4 % higher than that developed above a single tunnel. In addition, the settlement profile is asymmetric. This means that the maximum settlement is not located over the mid-point between the two tunnels. During the new tunnel advancement (right), the settlement trough shifts gradually from the left to the right. An asymmetric profile of the settlement trough has also been observed through field measurements obtained at shield tunnelling sites (Suwansawat and Einstein [2007], Chen et al. [2011]), analytical results using the superposition technique (Suwansawat and Einstein 2007) and laboratory model tests (Chapman et al. [2006], Chapman et al. [2007]).

In order to determine settlement trough developed over the twin tunnels, Suwansawat and Einstein [2007] and Chen et al. [2012b] suggested using Gaussian curve proposed by Peck (1969) to describe settlement developed over both tunnels. The final settlement trough is estimated on the basis of the superposition of individual settlement troughs caused by each tunnel:

$$S = S_1 \exp\left(-\frac{x^2}{2i_1^2}\right) + S_2 \exp\left(-\frac{\left(x-B'\right)^2}{2i_2^2}\right) \qquad (5\text{-}2)$$

In equation (5-2), S is the overall surface settlement; S_1 and S_2 are the maximum ground disturbance induced by the preceding tunnel and following tunnel, respectively; x is the horizontal distance from the preceding tunnel centerline in the transverse direction, i_1 and i_2 are the distance from the tunnel centerline to the inflexion point of the curve, B' is the distance between two tunnel centers (B' = B+D).

On the basis of the superposition method, Suwansawat and Einstein [2007] proposed a 2-step curve fitting method. The settlement curve caused by the preceding tunnel, which corresponds to that of a single tunnel, is first estimated using Peck's formula. Then the additional settlement developed over the centreline of the second tunnel, when the following tunnel passes through, is determined and the additional settlement curve is fitted by Peck's formula again. Finally, the two fitted curves caused by each tunnel are superposed to present

the overall ground settlement. Although the authors indicated that their simple method can be used to predict the settlement trough over twin tunnels excavated horizontally or stacked over each other, by adopting above procedure it is clear that the effect of the tunnel interaction between tunnels on the development of settlement curves has not yet been taken into consideration.
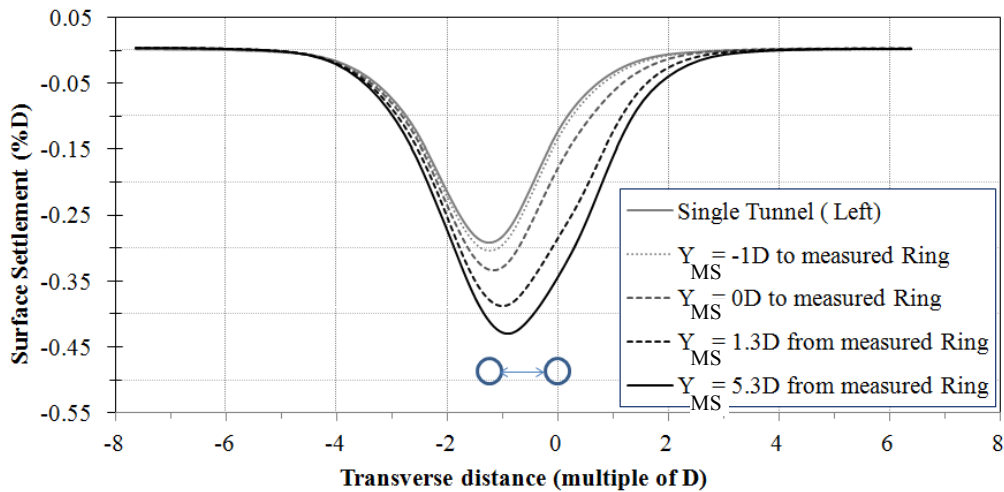
a) Development of the settlement trough in the transverse section during the new tunnel advancement (right), for the $L_F = 10D$ case
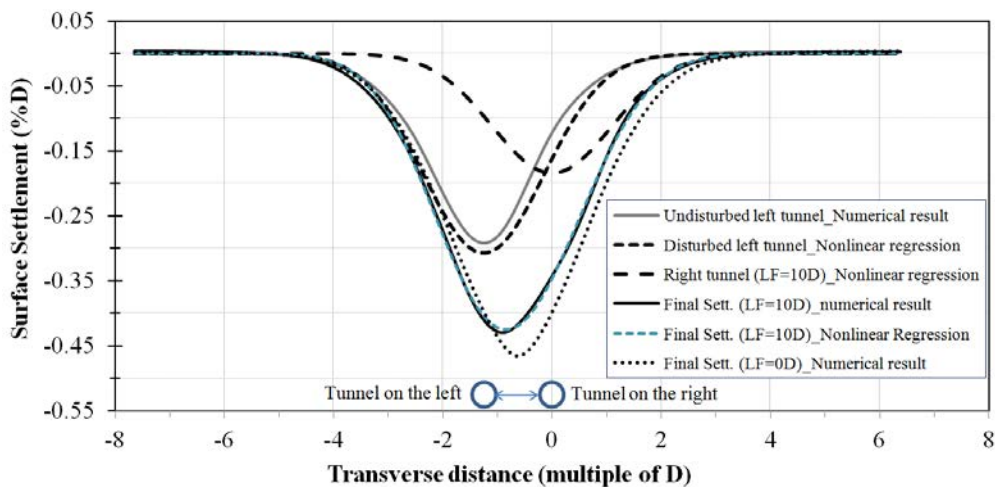
b) Comparison of the settlement trough in the transverse section of the twin tunnels

Figure 5-24. Surface settlements above the twin tunnels

It is reasonable to suppose that the excavation of the following tunnel will cause the development of a settlement curve over the tunnel and also disturb to the ground over the existing tunnel. Consequently, an additional settlement over the existing tunnel can be predicted. Due to this assumption, the final settlement curve over the twin tunnels is now a function of four unknown parameters, that is, maximum settlements over each tunnel S_1 and S_2, and distances from the inflexion point to the tunnel centreline i_1 and i_2 (see equation (5-2)) and it is therefore necessary to use an iterative procedure to obtain the best fitting curve. The

results obtained by Ma et al. [2014] indicated that Levenberg-Marquardt non-linear regression method provide an effective solution to fit the settlement curve over the twin tunnels.

Using Levenberg-Marquardt non-linear least-square criterion, a FEM code written in MATLAB programming language (The MathWorks, Inc., Natick, Massachusetts, USA) has been used to obtain the results in this paper with correlation coefficient of 0.99956.

Figure 5-24b shows the settlement curves caused by the construction of the tunnels. The settlement curve caused by the first tunnel on the left, before the excavation of the second tunnel on the right, is determined from numerical analysis. The additional settlement curves developed over each tunnel, after the advance of the tunnel on the right, are estimated using the FEM code on the basis of the nonlinear regression method. The final settlement curve obtained from numerical analysis has been used as input data. It can be seen from **Figure** 5-24b significant additional settlements induced over the existing tunnel on the left with the maximum settlement increases from 27.4 mm (0.291 % D) to 28.9 mm (0.307 % D), which correspond to an increase in volume loss ratios, determined at the final state as the ratio of settlement trough area developed on the ground surface to the cross-section area of the tunnel, from 0.915 % to 1.084 %.

The settlement trough developed over the following tunnel on the right is shallower the one developed on the existing tunnel. These conclusions are in good agreement with field observations made by Suwansawat and Einstein [2007], Chen et al. (2011) and He et al. (2012) during the excavation of twin tunnels through respectively stiff clay, silty and sandy soil. However, it should be noted that the distances from inflexion point of the curve to the centreline tunnel of each tunnel are rigorously similar and equal to approximately 10.4 m. The volume loss ratio of the following tunnel on the right is equal to about 0.647 %, and the total volume loss above the twin tunnels is therefore equal to 1.731 %.

Figure 5-24b also presents a comparison of the final settlement troughs for the different construction procedures ($L_F = 0D$ and 10D). The maximum settlement above the twin tunnels of about 43.8 mm (0.47%D) (**Table 5-13**) and the volume loss ratio of 1.81 % are observed in the $L_F = 0D$ case. These results are 9% and 6 % higher than the corresponding ones for the $L_F = 10D$ case. However, the widths of the settlement troughs are similar in both cases. In addition, as expected for the $L_F = 0D$ case, the settlement troughs that develop during tunnel face advancement are always symmetrical over the two tunnels. The larger of maximum surface settlement observed the $L_F = 0D$ case in the present study is different from that obtained through 2D numerical calculation conducted by Chen et al. [2012a]. They showed a smaller surface settlement caused by the simultneous excavation of the two tunnels compared to that observed when two tunnels are excavated successively. It should be noted that elements of shield tunnelling process have not taken into consideration in the model by Chen et al. [2012a]. Additionally, the Mohr-Coulomb has been adopted in their work, which is different from the CYsoil model used in the present study.

5.2.3.2. Horizontal ground displacement

The variations in the horizontal displacement along the PC axis, which is located at the centerline of the two tunnels, during the advancement of the single tunnel on the left are shown in **Figure** 5-25a. First, the soil mass between the tunnel crown and the invert moves outwards due to the thrust effects of the face pressure in the working chamber. Then, the ground moves toward the tunnel, due to the convergence displacement over the length of shield. The ground again moves outward at the shield tail, due to the action of the grouting pressure. These outward movements continue until the steady state is reached because of the grout consolidation and the low value of lateral earth pressure factor ($K_0 = 0.5$). The maximum horizontal displacement is about 6.0mm (0.064%D) at the ground surface.
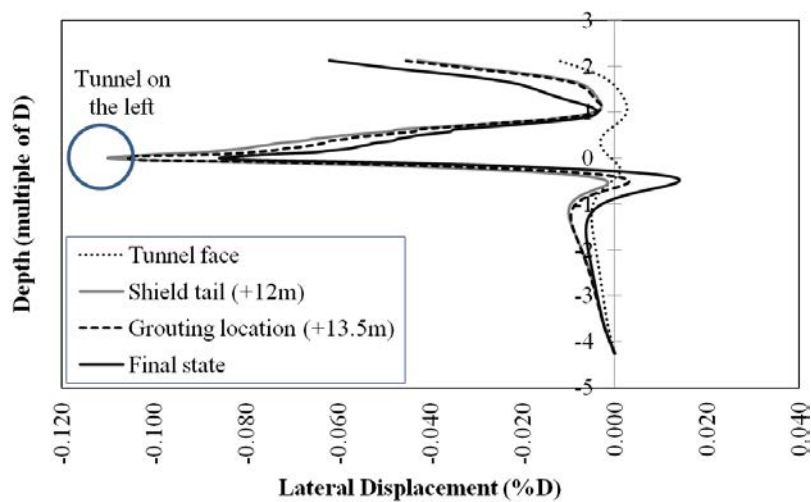
a) Lateral displacement along the PC axis during the advancement of the tunnel (single) on the left
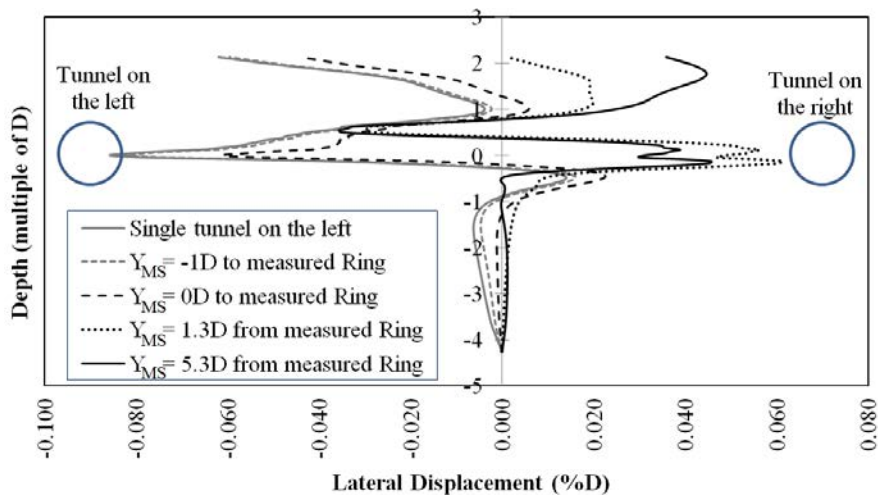
b) Lateral displacement along the PC axis during the advancement of the new tunnel on the right

Figure 5-25. Horizontal displacements between the twin tunnels, for the $L_F = 10D$ case

Figure 5-25b presents the effect of the advancement of the new tunnel on the right on the lateral displacement of the ground between the two tunnels. When the face of the new tunnel approaches the measured section, a soil mass movement towards the new tunnel caused by the convergence displacement along the length of the shield of the new tunnel is observed. These movements, which reach a peak value towards the new tunnel, correspond to the moment in which the shield tail of the new tunnel passes over the measured section (see line $Y_{MS} = 1.3D$ from the measured section in **Figure** 5-25b). When the shield in the new tunnel passes over the measured section, a ground movement towards the existing tunnel on the left can be observed due to the action of the grouting pressure, the grout consolidation, and the low lateral earth pressure factor value ($K_0 = 0.5$). The horizontal displacements at the measured section appear to have reached a steady state when the face of the new tunnel passes over the measured section at about 49.5 m, which corresponds to an Y_{MS} value of 5.3D.

It is necessary to mentioned that, compared to a corresponding 8.05 mm (0.86%D) inward movement at the spring line of a single tunnel (see the "single tunnel on the left" line in **Figure** 5-25b), the twin tunnel construction results in a 42 % reduction in lateral movement at the PC axis between the two tunnels. At the final state, the displacement of the soil mass zone below the tunnel base is almost zero.

On the basis of the above analyses on the surface settlement and lateral displacement, it is reasonable to conclude that, in the region between the two tunnels, the soil mass is subject to more vertical settlements and less horizontal displacements than in the case of a single tunnel. The same conclusion can be found through field observations obtained at a shield tunnelling site (see for example, Chen et al. [2011]).

For the case of the faces of two tunnels advancing simultaneously ($L_F = 0D$), as expected, the lateral displacements between the two tunnels are equal to zero.

5.2.3.3. Normal displacement in the tunnel lining

In this section, the positive and negative normal displacements correspond to the outward and inward deformations of the tunnel lining. As expected, the existing tunnel linings for the $L_F = 10D$ case are deformed during the passage of the new tunnel. The inward deflection at the tunnel crown and the outward displacement at the spring line gradually increase and reach values of about 271.2 % and 310.8 %, respectively, at the final state (see line $Y_{MS} = 5.3D$ in **Figure 5-26** and **Table 5-11**). These differences are important, in particular, at the right shoulder and the spring line on the right near the new tunnel (see arrows in **Figure 5-26**). Similar trends of lining deformations were observed through finite element analyses conducted by Addenbrooke and Potts [1996], laboratory 1 g tests performed by Kim et al. [1998], and measurement data collected during the excavation of twin bored tunnels at the Singapore Mass Rapid Transit (MRT) Circle Line 3, Contract 852 (Mohamad et al. [2012]), i.e., outward deformation (compressive strain) was found to be higher at the springline closer to the new tunnel, whereas inward deformation (tensile strain) was seen at the tunnel crown.

It should be noted that, at the moment in which the shield tail of the new tunnel passes over the measured section of the existing tunnel, the minimum value of the negative normal

displacement, which corresponds to a deformation ratio of 354.5 %, occurs at the spring line on the right (see line $Y_{MS} = 1.3D$ in **Figure 5-26** and **Table 5-11**).

Unlike the existing tunnel, the normal deformation of the new tunnel lining is similar to that of a single tunnel (see **Figure 5-26**) with the differences of the maximum normal displacement at the tunnel crown or invert and the minimum normal displacement at the spring line are 7.9 % and 9.9 %, respectively (**Table 5-11**).

Figure 5-27 and **Table 5-12** show gradual increases in the normal displacements induced in the tunnel on the left during the simultaneous advancement of the double tunnel faces in the $L_F = 0D$ case. When the twin tunnel faces are 5.3D from the measured ring, the normal displacements in the tunnel lining are steady. The maximum magnitudes of the normal displacement are similar in both tunnels but their diagrams are affected to a great extent by the interaction between the two tunnels. As expected, the final shapes of the normal displacements of the two tunnels are symmetrical over the vertical centerline of the tunnel (**Figure** 5-27).
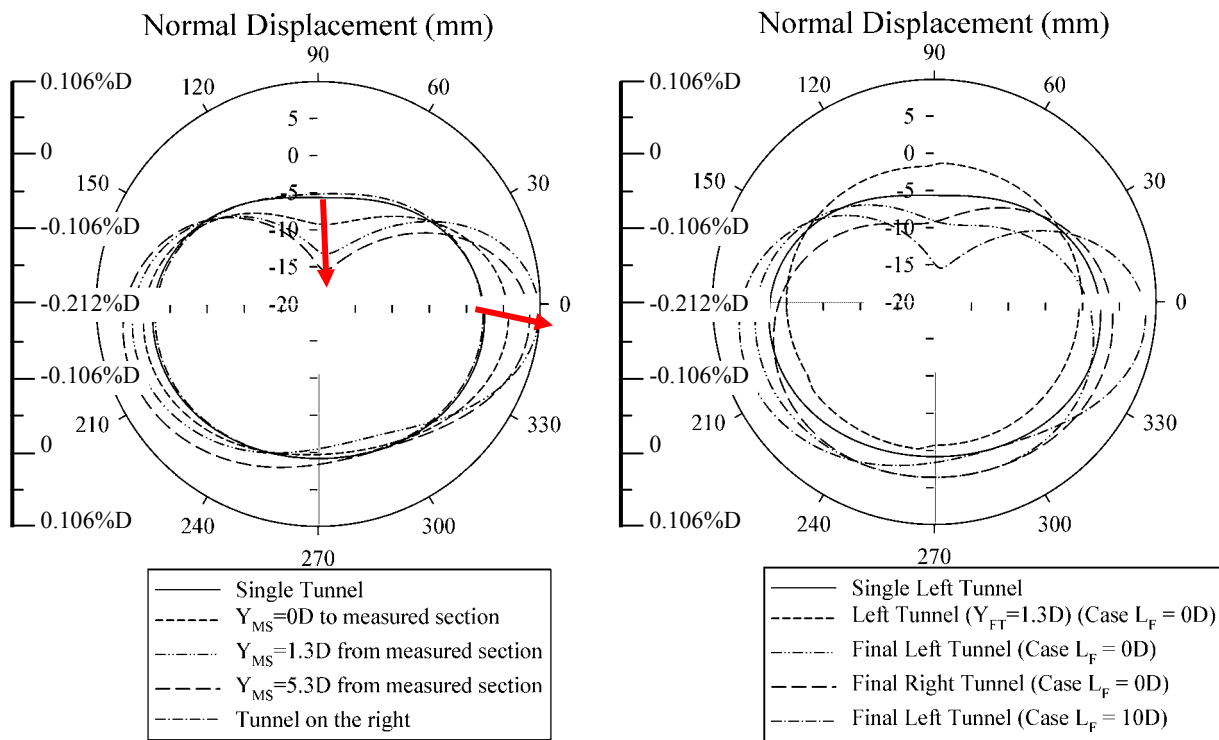
Figure 5-26. Normal displacement in measured lining ring 30 of the existing (left) tunnel, for the $L_F = 10D$ case

Figure 5-27. Normal displacement in measured lining ring 30 of the tunnel on the left, for the $L_F = 0D$ case

It can be seen in **Figure** 5-27 and **Table 5-13** that the normal displacements of the lining in the tunnel on the left in the $L_F = 0D$ case are more similar in shape and magnitude to those obtained in a single tunnel than the normal displacements determined in the $L_F = 10D$ case. These differences are important, in particular, at the tunnel side near the tunnel on the right.

5.2.3.4. Normal forces and longitudinal forces in the tunnel lining

Figure 5-28a and **Table 5-11** show the changes in the normal forces induced in the measured ring during advancement of the new tunnel on the right for the L_F = 10D case. When the face of the new tunnel approaches the measured section, there is a significant increase in the normal forces at the spring line on the right near to the new tunnel. This points out a load transfer from the new tunnel to the existing tunnel. At the moment when the face of the new tunnel is across the measured section, which corresponds to a distance Y_{MS} = 0D, an increase of 40.7 % in the normal forces occurs at the region of the spring line on the right near the new tunnel (see line Y_{MS} = 0D in **Figure** 5-28a and **Table 5-11**). After that, the movement of the ground towards the new tunnel (see line Y_{MS} = 1.3D from the measured section in **Figure** 5-25b), caused by the convergence displacement along the shield, is the main reason for the decrease in the normal forces measured at the region of the spring line on the right (see line Y_{MS} = 1.3D from the measured section in **Figure** 5-28a and **Table 5-11**). This means that there is a load transfer from the existing tunnel to the new tunnel.

When the shield in the new tunnel passes over the measured section, the movement of the ground in the opposite direction, from the new tunnel towards the existing tunnel (see line Y_{MS} = 5.3D from the measured section in **Figure** 5-25b), again causes a load transfer from the new tunnel to the existing tunnel that leads to an increase in the normal forces measured at the spring line on the right in the existing tunnel (see line Y_{MS} = 5.3D from the measured section in **Figure** 5-28a). At the final state, the maximum normal force in the measured lining ring in the existing tunnel is about 29.3 % higher than that of a single tunnel (**Table 5-11**).

Unlike the normal forces on the right side near the new tunnel, the advancement of the excavation of the new tunnel always shows an increase in the normal forces induced in the left side regions of the existing tunnel lining. This can be attributed to the fact that the ground regions on the left side of the existing tunnel show a general tendency to move to the right side, due to the effect of the excavation of the new tunnel. The tunnel linings on this side are deflected outwards (see **Figure 5-26**), caused by the large downward vertical movement of the tunnel crown. These phenomena lead to an increase in the external loads that act on the tunnel lining.

As for the longitudinal forces (see **Figure** 5-28b), when the face of the new tunnel approaches the measured section, an increase in longitudinal forces of about 6.6 %, measured at the spring line region on the right in the existing tunnel, can be observed (see line Y_{MS} = 0D to the measured section in **Figure** 5-28b and **Table 5-11**). This could be explained by the increase in the normal forces, as mentioned above, which produces an increase in the longitudinal force of the lining because of the Poisson effect caused by the transversal deformation. On the other hand, the longitudinal forces at the tunnel crown show a large decrease of about 27 % (see line Y_{MS} = 0D to the measured section in **Figure** 5-28b). These decreases could be attributed to the decrease in coupling effects between the lining rings in the existing tunnel, which is caused by the movement of ground ahead of the face of the new tunnel towards the shield space.
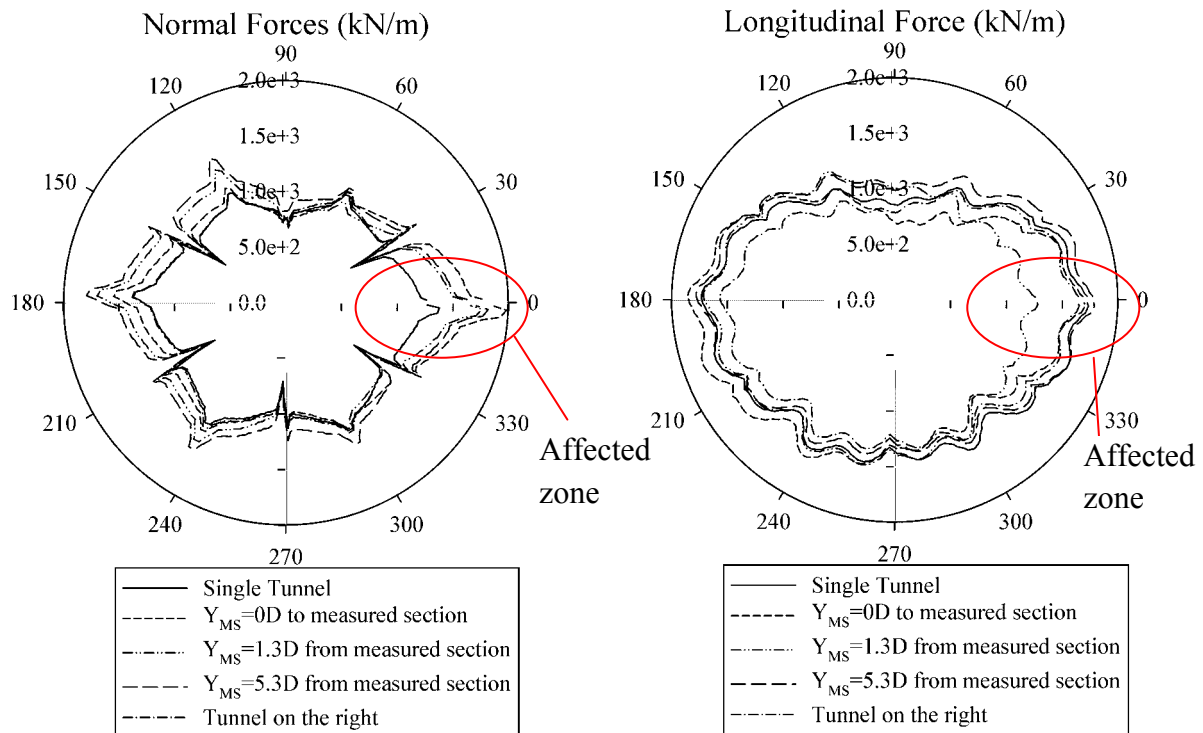
a) Normal force in measured lining ring 30 of the existing (left) tunnel

b) Longitudinal force in measured lining ring 30 of the existing (left) tunnel

Figure 5-28. Normal force and longitudinal force of the existing (left) tunnel lining during the advancement of the new (right) tunnel, for the $L_F = 10D$ case

When the face of the new tunnel passes over the measured section, a large decrease of about 24 % at the spring line regions on the right and an increase of about 23.5 % at the tunnel crown in the longitudinal forces, measured in the existing tunnel, are observed (see line $Y_{MS} = 1.3D$ from the measured section in **Figure** 5-28b). This could be explained by the lateral movement of the ground between the two tunnels towards the new tunnel which is caused by the ground loss along the shield in the new tunnel.

At the final state, as the new tunnel face becomes distant, due to the increase in normal forces, a gradual increase in the longitudinal forces caused by the Poisson effect can be expected and the maximum value of the longitudinal forces in the existing tunnel are more or less similar as that obtained before the passage of the new tunnel face (**Figure** 5-28b and **Table 5-11**).

Unlike the existing tunnel, both the normal forces and longitudinal forces induced in the new tunnel lining (right) are the same as those developed in a single tunnel, not only in terms of the distribution along the tunnel boundary but also in magnitude terms (**Figure** 5-28 and **Table 5-11**). This means that normal forces and longitudinal forces induced in the new tunnel lining are smaller than that developed in the existing tunnel. This suggests that the existing tunnel carries more external loads than the new tunnel.

Figure 5-29 and **Table 5-12** show gradual increases in the normal forces induced in the measured ring of the tunnel on the left during the simultaneous advancement of the double tunnel faces for the $L_F = 0D$ case. When the twin tunnel faces are 5.3D from the measured

ring, the normal forces and longitudinal forces in the tunnel lining are steady. The maximum magnitudes of normal forces and longitudinal forces are similar in both two tunnels, but occur at different locations on the tunnel boundary, which are symmetrical over the vertical centerline of each tunnel, due to the interaction between the two tunnels (see **Figure** 5-29).

Figure 5-29 also shows that the normal forces and longitudinal forces in the tunnel on the left in both the $L_F = 0D$ and 10D cases are similar in shape. However, the normal forces induced in the $L_F = 10D$ case are 11.4% higher than those of the $L_F = 0D$ case. As for the longitudinal forces, it is 87.4 % less than the one in the $L_F = 0D$ case (**Table 5-13**). It can be seen that the longitudinal forces obtained in the $L_F = 10D$ case is more similar in magnitude to those determined in a single tunnel than that obtained in the $L_F = 0D$ case. The longitudinal forces at the crown and bottom region of the tunnel are affected to a great extent by the simultaneous excavation of the two tunnels compared to those of a single tunnel, in the $L_F = 0D$ case.
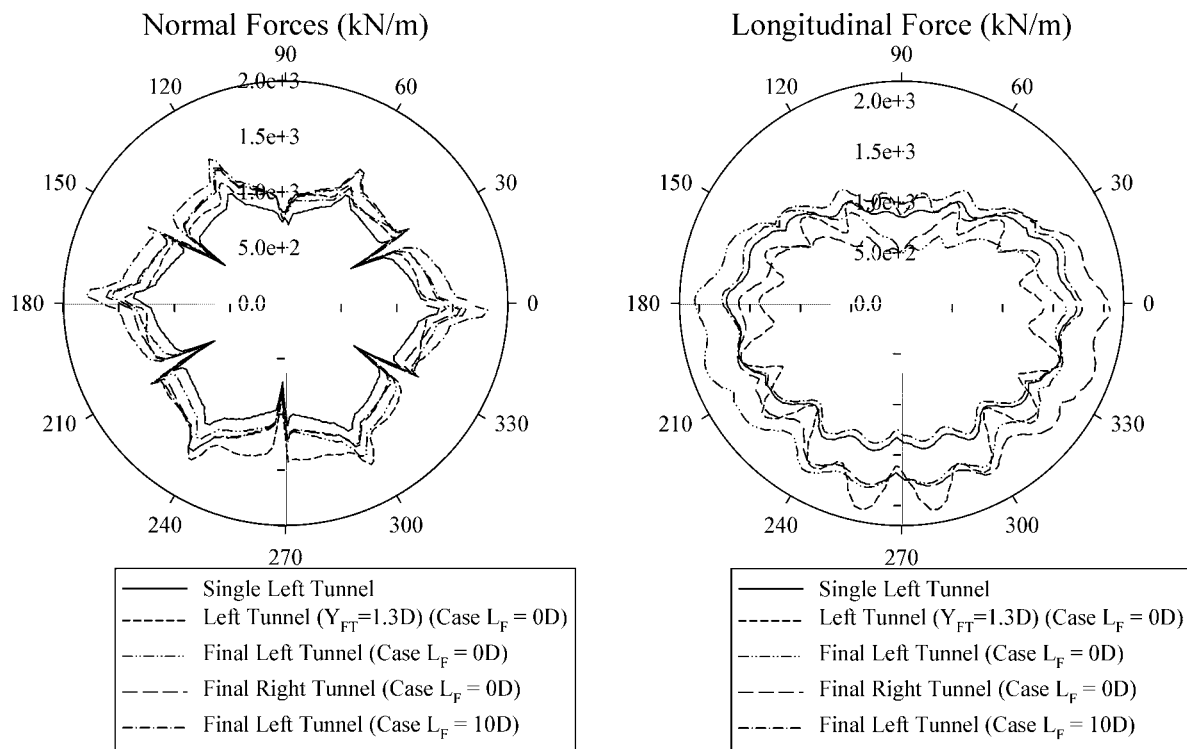
a) Normal force in measured lining ring 30 of the tunnel on the left

b) Longitudinal force in measured lining ring 30 of the tunnel on the left

Figure 5-29. Normal force and longitudinal force of the tunnel lining on the left during the simultaneous advancement of the double tunnel faces, for the $L_F = 0D$ case

5.2.3.5. Bending moment in the tunnel lining

Figure 5-30 shows the distribution of the bending moment in the measured ring of the existing tunnel (left) for the $L_F = 10D$ case. It can be seen that the excavation of the new tunnel (right) causes a significant increase in the bending moment induced in the existing

tunnel, in particular at the right side near the new tunnel. The results presented in **Figure** 5-30 and **Table 5-11** show a gradual increase in the absolute magnitude of the bending moment in the existing tunnel during the advancement of the face of the new tunnel. Generally, due to the loss of ground during the excavation of the new tunnel, the soil mass between the tunnels has a tendency to move towards to the new tunnel, as can be seen in **Figure** 5-25b. On the other hand, the ground above the existing tunnel moves downwards. These phenomena lead to an increase in the positive bending moment at the right shoulder and right base regions, for the measured ring in the existing tunnel, and an increase in the absolute magnitude of the negative bending moment at the spring line on the right. These changes are pointed out by the results presented in **Figure** 5-30 and **Table 5-11**. These results are consistent with the results of Kim et al. [1998], who reported that the incremental bending moment of an existing tunnel is at a maximum near a new tunnel. **Figure** 5-30 indicates that the changes in bending moment at the other locations around the existing tunnel (location on the left side) are relatively insignificant.
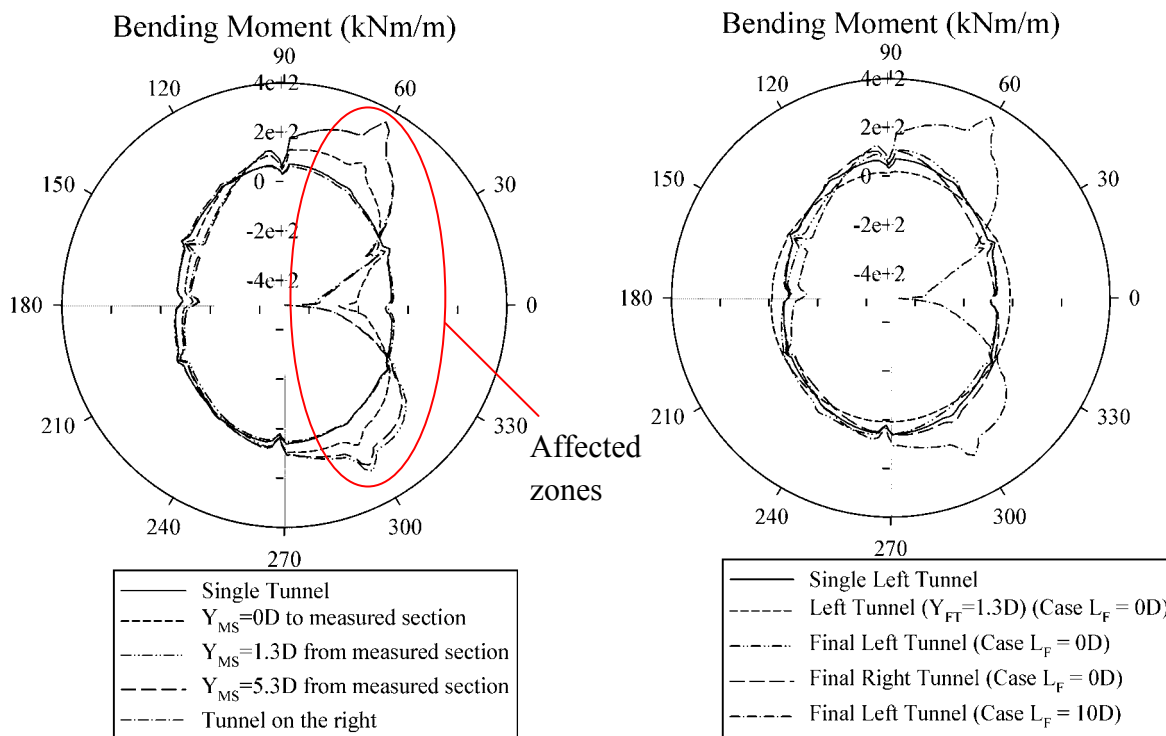
Figure 5-30. Bending moment in measured lining ring 30 of the existing (left) tunnel, for the L_F = 10D case

Figure 5-31. Bending moment in measured lining ring 30 of the tunnel on the left, for the L_F = 0D case

An increase of about 14.2 % can be seen for the positive bending moment when the new tunnel face approaches the Y_{MS} distance of -1D and the increase reaches a maximum value of 383.8 % at distance Y_{MS} = 1.3D, which corresponds to the moment at which the shield tail of the new tunnel passes over the measured section. After that, a negligible change in the positive bending moment can be seen (see **Figure** 5-30 and **Table 5-11**). A similar tendency

can be observed for the negative bending moment induced at the spring line in the measured ring in the existing tunnel (see **Figure** 5-30 and **Table 5-11**).

It should be noted that, in the existing tunnel lining, the change in the bending moment on the right side near the new tunnel is greater than the one that occur on the left side. The maximum changes in the absolute negative bending moment that occur at the right and left spring lines of the existing tunnel are equal to 516 % and to 176 %, respectively, compared to a single tunnel (see line Y_{MS} = 1.3D in **Figure** 5-30).

Table 5-11. Development of the structural forces and deformation in measured ring 30 of the existing tunnel (left) and surface settlement during the new tunnel advancement (right) (for the L_F = 10D case)

Parameters	*Single tunnel*	*Distance Y_{MS} (m)*						*Tunnel on the right*
	-	*-1D*	*0*	*1.3D*	*3D*	*4.5D*	*5.3D*	*-*
Max. pos. bending moment (kN.m/m)	71.9	82.2	162.8	348.1	343.9	347.2	348.1	65.8
R_{M+} *(%)*	*100.0*	*114.2*	*226.2*	*483.8*	*478.0*	*482.5*	*483.8*	*91.5*
Min. neg. bending moment (kN.m/m)	-93.8	-107.4	-279.5	-498.1	-481.6	-481.2	-480.6	-89.9
R_{M-} *(%)*	*100.0*	*114.5*	*297.8*	*530.7*	*513.1*	*512.8*	*512.0*	*95.8*
Max. Normal force (kN/m)	1490	1598	2096	1859	1948	1931	1927	1491
R_N *(%)*	*100.0*	*107.2*	*140.7*	*124.8*	*130.8*	*129.6*	*129.3*	*100.1*
Max. Longitudinal force (kN/m)	1745	1966	1861	1719	1736	1809	1798	1667
R_{LN} *(%)*	*100.0*	*112.7*	*106.6*	*98.5*	*99.5*	*103.6*	*103.0*	*95.5*
Max. normal displacement (mm)	5.69	6.72	9.28	13.18	14.33	15.09	15.42	5.24
R_{disp+} *(%)*	*100.0*	*118.2*	*163.1*	*231.8*	*252.0*	*265.3*	*271.2*	*92.1*
Min. normal displacement (mm)	-2.78	-3.40	-5.80	-9.86	-9.00	-8.70	-8.65	-2.51
R_{disp-} *(%)*	*100.0*	*122.2*	*208.6*	*354.5*	*323.8*	*312.9*	*310.8*	*90.1*
Max. settlement (%D)	-0.26	-0.30	-0.33	-0.39	-0.41	-0.42	-0.43	-
R_{set} *(%)*	*100.0*	*104.4*	*114.5*	*133.0*	*142.6*	*145.9*	*147.4*	*-*

Figure 5-30 and **Table 5-11** also show that, at the final state, the magnitude of the bending moments is higher in the existing tunnel than in the new tunnel. The maximum positive bending moments induced in the existing and new tunnel are about 483.8 % and 91.5 %, respectively, compared to the bending moment induced in a single tunnel. These values are 512.0 % and 95.8 %, respectively, for the minimum negative bending moment. This means that both the distribution and magnitude of the bending moments induced in the new tunnel are similar to those of a single tunnel.

Table 5-12. Development of the structural forces and deformation in measured ring 30 of the tunnel on the left and surface settlement during the simultaneous advancement of twin tunnels (for the $L_F = 0D$ case)

Parameters	Single tunnel	Distance Y_{FT} (m)			
	-	*1.3D*	*2.55D*	*3.8D*	*5.3D*
Max. pos. bending moment (kN.m/m)	71.9	19.1	101.3	108.9	109.9
R_{M+} *(%)*	*100.0*	*26.5*	*140.8*	*151.3*	*152.7*
Min. neg. bending moment (kN.m/m)	-93.8	-15.0	-85.1	-95.6	-97.4
R_{M-} *(%)*	*100.0*	*16.0*	*90.6*	*101.8*	*103.8*
Max. Normal force (kN/m)	1 490	1 669	1 715	1 726	1 730
R_N *(%)*	*100.0*	*112.0*	*115.1*	*115.9*	*116.1*
Max. Longitudinal force (kN/m)	1 745	2 081	1 652	1 913	2 057
R_{LN} *(%)*	*100.0*	*119.2*	*94.7*	*109.6*	*117.8*
Max. normal displacement (mm)	5.69	1.77	6.42	8.64	9.39
R_{disp+} *(%)*	*100.0*	*31.2*	*112.9*	*151.9*	*165.1*
Min. normal displacement (mm)	-2.78	-0.22	-3.34	-4.41	-4.74
R_{disp-} *(%)*	*100.0*	*8.1*	*120.0*	*158.4*	*170.6*
Max. settlement (%D)	-0.26	-0.36	-0.43	-0.46	-0.47
R_{set} *(%)*	*100*	*121.9*	*147.4*	*156.2*	*159.9*

Figure 5-31 and **Table 5-12** show a gradual increase in the bending moment induced in the measured ring in the tunnel on the left during the simultaneous advancement of the double tunnel faces ($L_F = 0D$). When the twin tunnel faces is 5.3D from the measured ring, the bending moments are steady. As expected, the maximum magnitudes of the bending moments in the two tunnels are similar.

Figure 5-31and **Table 5-13** show that the bending moments induced in the tunnel lining on the left for the $L_F = 0D$ case are similar in shape and magnitude to those obtained in a single tunnel, but are significantly different from that determined in the $L_F = 10D$ case. These differences are important, in particular, at the tunnel side near the new tunnel (right).

Generally, the comparative results presented in **Table 5-13** indicate that, for both cases of lagged distance between the tunnel faces (i.e. $L_F = 0$ and 10D), the excavation of twin tunnels always causes increases in the absolute maximum values of both the structural lining forces induced in the left (existing) tunnel and of the surface settlement compared to those of a single tunnel. The simultaneous excavation of twin tunnels (i.e. $L_F = 0D$) causes smaller structural forces and lining displacements than those determined in the case of twin tunnels excavated at a great lagged distance (i.e. $L_F = 10D$). However, the simultaneous excavation of twin tunnels could result in a higher settlement above the two tunnels.

Table 5-13. Comparisons of the structural forces and deformation in measured ring 30 of the tunnel on the left and surface settlement for the $L_F = 0D$ and 10D cases

Parameters	Single tunnel	$L_F = 0D$ (A)	$L_F = 10D$ (B)	B/A %
Max. pos. bending moment (kN.m/m)	71.9	109.9	348.1	316.7
R_{M+} (%)	*100.0*	*152.7*	*483.8*	
Min. neg. bending moment (kN.m/m)	-93.8	-97.4	-480.6	493.4
R_{M-} (%)	*100.0*	*103.8*	*512.0*	
Max. Normal force (kN/m)	1490	1730	1927	111.4
R_N (%)	*100.0*	*116.1*	*129.3*	
Max. Longitudinal force (kN/m)	1745	2057	1798	87.4
R_{LN} (%)	*100.0*	*117.8*	*103.0*	
Max. normal displacement (mm)	5.69	9.39	15.42	164.2
R_{disp+} (%)	*100.0*	*165.1*	*271.2*	
Min. normal displacement (mm)	-2.78	-4.74	-8.65	182.5
R_{disp-} (%)	*100.0*	*170.6*	*310.8*	
Max. settlement (%D)	*-0.26*	-0.47	-0.43	92.0
R_{set} (%)	*100.0*	*159.9*	*147.4*	

5.2.4. Conclusions

It is well known that the interaction between mechanized twin tunnels excavated in soft ground is complex. In this study, a 3D numerical model of the mechanized twin tunnelling process has been developed. This model can be used to predict the ground movements and structural forces induced in the lining of two tunnels excavated in parallel.

The main construction aspects of a mechanized tunnelling excavation process have been simulated in the model. On the basis of 3D numerical analyses, it is possible to draw the following conclusions:

(1) The excavation of the new tunnel has a high impact on the behaviour of the existing tunnel. The impact of excavation is important, in particular, on the tunnel side near the new tunnel. The maximum interaction between two tunnels occurs when the shield tail of the new tunnel passes over the measured section. Interaction of the twin tunnels gradually decreases when the new tunnel face is far from the measured section. The influence of the new tunnel on the existing tunnel can be negligible at a Y distance of about 5.3D. This length of influence is similar to that of a single tunnel.

(2) Due to the interaction of the twin tunnels, an increase in the surface settlement can be expected compared to that induced above a single tunnel. In addition, the settlement profile is asymmetric. However, the two settlement troughs caused by the construction of the tunnels on the left and right have a similar shape. Twin tunnel construction procedures have a great influence on the surface settlement.

(3) As the new tunnel face approaches the measured section, there is a significant increase in the normal forces at the spring line on the right near the new tunnel. This points out a load transfer from the new tunnel to the existing tunnel. Unlike in the existing tunnel,

both the normal forces and longitudinal forces induced in the new tunnel lining are the same as those developed in a single tunnel. This suggests that the existing tunnel bears more external loads than the new tunnel.

(4)   The excavation of the new tunnel causes a significant increase in the bending moment in the existing tunnel. At the final state, the magnitude of the bending moments is higher in the existing tunnel than in the new tunnel. Unlike the existing tunnel, both the distribution and magnitude of the bending moments induced in the new tunnel are similar to those of a single tunnel. The bending moments induced in the lining of the tunnel on the left in the $L_F = 0D$ case are similar in shape and magnitude to those obtained in a single tunnel, but they are significantly different to those determined in the $L_F = 10D$ case.

(5)   Both the inward deflection at the tunnel crown and invert and the outward displacement at the spring line gradually increase. Unlike the existing tunnel, the normal deformation of the lining of the new tunnel is similar to that of a single tunnel. The normal displacements of the lining of the tunnel on the left in the $L_F = 0D$ case are more similar in shape and magnitude to those obtained in a single tunnel than the normal displacements determined in the $L_F = 10D$ case.

(6)   Generally, the simultaneous excavation of twin tunnels (i.e. $L_F = 0D$) causes smaller structural forces and lining displacements than those induced in the case of twin tunnels excavated at a high lagged distance (i.e. $L_F = 10D$). However, the simultaneous excavation of twin tunnels could result in higher settlements above the two tunnels.

(7)   The behaviour of the new tunnel is similar to that of a single tunnel.

It should be noted that interaction between twin horizontal tunnels observed in this study could be changed when other value of the K_0 factor is applied

---

5.3. Numerical Investigation of Twin Stacked Tunnels

5.3.1. Introduction

In recent years, many tunnels have been built in urban environments; this often involves the construction of twin tunnels in close proximity to each other. In some cases, the twin tunnels are stacked over each other in order to avoid the pile foundations of existing building on the ground surface.

The main purpose of this study was to provide a complete 3D model which allows the mechanized twin stacked tunnels interaction behaviour to be evaluated in terms of the structural forces induced in the tunnel lining and ground displacement surrounding the two tunnels. Similar to the 3D model described in section 5.2, most of the main elements of a mechanized excavation are simulated in this model. The CYsoil model has been adopted. The Bologna-Florence high speed railway line has been adopted in this study as a reference case.

5.3.2. Numerical model

5.3.2.1. Three-dimensional numerical model

Generally, the numerical model, the 3D simulation procedure of tunnels and simulation parameters presented in section 5.2 has been adopted in this section. However, parameters concerning the pressure acting on the tunnel face and grouting pressure at the shield tail have been changed in order to take into consideration the effect of the change in the depth of stacked tunnels on their values.

5.3.2.2. Mechanised twin stacked tunnel simulation procedure

The twin stacked tunnel excavation was modelled as follows:
- Case 1: (i) excavation of the upper tunnel first; (ii) excavation of the lower tunnel at a lagged distance $L_F = 10D$ behind the first tunnel face.
- Case 2: (i) excavation of the lower tunnel first; (ii) excavation of the upper tunnel at a lagged distance $L_F = 10D$ behind the first tunnel face.
- Case 3: simultaneous excavation of the upper and lower tunnels, i.e. a lagged distance of $L_F = 0D$ is adopted.

A side view in the vertical plane and a typical cross-section of the twin stacked tunnels are illustrated in **Figure** 5-32. The two cases of $L_F = 10D$ in this work means that the second tunnel is excavated when the behaviour of the lining structure and ground displacement caused by the first tunnel excavation appear to have reached a steady state. These cases commonly occur in reality. In order to highlight the influence of the excavation process of a

new tunnel on an existing tunnel, a center-to-center distance of 11.75 m (B= 0.25D) in the vertical direction has been adopted in this study.
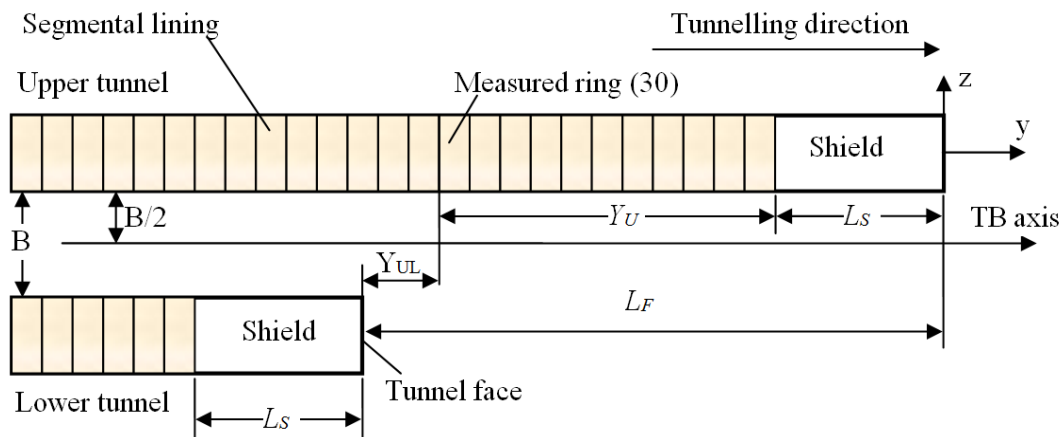
Figure 5-32. Side view of twin tunnels in a vertical plane (not scaled) (case 1)

A full model of twin tunnels, considering a height of 71.75 m and a width of 160 m, has been adopted in the present model. The mesh length of the model is equal to 120 m. The excavation step length is equal to 1.5 m, a distance which corresponds to the width of a lining ring. The nodes at all the sides of the model were fixed in the horizontal directions on the x-z and y-z planes (i.e. y = 0, y = 120, x = -80 and x = 80), while the nodes at the base of the model (z = -51.75) were fixed in the vertical (z) direction. A perspective view of half of the developed numerical model, which is composed of around 920,000 grid points and 800,000 zones, can be seen in **Figure 5-33**.
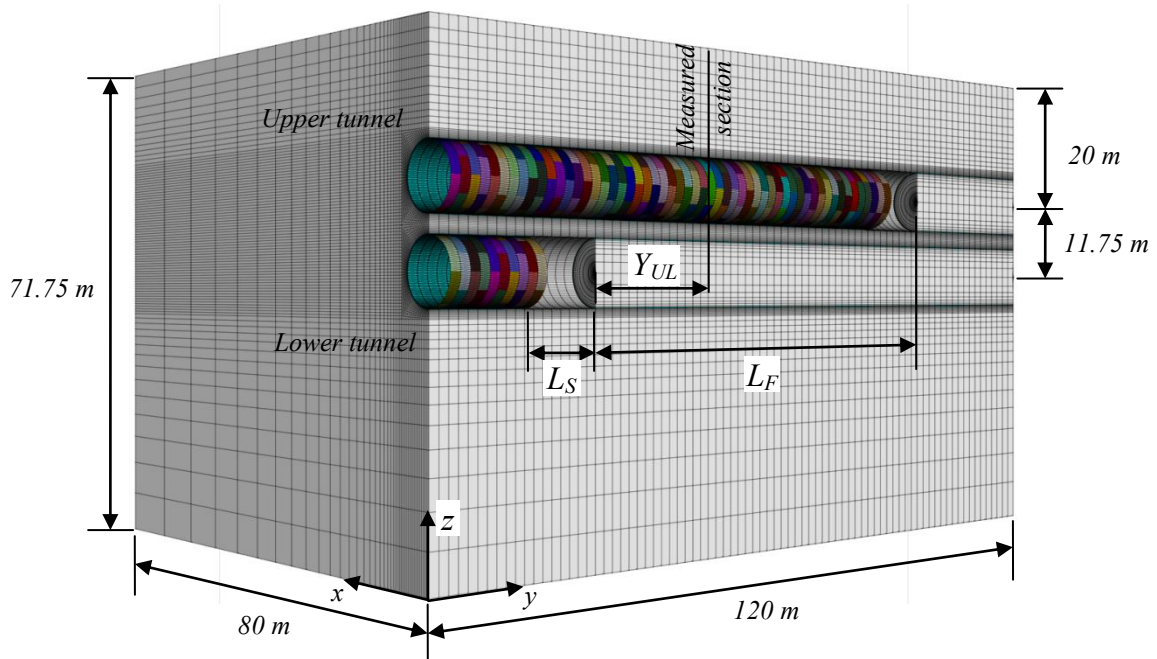
Figure 5-33. Perspective view of half of the developed numerical model introduced into FLAC^{3D} (case 1)

The positions of the segment joints in each ring are presented in **Table 5-10** and **Figure 5-33**. An alternation of type 1 and type 2 of the rings along the tunnel axis can be seen. Finally, it should be mentioned that the average time necessary for one calculation is approximately 340 hours, when a 2.67GHz core i7 CPU ram 24Go computer is used.

5.3.3. Numerical results and discussion

In order to understand the behaviour of stacked tunnels during the excavation of a new tunnel, this section presents the variations in the structural lining forces that are induced in both tunnels and in the ground displacements during the advancement of the new tunnel.

The variations in structural forces of both an existing and a new tunnel and in the ground displacement have been shown to occur at the section corresponding to the 30th ring, which is hereafter referred to as the measured section or measured ring in both tunnels, counting from the model boundary (y = 0 m). The influence of the boundary condition on tunnel behaviour is negligible at this section. The Y_{UL} value in **Figure 5-34**, **Figure 5-40**, **Figure 5-45**, **Figure 5-50** and **Table 5-14** represents the distance from the lower (new) tunnel face to the measured section in case 1. The Y_{LU} value in **Figure 5-36**, **Figure 5-41**, **Figure 5-46**, **Figure 5-51** and **Table 5-15** represents the distance from the upper (new) tunnel face to the measured section in case 2. The R values in **Table 5-14**, **Table 5-15**, **Table 5-17**, **Table 5-18** represents the ratios between the results obtained in the case of twin stacked tunnels and the corresponding ones obtained in the case of a single tunnel.

5.3.3.1. Surface settlements

The development of the surface settlement trough in the longitudinal section during the lower (new) tunnel face advancement is shown in **Figure 5-34** for case 1. This figure indicates that the stacked tunnels cause an increase in the surface settlements. This could be explained by the accumulation of the ground loss from both tunnels. The maximum settlement measured above the stacked tunnels is 40.1% higher than that developed above a single upper tunnel (see **Table 5-14**). **Figure 5-34** also indicates that the surface settlement at the measured section begins to be affected by the lower (new) excavation when the face of this tunnel approaches a distance of about 1.9D.

It can be seen in **Figure 5-35** that the two settlement troughs caused by the construction of the two tunnels are different. The settlement trough above the new tunnel is determined on the basis of the final settlement trough of the twin tunnels minus the settlement trough developed above the existing tunnel before it interacts with the new tunnel. The settlement trough caused by the new (lower) tunnel excavation is shallower and wider than that caused by the existing (upper) tunnel. The volume loss ratios, determined at the final state, of the upper (existing) and lower (new) tunnels are equal to about 0.875 % and 0.622 %, respectively, and the total volume loss above the stacked tunnels in case 1 is therefore 1.497 %.
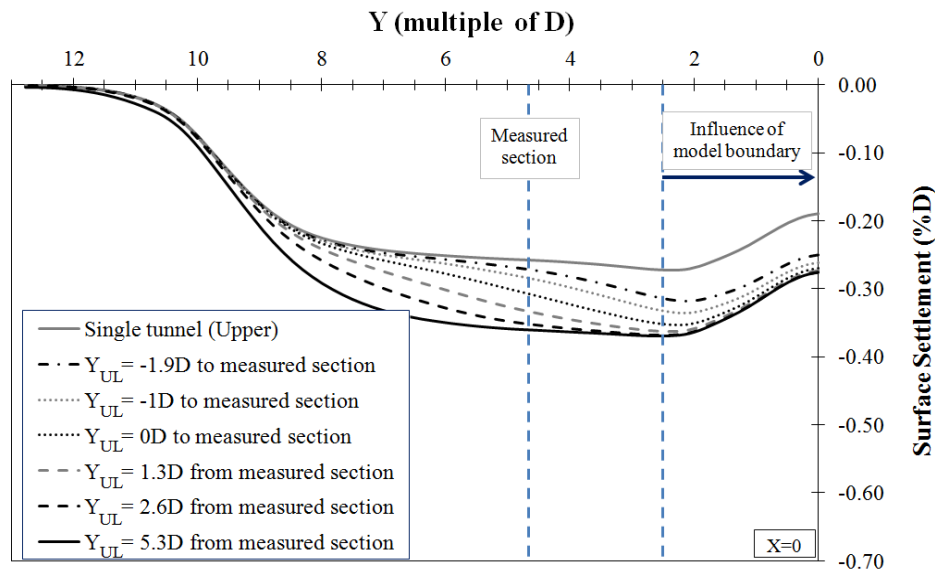
Figure 5-34. Longitudinal settlements on the ground surface above the stacked tunnels, case 1
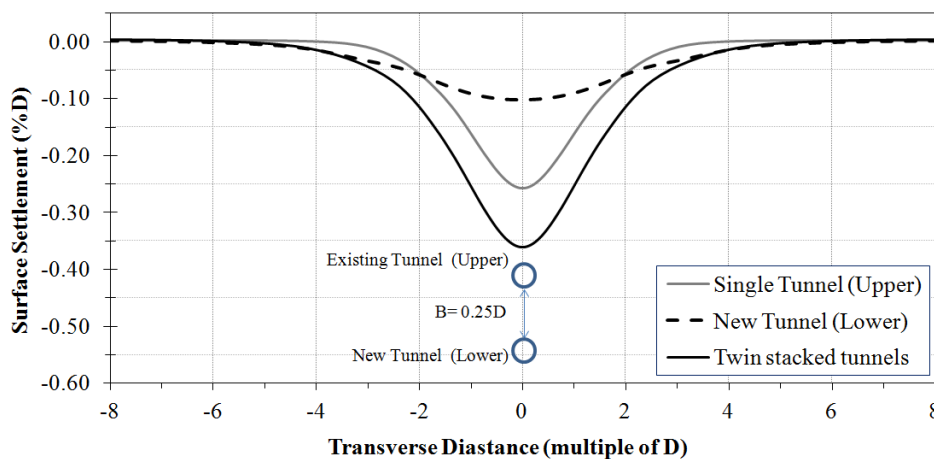
Figure 5-35. Comparison of the settlement troughs in the transverse section of the stacked tunnels, case 1

In case 2, when the lower tunnel is excavated first, the slopes of the longitudinal surface troughs are steeper than the ones observed in case 1 during the advancement of the new (upper) tunnel (see **Figure 5-34** and **Figure 5-36**). This could be explained by the shallower depth of the new tunnel in case 2. It can also be seen in **Figure 5-36** that the surface settlement at the measured section begins to be affected by the upper (new) excavation when the face of this tunnel approaches a distance of about 1D. This distance is shorter than that determined in case 1. The settlement trough caused by the new (upper) tunnel excavation is smaller and narrower than that caused by the existing (lower) tunnel. The volume loss ratios, determined at the final state, of the lower (existing) tunnel and upper (new) tunnel are similar and equal to about 0.933 % and 0.451 %, respectively, and the total volume loss above the twin tunnels is therefore 1.384 % (see **Figure 5-37**). Comparing these results with the results

obtained for case 1, it can be seen that the surface settlements above the stacked tunnels in case 1, in which the upper tunnel is excavated first, are more important than the surface settlements obtained in case 2 (**Figure 5-38**). This result is in good agreement with the 2D numerical results obtained by Hage Chehade and Shahrour [2008] and Channabasavaraj and Vishwanath [2012].

It can also be seen in **Figure 5-38** that the settlement value of 32.2 mm determined in case 3, in which two stacked tunnels are excavated simultaneously, falls in between those obtained in the two previous cases (i.e. case 1 and case 2). However, the widths of the settlement troughs are similar in all three cases. In addition, as for a single tunnel, the smaller the tunnel depth, the greater and the narrower the surface settlement trough. This result is in good agreement with the 2D numerical results obtained by Hejazi et al. [2008]. As expected, the settlement profiles in the traverse section in all three cases are always symmetric over the tunnel center.
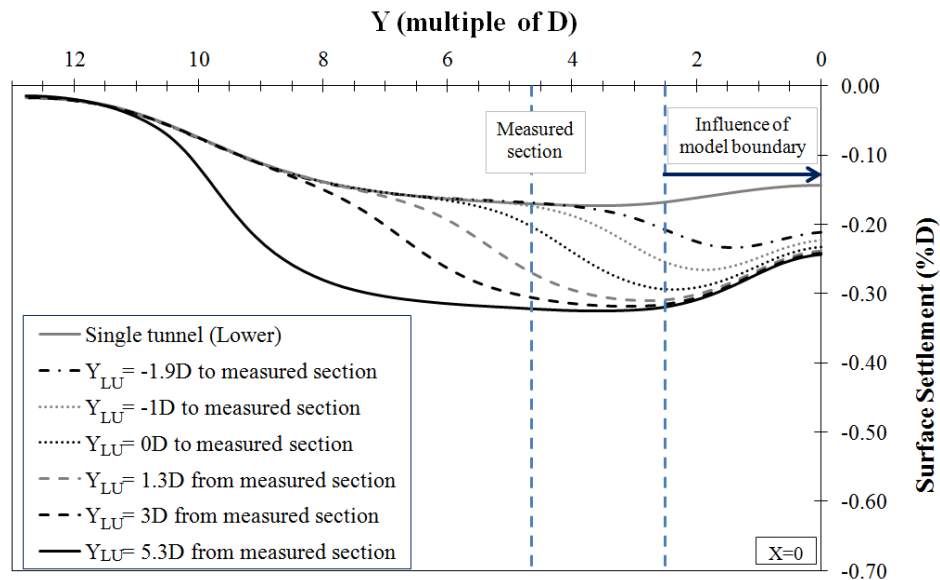
Figure 5-36. Longitudinal settlements on the ground surface above the stacked tunnels, case 2
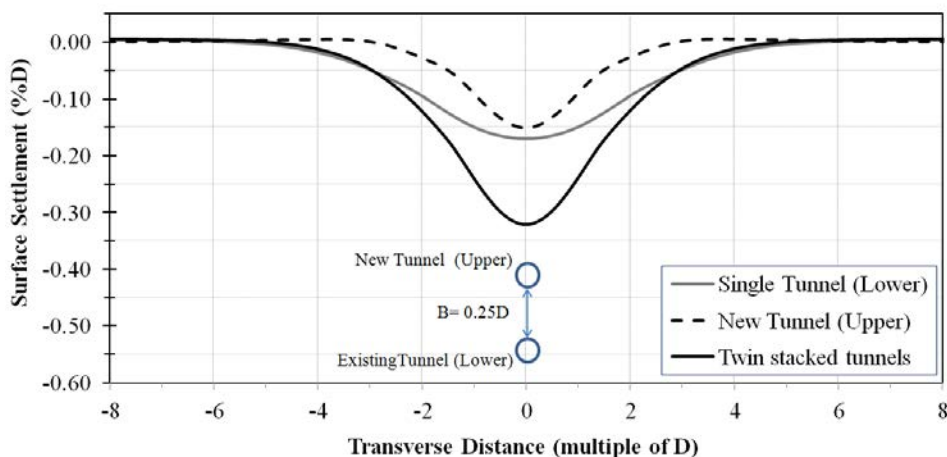
Figure 5-37. Comparison of the settlement trough in the transverse section of the stacked tunnels, case 2
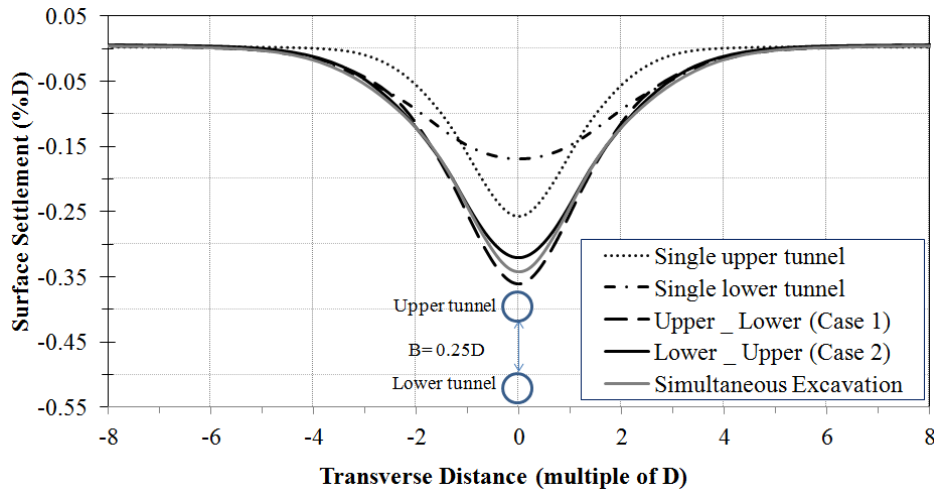
Figure 5-38. Comparison of the settlement trough in the transverse section of the stacked tunnels for different construction procedures

5.3.3.2. *Horizontal ground displacement*

The lateral displacements of the ground during the excavation of a single tunnel or stacked tunnels along the TS axis, which is placed on the right side of two tunnels at section of measured lining ring (ring 30) and at a distance of 1.25D from the tunnel centers, are shown in **Figure** 5-39. In the case of a single tunnel, an increase in tunnel depth is followed by a reduction in lateral displacements. This could be attributed to a greater lateral confinement stress, caused by the increase in tunnel depth.
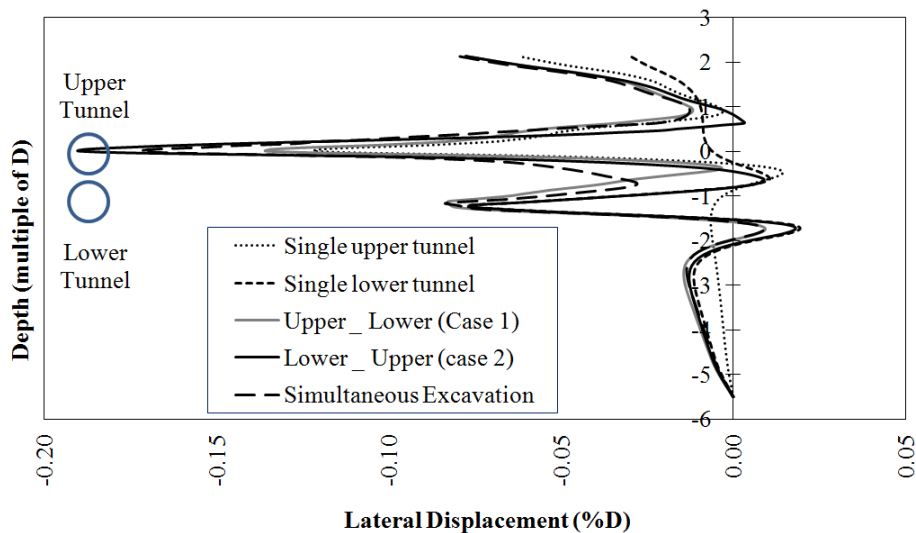
Figure 5-39. Horizontal displacements along the TS axis

For the case of stacked tunnels, the lateral displacements are affected to a great extent by the tunneling procedure. In case 1, when the upper tunnel is excavated first, the maximum final lateral displacement of about 12.8 mm (0.136 %D) is smaller than the corresponding one of about 17.9 mm (0.19 %D) obtained in case 2, in which the lower tunnel is excavated first,

and of about 16.2 mm (0.172 %D) in case 3, in which two tunnels are excavated simultaneously.

5.3.3.3. Normal displacement in the tunnel lining

In this section, the positive and negative normal displacements correspond to the outward and inward deformations of the tunnel lining. As expected, the existing tunnel linings in both cases 1 and 2 are deformed during the advancement of the new tunnel. As for case 1, in which the upper tunnel is excavated first, gradual increases in inward deformations at the crown and outward deformation at the bottom of the upper tunnel were observed during the advancement of the lower (new) tunnel (**Figure 5-40**) and they reached maximum values of about 319.1 % and 608.5 %, respectively, compared to those of a single tunnel at the final state (**Table 5-14**). This indicates that the deformation of the existing tunnel is a vertical expansion. This result is in good agreement with the measured results obtained by Yamaguchi et al. [1998]. The inward deformations at the two tunnel sides of the upper tunnel seem to be caused above all by the vertical expansion of the lining.
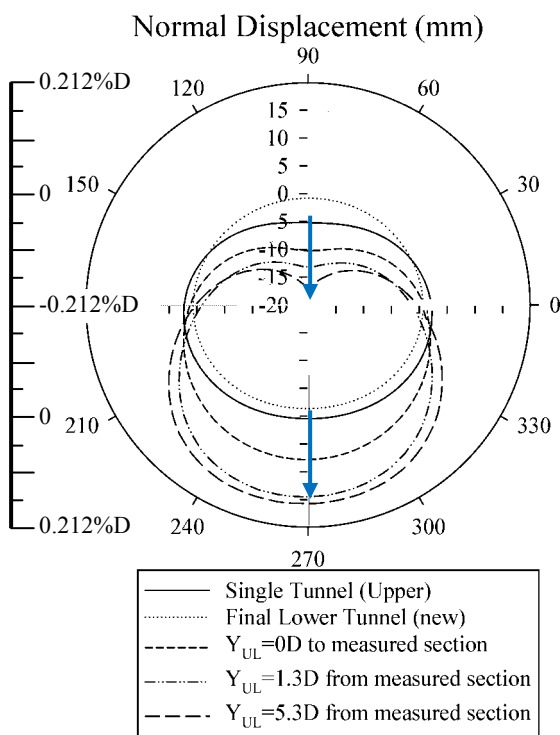
Figure 5-40. Normal displacement in measured lining ring 30 of the existing (upper) tunnel lining, case 1
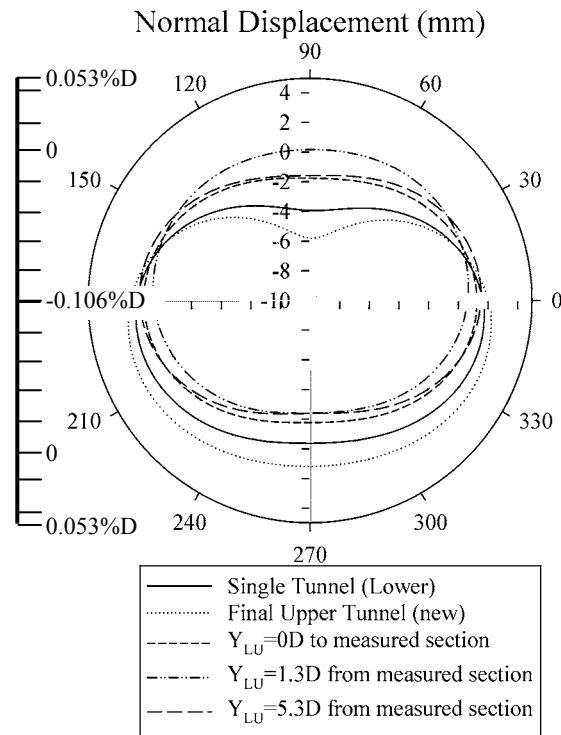
Figure 5-41. Normal displacement in measured lining ring 30 of the existing (lower) tunnel lining, case 2

On the other hand, the deformations of the lower tunnel lining are very small (**Figure 5-40**) The maximum and minimum deformations in the lower tunnel, at the steady state, are approximately 8.1 % and 4.4 %, respectively, compared to the corresponding ones in the

---

upper tunnel (**Table 5-14**). This shows that the external forces that act on the lower tunnel lining seem to be more uniform than those applied in the upper tunnel.

As in case 1, in case 2, in which the lower tunnel is excavated first, the changes in normal deformation of the lower (existing) tunnel lining basically occur at the tunnel crown (**Figure 5-41**). The maximum and minimum deformations in the lower tunnel lining, at the final state, are about 60.8 % and 82.9 % compared to those of a single tunnel. They are also 41.2 % and 60.8 % smaller than those induced in the upper (new) tunnel (**Table 5-15**).

In the case of stacked tunnels that are excavated simultaneously (case 3), the numerical results present a gradual increase in normal displacements in both tunnels during the tunnel face advancement. At the steady state, both the maximum and minimum normal displacements developed in the upper tunnel are larger than the corresponding ones in the lower tunnel (**Figure 5-42** and **Table 5-16**).
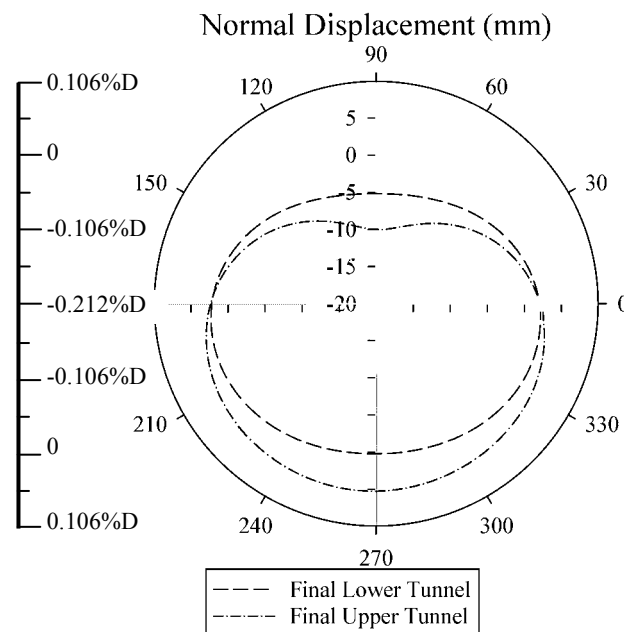
Figure 5-42. Normal displacement in measured lining ring 30 of the stacked tunnel linings, case 3

In order to highlight the effect of the tunnelling procedure, **Figure 5-43** and **Figure 5-44** show a comparison of the normal deformations in the two stacked tunnel linings. It is reasonable to conclude that the upper tunnel is more affected by the tunnelling procedure than the lower tunnel. **Figure 5-43** and **Table 5-17** point out smaller deformations of about 34.8 % and 16.2 %, corresponding to the maximum and minimum deformations, in the upper tunnel lining obtained in case 2 compared to those induced in case 1. Generally, in all three cases of stacked tunnels, the normal deformations in the upper tunnel are always greater than the ones that are developed in a single tunnel (**Table 5-17**).

Unlike the upper tunnel, except case 3, the normal deformations induced in the lower tunnel in the other cases of stacked tunnels (i.e. cases 1 and 2) are generally smaller than the ones developed in a single tunnel and the lining deformations in case 2, in which the lower

tunnel is excavated first, are higher than those obtained in case 1 (**Figure 5-44** and **Table 5-18**).
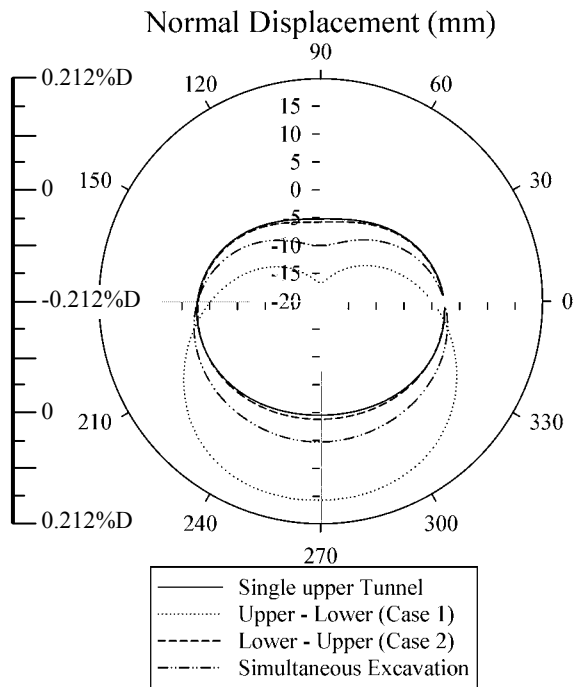
Figure 5-43. Comparison of the normal displacement in measured lining ring 30 of the upper tunnel lining
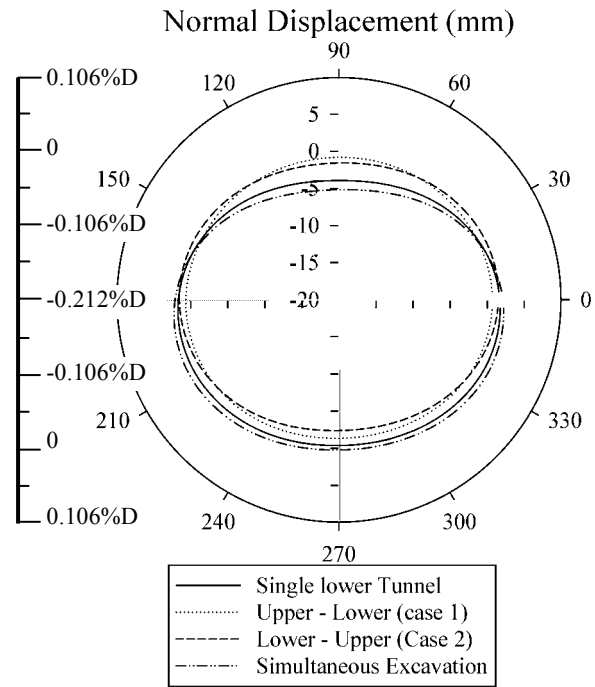
Figure 5-44. Comparison of the normal displacement in measured lining ring 30 of the lower tunnel lining

5.3.3.4. Normal forces and longitudinal forces in the tunnel lining

An important change in the normal forces induced in the measured ring of the upper (existing) tunnel during the advancement of the lower (new) tunnels (case 1) can be seen in **Figure 5-45**a and **Table 5-14**, in particular for the tunnel bottom region near the new tunnel.

When the advancement of the lower tunnel face approaches the measured section, a slight increase can be observed in the normal forces at the bottom of the upper tunnel, thus illustrating a load transfer to the upper tunnel, due to the effect of face pressure in the lower tunnel. At the moment in which the lower tunnel face crosses the measured section, which corresponds to a distance $Y_{UL} = 0D$, an increase in the normal forces of 8.9 % can be observed at the bottom region (**Figure 5-45**a and **Table 5-14**). The vertical movement of the ground towards the lower tunnel, caused by the convergence displacement along the shield in the lower tunnel, is the main reason for the decrease in the normal forces induced in the measured ring at the bottom region (see line $Y_{UL} = 1.3D$ from the measured section in **Figure 5-45**a and **Table 5-14**). The maximum normal force in the measured lining ring in the upper tunnel at the final state is about 69.4 % compared to that of a single tunnel. This suggests that a portion of the external load surrounding the upper tunnel is taken up by the lower tunnel. It

should be noted that the changes in normal forces at the crown region of the upper tunnel are insignificant during the advancement of the lower tunnel (**Figure 5-45**a).
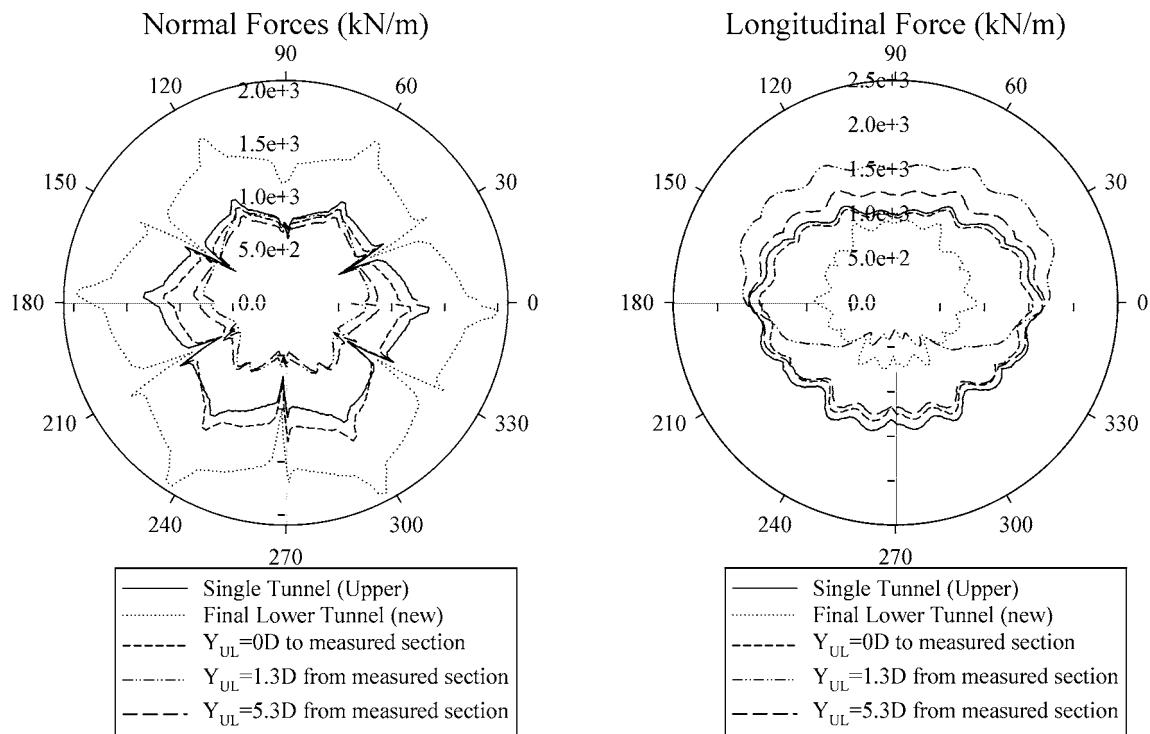
a) Normal forces in measured lining ring 30 of the existing (upper) tunnel lining

b) Longitudinal forces in measured lining ring 30 of the existing (upper) tunnel lining

Figure 5-45. Normal force and longitudinal force of the existing (upper) tunnel lining during the advancement of the new (lower) tunnel, case 1

As for the longitudinal forces (see **Figure 5-45**b), when the lower tunnel face approaches the measured section, a considerable increase in the longitudinal forces of about 32.5 %, measured at the bottom region in the upper tunnel, can be observed at moment Y_{UL} = -1D (**Table 5-14**). This could be attributed to the thrust forces acting on the face of the lower tunnel. When the lower tunnel face crosses and then goes away from the measured section, the longitudinal forces at the bottom regions of the upper tunnel show a gradual decrease, while their values at the tunnel crown indicate an increase (see line Y_{UL} = 1.3D from the measured section in **Figure 5-45**b). This could be explained by the downward movement of the ground at the bottom region of the upper tunnel, between the two tunnels. After installation of the segmental tunnel lining in the lower tunnel, a gradual increase in longitudinal forces can be observed at the bottom region of the upper tunnel as a result of the interaction between the two tunnels. The maximum longitudinal force in the measured lining ring of the upper tunnel at a steady state is similar to that of a single tunnel (**Table 5-14**).

As for the lower tunnel, unlike the upper (existing) tunnel, the advancement of the lower (new) tunnel shows a gradual increase in normal forces induced in the lower tunnel at the crown regions. On the other hand, the normal forces at the lower tunnel bottom are almost constant. The maximum normal force induced in the lower tunnel at a steady state is 216.6 %

Chapter 5: Three-dimensional numerical analyses   177

higher than the corresponding one in the upper tunnel (**Figure 5-45**a and **Table 5-14**). This shows that the external forces that act on the lower tunnel lining are greater than those applied to the upper tunnel. This could be attributed to the impact of a greater stress at the lower tunnel level, due to the effect of the tunnel depth from the ground surface, and greater grouting pressure that act at the shield tail during construction.

The numerical results point out a gradual decrease in longitudinal forces of the lower tunnel, especially at the bottom regions. This could be explained by the impact of the jacking forces at the shield tail which acts on the segmental lining. The effect of these forces is gradually reduced as the tunnel face becomes distant. The maximum longitudinal force induced in the lower tunnel at a steady state is 61.1 % smaller than the corresponding one in the upper tunnel (**Figure 5-45**b and **Table 5-14**).

When the lower tunnel is excavated first (case 2), an insignificant impact of the upper (new) tunnel on the normal forces induced in the lower (existing) tunnel can be observed in **Figure** 5-46a and **Table** 5-15. As shown in **Table** 5-17 and **Table** 5-18, because of different cover depth, generally the normal force of the lower tunnel is greater than that of the upper tunnel. However, the maximum variation of normal force of the upper tunnel in case 1 is greater than that of the lower tunnel in case 2, i.e., case 1 is relatively disadvantageous in terms of influence degree of normal force. The same conclusion was also obtained from the 3D numerical results performed by Zheng and Qiu [2005].
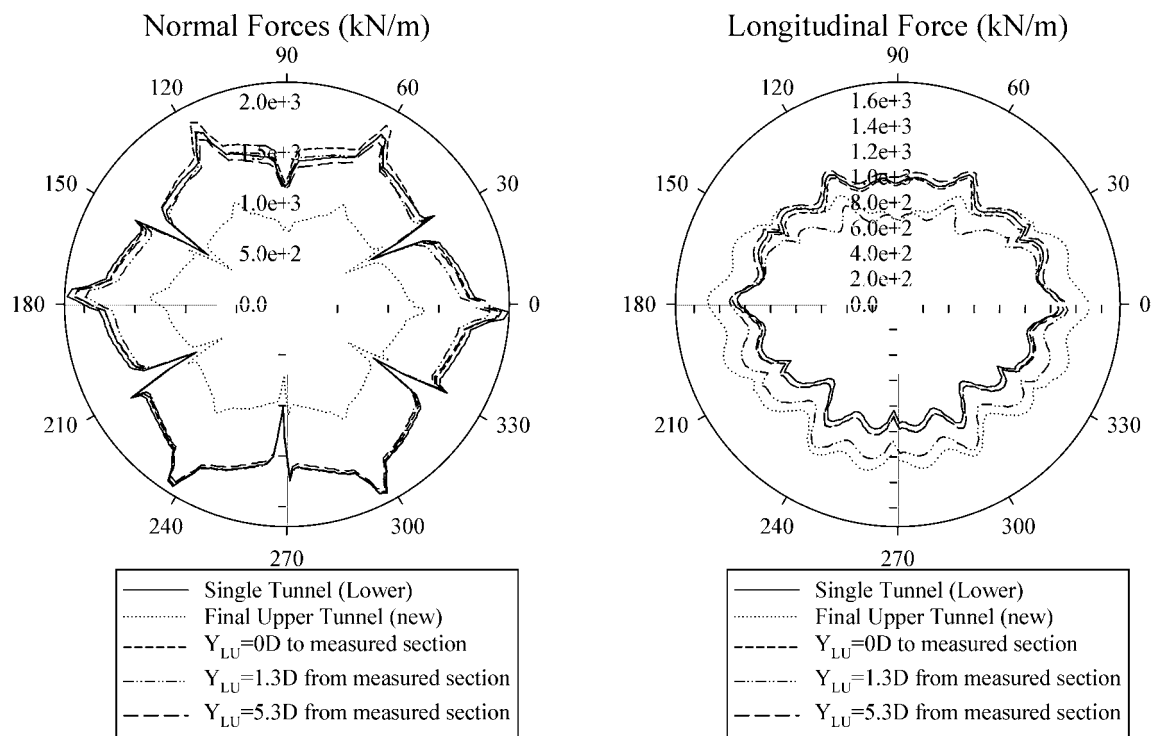
a) Normal forces in measured lining ring 30 of the existing (lower) tunnel lining

b) Longitudinal forces in measured lining ring 30 of the existing (lower) tunnel lining

Figure 5-46. Normal forces and longitudinal forces of the existing (lower) tunnel lining during the advancement of the new (upper) tunnel, case 2

A considerable change in the longitudinal forces in the lower tunnel lining can instead be observed in **Figure 5-46**b, especially at the crown region near the new tunnel. However, the maximum values of the two above forces at a steady state are similar to the corresponding ones of a single, lower tunnel (**Table 5-15**).

The numerical results point out significant changes in the normal forces and longitudinal forces in the upper tunnel, and in particular at the bottom region, during advancement of the upper (new) tunnel. When the tunnel face is distant, the maximum values of the normal forces and longitudinal forces induced in the lower tunnel are about 152.8 % and 87.1 %, respectively, compared to the corresponding ones induced in the upper tunnel (**Figure 5-46** and **Table 5-15**).

The results of normal forces obtained in this study are different from those obtained using a 2D simulation conducted by Hefny et al. [2004]. Through a parametric study on the effect of the new tunnel excavation on the existing tunnel, Hefny et al. [2004] showed that when the new tunnel is driven above the existing tunnel, the existing tunnel experiences a decrease in the maximum axial force. This conclusion is in good agreement with results observed in the present study. However, Hefny et al. [2004] pointed out that the excavation of the new tunnel below the existing tunnel has negligible effect on the maximum axial force induced in the lining. This observation is different from that obtained in the present study which shows a significant decrease in normal forces in this case. The difference could be attributed to the effect of 3D mechanised tunnelling process used in the present study, which has not been applied in study of Hefny et al. [2004].
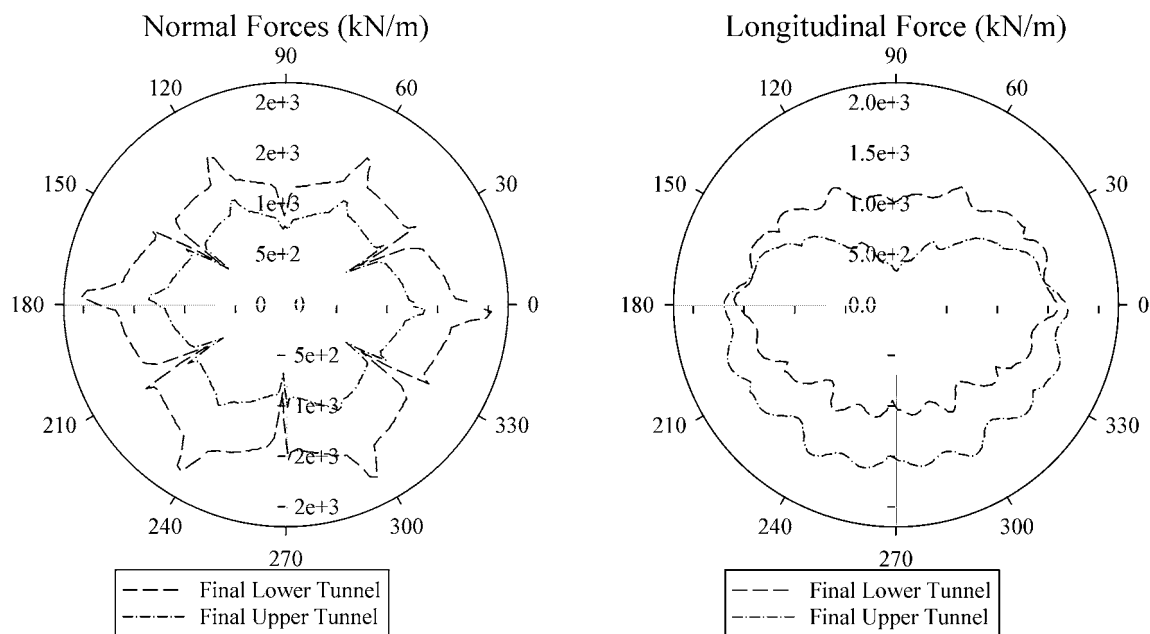
a) Normal forces in measured lining ring 30 of the stacked tunnel linings

b) Longitudinal forces in measured lining ring 30 of the stacked tunnel linings

Figure 5-47. Normal forces and longitudinal forces of the stacked tunnel linings, case 3

In the case of two stacked tunnels excavated simultaneously (case 3), the numerical results show that the normal forces induced in the two tunnels are similar in shape but their

values in the lower tunnel are significantly higher than those in the upper tunnel (**Figure 5-47**a and **Table 5-16**). The longitudinal forces developed in the upper tunnel are instead larger at the bottom region and smaller at the crow region compared to the corresponding ones induced in the lower tunnel (**Figure 5-47**b). This could be attributed to the important interaction at the ground zone between the two tunnels.

In order to illustrate the effect of the tunnelling procedure on tunnel behaviour, **Figure 5-48**, **Figure 5-49**, **Table 5-17** and **Table 5-18** show comparisons between the normal and longitudinal forces developed in the tunnel lining for the three considered cases. **Figure 5-48** shows that the tunnelling procedure has a considerable influence on both the longitudinal forces and the normal forces in the upper tunnel, and in particular case 1. However, as for the lower tunnel, the normal forces in the tunnel lining do not seem to be affected to any extent by the tunnelling procedure (**Figure 5-49**).
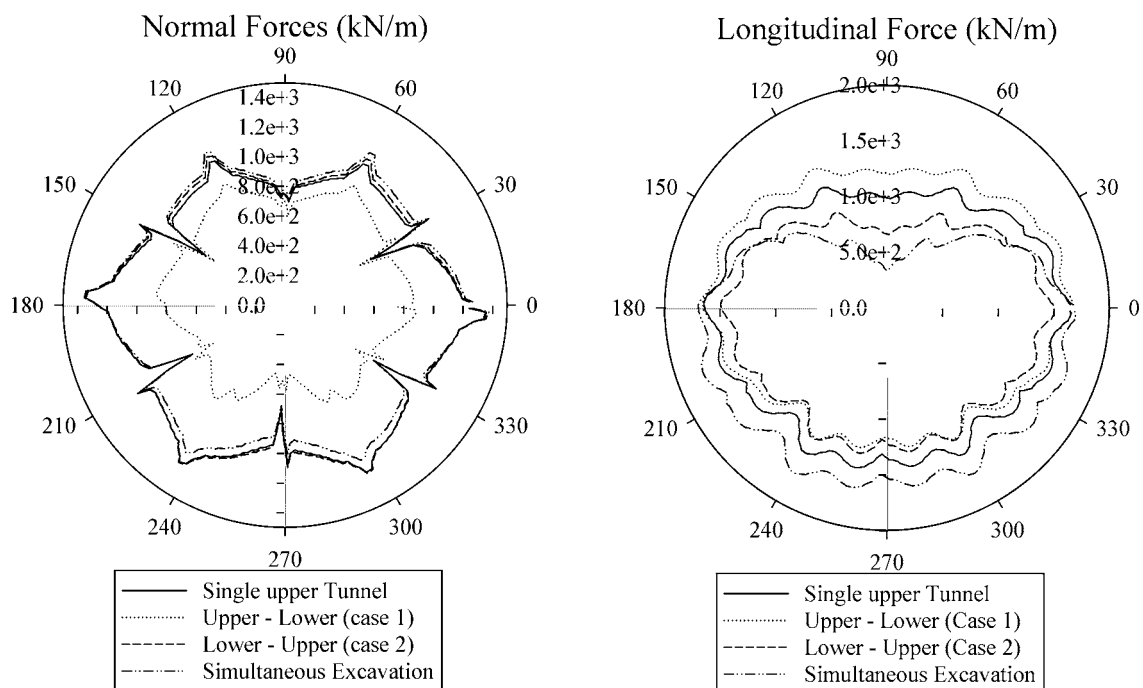
a) Normal forces in measured lining ring 30 of the upper tunnel lining

b) Longitudinal forces in measured lining ring 30 of the upper tunnel lining

Figure 5-48. Comparison of the normal forces and longitudinal forces of the upper tunnel lining

It is very interesting to note that the maximum normal forces and longitudinal forces in both stacked tunnels for case 2 are similar to those of a corresponding single tunnel. However, as for case 1, the maximum values induced in the two stacked tunnels are generally smaller than the corresponding ones in a single tunnel (see **Table 5-17** and **Table 5-18**). In other words, except for the longitudinal force in the upper tunnel, case 1, in which the upper tunnel is excavated first, leads to smaller internal forces in both stacked tunnels than case 2, in which the lower tunnel is excavated first.

The above results are different from the ones obtained, through the 2D numerical investigations, by Hage Chehade and Shahrour [2008] and Channabasavaraj and Vishwanath [2012], who concluded that the construction of the upper tunnel first leads to higher structural forces in the tunnel lining than those developed when the lower tunnel is constructed first. These differences could be attributed to the fact that, the influence of the main construction aspects of a mechanized tunnelling excavation process has not been simulated in their 2D analyses.

It can be seen in **Figure 5-48**, **Figure 5-49**, **Table 5-17** and **Table 5-18** that the simultaneous excavation of both tunnels (case 3) causes larger normal forces and longitudinal forces in both stacked tunnels than in the two other cases.
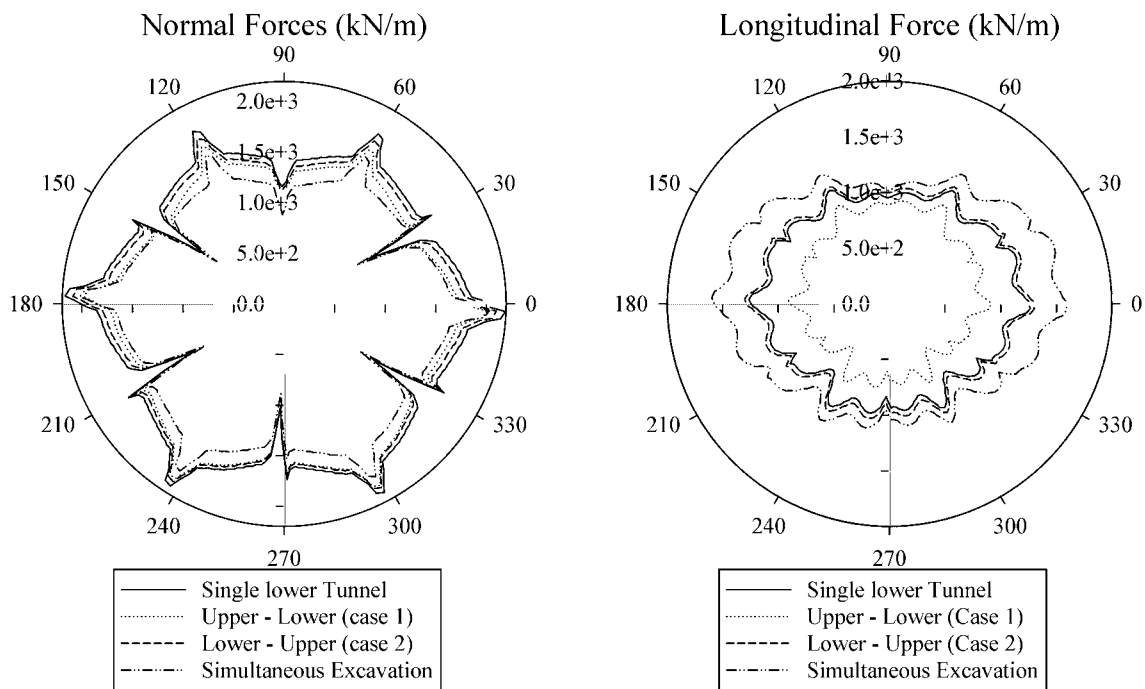
a) Normal forces in measured lining ring 30 of the lower tunnel lining   b) Longitudinal forces in measured lining ring 30 of the lower tunnel lining

Figure 5-49. Comparison of the normal forces and longitudinal forces of the lower tunnel lining

5.3.3.5. *Bending moment in the tunnel lining*

The distribution of the bending moment in the measured ring of the upper tunnel for case 1 can be seen in **Figure 5-50**. It can be seen that the excavation of the lower (new) tunnel causes important changes in the bending moment in the upper tunnel. In particular, changes in the bending moment from negative to positive values can be observed at the two lower sides of the upper tunnel near the spring line regions while changes from positive to negative values can be observed near the tunnel base, during the advancement of the lower (new) tunnel. This could be attributed to the downward movements of the soil above the lower tunnel during the lower tunnel advancement. For the same reason, a decrease in positive bending moment

induced at the bottom of the upper tunnel, when the shield machine in the lower tunnel pass over the measured section in the upper tunnel, can also be observed in **Figure** 5-50 (see line $Y_{UL} = 0D$). However, an increase of the positive bending moment at the tunnel bottom can after that be seen during the passage of the shield tail in the lower tunnel (see line $Y_{UL} = 1.3D$ in **Figure** 5-50). This could be attributed to the effect of the grouting pressure at the shield tail of the shield machine in the lower tunnel. These phenomena are different from that obtained with the 3D numerical results conducted by Zheng and Qiu [2005] and Li et al. [2010], in which a decrease of the positive bending moment at the bottom of the upper tunnel (existing tunnel), caused by the passage of the lower tunnel (new tunnel), has been seen. It should be noted that the effects of grouting pressure, jacking force, shield weight, etc. have not been considered in the works of Zheng and Qiu [2005] and Li et al. [2010].

As for the lower tunnel, the numerical results show a gradual increase in the positive bending moment at the crown and bottom regions and a negative bending moment at the two tunnel sides (due to the low K_0 value of 0.5). The absolute values of the maximum and minimum bending moments induced in the lower tunnel are approximately 43.6 % and 42.3 %, respectively, at the final state compared to those developed in the upper tunnel (see **Figure 5-50** and **Table 5-14**). An important difference in the shape of the bending moment at a steady state, induced in the two stacked tunnels in case 1, can also be observed in **Figure 5-50**.
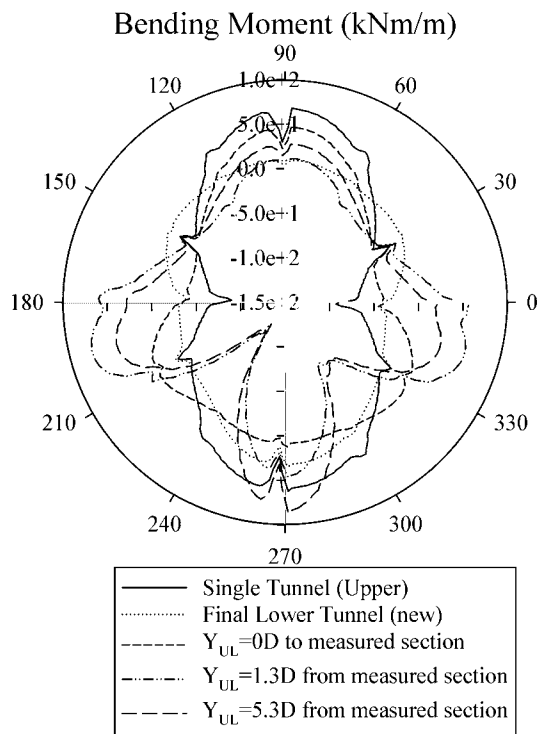
Figure 5-50. Bending moment in measured lining ring 30 of the existing (upper) tunnel lining, case 1
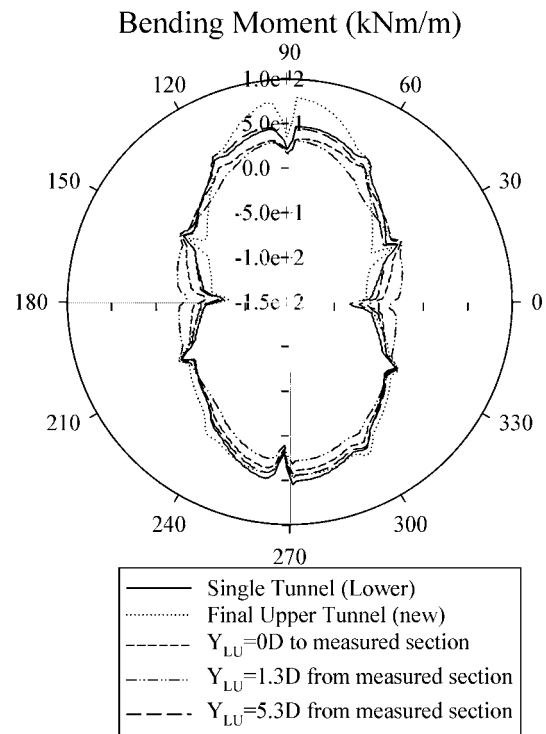
Figure 5-51. Bending moment in measured lining ring 30 of the existing (lower) tunnel lining, case 2
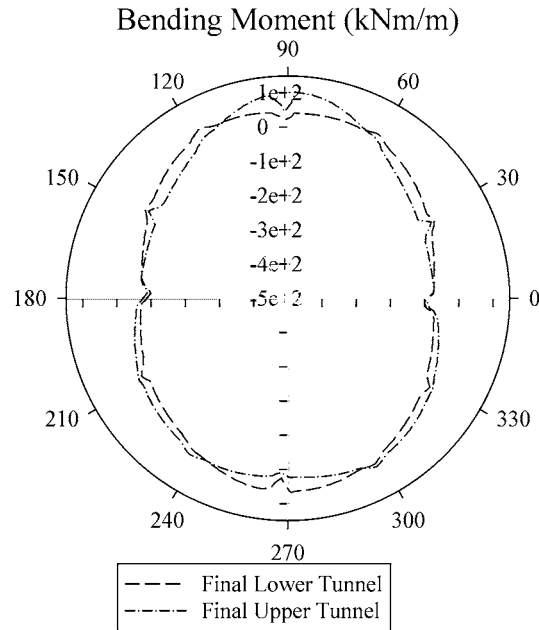
Figure 5-52. Bending moment in the measured lining ring of the stacked tunnel linings, case 3

As for case 2, in which the lower tunnel is excavated first, **Figure** 5-51 points out a slight decrease in bending moment at the crown region of the lower tunnel during the advancement of the upper (new) tunnel. This could be explained by the upward vertical movement of the soil at the bottom of the upper tunnel, due to low value of the earth lateral pressure coefficient ($K_0 = 0.5$). The bending moments induced in the upper tunnel show a gradual increase. When the upper tunnel face is at a distance, the absolute values of the maximum and minimum bending moments in the lower tunnel are approximately 66.3 % and 87.5 %, respectively, compared to the corresponding ones in the upper tunnel (**Figure 5-51** and **Table 5-15**). Unlike case 1, **Figure 5-51** and **Figure 5-52** indicate similar shapes of the bending moment induced in the two stacked tunnels for both case 2 and case 3.

It is interesting to note that the results obtained in the present study are in good agreement with that observed through 2D simulation conducted by Hefny et al. [2004]. Their results also indicated a decrease in the maximum bending moment induced in the lining of the existing tunnel after interaction with the new tunnel when the new tunnel is excavated above the existing tunnel. When the new tunnel is excavated below the existing tunnel, increases in the bending moment in the lining of the existing tunnel were also pointed out.

It can be seen in **Table 5-14** and **Table 5-15** that the bending moments induced in the lower tunnel are normally smaller than those in the upper tunnel. This means that, although the external loads that act on the lower tunnel lining are always higher than those acting on the upper tunnel, as mentioned above in **section** 5.3.3.4, the external loads determined in the lower tunnel are more uniform than those applied to the upper tunnel. This conclusion is in good agreement with the smaller deformation induced in the lower tunnel mentioned in **section** 5.3.3.3.

Comparisons of the bending moments induced in the stacked tunnel linings are presented in **Figure 5-53**, **Figure 5-54**, **Table 5-17** and **Table 5-18** for the three considered cases. **Figure 5-53** shows that the tunnelling procedure causes a considerable effect on the bending

moment in the upper tunnel, and in particular for case 1. However, as for the lower tunnel, the bending moment in the tunnel lining does not seem to be affected to any extent by the tunnelling procedure (**Figure** 5-54).

It is interesting to note that the successive excavation of stacked tunnels, i.e. case 1 and case 2, always cause an increase in the maximum bending moment induced in the upper tunnel at the final state (**Table** 5-17). However, a decrease in the maximum bending moment induced in the lower tunnel is usually observed (**Table** 5-18).
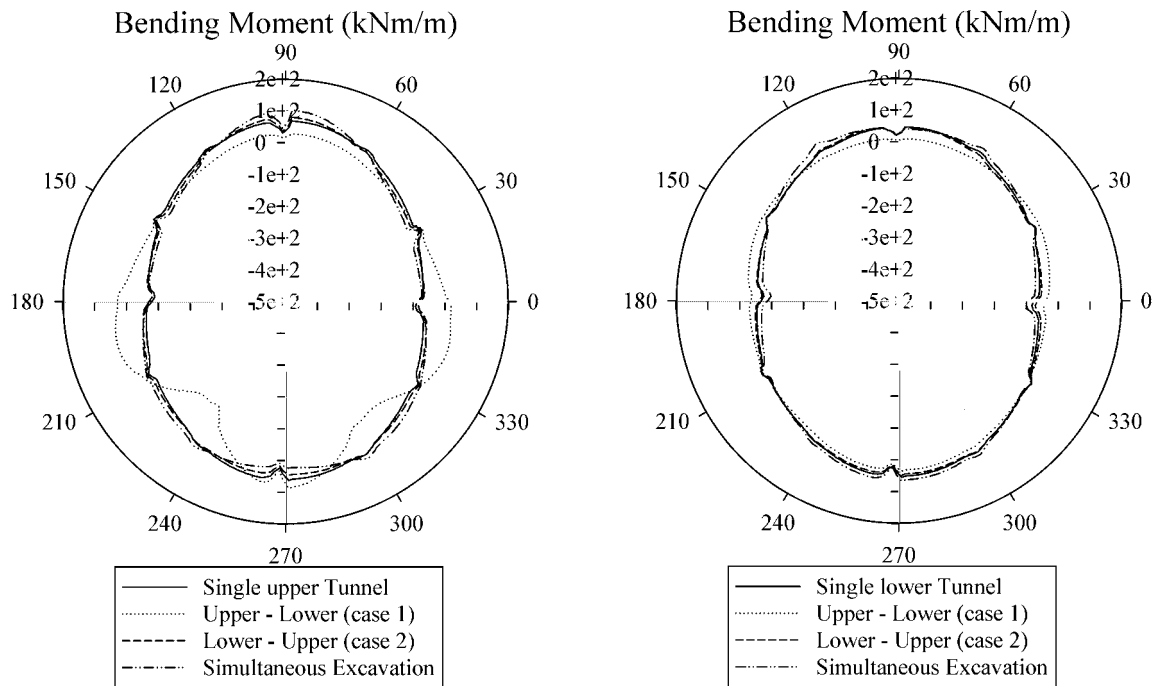
Figure 5-53. Comparison of the bending moment in measured lining ring 30 of the upper tunnel lining

Figure 5-54. Comparison of the bending moment in measured lining ring 30 of the lower tunnel lining

Table 5-14. Development of the structural forces and deformation in the measured ring (ring 30) of the upper (existing) tunnel and surface settlement during advancement of the lower (new) tunnel (case 1)

Parameters	Single upper tunnel	Distance Y_{UL} (m)						Final lower tunnel	B/A (%)
	-	-1.9D	-1D	0	1.3D	2.6D	5.3D (A)	(B)	
Max. pos. bending moment (kN.m/m)	69.2	78.3	84.3	48.9	73.7	89.1	92.9	40.5	43.6
R_{M+} (%)	100	113.2	121.8	70.7	106.5	128.8	134.2	58.5	
Min. neg. bending moment (kN.m/m)	-95.1	-109.8	-113.2	-48.1	-125.5	-117.6	-113.8	-48.1	42.3
R_{M-} (%)	100	115.5	119.0	50.6	132.0	123.7	119.7	50.6	
Max. Normal force (kN/m)	1466	1527	1622	1597	1107	1016	1017	2203	216.6
R_N (%)	100	104.2	110.6	108.9	75.5	69.3	69.4	150.3	
Max. Longitudinal force (kN/m)	1669	1965	2212	1565	1896	1604	1690	1033	61.1
R_{LN} (%)	100	117.7	132.5	93.8	113.6	96.1	101.3	61.9	
Max. normal displacement (mm)	5.24	6.37	7.88	10.27	13.17	15.79	16.72	1.36	8.1
R_{disp+} (%)	100	121.6	150.4	196.0	251.3	301.3	319.1	26.0	
Min. normal displacement (mm)	-2.59	-3.17	-3.85	-7.82	-14.54	-15.27	-15.76	-0.69	4.4
R_{disp-} (%)	100	122.4	148.6	301.9	561.4	589.6	608.5	26.6	
Max. settlement (%D)	-0.26	-0.27	-0.28	-0.30	-0.33	-0.36	-0.36	-	
R_{set} (%)	100	105.0	109.5	118.2	128.9	139.3	140.1	-	

Chapter 5: Three-dimensional numerical analyses

Table 5-15. Development of the structural forces and deformation in the measured ring (ring 30) of the lower (existing) tunnel and surface settlement during advancement of the upper (new) tunnel (case 2)

Parameters	*Single lower tunnel*	*Distance Y_{LU} (m)*						*Final upper tunnel*	*B/A (%)*
	-	*-1.9D*	*-1D*	*0*	*1.3D*	*2.6D*	*5.3D (B)*	*(A)*	
Max. pos. bending moment (kN.m/m)	60.5	64.6	62.9	48.1	36.5	44.4	53.4	80.6	66.3
R_{M+} *(%)*	*100*	*106.8*	*104.0*	*79.5*	*60.3*	*73.4*	*88.3*	*133.2*	
Min. neg. bending moment (kN.m/m)	-85.4	-91.4	-92.4	-67.1	-42.1	-61.5	-74.6	-85.3	87.5
R_{M-} *(%)*	*100*	*107.0*	*108.2*	*78.6*	*49.3*	*72.0*	*87.4*	*99.9*	
Max. Normal force (kN/m)	2335	2365	2374	2268	2265	2216	2247	1471	152.8
R_N *(%)*	*100*	*101.3*	*101.7*	*97.1*	*97.0*	*94.9*	*96.2*	*63.0*	
Max. Longitudinal force (kN/m)	1283	1353	1411	1286	1350	1270	1322	1517	87.1
R_{LN} *(%)*	*100*	*105.5*	*110.0*	*100.2*	*105.2*	*99.0*	*103.0*	*118.2*	
Max. normal displacement (mm)	3.95	3.84	3.54	1.78	2.42	2.89	2.40	5.82	41.2
R_{disp+} *(%)*	*100*	*97.2*	*89.6*	*45.1*	*61.3*	*73.2*	*60.8*	*147.3*	
Min. normal displacement (mm)	-1.87	-1.98	-1.96	-1.27	-0.88	-1.33	-1.55	-2.55	60.8
R_{disp-} *(%)*	*100*	*105.9*	*104.8*	*67.9*	*47.1*	*71.1*	*82.9*	*136.4*	
Max. settlement (%D)	-0.17	-0.17	-0.17	-0.20	-0.26	-0.30	-0.32	-	
R_{set} *(%)*	*100*	*99.4*	*101.9*	*116.4*	*155.3*	*179.2*	*189.9*	-	

Table 5-16. Comparison of the structural forces and deformation in the measured ring (ring 30) of the stacked tunnels at the final state in the case of simultaneous excavation (case 3)

Parameters	*Upper Tunnel (A)*	*Lower Tunnel (B)*	*B/A %*
	-	-	-
Max. pos. bending moment (kN.m/m)	103.0	72.6	*70.5*
Min. neg. bending moment (kN.m/m)	-93.5	-102.9	*110.1*
Max. Normal force (kN/m)	1483	2144	*144.6*
Max. Longitudinal force (kN/m)	1759	1608	*91.4*
Max. normal displacement (mm)	10.04	5.19	*51.7*
Min. normal displacement (mm)	-5.28	-2.57	*48.7*

Chapter 5: Three-dimensional numerical analyses

186

Table 5-17. Comparisons of the structural forces and deformation in the measured ring (ring 30) of the upper tunnel for the three construction procedure cases

Parameters	Single upper tunnel	Case 1 (A)	Case 2 (B)	Case 3	B/A %
	-	-	-	-	-
Max. pos. bending moment (kN.m/m)	69.2	92.9	80.6	103.0	86.8
R_{M+} (%)	100	134.2	116.5	148.8	
Min. neg. bending moment (kN.m/m)	-95.1	-113.8	-85.3	-93.5	75.0
R_{M-} (%)	100	119.7	89.7	98.3	
Max. Normal force (kN/m)	1466	1017	1471	1483	144.6
R_N (%)	100	69.4	100.3	101.2	
Max. Longitudinal force (kN/m)	1669	1690	1571	1759	93.0
R_{LN} (%)	100	101.3	94.1	105.4	
Max. normal displacement (mm)	5.24	16.72	5.82	10.04	34.8
R_{disp+} (%)	100	319.1	111.1	191.6	
Min. normal displacement (mm)	-2.59	-15.76	-2.55	-5.28	16.2
R_{disp-} (%)	100	608.5	98.5	203.9	
Max. settlement (%D)	-0.26	-0.36	-0.32	-0.34	89.1
R_{set} (%)	100	140.1	124.8	133.1	

Table 5-18. Comparisons of the structural forces and deformation in the measured ring (ring 30) of the lower tunnel for the three construction procedure cases

Parameters	Single lower tunnel	Case 1 (A)	Case 2 (B)	Case 3	B/A %
	-	-	-	-	-
Max. pos. bending moment (kN.m/m)	60.5	40.5	53.4	72.6	198.2
R_{M+} (%)	100.0	71.5	141.7	117.0	
Min. neg. bending moment (kN.m/m)	-85.4	-48.1	-74.6	-102.9	159.1
R_{M-} (%)	100.0	63.0	100.2	121.9	
Max. Normal force (kN/m)	2335	2203	2247	2144	105.9
R_N (%)	100.0	94.7	100.2	101.7	
Max. Longitudinal force (kN/m)	1283	1033	1322	1608	126.1
R_{LN} (%)	100.0	82.1	103.6	114.4	
Max. normal displacement (mm)	3.95	1.36	2.40	5.619	196.9
R_{disp+} (%)	100.0	44.6	87.9	128.4	
Min. normal displacement (mm)	-1.87	-0.69	-1.55	-2.57	195.3
R_{disp-} (%)	100.0	51.2	100.0	132.9	
Max. settlement (%D)	-0.17	-0.36	-0.32	-0.34	86.2
R_{set} (%)	100.0	209.6	180.7	202.5	

5.3.4. Conclusions

A 3D numerical model of the mechanized twin stacked tunnelling process has been developed in this study. This model can be used to predict the ground movements and structural forces induced in the lining of two stacked tunnels.

On the basis of the results of the 3D numerical analyses, it is possible to draw the following conclusions:

- The excavation of a new tunnel has an important impact on both the behaviour of the linings installed in the existing tunnel and the ground displacements surrounding twin stacked tunnels. The structural forces induced in the existing tunnel change during advancement of the new tunnel. The maximum interaction between the two tunnels occurs when the shield of the new tunnel passes over the measured section. The greatest impacts have been observed for case 1 in which the upper tunnel is excavated first.

- An increase in the surface settlement, compared to that induced above a single tunnel, is expected due to interactions between the twin stacked tunnels. The tunnelling procedure is responsible for the difference in surface settlement developed during the excavation of each tunnel. The excavation of the upper tunnel first causes a greater surface settlement than those of the other two cases.

- The lateral displacements are affected to a great extent by the tunnel depth and tunnelling procedure. The deeper the tunnel, the smaller the lateral displacement. The case in which the lower tunnel is excavated first causes a greater lateral displacement.

- The normal deformations in the upper tunnel are always greater than those developed in a single tunnel. Unlike the upper tunnel, the normal deformations induced in the lower tunnel are usually smaller than those developed in a single tunnel, except for in case 3 in which two stacked tunnels are excavated simultaneously. In other words, the normal displacements induced in the lower tunnel are usually smaller than those developed in the upper tunnel.

- The normal forces induced in the lower tunnels are always greater than the ones developed in the upper tunnel due to the impact of the higher stress at a greater depth. Case 1, in which the upper tunnel is excavated first, leads to smaller normal forces than in case 2. The simultaneous excavation of both tunnels causes greater longitudinal forces in both stacked tunnels.

- The bending moments induced in the lower tunnel are usually smaller than those in the upper tunnel. This means that the external loads that act on the lower tunnel lining are more uniform than those applied to the upper tunnel. This conclusion can be confirmed considering the smaller deformation induced in the lower tunnel.

- Generally, the structural forces induced in both stacked tunnels for case 3 are greater than those obtained for case 1 and case 2.

- The successive excavation of stacked tunnels, i.e. case 1 and case 2, causes an increase in the maximum bending moment in the upper tunnel and a decrease in the bending moment in the lower tunnel at the final state.

- The upper tunnel is affected to a greater extent by the excavation procedure.

5.4. General conclusions

3D numerical analyses have been conducted to investigate the behaviour of single tunnel or twin tunnels excavated in close proximity. Most of the processes that occur during mechanized excavation have been simulated in this model. The influence of the lining joint pattern, including segmental lining joints and their connections, has in particular been taken into consideration.

As for a single tunnel, the results have shown a negligible influence of the initial condition on tunnel behaviour. In contrast, a great influence of the constitutive model of the ground on the tunnel behaviour and ground displacement has been pointed out. The impact of the processes during mechanized excavation, such as the grouting pressure and the jacking forces in the structural forces induced in the tunnel lining, has been presented. These values depend on the tunnel advancement. However, a negligible influence of the joint pattern on the ground displacement field surrounding the tunnel has been observed. Generally, a variation in the structural forces in successive rings along the tunnel axis has been found in a staggered segmental lining, indicating the necessity of simulating the joints in the tunnel lining and using a full 3D numerical model to obtain an accurate estimation. In addition, the considerable influence of the coupling effect between successive rings on the lining behaviour has been highlighted.

As far as twin horizontal tunnels are concerned, the results of the numerical analysis have also indicated a great impact of a new tunnel construction on an existing tunnel. The influence of the lagged distance between the two tunnels faces has also been highlighted. Generally, the simultaneous excavation of twin tunnels causes smaller structural forces and lining displacements than those induced in the case of twin tunnels excavated at a large lagged distance. However, the simultaneous excavation of twin tunnels could result in a higher settlement above the two tunnels.

In the case of stacked tunnels, the results of the numerical analysis have indicated a great impact of a new tunnel construction on an existing tunnel. The greatest impacts are observed when the upper tunnel is excavated first and the upper tunnel is affected to a greater extent by the excavation procedure. The excavation of the upper tunnel generally leads to greater surface settlements than those obtained for the case in which the lower tunnel is excavated first. On the other hand, the structural forces induced in stacked tunnels, when they are excavated simultaneously, are greater than those obtained in other cases.

Obviously, numerical analysis allows one to consider in a rigorous way the behaviour of segmental tunnel lining. However, they are usually time consuming. This is why simplified methods such as empirical and analytical methods are still developed continuously and used widely.

Chapter 6

A New Approach to the Hyperstatic Reaction Method

6.1. Introduction

Numerical results presented in chapter 4 and 5 indicated that one of the most important factors in the design of a segmental tunnel lining is the influence of the segmental joints on its overall behaviour. In the literature, the effects of segmental joints on tunnel lining behaviour have usually been considered through direct and indirect methods. In indirect methods, the segmental tunnel lining is considered as a continuous lining ring embedded in a continuous soil mass (Muir Wood [1975], Einstein and Schwartz [1979], Duddeck and Erdmann [1985], Takano [2000], Oreste, [2007]). The effect of joints is usually taken into account through the reduction factor of the flexural rigidity of the lining, which can be determined empirically (e.g. Muir Wood [1975]), analytically (Blom [2002], Liu and Hou [1991], Lee and Ge [2001]) or experimentally (Teachavorasinskun and Chub-Uppakarn [2008]). Due to their simplicity, these indirect methods are still considered very useful for the design of a segmental lining.

In direct methods, segmental joints are added directly to the tunnel lining structure (Lee et al. [2002], Blom [2002], Naggar and Hinchberger [2008]). Although a useful step forward, the solution proposed by Lee et al. [2002] is limited to very soft soil and does not explicitly consider the soil structure interaction. Furthermore, in this method, the structures and external loads are assumed to be symmetric, with respect to the vertical center line, and cannot be applied when the distribution of the joints over the vertical tunnel axis is asymmetrical. To overcome some limitations of the methods so far mentioned, Blom [2002] proposed an analytical method that takes into account both segment joints and soil-structure interaction but only radial springs around the lining were modelled. Naggar and Hinchberger [2008] introduced a closed-form solution for segmental linings in elastic soil or rock in which both slip and no slip conditions at the lining ground interface can be considered. Like the above methods, the main drawback of this solution is the symmetrical assumption of external load and joint distribution over the vertical tunnel axis. In addition, the behaviour of the segment joints in all the above methods is taken into account through linear rotational stiffness.

Rapid progress in the development of user friendly computer codes and the limitations of analytical methods have led to an increase in the use of numerical methods for the design of tunnel lining. Less works, however, take into account the influence of segmental lining joints on the tunnel behaviour. Section 4.1 (also see Do et al. [2013a]) presented a 2D parametric study on the segmental tunnel lining, which showed that the influence of joint rotational stiffness should not be neglected. On the other hand, the results have also shown an insignificant influence of the axial and radial stiffness of the joints on segmental tunnel lining behaviour.

The HRM method [Duddeck and Erdmann [1985], Takano [2000], Oreste [2007], ITA [1988], AFTES [1997b]) (**Figure 6-1**), which is part of the numerical methods category, is particularly suitable for the design of support structures. This method simulates the interaction between the support and ground surrounding the tunnel through a number of independent "Winkler" type springs (Schulze and Duddeck [1964]). The reason why it is named hyperstatic is because of the high number of support structure connections to the soil mass. The method requires the definition of the active loads that apply directly to the support

---

structure. These loads can be estimated using different methods that are known in the scientific literature (Mashimo and Ishimura [2003]). Other passive loads are due to the reaction of the ground to the displacement of the support structure.
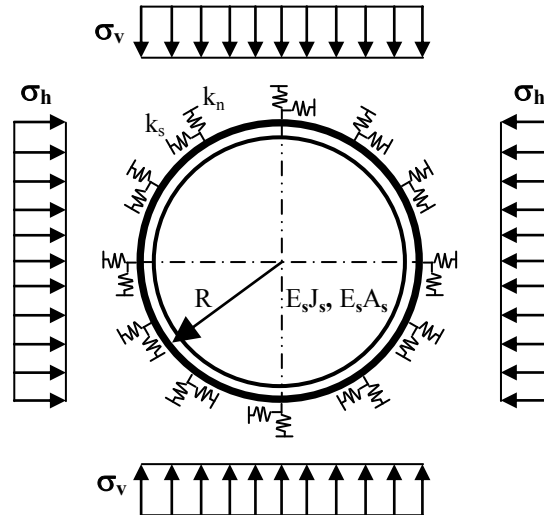
Figure 6-1. Calculation scheme of support structures with the hyperstatic method. Active loads are applied to the tunnel support through vertical loads, σ_v, and horizontal loads, σ_h. Key: σ_v: vertical load; σ_h: horizontal load; k_n: normal stiffness of the interaction springs; k_s: tangential stiffness of the interaction springs; R: tunnel radius; E_sJ_s and E_sA_s: bending and normal stiffness of the support (Do et al. [2014d]).

The support-ground interaction influences the stress state in the structure and this interaction depends on the mechanical characteristics of the ground. As these are only generally known with a certain approximation, it is often necessary to carry out parametric or probabilistic type analyses in order to be able to completely describe the uncertainty on the stress state of the support structure. These types of analyses need many calculations and the HRM method results to be particularly suitable for this purpose, due to its short calculation time.

This chapter proposes a numerical HRM approach for the analysis of segmental tunnel linings. This approach has been developed on the basis of the model which was proposed by Oreste [2007]. The influence of segmental joints has been directly considered using a lenghtless rotational spring, which is represented by a fixity ratio that is determined on the basis of a nonlinear rotational stiffness. The parameters necessary for the calculation have been presented. A specific implementation has been developed using a FEM framework, which is able to consider the effect of segment joints in successive rings on the tunnel lining. The present HRM method allows the arbitrary distribution of segment joints along the tunnel boundary to be taken into consideration. In addition, the rotational stiffness of the segment joints has been simulated using nonlinear behaviour, as it is closer to the true behaviour of a joint than linear or bilinear behaviour.

Besides the HRM method, a simplified 3D numerical model of the segmental tunnel lining has also been developed in this study, using the FLAC^{3D}finite difference software. This model

allows the segmentation of the lining to be taken into account. The HRM results of three ring interaction assumptions have been compared and validated with the 3D numerical results. The main content of this section has been presented in Do et al. [2014b, 2014d].

6.2. The Mathematical Formulation of the HRM

The fundamental hypothesis, on which the numerical approach of the HRM method is based, is the subdivision of the support structure into a finite number of linear sub-dominions, called elements (for which it is possible to describe the stress-strain law in a simple way). They are connected to the outside through stiffnesses that are distributed over the nodes. The support structure is therefore represented, in the calculation, by mono-dimensional elements that are able to develop bending moments, axial forces and shear forces (**Figure** 6-2).
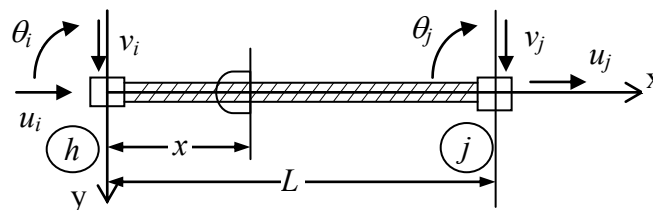
Figure 6-2. Scheme of the behaviour of a beam-type finite element with reference to the local Cartesian coordinates. Key: *h*: the initial node; *j*: the final node; *u*: the axial displacement; *v*: the transversal displacement; *θ*: the rotation; *x* and *y*: the local Cartesian coordinates.

The beam element *i* is defined by means of the following parameters: the inertia modulus *J* and area *A* of the transversal section, the elastic modulus *E* of the constituent material and length L_i (distance between the terminal connecting nodes). In bi-dimensional methods, reference is made to a unitary thickness and therefore the parameters *J* and *A* should also be calculated considering the sum of the inertia modules and the areas that are involved in the support for a unitary length in the direction of the tunnel axis.

The ground interacts with the support in two ways: through the normal and tangential springs connected to the nodes of the structure and through applied active loads (σ_v and σ_h) (**Figure 6-1**).

The unknown parameters of the problem are the displacement components of the nodes of the discretized structure. Once these unknown displacements are known, it is possible to obtain the stress characteristics inside each element and therefore also along the entire support structure length.

The evaluation of the unknown displacements is made through the definition of the global stiffness matrix of the entire structure and of its connections to the surrounding environment. The global stiffness matrix is obtained by considering the local stiffness matrices of each single element, and then passing to their assembly.

The local stiffness matrix Z_i of the i element is obtained by placing the work produced by the inner forces of the finite element equal to that produced by the external nodal forces, which are evaluated according to a local reference system (Huebner et al. [2001]).

One therefore obtains:

$$Z_i \cdot S_i = G_i + R_i \tag{6-1}$$

S_i: the vector of the displacements in nodes h and j of element i, evaluated according to the local reference system:

$$S_i = [u_{h,i} \; v_{h,i} \; \theta_{h,i} \; u_{j,i} \; v_{j,i} \; \theta_{j,i}] \tag{6-2}$$

u and v: the axial and transversal displacement in the local reference system;

θ: the rotation of the element in correspondence to the nodes;

G_i and R_i: the external nodal forces and the nodal forces applied by the neighbouring elements, which are evaluated according to the local reference system;

$$G_i^T = \begin{bmatrix} G_{xh,i} & G_{yh,i} & G_{zh,i} & G_{xj,i} & G_{yj,i} & G_{zj,i} \end{bmatrix}^T$$
$$R_i^T = \begin{bmatrix} R_{xh,i} & R_{yh,i} & R_{zh,i} & R_{xj,i} & R_{yj,i} & R_{zj,i} \end{bmatrix}^T \tag{6-3}$$

$G_{xh,i}$, $G_{yh,i}$ and $G_{zh,i}$ are respectively the axial force, the transversal force and the bending moment, corresponding to the initial node h of the ith element; $G_{xj,i}$, $G_{yj,i}$ and $G_{zj,i}$ are the corresponding ones for the final node j of the ith element (**Figure** 6-2). The same writing conventions were used for R_i^T.

Equation (6-1), re-written in explicit form, becomes:

$$
\underbrace{\begin{bmatrix}
\dfrac{E \cdot A}{L_i} & 0 & 0 & -\dfrac{E \cdot A}{L_i} & 0 & 0 \\[2mm]
 & \dfrac{12 \cdot E \cdot J}{L_i^3} & \dfrac{6 \cdot E \cdot J}{L_i^2} & 0 & -\dfrac{12 \cdot E \cdot J}{L_i^3} & \dfrac{6 \cdot E \cdot J}{L_i^2} \\[2mm]
 & & \dfrac{4 \cdot E \cdot J}{L_i} & 0 & -\dfrac{6 \cdot E \cdot J}{L_i^2} & \dfrac{2 \cdot E \cdot J}{L_i} \\[2mm]
 & & & \dfrac{E \cdot A}{L_i} & 0 & 0 \\[2mm]
 & & & & \dfrac{12 \cdot E \cdot J}{L_i^3} & -\dfrac{6 \cdot E \cdot J}{L_i^2} \\[2mm]
\text{SYM} & & & & & \dfrac{4 \cdot E \cdot J}{L_i}
\end{bmatrix}}_{Z_i}
\cdot
\begin{bmatrix}
u_{h,i} \\ v_{h,i} \\ \theta_{h,i} \\ u_{j,i} \\ v_{j,i} \\ \theta_{j,i}
\end{bmatrix}
=
\begin{bmatrix}
R_{xh,i} + G_{xh,i} \\ R_{yh,i} + G_{yh,i} \\ R_{zh,i} + G_{zh,i} \\ R_{xj,i} + G_{xj,i} \\ R_{yj,i} + G_{yj,i} \\ R_{zj,i} + G_{zj,i}
\end{bmatrix}
\tag{6-4}
$$

In the global Cartesian reference system, the nodal displacements $q_{h\div j,i}$ are connected to S_i through the following matrix expression:

$$S_i = \lambda_i \cdot q_{h\div j,i} \tag{6-5}$$

where:

$$q_{h \div j,i} = \begin{bmatrix} w_{h,i} \\ z_{h,i} \\ \varphi_{h,i} \\ w_{j,i} \\ z_{j,i} \\ \varphi_{j,i} \end{bmatrix} = \begin{bmatrix} q_i \\ q_{i+1} \end{bmatrix} \qquad (6\text{-}6)$$

$$\lambda_i = \begin{bmatrix} \cos\alpha_i & \sin\alpha_i & 0 & 0 & 0 & 0 \\ -\sin\alpha_i & \cos\alpha_i & 0 & 0 & 0 & 0 \\ 0 & 0 & 1 & 0 & 0 & 0 \\ 0 & 0 & 0 & \cos\alpha_i & \sin\alpha_i & 0 \\ 0 & 0 & 0 & -\sin\alpha_i & \cos\alpha_i & 0 \\ 0 & 0 & 0 & 0 & 0 & 1 \end{bmatrix} \qquad (6\text{-}7)$$

$q_{h \div j,i}$: the vector of the nodal displacements of element i; q_i: the vector of the nodal displacements of node i; w and z: the displacements along axis x and along axis y of the global Cartesian reference system; φ: rotation of node in the global Cartesian reference system; α_i: the angle that forms the local Cartesian reference system of element i with respects to the global Cartesian reference system.

In the same way, in the global Cartesian reference system, the nodal forces are given by the following matrix expressions:

$$G_i = \lambda_i \cdot F_{h \div j,i} \qquad (6\text{-}8)$$

$$R_i = \lambda_i \cdot Q_{h \div j,i} \qquad (6\text{-}9)$$

where:

$$F_{h \div j,i} = \begin{bmatrix} F_{xh,i} \\ F_{yh,i} \\ M_{h,i} \\ F_{xj,i} \\ F_{yj,i} \\ M_{j,i} \end{bmatrix} = \begin{bmatrix} F_i \\ F_{i+1} \end{bmatrix} \qquad Q_{h \div j,i} = \begin{bmatrix} Q_{xh,i} \\ Q_{yh,i} \\ Q_{Mh,i} \\ Q_{xj,i} \\ Q_{yj,i} \\ Q_{Mj,i} \end{bmatrix} = \begin{bmatrix} Q_i \\ -Q_{i+1} \end{bmatrix} \qquad (6\text{-}10)$$

Making the necessary substitutions, it becomes possible to write the following equation in the global Cartesian reference system:

Chapter 6: A new approach to the Hyperstatic-Reaction Method   197

$$Z_i \cdot \lambda_i \cdot q_{h\div j,i} = \left(G_i + R_i\right) = \lambda_i \cdot \left(F_{h\div j,i} + Q_{h\div j,i}\right) \tag{6-11}$$

and therefore:

$$\left(\lambda_i^T \cdot Z_i \cdot \lambda_i\right) \cdot q_{h\div j,i} = F_{h\div j,i} + Q_{h\div j,i} \tag{6-12}$$

which can be re-written in the following form:

$$k_i \cdot q_{h\div j,i} = F_{h\div j,i} + Q_{h\div j,i} \tag{6-13}$$

where k_i: the local stiffness matrix of element i in the global Cartesian reference system:

$$k_i = \lambda_i^T \cdot Z_i \cdot \lambda_i \tag{6-14}$$

The local stiffness matrices are assembled in the global stiffness matrix using the criteria illustrated in Huebner et al. [2001].

At the end of this stage, the matrix of the global stiffness, K, is obtained. This is constituted by (3n) x (3n) elements, where n is the total number of nodes, and the vectors of the unknown displacements q and the nodal forces F, both of which are constituted by (3n) elements. It should be noted that since the full cross-section of the tunnel lining is considered, the local stiffness matrix of the last element must be assembled with the corresponding ones of the first element.

$$K.q = F \tag{6-15}$$

or written in explicit form:

$$\begin{bmatrix} (k_{n,d} + k_{1,a}) & k_{1,b} & 0 & 0 & 0 & k_{n,c} \\ k_{1,c} & (k_{1,d} + k_{2,a}) & k_{2,b} & 0 & 0 & 0 \\ 0 & k_{2,c} & (k_{2,d} + k_{3,a}) & k_{3,b} & 0 & 0 \\ 0 & 0 & k_{3,c} & (k_{3,d} + k_{4,a}) & \cdots & 0 \\ 0 & 0 & 0 & \cdots & \cdots & k_{n-1,b} \\ k_{n,b} & 0 & 0 & 0 & k_{n-1,c} & (k_{n-1,d} + k_{n,a}) \end{bmatrix} \cdot \begin{bmatrix} q_1 \\ q_2 \\ q_3 \\ \cdots \\ \cdots \\ q_n \end{bmatrix} = \begin{bmatrix} F_1 \\ F_2 \\ F_3 \\ \cdots \\ \cdots \\ F_n \end{bmatrix}$$

$$\tag{6-16}$$

where: $k_{i,a}, k_{i,b}, k_{i,c}, k_{i,d}$: the sub-matrices of k, each of which has 3 x 3 dimension:

$$k_i = \begin{bmatrix} k_{i,a} & k_{i,b} \\ k_{i,c} & k_{i,d} \end{bmatrix} \tag{6-17}$$

where:

Chapter 6: A new approach to the Hyperstatic-Reaction Method   198

q_1 , q_2 , q_3 , ... q_n : the sub-vectors composed of the three displacements of each node;
F_1 , F_2 , F_3 , ... F_n : the sub-vectors composed of the three external forces applied to each node.

The presence of normal and tangential node springs (see **Figure** 6-3) along the structure causes stiffness changes in the structural elements in the corresponding directions. These changes are taken into consideration by the modification of the corresponding elements along the diagonal of the local stiffness matrix of each element and then of the global stiffness structure matrix:

$$K^*_{3i-2,3i-2} = K_{3i-2,3i-2} + k_{n,i} \cdot \cos^2\left(\frac{\alpha_{i+1}}{2} + \frac{\alpha_i}{2} - \frac{\pi}{2}\right) + k_{s,i} \cdot \sin^2\left(\frac{\alpha_{i+1}}{2} + \frac{\alpha_i}{2} - \frac{\pi}{2}\right)$$

$$K^*_{3i-1,3i-1} = K_{3i-1,3i-1} + k_{n,i} \cdot \sin^2\left(\frac{\alpha_{i+1}}{2} + \frac{\alpha_i}{2} - \frac{\pi}{2}\right) + k_{s,i} \cdot \cos^2\left(\frac{\alpha_{i+1}}{2} + \frac{\alpha_i}{2} - \frac{\pi}{2}\right)$$

$$K^*_{3i-1,3i-2} = K_{3i-1,3i-2} + (k_{n,i} - k_{s,i}) \cdot \sin\left(\frac{\alpha_{i+1}}{2} + \frac{\alpha_i}{2} - \frac{\pi}{2}\right) \cdot \cos\left(\frac{\alpha_{i+1}}{2} + \frac{\alpha_i}{2} - \frac{\pi}{2}\right)$$

$$K^*_{3i-2,3i-1} = K_{3i-2,3i-1} + (k_{n,i} - k_{s,i}) \cdot \sin\left(\frac{\alpha_{i+1}}{2} + \frac{\alpha_i}{2} - \frac{\pi}{2}\right) \cdot \cos\left(\frac{\alpha_{i+1}}{2} + \frac{\alpha_i}{2} - \frac{\pi}{2}\right)$$

(6-18)

where: i: the number of the generic node;

$k_{n,i}$: the stiffness of the normal interaction spring connected to node i;

$k_{s,i}$: the stiffness of the tangential interaction spring connected to node i;

α_i and α_{i+1}: the angle between the local and global reference systems, for element i and for element $i+1$ (see **Figure 6-3**).
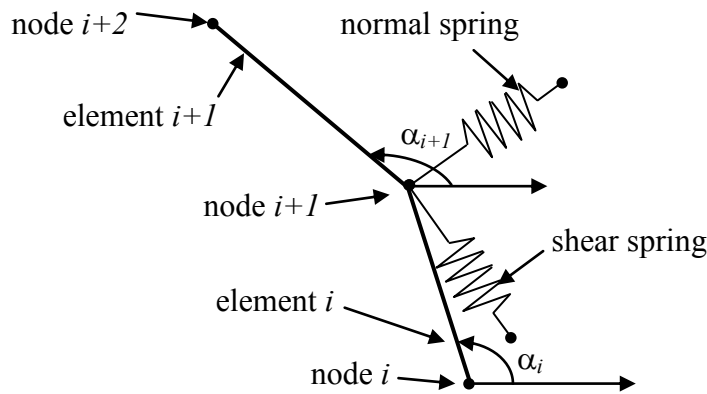
Figure 6-3. Details of the ground-support interaction through the Winkler springs connected to the support nodes

The vector of the nodal displacements q has been obtained from **Equation 6-16**. It is thus possible to evaluate the stress characteristics at the nodes of the structure. In practice, a

conversion of the nodal displacements $q_{h \div j,i}$ is performed at the local reference system of the generic element i and, once the vector S_i has been calculated, the characteristics of stress T_i can immediately be determined at the nodes through the local stiffness matrix:

$$S_i = \lambda_i \cdot q_{h \div j,i} \tag{6-19}$$

$$T_i = Z_i \cdot S_i \tag{6-20}$$

The ground-support interaction

The ground interacts with the tunnel support in two ways: through the normal springs and tangential springs connected to the nodes of the structure (**Figure 6-3**) and through the applied active loads. The normal springs allow the reaction produced by the ground to be simulated when the support, which deforms under the action of applied active loads, moves towards the ground. Instead, the shear springs allow the tangential deformations of the support in the circumferential direction under the action of applied active loads to be taken into consideration. The values of normal springs (k_n) and tangential springs (k_s) could be determined on the basis of the normal ground stiffness (η_n) and of the tangential ground stiffness (η_s).

Unlike the other methods in which the ground stiffness is considered as a constant value and is determined, on the basis of the dimension of the tunnel through the tunnel radius R and soil parameters, such as elastic modulus E_S and Poisson's factor v_S, Oreste [2007] introduced a non-linear (hyperbolic) relationship between reaction pressure p and support deformation δ (**Figure** 6-4):

$$p = p_{\lim}\left(1 - \frac{p_{\lim}}{p_{\lim} + \eta_0 \delta}\right) \tag{6-21}$$

where p_{lim} is the maximum reaction pressure that the ground can offer and η_0 is the initial stiffness (for values of δ close to 0) of the ground. By conducting a plate loading test in the ground, it is possible to note a curve load-displacement that is very similar to the hyperbolic one (AFTES [1997a]).

The apparent stiffness η^* of the ground is given by the p/δ ratio that can be obtained at each node of the support structure, that is, from:

$$\eta^* = \frac{p_{\lim}}{\delta}\left(1 - \frac{p_{\lim}}{p_{\lim} + \eta_0 \delta}\right) \tag{6-22}$$

The above non-linear relationship will be applied to both the normal ground stiffness and tangential ground stiffness in this study. For a circular tunnel in elastic ground under axisymmetric loading, the ground reaction only depends on the radius of the tunnel and the

ground elasticity parameters. In this case, the following empirical formula detailed in Möller [2006] can be applied to determine the initial normal ground stiffness:

$$\eta_{n,0} = \beta \frac{1}{1+v_s} \cdot \frac{E_S}{R} \qquad (6\text{-}23)$$

where v_s is the Poisson's ratio of the ground, R is the tunnel radius, and E_s is Young's modulus of the ground, β is a dimensionless factor.
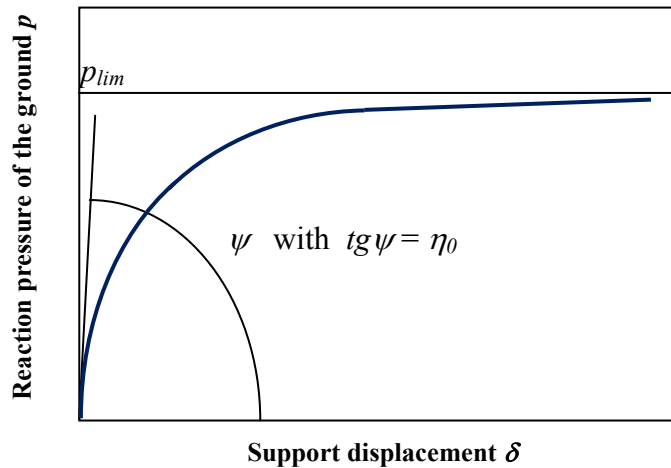
Figure 6-4. Non-linear relation between the reaction pressure of the ground and the displacement of the support (p-δ). The value of the initial stiffness of the ground is equal to η_0 and the maximum pressure p_{lim} is reached for very high values of δ while ψ is equal to $\arctan(\eta_0)$.

For engineering practice, the β factor is difficult to assess, as ground stiffness is not a material constant, but depends to a significant extent on the geometry of the structure. In situ tests, such as plate loading tests, although not representative of the final tunnel geometry, are often used to estimate the normal stiffness of the ground. In the literature, most authors adopted the β value of unity in their calculation (AFTES [1976], ITA [1982], USACE [1997], Kolymbas [2005]). However, in this study, a β value of 2 has been adopted on the basis of parametric analyses that were conducted using the HRM method, compared with those obtained with the Einstein & Schwartz's well-known analytical method.

Unlike the model proposed by Oreste [2007], the presence of tangential springs has been taken into consideration in this study. The frictional or shear stiffness at the ground-support interface is very difficult to estimate. The following simple relationship between the normal stiffness (η_n) and tangential stiffness (η_s) can be adopted (Mashimo and Ishimura [2005], Plizzari and Tiberti [2006], Arnau and Molins [2011b], Barpi et al. [2011]):

$$\eta_s = \frac{1}{3}\eta_n \tag{6-24}$$

The value of the maximum reaction pressure $p_{n,\lim}$ can be estimated, starting from the cohesion values c and the friction angle ϕ of the ground, considering the effect of confining pressure:

$$p_{n,\lim} = \frac{2 \cdot c \cdot \cos\phi}{1 - \sin\phi} + \frac{1 + \sin\phi}{1 - \sin\phi} \cdot \Delta\sigma_{conf} \tag{6-25}$$

where $\Delta\sigma_{conf}$ is the confining pressure on the tunnel perimeter defined by the following expression:

$$\Delta\sigma_{conf} = \frac{\sigma_h + \sigma_v}{2} \frac{\nu_s}{1 - \nu_s} \tag{6-26}$$

The value of the maximum shear reaction pressure $p_{s,lim}$ can be preliminarily and prudently estimated as followed:

$$p_{s,\lim} = \frac{\sigma_h + \sigma_v}{2} tg\phi \tag{6-27}$$

where σ_v and σ_h are the vertical and horizontal loads, respectively.

The stiffnesses $k_{n,i}$ and $k_{s,i}$ of each spring are simply given by the formula:

$$k_{n,i} = \eta_{n,i}^* \cdot \left[\frac{(L_{i-1} + L_i)}{2} \cdot 1 \right] = \frac{p_{n,\lim}}{\delta_{n,i}} \cdot \left(1 - \frac{p_{n,\lim}}{p_{n,\lim} + \eta_{n,0} \cdot \delta_{n,i}} \right) \cdot \frac{(L_{i-1} + L_i)}{2} \tag{6-28}$$

$$k_{s,i} = \eta_{s,i}^* \cdot \left[\frac{(L_{i-1} + L_i)}{2} \cdot 1 \right] = \frac{p_{s,\lim}}{\delta_{s,i}} \cdot \left(1 - \frac{p_{s,\lim}}{p_{s,\lim} + \eta_{s,0} \cdot \delta_{s,i}} \right) \cdot \frac{(L_{i-1} + L_i)}{2} \tag{6-29}$$

The normal springs disappear in zones where the support structure moves towards the tunnel: this is generally the case of the roof, but when the horizontal active loads are higher than the vertical ones, it occurs at the sidewalls. Therefore, only compressive loads are possible in the normal direction, where the tunnel support moves towards the ground: normal springs only work in compression. Shear springs instead allow both the positive and negative stresses in the tangential direction to be taken into consideration.

The active loads

The active vertical load σ_v can be estimated using Terzaghi's formula (Takano [2000], Ding [2004]). If the overburden thickness is two times larger than the external diameter D of

the shield lining, an effective overburden thickness h_0 ($h_0 \geq 2D$) should be used and is determined by means of the following formula (Takano [2000]):

$$h_0 = \frac{B_1\left(1-\left(c/B_1\gamma_s\right)\right)}{K\tan\phi}\left(1-e^{-K\tan\phi(H/B_1)}\right) + \frac{P_0}{\gamma_s}\left(e^{-K\tan\phi(H/B_1)}\right) \qquad (6\text{-}30)$$

$$B_1 = R_0 \cot\left(\frac{\left(\pi/4\right)+\left(\phi/2\right)}{2}\right) \qquad (6\text{-}31)$$

where c, ϕ and γ_s are the cohesion, internal friction angle and unit weight of the ground respectively; K is the ratio of horizontal earth pressure to vertical earth pressure (usually, 1.0 can be adopted as K (Takano [2000]), and H is the overburden.

Unlike the model introduced by Oreste [2007], an active external load, which acts at the tunnel bottom in the upward direction, is considered in this study that allow simulating the same external load scheme as the one used in the Einstein & Schawrtz's method.

The horizontal loads σ_h that are applied to the sidewall are usually considered to be a certain percentage of the vertical ones, depending on the lateral earth pressure coefficient K_0:

$$\sigma_h = K_0 . \sigma_v \qquad (6\text{-}32)$$

6.3. Evaluation of the HRM method

This section presents a comparison between the HRM and a numerical method, which allows one to estimate the accuracy that can be achieved using the present improved HRM approach. The numerical simulation has been performed by means of the FLAC^{3D} finite differences program (Itasca [2009]). Parameters from the Bologna-Florence high-speed railway line tunnel project in Bologna have been adopted in this numerical modelling for the evaluation purpose (Croce [2011]). The properties of the soil and tunnel lining can be found in **Table** 4-1.

Figure 6-5 shows a 2D numerical model, assuming plane-strain conditions. The FLAC^{3D} model grid contains a single layer of zones in the y-direction, and the dimension of the elements increases as one moves away from the tunnel. The numerical model is 120 m wide in the x-direction, 60 m in the z-direction. The nodes were fixed in the directions perpendicular to the x-z and the y-z planes (i.e. y = 0, y = 1, x = -60 and x = 60), while the nodes at the base of the model (z = -40) were fixed in the vertical (z) direction.

The volume under study was discretized into hexahedral zones. The tunnel lining have been modelled using linear-elastic embedded liner elements. In the present work, a continuous lining has been simulated in order to compare with the results of the HRM.

The ground is assumed to be a linear elastic and massless material which corresponds to the boundary conditions applied in the HRM method. The external loads, which are

represented by a vertical load σ_v and a horizontal load σ_h, have been applied at the external boundaries of the model (**Figure 6-5**).
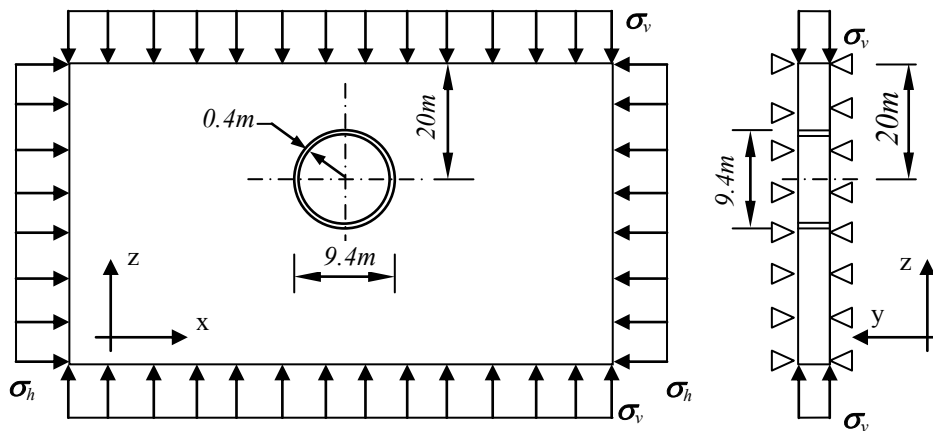
Figure 6-5. Numerical model under consideration

Figure 6-6 and **Figure 6-7** illustrate the lining displacements and structural forces, respectively, at ring 582. **Figure 6-6**b shows that tangential displacements obtained with the HRM are quite similar to the one obtained with the FLAC^{3D} model. Nevertheless, noticeable differences in radial displacements obtained with the two methods can be observed (**Figure 6-6**a). This could be attributed to the fact that the loading condition that acts on the tunnel lining is not the same in the two methods. In the case of the HRM method, the external loads act directly and explicitly on the beam elements. The external loads in the FLAC^{3D} model are instead applied at the model's boundary that act on the tunnel support through the continuous soil and an arch effect can be created in the ground around the tunnel (**Figure 6-5**).

It can be seen in **Figure 6-7** that both normal forces and bending moment obtained with the HRM are slightly greater than the FLAC^{3D} ones. A considerable difference in the shape of the normal forces along the tunnel periphery can be observed. Like for the lining displacements, the difference in the normal forces could be attributed to the effect of external loads that act on the tunnel lining, which are not similar in the two methods.

On the basis of above results, it is reasonable to conclude that the structural forces and the lining displacement results obtained using the HRM method are basically in good agreement with the numerical FLAC^{3D} results with respect to the tunnel location
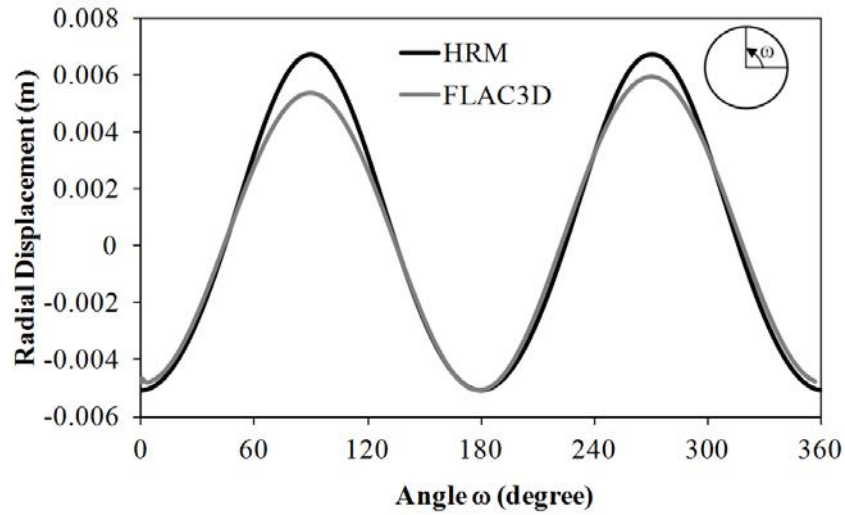
a) Radial displacements
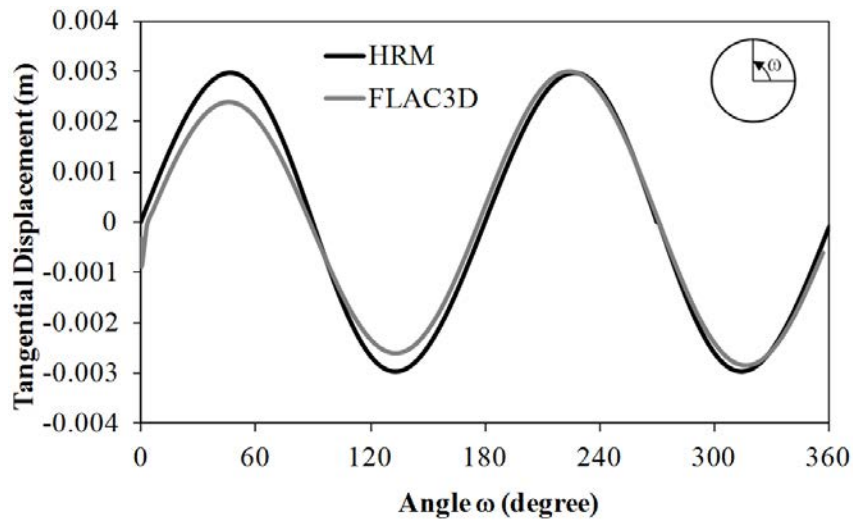
b) Tangential displacements

Figure 6-6. Displacement in the tunnel lining, comparison between the HRM method and FLAC^{3D} model
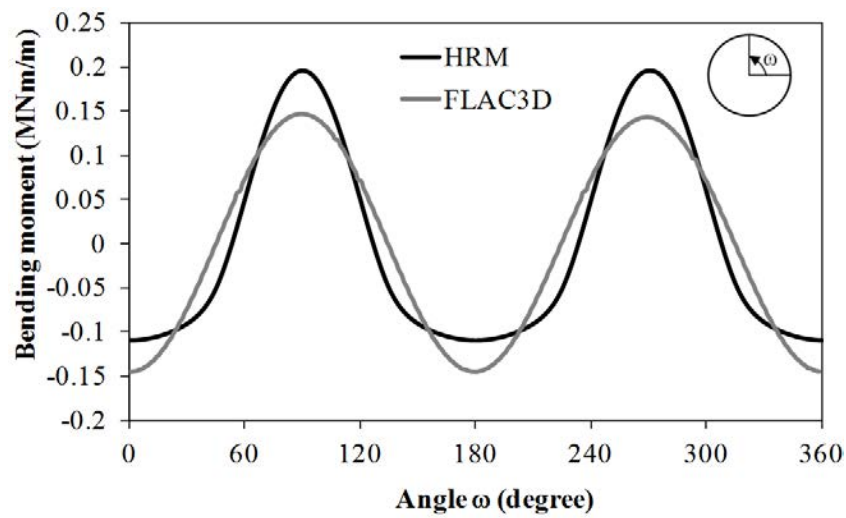
a) Bending moment
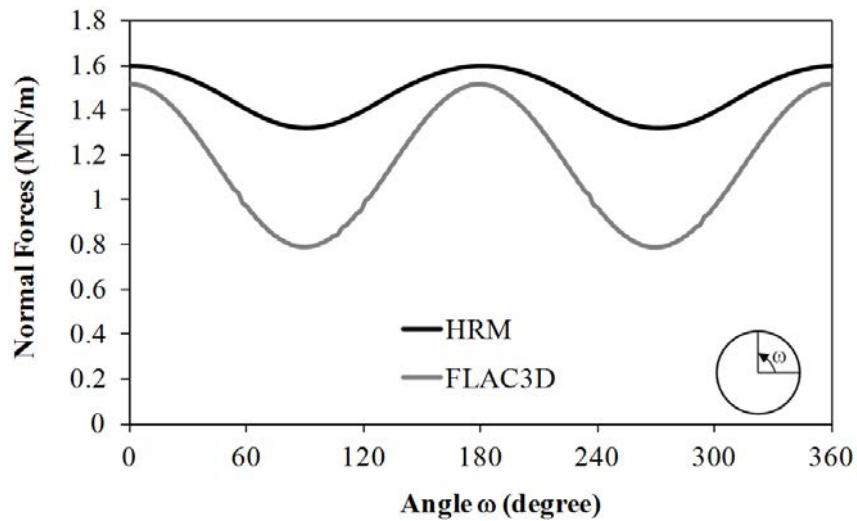
b) Normal forces

Figure 6-7. Structural forces in the tunnel lining, comparison between the HRM method and FLAC³ᴰ model

6.4. The Behaviour of Segmental Tunnel Lining studied by the HRM

An extensive parametric analysis has been developed to investigate the effect of the geo-mechanical parameters of the soil, the segmental tunnel lining stiffness and the applied loads, in terms of bending moment (M), normal force (N), and shear force (Q), the normal lining displacement value (δ_n), and the normal pressure (p_n). Three types of ground were considered in the calculation to cover weak and good ground. Two values of lateral earth pressure coefficient K_0 were considered ($K_0 = 0.5$ and $K_0 = 1.5$). The tunnel dimension, represented here by the radius R, is in a range between 2 m and 5 m. Vertical loads, determined using Terzaghi's formula, for two cases corresponding to a shallow tunnel ($H = 4R$) and a deep tunnel ($H = 20R$) were investigated.

Generally, the presence of joints leads to a reduction in the flexural stiffness of a segmental lining. In other words, the deformability of a segmental lining is higher than that of a continuous lining. In this study, a reduction factor, η, has been applied to the bending rigidity (EJ) of the segmental tunnel lining (see equation 1-1). In general, its values are in 0.6 to 0.8 ranges (JSCE [1996]). Four values of η, equal to 0.4, 0.6, 0.8 and 1, were however investigated in the parametric analyses. Details of the cases adopted for the parametric analyses are illustrated in **Table** 6-1.

Table 6-1. Details of the cases adopted for the parametric analyses

Descriptions/Case	1	2	3	4	5	6	7	8	9	10	11	12
Ground properties	A	A	B	B	C	C	A	A	B	B	C	C
Young's modulus E_S (MN)	500	500	150	150	50	50	500	500	150	150	50	50
Friction angle ϕ (degree)	35	35	31	31	28	28	35	35	31	31	28	28
Cohension c (MN)	0.05		0.02		0.005		0.05		0.02		0.005	
Unit weight γ (MN/m³)					0.017							
Lateral earth pressure coefficient K_0	0.5	1.5	0.5	1.5	0.5	1.5	0.5	1.5	0.5	1.5	0.5	1.5
Tunnel depth H	4R	4R	4R	4R	4R	4R	20R	20R	20R	20R	20R	20R
Tunnel outer radius R (m)	Changed for three cases: R_1=2m; R_2=3.5m; R_3=5m											
Lining thickness t (m)	Changed for three cases: t_1=0.3m; t_2=0.4m; t_3=0.5m											
Reduction factor of rigidity η	Changed for four values: η=0.4, 0.6, 0.8 (*segmental lining*); η=1 (*continuous lining*)											

The parametric analyses calculated 432 cases using the FEMCL code, thus covering most of the possible situations that could be encountered in shield-driven segmental tunnel lining design practice.

The values of the bending moment, the normal force, and the normal displacement at the tunnel crown and the right sidewall corresponding to a θ angle of 90^0 and 0^0, where the maximum values can occur, have been determined. Furthermore, the maximum values of the

shear force and normal pressure around the segmental tunnel lining are also estimated. The results obtained with parameters in **Table** 6-1 have been presented in **Appendix A**.
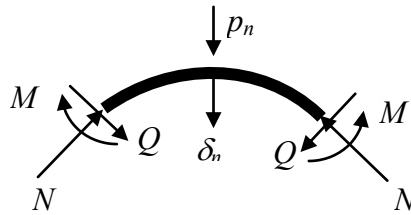
Figure 6-8. Positive direction of the structural forces (M, N, Q), normal lining displacement (δ_n), and normal pressure (p_n).

From the parametric analyses, as shown in **Appendix A**, some conclusions can be drawn:

- The higher the ground quality, the lower the bending moment, the normal force, and the tunnel lining displacement, but the higher the maximum shear force;

- The thicker the tunnel lining, the lower the passive normal pressure (except the small tunnel excavated through strong ground), and the higher the bending moment, but the lower the normal force, the maximum shear force and the normal displacement;

- The decrease in Young's modulus E of the concrete segmental tunnel lining, due to the effect of joints, is followed by a decrease in the absolute bending moment measured at both the tunnel sidewall and the tunnel crown. The dependence of the bending moment on the reduction factor, η, is almost linear and can be expressed by the relationship equation $y = ax + b$. The larger the tunnel diameter and the thicker the tunnel lining, the higher the influence of the reduction factor, η, on the bending moment values. The effect of the lining thickness on the bending moment is higher for large tunnels (R = 5 m) than that induced in small tunnel (R = 2 m). For example, with the input data of case 1, the *a* value in the above relationship equation applied for the bending moment induced at the spring line changes from -0.012 to -0.022 when the tunnel radius is of 2 m and the lining thickness changes from 0.3 m to 0.5 m, respectively. On the other hand, when the tunnel radius is of 5m, the corresponding *a* value changes from -0.0055 to -0.07 (e.g., see **Figure** A.1a);

- The lower the ground quality, the higher the influence of reduction factor, η, on the bending moment. For example, the absolute maximum *a* values in the relationship equation applied for the bending moment induced at the spring line, obtained with a tunnel radius of 5m and a lining thickness of 0.5m are about 0.07, 0.2, and 0.322, for case 1 (ground type A, see **Figure** A.1a), case 3 (ground type B, see **Figure** A.3a) and case 5 (ground type C, see **Figure** A.5a), respectively;

- Reduction factor, η, has an insignificant impact on the normal force induced in the segmental tunnel lining;

- The normal force at the tunnel crown when the K_0 values is smaller than unity depends more on the lining thickness, especially for a small tunnel, than the normal force determined at the tunnel sidewall. For example, with the case 1 input data, the absolute maximum

discrepancies between the normal force determined in small tunnel (R = 2 m) and large tunnel (R = 5 m) caused by a change in lining thickness from 0.3 m to 0.5 m are about 15.92 % and 5.37 %, respectively (e.g., see **Figure** A.1d). On the other hand, when the K_0 value is larger than unity, the lining thickness has more effect on the normal force determined at the tunnel sidewall;

- The absolute discrepancies of the normal forces determined at locations that lie along and perpendicular to the direction of the larger external ground loads, when the lining thickness changes from 0.3m to 0.5m, increase and decrease, respectively, due to the reduction in the η value. For example, with the case 1 input data, the absolute discrepancies of the normal force induced at the tunnel crown decrease from 15.92 % to 11.81 % for the case of a reduction factor, η, of 1 and 0.4, respectively. The corresponding values for absolute discrepancies of the normal forces at the spring line are 0.04% and 0.91% (e.g., see **Figure** A.1c,d).

- For high quality ground (ground type A), the impact of reduction factor, η, on the normal pressure, p_n, depends to a great extent on the tunnel dimensions and lining thickness. For large tunnels ($R = 5$ m), an increase in η values and an increase in lining thickness cause an increase in normal pressure p_n. On the other hand, for small tunnels ($R = 2$ m), the normal pressure acting on the lining is higher when the reduction factor is lower and the tunnel lining is thinner. The normal pressures for medium tunnel dimensions ($R = 3.5$ m) are almost constant (e.g., see **Figure** A.1f);

- For medium quality ground (ground type B) and weak ground (ground type C), the effects of reduction factor, η, and the lining thickness on the normal pressure are similar (e.g., see **Figure** A.3f and **Figure** A.5f). The higher the η value and the thicker the tunnel lining, the lower the normal pressure p_n;

- The larger the tunnel dimension, the higher the dependence of shear forces on reduction factor, η. Generally, an increase in η values leads to a decrease in shear force. This relation is almost linear and can also be expressed by relationship equation $y = ax + b$. The larger the tunnel, the higher the a value. For example, with the case 1 input data, the absolute maximum values of a, when the tunnel radius is 2m or 5m, are 0.008 and 0.03, respectively (e.g., see **Figure** A.1e).

- For high quality ground (ground type A), the influence of reduction factor, η, on the normal displacement, measured in the direction of smaller external load, depends to a great extent on the tunnel dimension. The increase in η values for a small tunnel ($R = 2$ m) leads to a decrease in the absolute normal displacement. Instead, for large tunnel ($R = 5$ m), the behaviour is the opposite. In the case of medium tunnels ($R = 3.5$ m), the normal displacement is only effected slightly by the reduction factor (e.g., see **Figure** A.1g);

- For medium quality ground (ground type B), and weak ground (ground type C), the higher the reduction factor, generally the lower the absolute normal displacement measured in the direction of the smaller external load (e.g., see **Figure** A.3g and **Figure** A.5g);

- The larger the tunnel, the higher the impact of the lining thickness on the normal displacement;

- The influence of the reduction factor, η, on the normal displacement can be approximately by means of a linear relation;

From these parametric analyses, once the tunnel dimension (radius R), ground condition (cohesion, internal friction angle, Young's modulus, lateral earth pressure coefficient), lining thickness and a value of reduction factor, η, assumed on the basis of the analytical or empirical methods and/or experimental data introduced above are known, the structural forces, lining displacement, and normal pressure can be estimated. It is then possible to conduct a detailed design of the structure of the segmental tunnel lining, in terms of necessary reinforcements, concrete quality, etc. Using these design figures, it is also possible to verify the influence of the various calculation parameters on the support structure behaviour, in order to decide whether it is necessary to study the unknown parameters in more detail. The preliminary results that are acquired from design figures help one to start with the further numerical calculations considering types of support that are close to the final ones, thus saving precious time.

If, for example, it is necessary to estimate the critical cases of structural forces induced in a shield-driven segmental tunnel lining with an external radius of 3.5m and an assumed support thickness of 0.3m, which is excavated through strong ground (ground type A with lateral earth pressure coefficient K_0 of 0.5) at a depth of $4R$ (14m), assuming a reduction factor of 0.9, which is similar to the one determined in the above case study, using **Figure** A.1 in **Appendix A** for this example case, the following tunnel behaviour data can be obtained:

- Bending moment at the tunnel sidewall M_0 (MN.m/m):   -0.0065;
- Bending moment at the tunnel crown M_{90} (MN.m/m):   0.04
- Normal force at the tunnel sidewall N_0 (MN/m):   0.8
- Normal force at the tunnel crown N_{90} (MN/m):   0.73
- Maximum shear force Q_{max} (MN/m):   0.038
- Maximum normal pressure p_n (MN):   0.12
- Normal displacement at the tunnel sidewall δ_{n0} (m):   -0.00072
- Normal displacement at the tunnel crown δ_{n90} (m):   0.0017

Obviously, in this case, the critical values of the structural forces and lining displacement are at the tunnel crown and the lining should be designed considering this location.

6.5. A New Approach to the HRM for the Design of Segmental Linings

This section proposes a new numerical HRM approach for the analysis of segmental tunnel linings. This approach has been developed on the basis of the model which was proposed by Oreste [2007] and then improved in section 6.2 (also see Do et al. [2014d]). The influence of segmental joints has been directly considered using a lenghtless rotational spring, which is represented by a fixity ratio that is determined on the basis of a nonlinear rotational stiffness. The parameters necessary for the calculation have been presented. A specific implementation

has been developed using a FEM framework, which is able to consider the effect of segment joints in successive rings on the tunnel lining. The present HRM method allows the arbitrary distribution of segment joints along the tunnel boundary to be taken into consideration. In addition, the rotational stiffness of the segment joints has been simulated using nonlinear behaviour, as it is closer to the true behaviour of a joint than linear or bilinear behaviour.

The HRM results of three ring interaction assumptions have been compared and validated with the 3D numerical results. The work presented in this section shows that the proposed HRM method can be used to investigate the behaviour of a segmental tunnel lining.

6.5.1. Characteristics of the joints in the segmental tunnel lining

As far as a segmental tunnel lining is concerned, it is very important to take into consideration the effect of the joints in the lining on its behaviour. In structural analyses, a segmental joint can be considered as an elastic pin and its stiffness characteristics are specified by the rotational stiffness K_{RO}, the axial stiffness K_A, and the radial stiffness K_R (see section 4.1 and Do et al. [2013a]). The K_{RO} value is defined as the bending moment-per-unit length required to develop a unit rotation angle along the joints of the assembled segments. Similarly, axial stiffness, K_A, and radial stiffness, K_R, are defined as the axial force and the shear force-per-unit length required to develop a unit axial and radial displacement at a given joint, respectively. In a study performed in section 4.1 (also see Do et al. [2013a]), the 2D numerical results pointed out that the influence of radial and axial stiffness can be ignored. However, the impact of the rotational stiffness should be considered. For this reason, segmental joints in numerical models, which are introduced in this study, are simulated by means of only rotational springs.

6.5.2. The new HRM method

On the basis of the work of Oreste [2007], Do et al. [2014d] developed a numerical HRM approach for the analysis of tunnel linings in which the influence of segmental joints was considered indirectly through the use of a reduction factor applied to the flexural rigidity of the lining. The details of the HRM model presented in section 6.2 can be found in Do et al. [2014d].

6.5.2.1. Simulation of segmental joints in the HRM

6.5.2.1.1. Introduction

Joint connections in a segmental lining present intermediate behaviour between the two extreme cases: a pinned-joint connection and a rigid-joint connection in which the joint is considered totally pinned and totally rigid, respectively. This behaviour is similar to that of a semi-rigid connection, which has been adopted extensively in the design of frame structures

(Burn et al. [2002] and Filho et al. [2004]). Theoretically, the joint connections in a segmental lining should therefore be classified as semi-rigid connections.

A semi-rigid connection is one that has a moment transmission capacity. The main characteristic of the semi-rigid connection is a continuous change in the rotational stiffness under the action of the loads (see **Figure** 6-9) (Kartal et al. [2010]).
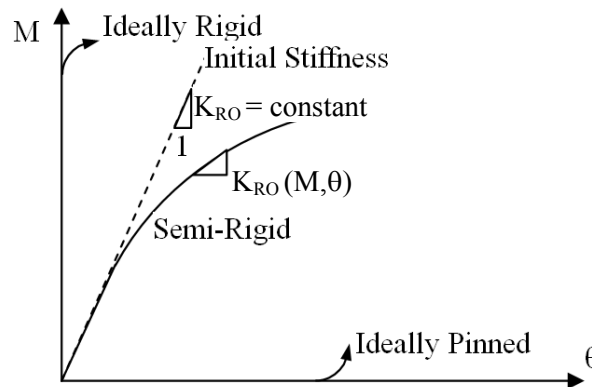
Figure 6-9. M-θ relation for rotational connection in the semi-rigid condition for the segment connections (Kartal et al. [2010]). In the ideally-rigid connection (no rotation admitted) the moment increases with nil rotation (the representative curve is the ordinate axis); in the perfect pinned condition (no moment transmitted through the connection) the rotation increases with nil moment (the representative curve is the abscissa axis).

In general, two different approaches can be followed to incorporate a semi-rigid joint connection into numerical analysis. The first one is to introduce additional "connection elements" that directly model the joint connections (e.g. Ding et al. [2004]). However, when this approach is used, it is difficult to obtain a physical sense of the stiffness of each connecting member since they are separated from the attached end-connections. In the second approach, each beam member has a lengthless rotational spring attached at each end. Most research applications have adopted the second approach rather than the first one to incorporate connection behaviour into frame analysis Burn et al. [2002]. If the second approach is adopted, an increase in the number of elements in the analysis is avoided and the number of degrees of freedom is the same as for the system with ideally rigid-connections (no rotation admitted).

6.5.3.1.2. Behaviour of the semi-rigid joint connection

As for the relationship between the bending moment and the angular rotation at the joint, the nonlinear behaviour was back analysed on experimental data (Hordijk and Gijsbers [1996]). This means that the rotational stiffness can be considered to depend on the rotation of the segmental joints.

There are two models in the literature that are now generally used to simulate segmental joint behaviour. The first is the single-stiffness linear model, and it is the simplest connection model, which is applied extensively in semi-rigid joint analysis methods, especially in

analytical methods (e.g. Lee, Hou, Ge and Tang [2002], Naggar and Hinchberger [2008]). The second is the bilinear models, which has been proposed in the numerical analyses of tunnels to provide a better approximation (Zhong et al. [2006], Van Oorsoiw [2010], Thienert and Pulsfort [2011]).

In the present model, nonlinear behaviour has been adopted to simulate the segmental joint behaviour. This has been done by continuously updating the rotational stiffness values during the analysis process.

Janssen's formulas, which are based on the investigation by Leonhardt and Reimann [1966], are used to determine the rotational stiffness of the segmental joints (Gruebl [2006], Groeneweg [2007]). As described in Chapter 1, Janssen's analytical results have been proved to closely match the experimental results introduced by Hordijk and Gijsbers [2007] . The so-called Janssen joint assumes that the contact area (shadow zone in **Figure** 6-10) can be represented by a concrete beam with a depth equal to the width of the joint contact area (segment width) and a height equal to the contact height of the joint (see **Figure** 6-10). Opening of the joint is considered as the concrete beam is unable to bear any tensile stresses.
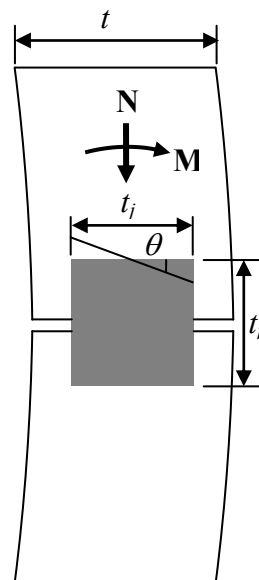
Figure 6-10. Cross-section of the longitudinal joint (Groeneweg [2007])

Two stages are distinguished for an increasing rotation of the joint or beam (Groeneweg [2007]):

1. Closed joint (rotation $\theta \leq \dfrac{2N}{E_s W t_j}$)   (6-33)

2. Opened joint (rotation $\theta > \dfrac{2N}{E_s W t_j}$)   (6-34)

where: W = Width of the longitudinal joint (segment width), m;
        E_s = Young's modulus of the lining, kN/m^2;
        t_j= Height of the contact in the longitudinal joint, m;
        N = Normal forces, kN;

θ = Rotation, degree.

The Janssen rotation stiffness K_{RO} is given for all stages (see **Figure** 6-11):

1. Closed joint:

$$K_{RO} = \frac{Wt_j^2 E_s}{12}$$ (6-35)

2. Opened joint:

$$K_{RO} = \frac{9Wt_j E_s M \left(\frac{2M}{Nt_j} - 1 \right)^2}{8N}$$ (6-36)

where K_{RO} = rotation stiffness, kN.m/rad;
   M = Bending moment present in the joint, kN.m/m.
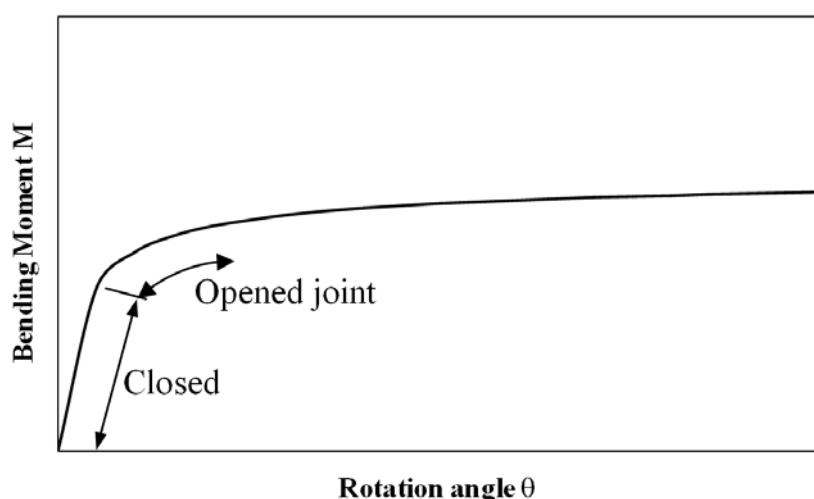
Figure 6-11. Relationship between the bending moments and rotations in a Janssen joint (Groeneweg [2007])

Fixity factor

The simulation of the joint connection as a lengthless rotational spring is widely used in the semi-rigid analysis of frames, but the implementation of this approach requires small modifications to the existing analysis programmes generally applied for a rigidly connected frame, for example the HRM method presented by Oreste [2007] and Do et al. [2014d].

Using a simulation approach in which each semi-rigid connection member is comprised of a finite-length member with a lengthless rotational spring attached at each end, Monforton and Wu [1963] defined the so-called "fixity factor" in order to reflect the relative stiffness of the beam and the rotational springs, as shown in **Figure** 6-12. In **Figure** 6-12, K_{RO1} and K_{RO2} are the rotational spring stiffnesses of the end-connections, and $E_s J_s / L_i$ is the bending stiffness

of the attached member. The "fixity factor", r_j, is used extensively in semi-rigid frame analysis and determined at each end-connection of the beam using the following formula (Burn et al. [2002], Filho et al. [2004], Kartal et al. [2010], Pinheiro and Silveira [2005], Xu [1992], Sekulovic and Salatic [2001], Csébfalvi [2007], Kaveh and Moez [2008], Hasan et al. [2011]):

$$r_j = \frac{1}{1 + \dfrac{3E_S J_S}{K_{RO} L_i}} \tag{6-37}$$

where K_{RO} is the rotational spring stiffness of the end-connection, E_s is the Young's modulus of the lining material, J_S is the inertia moment of the beam, and L_i is the length of each beam element.

6.5.2.1.3. *Semi-rigid joint connection analysis using a lengthless rotational spring in a numerical approach*

The fixity factor r_j defines the rotational stiffness of each end connection relative to that of the attached member. For a pinned connection, the fixity factor is zero ($r_j = 0$), and for a fully-rigid connection the fixity factor is unity ($r_j = 1$). Therefore, a semi-rigid joint connection has a fixity factor somewhere between zero and unity ($0 < r_j < 1$).

Upon the introduction of the fixity factor, different member end-restraint conditions are then readily modelled, such as rigid-pinned, rigid-semi-rigid or pinned-semi-rigid, simply by setting the fixity factors at the two ends of the member to appropriate values. Therefore, this analysis approach is comprehensive regardless end-rotational conditions of the member and can be applied to the analysis of frames with pinned, rigid and/or semi-rigid connections.
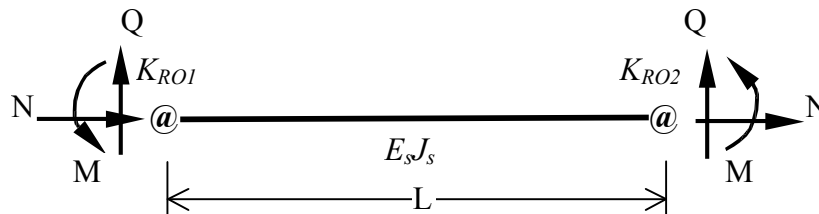
Figure 6-12. Semi-rigid member (Burns et al. [2002])

Stiffness matrix of a semi-rigid connected element

On the basis of an existing rigid connected frame, only minor modifications to the member stiffness matrix are necessary.

The elastic stiffness matrix of a member i, with two semi-rigid end-connections and with rotational stiffness modulus K_{RO1} and K_{RO2}, as shown in **Figure** 6-12, can be represented by the stiffness matrix of the member considered to have rigid end-connections modified by a semi-rigid correction matrix (Burn et al. [2002], Chen [2000]), i.e.:

$$K_i^{SR} = Z_i . C_i \tag{6-38}$$

where K_i^{SR} is the stiffness matrix of member i, with semi-rigid end-connections taken into account, Z_i is the stiffness matrix of the member considered to have rigid ends and C_i is the correction matrix.

For a planar beam element with six degrees of freedom, the correction matrix C_i has the following form (Burn et al. [2002], Chen [2000]):

$$C_i = \begin{bmatrix} 1 & 0 & 0 & 0 & 0 & 0 \\ 0 & \dfrac{4r_2 - 2r_1 + r_1 r_2}{4 - r_1 r_2} & \dfrac{-2L_i r_1 (1 - r_2)}{4 - r_1 r_2} & 0 & 0 & 0 \\ 0 & \dfrac{6(r_1 - r_2)}{L_i(4 - r_1 r_2)} & \dfrac{3r_1(2 - r_2)}{4 - r_1 r_2} & 0 & 0 & 0 \\ 0 & 0 & 0 & 1 & 0 & 0 \\ 0 & 0 & 0 & 0 & \dfrac{4r_1 - 2r_2 + r_1 r_2}{4 - r_1 r_2} & \dfrac{2L_i r_2 (1 - r_1)}{4 - r_1 r_2} \\ 0 & 0 & 0 & 0 & \dfrac{6(r_1 - r_2)}{L_i(4 - r_1 r_2)} & \dfrac{3r_2(2 - r_1)}{4 - r_1 r_2} \end{bmatrix} \tag{6-39}$$

where L_i is the length of member i.

The fixity factors r_1 and r_2 in Equation (6-39), which correspond to K_{RO1} and K_{RO2} at two ends, are defined by means of Equation (6-37). When the semi-rigid beam member stiffness matrix K_i^{SR} from Equation (6-38) has been determined for specified values of fixity factors that reflect connection stiffness, frames with semi-rigid connections can be analysed directly by means of the semi-rigid beam member stiffness matrix K_i^{SR} to replace the local stiffness matrix Z_i of the ith element. All the other calculations are performed in the same way as for a rigid frame using the "displacement method", described in section 6.2 (also see Do et al. [2014d]). An iterative procedure is applied to take the nonlinear behaviour of semi-rigid connections into account. The member stiffness matrix K_i^{SR} is modified at each iteration using the correction matrix C_i with updated fixity factors r_j.

On the basis of mathematical formulation of the HRM method and correction matrix C_i of a semi-rigid connected element, the FEMSL code has been written in MATLAB programming language. It should be mentioned that the necessary time for each calculation, used for a numerical model including 360 beam elements per lining ring divided by 6 segmental joints, is very short (about 5 seconds).

It is necessary to note that the present HRM method allows the arbitrary distribution of segmental joints along the tunnel boundary to be taken into account.

6.5.2.2. Assumptions on the 3D effect between successive rings in the HRM method

The behaviour of segmental tunnel lining is a 3D problem. Segment joints in successive lining rings usually have different positions which make a staggered pattern of the joints in

the segmental tunnel lining. This feature plays a crucial role and may lead to completely different results from the case in which segmental joints are at the same position at all the segments along the axis of the lining.

In order to take into consideration the 3D effect of a segmental tunnel lining, three assumptions on the segmental joints simulation have been developed to model the interaction between segment joints in successive rings (**Figure 6-14**). The number of numerical joint is equal to double of the true joint number.

r_1 and r_2 in **Figure 6-14** are fixity factors that are determined, using Equation (6-37), at the concrete section and at the true joint, respectively, in a lining ring. In this study, a r_1 value of unity is adopted for concrete section on the basis of the assumption that the concrete is a completely rigid connection. The values of r_2 of true joints are automatically recalculated, after each iterative procedure, during the FEM analysis process on the basis of the bending moment, M, and rotational angle, θ, measured at each joint along the tunnel structure. The value r_3 is defined as the average value of r_1 and r_2 (i.e. $r_3 = 0.5(r_1+r_2)$). r_1, r_2 and r_3 are used to simulate the flexural behaviour of segments due to the presence of segmental joints.

In hypothesis 1, the fixity factors assigned at nodes, which lie between numerical joints, are the same and do not depend on the distance to the numerical joints (see **Figure 6-14**a). On the other hand, the fixity factors assigned at these nodes in hypotheses 2 and 3 are not the same; they increase gradually from the node, which is close to the numerical joint, to the middle node, which lie between two numerical joints (see **Figure 6-14**b and c).

In order to estimate the effectiveness of the above three assumptions, the numerical results of the three assumptions have been compared with data obtained from the shield-driven tunnel of the Bologna-Florence high speed railway line project, as mentioned later on in section 6.5.4. It should be noted that both position of true joints in a lining ring, L_j, and position of two numerical joints, a_i, which depends on the joint distribution in successive rings, can in fact be changed (see **Figure 6-13** and **Figure 6-14**). These characteristics are also taken into consideration in the FEMSL code.
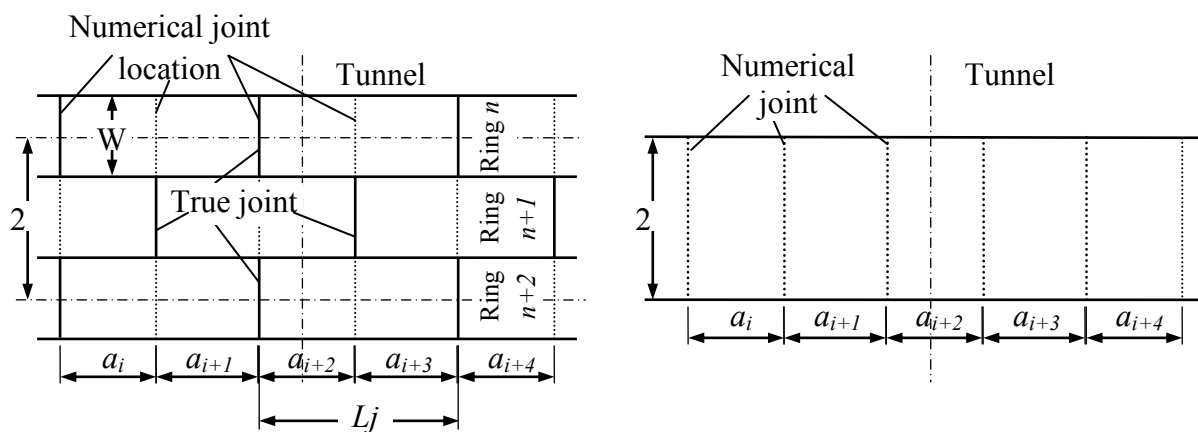
a) True segmental tunnel lining   b) Simplified model in the HRM method

Figure 6-13. Segmental lining scheme

a) Assumption 1   b) Assumption 2
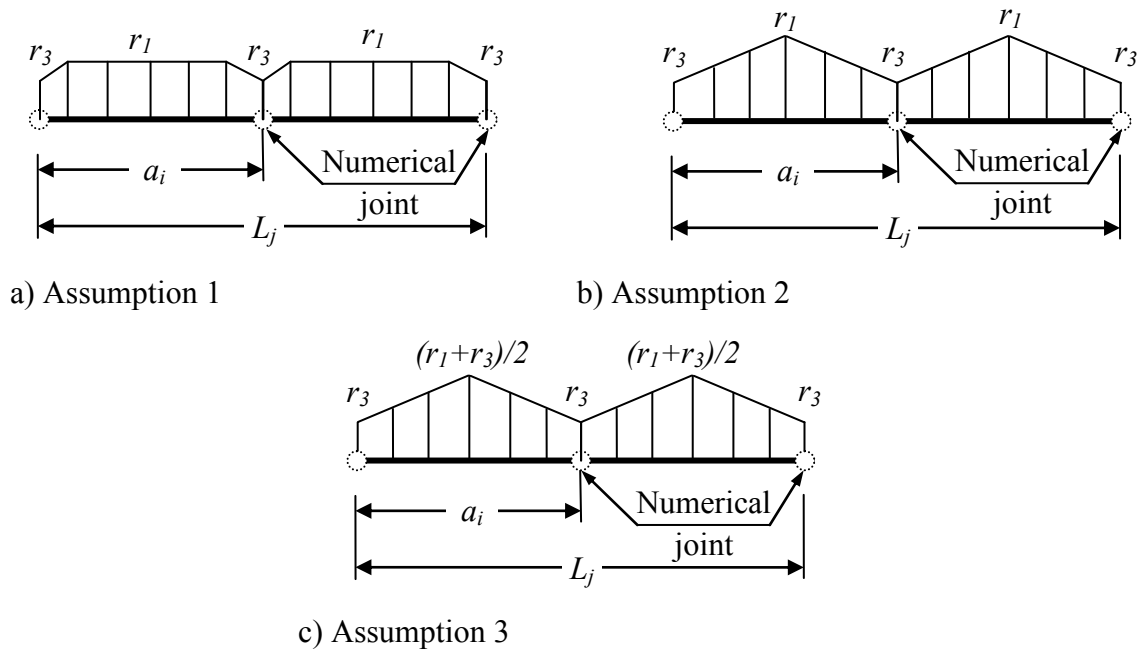
c) Assumption 3

Figure 6-14. Assumptions on the 3D effect simulation of a segmental tunnel lining

6.5.3. 3D numerical model description

A simplified model has been developed using the FLAC^{3D} software (Itasca [2009]), which is based on the Generalised Finite Difference Method. The analyses have been performed using small strain calculations. In the simplified model, a 3D simulation of a tunnel supported by means of segmental lining has been modelled. The influence tunnelling process such as the shield machine and the construction loads (face support pressure, grouting pressure, jacking force loads, etc.) was however not taken into consideration. The main purpose of the simplified model is to take into account the effect of the tunnel lining segmentation.

As in Chapters 4 and 5 (also see Do et al. [2013a, 2013b, 2014a, 2014c, 2014f]), the tunnel segments have been modelled using a linear-elastic embedded liner element. The segment joints have been simulated using double node connections (see **Figure 5-2**). The values of the spring constants used to simulate the segment joints can be determined on the basis of the simplified procedures presented by Thienert and Pulsfort [2011] and Do et al. [2013a]. The attachment conditions of the translational components and two rotational components around the x and z directions were assumed to be rigid for all the investigated cases.

In the same way as for the segment joint, the ring joints have also been simulated using double connections (see **Figure 5-2**). In this section, like the simulation in the HRM method, connections between lining rings have been assumed to be rigid. A discussion on the influence of this assumption on the tunnel behaviour is mentioned in the following section.

The ground is assumed to be a linear elastic and massless material which corresponds to the boundary conditions applied in the HRM method. The external loads, which are

represented by a vertical load σ_v and a horizontal load σ_h, have been applied at the external boundaries of the model (**Figure** 6-15).
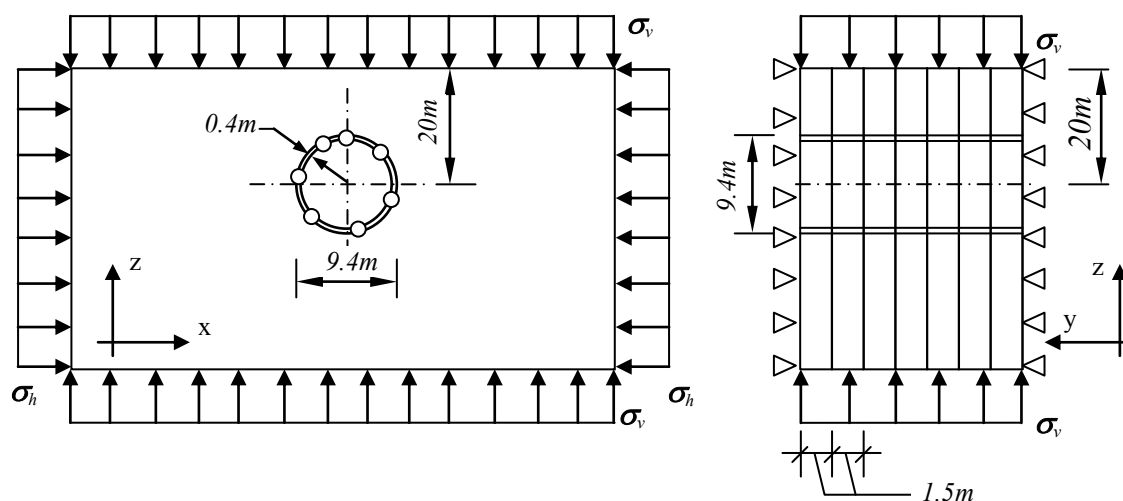
Figure 6-15. Simplified 3D model under consideration

A parametric analysis has been performed in the present study in order to determine the minimum dimension of the numerical model along the y-direction (parallel to the longitudinal axis of the tunnel) which allows the influence of the model boundaries on the behaviour of the monitored lining to be reduced. The numerical results have showed that a model with seven rings, which corresponds to 10.5 m length in the y-direction, is sufficient to determine the structural behaviour of the middle lining ring (ring 4) without the effect of the model boundaries (**Figure** 6-15). The time requested for the FLAC³ᴰ analysis of the model presented in **Figure** 6-15 is about 15 minutes when using a 2.67GHz core i7 CPU computer.

6.5.4. Evaluation of the FLAC³ᴰ model

Parameters from the Bologna-Florence high speed railway line tunnel project in Bologna have been adopted in this numerical modelling for the evaluation purpose (Croce [2011]). It is assumed that the behaviour of the soil and the tunnel structure is linear-elastic. The properties of the soil and tunnel lining can be found in **Table** 4-1.

The 3D numerical model (**Figure** 6-16) is 120 m wide in the x-direction, 10.5m thick in the y-direction, 60 m high in the z-direction and consists of approximately 42,000 zones and 55,000 grid points. Two lining joint patterns, that are staggered and straight patterns (see **Figure** 6-17), have been simulated. Obviously, a staggered pattern allows the tunnel lining to be simulated in a more realistic way in case of the Bologna-Florence tunnel. However, the straight pattern has also been simulated in order to highlight the effect of tunnel lining segmentation on the lining behaviour.
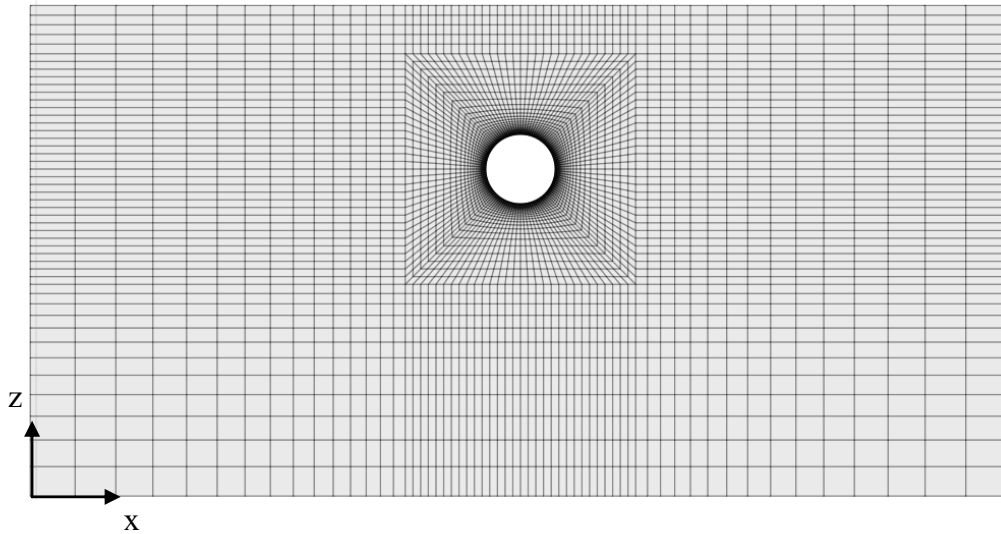
Figure 6-16. FLAC³ᴰ numerical model

Figure 6-18 illustrates the structural forces determined using the simplified 3D model. It can be seen that the segmentation in the tunnel lining has an insignificant influence on the normal forces induced in the lining. This is in good agreement with the 2D results introduced in section 4.1 (also see Do et al. [2013a]). However, as far as bending moment is concerned, **Figure** 6-18 points out a noticeable difference in the results obtained with a straight pattern and with a staggered pattern of the joints.

a)   b)
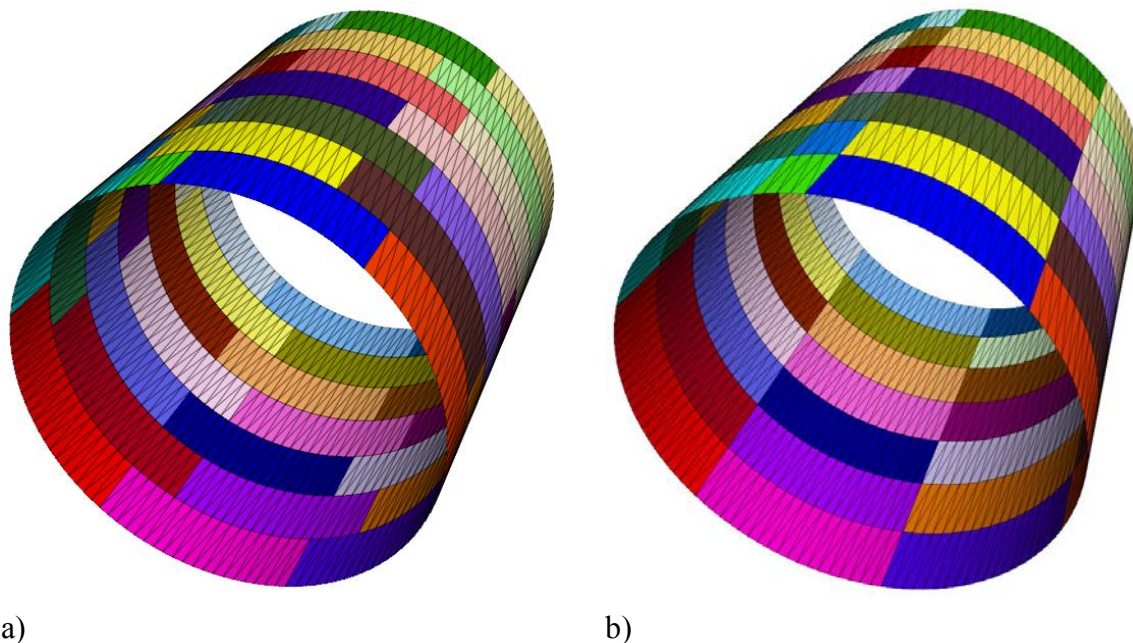
Figure 6-17. Segmental lining patterns: staggered lining (a) and straight lining (b)

As expected, the bending moments induced in a staggered lining are higher than the ones induced in a straight lining. This could be attributed to the stiffer tunnel lining in case of using a staggered pattern. The maximum differences of about 50% are observed at the crown and bottom of the tunnel (**Figure** 6-18).

Chapter 6: A new approach to the Hyperstatic-Reaction Method   220
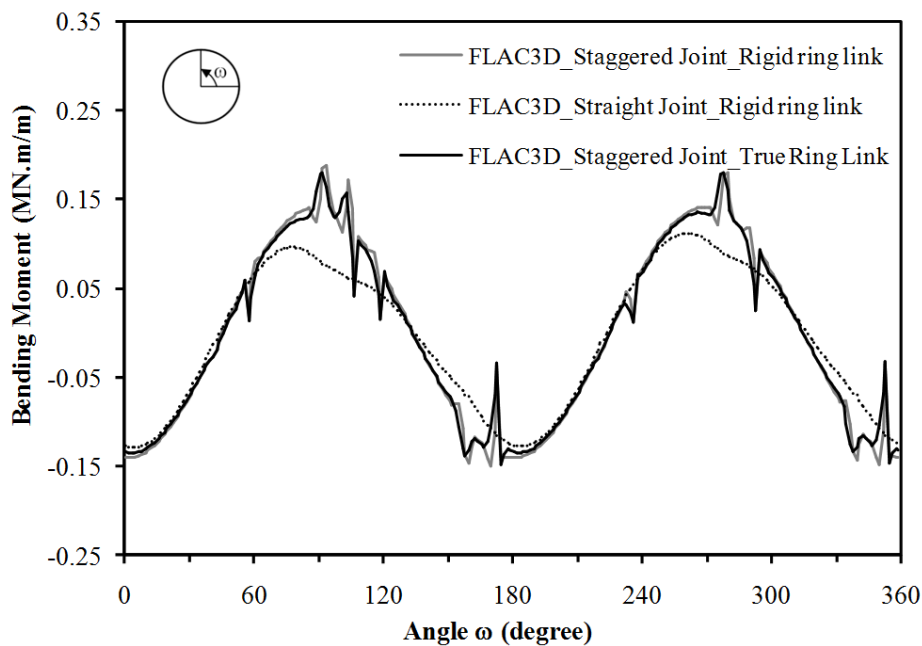
a) Bending moment
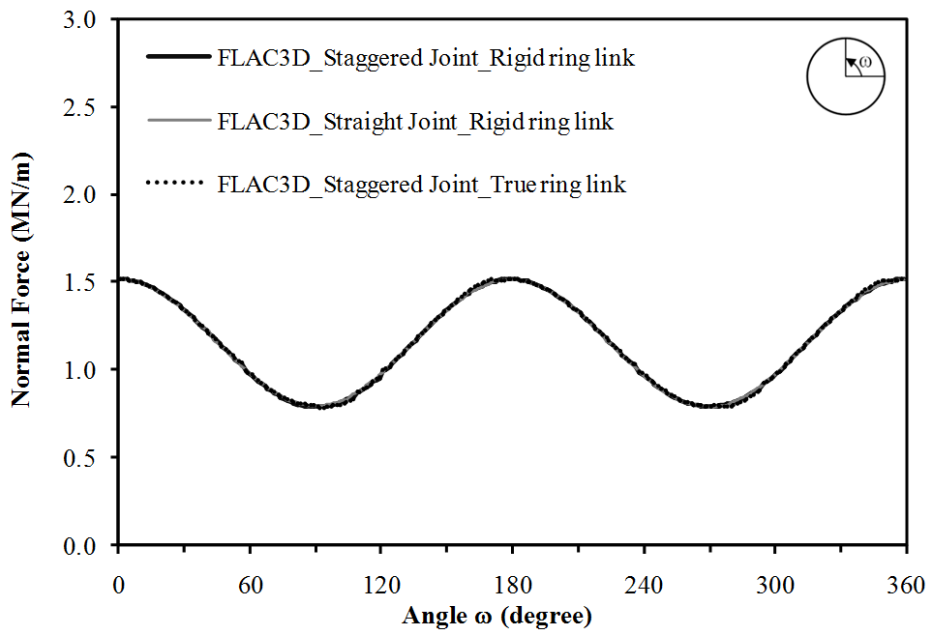
b) Normal forces

Figure 6-18. Structural forces in the tunnel lining

In order to highlight the effect of the connections between successive rings along the tunnel direction, an additional case in which the true connections between lining rings was considered has been performed. The rigidity characteristics of the ring joint connection have been represented by a set of rotational, axial and radial springs. The interaction mechanism of each spring is the same as the ones described by the same authors (Do et al. [2013a]). Owing to the presence of the true connection between successive rings, the lining rings in the additional case are more flexible than the ones simulated in previous case in which the ring connections are assumed to be rigid. As a consequence, the bending moments induced in the

lining are reduced while the normal forces are quite similar (**Figure** 6-18a). The maximum difference in the bending moment is about 5%.

On the basis of the above results, it is reasonable to conclude that a 3D numerical model, which allows the staggered pattern of the lining to be taken into consideration, is necessary to accurately simulate the behaviour of a segmental tunnel lining. In addition, the assumption of rigid connection between successive rings, which has been applied in the present HRM method, could be adopted from the design point of view.

6.5.5. Comparison between the HRM and FLAC³ᴰ numerical methods

As described in section 6.5.2.2, three assumptions on the segmental joints simulation have been developed in the HRM method to model the staggered pattern between successive lining rings. On the basis of comparison with the FLAC³ᴰ numerical results, using the same joint pattern with 6 segmental joints on a lining ring, the main purpose of this section is to determine which assumption is the most appropriate to simulate the staggered characteristics of a segmental tunnel lining.

For comparison purpose, instead of using the non-linear behaviour in section 6.2. and as described by Do et al. [2014d], the linear elastic soil springs in the HRM model have been adopted in this section. This assumption permits to better compare the two models (3D numerical one and HRM). This means that the normal spring stiffness, k_n, and tangential spring stiffness, k_s, at nodes along the tunnel lining in the HRM model are constant. Their values have been determined on the basis of the comparison of results obtained with the HRM and the FLAC³ᴰ model (case of a continuous lining). Using the determined spring stiffnesses, comparison between the HRM and FLAC³ᴰ model has been conducted for segmental linings.

Figure 6-19 and **Figure** 6-20 illustrate the lining displacements and structural forces, respectively, using a staggered joint pattern with rigid ring connections, at ring 582. **Figure** 6-19 shows an insignificant influence of the three assumptions in the HRM method for the lining displacements. Their tangential displacement results are quite similar to the one obtained with the FLAC³ᴰ model (**Figure** 6-19b). Nevertheless, noticeable differences in radial displacements obtained by the two methods can be observed (**Figure** 6-19a). This could be attributed to the fact that the loading condition acting on the tunnel lining is not the same in the two methods. In the case of the HRM method, the external loads act directly and explicitly on the beam elements. The external loads in the FLAC³ᴰ model are instead applied at the model's boundary that act on the tunnel support through the continuous soil and an arch effect can be created in the ground around the tunnel (**Figure** 6-15).

It can be seen from **Figure** 6-20 that the structural lining force results of the HRM method using the three assumptions on the 3D effect of the segmental tunnel lining (see **Figure** 6-14) are similar. The normal forces are quite similar for all the three assumptions in the HRM method (**Figure** 6-20b). A considerable difference in the shape of the normal forces along the tunnel periphery can be observed. Like for the lining displacements, the difference in the normal forces could be explained by the impact of external loads that act on the tunnel lining, which are not similar in the two methods. Additionally, this could also be attributed to

the effect of the interaction between the beam elements in the HRM model. Indeed, when the tunnel lining moves toward the soil, reaction forces from the surrounding soil mass acting on the tunnel lining through springs placed at nodes along the tunnel section in the HRM (at angles ω of 0^0 and 180^0 in this study) will appear. The compressive normal forces induced in the tunnel lining at these sections will therefore be transferred to the section at which normal forces are currently smaller (at angles ω of 90^0 and 270^0 in this study). Consequently, normal forces at these sections which are originally small will increase as observed in the HRM results.
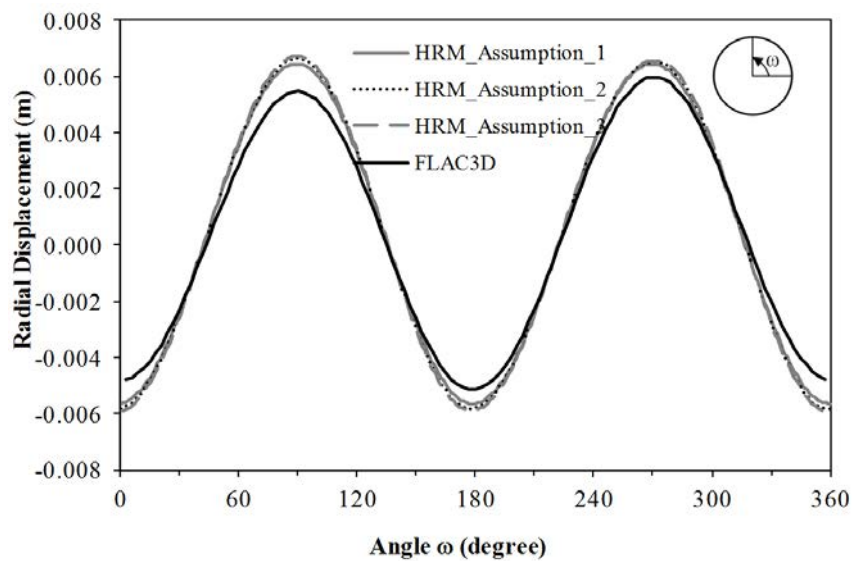
a) Radial displacements
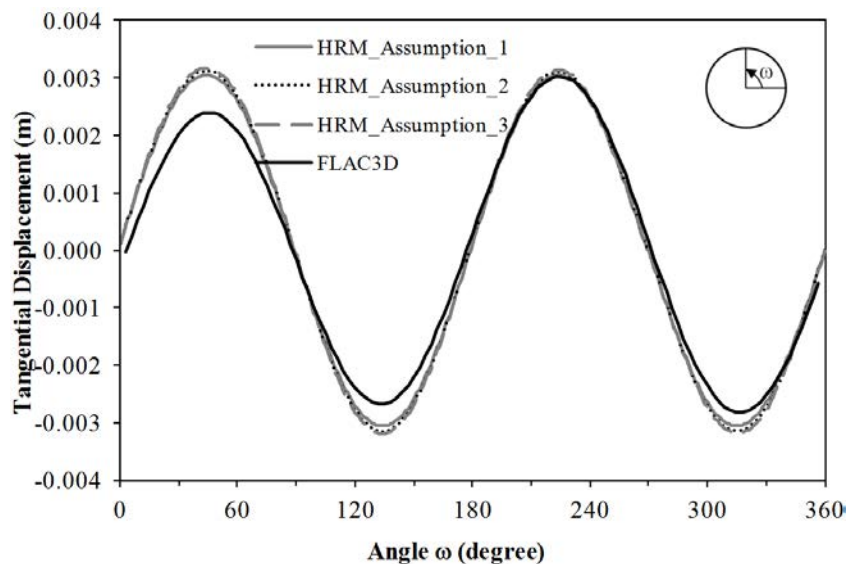
b) Tangential displacements

Figure 6-19. Displacement in the tunnel lining, comparison between the HRM method and FLAC^{3D} model

Chapter 6: A new approach to the Hyperstatic-Reaction Method   223

Without considering the suddenly change of the bending moment value at the segmental joint location, **Figure** 6-20a shows that the mean line of the bending moment obtained with the FLAC[3D] numerical analysis is closer to the corresponding value obtained by the HRM model in case of using the assumption 1 than with the two other assumptions. Indeed, the maximum differences between the bending moment obtained with FLAC[3D] model and that of assumptions 1, 2 and 3 introduced in the HRM are 6 %, 9.8 % and 18.1 %, respectively, which are observed at locations corresponding to angles ω of 0^0 or 180^0.
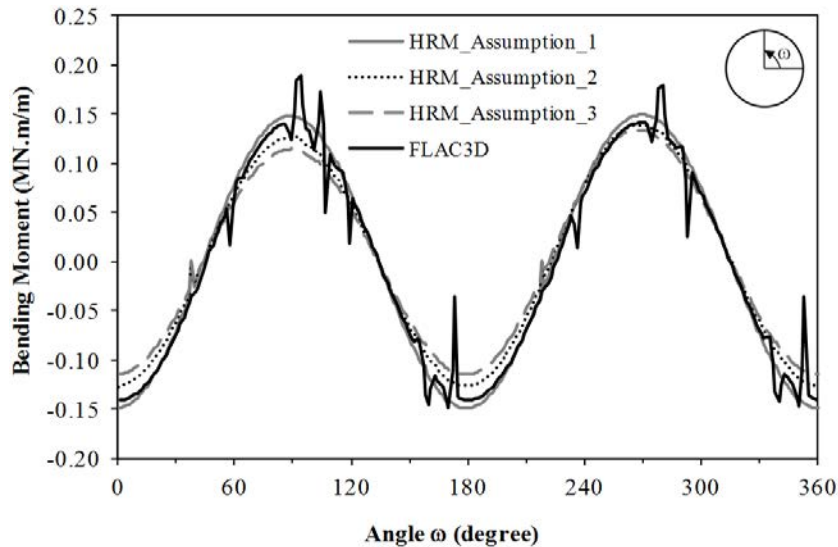
a) Bending moment
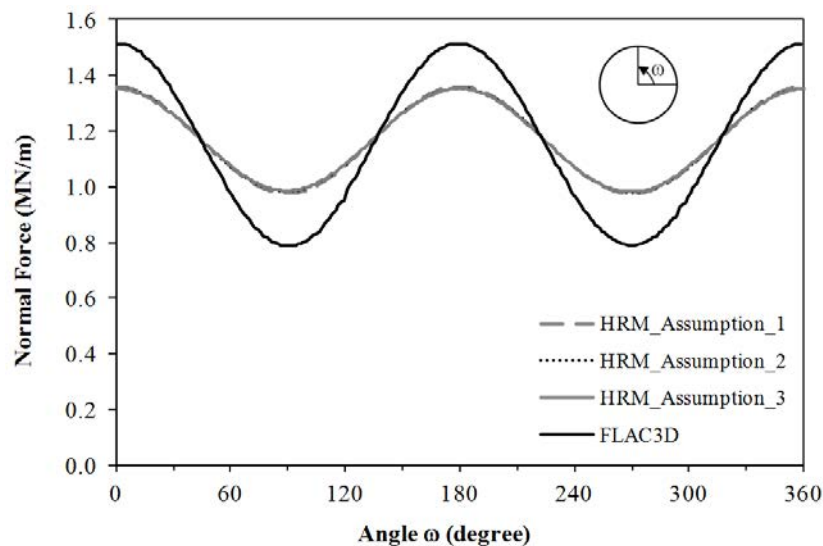
b) Normal forces

Figure 6-20. Structural forces in the tunnel lining, comparison between the HRM method and FLAC[3D] model

The following comments can be made on the basis of the previous analysis:
 (a) The structural force and lining displacement results obtained using the HRM method are basically in reasonable agreement with the numerical FLAC[3D] results;

(b) The influence of the joints between successive rings in segmental linings can be taken into consideration through numerical joints using one of above the three proposed assumptions in the HRM method. In this case study, assumption 1 produces the numerical results obtained using the FEMSL code to be in better agreement with the FLAC^{3D} results than the two others.

6.6. Conclusions

The HRM is particularly suitable for the estimation of tunnel lining behaviour, in terms of structural forces, lining displacement, and passive ground pressure along the support profile. The method allows results to be obtained in short calculation times.

An improved numerical approach to the HRM, which was firstly developed using reduction factor, η, on the basis of the model proposed by Oreste [2007], has been presented in this section.

An extensive parametric analysis has made it possible to estimate the segmental tunnel lining behaviour in a large number of cases which cover the conditions that are generally encountered in excavation practice. The influence of three typical types of grounds, that is weak, medium, and strong quality grounds, of two values of lateral earth pressure coefficient K_0, of two values of tunnel depth, of three values of tunnel radius, of three values of tunnel lining thickness, and of four values of reduction factor have been investigated. The results, have presented as design figures, can be used for a preliminary estimation of the structural forces, lining displacement and passive pressure induced in the segmental tunnel lining under the action of external active loads. In order to use these figures for a preliminary segmental tunnel lining design, it is necessary to know the external loads that are applied to the tunnel structure, in terms of vertical load σ_v and lateral earth pressure coefficient K_0. The vertical load should be estimated from back analysis obtained results from convergence measurements made during the construction of a tunnel or could be preliminarily evaluated using Terzaghi's formula. An example in which these figures have been utilized has also been introduced in this study.

A numerical type approach to the HRM method applied to a segmental tunnel lining has also been presented in this section. The influence of segmental joints has been considered directly using a lenghtless rotational spring, which is represented by a fixity ratio that has been determined on the basis of the nonlinear rotational stiffness. A specific implementation has been developed using a FEM framework. This code is able to consider the effect of segmental joints in successive rings on the tunnel lining. The present HRM method allows the arbitrary distribution of segmental joints along the tunnel boundary to be taken into consideration. In addition, the rotational stiffness of the segmental joints has been simulated using nonlinear behaviour, which is closer to the true behaviour of a joint than linear or bilinear behaviour.

In order to estimate the efficiency of the HRM method, the numerical results of the three assumptions on the segmental joints have been compared with numerical results obtained with a simplified 3D numerical model. The results have pointed out that the assumption 1 gives the

structural lining forces and lining displacements which are in better agreement with those of the 3D numerical model than the two others. In addition, the results of a 3D numerical model pointed out that a rigid connection between successive rings is an acceptable assumption.

The numerical results presented in the study show that the proposed HRM method can be used to investigate directly the behaviour of a segmental tunnel lining instead of a 3D numerical modelling. The HRM method allows the results to be obtained in short calculation time.

Third part

Dynamic Analyses of Segmental Tunnel Linings

Introduction

This third part focuses on estimating the behaviour of the tunnel exposed to dynamic loads. Due to the calculation time, the works have been conducted using 2D numerical analyses and Hyperstatic Reaction Method.

A 2D numerical model in which the ovaling deformation of the tunnel cross-section has been adopted to simulate dynamic conditions is developed in **Chapter 7**. This model has been validated by comparing with the analytical results obtained through the well known closed-form solution of Wang (1993). The influence of parameters, that is, the rotational, axial and radial stiffnesses of longitudinal joints, the lateral earth pressure factor, the deformability of the soil and the maximum shear strain, on the tunnel behaviour under seismic loadings is considered in detail. The numerical results allow highlighting the differences of tunnel behaviour under static and seismic loadings.

Full dynamic analysis, which is introduced in **Chapter 8,** is the most complex level of dynamic analysis. Two different ground motions have been applied in the model, which allow highlighting the effect of the joints on the tunnel lining during a seismic event with different maximum amplitude of the input signal.

Finally, **Chapter 9** introduces the new HRM which is developed on the basis of the HRM model presented in **Chapter 6** and taking into consideration the impact of dynamic loads by using quasi-static method. Different from the ovaling deformation which is called the deformation based method presented in **Chapter 7**, the new HRM is developed on the basis of the force based method. Parametric analysis has been conducted, which allow the effects of tunnel dimension, magnitude of seismic event and segmental joints on the tunnel lining to be highlighted.

Chapter 7

Numerical Analyses under Dynamic Loads: Quasi-Static Analysis

7.1. Introduction

In this chapter, a 2D finite difference model of segmental tunnel lining where the distribution of segment joints and their characteristics are taken into consideration is proposed. The joint has been considered as an elastic pin and its stiffness characteristics are influenced by rotational stiffness K_{RO}, axial stiffness K_A, and radial stiffness K_R. The influence of parameters, that is, the rotational, axial and radial stiffnesses of longitudinal joints, the lateral earth pressure factor, the deformability of the soil and the maximum shear strain, on the tunnel behaviour under seismic loadings is considered in detail. The numerical results allow highlighting the differences of tunnel behaviour under static and seismic loadings.

7.2. Numerical modelling of tunnel ovaling

Figure 7-1 shows the 2D numerical model used in the present study, using the finite difference program FLAC^{3D}. It is assumed that the behaviour of the tunnel structure and of the soil mass are linear-elastic. As described in Chapter 4, the tunnel segments are modelled using the embedded liner elements. The segment joint is simulated using double node connections (see **Figure** 4-5). The behaviour of axial springs has been approximately represented by a linear relation, using a constant coefficient spring. The radial stiffness and rotational stiffness of a segment joint have instead been modelled by means of a bi-linear relation that is characterized by a stiffness factor and maximum bearing capacity. The attachment conditions of the translational component in the y direction (parallel to the longitudinal axis of the tunnel) and two rotational components around the x and z directions have been assumed to be rigid for all the investigated cases.
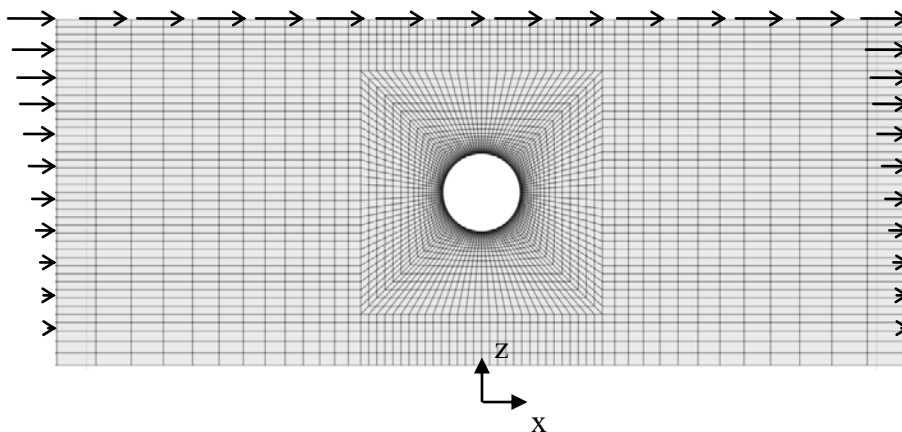
Figure 7-1. Geometry and boundary condition

The FLAC^{3D} model grid contains a single layer of zones in the y-direction, and the dimension of elements increases as one moves away from the tunnel (see **Figure** 7-1). The

Chapter 7: Numerical analyses under dynamic loads: Quasi-static analysis 233

numerical model is 120 m wide in the x-direction, 40 m high in the z-direction and consists of approximately 5,700 zones and 11,800 grid points.

In this study, like the works of Kramer et al. [2007], Kontoe et al. [2008], Sederat et al. [2009], Zurlo [2012] and Naggar and Hinchberger [2012], ovaling deformations due to seismic loading are imposed as inverted triangular displacements along the lateral boundaries of the model and uniform lateral displacements along the top boundary (see **Figure** 7-1). The magnitude of the prescribed displacement at the top of the model is related to the maximum shear strain γ_{max} and to the height of the model. The horizontal base is restraint in all directions It should be noted that the proposed solution ignore seismic (inertial) interaction effect.

Prior to application of ovaling deformation due to seismic loading, it is necessary to establish the steady state of the excavated tunnel under static condition. When tunnelling process is performed in 2D plane strain model, an assumption that takes into account the pre-displacement of the ground surrounding the tunnel boundary prior to the structural elements installation must be adopted. The convergence confinement method has been chosen in the present study using a relaxation factor, λ_d, of 0.3 (Möller & Vermeer [2008]). The numerical modelling of tunnel ovaling has been therefore performed through the following steps:

- Step 1: Establishing the in situ state of stress in the soil prior to tunnel construction.
- Step 2: Deactivating the excavated soil inside the tunnel and applying simultaneously the convergence-confinement process using a relaxation factor, λ_d, of 0.3. After that the concrete lining is actived on the tunnel's periphery. The computation process is stopped when the equilibrium state is reached.
- Step 3: Assigning ovaling deformation due to seismic loading on the model boundaries using prescribed displacements as mentioned above and a new computation process is allowed.

It should be noted that all values presented in the present study are determined by subtracting the lining forces computed at the end of tunnel construction (step 2) from those at the end of ovaling deformation (step 3).

7.3. Validation of the numerical model

Numerical simulations of the circular tunnel ovaling are conducted and compared with the well known closed-form solution of Wang [1993], according to what suggested by Hashash et al. [2005], to validate the numerical model for further studies. The soil and tunnel lining material properties are assumed to be linear elastic and massless (see **Table 7-1**). An anisotropic stress field has been assigned in the model with a lateral earth pressure factor, K_0, of unity. A parameter set has been used that is the case found in the work performed by Hashash et al. [2005]. The prescribed displacements that correspond to a shear strain equal to 0.252 % are applied (Hashash et al. [2005]). The comparative results are presented in **Figure 7-2** and **Table 7-2**.

It can be seen that, when using the same assumptions, the numerical model results in a normal forces and bending moment which are in good agreement with the ones obtained using

the Wang solution (Wang [1993]). The error (20.08 %) is high because the normal force in this full slip condition is numerically small. The difference is about 15.8 kN/m compared to the normal forces of about 62.9 kN/m.

Table 7-1. Parameters used in the validating analysis

Parameters	Unit	Value
Tunnel lining		
Young's modulus E_l	kN/m^2	24,800,000
Poisson's ratio v_l	-	0.2
Moment inertia	m^4/m	0.00225
Area (per unit width)	m^2/m	0.3
Lining thickness	m	0.3
Soil		
Young's modulus E	kN/m^2	312,000
Poisson's ratio v_S	-	0.3

Note: Parameter from Table 2 in Hashash et al. [2005]

Table 7-2. Comparison of analytical solution with numerical analysis

	Wang (1993)		Flac^{3D}		% Difference	
	Full slip	No slip	Full slip	No slip	Full slip	No slip
Maximum normal forces N (kN/m)	62.94 [a]	1045.38 [a]	78.7	1036.8	-20.08	0.83
Maximum bending moment M (kNm/m)	188.81 [a]	-	184.1	156.0	2.55	-

Note: [a] Parameter from Table 3 in Hashash et al. [2005]

7.4. Parametric study

Parameters from the Bologna-Florence high speed railway line tunnel project in Bologna have been adopted (see **Table** 4-1) (Croce [2011]). This case is named the reference case.

The numerical model described in section 7.2 is used. The effect of the gravity field has been taken into consideration. In the reference case, after establishing initial stress conditions, racking deformations corresponding to a soil shear strain equal to 0.5% are applied (Sederat et al. [2009]). All investigated cases are performed using the no slip condition between the soil and the tunnel lining. This process has been adopted in order to consider the worst case for the normal forces.
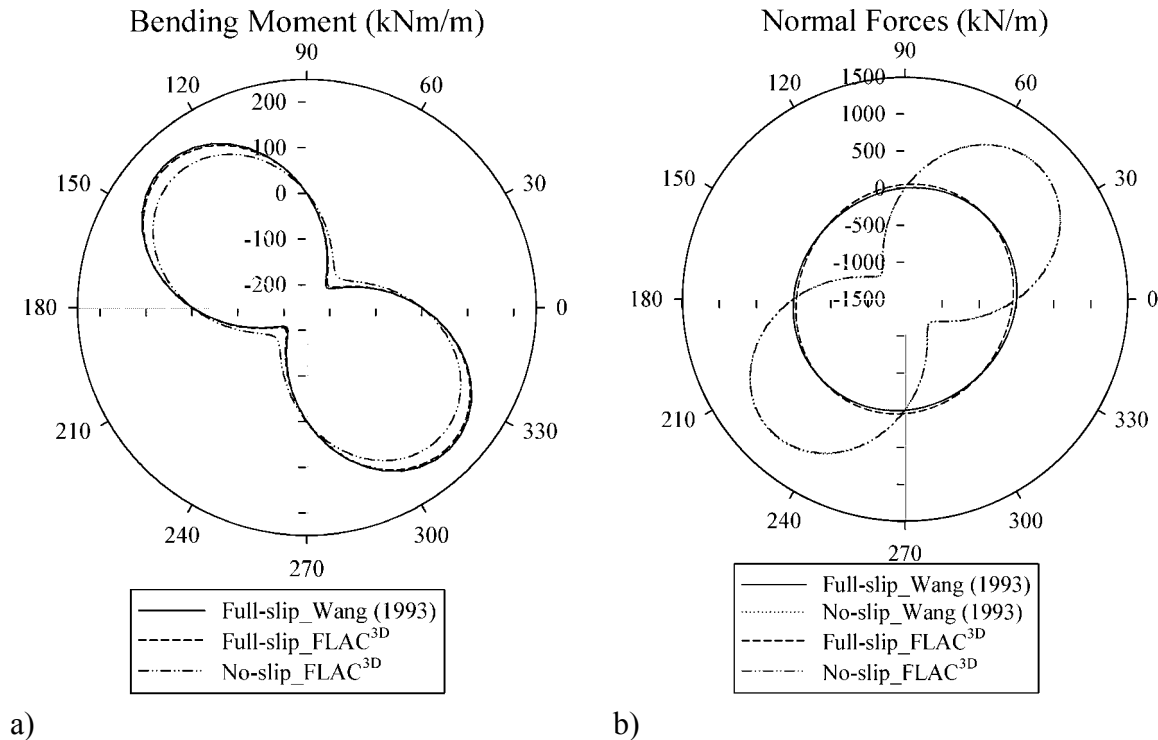
Figure 7-2. Comparison between Wang closed-form solution (see Wang [1993]) and numerical method: a) bending moment, b) normal forces - (refer to Hashash et al. [2005])

7.4.1. Influence of the joint parameters

7.4.1.1 Influence of the joint distribution

As in section 4.1 (also see Do et al. [2013a]), the influence of joint distribution on the behaviour of a segmental lining can be established, considering the change in joint number and joint orientation in a lining ring. The location of the joints in a lining ring is represented by the reference joint that is closest to the tunnel crown, considering the angle "ω" between the reference joint and the crown and measuring it in the clockwise direction starting from the tunnel crown. An ω angle of zero means the reference joint has been positioned at the tunnel crown, while an ω angle of 90° means the reference joint has been located at the right spring line. The joint distribution is assumed to be uniform.

In this section, the influence of the joints has been taken into consideration by means of only the rotational spring. A bi-linear relationship has been adopted for the rotational springs. A discussion on the justification and the influence of considering bi-linear springs on segment joint behaviour can be found in section 4.1 (also see Do et al. [2013a]). The values of the spring constants used to simulate the segment joints have been determined on the basis of the simplified procedures presented by Thienert and Pulsfort [2011] and Do et al. [2013a], using the Janssen's formulas (Janssen [1983]). It should be noted that rotational spring parameters depend on the normal stress induced at joint surface. These forces are different in static and in seismic circumstances. The rotational parameters of the joint have been therefore updated

when the numerical model transform from a static to a seismic circumstance. Accordingly, the maximum limit bending moment, M_{yield}, and the rotational stiffness, K_{RO}, assigned at a joint under static condition are 150 kN.m/m and 98,410 kN.m/rad/m, respectively (Do, et al. [2013]. Their corresponding values applied under seismic circumstance are 700 kN.m/m and 158,800 kN.m/rad/m.

Besides the K_0 value of 0.5 in the reference case, the K_0 values of 1.0 and 2.0 have also been considered. The K_0 values of 0.5 and 1.0 were adopted to represent normally consolidated ground, while K_0 value of 2.0 were adopted for over-consolidated ground.

A comparative study has been performed for the tunnel lining with the joint number varying from 4 to 9, using the parameters from the reference case. The results show the same change in tendency of the bending moment and normal forces due to the variation in the joint distribution when the K_0 values are equal to 0.5, 1, and 2. Only the maximum/minimum bending moment and normal forces, corresponding to different joint orientations for each joint number obtained in the case of a K_0 value of 0.5, are therefore presented hereafter.

The results show an important influence of joint distribution on the bending moment induced in the tunnel lining. **Figure 7-3**a, b and **Figure 7-4**a, b indicate that an increase in joint number would result in a reduction in the absolute magnitude of the maximum and minimum values of both bending moment and normal forces induced in a segmental tunnel lining. Moreover, the difference in the absolute values of maximum and minimum structural forces resulting from the change in joint locations reduces when the joint number increases. This means that the higher the joint number, the lower the influence of the joint orientation. The phenomena are in good agreement with the results obtained under static loading by Hefny and Chua [2006] and that in section 4.1 (also see Do et al. [2013a]) and can be explained by the effect of segment span on the structural lining force. When the joint number is constant, the maximum or minimum values of bending moment and normal forces are affected by the joint location. This indicates that the joint orientation has a significant influence on the structural forces that develops in a segmental lining under seismic loading.

As far as the bending moment is concerned, this dependence can be attributed to the fact that the influence of a joint is less important when it is located near a point where the bending moment is equal to zero. The influence of a joint on the reduction of the bending moment will be higher when the joint is located near a point where the bending moments are maximum (Do, et al. [2013]).

Using the same calculated results presented in **Figure 7-3**a and b, **Figure 7-3**c and d show the effect of the joint orientation on the bending moment in another way. However, a conclusion on the influence of joint orientation as the one obtained from the analyses which were performed under static condition (see section 4.1 and Do et al. [2013a]) is not shown. This indicated that the influence of the joint distribution on the segmental tunnel lining under the seismic and static conditions is not similar. Additionally, the difference could be also attributed to the fact that the soil constitutive model used under static condition (see section 4.1 and Do et al. [2013a]) was assumed to be an elasto-plastic model governed by the Mohr-Coulomb criteria. This is different from a linear elastic model used in the present study.
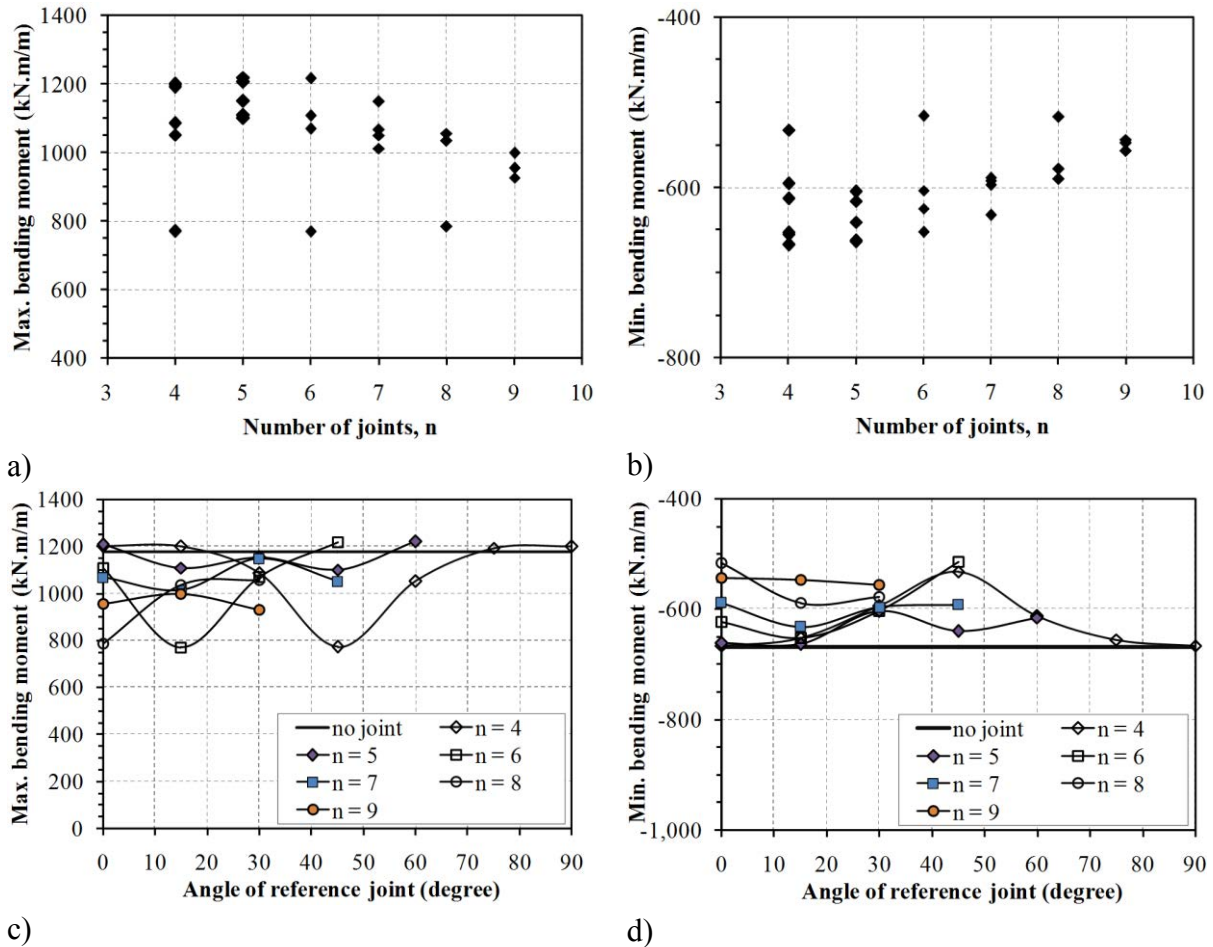
Figure 7-3. The maximum and minimum bending moment vs. joint number and joint orientation, lateral earth pressure factor K_0 equal to 0.5

Figure 7-5 shows an example of the joint orientation effect on the structural forces in a segmental lining, which are determined for a joint number of 6. It can be seen that the bending moments are considerably affected by the joint orientation. Locations of the maximum/minimum bending moment change, depending on the joint orientation. Its effect on the normal force diagrams is instead insignificant. The same observations have been obtained with the other joint number cases.

It is important to note that the bending moment and normal forces induced in a segmental tunnel lining are generally smaller than the corresponding ones induced in a continuous lining (**Figure 7-3** and **Figure 7-4**), except for the minimum normal forces. This means that a segmental lining can perform better than a continuous lining during earthquake. This conclusion is in good agreement with that of Dean et al. [2006], Kaneshiro and Sinha [2008] and Hashash et al. [2001]. The differences are about 33 % and 24 % for the maximum and minimum bending moment, respectively. As for the normal forces, the corresponding values are 4.5 % and 41.7%.
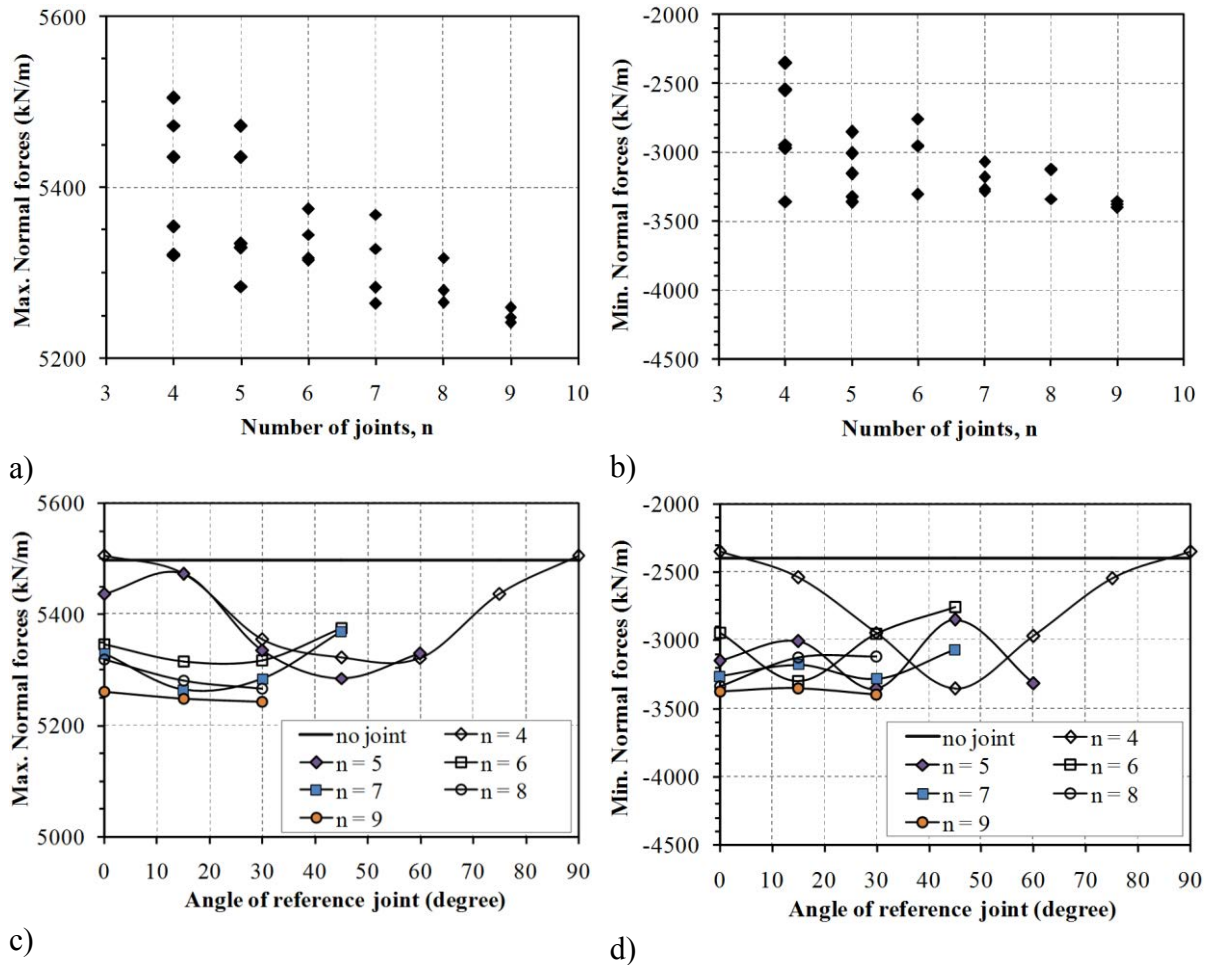
Figure 7-4. The maximum and minimum normal forces vs. joint number and joint orientation, lateral earth pressure factor K_0 equal to 0.5

It should also be noted that absolute values of the maximum/minimum bending moment and normal forces induced in the tunnel lining are not similar. The results are different from those obtained with the analytical methods (e.g. Wang [1993]). In analytical solutions, the absolute magnitudes of the maximum/minimum bending moment and normal forces are always similar. The same observations could be found in the numerical study of Sederat et al. [2009].

7.4.1.2. Effect of joint stiffness

7.4.1.2.1. Influence of rotational stiffness

The dimensionless factor, called the rotational stiffness ratio, $\lambda = K_{RO}l/E_lI_l$, proposed by Lee et al. [2001], is adopted to represent the relative joint stiffness over the lining segment bending stiffness. A calculation length, l, of 1 m is usually taken to present a typical unit lining segment length.

The reference case with a joint number equal to 6 and the reference joint of 45 degrees has

---

Chapter 7: Numerical analyses under dynamic loads: Quasi-static analysis   239

been adopted in this study, which corresponds to the case in which the structural forces induced in the segmental lining is maximum (see **Figure 7-3** and **Figure 7-4**).

a)   b)
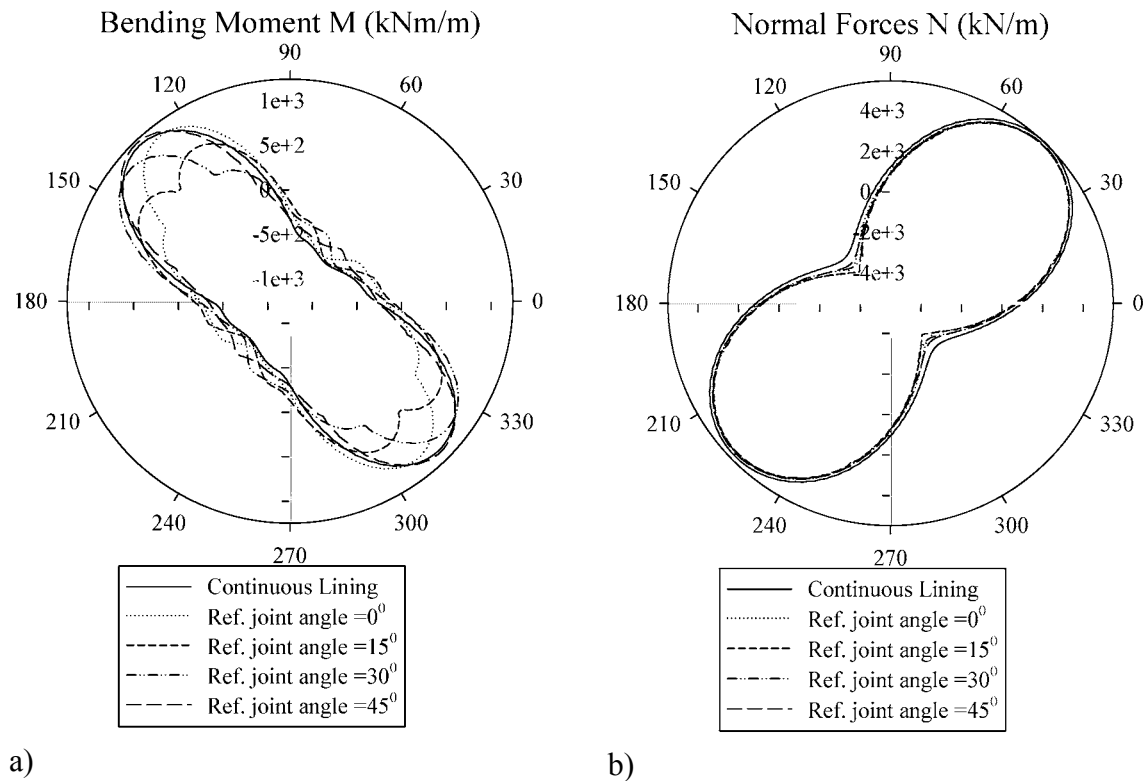
Figure 7-5. Bending moment (a) and normal forces (b) vs. joint orientations, joints number equal to 6, lateral earth pressure factor K_0 equal to 0.5

The bending moment ratio, R_M, and the normal force ratio, R_N, are defined as the ratio of the maximum absolute value of the bending moment and the maximum normal force, respectively, induced in a segmental lining to the corresponding value developed in a continuous lining.

A dependence of the bending moment and normal forces ratios on the rotational stiffness ratio, λ, is indicated in **Figure 7-6**. For a given value of Young's modulus ($E = 500$ MPa), the development of the bending moment is affected by the rotational stiffness ratio, particular in negative bending moment. A higher rotational stiffness ratio results in a higher magnitude of both positive and negative bending moment ratios (**Figure 7-6**a). The results are in good agreement with those obtained under static condition (Do, et al. [2013]). It should be noted that while the negative bending moment ratio is always smaller than unity, the positive bending moment ratio is instead higher than unity.

As far as the normal forces are concerned, **Figure 7-6**b shows an insignificant effect of the rotational stiffness ratio, in particular, when the rotational stiffness ratio is larger than 0.5. However, it is necessary to note that while the positive normal force ratio is approximately equal to unity, the negative normal force ratio is always higher than 1.1. These results are consistent with those introduced in **Figure 7-4**d.

a)   b)
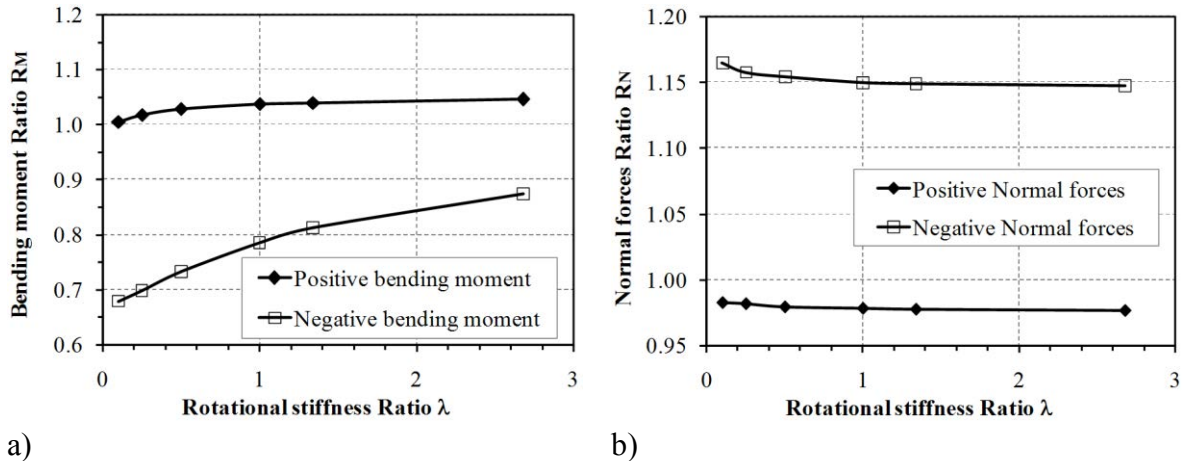
Figure 7-6. The bending moment (a) and normal forces (b) ratio under the influence of the rotational stiffness, joints number equal to 6, lateral earth pressure factor K_0 equal to 0.5

7.4.1.2.2. Influence of axial stiffness

The effect of the axial stiffness (K_A) of a joint has been considered using the reference case (six joints located on the tunnel lining with the reference joint of 45 degrees). The rotational stiffness of a joint is considered. The effect of radial stiffness is neglected. A range of axial stiffness, K_A, is chosen on the basis of experimental results presented by Cavalaro and Aguado [2011]. As in section 4.1 (also see Do et al. [2013a]), it is necessary to know the normal stress that acts on the joint surface in order to determine the K_A value. On the basis of the normal stress, the K_A value can be deduced from the work of Cavalaro and Aguado [2011].

In the present study, $R_{M-axial}$ and $R_{N-axial}$ are defined as the ratio of the absolute magnitude of the maximum/minimum bending moment and normal force, respectively, induced in a segmental lining where a certain axial stiffness of the joint has been assigned, to the corresponding values developed in a segmental lining in which the axial stiffness of the joint goes to infinity. For investigation purposes, the K_A value was chosen over a range from 1,500 MN/m to 15,000 MN/m. **Figure 7-7** indicates that the ratios of the bending moment and the normal force are highly affected by the axial stiffness, particular in the ratios of the negative bending moment and negative normal forces. These results are different from those obtained in the numerical analyses performed under static condition (see section 4.1 and Do et al. [2013a]). This means that the influence of the axial stiffness needs to be considered under seismic loading.
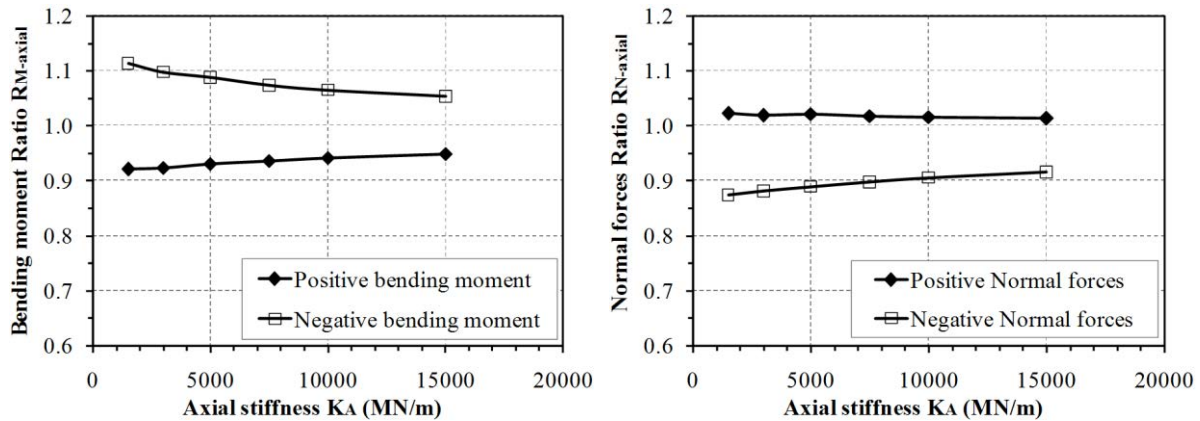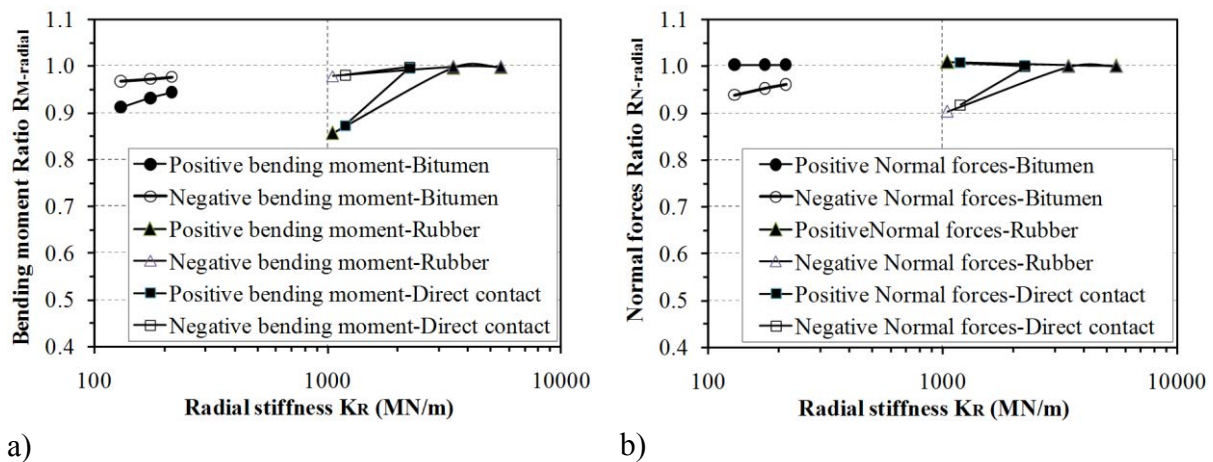
Figure 7-7. The bending moment (a) and normal forces (b) ratio under the influence of the axial stiffness, joints number equal to 6, lateral earth pressure factor K_0 equal to 0.5

7.4.1.2.3. Influence of radial stiffness

The effect of the radial stiffness (K_R) of a joint has been investigated using the reference case (six joints located on the tunnel lining with the reference joint of 45 degrees). In order to quantify the effect of the radial stiffness of joint, K_R, on the behaviour of a segmental tunnel lining, the experimental results presented by (Cavalaro & Aguado [2011]) were adopted and three main materials used for segment joints were considered: packers made of plastic (rubber), packers made of bitumen and contact without packers (direct contact between the concrete surfaces). The rotational stiffness of a joint is considered. The effect of axial stiffness is neglected. **Table** 4-2 presents parameters used in this study (Do, et al. [2013]). It should be noted that the radial stiffness depends on the normal stress that acts on the joint surface. This means that parameters corresponding to the normal stresses of 1.5 and 4 MPa are not consistent with the reference case in this study, in which the normal stress is determined about 15 MPa as mentioned earlier. However, for investigation purposes, all parameters in **Table** 4-2 are still used in this study.

Figure 7-8 shows the results of the bending moment ratio, R_{M_radial} and the normal force ratio, R_{N_radial} defined as the ratio of the absolute magnitude of the maximum/minimum bending moment and normal force, respectively, which are induced in a segmental lining, to the corresponding ones developed in a tunnel lining with an infinite radial stiffness of the joints.

The bending moment ratio generally approaches unity when the joint radial stiffness increases (**Figure 7-8**). As expected, the lower the radial stiffness (K_R) and the maximum shear stress (τ_{yield}), the lower the bending moment and normal force ratios. The absolute values of the maximum/minimum bending moment and normal forces induced in a segmental lining with a finite radial stiffness of the joints are usually lower than those developed in a tunnel lining with an infinite radial stiffness. This means that the bending moment ratio, R_{M_radial}, and the normal force ratio, R_{N_radial}, are smaller than unity. It is possible to conclude that the radial stiffness assigned to the segment joint has a negligible effect on the segmental lining behaviour.

a)   b)

Figure 7-8. The bending moment (a) and normal forces (b) ratio under the influence of the radial stiffness, joints number equal to 6, lateral earth pressure factor K_0 equal to 0.5

It is necessary to note that the influence of the radial stiffness on the positive bending moment ratio is greater than that of the negative bending moment. On the contrary, as far as normal force is concerned, its effect on the negative normal forces is larger than that of the positive normal forces. Moreover, the tunnel lining behaviour under seismic condition is more affected than in static condition that was introduced in section 4.1 (also see Do et al. [2013a]).

7.4.2. Influence of the geotechnical parameters of the ground mass

7.4.2.1. Effect of the lateral earth pressure factor

The effect of the lateral earth pressure factor, K_0, on segmental tunnel lining behaviour is studied in this section. Other parameters based on the reference case have been assumed (**Table** 4-1). The effects of the joint axial and radial stiffness are neglected. For each case of joint number and lateral earth pressure factor, all joint orientation cases are investigated.

Figure 7-9a and b shows that the highest maximum bending moment induced in the segmental lining are considerably affected by the joint number and the lateral earth pressure factor. Generally, the higher the lateral earth pressure factor, K_0, the lower the maximum bending moment (**Figure 7-9**a). On the other hand, the minimum bending moments are not affected to any extent by the K_0 values (**Figure 7-9**b). These results are different from those obtained in the analyses performed under static loading (see section 4.1 or Do et al. [2013a]). Their results indicated that the maximum bending moment, induced under static condition, in case of K_0 value of unity is considerably smaller than those of the other K_0 values. It should be noted that the influence of the lateral earth pressure factor, K_0, could not be observed when analytical methods (e.g. Wang [1993]) are used.

When the joint number is smaller than 6, the maximum bending moments are quite similar for a given K_0 value. However, as for a larger joint number, **Figure 7-9**a shows a

Chapter 7: Numerical analyses under dynamic loads: Quasi-static analysis   243

significant dependence of the maximum bending moment on the joint number. This dependence is approximately linear. The same conclusion can be adopted for the minimum bending moment (**Figure 7-9**b).

a)   b)

c)   d)
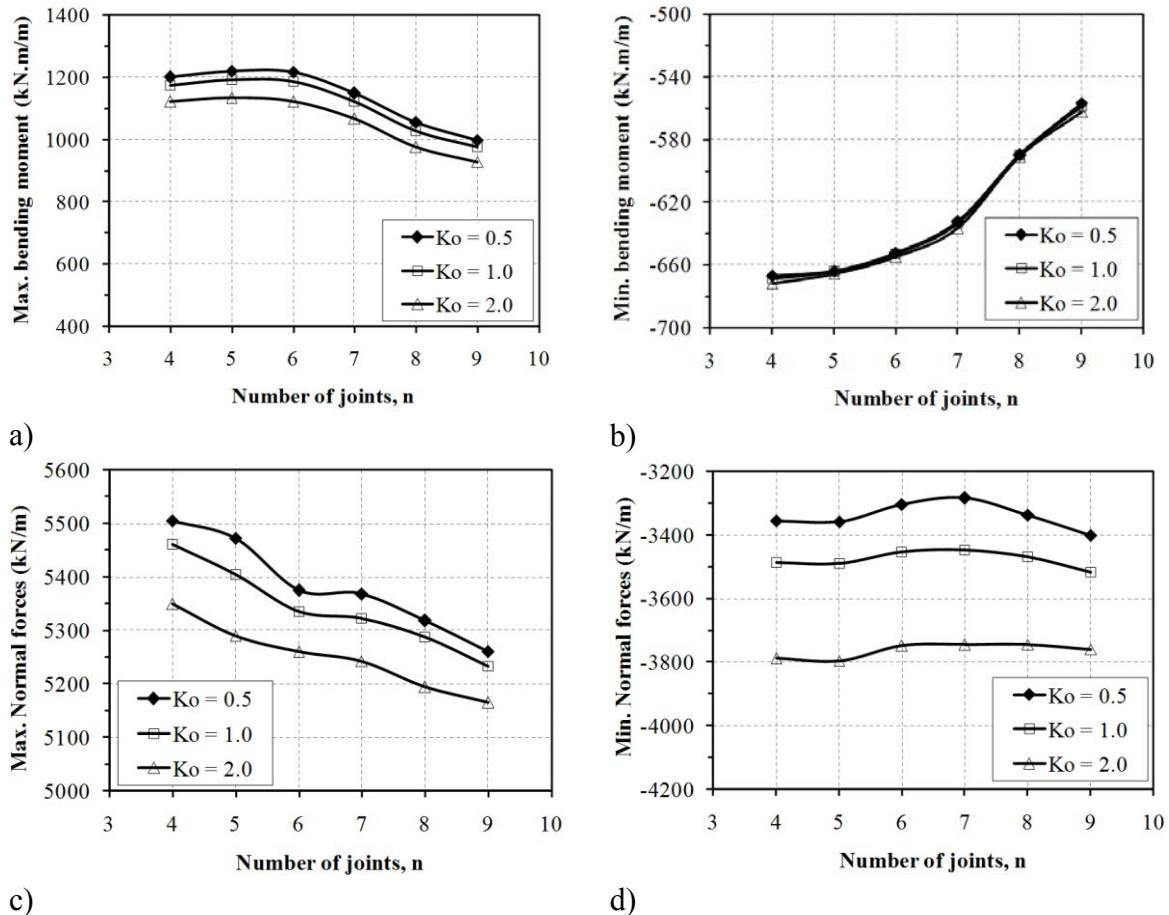
Figure 7-9. The maximum/minimum bending moment and normal forces vs. joint numbers and lateral earth pressure factors, joints number equal to 6

As far as the normal forces are concerned, a high effect of the lateral earth pressure factor and joint number is indicated in **Figure 7-9**c and d. Generally, the higher the lateral earth pressure factor, the lower the maximum and minimum normal forces. These results are contrary to those obtained under static condition introduced in section 4.1 (also see the work of the same authors (Do et al. [2013a]). Under static condition, the higher the lateral earth pressure factor, the higher the maximum normal forces. In addition, the influence of the lateral earth pressure factor on the maximum normal force obtained in the present study is also different from the numerical results which were performed under the same seismic condition by Sederat et al. [2009]. In study of Sederat et al. [2009], two K_0 values of 0.5 and 1.0 were considered. They showed that the larger the K_0 value, the higher the maximum normal forces. The difference could be attributed to the influence of the contact condition between the lining and the soil. In the present study, the no slip condition has been adopted. However, a frictional contact interface was used in study of Sederat et al. [2009].

It should be noted that, for the same K_0 value, while the minimum normal forces are quite

similar, the reduction in the magnitude of the maximum normal forces developed in the segmental lining is approximately linear when the joint number increases.

7.4.2.2. Effect of ground deformability

The change in structural forces has been investigated over a Young's ground modulus range that varies from 250 MPa to 1,500 MPa, which corresponds to a range of ground condition from the soft soils to the soft rocks under the impact of seismic loading, in order to study the effect of ground deformability surrounding the tunnel. The shear strains that cause the tunnel ovaling deformation change over a range from 0.01 to 1 % (Sederat et al. [2009]). Other parameters are assumed considering the reference case (**Table** 4-1) and six joints located on the tunnel lining with the reference joint of 45 degrees. The axial and radial stiffness effects are neglected.

a)   b)

c)   d)
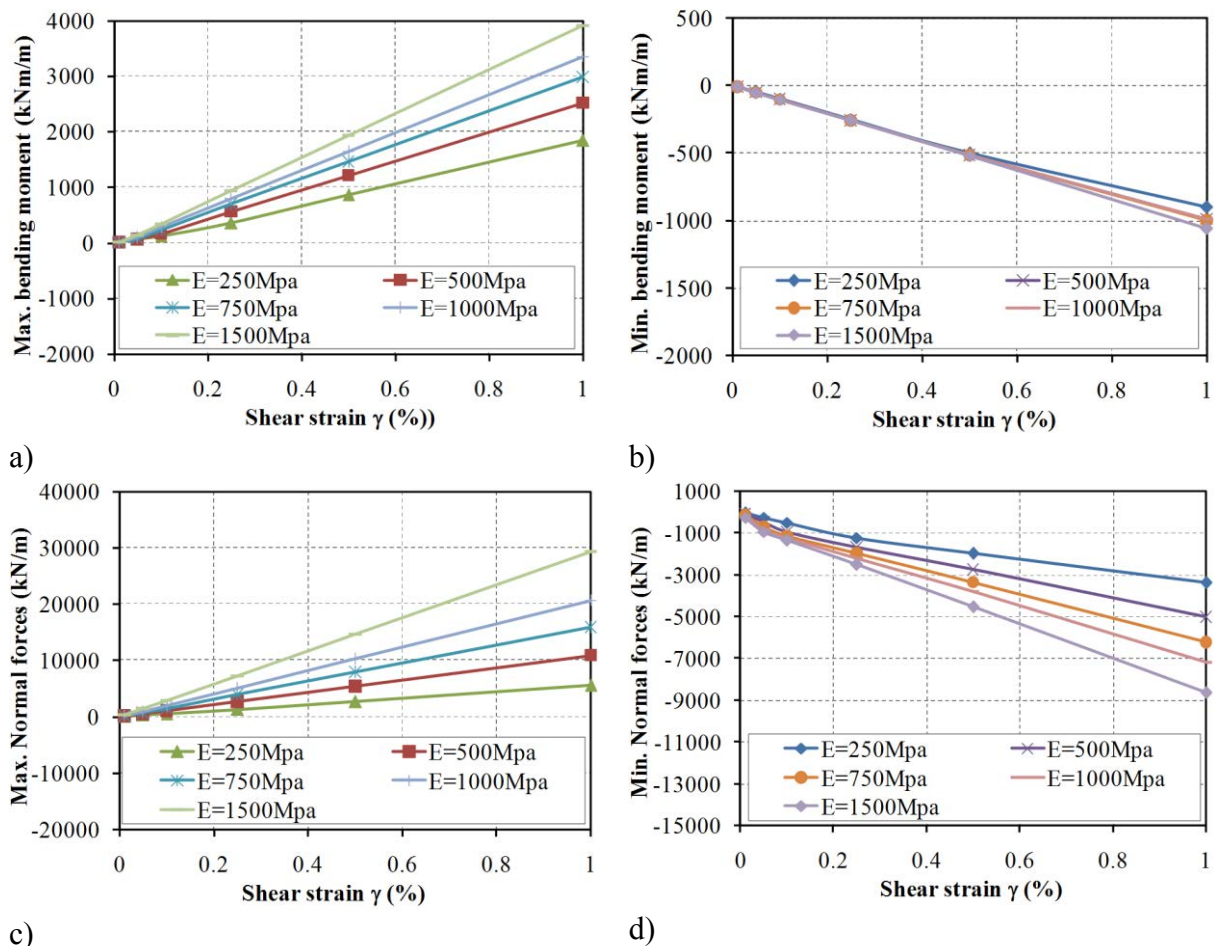
Figure 7-10. The maximum/minimum bending moment and normal forces vs. Young's modulus of the soil and shear strain, joints number equal to 6

The development of the bending moment and normal forces are highly affected by Young's modulus of the ground surrounding the tunnel and the shear strain, γ. For each given values of Young's modulus of the soil, *E*, a higher shear strain value, γ, results in a higher

maximum bending moment (**Figure 7-10**a) and a lower minimum bending moment (**Figure 7-10**b). The dependences of the maximum/minimum bending moment on the shear strain, γ, are quite linear, which can be displayed by an equation $y = ax$. As far as the maximum bending moment is concerned, the higher Young's modulus of the soil, E, the higher a parameter. However, a parameter is quite similar for all E values. The same observations are obtained as far as the normal forces are concerned (**Figure 7-10**c and d). In other words, when the E values increase, the structural forces induced in a tunnel lining are more sensitive to the change in shear strain, γ.

a)

b)

c)

d)
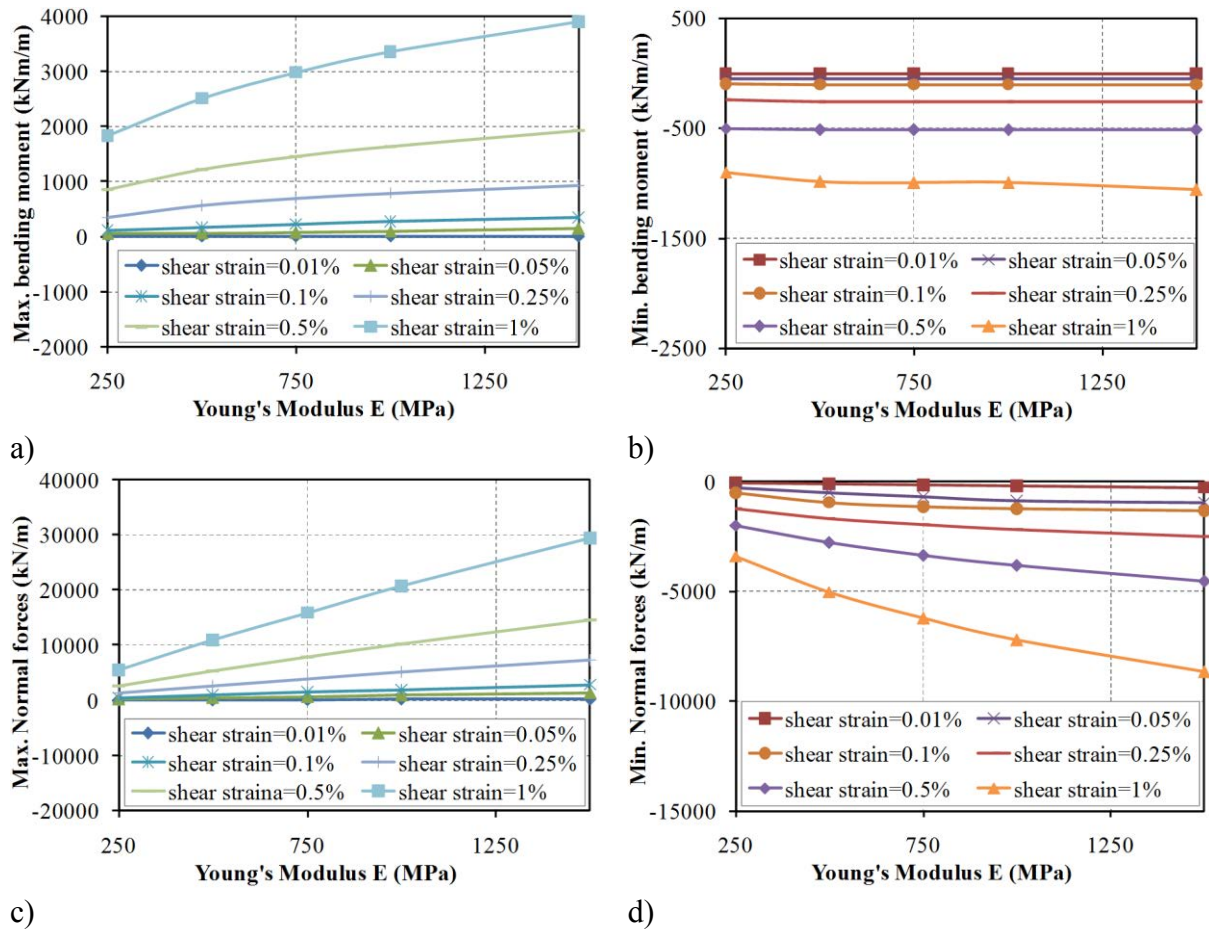
Figure 7-11. The maximum/minimum bending moment and normal forces vs. Young's modulus of the soil and shear strain, joints number equal to 6

Using the same data, **Figure 7-11** is introduced in order to show in a clearer way the influence of Young's modulus of the soil on the segmental lining. For each given shear strain, γ, which is quite small (i.e. γ = 0.01; 0.05 and 0.1 %), the influence of E values on the tunnel lining behaviour is insignificant. However, when the shear strain, γ, is larger, both the bending moment and normal forces induced in the tunnel lining are affected by Young's modulus of the soil. This influence can be displayed by a linear relationship. For each given shear strain, the higher the E values, the larger the maximum bending moment and normal forces and the lower the minimum normal forces (**Figure 7-11**a, b, c). This could be attributed to the higher reaction forces originated from the surrounding ground which act on the tunnel lining when

Chapter 7: Numerical analyses under dynamic loads: Quasi-static analysis   246

the E values increase. On the other hand, the effect of the E values on the minimum bending moment can be ignored (**Figure 7-11**b).

Besides Young's modulus, E, and lateral earth pressure factor, K_0, the influence of Poisson's ratio, ν_S, of the soil on the tunnel lining has also been investigated. The Poisson's ratio is assumed to be on the range from 0.25 to 0.45. The other parameters of the reference case have been adopted. An insignificant influence of Poisson's ratio on the structural lining forces is however observed. The results are therefore not presented in this study.

7.5. Conclusions

A 2D numerical study has been used to investigate the factors that affect the behaviour of segmental tunnel linings under seismic conditions. The influences of the joint distribution, joint stiffness (including the rotational stiffness, the axial stiffness and the radial stiffness assigned at the joints), the ground conditions, that is, Young's modulus and lateral earth pressure factor, and the seismic racking loads represented by the maximum shear strain, have been studied in detail.

The results pointed out that the influence of the joint distribution on the segmental tunnel lining under the seismic and static conditions is not similar. The same change in tendency of the bending moment due to the variation in the joint distribution when the K_0 values are equal to 0.5, 1, and 2 has been obtained. An increase in joint number would generally result in a reduction in the absolute magnitude of the maximum/minimum values of both bending moment and normal forces induced in a segmental tunnel lining. In addition, the higher the joint number, the lower the influence of the joint orientation. The bending moment and normal forces induced in a segmental tunnel lining are generally smaller than the corresponding ones induced in a continuous lining, except for the minimum normal forces. This means that a segmental lining can perform better than a continuous lining during earthquake.

The development of the bending moment is affected by the rotational stiffness ratio, particular in negative bending moment. A higher rotational stiffness ratio results in a higher magnitude of both positive and negative bending moment ratios. As far as the normal forces are concerned, the results has shown an insignificant effect of rotational stiffness ratio, especially when the rotational stiffness ratio is larger than 0.5.

The bending moment and the normal force are highly affected by the axial stiffness, especially the negative bending moment and negative normal forces. On the other hand, under an actual normal stress of about 15 MPa which acts on the joint surface, the radial stiffness assigned to the segment joint has a negligible effect on the segmental lining behaviour.

The tunnel lining behaviour under the effect of lateral earth pressure factor, K_0, are different from that obtained under static loading. The higher the lateral earth pressure factor, K_0, the lower the maximum bending moment and the maximum/minimum normal forces.

Under seismic loading, the development of the bending moment and normal forces are affected by the change in Young's modulus of the soil and shear strain. For each given values of Young's modulus, E, the dependences of maximum/minimum bending moment on the

shear strain, γ, are quite linear. When the E values increase, the structural forces induced in a tunnel lining are more sensitive to the change in shear strain. For each given of shear strain, γ, which is quite small (i.e. γ = 0.01; 0.05 and 0.1 %), the influence of E values on the tunnel lining behaviour is insignificant. However, when the shear strain, γ, is larger, both the bending moment and normal forces induced in the tunnel lining are affected to a great extent by Young's modulus of the soil. This influence can be displayed by a linear relationship.

Chapter 8

Numerical Analyses under Dynamic Loads: Full Dynamic Analysis

8.1. Introduction

While tunnels generally perform better than above ground structures during earthquakes, the damage to some important structures during earthquake events has highlighted the need to account for seismic load in the design of underground structures (Park and Yareevand [2005]).

A 2D finite difference model of a segmental tunnel lining exposed to a full seismic excitation in which the segment joints are taken into consideration has been proposed in this chapter. The joint has been considered as an elastic pin and its stiffness characteristics have been specified by rotational stiffness K_{RO}, axial stiffness K_A, and radial stiffness K_R. The numerical results allow the differences in tunnel behaviour under seismic excitation due to the effect of the segmental joints and of the soil constitutive model to be highlighted. Additionally, significant differences in structural lining forces when quasi-static solutions and a full dynamic analysis have been used have also been introduced.
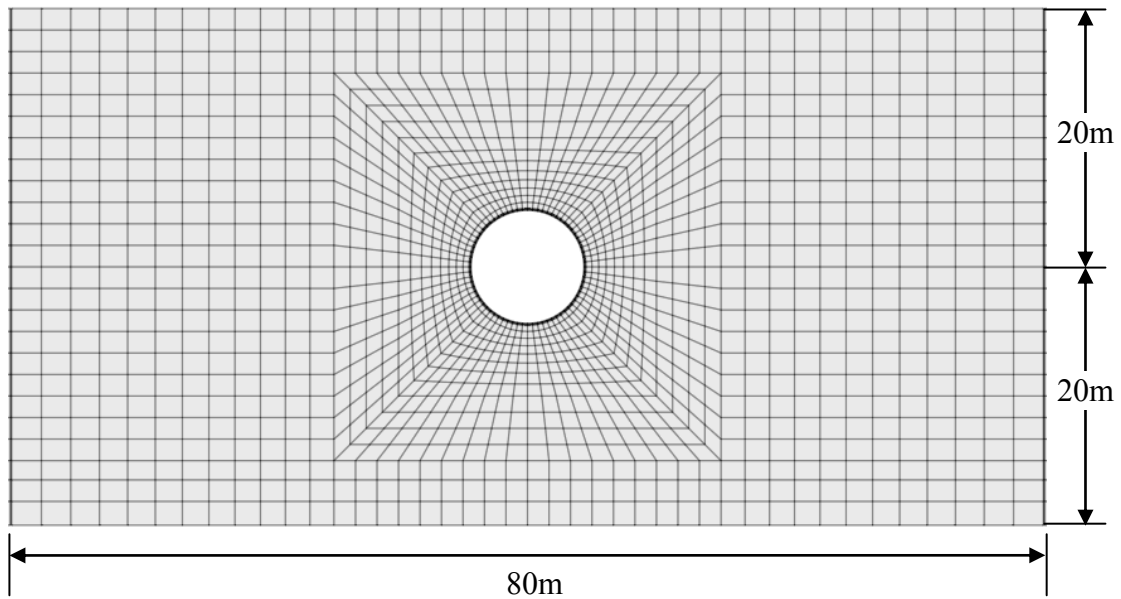
8.2. Numerical modelling

8.2.1. Ground parameters

Parameters from the Bologna-Florence high-speed railway line tunnel project in Bologna have been adopted (see **Table** 4-1). This case is named the reference case.

8.2.2. Numerical model description

Figure 8-1 illustrates the 2D plane-strain numerical model which has been set up using the finite difference software FLAC^{3D}. It has been assumed that the behaviour of the tunnel structure is linear-elastic. In order to highlight the effect of the soil constitutive model, the behaviour of the soil has been assumed to be linear-elastic and elastic perfectly plastic. The later constitutive model of the soil is based on the Mohr-Coulomb failure criterion. The effect of the gravity field has also been taken into consideration.

Like the 2D model described in section 4.1.3, the volume under study is discretized into hexahedral zones. The tunnel lining is modelled using embedded liner elements. No relative movement (no-slip) was allowed at the tunnel lining-soil interface. The segment joint is simulated using double nodes.

In this study, the stiffness characteristics of the joint connection are represented by a set composed of a rotational spring (K_{RO}), an axial spring (K_A) and a radial spring (K_R), as presetned in section 4.1.3.

Chapter 8: Numerical analyses under dynamic loads: Full dynamic analysis   251

Figure 8-1. Plane strain model under consideration

In the seismic analysis, the width of the model plays an important role in ensuring the development of the free-field deformation far away from the tunnel. A sensitivity study found that the soil-tunnel structure interaction region may be extended up to three diameters from the tunnel center (Gomes [2000]). In this analysis, the lateral boundaries of the mesh were placed approximately 4.5 diameters from the tunnel center. The FLAC^{3D} model grid contains a single layer of zones in the y-direction, and the dimension of elements increases as one moves away from the tunnel (see **Figure** 8-1). The numerical model is 80 m wide in the x-direction, 40 m high in the z-direction and consists of approximately 2070 zones and 4280 grid points.

During the static analysis, the nodes were fixed in the directions perpendicular to the x-z and the y-z planes (i.e. y = 0, y = 1, x = -40 and x = 40), while the nodes at the base of the model (z = -20) were fixed in both the horizontal (x) and vertical (z) directions. During the dynamic stage, the nodes along the base of the model were freed in the horizontal direction in order to apply seismic input motion.

The seismic signal from the Nice earthquake case has been adopted in the study. This accelerogram is representative of the French design spectrum (Grange [2008]). It has a maximum acceleration of 0.35g. The spectrum of the corresponding Fourier amplitude is shown in **Figure 8-3**. Moreover, a lower signal (maximum acceleration of 0.0035g) has also been used. The acceleration time histories of a 21 seconds duration are presented in **Figure 8-2**. These records were integrated to provide velocity histories which were then applied in the horizontal direction to all the nodes along the bottom boundary of the model.

The dynamic simulations were performed using Rayleigh damping. The center frequency for Rayleigh damping is 1.99 Hz, which was determined from an undamped analysis. The Rayleigh damping ratios of the soil and of the tunnel lining were fixed at 5 % and 2 %, respectively. In order to simulate a semi-infinite elastic space, quiet boundaries are placed at the borders of the model in order to avoid wave reflection. Since a dynamic source is applied

as a boundary condition at the bottom of the model, a free filed boundary was applied at the sides of the model (Itasca [2009]). In order to accurately represent wave transmission through the model mesh, it is necessary to ensure that the size of the element is small compared to the transmitted wavelength. Therefore, the side length of the element (Δl) was chosen accordingly on the basis of the recommendation by Kuhlemeyer and Lysmer [1973]:

$$\Delta l \leq \frac{V_{S,\min}}{10 f_{\max}} \qquad (8\text{-}1)$$

where $V_{s,min}$ is the lowest shear wave velocity that is of interest in the simulation, and f_{max} is the highest frequency of the input wave.

As far as the higher signal is concerned, the Fourier amplitude of the uncorrected Nice record indicates that the highest frequency f_{max} is less than 5 Hz (**Figure 8-3**). The Fourier spectrum obtained in the case in which a low signal was used indicated the same highest frequency. All the parameters of the FLAC^{3D} model applied in the case in which a low signal was used were therefore similar to those applied in the case of a high signal.

a) Low acceleration time history   b) High acceleration time history
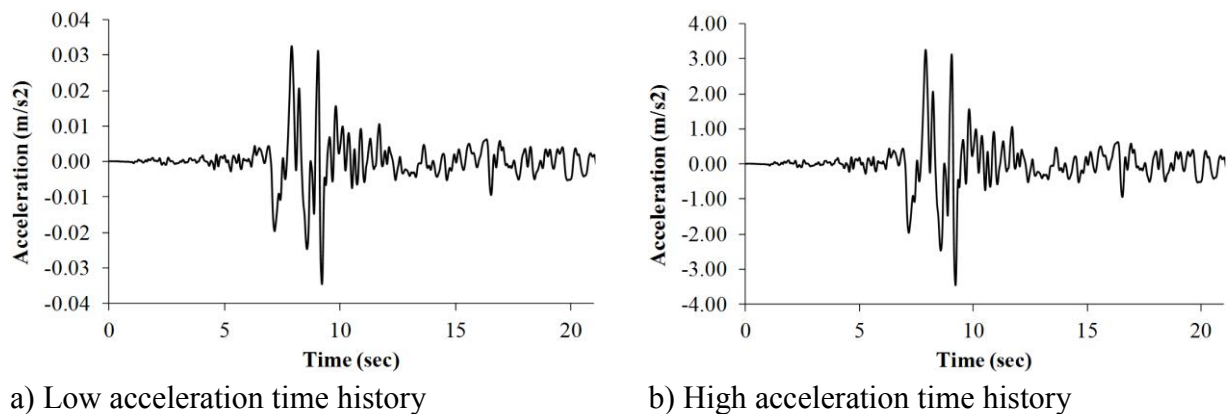
Figure 8-2. Seismic input signals
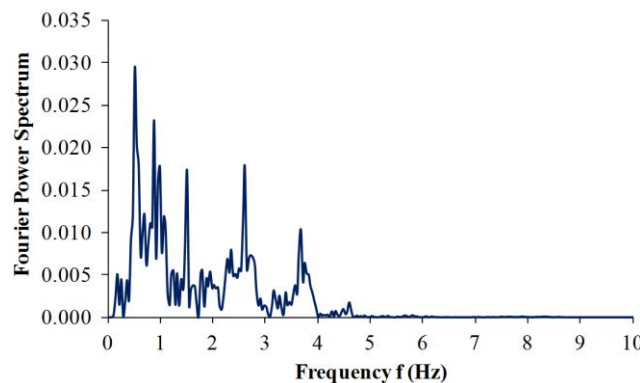
Figure 8-3. Input acceleration power spectrum (e.g., high signal case)

8.2.3. Construction simulation

Prior to the application of the seismic load, it is necessary to establish the steady state of the excavated tunnel under static condition. When a tunnelling process is performed in a 2D plane strain model, an assumption that takes into account the pre-displacement of the ground surrounding the tunnel boundary prior to installation of the structural elements must be adopted. The convergence confinement method has been chosen in the present study with a relaxation factor, λ_d, of 0.3. The numerical modelling of tunnel ovaling was performed through the following steps:

- *Step 1*: Establishing the in situ state of stress in the soil prior to tunnel construction.
- *Step 2*: Deactivating the excavated soil inside the tunnel and simultaneously applying the convergence-confinement process using a relaxation factor, λ_d, of 0.3. The concrete lining is then actived on the tunnel periphery. The computation process is stopped when the equilibrium state is reached.
- *Step 3*: Assigning a seismic load to the bottom of the model thus allowing a new computation process to be made.

It should be noted that all the values presented in the present study are determined by subtracting the lining forces computed at the end of tunnel construction (step 2) from those at the end of the seismic load (step 3). In addition, all the calculations were performed under drained conditions.

It is important to mention that the average time necessary for the calculations with a continuous lining and a segmental lining is approximately 30 days and 40 days, respectively, when a 2.67GHz core i7 CPU ram 24Go computer is used.

8.3. Numerical analyses

### 8.3.1. Behaviour of a tunnel under a low seismic load

This section highlights the effect of segmental joints and a soil constitutive model on the lining behaviour of a tunnel under low seismic excitation.

The obtained numerical results have pointed out an insignificant influence of the soil constitutive model on the maximum absolute bending moment change developed in a tunnel lining during seismic loads. When the seismic loading is low, only a few of plastic zones occurs in the soil mass. It can be seen that the largest variation in structural lining forces occurs between 7 and 11 s approximately, which corresponds to the most intense part of the seismic excitation (see **Figure 8-4**, for example).

In order to highlight the effect of the joints, **Figure 8-4** compares the maximum absolute bending moment change induced in a continuous lining and a segmental lining in the elastic case. During seismic excitation, the change in the maximum absolute bending moment induced in a segmental lining is larger than that induced in a continuous lining when the acceleration of the input motion is small. However, a reverse phenomenon is observed when the acceleration of the input is increased (see **Figure 8-4**b).

As far as the influence of the constitutive model is concerned, the changes in the maximum absolute bending moment induced in segmental and continuous linings when elastic and elastic-perfectly plastic models are used are not similar. In the case in which a continuous lining is used, the obtained value with Mohr-Coulomb is approximately 2 % smaller than the one with the elastic soil constitutive model. On the other hand, in the case in which a segmental lining is used, Mohr-Coulomb gives a value which is 15 % larger than the elastic one (**Table 8-1**).
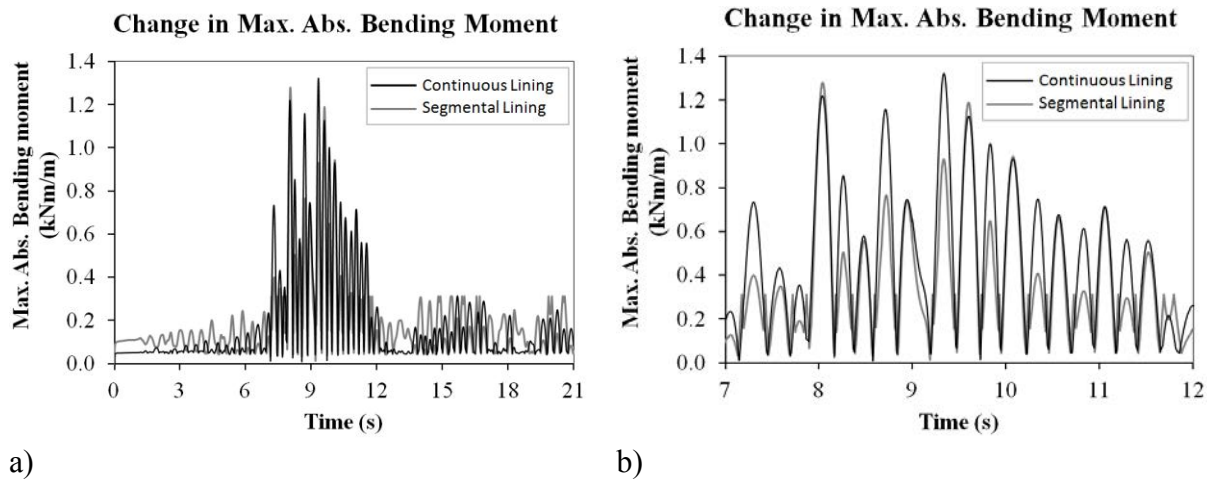
Figure 8-4. Change in maximum absolute bending moment during 21 seconds (a) and during the most intense part of seismic excitation (b) - Influence of segmental joints when an elastic constitutive model is used

It can be seen that the joints have a negligible effect on the change in the maximum normal forces induced in a continuous lining and in a segmental lining in the case in which an elastic soil model is used (**Table 8-1**). The same conclusion is obtained when the Mohr-Coulomb soil model is used. As far as the influence of the constitutive model on the change in maximum normal forces is concerned, both continuous and segmental linings show a difference of about 10 % (**Table 8-1**).

Table 8-1. Maximum changes in structural forces, lining deformation and surface settlement (low signal case)

	Elastic model		*Mohr-Coulomb model*	
	Cont. lining	Seg. lining	Cont. lining	Seg. lining
Change in max. absolute M (kNm/m)	1.32	1.28	1.30	1.47
Change in max. N (kN/m)	5.55	5.49	5.14	4.91
Change in max. Normal Disp (mm)	0.500	0.527	0.499	0.532
Change in max. Settlement (mm)	0.038	0.020	0.043	0.038

As can be seen in **Figure** 8-5 and **Table** 8-1, the maximum value of the change in the maximum normal displacement induced in a segmental lining is approximately 5 % higher than that of a continuous lining for the two constitutive models. It is interesting to note that, during seismic excitation, when the acceleration of the input motion is large enough, the

change in maximum normal displacement induced in a segmental lining is usually larger than that of a continuous lining. However, an opposite effect is observed at low accelerations of the input motion. This could be explained by the fact that the movement of the tunnel lining under seismic loading is absorbed by the segmental joints. Nevertheless, when acceleration of the input motion is large enough, the effect of the deformation absorbability of the joint on the overall deformation of the lining is negligible.
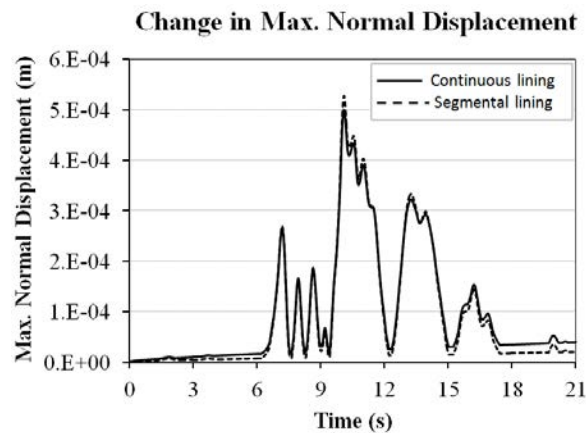
Figure 8-5. Change in normal displacement - Influence of segmental joints when an elastic soil constitutive model is used

As far as surface settlement during seismic excitation is concerned, the results indicate that the change in surface settlement when a segmental lining is used is less sensitive to seismic loads than that of a continuous lining. Similarly, a less sensitive surface settlement to seismic loads when the elastic soil model is applied compared to that of the Mohr-Coulomb model can also be observed. The change in surface settlement when the Mohr-Coulomb model is used is greater than that of the elastic model. However, the absolute differences are negligible. It should be mentioned that a positive value of the change in surface settlement corresponds to heave of the soil.

8.3.2. Behaviour of a tunnel under a high seismic load

This section highlights the effect of segmental joints and a soil constitutive model on the lining behaviour of a tunnel under high seismic excitation.

In contrast to the results obtained when the low seismic signal presented in the above section was used, **Figure 8-6**b shows a significant effect of the soil constitutive model on the change in maximum absolute bending moment developed in a tunnel lining. The changes in maximum bending absolute moment in the case in which the Mohr-Coulomb model is used are usually higher than those determined when elastic material is used and reach a maximum differences of about 250 % in a segmental lining (**Table 8-2**). The same phenomena were observed in the numerical work of Sliteen [2013] and Sliteen et al. [2013]. However, the present results appear to be in contrast those obtained by Shahrour et al. [2010], who showed an important decrease of about 50% in the seismic-induced bending moment in a tunnel when

a soil constitutive model, which took into consideration plastic deformations, was used. It should be noted that an elastic-perfectly plastic constitutive model with a Mohr-Coulomb failure criterion has been used in the present study and in the work of Sliteen [2013] and Sliteen et al. [2013]. Nevertheless, Shahrour et al. [2010] used an advanced cyclic elastoplastic model, Modsol (Khosnoudian and Sharour [2002]), which is based on the bounding surface concept. Another reason for the discrepancy could be the effect of the soil type, as found in the work by Amorosi and Boldini [2009]. While medium Nevada sand was used in the study by Shahrour et al. [2010], clayey sand has been used in the present study. It should also be noted that the accumulation of plastic strain during seismic loading could result in difference in the locations on the tunnel structure at which the induced-maximum bending moment is observed when Mohr-Coulomb and elastic models are used.
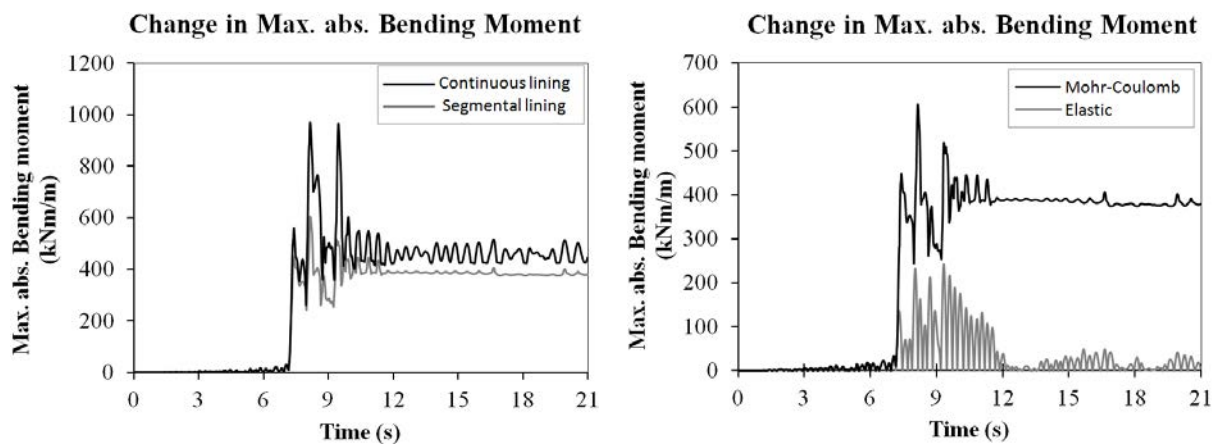
a) Influence of segmental joints when the Mohr-Coulomb constitutive model is used

b) Influence of the soil constitutive model when a segmental lining is used

Figure 8-6. Change in the maximum absolute bending moment

It is interesting to note that although the residual bending moment is almost zero in the case in which elastic soil constitutive model is used, significant residual maximum absolute bending moment of about 58 %, compared to the maximum value, can be observed 21 seconds after the end of the seismic load when the Mohr-Coulomb constitutive model is used. The residual bending moment is due to irreversible deformations cumulated by the soil during seismic excitation. This statement can be also confirmed by considering the residual normal displacement of the tunnel lining presented in **Figure 8-8**b. It should be mentioned that these residual bending moments are not so obvious when a low seismic signal is used.
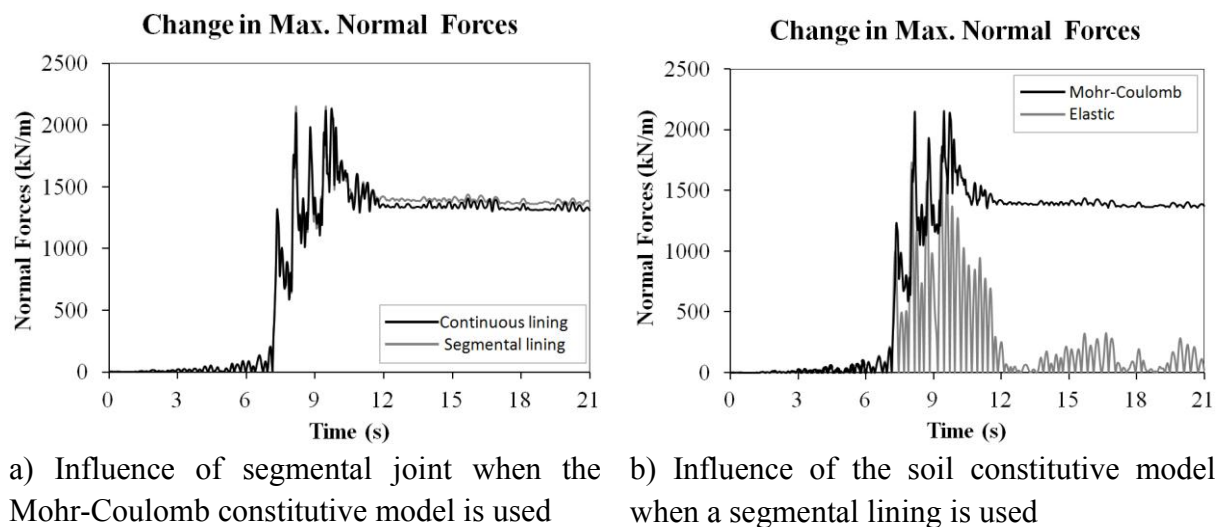
It is reasonable to conclude, on the basis of above analysis, that the effect of the soil constitutive model on the tunnel behaviour depends on the amplitude of the seismic excitation. In addition, the irreversible soil behaviour significantly modifies the tunnel loads both during the seismic excitation and, more importantly, after it. This finding is consistent with what was observed by Amorosi and Boldini [2009].

Besides the soil constitutive model, the numerical results also introduce a significant influence of the segmental joints on the tunnel lining behaviour during seismic loading. Like the phenomena observed and explained in the case in which the low seismic signal presented in the above section is used, important decreases in the changes of the maximum absolute

bending moment induced in a segmental lining, compared to the corresponding ones of a continuous lining, can be seen (see **Figure 8-6**a). The maximum differences in the changes in maximum absolute bending moment are 160 %. The same result was found in the analytical analyses by Naggar et al. [2008]. It is necessary to note that segmental joints perform like yield joints in a concrete lining during the impact of high seismic loads and the concrete segments continue to behave like elastic material. This means that the elastic material assumption applied to the concrete lining can be considered for segmental linings. However, the assumption of elastic material for a continuous lining does not lead to the appearance of yield joints in the lining structure. Consequently, adopting elasticity in a constitutive model for a continuous lining is not realistic. This assumption is too simple and it also represents a limitation of the present study.

After the end of seismic excitation, residual maximum absolute bending moments exist in both continuous and segmental linings. It should be mentioned that the residual absolute bending moment ratio in a segmental lining is usually higher than that of a continuous lining. For instance, the residual maximum absolute bending moments of a segmental lining and a continuous lining are 57 % and 45 %, respectively (**Figure 8-6**a). This could be attributed to the nonlinear (bilinear) rotational stiffness behaviour of the joints that have been applied in this study.

Figure 8-7 presents the effects of segmental joints and a soil constitutive model on the change in maximum normal forces during seismic excitation. It can be seen from **Figure 8-7**a that segmental joints have a negligible influence on the normal forces, in particular at the beginning when the seismic amplitude is small and seismic excitation increases. However, when seismic excitation gradually decreases, the decreases in the residual maximum normal forces induced in continuous and segmental linings are not similar. Consequently, the residual maximum normal forces in a segmental lining are about 5 % higher than that of a continuous lining. This difference can also be explained by the nonlinear behaviour of the segmental joints during seismic loads. A limited influence of the segmental joints on the induced normal forces was also observed in the analytical analyses performed by Naggar et al. [2008].

a) Influence of segmental joint when the Mohr-Coulomb constitutive model is used

b) Influence of the soil constitutive model when a segmental lining is used

Figure 8-7. Change in maximum normal forces

Like the bending moment, the normal forces are affected to a large extent by the soil constitutive model during seismic excitation. The maximum change in the maximum normal forces in the case in which Mohr-Coulomb model is used is about 19 % higher than that determined in the case when the elastic soil model is used. This could be attributed to the fact that the progressive plastification of the soil during seismic excitation increases the load transmitted to the tunnel lining (Gomes [2013]). The same tendency has been observed in the work by Sliteen [2013] and Sliteen et al. [2013]. At the end of the seismic excitation, the change in the normal forces induced in the tunnel lining when elastic material is used decrease to till zero. Nevertheless, a change in the residual value of the normal forces of about 61 % can be observed in **Figure 8-7**b for the Mohr-Coulomb. This phenomenon might not be seen clearly in the case in which a low seismic signal is used.

As explained in section 8.3.1 concerning the negligible effect of deformation absorbability of the segmental joints on the overall tunnel lining deformation, **Figure 8-8**a shows an insignificant difference in the change in the maximum normal displacement induced in the tunnel lining when both a continuous lining and a segmental lining are used. On the other hand, the maximum change in normal displacement observed in the case in which the Mohr-Coulomb constitutive model is used is about 9 % smaller than that obtained when elastic material is used (**Figure 8-8**b). A larger residual value of normal displacement can be seen when the Mohr-Coulomb model is applied due to the effect of irreversible deformation.
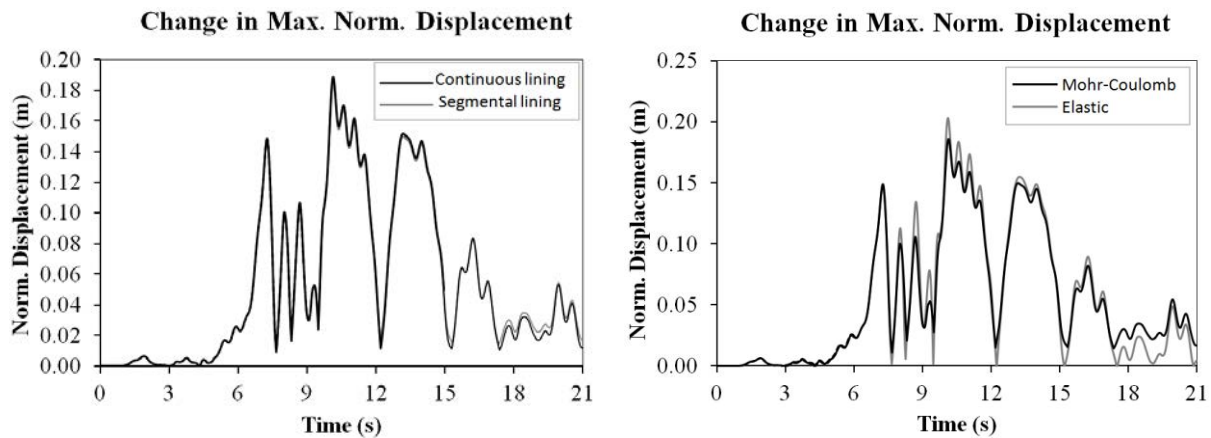
a) Influence of segmental joints when the Mohr-Coulomb constitutive model is used

b) Influence of the soil constitutive model when a segmental lining is used

Figure 8-8. Change in normal displacement

Figure 8-9 illustrates an insignificant effect of the joints on the surface settlement. The results indicate that an elastic analysis is inadequate in determining the induced settlement on the ground surface. The values are almost zero (around 2 mm) which is not realistic (**Table 8-2**). The same conclusion was also reached in the work by Sliteen et al. [2013].
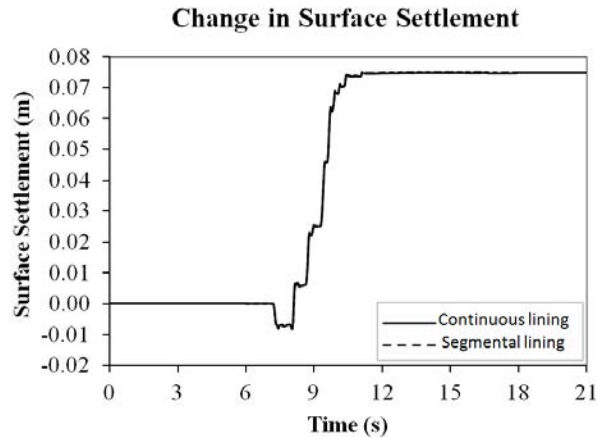
Figure 8-9. Change in surface settlement - Influence of segmental joints when the Mohr-Coulomb constitutive model is used

Table 8-2. Maximum changes in structural forces, lining deformation and surface settlement (high signal case)

	Elastic model		Mohr-Coulomb model	
	Cont. lining	Seg. lining	Cont. lining	Seg. lining
Change in max. absolute M (kNm/m)	277.83	242.18	970.27	605.55
Change in max. N (kN/m)	1811.44	1796.61	2133.13	2154.37
Change in max. Normal Disp (mm)	203.42	203.39	189.09	186.24
Change in max. Settlement (mm)	2	2	74.91	75.12

8.4. Comparison with simplified methods

Due to the complexity and high computational costs of a full dynamic numerical analysis, it is often preferred to use simplified analytical solutions and/or quasi-static numerical methods to study the seismic response of tunnels.

A quasi-static numerical analysis usually approximates the seismic-induced inertia forces as a constant horizontal body force applied through a mesh (Debiasi et al. [2013]). Horizontal accelerations that correspond to the peak acceleration obtained in the cases in which low and high seismic signals are used (**Figure 8-2**) have been applied in the present study. The vertical and horizontal displacements were restricted along the base of the model during the application of horizontal acceleration while the horizontal displacements were left free along both sides of the model.

Besides the horizontal acceleration method, a 2D numerical model based on the ovaling deformations has been developed and presented in Chapter 7, in which seismic loads are imposed as inverted triangular displacements along the lateral boundaries of the model and uniform lateral displacements are imposed along the top boundary. The magnitude of the prescribed displacement at the top of the model is related to the maximum shear strain γ_{max} and to the height of the model, in which the maximum shear strain γ_{max} is equal to the maximum shear strain determined through the horizontal-acceleration method.

8.4.1. Validation of the quasi-static models

The parameter set that has been used here was taken from the work performed by Hashash et al. [2005]. Comparisons of the results obtained using quasi-static methods with those of Wang's well-known analytical method (Wang [1993]) have been made and are presented in **Table** 8-3. All of the calculations have been performed using the assumptions of Wang's solution.

Wang's solution is considered by many authors (e.g., Hashash et al. [2005]) as a realistic way of estimating structural forces induced in a tunnel lining. It should be noted that Wang's well-known analytical method and the prescribed shear strain method are built on the basis of the same assumptions. Unlike Wang's solution, the prescribed shear strain and horizontal acceleration methods both allow one to take the effect of gravity and the soil-structure interface contact into consideration.

It can be seen that both quasi-static numerical models result in normal forces and in bending moments which are in good agreement with the ones obtained using Wang's well-known analytical solution. The difference between the results of horizontal acceleration method and those of the prescribed shear strain method could be attributed to the difference in shear displacements applied to the tunnel structure in each case, as illustrated in **Figure** 8-10.

Table 8-3. Summary of quasi-static methods

|	Full Slip			No Slip		
	Wang	Pre. Shear Strain	Hor. Acce.	Wang	Pre. Shear Strain	Hor. Acce.
Max. Normal Forces (kN/m)	62.9[a]	78.7	77.6	1045.4[a]	1036.8	1154.2
Ratio N (%)	*100.0*	*125.1*	*123.3*	*100.0*	*99.2*	*110.4*
Max. Bending Moment (kNm/m)	188.8[a]	184.1	201.5	-	156.0	169.1
Ratio M (%)	*100.0*	*97.5*	*106.7*		*100*	*108.4*

Note: [a] Parameter from Table 3 in Hashash et al. [2005]

Due to the fact that three above methods give more or less similar results, only the horizontal acceleration method will be used in the next section for comparison with the results of full dynamic analyses.

8.4.2. Comparison between quasi-static analysis and full dynamic analysis

Table 8-4 illustrates the maximum normal forces and the bending moment induced in a tunnel lining determined using quasi-static and full seismic analyses. All the calculations have been performed using elastic soil material and applying the no-slip condition at the soil-tunnel interface. It can be seen that the quasi-static analysis gives results that are in good agreement with those predicted with a full seismic analysis, when a low seismic excitation is considered. However, quasi-static analysis is inadequate, under the impact of a high seismic excitation, in determining the normal forces and bending moment induced in a tunnel lining (**Figure** 8-11

and **Table** 8-4). It has been suggested that an equivalent static solution could yield smaller structural lining forces than those of a true dynamic solution. This finding is consistent with the results of Lee et al. [2007], who pointed out that the bending moment in a segmental lining is about 0.3 to 0.7 times smaller in a quasi-dynamic method than in a full dynamic analysis. Similarly, Akhlaghi and Nikkar [2014] indicated the maximum values of bending moment and normal forces induced in a circular tunnel determined using analytical method (Wang [1993]) are 0.7 and 0.65 times, respectively, smaller than those estimated using numerical model subjected to a true seismic signal. The same conclusion can also be found in the literature (e.g., Hung et al. [2009], Romero and Caufield [2012]).
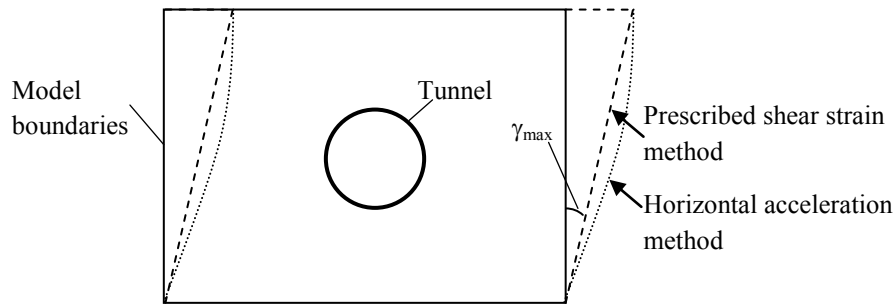
Figure 8-10. Comparison of shear displacements

Table 8-4. Summary of quasi-static and full seismic analyses (no slip condition)

| | Low seismic signal | | | | High seismic signal | | | |
| | Cont. Lining | | Seg. Lining | | Cont. Lining | | Seg. Lining | |
	Quasi-static	Full dynamic	Quasi-static	Full dynamic	Quasi-static	Full dynamic	Quasi-static	Full dynamic
Max. Normal Forces (kN/m)	5.99	5.55	5.85	5.49	703.8	1811.4	703.7	1796.6
Max. Bending moment (kNm/m)	1.53	1.32	1.35	0.75	106.0	277.8	97.0	219.7
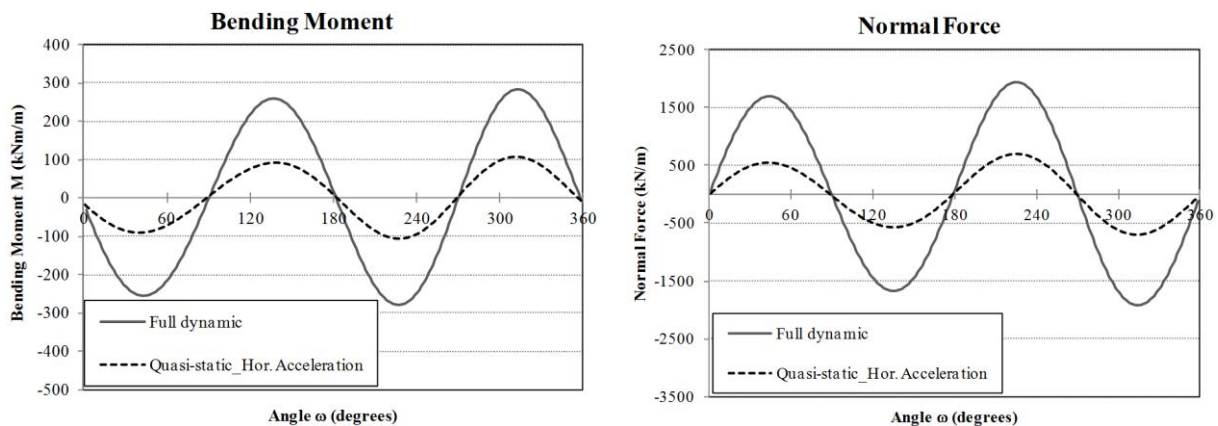
a) Bending moment   b) Normal forces

Figure 8-11. Comparison between quasi-static analysis and full dynamic analysis (high seismic signal case)

8.5. Conclusions

This chapter presents a numerical study that investigates the performance of segmental tunnel linings under seismic loads. Analyses have been carried out using a 2D finite difference element model. Two typical seismic signals, obtained using Nice earthquake data, which correspond to a low seismic signal and a high seismic signal, have been adopted as input.

Several conclusions can be drawn from the results of the present study:

- A segmental lining can perform better than a continuous lining during an earthquake. The maximum bending moment induced in a segmental lining is significantly smaller than that developed in a continuous lining;

- Although there are differences between the behaviour of a segmental lining and that of a continuous lining, the effect of the joints under a low seismic excitation could be neglected;

- The effect of the soil constitutive model on the tunnel behaviour depends to a great extent on the amplitude of the seismic excitation and it could be neglected under low seismic excitation. However, this effect must be taken into consideration under a high seismic excitation;

- The irreversible behaviour of the soil significantly modifies the tunnel loads both during seismic excitation and, more importantly, after it. Significant residual structural lining forces should be predicted when plasticity of the soil is taken into account;

- An elastic analysis is not sufficient to determine the seismic induced response of a soil-tunnel system;

- An equivalent static solution would yield smaller structural lining forces than those of a true dynamic solution.

Further comparisons with experimental data, obtained from real tunnel excavations, should be made in order to improve the quality of the numerical simulation.

Chapter 9

The Hyperstatic Reaction Method under Dynamic Loads

9.1. Introduction

Generally, the impact of seismic loads on tunnels can be taken into consideration through full dynamic analysis or quasi static analysis. Full dynamic analysis, which is also called time history analysis, represents the most complex level of seismic analysis, and, as a result, it is also the most precise method. This type of analysis is generally conducted using a numerical tool. However, this method is not economic, due to the long calculation time that is necessary. This is why the application of full dynamic analysis is still limited. The recently common trend is to use quasi-static analysis techniques with analytical methods or numerical analyses.

The implementation of tunnel response analysis using the quasi static approach can be grouped into two approaches: (1) the deformation based method and (2) the force based method. The deformation based method, which is described in detail in Hashash et al. [2001], is based on the calculation of the shear strain due to earthquakes at a tunnel depth and then applying this strain to the tunnel structure. The force based method instead usually assumes that the earthquake loads are caused by the inertial forces from the surrounding ground. The additional inertial force is equal to the product of the seismic coefficient, related to the peak ground acceleration, and the weight of the element in the model. While the deformation based method is developed in both analytical solutions and numerical analyses, the application of the force based method to tunnels is usually carried out using commercial software (e.g., Debiasi et al. [2013], Papanikolaou and Kappos [2013]).

In order to use the force based method in an analytical model, it is necessary to estimate the dynamic loads that act on the tunnel structure. One procedure that is commonly used to determine the increase in lateral earth pressure under seismic circumstance is the Mononobe-Okabe method (Hashash et al. [2001]). However, the Mononobe-Okabe method was originally developed for aboveground earth retaining walls, assuming that the retaining wall yields sufficiently to develop minimum active and maximum passive earth pressure. Obviously, the behaviour of a tunnel and that of a retaining wall structure under dynamic conditions are not similar in many cases.

The component that has the most significant influence on the behaviour of a tunnel lining under seismic loads, except for the case of a tunnel sheared by a fault, is the ovaling or racking deformation generated by seismic shear or S-wave propagation (Hashash et al. [5], Peinzen [2000]). Wang [1993] suggested two separate load schemes for rectangular tunnels: a quasi-static concentrated force for deep tunnels, and a quasi-static triangular pressure for shallow tunnels. However, this kind of cross-section shows different behaviour from that of the circular tunnel studied in this study, under seismic loads.

As far as circular tunnels are concerned, Naggar et al. [2008] developed a closed-form solution for moments and thrusts in a jointed composite tunnel lining, on the basis of external load scheme that was proposed by Peinzen and Wu [1998], which is also used in this study. This solution has been adapted to evaluate the effect of in-plane shear stresses induced by ovaling deformation.

This chapter has the aim of proposing the use of a numerical procedure to the hyperstatic reaction method (HRM) in order to analyse of segmental tunnel linings exposed to seismic loads. This method has been developed on the basis of the HRM that was proposed by Oreste [2007], and then developed in Chapter 6 (also see Do et al. [2014b, 2014d]). Seismic loads are determined on the basis of in-plane shear stresses which were introduced in the works of Peinzen and Wu [1998] and Naggar et al. [2008]. The parameters that are necessary to calculate the tunnel lining under seismic loads are presented. A specific implementation has been developed using a finite element (FEM) framework.

The HRM results have been compared and validated with the numerical results obtained using the FLAC^{3D} model. A parametric study has been performed which allows the effect of seismic magnitude, tunnel dimension and segmental joints on the seismic-induced bending moment and normal forces in a tunnel lining to be evaluated.

9.2. The mathematical formulation of the HRM

9.2.1. The HRM under static conditions

On the basis of the work by Oreste [2007], the content in Chapter 6 (also see Do et al. [2014b, 2014d]) has introduced a numerical HRM approach for the analysis of segmental tunnel linings under static loads. The problem geometry under static conditions can be seen in **Figure 6-1**.

9.2.2. The HRM under seismic conditions

In the HRM, it is necessary to estimate the active loads that act on the tunnel lining. Ovaling deformation can develop in a circular tunnel during a seismic event due to the in-plane shear stresses caused by vertically propagating horizontal shear waves (Peinzen and Wu [1998] and Naggar et al. [2008]).

For the quasi-static analysis of circular tunnels, the in-plane shear stress is calculated as follows (Peinzen and Wu [1998] and Naggar et al. [2008]):

$$\tau = \gamma_{c.} G \qquad\qquad (9\text{-}1)$$

where γ_c is the shear strain that is deduced from a ground-response analysis, and G is the shear modulus of the soil.

Assuming that the in-plane shear stress is constant at the depth of the tunnel, the free-field shear stress is usually applied as a far-field stress in analytical solutions (e.g., Peinzen and Wu [1998] and Naggar et al. [2008]).

It should be noted that, in the HRM, beam elements interact with the neighbouring ones through nodes. Compressive external loads applied in one direction will also yield tensile

loads in a perpendicular direction. Therefore, the external loads caused by shear stress under seismic events, which act on the tunnel lining in the HRM, can be different from those applied in the analytical solution proposed by Naggar et al. [2008]. The two parameters, *a* and *b*, presented in **Figure 9-1** have been adopted to represent the change in external loads under seismic condition in the HRM.

On the basis of the seismic load scheme that acts on the tunnel lining in the HRM method presented in **Figure 9-1**, it can be seen that this load scheme is more or less identical to that of the load components under the static condition presented in **Figure 6-1**, but the horizontal loads are in opposite directions and all the external loads are rotated counter-clockwise by $\pi/4$. This would therefore seem to suggest that the HRM approach (see Chapter 6 or Do et al. [2014b, 2014d]), which was developed under static loads, could also be used to calculate the seismic-induced stresses in the HRM, while recalling that all the results need to be rotated counter-clockwise along the tunnel lining by $\pi/4$, in order to obtain the results under seismic conditions.
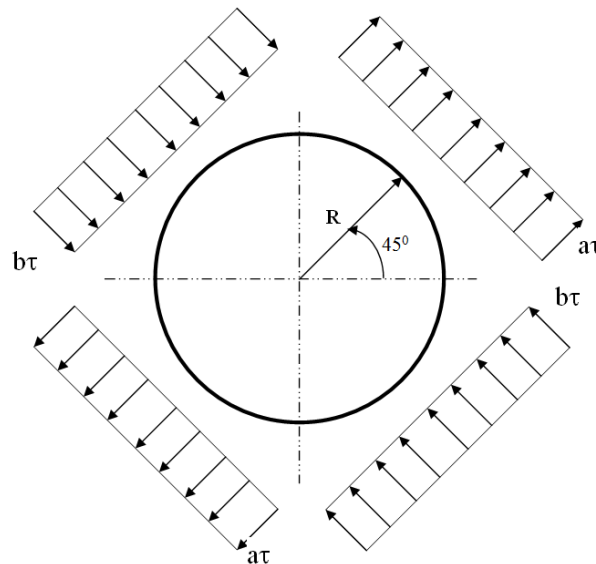
Figure 9-1. Proposed equivalent external forces under a seismic event in the HRM

The maximum shear reaction pressure, $p_{s,lim}$, introduced in Chapter 6 (also see Do et al. [2014b, 2014d]) for the static load case, must be changed, due to the change in the external load scheme, as follows:

$$p_{s,\lim} = \frac{(b-a)\tau}{2} tg\phi \qquad (9-2)$$

where   *a* and *b* are the parameters shown in **Figure 9-1**;
and ϕ is the internal friction angle of the soil.

Similarly, the confining pressure, $\Delta\sigma_{conf}$, introduced on the tunnel perimeter in Chapter 6 (also see Do et al. [2014d]) also has to be changed as follows:

$$\Delta\sigma_{conf} = \frac{(b-a)\tau}{2}\frac{v_S}{1-v_S}$$ (9-3)

where a and b are the parameter shown in **Figure 9-1**;

              and v_s is Poisson's ratio of the soil.

A parametric analysis was then conducted in order to estimate two parameters, a and b, which represent the external loads caused by seismic-induced shear stress, as mentioned above. For this purpose, the results obtained using the HRM were compared with those determined using the numerical FLAC^{3D} model which is introduced in the next section. The results indicate that while parameter b is constant and equal to 1.25, parameter a depends on the change in tunnel dimension (tunnel radius R), and can be estimated using the following expression:

$$a = -0.7\ln(R) + 0.885$$ (9-4)

where R is the tunnel radius (m).

Finally, in order to obtain the overall stresses in the tunnel lining, the seismic-induced (incremental) stresses are superimposed onto the stresses determined under static conditions.

9.3. 2D numerical modelling FLAC^{3D}

The 2D numerical model developed in Chapter 7 using the FLAC^{3D} finite difference program (Itasca [2009]) has been adopted in this section in order to investigate the behaviour of tunnel linings under seismic loads (see **Figure** 7-1). This model assumes the behaviour of the tunnel structure and of the soil mass is linear-elastic and mass less.

This model is developed on the basis of the deformation based method, in which ovaling deformations, due to seismic loads, are imposed as inverted triangular displacements along the lateral boundaries of the model and uniform lateral displacements along the top boundary (quasi static using the deformation based method, see **Figure** 7-1). The magnitude of the prescribed displacement at the top of the model is related to the maximum shear strain, γ_c, and to the height of the model.

This FLAC^{3D} model was validated on the basis of a comparison with the results obtained with Wang's well known closed-form analytical solution (Wang [1993]), under the same hypotheses (see Chapter 7 and Do et al. [2014]).

9.4. Evaluation of the HRM under seismic loads applied to a continuous lining

The results of the HRM have been compared with those obtained from the FLAC^{3D} model. The external loads presented in **Figure 9-1**, with the *a* parameter determined from **Equation** 9-4, have been used for all the calculations with the HRM. Parameters of the tunnel lining and of the soil from the Bologna-Florence high speed railway line tunnel project in Bologna have been adopted (Croce [2011]).

The tunnel lining considered in this section is a continuous cast-in-place concrete lining. It should be mentioned that all the FLAC^{3D} calculations have been performed using the no-slip condition between the soil and the tunnel lining. This process has been adopted in order to consider the worst case for the normal forces. The results presented in this study all refer to only the increment in the structural forces caused by seismic loads (seismic-induced structural forces).

A parametric study has been conducted to investigate the effects of seismic loads, which, in this study, are represented by the maximum horizontal seismic acceleration, a_H, shear strain, γ_c, and the tunnel dimension, R. A maximum horizontal acceleration, which changes over a range of 0.1g to 0.75g, has been adopted in this study. The maximum shear strain, γ_c, which is determined according to Power et al. [2004], changes over a corresponding range of 0.035 % to 0.26 %. The tunnel radius is assumed to change in a range of 1.25 m to 7.5 m, a range that covers most of the tunnel cases observed in practice (see **Table 9-1**).

Table 9-1. Parameters used in the analysis

Parameters	Unit	Value						
Tunnel lining properties								
Young's modulus E_l	kN/m^2	35,000,000						
Poisson's ratio ν_l	-	0.15						
Lining thickness t_l	m	0.4						
Tunnel radius R	m	1.25	2	2.5	3	4.5	6	7.5
Flexibility ratio F	-	0.59	2.42	4.72	8.16	27.53	65.26	127.45
Soil properties								
Young's modulus E_S	kN/m^2	450,000						
Poisson's ratio ν_S	-	0.3						
Internal friction angle ϕ	degrees	37						
Seismic parameters								
Horizontal acceleration a_H	(g)	0.1 - 0.2 - 0.35 - 0.5 - 0.75						
Corresponding shear strain γ_c	(%)	0.035 - 0.07 - 0.1212 - 0.173 - 0.26						

Due to the fact that other parameters are assumed to be constant, the flexibility ratio F suggested by Peck [1972] can be used to represent the change of the tunnel radius, R. This ratio is usually used in the tunnel design to express the relative stiffness of the surrounding soil and of the lining structure:

$$F = \frac{E_S\left(1-v_l^2\right)R^3}{6E_l I\left(1+v_S\right)} \tag{9-5}$$

where E_l and v_l are modulus of elasticity and Poisson's ratio of the lining; E_S and v_S modulus of elasticity and Poisson's ratio of the soil; R, radius of the tunnel; I, moment of inertia of the lining.

Figure 9-2 and **Figure** 9-3 show a comparison of the incremental bending moment and normal forces, using the HRM and FLAC^{3D} model for the case in which tunnel radius R is equal to 2.5 m. This case has been chosen due to the fact that the incremental bending moment induced in the tunnel lining, caused by the impact of seismic loads, reaches the maximum value for this tunnel radius values as can be seen in the next section. This case has been adopted as the reference case in this study.
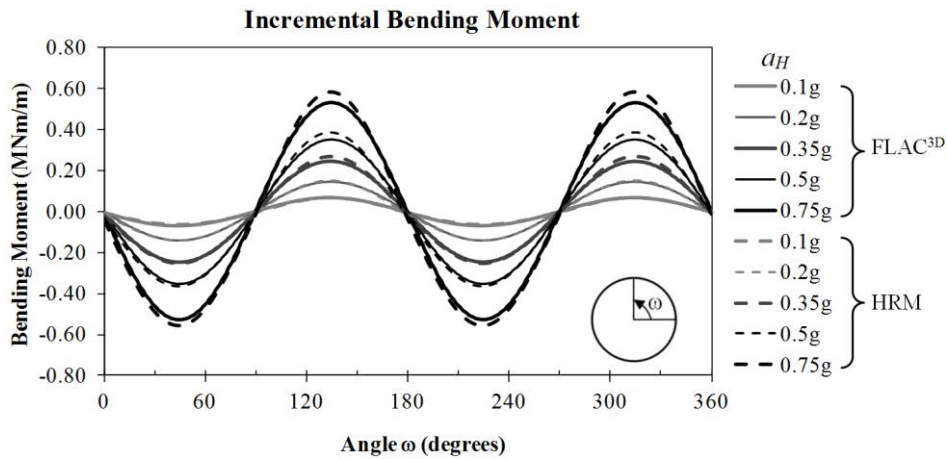
Figure 9-2. Comparison of the incremental bending moment for $F = 4.72$, ($R = 2.5$m only seismic-induced loads)
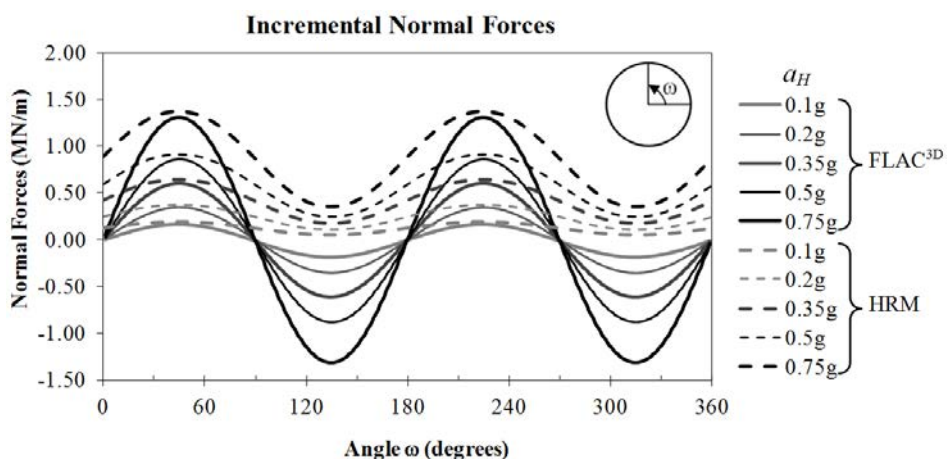
Figure 9-3. Comparison of the incremental normal forces for $F = 4.72$, ($R = 2.5$m only seismic-induced loads)

It can be seen, from **Figure** 9-2, that the bending moment obtained using the HRM method for all the considered horizontal seismic accelerations is similar to that of the FLAC^{3D}

Chapter 9: The Hyperstatic-Reaction Method under dynamic loads
270

model, not only as far as the maximum value is concerned but also for the distribution along the tunnel periphery. However, a considerable difference in the shape of the normal forces along the tunnel periphery can be observed (**Figure** 9-3). In other words, the negative normal forces determined with the HRM are not seen as that obtained with the FLAC^{3D} model. This could be attributed to the effect of interaction between the beam elements in the HRM model. In fact, the restraining of the surrounding soil yields reaction forces that act on the tunnel lining through springs placed at nodes in the HRM along the tunnel sections at which the tunnel lining move toward the soil. The compressive (positive) normal forces induced in the lining at these sections are therefore transferred to the lining sections at which the normal forces are currently tensile (negative). Consequently, the incremental normal forces at these sections, which are originally negative, increase and change to compressive (positive) values, as can be seen in the HRM results.

In addition, as expected, **Figure** 9-2 and **Figure** 9-3 show that the peak values of the incremental bending moment and normal force are observed at angles of ($\pi/4 + n\pi/2$, n ∈ IN) degrees measured from the right spring line.

On the basis of the above analysis, it is reasonable to conclude that the maximum seismic-induced (incremental) bending moment and normal forces obtained from the FLAC^{3D} model and the HRM are more or less similar. The HRM can therefore be used to investigate the behaviour of a tunnel lining under seismic loads.

The effect of the tunnel radius, R, or flexibility ratio, F, on the behaviour of a tunnel lining under seismic loads is studied in the following section. The other parameters presented in **Table 9-1** have been fixed. All tunnel radius cases are investigated for each value of shear strain, γ_c. **Figure** 9-4 to **Figure** 9-8 illustrate the maximum incremental (seismic-induced) bending moment and normal forces determined using the HRM and the FLAC^{3D} model. These figures show a good agreement between the HRM results and those of the FLAC^{3D} model for all the studied cases.

It can be seen that the development of the maximum incremental bending moment is affected to a great extent by the change in the tunnel radius for a given shear strain, γ_c. The highest maximum incremental bending moment is obtained for a tunnel radius R of approximately 2.5 m (F = 4.72) for all the shear strain, γ_c, values. When the tunnel radius increases (till 2.5m), the maximum incremental bending moment also increases. This increase in bending moment could be attributed to the increase in external seismic-induced loads that act on the tunnel lining, due to the increase in the tunnel radius. Over this critical value of tunnel radius (R = 2.5 m), an increase in the tunnel radius would result in a decrease in the maximum incremental bending moment. Theoretically, as mentioned above, an increase in the tunnel radius is followed by an increase in the external seismic-induced loads. However, when the same lining thickness is used, the increase in the tunnel radius also leads to an increase in the flexibility of the tunnel lining, F, as described in Peck [1972]. Consequently, a decrease in the bending moment induced in the tunnel lining can be observed. It is interesting to note that all the increases or decreases in the maximum incremental bending moment are approximately linear.

Unlike for the bending moment, **Figure** 9-4 to **Figure** 9-8 indicates a linear increase in the maximum incremental normal forces, when the tunnel radius increases. It should

Chapter 9: The Hyperstatic-Reaction Method under dynamic loads   271

mentioned that significant differences in the maximum incremental normal forces obtained with the HRM and the FLAC^{3D} model are observed as the tunnel radius increase over a range of 4 m to 7.5 m. The maximum differences obtained at a tunnel radius value of 7.5 m are about 20% for a_H values which change over a range of 0.1g to 0.35g. The differences decrease to 17 % and 13 % for a_H values of 0.5g and 0.75g, respectively. Due to the fact that the result obtained with the HRM is higher than the corresponding result of FLAC^{3D}, these differences make the HRM calculations secure and can therefore be adopted from a design point of view.


a)   b)
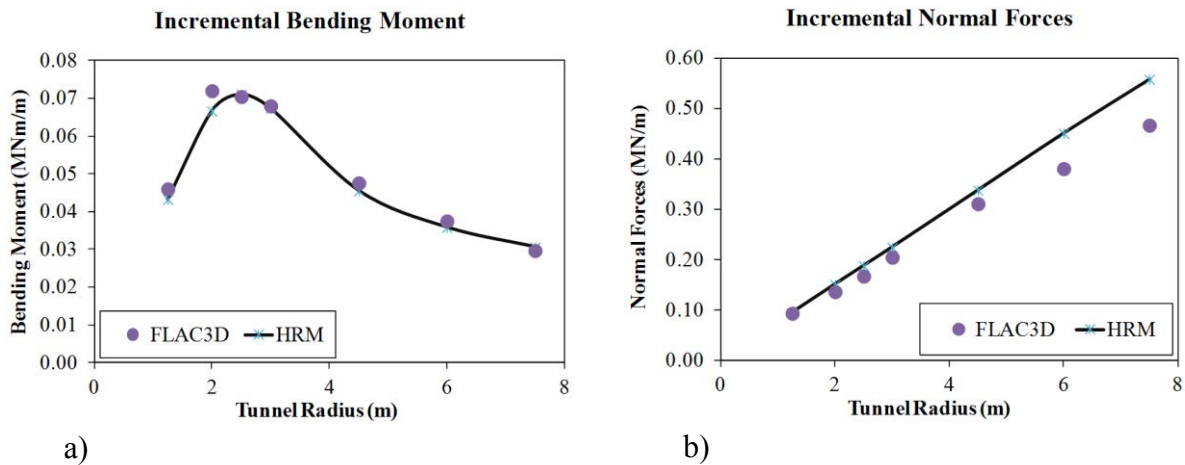
Figure 9-4. The effect of the tunnel radius on the maximum incremental bending moment (a) and normal forces (b) for a shear strain, γ_c, of 0.035 % (a_H = 0.1g) (only seismic-induced loads)

a)   b)
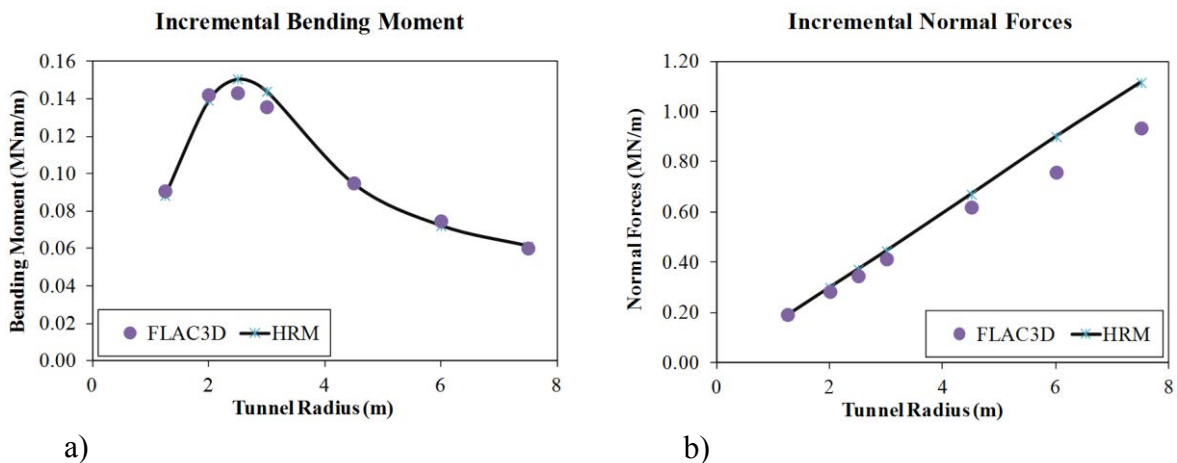
Figure 9-5. The effect of tunnel radius on the maximum incremental bending moment (a) and normal forces (b) for the shear strain, γ_c, of 0.07 % (a_H = 0.2g) (only seismic-induced loads)

a)   b)
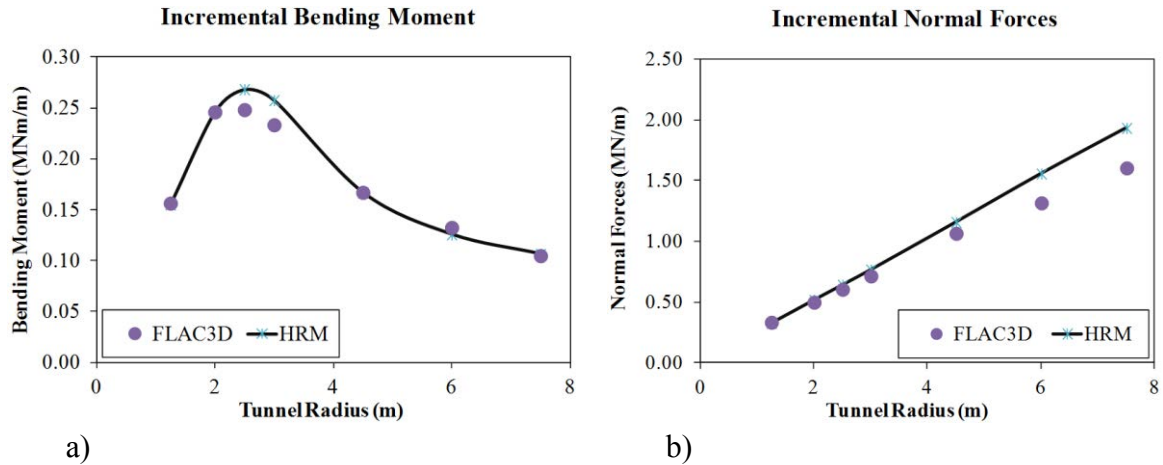
Figure 9-6. The effect of the tunnel radius on the maximum incremental bending moment (a) and normal forces (b) for a shear strain, γ_c, of 0.1212 % (a_H = 0.35g) (only seismic-induced loads)

a)   b)
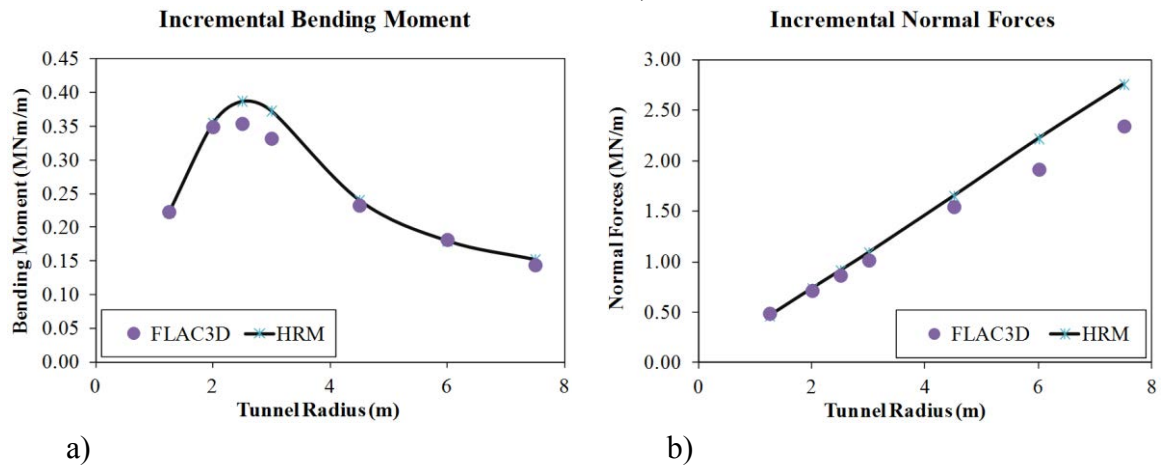
Figure 9-7. The effect of tunnel radius on the maximum incremental bending moment (a) and normal forces (b) for the shear strain, γ_c, of 0.173 % (a_H = 0.5g) (only seismic-induced loads)

a)   b)
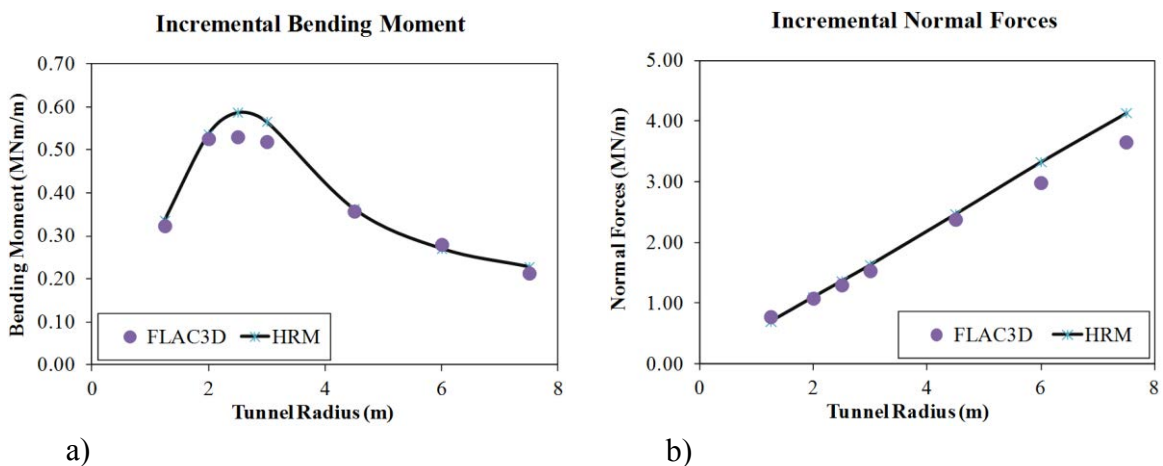
Figure 9-8. The effect of the tunnel radius on the maximum incremental bending moment (a) and normal forces (b) for a shear strain, γ_c, of 0.26 % (a_H = 0.75g) (only seismic-induced loads)

Chapter 9: The Hyperstatic-Reaction Method under dynamic loads   273

It should be mentioned that the same change in tendency, caused by the change in the tunnel radius, can be observed for both the maximum incremental bending moment and the maximum incremental normal forces when Wang's well-known analytical method (Wang [1993]) is used.

9.5. Effect of seismic loads on a continuous lining

Considering the results of the above section, **Figure** 9-9 shows the effect of seismic loads on the maximum incremental bending moment and on the extremum incremental normal forces for each given tunnel radius. It can be seen that the development of the maximum incremental bending moment and maximum incremental normal forces are affected to a great extent by the seismic loads represented in this study by the shear strain, γ_c. A higher shear strain value, γ_c, would result in a higher maximum incremental bending moment (**Figure** 9-9a) and a higher maximum incremental normal forces for each given value of the tunnel radius, R (**Figure** 9-9b).

a)

b)

c)
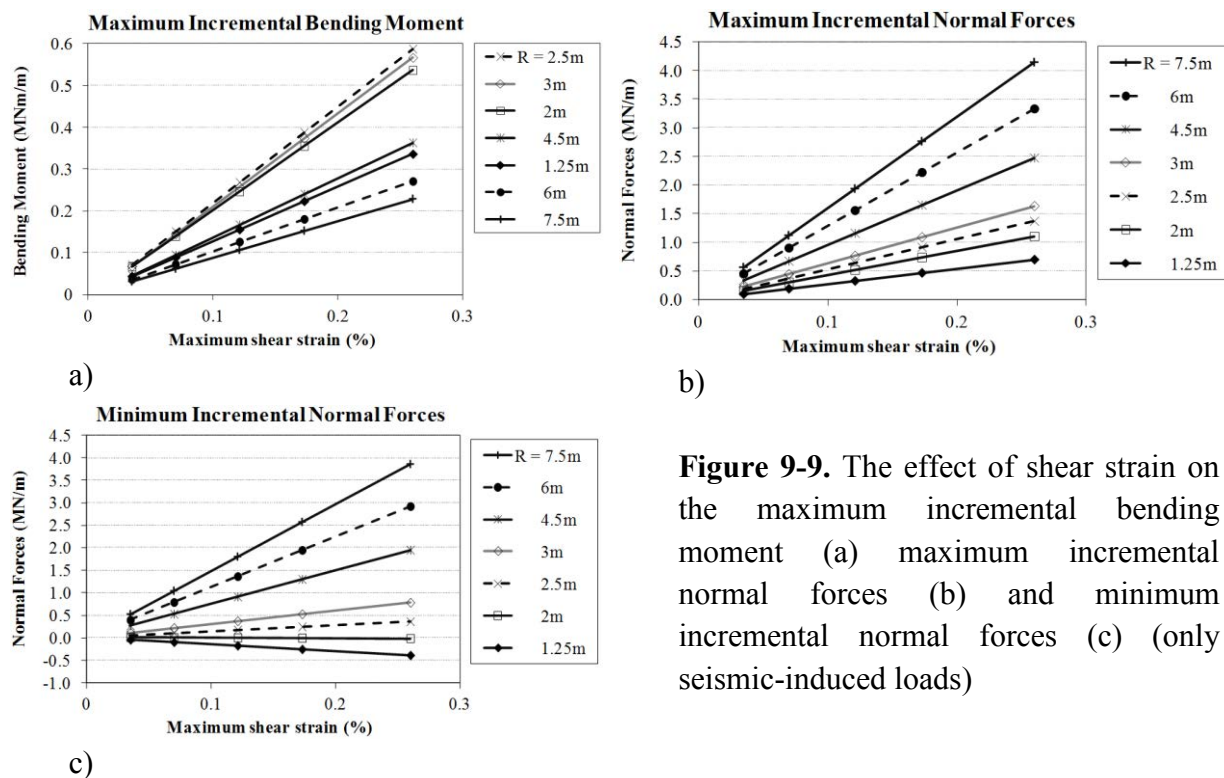
Figure 9-9. The effect of shear strain on the maximum incremental bending moment (a) maximum incremental normal forces (b) and minimum incremental normal forces (c) (only seismic-induced loads)

The dependence of the maximum incremental bending moment and the maximum incremental normal forces on shear strain, γ_c, is quite linear, and can be illustrated by an equation $y = kx$. As far as the maximum incremental bending moment is concerned, the k parameter has the highest value for a tunnel radius of 2.5 m and the lowest value for a tunnel radius of about 7.5 m (see **Figure** 9-9a).

Unlike for the bending moment, as far as the maximum incremental normal forces are

concerned, the larger the tunnel radius, the greater the *k* parameter (i.e. the steeper the relationship line) (see **Figure** 9-9b). In other words, as the tunnel radius *R* increases, the normal forces induced in the tunnel lining are more sensitive to change in shear strain, γ_c.

The results presented in **Figure** 9-9c also indicate a linear dependence of the minimum incremental normal forces on shear strain, γ_c, for each tunnel radius value. It should be noted that the minimum incremental normal forces are more affected by shear strain, γ_c, when larger tunnels with radiuses from 4.5 m to 7.5 m are considered. On the other hand, this effect is reduced for smaller tunnels, particularly for tunnels with radius of 2 m.

9.6. Effect of segmental joints under seismic loads

This section has the aim of showing how the proposed HRM can be used to analyse the behaviour of segmental tunnel linings under seismic loads. A parametric analysis has been conducted using the proposed HRM, in which the effect of tunnel radius, *R*, and seismic-induced shear strain (γ_c) on the segmental tunnel lining has been taken into consideration assigning different values of rotational stiffness.

The tunnel lining considered in this study is made up of 6 segments, which are distributed evenly along the tunnel periphery. The joints are located at angles of $0°$, $60°$, $120°$, $180°$, $240°$ and $300°$, measured counter-clockwise from the spring line on the right. The effect of circumferential joints between successive rings has not been considered. As for the longitudinal joints in a ring, only the influence of the rotational stiffness, K_{RO}, has been taken into account through the rotational stiffness ratio, $\lambda = K_{RO}l/E_lI_l$, proposed by Lee et al. [20]. A calculation length, *l*, of 1 m is usually considered to represent a typical unit length of a lining segment. The effect of radial and axial stiffness has been neglected. Segmental linings with rotational stiffness ratios, λ, of 0.25, 0.5, 1.0 and 1.5 have been investigated (Naggar et al. [2008]). The maximum seismic-induced shear strain, corresponding to a horizontal seismic acceleration which changes over a range of 0.1g to 0.75g, has been adopted for this study. The other parameters presented in **Table 9-1** have been assumed.

The distributions of the incremental bending moment and normal forces in the reference case for the tunnel radius of 2.5 m are presented in **Figure** 9-10 and **Figure** 9-11. A peak horizontal acceleration seismic load of 0.35g, which is consistent with the value suggested in Eurocode 8 for a highly seismic zone (CEN [2004]), has been adopted (Debiasi et al. [2013]).

Figure 9-10 shows that, for a given value of tunnel radius (*R* = 2.5 m), the development of the bending moment under seismic loads is affected to a great extent by the rotational stiffness ratio. As the joint rotational ratio, λ, decreases (i.e. the rotational stiffness, K_θ, decreases), the bending moments also decrease. These results are in good agreement with the numerical results obtained by Naggar et al. [2008], and can be explained by the increase in the flexibility of the tunnel lining when the joint rotational ratio, λ, decreases. Unlike for the bending moment, while the minimum incremental normal force is affected in a great extent by the joint rotational ratio, the maximum incremental normal force that develops in the lining is not sensitive to the change in the rotational stiffness (**Figure** 9-11).
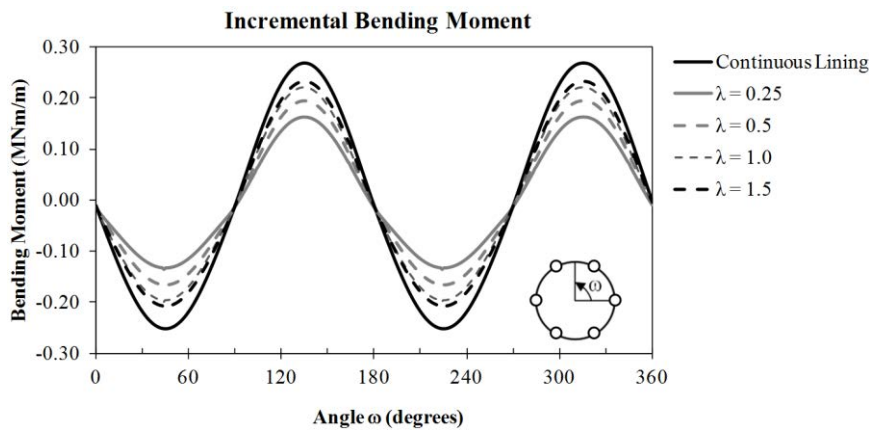
Figure 9-10. Incremental bending moment distribution around the tunnel (only seismic induced-loads) ($F = 4.72$ or $R = 2.5$ m, $a_H = 0.35$g)
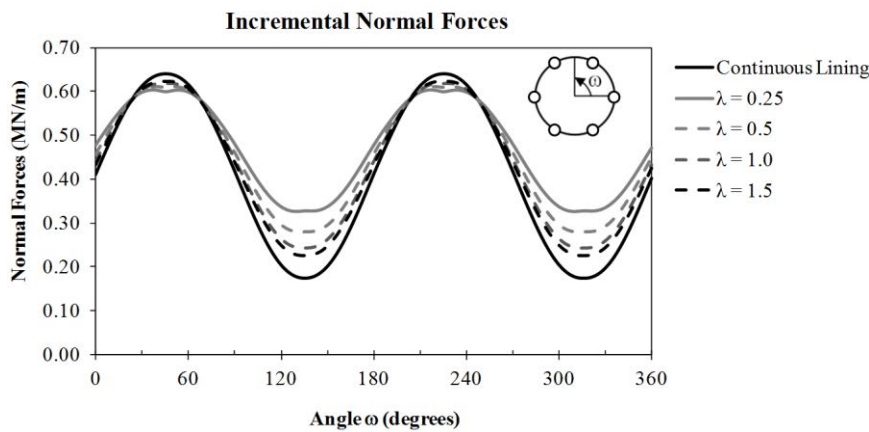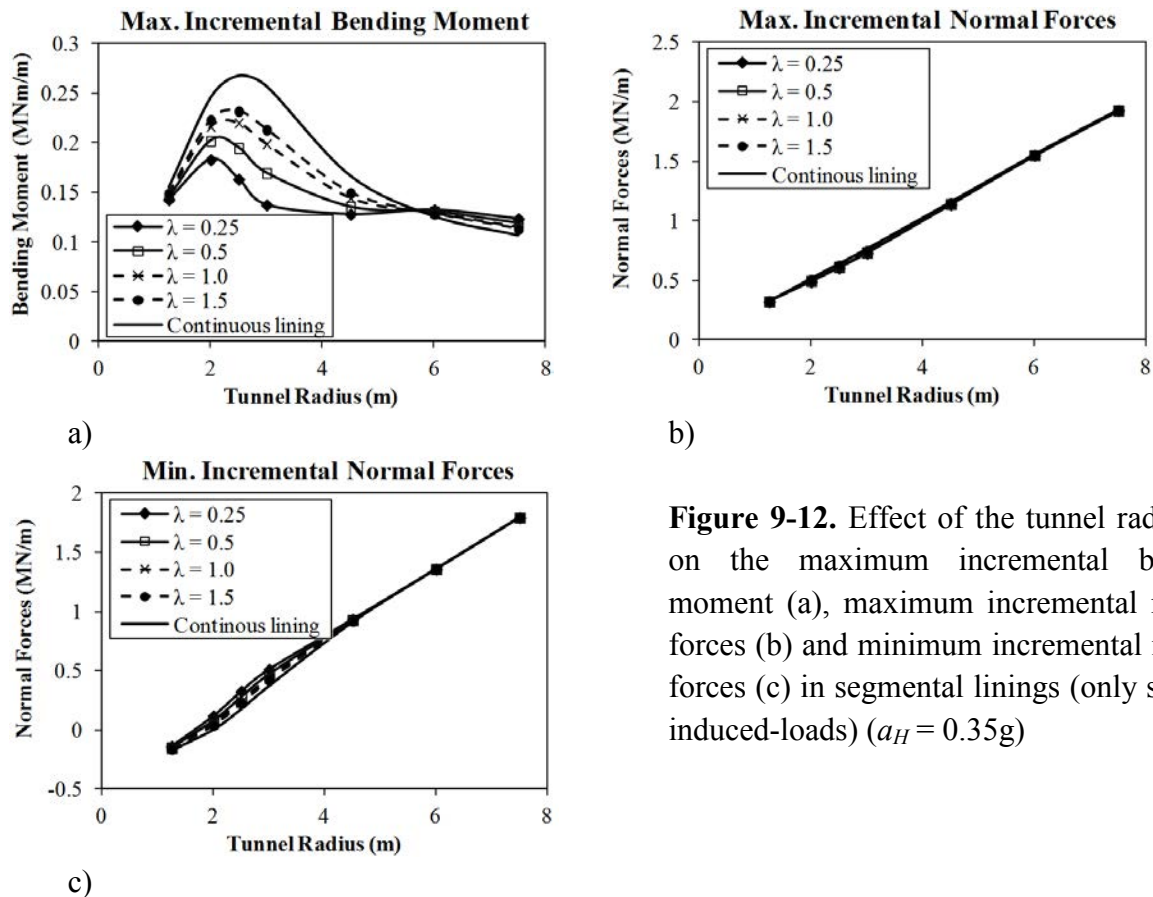

Figure 9-11. Incremental normal force distribution around the tunnel (only seismic induced-loads) ($F = 4.72$ or $R = 2.5$ m, $a_H = 0.35$g)

A parametric analysis, which focuses on the effect of the tunnel radius on the maximum incremental bending moment, and on the maximum/minimum incremental normal forces induced in a segmental lining when different rotational stiffness ratios, λ, are used, has been conducted. The results show the same change in tendency of the structural forces, due to the tunnel radius variation, when the horizontal seismic acceleration values are equal to 0.1g, 0.2g, 0.35g, 0.5g and 0.75g. Therefore, only the results of the maximum incremental bending moment and maximum/minimum incremental normal forces, corresponding to different tunnel radius for each rotational stiffness ratio, λ, obtained for a a_H value of 0.35g, are presented hereafter (**Figure** 9-12).

The results presented in **Figure** 9-12a indicate that the effect of the tunnel radius on the maximum incremental bending moment depends on the rotational stiffness ratio, λ. The higher the rotational stiffness ratio, λ, the greater the effect of the tunnel radius. However, the same change in tendency of the maximum incremental bending moment, which depends on the tunnel radius when different rotational stiffness ratio values are used can be observed (**Figure** 9-12a). It is interesting to note that, at a tunnel radius of about 6m, the influence of

the rotational stiffness ratio on the maximum incremental bending moment can be neglected. This phenomenon is again highlighted in **Figure** 9-13a. Unlike for the bending moment, **Figure** 9-12b and c show an insignificant effect of the rotational stiffness ratio on the extremum incremental normal forces.

a)

b)

c)

Figure 9-12. Effect of the tunnel radius, R, on the maximum incremental bending moment (a), maximum incremental normal forces (b) and minimum incremental normal forces (c) in segmental linings (only seismic induced-loads) ($a_H = 0.35g$)

Considering the results presented in **Figure** 9-12, **Figure** 9-13 shows the effect of the tunnel radius and of the rotational stiffness ratio on the maximum incremental bending moment and on the extremum incremental normal forces in another way. The maximum incremental bending moment ratio, R_M, the maximum incremental normal force ratio, R_{N-max}, and the minimum incremental normal force ratio, R_{N-min}, are defined as the ratio of the maximum incremental bending moment, the maximum incremental normal forces, and the minimum incremental normal forces, respectively, induced in a segmental lining under seismic loads to the corresponding value developed in a continuous lining. It can be seen from **Figure** 9-13a that the R_M ratio is affected more by the rotational stiffness ratio when medium tunnels with radiuses of 2 m to 4.5 m are considered. This effect is reduced when smaller or larger tunnels are considered.

It should be mentioned that when large tunnels with radiuses of 6 m and 7.5 m are considered, larger maximum incremental bending moment ratios, R_M, than unity are observed (**Figure** 9-13a). This phenomenon can be explained considering the effect of the joint distribution along the segmental tunnel lining on the worst case of the maximum incremental

bending moment under seismic loads, as described in the work presented in Chapter 7 (also see Do et al. [2014]).
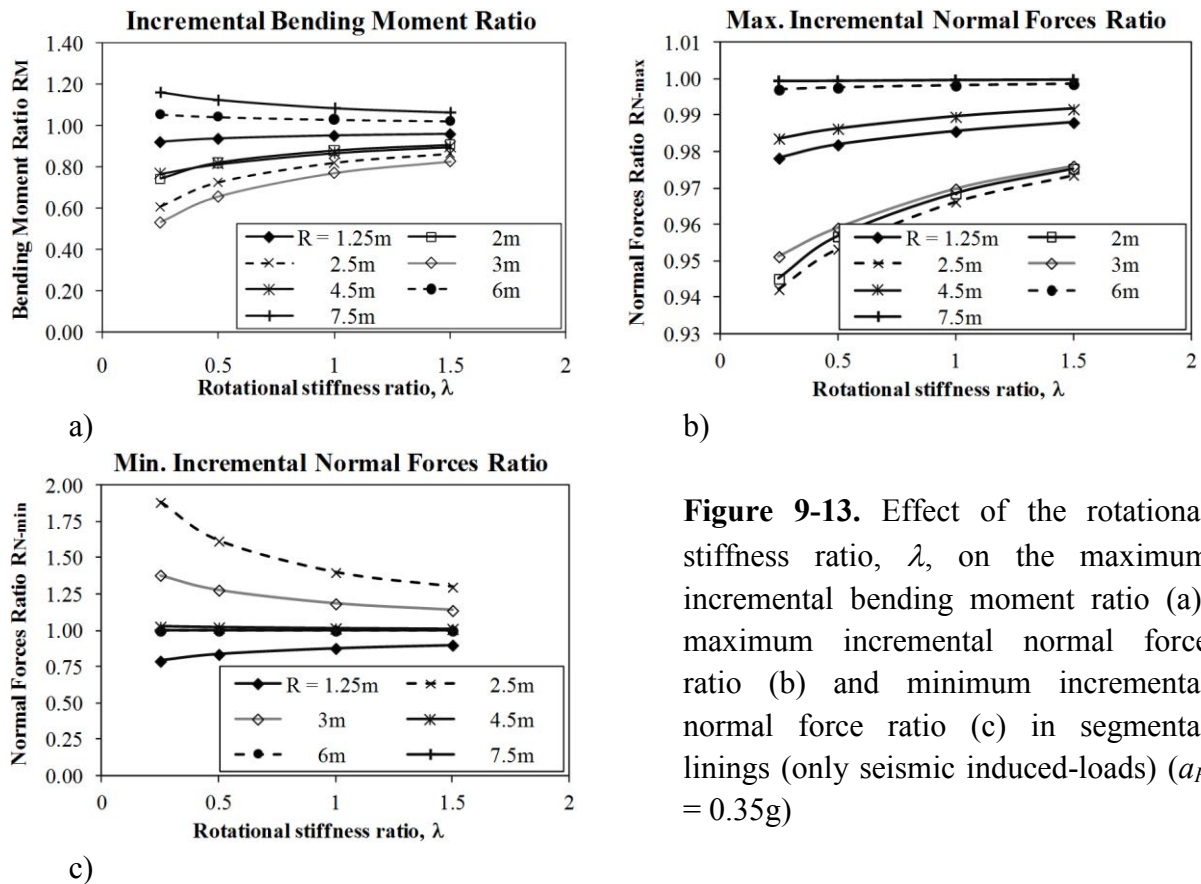
Figure 9-13. Effect of the rotational stiffness ratio, λ, on the maximum incremental bending moment ratio (a), maximum incremental normal force ratio (b) and minimum incremental normal force ratio (c) in segmental linings (only seismic induced-loads) ($a_H = 0.35g$)

In the same way as for the bending moment, the maximum incremental normal force ratio, R_{N-max}, is affected more by the rotational stiffness ratio when medium tunnel radiuses between 2 m to 3 m are used. This effect is reduced for smaller or larger tunnels. However, the change in ratio R_{N-max} is very small and can be neglected (**Figure** 9-13b).

Like for the maximum incremental normal force, **Figure** 9-13c indicates that the minimum incremental normal force ratio, R_{N-min}, is more affected by the rotational stiffness ratio when medium tunnel radiuses between 2,5 to 3 m are used. However, unlike the change in ratio R_{N-max}, which is very small and can be neglected, the change in ratio R_{N-min} for medium tunnels is significant and cannot be neglected. The R_{N-min} ratio is larger than unity for medium tunnels with radiuses of 2.5 m to 3 m, and smaller than unity for small tunnel with radius of 1.25 m. The effect of the rotational stiffness ratio on the R_{N-min} ratio can be neglected for larger tunnels with radiuses of 4.5 m to 7.5 m. It should be mentioned that the R_{N-min} ratio determined for a tunnel with radius of 2 m is not presented here, due to the fact the minimum incremental normal forces induced in a continuous lining are approximately equal to zero (see **Figure** 9-12c). This leads to high values of the R_{N-min} ratio, from 22 to 64, which do not really reflect the effect of the rotational stiffness ratio on the R_{N-min} ratio.

As shown from above analysis, the R_M and R_{N-min} ratios are affected more by the rotational stiffness ratio of segmental joints for medium tunnels with radiuses of 2 m to 3 m.

The presence of joints suppresses the incremental bending moments developed in the tunnel lining by up to approximately 50% compared with the continuous lining case (case R = 2 m in **Figure** 9-13a). On the other hand, the segmental joints lead to an increase in the minimum incremental normal forces by up to approximately 88 % (case R = 2.5 m in **Figure** 9-13c). Theoretically, for a tunnel lining design, the more critical situation necessary to consider is the combination of a peak of bending moments and a lower value of normal forces. This means that the stability of the tunnel lining increases as whether the peak of bending moment decreases or the lower value of normal forces increases. Thus, the effect of the joints on the internal forces should be considered to achieve an economical design of segmental lining exposed to seismic loads. In order to highlight the effect of seismic-induced loads on segmental lining behaviour, a reference case with a tunnel radius of 2.5 m has been adopted in the following section. The horizontal seismic acceleration values have been changed from 0.1g to 0.75g. **Figure** 9-14 shows the same change in tendency of the maximum incremental bending moment ratio, R_M, the maximum incremental normal force ratio, R_{N-max}, and the minimum incremental normal force ratio, R_{N-min}, for each given horizontal acceleration value, when the rotational stiffness ratio, λ, is changed from 0.25 to 1.5. It is interesting to note that, for a given tunnel radius of 2.5 m, while the R_M and R_{N-max} ratios are always smaller than unity, the R_{N-min} ratio is larger than unity for all the horizontal seismic acceleration values (**Figure** 9-14).

a)

b)

c)
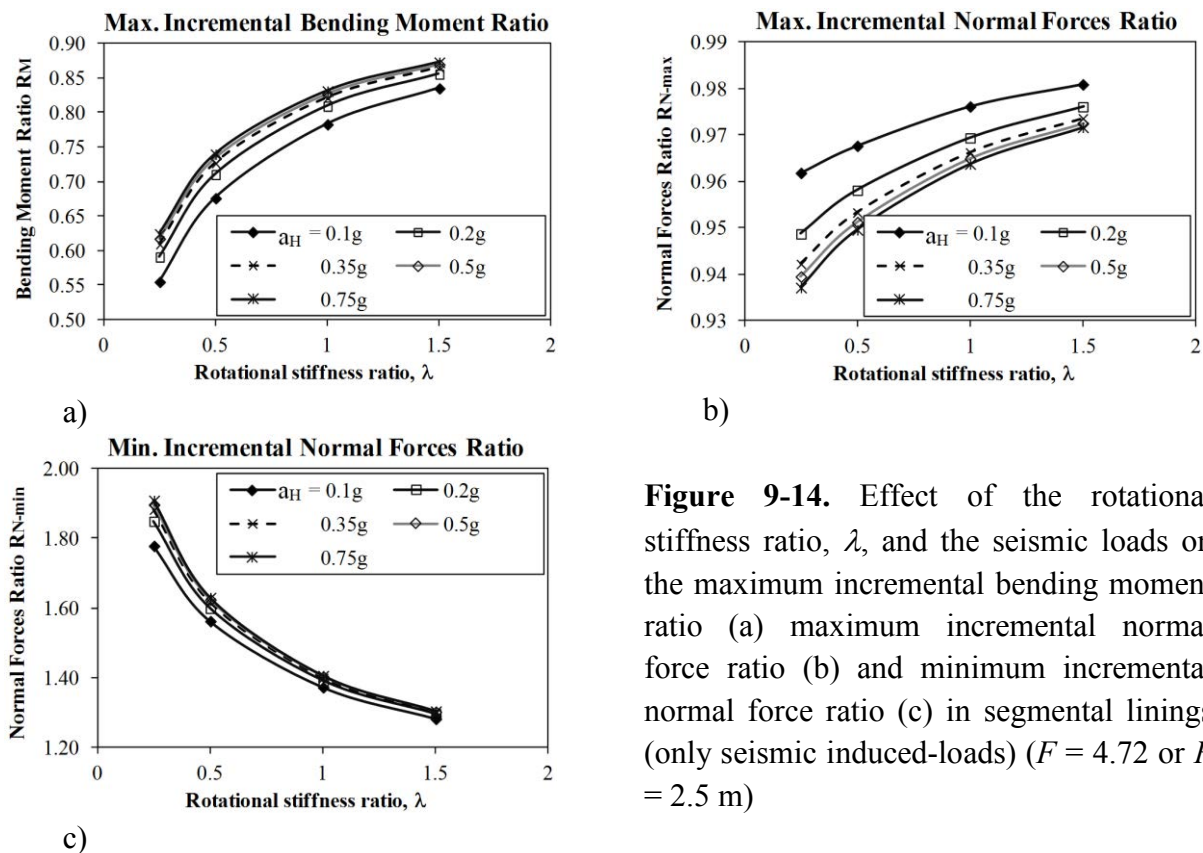
Figure 9-14. Effect of the rotational stiffness ratio, λ, and the seismic loads on the maximum incremental bending moment ratio (a) maximum incremental normal force ratio (b) and minimum incremental normal force ratio (c) in segmental linings (only seismic induced-loads) (*F* = 4.72 or *R* = 2.5 m)

It can be seen that, for each given rotational stiffness ratio, λ, as the horizontal seismic acceleration increases, the R_M and R_{N-min} ratios also increase (**Figure** 9-14a and c), while the

R_{N-max} ratio decreases (**Figure** 9-14b). It is interesting to note that the influence of the horizontal seismic acceleration on R_M, R_{N-max} and R_{N-min} values is very small for a high horizontal seismic acceleration range (from 0.35g to 0.75g) and can be neglected. The maximum differences in R_M, R_{N-max} and R_{N-min}, for each given rotational stiffness ratio, λ, when the horizontal seismic acceleration is changed from 0.35g to 0.7g, are in fact about 2.5 %, 0.5 %, and 1.3 %, respectively (see **Figure** 9-14).

Figure 9-14 also shows that, for each given horizontal acceleration value, as the rotational stiffness ratio increases, the R_M and R_{N-max} ratios also increase (**Figure** 9-14a and b), while the R_{N-min} ratio decreases (**Figure** 9-14c). In other words, segmental tunnel linings with smaller joints rotational stiffness can perform better under seismic loads. It is necessary to note that the change in R_M, R_{N-max} and R_{N-min} values is reduced gradually as the rotational stiffness ratio increases.

9.7. Conclusion

A numerical type of approach, named the HRM, has been applied to segmental tunnel linings under seismic loads and the results are presented in this chapter. This approach allows the effects of in-plane shear stress induced by seismic loads on segmental tunnel linings to be studied. A specific implementation has been conducted using a FEM framework. The presented HRM method allows an arbitrary distribution of segmental joints along the tunnel boundary to be taken into consideration. The solution is appropriate for the analysis of circular tunnels, embedded in either rock or soil, that remain predominantly elastic during construction.

In order to estimate the performance of the HRM method under seismic loads, the numerical results of the HRM, on pertaining to a continuous lining, have been compared with numerical results obtained using a $FLAC^{3D}$ model. The results have pointed out that the HRM gives bending moment distribution, which are in good agreement with that of the $FLAC^{3D}$ model. However, an important difference in the normal force distribution can be seen.

On the basis of the parametric analysis on segmental linings presented here, the following conclusions can be drawn:
- The effect of the joints on the internal forces should be considered to achieve an economical design of segmental lining exposed to seismic loads;
- The maximum incremental bending moment and normal forces are affected to a great extent by changes in the tunnel dimension. The highest maximum incremental bending moment is obtained for a tunnel radius, R, of approximately 2.5 m for all shear strain values. A linear increase in the maximum incremental normal forces when the tunnel radius increases, which is not observed for the bending moment, has been observed.
- Significant dependences of the maximum incremental bending moment and normal forces on the shear strain, γ_c, are quite linear.
- The development of the bending moment under seismic loads is affected to a great extent by the rotational stiffness ratio. Unlike the bending moment, the maximum incremental

normal force that develops in the lining is not sensitive to the magnitude of the rotational stiffness.

- The effect of the tunnel radius on the maximum incremental bending moment depends on the rotational stiffness ratio. The higher the rotational stiffness ratio, the greater the effect of the tunnel radius.

- The R_M, R_{N-max} and R_{N-min} ratios, defined as the ratio of the maximum incremental bending moment and the maximum/minimum incremental normal force, respectively, induced in a segmental lining under seismic loads to the corresponding value developed in a continuous lining, are affected more by the rotational stiffness ratio when medium sized tunnels with radiuses of 2 m to 3 m are considered.

- For each given rotational stiffness ratio, λ, if the horizontal seismic acceleration increases, the R_M and R_{N-min} ratios also increase and the R_{N-max} ratio decreases. Under high horizontal seismic accelerations, from 0.35g to 0.75g, the influence of horizontal seismic acceleration on the R_M, R_{N-max} and R_{N-min} values can be neglected.

- For each given horizontal acceleration value, as the rotational stiffness ratio increases, the R_M and R_{N-max} ratios also increase and the R_{N-min} ratio decreases. In other words, segmental tunnel linings with smaller rotational stiffness of the joints can perform better under seismic loads.

The proposed HRM method could be used to investigate directly the behaviour of segmental tunnel linings under seismic loads. The method allows results to be obtained with short calculation times (5 seconds).

GENERAL CONCLUSIONS

General Conclusions

The present thesis has allowed achieving several conclusions that represent innovative contributions to the knowledge of the segmental tunnel lining design under both static and dynamic loads.

After the bibliography study presented in the first part, in the second part that aims to study the behaviour of segmental tunnel lining under static loads, 2D and 3D numerical analyses performed in the present research pointed out the importance of taking into consideration the effect of the joints during segmental tunnel lining design. A significant reduction in the bending moment induced in the tunnel lining as the joint number increases has been shown. It has been seen that the influence of joint rotational stiffness, the reduction in joint rotation stiffness under the negative bending moment, the lateral earth pressure factor and Young's modulus of ground surrounding the tunnel should not be neglected. On the other hand, the results have also shown an insignificant influence of the axial and radial stiffness of the joints on segmental tunnel lining behaviour.

When the volume loss method and the convergence-confinement method are used to represented 3D tunnelling effect in a 2D model, significant difference has been shown between the structural lining forces and the surface settlement obtained. A comparison with 3D numerical results indicated that, for the same surface settlement, the structural lining forces determined with the CCM method are in better agreement with the 3D numerical results than those obtained with the VLM method. A technique that can be used to simulate the tunnel wall displacement process, based on the principles of the VLM, has been developed using the FLAC^{3D} finite difference program.

A 2D model has been developed for twin horizontal tunnels. The results showed that the impact between two tunnels is more considerable when the tunnel distance is less than 1D. At a tunnel distance of about 2D, the impact of the first tunnel construction process on the second tunnel behaviour can be negligible.

Due to the complexity of the mechanized tunnelling process, 3D numerical models of a single tunnel and of twin horizontal/twin stacked tunnels have been developed, which would allow the tunnel lining behaviour, the displacement of the ground surrounding the tunnel and the interaction between tunnels to be evaluated. The numerical results have shown a negligible influence of the initial conditions on the tunnel behaviour. In contrast, a great influence of the constitutive model of the ground on the tunnel behaviour and ground displacements has been pointed out. The impact of the processes during mechanized excavation, such as the grouting pressure and the jacking forces in the structural forces induced in the tunnel lining depend on the tunnel advancement.

In above 3D models, the influence of the joint pattern of the lining has in particular been taken into consideration. A negligible influence of the joint pattern on the ground displacement field surrounding the tunnel has been observed. Generally, a variation in the structural forces in successive rings along the tunnel axis has been found in a staggered segmental lining, indicating the necessity of simulating the joints in the tunnel lining and using a full 3D numerical model to obtain an accurate estimation of the lining efforts. In

addition, the considerable influence of the coupling effect between successive rings on the lining behaviour has been highlighted.

In the case of stacked tunnels, the results of the numerical analysis have indicated a great impact of a new tunnel construction on an existing tunnel. The greatest impacts are observed when the upper tunnel is excavated first and the upper tunnel is also affected to a greater extent by the excavation procedure. The excavation of the upper tunnel generally leads to greater surface settlements than those obtained for the case in which the lower tunnel is excavated first. On the other hand, the structural forces induced in stacked tunnels, when they are excavated simultaneously, are greater than those obtained in other cases.

As far as twin horizontal tunnels are concerned, the results of the numerical analysis have also indicated a great impact of a new tunnel construction on an existing tunnel. Generally, the simultaneous excavation of twin tunnels causes smaller structural forces and lining displacements than those induced in the case of twin tunnels excavated at a large lagged distance. However, the simultaneous excavation of twin tunnels could result in a higher settlement above the two tunnels.

Although numerical analyses using commercial softwares allow most of complicated processes during the mechanized tunnelling to be simulated but they are generally time consuming. The HRM is particularly suitable for the estimation of tunnel lining behaviour, in terms of structural forces, lining displacements, and passive ground pressure along the support profile. The method allows results to be obtained in short calculation times.

An improved numerical approach to the HRM, which was firstly developed using reduction factor, η, on the basis of the model proposed by Oreste [2007], has been presented in this research. An extensive parametric analysis has made it possible to estimate the segmental tunnel lining behaviour in a large number of cases which cover the conditions that are generally encountered in excavation practice. The influence of three typical types of grounds, that is weak, medium, and strong quality ground, of two values of lateral earth pressure coefficient K_0, of two values of tunnel depth, of three values of tunnel radius, of three values of tunnel lining thickness, and of four values of reduction factor, have been investigated. The results, have presented as design figures, can be used for a preliminary estimation of the structural forces, lining displacements and passive pressure induced in the segmental tunnel lining.

On the basis of the above HRM model, a new approach to the HRM method applied to a segmental tunnel lining has also been presented in this thesis. The influence of segmental joints has been considered directly using a lenghtless rotational spring, which is represented by a fixity ratio that has been determined on the basis of the nonlinear rotational stiffness. A specific implementation has been developed using a FEM framework. This code is able to consider the effect of segmental joints in successive rings on the tunnel lining. The present HRM method allows the arbitrary distribution of segmental joints along the tunnel boundary to be taken into consideration. In addition, the rotational stiffness of the segmental joints has been simulated using nonlinear behaviour, which is closer to the true behaviour of a joint than linear or bilinear behaviour. This new HRM approach has been validated using a simplified 3D numerical model. Additionally, one of the main advantages of the new HRM approach is the short time of about 5seconds for each calculation.

The third part has focused on estimating the behaviour of the tunnel exposed to dynamic loads. The works have been conducted using 2D numerical analyses and the HRM method.

Firstly, a 2D numerical model in which the ovaling deformation of the tunnel cross-section is adopted to simulate dynamic conditions has been developed. The influences of the joint distribution, joint stiffness (including the rotational stiffness, the axial stiffness and the radial stiffness assigned at the joints), the ground conditions, that is, Young's modulus and lateral earth pressure factor, and the seismic racking loads represented by the maximum shear strain, have been studied in detail. The results pointed out that the influence of the joint distribution on the segmental tunnel lining under the seismic and static conditions is not similar. The bending moment and normal forces induced in a segmental tunnel lining are generally smaller than the corresponding ones induced in a continuous lining, except for the minimum normal forces. This means that a segmental lining can perform better than a continuous lining during earthquake.

Compared to quasi-static models, full dynamic analysis is obviously the most complex level of dynamic analysis, which is therefore also the most precise method. In this research, two different ground motions have been applied in the model, which allow highlighting the effect of the joints on the tunnel lining during a seismic event with different maximum amplitude of the input signal. Although there are differences between the behaviour of a segmental lining and that of a continuous lining, the effect of the joints under a low seismic excitation could be neglected. The effect of the soil constitutive model on the tunnel behaviour depends to a great extent on the amplitude of the seismic excitation and it could be neglected under low seismic excitation. However, this effect must be taken into consideration under a high seismic excitation. The results also indicated that an elastic analysis is not sufficient to determine the seismic induced response of a soil-tunnel system and an equivalent static solution would yield smaller structural lining forces than those of a true dynamic solution.

The present work ends by the development of a new solution applied to the HRM to consider the effect of dynamic loads on the segmental tunnel lining. This new HRM model allows the effects of in-plane shear stress induced by seismic loads on segmental tunnel linings to be studied. Parametric results indicated that the effect of the joints on the internal forces should be considered to achieve an economical design of segmental lining exposed to seismic loads.

Perspectives

It is important to note that all of numerical models developed in this research have been performed using drained condition and with tunnels embedded at shallow depth. Additionally, due to the fact that the authors have not found an appropriate data set, all of numerical results have not been yet compared and validated with experimental data.

Therefore, the research works listed below are proposed for the short-term stage:

- Validate all numerical models using real or laboratory data;
- Improve constitutive model for concrete;
- Develop and perform 3D numerical analyses at higher depths;
- Perform dynamic calculations using more complicated constitutive model of the soil and apply to the case of twin tunnels.

and for the long-term stage:

- Develop and perform 3D numerical analyses considering the effect of water on the tunnel lining behaviour for undrained analyses;
- Develop a new approach to the HRM under seismic loads, in which true seismic signal is applied directly on the HRM model but not by using quasi-static loads.

REFERENCES

Addenbrooke, T. I., & Potts, D. M. (1996). Twin tunnel construction - Ground movements and lining behaviour. *Proc. International Symposium on Geotechnical Aspects of Underground Construction in Soft Ground*, (pp. 441-446).

Addenbrooke, T. I., Potts, D. M., & Puzrin, A. M. (1997). The influence of pre-failure soil stiffness on the numerical analysis of tunnel construction. *Géotechnique, 47(3)*, 693-712.

Afifipour, M., Sharifzadeh, M., Shahriar, K., & Jamshidi, H. (2011). Interaction of twin tunnels and shallow foundation at Zand underpass, Shiraz metro, Iran. *Tunnelling and Underground Space Technology*, *26*, 356-363.

AFPS/AFTES. (2001). *Earthquake design and protection of underground structures*. Tech. rep.

AFTES. (1976). *Consideration on the usual method of tunnel lining design*. Tech. rep., French Association of Tunnels and Undergrouns Spaces.

AFTES. (1997a). *Guidelines on the plate loading test of the rockmass, Tunnel et ouvrages souterrain*. Tech. rep., French Association of Tunnels and Undergrouns Spaces.

AFTES. (1997b). *The design, sizing and construction of precast concrete segments installed at the rear of a tunnel boring machine (TBM)*. Tech. rep., French Association of Tunnels and Undergrouns Spaces.

Akhlaghi, T. and Nikkar, A. (2014). *Effect of vertically propagating shear waves on seismic behavior of circular tunnels*. The Scientific World Journal, doi.org/10.1155/2014/806092.

Amorosi, A., & Boldini, D. (2009). Numerical modeling of the transverse dynamic behaviour of circular tunnels in clayey soils. *Soil Dynamics and Earthquake Engineering*, *29*, 1059-1072.

Anastasopoulos, L., Gerolymos, N., & Drosos, L. (2007). Nonlinear response of deep immersed tunnel to strong seismic shaking. *Journal of Geotechnical and Geoenvironmental Engineering*, *133(9)*, 1067-1090.

Arnau, O., & Molins, C. (2011a). Experimental and analytical study of the structural response of segmental tunnel linings based on an in situ loading test. Part 1: Test configuration and execution. *Tunnelling and Underground Space Technology*, *26*, 764-777.

Arnau, O., & Molins, C. (2011b). Experimental and analytical study of the structural response of segmental tunnel linings based on an in situ loading test. Part 2: Numerical simulation. *Tunnelling and Underground Space Technology*, *26*, 778-788.

Arnau, O., & Molins, C. (2012). Three dimensional structural response of segmental tunnel linings. *Engineering Structures*, *44*, 210-221.

Barla, G., Barla, M., Bonini, M., & Gamba, F. (2005). Two and three dimensional modelling and monitoring of the Metro Torino. *11th International Conference of Iacmag, Turin (Italy)*.

Barpi, F., Barbero, M., & Peila, D. (2011). Numerical modelling of ground-tunnel support interaction using bedded-beam-spring model with fuzzy parameters. *Gospodarka Surowcami Mineralnymi (Mineral Resources Management)*, *27(4)*, 71-87.

Bazaz, J. B., & Besharat, V. (2008). An investigation on seismic analysis of shallow tunnels in soil medium. *The 14th World Conference on Earthquake Engineering October 12-17, 2008, Beijing, China*.

Benmebarek, S., Kastner, R., & Ollier, C. (1998). Auscultation et modélisation numérique du processus de creusement à l'aide d'un tunnelier. *Geotechnique*, *48(6)*, 801-818.

Bernat, S. (1996). *Modélisation des déformations induites par le creusement d'un tunnel-Application au métro de Lyon-Vaise.* Ph.D. dissertation, Ecole Centrale de Lyon.

Bernat, S., & Cambou, B. (1998). Soil-Structure interaction in shield tunnelling in soft soil. *Computers and Geotechnics*, *22(3/4)*, 221–242.

Bezuijen, A., & Talmon, A. M. (2004). Grout pressures around a tunnel lining, influence of grout consolidation and loading on lining. *Proceedings of World Tunnel Congress and 13th ITA Assembly, Singapore*, (pp. 22–27).

Bilotta, E., & Russo, G. (2013). Internal forces arising in the segmental lining of an EPB bored tunnel. *J. Geotech. Geoenviron. Eng.*, *10.1061/(ASCE)GT.1943-5606.0000906*.

Bilotta, E., Lanzano, G., Russo, G., Silvestri, F., & Madabhushi, S. P. (2009). Seismic analyses of shallow tunnels by dynamic centrifuge tests and finite elements. *Proc. 17th Int. Conf on Soil Mechanics and Geotechnical Engineering, Alexandrìa, Egypt*.

Blom, C. B. (2002). *Design philosophy of concrete linings for tunnel in soft soils.* Ph.D. dissertation, Delft University, Netherlands.

Blom, C. B., Van der Horst, E. J., & Jovanovis, P. S. (1999). Three-dimensional structural analyses of the shield-driven "Green Heart" tunnel of the high-speed line South. *Tunnelling and Underground Space Technology*, *14(2)*, 217-224.

Bobet, A. (2003). Effect of pore water pressure on tunnel support during static and seismic. *Tunnelling and Underground Space Technology*, *18*, 377–393.

Bolton, M. D., Dasari, G. R., & Britto, A. M. (1994). Putting small-strain non-linearity into modified cam clay model. *In: Proceedings of the 8th international conference on*

computer methods and advances in geomechanics, Morgantown, West Virginia, (pp. 537-542).

Boubou, R. (2010). *Prise en compte du mode de pressurisation du front et de la géologie dans l'étude de l'impact du creusement de tunnels.* Ph.D. dissertation, Doctor's thesis. INSA de Lyon. N° d'ordre 2010ISAL0093.

Brinkgrave, R. B., & Broere, W. (2003). The influence of tunnel boring on foundations and buildings in urban areas – A numerical study. *Int. Workshop on Getechnics of Soft Soil-Theory and Practice. Vermeer, Schweiger, Harstunen \& Cudny (eds)*, (pp. 257-263).

Broere, W., & Brinkgreve, R. B. (2002). Phased simulation of a tunnel boring process in soft soil. *Numerical methods in Geotechnical Engineering, Mestat (ed.), Presses de l'ENPC/LCPC, Paris*, (pp. 529-536).

Burns, S. A., Arora, J. S., Balling, R., Cheng, F. Y., Estes, A. C., Foley, C. M., et al. (2002). *Recent advances in optimal structural design.* (S. A. Burns, Éd.)

Cao, X., & Yan, S. (2013). Numerical analysis for earthquake dynamic responses of tunnel with different lining rigidity based on finite element method. *Information Technology Journal*, *12*, 2599-2604.

Cavalaro, S. H., & Aguado, A. (2011). Packer behavior under simple and coupled stresses. *Tunnelling and Underground Space Technology*, *28*, 159-173.

Cavalaro, S. H., Blom, C. B., Walraven, J. C., & Aguado, A. (2012). Structural analysis of contact deficiencies in segmented lining. *Tunnelling and Underground Space Technology*, *26*, 734-749.

CEN. *Eurocode 8: Design of Structures for Earthquake Resistance. Part 1-1: General Rules, Seismic Actions and Rules for Buildings. European Committee for Standardization 2004, Bruxelles, Belgium.*

Chakeri, H., Hasanpour, R., Hindistan, M., & Ünver, B. (2011). Analysis of interaction between tunnels in soft ground by 3D numerical modeling. *Bull Eng Geol Environ*, *70*, 439-448.

Chakeri, H., Ozcelik, Y., & Unver, B. (2013). Effects of important factors on surface settlement prediction for metro tunnel excavated by EPB. *Tunnelling and Underground Space Technology*, *36*, 14–23.

Channabasavaraj, W., & Vishwanath, B. (2012). Influence of relative position of the tunnels - Numerical analysis on interaction between twin tunnels. *Proceedings of Indian Geotechnical Conference December 13-15, 2012, Delhi*, (pp. 500-503).

Chapman, D. N., Ahn, S. K., & Hunt, D. V. (2007). Investigating ground movements caused by the construction of multiple tunnels in soft ground using laboratory model tests. *Canadian Geotechnical Journal, 44(6)*, 631-643.

Chapman, D. N., Ahn, S. K., Hunt, D. V., & Chan, A. H. (2006). The use of model tests to investigate the ground displacements associated with multiple tunnel construction in soil. *Tunnelling and Underground Space Technology*, *21*, 413.

Chen, J., Jiang, L., Li, J., & Shi, X. (2012). Numerical simulation of shaking table test on utility tunnel under non-uniform earthquake excitation. *Tunnelling and Underground Space Technology*, *30*, 205-216.

Chen, R. P., Zhu, J., Liu, W., & Tang, X. W. (2011). Ground movement induced by parallel EPB tunnels in silty soils. *Tunnelling and Underground Space Technology*, *26*, 163-171.

Chen, S. L., & Gui, M. W. (2011). Seismic performance of tunnel lining of side-by-side and vertically stacked twin-tunnels. *Journal of Cent. South Univ. Technol.*, *18*, 1226-1234.

Chen, S. L., Gui, M. W., & Yang, M. C. (2012). Applicability of the principle of superposition in estimating ground surface settlement of twin- and quadruple-tube tunnels. *Tunnelling and Underground Space Technology*, *28*, 135–149.

Chen, W. (2000). *Practical analysis for semi-rigid frame design.* World Scientific Pub Co Inc.

Chen, S., Gui, M., & Yang, M. (2012b). Applicability of the principle of superposition in estimating ground surface settlement of twin- and quadruple-tube tunnels. *Tunnelling and Underground Space Technology*, *28*, 135-149.

Cheng, S. J. (1985). *The analysis of the joint mechanism of shield-driven tunnel lining.* M. Phil. Thesis,, Dept. of Geotechnics, Tongji University, P.R. China.

Choi, J. I., & Lee, S. W. (2010). Influence of existing tunnel on mechanical behaviour of new tunnel. *KSCE Journal of Civil Engineering*, *14(5)*, 773-783.

Chong, P. T., Tang, S. K., Lim, T. L., Sugawara, S., & Furusono, T. (2004). Bored tunnel lining design in soft soils - A comparison between analytical and numerical analyses. *Tunnelling and Underground Space Technology. Underground space for sustainable urban development. Proceedings of the 30th ITA-AITES World Tunnel Congress*, *19(4-5)*, 456.

Chow, W. L., Tang, S. K., & Tong, S. Y. (2009). Design of segmental tunnel lining in an earthquake zone. *ITA-AITES World Tunnel Congress 2009 "Safe Tunnelling For The City and Environment", Budapest.*

Cilingir, U., & Madabhushi, S. P. (2010). Effect of depth on seismic response of circular tunnels. *Canadian Geotechnical Journal*, *48*, 117-127.

Conti, R., Viggiani, G. M., & Perugini, F. (2013). Numerical modelling of centrifuge dynamic tests of circular tunnels in dry sand. *Acta Geotechnica, doi: 10.1007/s11440-013-0286-8*.

Corigliano, M., Scandella, L., Lai, C. G., & Paolucci, R. (2011). Seismic analysis of deep tunnels in near fault conditions: a case study in Southern Italy. *Bull Earthquake Eng.*, *9*, 975-995.

Croce, A. (2011). *Analisi dati di monitoraggio del rivestimento della galleria del passante ferroviario di Bologna.* Ph.D. dissertation, Polytechnics of Turin, Italy.

Csébfalvi, A. (2007). Optimal design of frame structures with semi-rigid joints. *Civil Engineering*, *51(1)*, 9-15.

De Brost, K., Van de Broek, W. L., & Groen, A. E. (1996). Two and three dimensional numerical modelling of a guided pipejacking in soft soil. *Geotechnical aspects of underground construction in soft ground, London, April 1996. Balkema, Rotterdam.*

Dean, A., Young, D. J., & Kramer, G. J. (2006). The use and performance of precast concrete tunnel linings in seismic areas. *IAEG2006 Paper number 679.*

Debiasi, E., Gajo, A., & Zonta, D. (2013). On the seimic response of shallow-buried rectangular structures. *Tunnelling and Underground Space Technology*, *38*, 99-113.

Dias, D., & Kastner, R. (2013). Movements caused by the excavation of tunnels using face pressurized shields - Analysis of monitoring and numerical modelling results. *Engineering Geology, 152(1)*, 17-25.

Dias, D., & Kastner, R. (2000). Slurry shield tunneling: Comparison between in situ data and three dimensional numerical simulations. *Geotech-Year 27-30 Nov. 2000, Bangkok, Thailand.*

Dias, D., Kastner, R., & Maghazi, M. (2000). Three dimensional simulation of slurry shield tunnelling. *Geotechnical Aspects of Underground Construction in Soft Ground, Kusakabe, Fujita and Miyazaki (eds.), Balkema, Rotterdam*, (pp. 351-356).

Ding, W. Q., Yue, Z. Q., Tham, L. G., Zhu, H. H., Lee, C. F., & Hashimoto, T. (2004). Analysis of shield tunnel. *International Journal for Numerical and Analytical Methods in Geomechanics*, *28*, 57-91.

Divall, S. (2013). *Ground movements associated with twin-tunnel construction in clay. (Unpublished Doctoral thesis, download from the link: openaccess.city.ac.uk/2437/1/Divall,_Sam.pdf?).* Ph.D. dissertation, City University London.

Divall, S., Goodey, R. J., & Taylor, R. N. (2012). Ground movements generated by sequential twin-tunnelling in over-consolidated clay. *2nd European Conference on Physical Modelling in Geotechnics, Delft, The Netherlands.*

Do, N. A., Dias, D., Oreste, P. P., & Djeran-Maigre, I. (2012). Numerical investigation of surface settlements above a tunnel: Influence of segmental joints and deformability of ground. *Proceeding of 2nd International Conference on Advances in Mining and Tunnelling, Vietnam, ISBN: 978-604-913-081-6*, (pp. 251-258).

Do, N. A., Dias, D., Oreste, P. P., & Djeran-Maigre, I. (2013a). 2D numerical investigation of segmental tunnel lining behavior. *Tunneling and Underground Space Technology*, *37*, 115-127.

Do, N. A., Dias, D., Oreste, P. P., & Djeran-Maigre, I. (2013b). 3D Modelling for mechanized tunnelling in soft ground - Influence of the consititutive model. *American Journal of Applied Sciences*, *10(8)*, 863-875.

Do, N. A., Dias, D., Oreste, P. P., & Djeran-Maigre, I. (2014a). 2D tunnel numerical investigation - the influence of the simplified excavation method on tunnel behaviour. *Geotechnical and Geological Engineering*, *32(1)*, 43-58.

Do, N. A., Dias, D., Oreste, P. P., & Djeran-Maigre, I. (2014b). A new numerical approach to the Hyperstatic Reaction Method for segmental tunnel linings. *International Journal for Numerical and Analytical Methods in Geomechanics*, *in press*.

Do, N. A., Dias, D., Oreste, P. P., & Djeran-Maigre, I. (2014c). Three-dimensional numerical simulation of a mechanized twin tunnels in soft ground. *Tunnelling and Underground Space Technology*, *42,* 40-51.

Do, N. A., Dias, D., Oreste, P. P., & Djeran-Maigre, I. (2014d). The behaviour of the segmental tunnel lining studied by the Hyperstatic Reaction Method. *European Journal of Environmental and Civil Engineering, 18(4),* 489-510.

Do, N. A., Dias, D., Oreste, P. P., & Djeran-Maigre, I. (2014e). 2D Numerical investigation of twin tunnel interaction. *Geomechanics and Engineering, 6(3),* 263-275.

Do, N. A., Dias, D., Oreste, P. P., & Djeran-Maigre, I. (2014f). Three-dimensional numerical simulation for mechanized tunnelling in soft ground: the influence of the joint pattern. *Acta Geotechnica*, *Doi: 10.1007/s11440-013-0279-7*.

Duddeck, H., & Erdmann, J. (1985). On structural design models for tunnels in soft soil. *Underground Space*, *9(5-6)*, 246-253.

Einstein, H. H., & Schwartz, C. W. (1979). Simplified analysis for tunnel supports. *Journal of Geotechnical Engineering, 105, GT4*, 499-517.

Ercelebi, S. G., Copour, H., & Ocak, I. (2011). Surface settlement predictions for Istanbul metro tunnels excavated by EPB-TBM. *Springer. Environ Earth Sci*, *62*, 357-365.

Fahimifar, A., & Vakilzadeh, A. (2009). Numerical and analytical solutions for ovaling deformation in circular tunnels under seismic loading. *International Journal of Recent Trends in Engineering*, *1(6)*, 30-35.

Fattah, M. Y., Shalash, K. T., & Salim, N. M. (2013). Prediction of settlement trough induced by tunnelling in cohesive ground. *Acta Geotechnica*, *8*, 167-179.

Filho, M. S., Guimarães, M. J., Sahlit, C. L., & Brito, J. L. (2004). Wind pressures in frame structures with semi-rigid connections. *Journal of the Brazilian Society of Mechanical Sciences and Engineering*, *26(2)*, 180-189.

Franzius, J. N. (2004). *Behaviour of buildings due to tunnel induced subsidence.* Ph.D. dissertation, Imperial College of Science, Technology and Medicine, University of London.

Franzius, J. N., & Potts, D. M. (2005). Influence of mesh geometry on three-dimensional finiteelement analysis of tunnel excavation. *ASCE Int. J. Geomech.*, *5(3)*, 256-266.

Franzius, J. N., Potts, D. M., & Burland, J. B. (2005). The influence of soil anisotropy and K0 on ground surface movements resulting from tunnel excavation. *Geotechnique*, *55(3*, 189–199.

Gomes, R. C. (2013). Effect of stress disturbance induced by construction on the seismic response of shallow bored tunnel. *Computer and Geotechnics*, *49*, 338-351.

Gomes, R. C. (2000). *Seismic behaviour of tunnels under seismic load.* Master's thesis, Instituto Superior Técnico, Technical University of Lisbon.

Grange, S. (2008). *Risque sismique: stratégie de modélisation pour simuler la réponse des structures en béton et leurs interactions avec le sol.* Ph.D. dissertation, INPG.

Groeneweg, T. W. (2007). *Shield driven tunnels in ultra high strength concrete, reduction of the lining thickness.* Master's thesis, Delft University of Technology, Delft, The Netherlands.

Gruebl, F. (2006). Modern design aspects of segmental lining. *CPT-ITA Congress.*

Hage Chehade, F., & Shahrour, I. (2008). Numerical analysis of the interaction between twin-tunnels: Influence of the relative position and construction procedure. *Tunnelling and Underground Space Technology*, *23*, 210-214.

Hasan, S., Elliot, K. S., & Ferreira, M. A. (2011). Experimental in investigation on the moment continuity of precast concrete beam-column connections under gravity loads. *In: Symposium Prague 2011*, (pp. 395-398).

Hasanpour, R., Chakeri, H., Ozcelik, Y., & Denek, H. (2012). Evaluation of surface settlements in the Istanbul metro in terms of analytical, numerical and direct measurements. *Bull Eng Geol Environ*, *71*, 499-510.

Hashash, Y. M., Hook, J. J., Schmidt, B., & Yao, J. I. (2001). Seismic design and analysis of underground structures. *Tunnelling and Und*, *16(4)*, 247-293.

Hashash, Y. M., Park, D., & Yao, J. I. (2005). Ovaling deformations of circular tunnels under seismic loading, an update on seismic design and analysis of underground structures. *Tunnelling and Underground Space Technology*, *20*, 435–441.

Hasimoto, T., Brinkman, J., Konda, T., Kano, Y., & Fedema, A. (2004). Simultaneous backfill grouting, pressure development in construction phase and in the long-term. *Proceeding of the 30th ITA-AITES World Congress, Singapore*, (pp. 52-59).

He, C., & Koizumi, A. (2000). Dynamic behaviour in transverse direction of shield tunnel with considering effect of segment joints. *12WCEE2000, paper 0362*.

He, C., Feng, K., Fang, Y., & Jiang, Y. C. (2012). Surface settlement caused by twin-parallel shield tunnelling in sandy cobble strata. *Journal of Zhejiang University-SCIENCE A (Applied Physics \& Engineering) ISSN 1673-565X (Print); ISSN 1862-1775 (Online)*, *13(11)*, 858-869.

Hefny, A., & Chua, H. (2006). An investigation into the behavior of jointed tunnel lining. *Tunnelling and Underground Space Technology*, *21*, 428.

Hefny, A., Chua, H., & Jhao, J. (2004). Parametric studies on the interaction between existing and new bored tunnels. *Tunnelling and Underground Space Technology*, *19*, 471.

Hejazi, Y., Dias, D., & Kastner, R. (2008). Impact of constitutive models on the numerical analysis of underground constructions. *Acta Geotechnica*, *3*, 251-258.

Hordijk, D. A., & Gijsbers, F. B. (1996). *Laboratoriumproeven tunnel segmenten.* Tech. rep., TNO-rapport 96-CON-R0708/03 (COB-K100-rapport K100-W-026), TNO Bouw.

Hossaini, S. M., Shaban, M., & Talebinejad, A. (2012). Relationship between twin tunnels distance and surface subsidence in soft ground of Tabriz metro - Iran. *12th Coal Operator's Conference, University of Wollongong \& the Australasian Institute of mining and Metallurgy*, (pp. 163-168).

Hudoba, I. (1997). Contribution to static analysis of load-bearing concrete tunnel lining built by shield-driven technology. *Tunnelling and Underground Space Technology*, *12(1)*, 55-58.

Huebner, K. H., Dewhirst, D. L., Smith, D. E., & Byrom, T. G. (2001). *The finite element method for engineers.* John Wiley and Sons, inc., New York.

Hung, C. J., Monsees, J., Munfah, N., & Wisniewski, J. (2009). *Technical manual for design and construction of road tunnels - Civil elements.* Tech. rep., Report N° FHWA-NHI-10-034.

Hunt, D. V. (2005). *Predicting the ground movements above twin tunnels constructed in London Clay*. Ph.D. dissertation, University of Birmingham.

ITA. (1988). ITA guidelines for the design of tunnels. *Tunnelling and Underground Space Technology*, *3(3)*, 237-249.

ITA. (1982). Views on structural design models for tunnelling. *Advances in tunneling technology and subsurface use*, *2(3)*, 153-228.

Itasca. (2009). FLAC Fast Lagrangian Analysis of Continua, Version 4.0. User's manual. *FLAC Fast Lagrangian Analysis of Continua, Version 4.0. User's manual* .

Janin, J. P. (2012). *Tunnels en milieu urbain: Prévisions des tassements avec prise en compte des effets des pré-soutènements (renforcement du front de taille et voûte-parapluie)*. Ph.D. dissertation, N° d'ordre 2012ISAL0038, INSA de Lyon.

Janin, J. P., Dias, D., Kastner, R., Emeriault, F., Le Bissonnais, H., & Guillou, A. (2013). South Toulon tube: numerical back-analysis of in situ measurements. *Plaxis Bull*, *33*, 10–13.

Janssen, P. (1983). Tragverhalten von Tunnelausbauten mit Gelenktübbings. *Report-No. 83-41 University of Braunschweig, Department of civil engineering, Institute for structural analysis.*

Jenck, O., & Dias, D. (2004). Analyse tridimensionnelle en différences finies de l'interaction entre une structure en béton et le creusement d'un tunnel à faible profondeur. *Géotechnique*, *54(8)*, 519-528.

Jenck, O., & Dias, D. (2003). Numerical analysis of the volume loss influence on building during tunnel excavation. *Third Int, FLAC Symp. - FLAC and FLAC3D Numerical Modelling in Geomechanics, Sudbury, Canada.*

JSCE. (1996). *Japanese standard for shield tunnelling*. Tunnel Engineering Committee English Edition of Japanese Standard for Tunnelling, Subcommitteee Japan Scociety of Civil Engineers, The third edition, Tokyo.

Kaneshiro, J., & Sinha, M. (2008). Simplified seismic design approach using pushover considerations and ring compression theory for a concrete segmented liner. *World Tunnel Congress 2008 - Underground Facilities for Better Environment and Safety - India*, (pp. 462-472).

Karakus, M. (2007). Appraising the methods accounting for 3D tunnelling effects in 2D plane strain FE analysis. *Tunnelling and Underground Space Technology*, *22*, 47-56.

Karakus, M., Ozsan, A., & Basarir, H. (2007). Finite element analysis for the twin metro tunnel constructed in Ankara Clay, Turkey. *Bull Eng Geol Env*, *66*, 71-79.

Kartal, M. E., Basaga, H. B., Bayraktar, A., & Muvafik, M. (2010). Effects of semi-rigid connection on structural responses. *Electronic journal of structural Engineering*, *10*, 22-35.

Kasper, T., & Meschke, G. (2004). A 3D finite element simulation model for TBM tunnelling in soft ground. *International Journal for Numerical and Analytical Methods in Geomechanics*, *28*, 1441-1460.

Kasper, T., & Meschke, G. (2006). A numerical study of the effect of soil and grout material properties and cover depth in shield tunnelling. *Computers and Geotechnics*, *33(4-5)*, 234-247.

Kasper, T., & Meschke, G. (2006). On the influence of face pressure, grouting pressure and TBM design in soft ground tunneling. *Tunnelling and Underground Space Technology*, *21*, 160-171.

Kaveh, A., & Moez, H. (2008). Minimal cycle bases for analysis of frames with semi-rigid joints. *Computers and Structures*, *86*, 503-510.

Khoshnoudian, F., & Shahrour, I. (2002). Numerical analysis of the seismic behaviour of tunnels constructed in liquefiable soils. *Journal Soils and Foundation*, *42(6)*, 1-8.

Kim, S. H., Burd, H. J., & Milligan, G. W. (1996). Interaction between closely spaced tunnel in clay. *Proc. International Symposium on Geotechnical Aspects of Underground Construction in Soft Ground*, (pp. 543-548).

Kim, S. H., Burd, H. J., & Milligan, G. W. (1998). Model testing of closely spaced tunnels in clay. *Geotechnique*, *48(3)*, 375-388.

Klappers, C., Grübl, F., & Ostermeier, B. (2006). Structural analyses of segmental lining - coupled beam and spring analyses versus 3D-FEM calculations with shell elements. *Tunnelling and Underground Space Technology*, *21*, 254-255.

Klotz, U., Vermeer, P. A., Klotz, C., & Moller, S. (2006). A 3D finite element simulation of a shield tunnel in weathered Singapore Bukit Timah Granite. *Tunnelling and Underground Space Technology (AITES-ITA world tunnel congress; Safety in the underground space)*, *21(3/4)*, 272.

Koelewijn, A. R., & Verruijt, A. (2001). Simplified three-dimensional numerical modelling of shield tunnel advancement. *Proc. XV Int. Conf. Soil Mech. And Geotech. Engng., Istanbul 27–31, August*, (pp. 1463–1466).

Kolymbas, D. (2005). *Tunnelling and tunnel mechanics* (Vol. ISBN-10 3-540-25196-0). Springer Berlin Heidelberg New York.

Kontoe, S., Zdravkovic, L., Potts, D. M., & Menkiti, C. O. (2008). Case study on seismic tunnel response. *Canadian Geotechnical Journal*, *45*, 1743-1764.

Kouretzis, G., Sloan, S. W., & Carter, J. P. (2013). Effect of interface friction on tunnel liner internal forces due to seismic S- and P-wave propagation. *Soil Dy*, *46*, 41-51.

Koyama, Y. (2003). Present status and technology of shield tunneling method in Japan. *Tunneling and Underground Space Technology*, *18*, 145-159.

Kramer, G. J., Sederat, H., Kozak, A., Liu, A., & Chai, J. (2007). Seismic response of precast tunnel lining. *Proceedings of the Rapid Exacavation and Tunnelling Concference*, (pp. 1225-1242).

Kuhlemeyer, R. L., & Lysmer, J. (1973). Finite element method accuracy for wave propagation problems. *Journal of Soil Mech. \& Foundations, Div. ASCE*, *99(SM5)*, 421-427.

Lambrughi, A., Rodríguez, L. M., & Castellanza, R. (2012). Development and validation of a 3D numerical model for TBM-EPB mechanised excavations. *Computers and Geotechnics, 40*, 97-113.

Lanzano, G., Bilotta, E., Russo, G., Silvestri, F., & Madabhushi, S. P. (2010). Dynamic centrifuge tests on shallow tunnel models in dry sand. *VII International Conference on Physical Modelling in Geotechnics, Zurich*.

Laver, R. (2010). *Long-term behaviour of twin tunnels in London Clay*. Ph.D. dissertation, Corpus Christi College, University of Cambridge.

Leca, E. (1989). *Analysis of NATM and shield tunnelling in soft ground*. Ph.D. dissertation, Virginia Institute and State University, Blacksburg, Va.

Lee, D. H., Choi, Y. T., & Kim, D. H. (2007). A study on the seismic design methods for precast concrete lining (PCL). *Underground Space - the 4th Dimension of Metropolises - Barták, Hrdina, Romancov \& Zlámal (eds)© 2007, Taylor \& Francis Group, London, ISBN 978-0-415-40807-3*.

Lee, K. M., & Ge, X. W. (2001). The equivalence of a jointed shield-driven tunnel lining to a continuous ring structure. *Canadian Geotechnical Journal*, *38(3)*, 461-483.

Lee, K. M., & Rowe, R. K. (1991). An analysis of three-dimensional ground movements: the Thunder Bay tunnel. *Canadian Geotechnical Journal*, *28*, 25-41.

Lee, K. M., Hou, X. Y., Ge, X. W., & Tang, Y. (2001). An analytical solution for a jointed shielddriven tunnel lining. *International Journal of Analytical and Numerical Methods in Geomechanics*, *25*, 365-390.

Leonhard, F., & Reimann, H. (1966). Betongelenke. *Der Bauingenieur*, *41*, 49-56.

Li, X., Du, S., & Zhang, D. (2010). Numerical simulation of the interaction between two parallel shield tunnels. *Proceeding of ICPTT 2012: Better Pipeline Infrastructure for a Better Life*, (pp. 1521-1533).

Liu, H. Y., Small, J. C., & Carter, J. P. (2008). Full 3D modeling for effects of tunnelling on existing support systems in the Sydney region. *Tunnelling and Underground Space Technology*, *23*, 399-420.

Liu, J. H., & Hou, X. Y. (1991). Shield-driven tunnels. *China Railway Press, Beijing, China*, 152-303.

Lu, L., Lu, X. L., Fan, P. F., & Guo, Z. J. (2005). Experimental study of a double-circular shield tunnel lining. *Proc. of the First International Conference on Advances in Experimental Structural Engineering, Nagoya, Japan, July 2005*, (pp. 127-134).

Lu, L., Lu, X., & Fan, P. (2006). Full-ring experimental study of the lining structure of Shanghai Changjiang tunnel. *4th International Conference on Earthquake Engineering Taipei, Taiwan October 12-13, 2006.*

Luttikholt, A. (2007). *Ultimate limit state analysis of a segmented tunnel lining - Results of full-scale tests compared to finite element analysis.* Master's thesis, Delft University.

Lyngs, J. H. (2008). *Model accuracy in a seismic design of immersed tunnel.* Master's thesis, Master of Science in Civil and Structural Engineering The School of Civil Engineering, Aalborg University.

Ma, L., Ding, L., & Luo, H. (2014). Non-linear description of ground settlement over twin tunnels in soil. *Tunnelling and Underground Space Technology*, *42*, 144-151.

Maidl, B., Herrenknecht, M., & Anheuser, L. (1996). *Mechanized shield tunnelling.* Ernst and Sohn, Berlin.

Maranha, J. R., & Neves, E. M. (2000). 3D analysis of ground displacements due to the construction of Lisbon underground. *Proceedings of the International Conference on Geotechnical \& Geological Engineering (GeoEng 200), Melbourne.*

Mashimo, H., & Ishimura, T. (2003). Evaluation of the load on a shield tunnel lining in gravel. *Tunnelling and Underground Space Technology*, *18*, 233-241.

Mashimo, H., & Ishimura, T. (2005). Numerical modelling of the behavior of shield tunnel lining during assembly of a tunnel ring. *5th International Symposium Geotechnical Aspects of Underground Construction in soft ground.*

Mašin, D. (2009). 3D modelling of a NATM tunnel in high K0 clay using two different constitutive models. *Journal of Geotechnical and Geoenvironmental Engineering ASCE*, *135(9)*, 1326–1335.

Mašin, D., & Herle, I. (2005). Numerical analyses of a tunnel in London clay using different constitutive models. *In: Proceedings of the 5th international symposium TC28 geotechnical aspects of underground construction.*

Medina Rodríguez, L. E. (2000). *Estudio de los movimientos originados por la excavación de túneles con escudos de presión de tierras en los suelos tosquizos de Madrid.* Ph.D. dissertation, University of La Coruña. (in Spanish).

Medina Rodríguez, L. E. (2008). Modelizacion de la excavacion de tuneles mediante EPB: Diferencias finitas y elementos discretos. *Technical Seminar: Tunnels with EPB Simulation and Control of TBM Barcelona*, (pp. 73-104).

Melis, M., Medina, L., & Rodriguez, J. M. (2002). Prediction and analysis of subsidence induced by shield tunneling in the Madrid Metro extension. *Canadian Geotechnical Journal*, *39*, 1273-1287.

Migliazza, M., Chiorboli, M., & Giani, G. P. (2009). Comparison of analytical method, 3D finite element model with experimental subsidence measurements resulting from the extension of the Milan underground. *Computers and Geotechnic*, *36*, 113-124.

Mirhabibi, A., & Soroush, A. (2012). Effects of surface buildings on twin tunnelling-induced ground settlements. *Tunnelling and Underground Space Technology*, *29*, 40-51.

Mohamad, H., Soga, K., Bennett, P. J., Mair, R. J., & Lim, C. S. (2012). Monitoring twin tunnel interaction using distributed optical fiber strain measurements. *Journal of Geotechnical and Geoenvironmental Engineering*, *138*, 957-967.

Möller, S. C., & Vermeer, P. A. (2008). On numerical simulation of tunnel installation. *Tunnelling and Underground Space Technology*, *23*, 461-475.

Möller, S. (2006). *Tunnel induced settlements and structural forces in linings.* Ph.D. dissertation, Stuttgart University.

Mollon, G. (2010). *Etude déterministe et probabiliste du comportement des tunnels.* Ph.D. dissertation, INSA de Lyon. N° d'ordre 2010ISAL0110.

Mollon, G., Dias, D., & Soubra, A. H. (2013). Probabilistic analyses of tunnelling-induced ground movements. *Acta Geotechnica*, *8*, 181-199.

Monforton, G. R., & Wu, T. S. (1963). Matrix analysis of semi-rigidly connected frames. *Journal of Structural Engineering, ASCE, 89, ST6*, 13-42.

Mroueh, H., & Shahrour, I. (2008). A simplified 3D model for tunnel construction using tunnel boring machines. *Tunnelling and Underground Space Technology*, *23*, 38-45.

Muir Wood, A. M. (1975). The circular tunnel in elastic ground. *Géotechnique, 25(1)*, 115-127.

Muniz de Farias, M., Júnior, A. H., & Pacheco de Assis, A. (2004). Displacement control in tunnels excavated by the NATM: 3-D numerical simulations. *Tunnelling and Underground Space Technology*, *19(3)*, 283-293.

Naggar, H. E., & Hinchberger, S. D. (2008). An analytical solution for jointed tunnel linings in elastic soil or rock. *Canadian Geotechnical Journal*, *45*, 1572-1593.

Naggar, H. E., & Hinchberger, S. D. (2012). Approximate evaluation of stresses in degraded tunnel linings. *Soil Dynamics and Earthquake Engineering*, *43*, 45-57.

Naggar, H. E., Hinchberger, S. D., Hesham, M., & Naggar, E. I. (2008). Simplified analysis of sesmic in-plane stresses in composite and jointed tunnel linings. *Soil Dynamics and Earthquake Engineering*, *28(12)*, 1063–1077.

Negro, A., & Queiroz, B. I. (1999). Prediction and performance of soft ground tunnels. *Geotechnical Aspects of Underground Construction in Soft Ground, 1999. Balkema, Tokyo, Japan*, (pp. 409-418).

Ng, C. W., & Lu, H. (2014). Effects of the construction sequence of twin tunnels at different depths on an existing pile. *Canadian Geotechnical Journal*, *51*, 173-183.

Ng, C. W., Lee, K. M., & Tang, D. K. (2004). Three-dimensional numerical investigations of new Austrian tunnelling method (NATM) twin tunnel interactions. *Canadian Geotech. Journal*, *41*, 523-539.

Ng, C. W., Lu, H., & Peng, S. Y. (2013). Three-dimensional centrifuge modelling of the efects of twin tunnelling on an existing pile. *Tunnelling and Underground Space*, *35*, 189-199.

Nguyen, D. T. (2006). *TBM and Lining - Essential Interfaces.* Master's thesis, Politecnico of Torino.

Nishida, M., & Matsui, T. (2004). Applicability of seismic deformation method to aseismic analysis of underground linear structure. *Proceedings of the 14th International Offshore and Polar Engineering Conference, Toulon, France.*

Nishikawa, K. (2003). Development of a prestressed and precast concrete segmental lining. *Tunnelling and Underground Space Technology*, *18*, 243-251.

Ocak, I. (2013). Interaction of longitudinal surface settlements for twin tunnels in shallow and soft soils: the case of Istanbul Metro. *Environ Earth Sci.*, *69*, 1673–1683.

Oreste, P. P. (2007). A numerical approach to the hyperstatic reaction method for the dimenshioning of tunnel supports. *Tunnelling and Underground space technology*, *22*, 185-205.

Oreste, P. P. (2003). Analysis of structural interaction in tunnels using convergence-confinement approach. *Tunnelling and Underground space technology*, *18*, 347-363.

Owen, G. N., & Scholl, R. E. (1981). *Earthquake engineering of large underground structures.* Tech. rep., Report N°. FHWA/RD-80/195. Federal Highway Administration and National Science Foundation.

Pakbaz, M. C., & Yareevand, A. (2005). 2-D analysis of circular tunnel against earthquake loading. *Tunnelling and U*, *20*, 411-417.

Panet, M., & Guenot, A. (1982). Analysis of convergence behind the face of a tunnel. *Proceedings of the International Symposium. Tunneling-82*, (pp. 187-204).

Papanikolaou, V. K., & Kappos, A. J. (2013). Practical nonlinear analysis of unreinforced concrete tunnel linings. *Tunnelling and Underground Space Technology*, *40*, 127-140.

Park, K. H., Tantayopin, K., & Tontavanich, B. (2006). Analytical solutions for seismic design of tunnel lining in Bangkok MRT subway. *International Symposium on Underground Excavation and Tunnelling 2-4 February 2006, Bangkok, Thailand.*

Park, K. H., Tantayopin, K., Tontavanich, B., & Owatsiriwong, A. (2009). Analytical solution for seismic-induced ovaling of circular tunnel lining under no-slip interface conditions: A revisit. *Tunnelling and*, *24*, 231-235.

Peck, R. B., Hendron, A. J., & Mohraz, B. (1972). State of the art of soft ground tunneling. *In: Proceedings of 1st Rapid Excavation and Tunneling Conference, AIME Chicago; vol 1: 259–285.*

Penzien, J., & Wu, C. L. (1998). Stresses in linings of bored tunnels. *Int. J. Earthquake Eng. Struct. Dynamics*, *27*, 283–300.

Penzien, Z. (2000). Seismically induced racking of tunnel linings. *Int. J. Earthquake Eng. Struct. Dynamic*, *29*, 683–691.

Phienwej, N., Hong, C. P., & Sirivachiraporn, A. (2006). Evaluation of ground movements in EPB-shield tunnelling for Bangkok MRT by 3D-numerical analysis. *Tunnelling and Underground Space Technology*, *21(3-4)*, 273.

Pinheiro, L., & Silveira, R. A. (2005). Computational procedures for nonlinear analysis of frames with semi-rigid connections. *Latin American Journal of Solids and Structures*, *2*, 339-367.

Plizzari, G. A., & Tiberti, G. (2006). Steel fibers as reinforcement for precast tunnel segments. *Tunnelling and Underground Space Technology*, *21(3-4)*, 438-439.

Rijke, Q. C. (2006). *Innovation of stress and damage reduction in bored tunnels during construction based on a shield equilibrium model.* Ph.D. dissertation, Utrecht: Delft University of Technology and Holland Railconsult.

Romero, V. S., & Caufield, R. J. (2012). Improving the seismic resilience of lifeline tunnels. *2012 NZSEE conference, paper 064.*

Rowe, R. K., Lo, K. Y., & Kack, K. J. (1983). A method of estimating surface settlement above shallow tunnels constructed in soft ground. *Canadian Geotechnical Journal*, *20*, 11-22.

Sagaseta, C., Sanchez-Alciturri, J. M., Gonzalez, C., Lopez, A., P., G., & Pina, R. (1999). Soil deformations due to the excavation of two parallel underground cavern. *Proc. 12th European Conference Soil Mechanics and Foundation Engineering, Amsterdam, vol. 3*, (pp. 2125-2131).

Schreyer, J., & Winselmann, D. (2000). Suitability tests for the lining for the 4th Elbe tunnel tube - Results of large-scale tests. *Tunnel, 1*, 34-44.

Schulze, H., & Duddeck, H. (1964). Spannungen in schildvorgetrieben tunneln. *Beton and Stahlbetonbau, 8*, 169-175.

Sederat, H., Kozak, A., Hashash, Y. M., Shamsabadi, A., & Krimotat, A. (2009). Contact interface in seismic analysis of circular tunnels. *Tunnelling and Underground Space Technology, 24*, 482-490.

Sekulovic, M., & Salatic, R. (2001). Nonlinear analysis of frames with flexible connections. *Computers and structures, 79*, 1097-1107.

Shahrour, I., Khoshnoudian, F., Sadek, M., & Mroueh, H. (2010). Elastoplastic analysis of the seismic response of tunnels in soft soils. *Tunnelling and Under, 25*, 478-482.

Simic, D. (2006). Building damage potential due to tunnel settlements. *4th International FLAC Symposium on Numerical Modelling in Geomechanics - 2006 - Hart \& Varona (eds.)*, (pp. 63-69).

Sliteen, L. (2013). *Modélisation Tridimensionnelle du comportement sismique des tunnels en terrain meuble.* Ph.D. dissertation, Université Lille1 Sciences et Technologies.

Sliteen, L., Mroueh, H., & Sadek, M. (2013). Three-dimensional modeling of the behaviour of shallow tunnel under seismic load. *20ème Congrès Francais de Méchanique (CFM2011)*.

Surarak, C. (2010). *Geotechnical aspects of the Bangkok MRT blue line project.* Ph.D. dissertation, Griffith University.

Suwansawat, S. (2007). Lining response of twin tunnels affected by EPB shield operation. *Underground Space – the 4th Dimension of Metropolises – Barták, Hrdina, Romancov\& Zlámal (eds) © 2007 Taylor \& Francis Group, London*, (pp. 1261-1266).

Suwansawat, S., & Einstein, H. H. (2007). Describing settlement troughs over twin tunnels using a superposition technique. *Journal of Geotechnical and Geoenvironmental Engineering, 133(4)*, 445-468.

Svoboda, T., & Mašin, D. (2009). Comparison of displacement field predicted by 2D and 3D finite element modelling of shallow NATM tunnels in clays. *Geotechnik, 34*, 115-126.

Svoboda, T., Mašin, D., & Bohac, J. (2010). Class A predictions of a NATM tunnel in stiff clay. *Computers and Geotechnics, 37(6)*, 817–825.

Swoboda, G. (1979). Finite element analysis of the New Austrian Tunnelling Method (NATM). *Proc. 3rd Int. Conf. Num. Meth. Geomech., Aachen, Vol 2*, (p. 581).

Swoboda, G., Kenawi, M. A., & Ramadan, E. H. (2004). Numerical investigation of TBM tunnelling in consolidated clay. *Tunnelling and Underground Space Technology*, *19(4)*, 459.

Takano, Y. H. (2000). Guidelines for the design of shield tunnel lining. *Tunneling and Underground Space Technology*, *15(3)*, 303-331.

Talmon, A. M., & Bezuijen, A. (2009). Simulating the consolidation of TBM grout at Noordplaspolder. *Tunnelling and Underground Space Technology*, *24(5)*, 493–499.

Teachavorasinskun, S., & Chub-Uppakarn, T. (2008). Experimental verification of joint effects on segmental tunnel lining. *Electronic Journal of Geotechnical Engineering*, *14*.

Teachavorasinskun, S., & Chub-Uppakarn, T. (2010). Influence of segmental joints on tunnel lining. *Tunnelling and Underground Space Technology*, *25*, 490-494.

Thienert, C., & Pulsfort, M. (2011). Segment design under consideration of the material used to fill the annular gap. *Geomechanics and Tunneling*, *4*, 665-679.

Torcato, D. M. (2010). *Seismic behaviour of shallow tunnels in stratified ground.* Master's thesis, Univeridade Ténica de Lisboa.

USACE. (1997). *Tunnels and shafts in rock, Engineer manual EM 1110-2-2901.*

Van Oorsouw, R. S. (2010). *Behaviour of segment joints in immersed tunnels under seismic loading.* Master's thesis, Delft University of Technology.

Vermeer, P. A., & Brinkgreve, R. (1993). *Plaxis version 5 manual.*

Wang, J. G., Kong, S. L., & Leung, C. F. (2003). Twin tunnels-induced ground settlement in soft soil. *Proceeding of the Sino-Japanese Symposium on Geotechnical Engineering, Beijing, China, 29-30 October 2003*, (pp. 241-244).

Wang, J. N. (1993). *Seismic design of tunnels: A state-of-the-art approach,.* (m. 7. Monograph, Éd.) Brinckerhoff Quade and Douglas Inc., New York.

Wittke, W., Druffel, R., Erichsen, C., Gattermann, J., Kiehl, J., Schmidt, D., et al. (2007). *Stability analysis and design for mechanized tunnelling.* (W. WBI Professor Dr.-Ing. Wittke, Éd.) Grundbau und Felsbau GmbH, Aachen.

Xu, L. (1992). Geometrical stiffness and sensitivity matrices for optimization of semi-rigid steel frameworks. *Structural Optimization*, *5*, 95-99.

Yamaguchi, I., Yamazaki, I., & Kiritani, Y. (1998). Study of ground-tunnel interactions of four shield tunnels driven in close proximity, in relation to design and construction of parallel shield tunnels. *Tunnelling and Underground Space Technology*, *13(3)*, 289-304.

Yang, X. L., & Wang, J. M. (2011). Ground movement prediction for tunnels using simplified procedure. *Tunnelling and Underground Space Technology*, *26*, 462-471.

Zhang, Z., & Huang, M. (2014). Geotechnical influence on existing subway tunnels induced by multiline tunnelling in Shanghai soft soil. *Computers and Geotechnics 2014*, *56*, 121-132.

Zheng, Y., & Qiu, W. (2005). 3-D FEM analysis of closely spaced vertical twin tunnel. *Underground Space Use: Analysis of the Past and Lessons for the Future – Erdem \& Solak (eds) © 2005 Taylor \& Francis Group, London, ISBN 04 1537 452 9*, (pp. 1155-1160).

Zheng-Rong, H., Wei, Z., Jing-Hua, L., Jian, L., & Rui, J. (2006). Three dimensional numerical modelling of shield tunnel lining. *Tunnelling and Underground Space Technology*, *21 (3-4)*, 434.

Zhong, X., Zhu, W., Huang, Z., & Han, Y. (2006). Effect of joint structure on joint stiffness for shield tunnel lining. *Tunneling and Underground Space Technology*, *21*, 406-407.

Zhou, J. Y. (1988). The analysis of segmental circular tunnel lining. *Underground Engineering and Tunnels*, *4*, 2-6.

Zurlo, M. A. (2012). Seismic response of circular tunnels: Numerical validation of closed form solutions. *1st Civil and Environmental Engineering Student Conference 25-26 June 2012 Imperial College London.*

Appendix A

Parametric analyses/Design figures

This appendix presents parametric analyses in Chapter 6, using the FEMCL code, on the basis of the input data introduced in **Table** 6-1. The R and T symbols in figures correspond to different cases of tunnel radius and lining thickness.
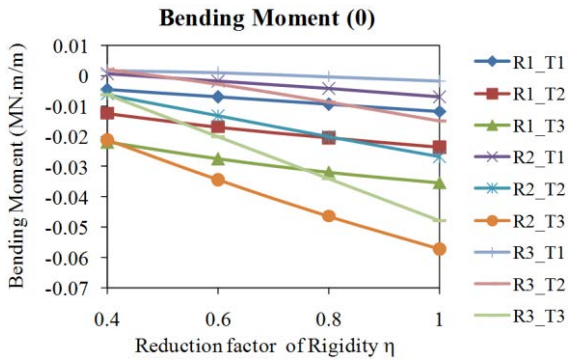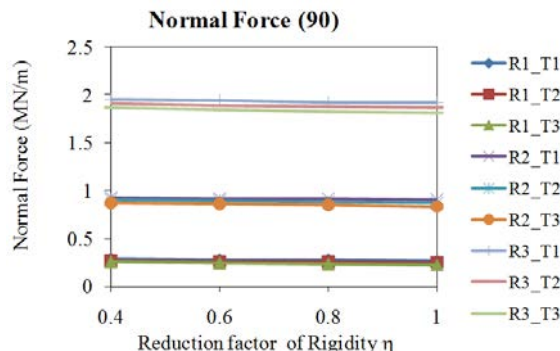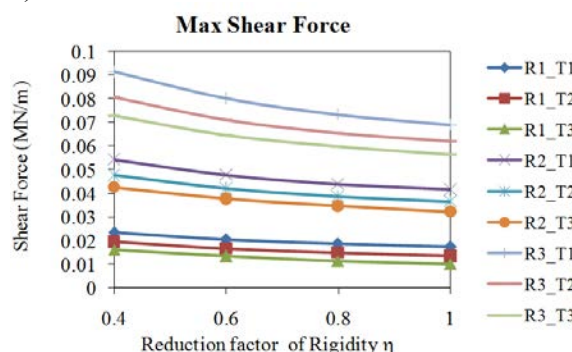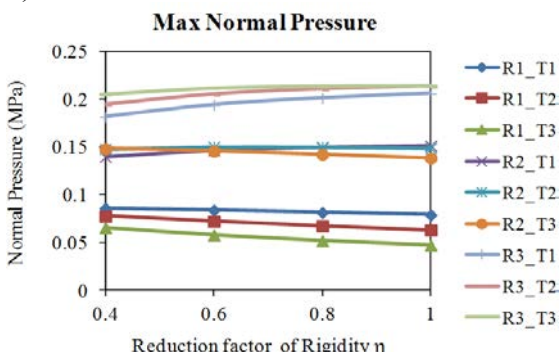
a) Bending moment at the tunnel sidewall
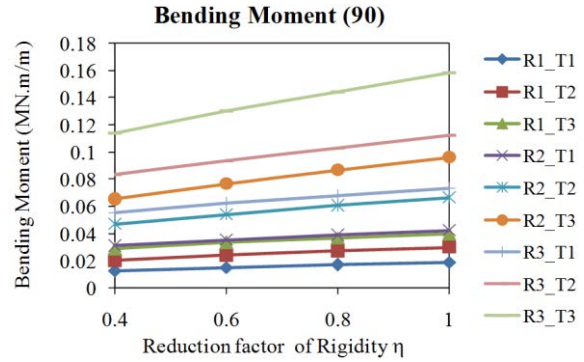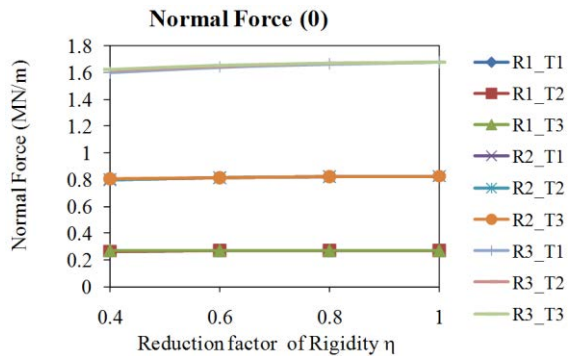
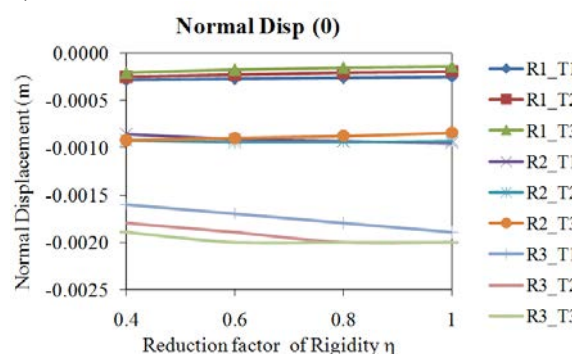b) Bending moment at the tunnel crown

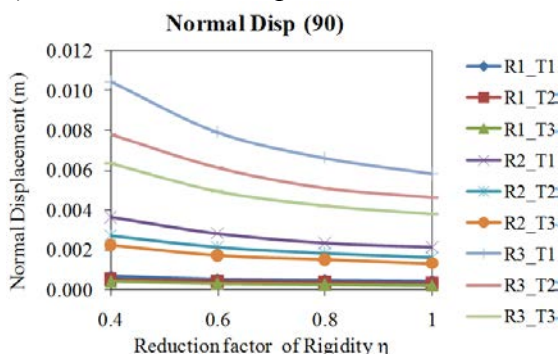c) Normal force at the tunnel sidewall
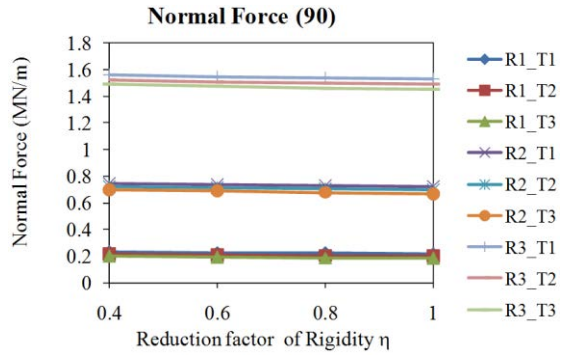
d) Normal force at the tunnel crown
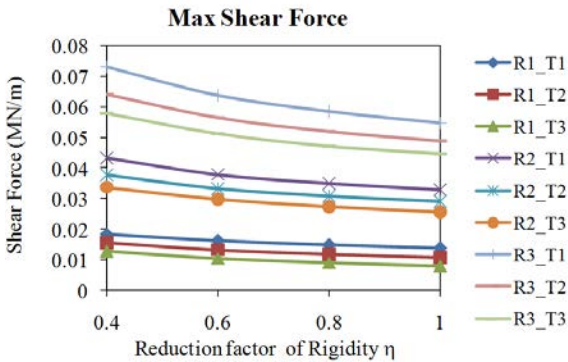
e) Maximum shear force
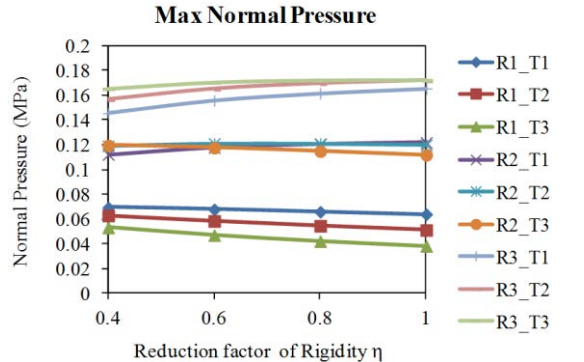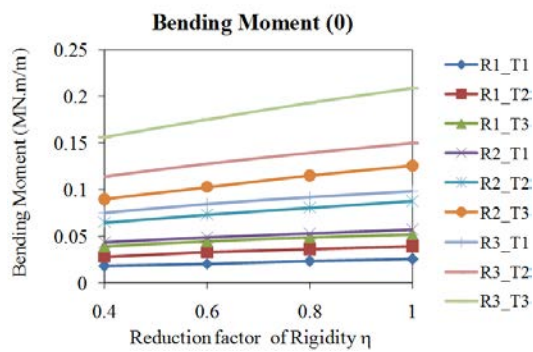
f) Maximum normal pressure
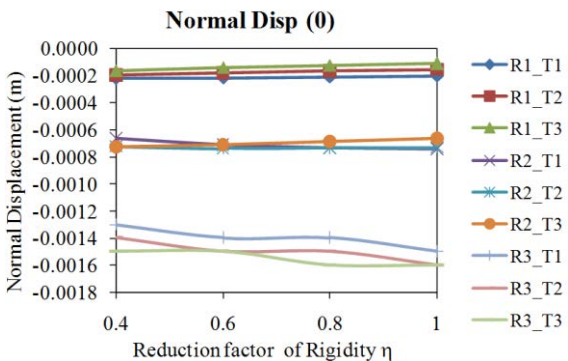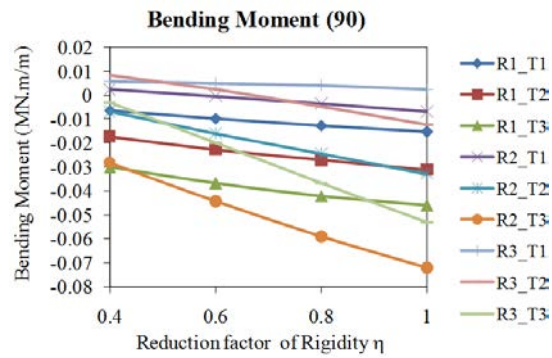
g) Normal displacement at the tunnel sidewall
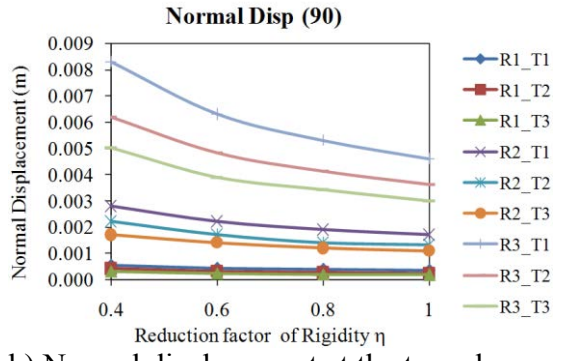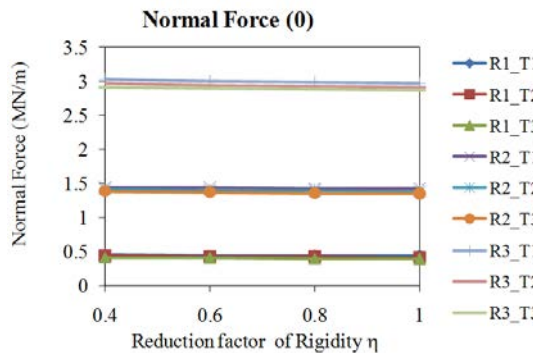
h) Normal displacement at the tunnel crown

Figure A.1. Behaviour of the tunnel lining considering changes in the tunnel dimensions (diameter D), lining thickness, and reduction factor of rigidity, η, (ground type A: cohesion c = 0.05MPa, friction angle $\phi = 35^0$, Young's modulus $E_S = 500$MPa; $K_0 = 0.5$; $H = 4R$) (Case 1)
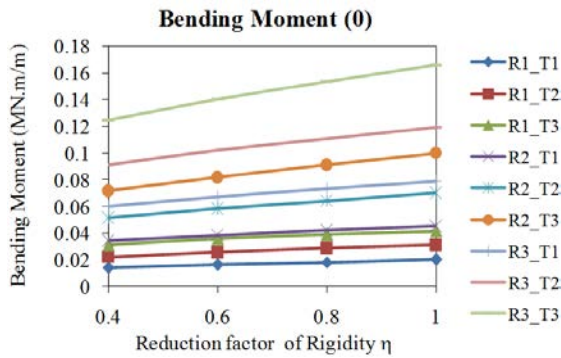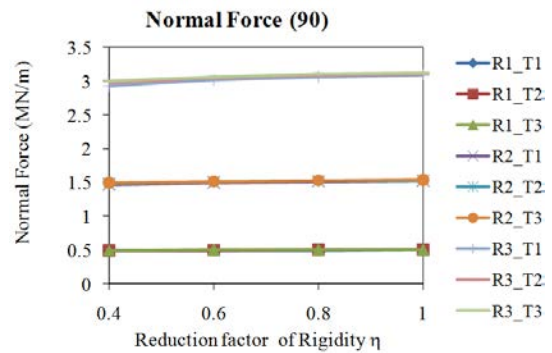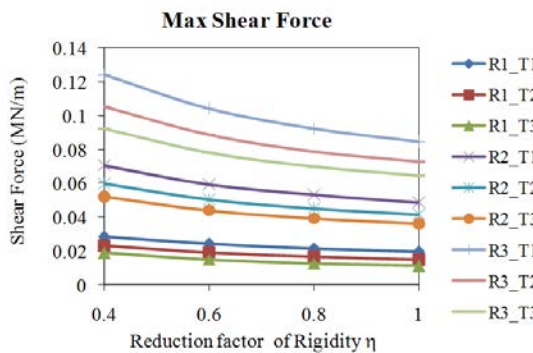
a) Bending moment at the tunnel sidewall
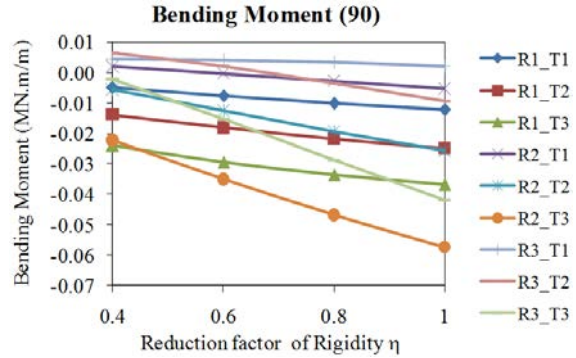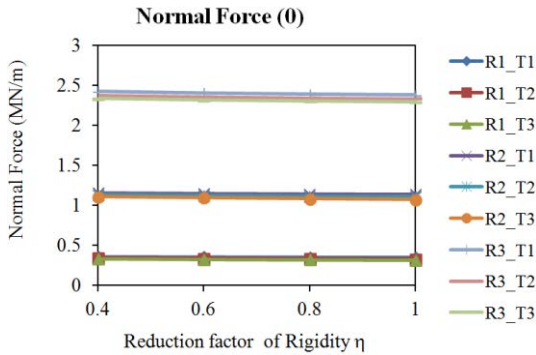
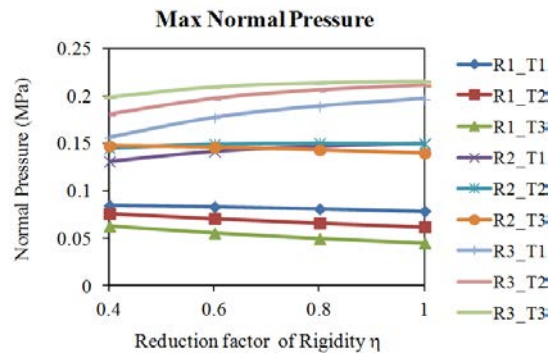b) Bending moment at the tunnel crown

c) Normal force at the tunnel sidewall
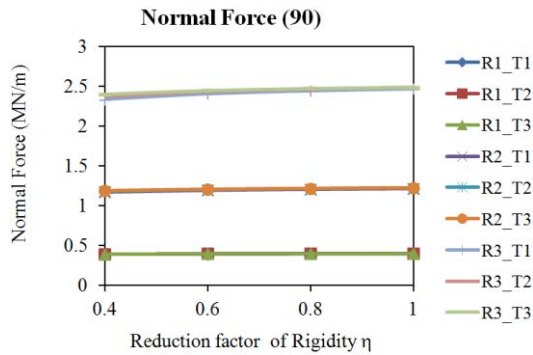
d) Normal force at the tunnel crown
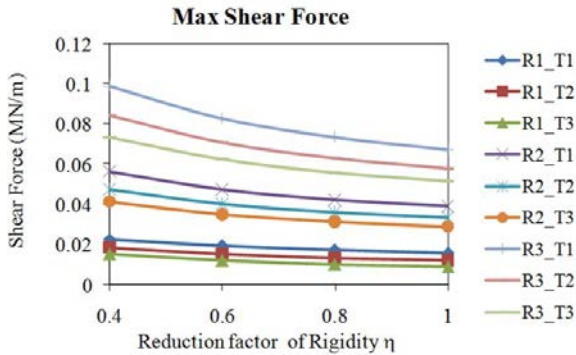
e) Maximum shear force
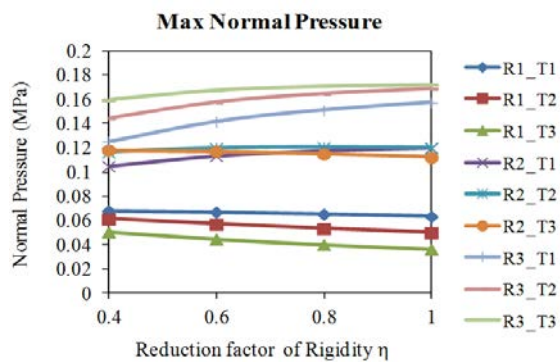
f) Maximum normal pressure
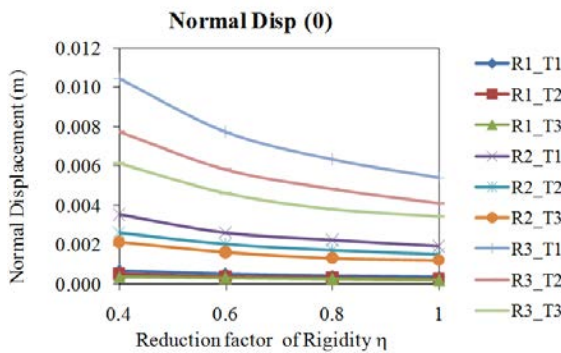
g) Normal displacement at the tunnel sidewall
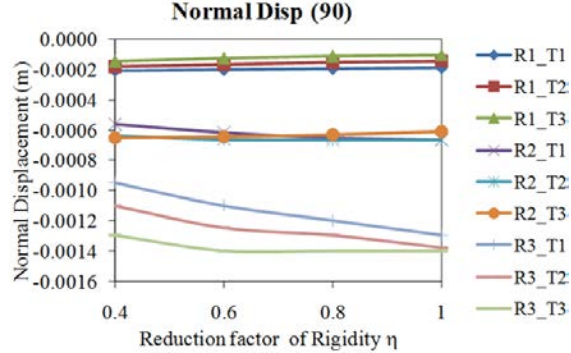
h) Normal displacement at the tunnel crown

Figure A.2. Behaviour of the tunnel lining considering changes in the tunnel dimensions (diameter D), lining thickness, and reduction factor of rigidity, η, (ground type A: cohesion $c = 0.05$MPa, friction angle $\phi = 35^0$, Young's modulus $E_S = 500$MPa; $K_0 = 1.5$; $H = 4R$) (Case 2).
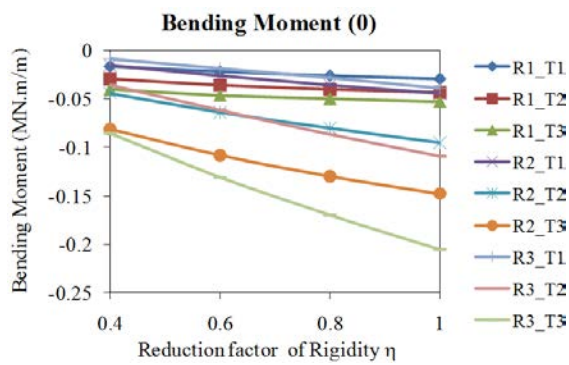
a) Bending moment at the tunnel sidewall
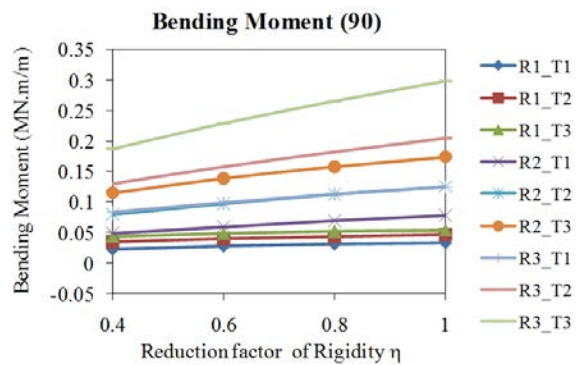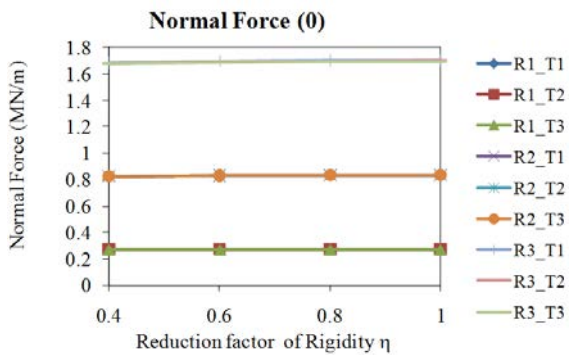
b) Bending moment at the tunnel crown
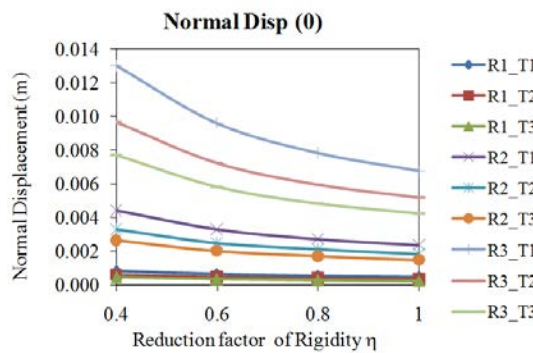
c) Normal force at the tunnel sidewall
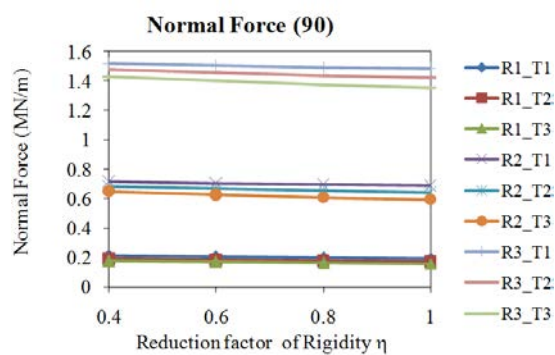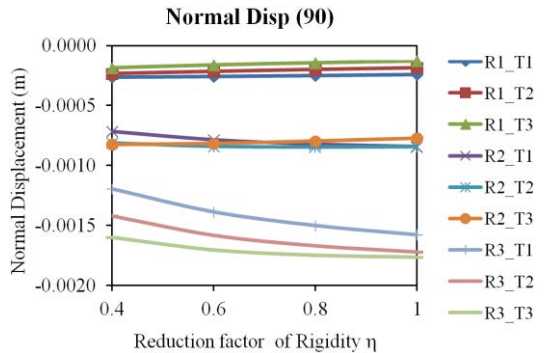
d) Normal force at the tunnel crown
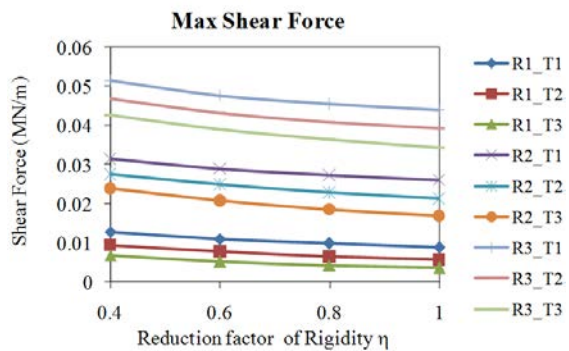
e) Maximum shear force
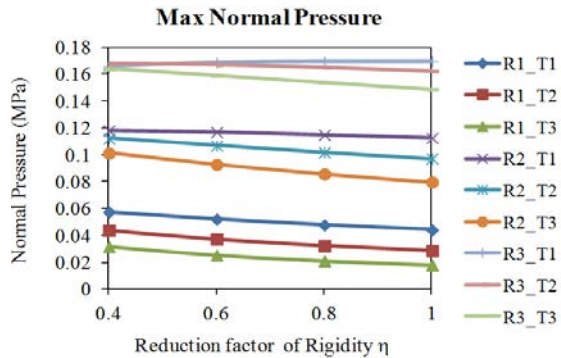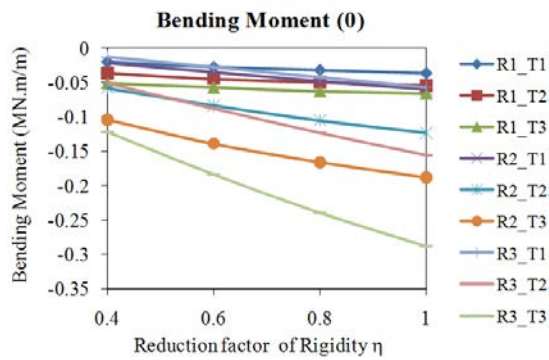
f) Maximum normal pressure
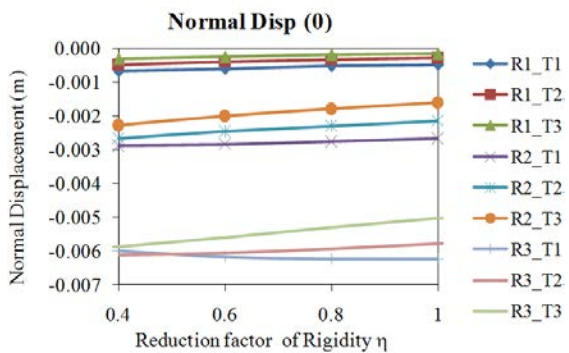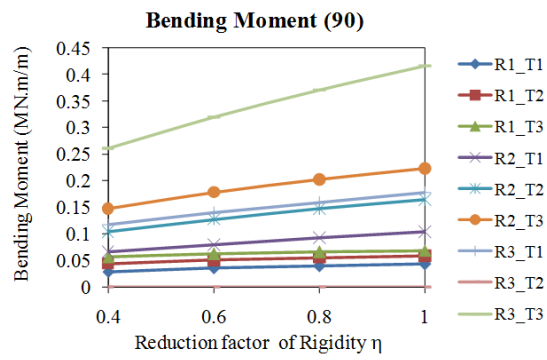
g) Normal displacement at the tunnel sidewall
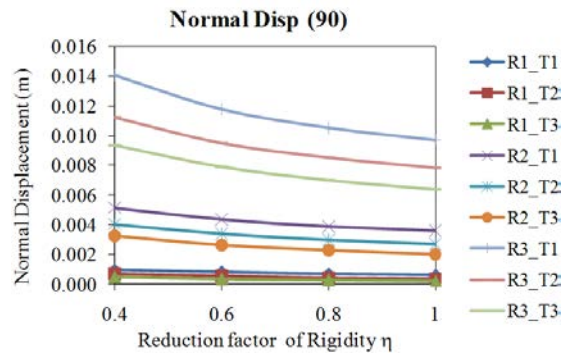
h) Normal displacement at the tunnel crown

Figure A.3. Behaviour of the tunnel lining considering changes in the tunnel dimensions (diameter D), lining thickness, and reduction factor of rigidity, η, (ground type B: cohesion $c = 0.02$MPa, friction angle $\phi = 31^0$, Young's modulus $E_S = 150$MPa; $K_0 = 0.5$; $H = 4R$) (Case 3).
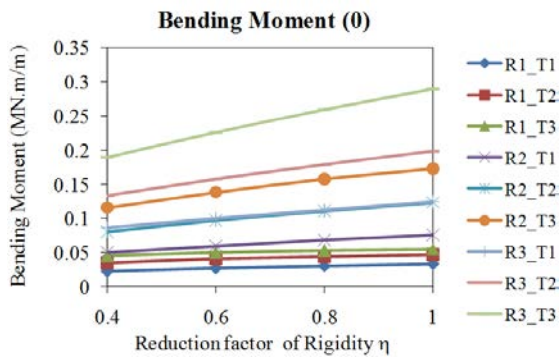
a) Bending moment at the tunnel sidewall   b) Bending moment at the tunnel crown
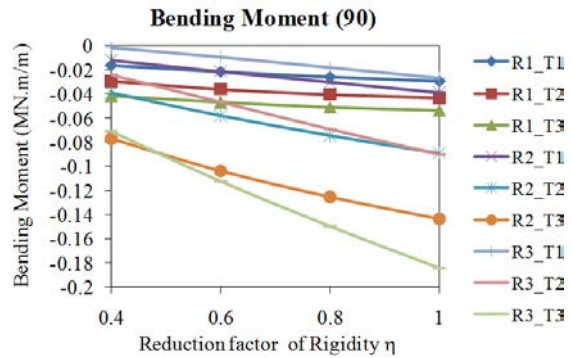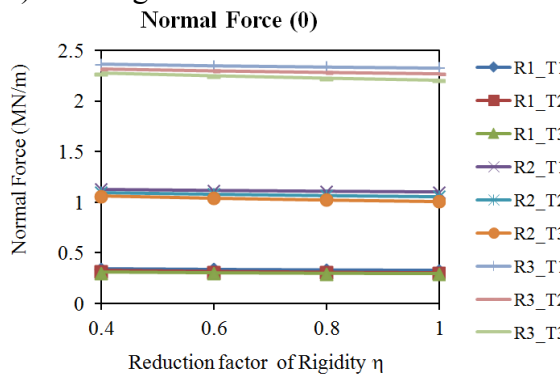
c) Normal force at the tunnel sidewall   d) Normal force at the tunnel crown
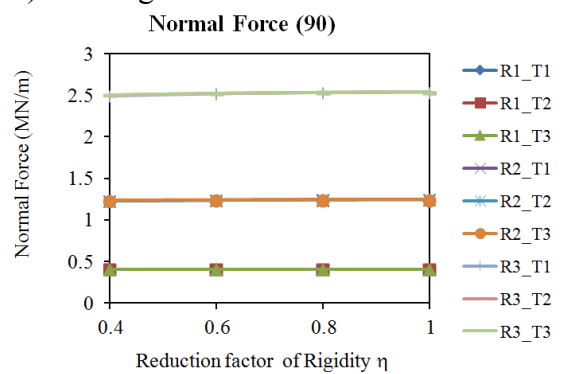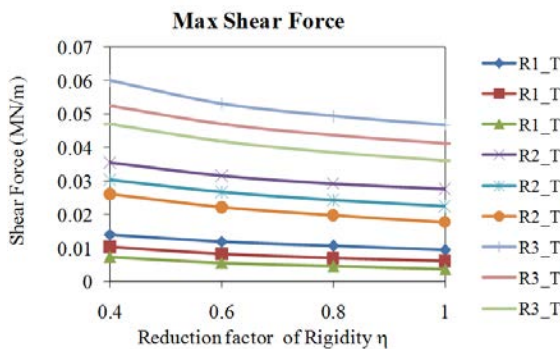
e) Maximum shear force   f) Maximum normal pressure
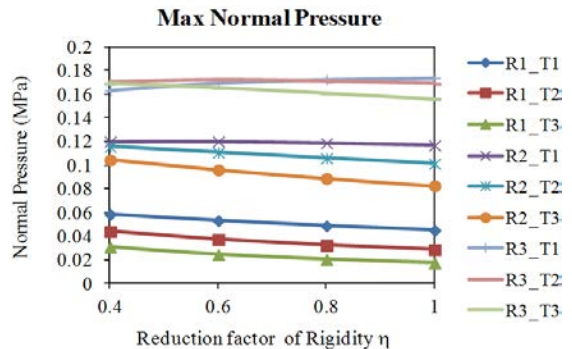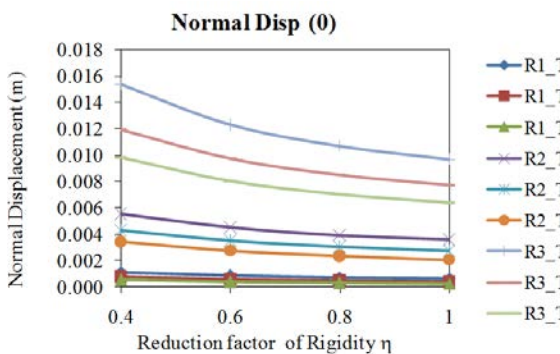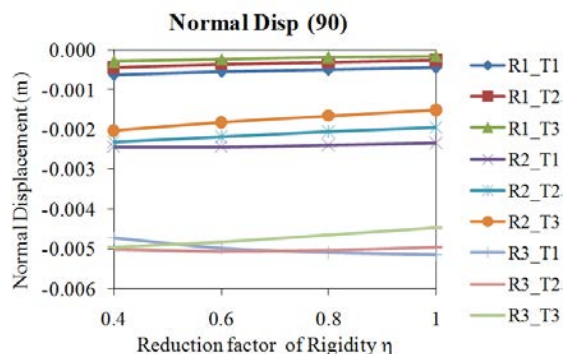
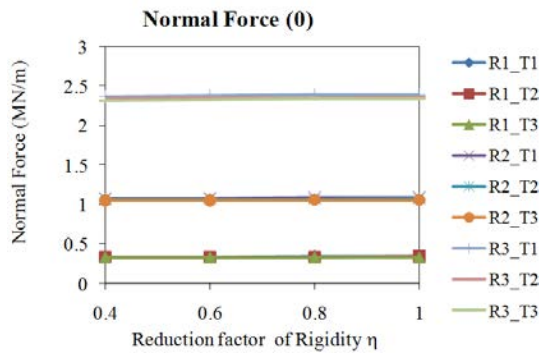g) Normal displacement at the tunnel sidewall   h) Normal displacement at the tunnel crown

Figure A.4. Behaviour of the tunnel lining considering changes in the tunnel dimensions (diameter D), lining thickness, and reduction factor of rigidity, η, (ground type B: cohesion c = 0.02MPa, friction angle $\phi = 31^0$, Young's modulus E_S = 150MPa; K_0= 1.5; $H = 4R$) (Case 4).
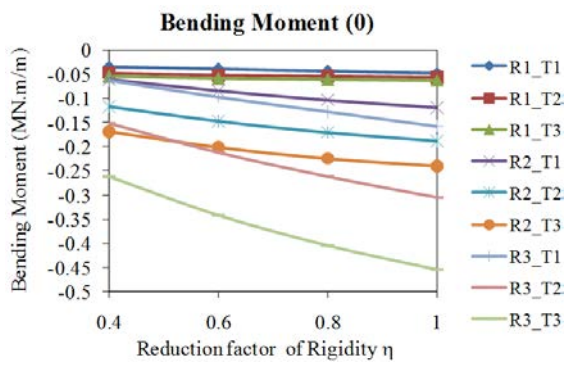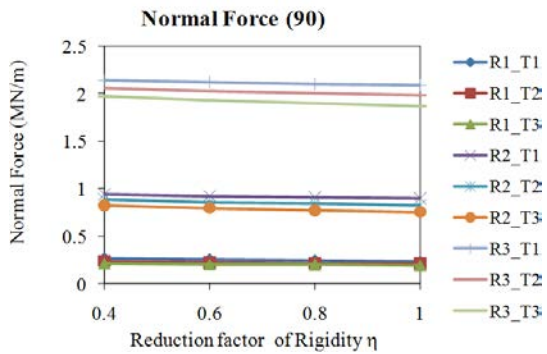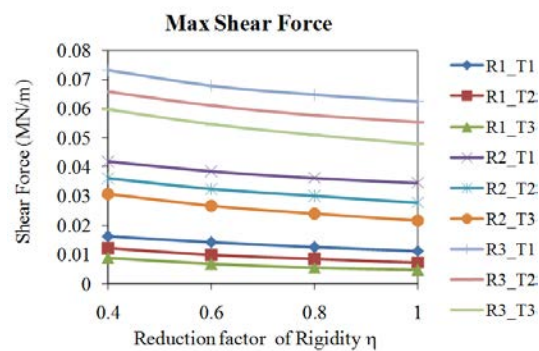
a) Bending moment at the tunnel sidewall
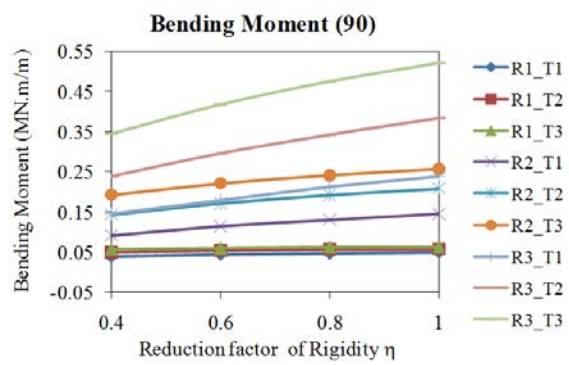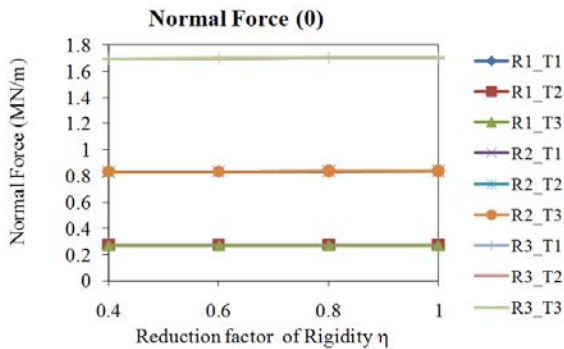
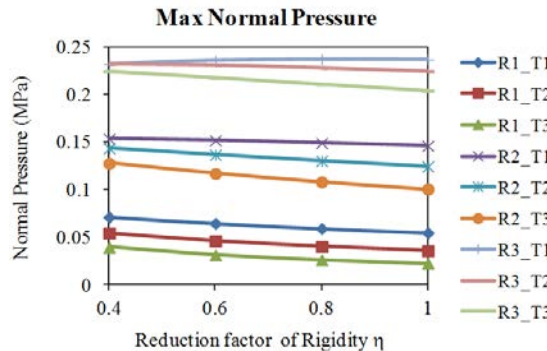b) Bending moment at the tunnel crown

c) Normal force at the tunnel sidewall
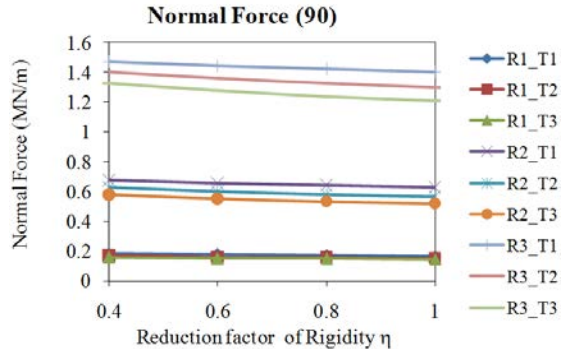
d) Normal force at the tunnel crown
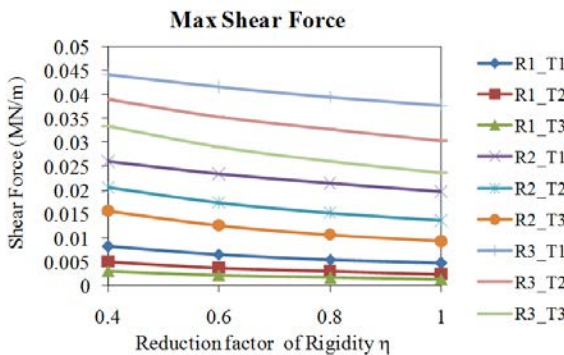
e) Maximum shear force
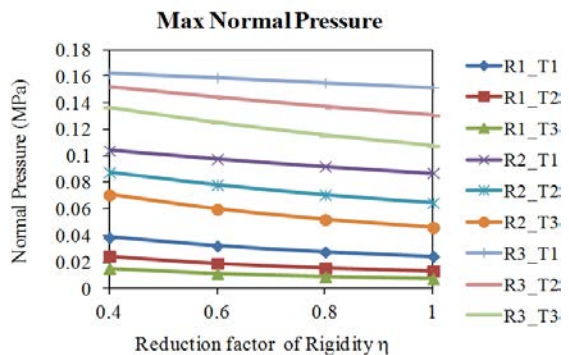
f) Maximum normal pressure
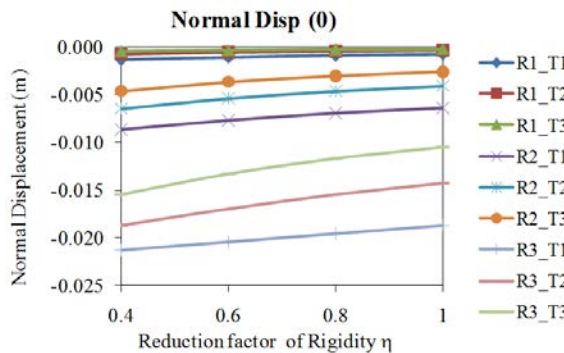
g) Normal displacement at the tunnel sidewall
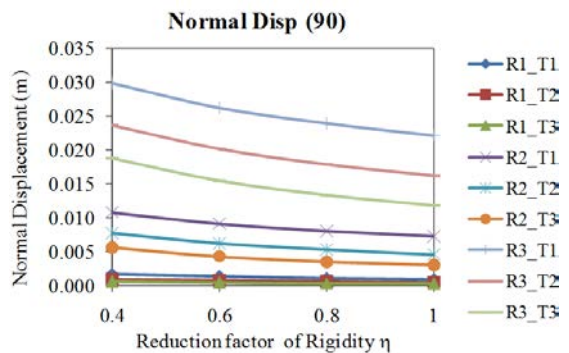
h) Normal displacement at the tunnel crown

Figure A.5. Behaviour of the tunnel lining considering changes in the tunnel dimensions (diameter D), lining thickness, and reduction factor of rigidity, η, (ground type C: cohesion c = 0.005MPa, friction angle ϕ = 28^0, Young's modulus E_S = 50MPa; K_0= 0.5; H = 4R) (Case 5).
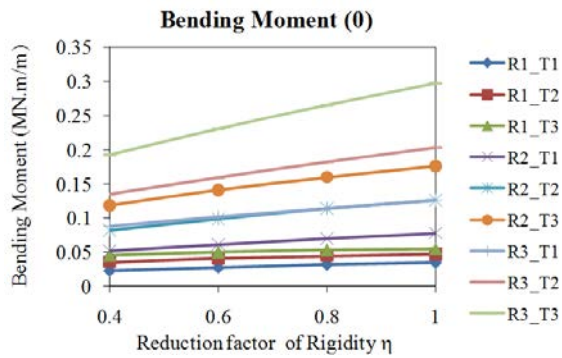
a) Bending moment at the tunnel sidewall
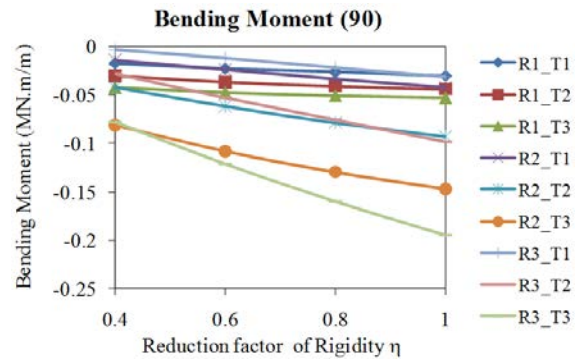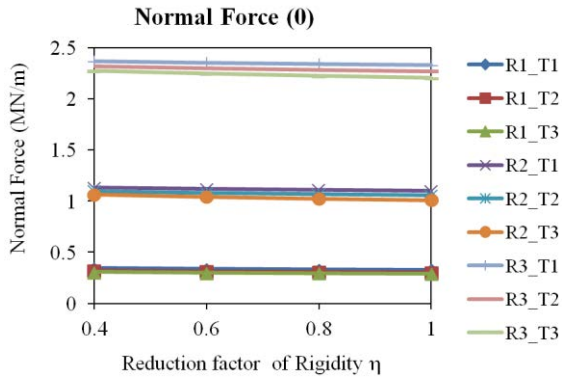
b) Bending moment at the tunnel crown
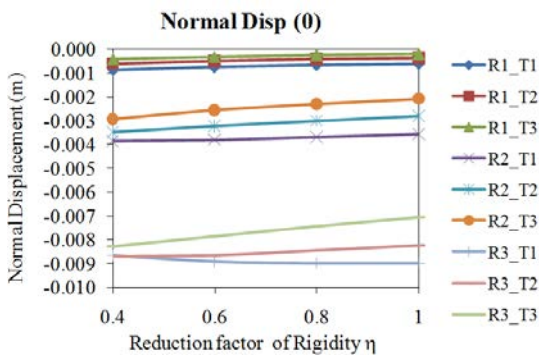
c) Normal force at the tunnel sidewall
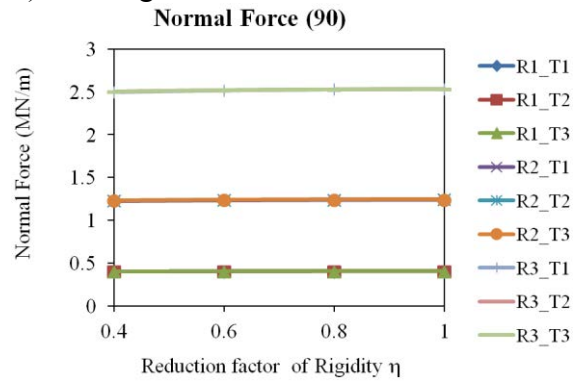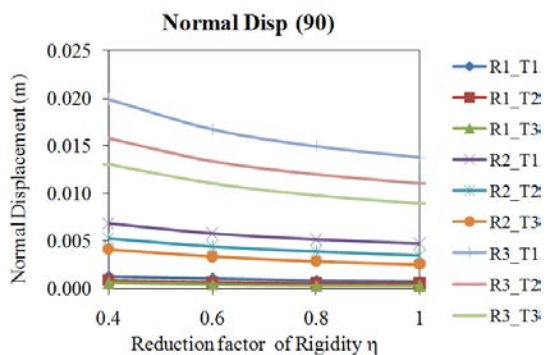
d) Normal force at the tunnel crown
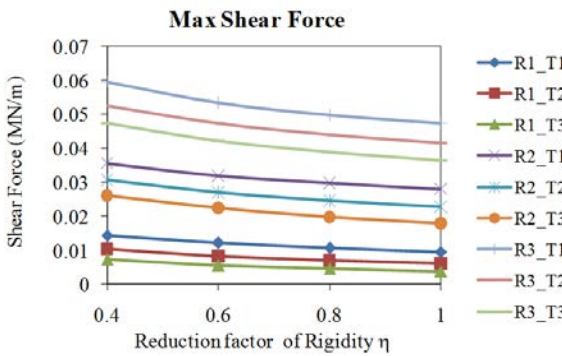
e) Maximum shear force
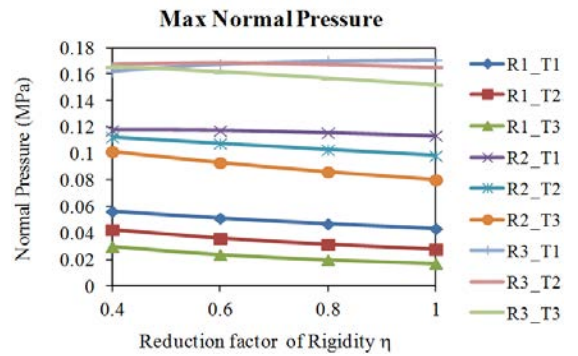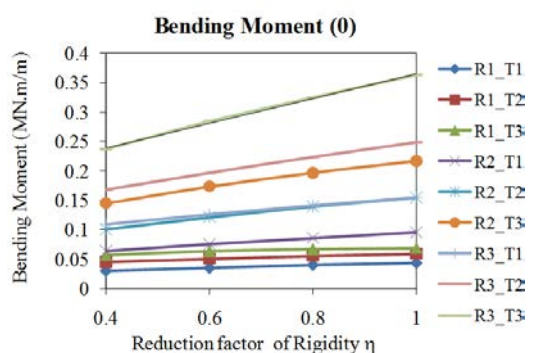
f) Maximum normal pressure
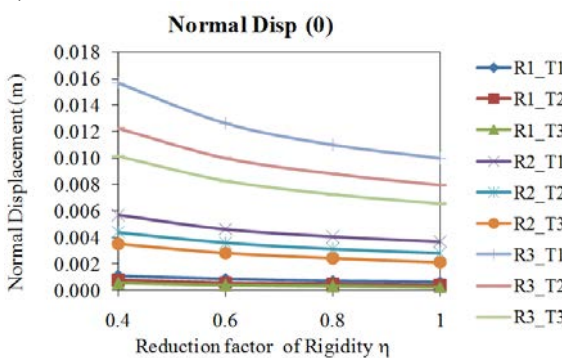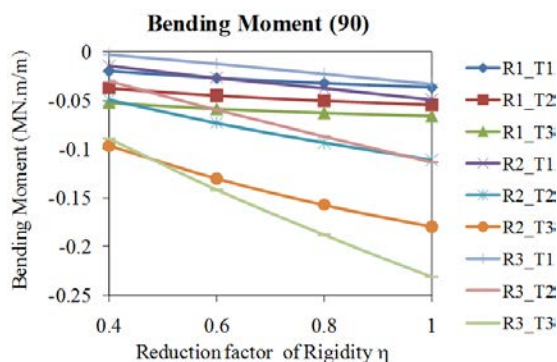
g) Normal displacement at the tunnel sidewall
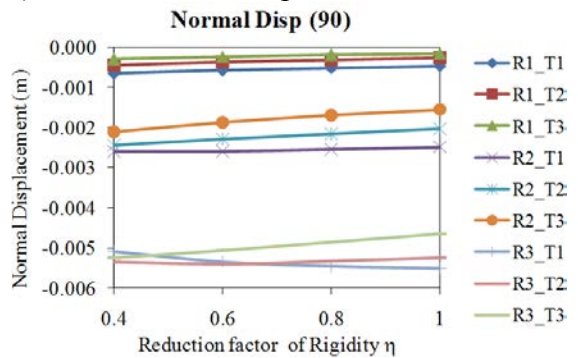
h) Normal displacement at the tunnel crown

Figure A.6. Behaviour of the tunnel lining considering changes in the tunnel dimensions (diameter D), lining thickness, and reduction factor of rigidity, η, (ground type C: cohesion c = 0.005MPa, friction angle $\phi = 28^0$, Young's modulus E_S = 50MPa; K_0 = 1.5; $H = 4R$) (Case 6).
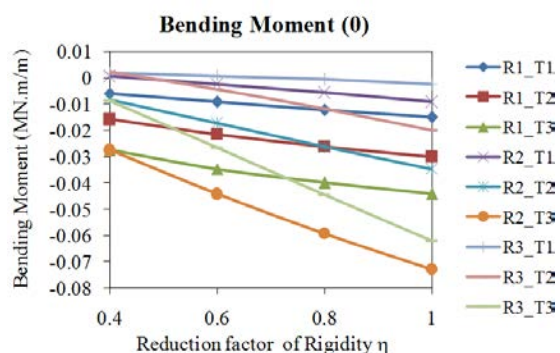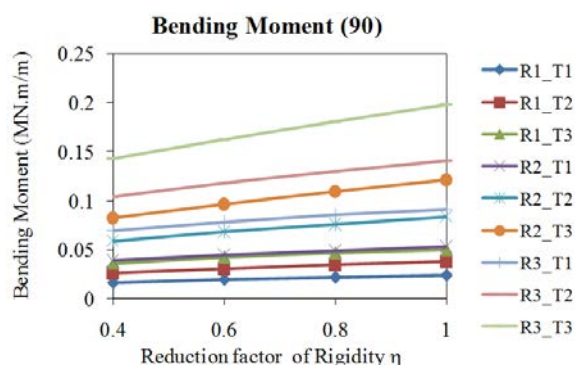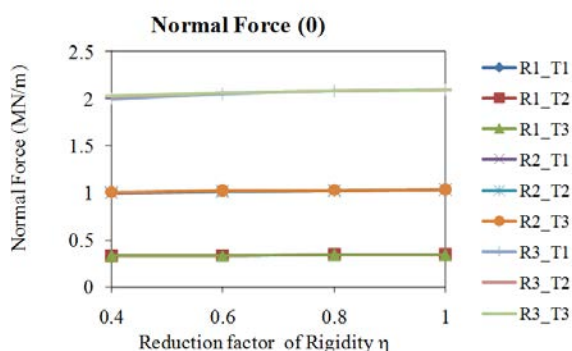
a) Bending moment at the tunnel sidewall
b) Bending moment at the tunnel crown
c) Normal force at the tunnel sidewall
d) Normal force at the tunnel crown
e) Maximum shear force
f) Maximum normal pressure
g) Normal displacement at the tunnel sidewall
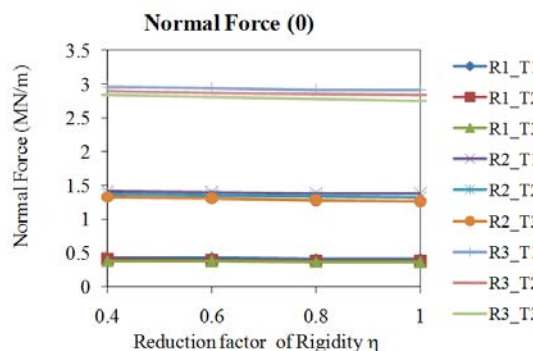h) Normal displacement at the tunnel crown

Figure A.7. Behaviour of the tunnel lining considering changes in the tunnel dimensions (diameter D), lining thickness, and reduction factor of rigidity, η, (ground type A: cohesion c = 0.05MPa, friction angle ϕ = 35^0, Young's modulus E_S = 500MPa; K_0= 0.5; H = 20R) (Case 7).
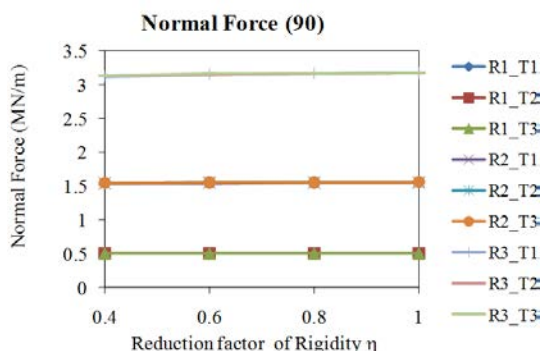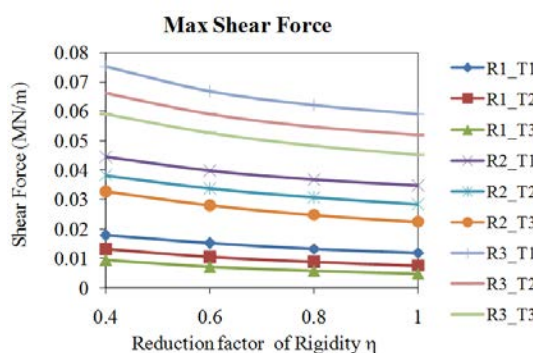
a) Bending moment at the tunnel sidewall

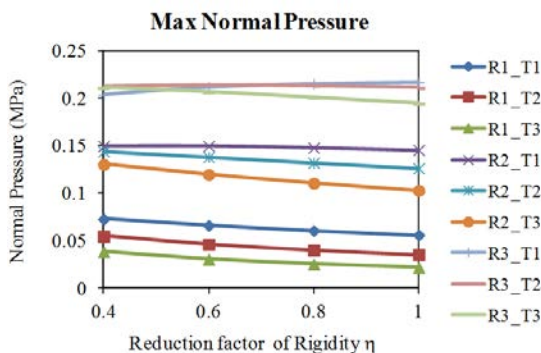b) Bending moment at the tunnel crown

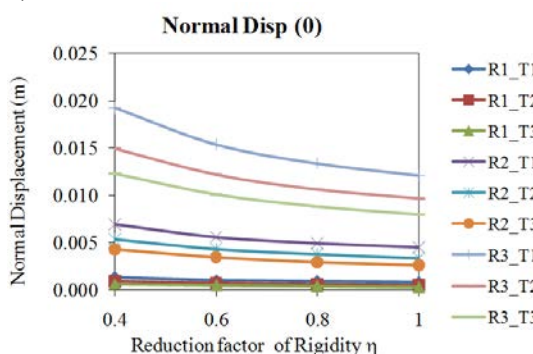c) Normal force at the tunnel sidewall

d) Normal force at the tunnel crown

e) Maximum shear force

f) Maximum normal pressure

g) Normal displacement at the tunnel sidewall

h) Normal displacement at the tunnel crown

Figure A.8. Behaviour of the tunnel lining considering changes in the tunnel dimensions (diameter D), lining thickness, and reduction factor of rigidity, η, (ground type A: cohesion c = 0.05MPa, friction angle ϕ = 35^0, Young's modulus E_S = 500MPa; K_0= 1.5; H = 20R) (Case 8).

a) Bending moment at the tunnel sidewall

b) Bending moment at the tunnel crown

c) Normal force at the tunnel sidewall
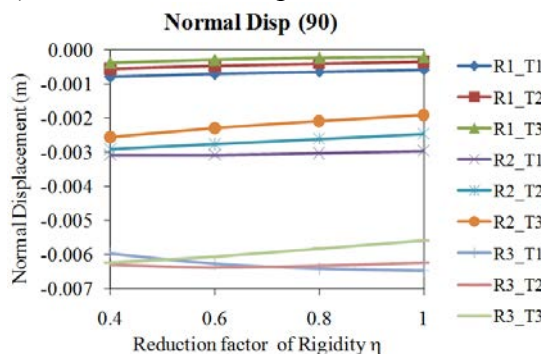
d) Normal force at the tunnel crown
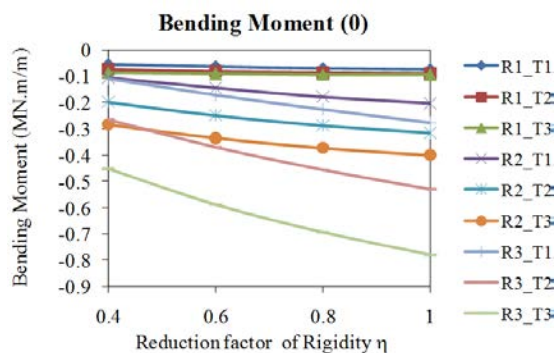
e) Maximum shear force

f) Maximum normal pressure
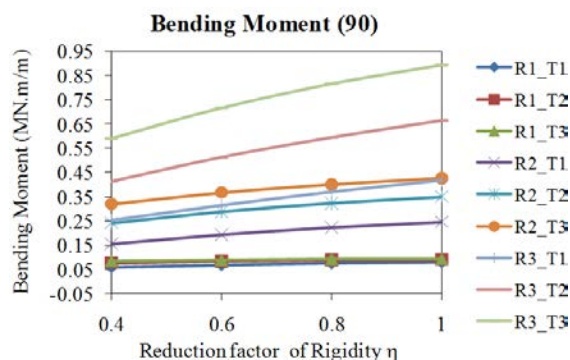
g) Normal displacement at the tunnel sidewall
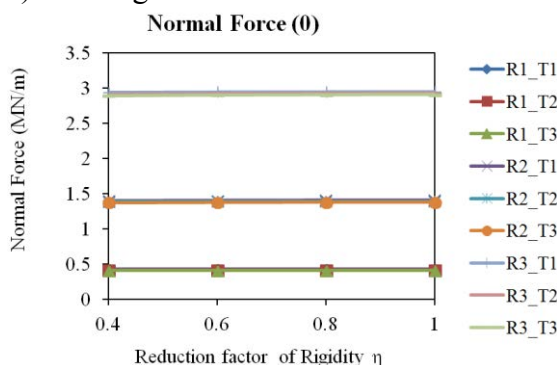
h) Normal displacement at the tunnel crown

Figure A.9. Behaviour of the tunnel lining considering changes in the tunnel dimensions (diameter D), lining thickness, and reduction factor of rigidity, η, (ground type B: cohesion c = 0.02MPa, friction angle ϕ = 31^0, Young's modulus E_S = 150MPa; K_0= 0.5; H = 20R) (Case 9).

a) Bending moment at the tunnel sidewall

b) Bending moment at the tunnel crown

c) Normal force at the tunnel sidewall

d) Normal force at the tunnel crown

e) Maximum shear force

f) Maximum normal pressure

g) Normal displacement at the tunnel sidewall

h) Normal displacement at the tunnel crown

Figure A.10. Behaviour of the tunnel lining considering changes in the tunnel dimensions (diameter D), lining thickness, and reduction factor of rigidity, η, (ground type B: cohesion c = 0.02MPa, friction angle ϕ = 31^0, Young's modulus E_S = 150MPa; K_0= 1.5; H = 20R) (Case 10).
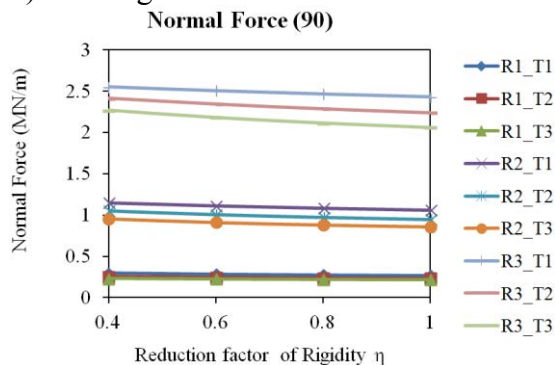
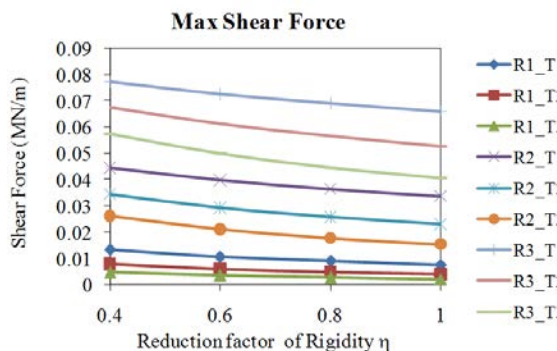a) Bending moment at the tunnel sidewall

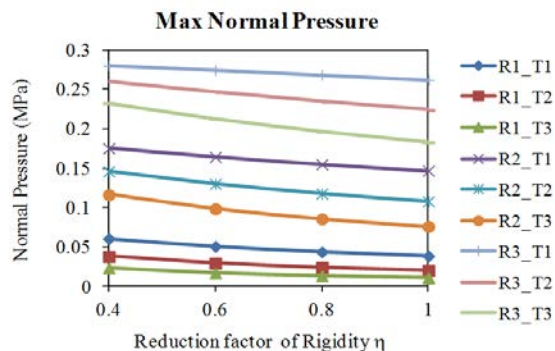b) Bending moment at the tunnel crown

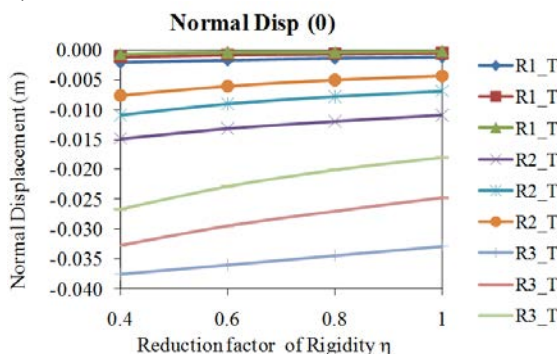c) Normal force at the tunnel sidewall

d) Normal force at the tunnel crown

e) Maximum shear force

f) Maximum normal pressure

g) Normal displacement at the tunnel sidewall

h) Normal displacement at the tunnel crown

Figure A.11**.** Behaviour of the tunnel lining considering changes in the tunnel dimensions (diameter D), lining thickness, and reduction factor of rigidity, η, (ground type C: cohesion c = 0.005MPa, friction angle ϕ = 28^0, Young's modulus E_S = 50MPa; K_0 = 0.5; H = 20R) (Case 11).

a) Bending moment at the tunnel sidewall   b) Bending moment at the tunnel crown

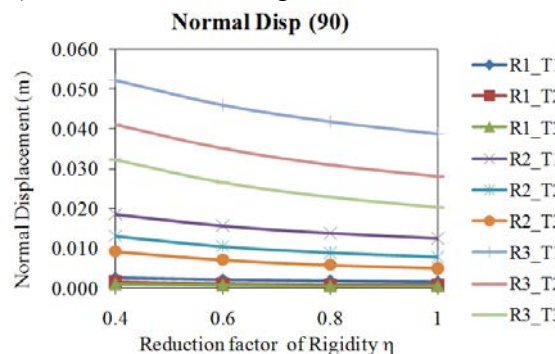c) Normal force at the tunnel sidewall   d) Normal force at the tunnel crown
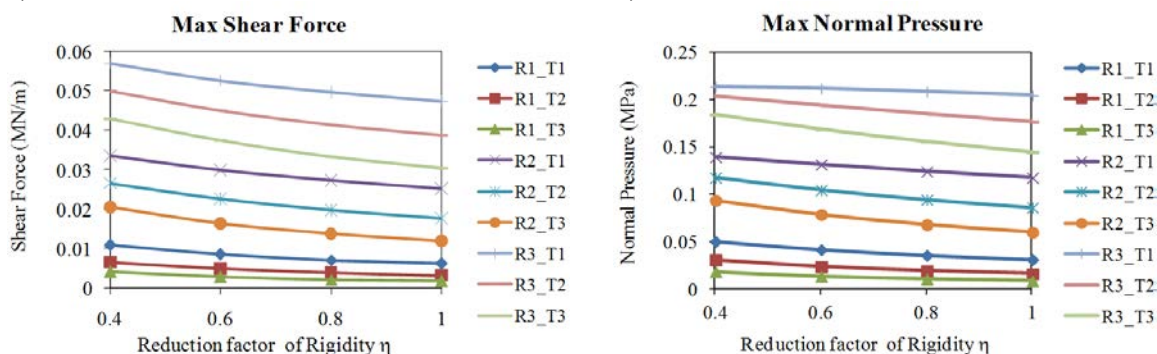
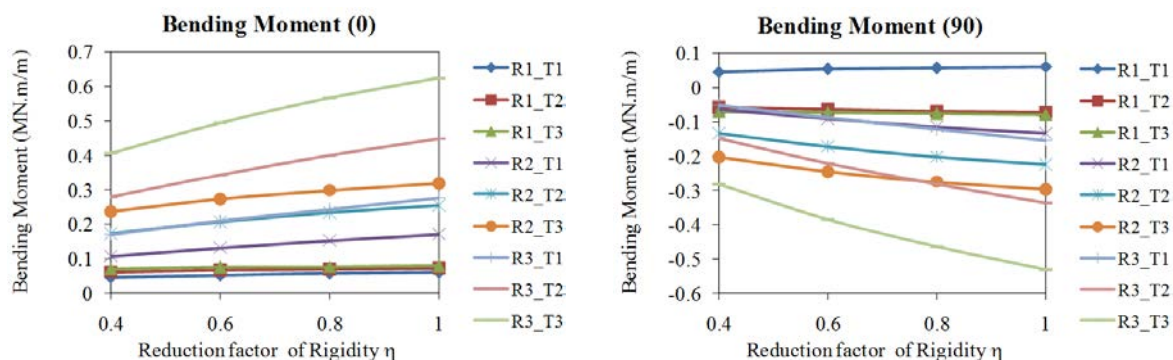e) Maximum shear force   f) Maximum normal pressure

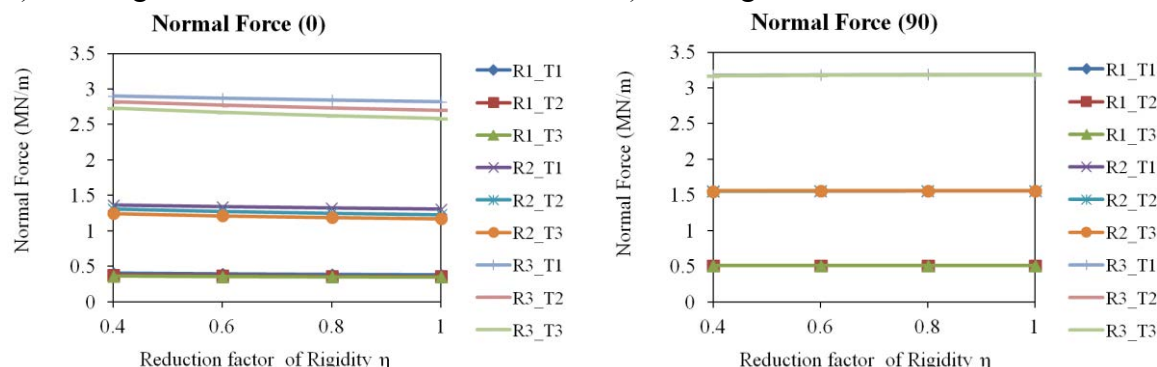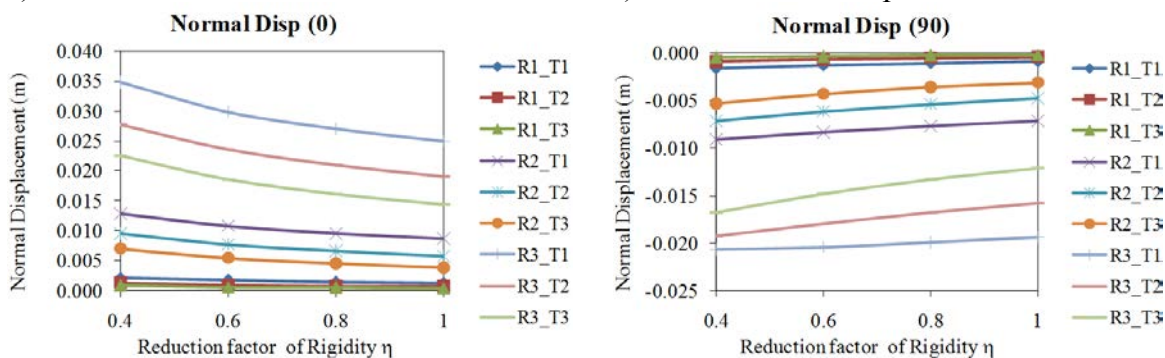g) Normal displacement at the tunnel sidewall   h) Normal displacement at the tunnel crown

Figure A.12. Behaviour of the tunnel lining considering changes in the tunnel dimensions (diameter D), lining thickness, and reduction factor of rigidity, η, (ground type C: cohesion c = 0.005MPa, friction angle ϕ = 28^0, Young's modulus E_S = 50MPa; K_0= 1.5; H = 20R) (Case 12).

FOLIO ADMINISTRATIF

THESE SOUTENUE DEVANT L'INSTITUT NATIONAL DES SCIENCES APPLIQUEES DE LYON

NOM : DO   DATE de SOUTENANCE : 07 juillet 2014

Prénoms : Ngoc Anh

TITRE : Numerical analyses of segmental tunnel lining under static and dynamic loads

NATURE : Doctorat   Numéro d'ordre : 2014ISAL0042

Ecole doctorale : Mécanique, Energétique, Génie civil, Acoustique

Spécialité : Génie Civil

RESUME : This PhD thesis has the aim to study the behaviour of segmental tunnel lining by developing a new numerical approach to the Hyperstatic Reaction Method (HRM) and producing two-dimensional (2D) and three-dimensional (3D) numerical models using the finite difference method (FDM). The study first deals with under static loads, and then performs under dynamic loads.
Firstly, a literature review has been conducted. A new numerical approach applied to the HRM has then been developed. At the same time, a 2D numerical model is programmed regarding static loading conditions in order to evaluate the influence of the segmental joints, in terms of both joint distribution and joint stiffness characteristics, on the tunnel lining behaviour. After that, full 3D models of a single tunnel, twin horizontal tunnels and twin tunnels stacked over each other, excavated in close proximity in which the joint pattern is simulated, have been developed. These 3D models allow one to investigate the behaviour of not only the tunnel lining but also the displacement of the ground surrounding the tunnel during the tunnel excavation. A simplified 3D numerical model has then been produced in order to validate the new numerical approach applied to the HRM.
In the last part of the manuscript, the performance of the segmental tunnel lining exposed to dynamic loading is taken into consideration through quasi-static and full dynamic analyses using 2D numerical models (FDM). A new HRM model has also been developed considering quasi-static loading. The differences of the tunnel behaviour under static and seismic loadings are highlighted.

MOTS-CLES : Tunnel; Segmental lining; Hyperstatic Reaction Method; Numerical model; Quasi static; Dynamic; Soft ground

Laboratoire (s) de recherche : LGCIE – Laboratoire de Génie Civil et d'Ingénierie Environnementale

Directeur de thèse: Professeur Daniel DIAS et Professeur Irini DJERAN-MAIGRE

Président de jury : Professeur Richard KASTNER

Composition du jury :

Richard KASTNER	Professeur, Lab. LGCIE, INSA de Lyon, France	Président
Tarcisio CELESTINO	Professeur, University of São Paulo, Brazil	Rapporteur
Günther MESCHKE	Professeur, Ruhr-Universität Bochum, Germany	Rapporteur
Pierpaolo ORESTE	Professeur associé, Politecnico di Torino, Italie	Examinateur
Irini DJERAN-MAIGRE	Professeur, Lab. LGCIE, INSA de Lyon, France	Directrice de thèse
Daniel DIAS	Professeur, Lab. LTHE, Grenoble Alpes Université	Directeur de thèse

SUMMARY: This PhD thesis has the aim to study the behaviour of segmental tunnel lining by developing a new numerical approach to the Hyperstatic Reaction Method (HRM) and producing two-dimensional (2D) and three-dimensional (3D) numerical models using the finite difference method (FDM). The study first deals with under static loads, and then performs under dynamic loads.

Firstly, a literature review has been conducted. A new numerical approach applied to the HRM has then been developed. At the same time, a 2D numerical model is programmed regarding static loading conditions in order to evaluate the influence of the segmental joints, in terms of both joint distribution and joint stiffness characteristics, on the tunnel lining behaviour. After that, full 3D models of a single tunnel, twin horizontal tunnels and twin tunnels stacked over each other, excavated in close proximity in which the joint pattern is simulated, have been developed. These 3D models allow one to investigate the behaviour of not only the tunnel lining but also the displacement of the ground surrounding the tunnel during the tunnel excavation. A simplified 3D numerical model has then been produced in order to validate the new numerical approach applied to the HRM.

In the last part of the manuscript, the performance of the segmental tunnel lining exposed to dynamic loading is taken into consideration through quasi-static and full dynamic analyses using 2D numerical models (FDM). A new HRM model has also been developed considering quasi-static loads. The differences of the tunnel behaviour under static and seismic loadings are highlighted.

Keywords: Tunnel; Segmental lining; Hyperstatic Reaction Method; Numerical model; Quasi static; Dynamic; Soft ground.

_____

RÉSUMÉ : Cette thèse vise à étudier le comportement de revêtement articulé du tunnel en développant une nouvelle approche numérique à la Méthode de Réaction Hyperstatique (HRM) et la production des modèles numériques en deux dimensions et trois dimensions à l'aide de la méthode des différences finies (FDM). L'étude a été traitée d'abord sous charges statiques, puis effectuée sous charges dynamiques.

Tout d'abord, une étude bibliographique a été effectuée. Une nouvelle approche numérique appliquée à la méthode HRM a ensuite été développée. En même temps, un modèle numérique en deux dimensions est programmé sur les conditions de charge statique dans le but d'évaluer l'influence des joints, en termes de la distribution et des caractéristiques des joints, sur le comportement du revêtement articulé de tunnel. Après cela, des modèles complets en trois dimensions d'un seul tunnel, de deux tunnels horizontaux et de deux tunnels empilés, dans lesquels le système des joints est simulé, ont été développés. Ces modèles en trois dimensions permettent d'étudier le comportement non seulement du revêtement du tunnel, mais encore le déplacement du sol entourant le tunnel lors de l'excavation. Un modèle numérique en trois dimensions simplifié a ensuite été réalisé afin de valider la nouvelle approche numérique appliquée à la méthode HRM.

Dans la dernière partie de ce mémoire, la performance du revêtement articulé du tunnel sous chargements dynamiques est prise en compte par l'analyse quasi-statique et dynamique complète en utilisant le modèle numérique en deux dimensions (FDM). Un modèle HRM a également été développé prenant en compte des charges quasi-statiques. Les différences de comportement de tunnel sous chargements statiques et sismiques sont mises en évidence et expliquées.

Mots-clés: Tunnel; Revêtement articulé; Méthode de Réaction Hyperstatiques; Modèle numérique; Quasi statique; Dynamique; Sol souple.